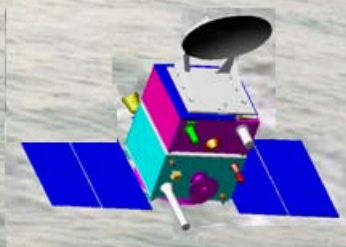




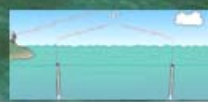
nrsc

**Proceedings of the workshop
on
Utilisation of Satellite Derived Oceanic
Heat Content for Cyclone Studies**



held at

**National Remote Sensing Centre
Indian Space Research Organisation
Hyderabad, India
During March 25-26, 2010**



INTRODUCTION:

National Remote Sensing Centre (NRSC), Indian Space Research Organisation (ISRO), Hyderabad organized a two day workshop on “Utilisation of satellite derived oceanic heat content for cyclone studies” during 25-26 March 2010 at NRSC. The programme of the workshop is given in annexure-1. 52 Participants from 16 institutions attended the workshop. The list of participants with their designations and institutions is given in annexure-2. The workshop has seven components: Inaugural session, invited special talks session, four technical sessions and the concluding session. Each technical session has a lead talk followed by the invited talks. The presentations are made by invitations.

INAUGURAL SESSION:

In the inaugural session while introducing the workshop M M Ali, convener of the workshop, mentioned that satellite derived oceanic heat content is being extensively used for the cyclone track and intensity prediction (CTIP) in the Atlantic and Pacific Oceans. However, the potential of this parameter in the North Indian Ocean is yet to be realised. In view of the varying coastal bathymetry adjoining the Indian seas accurate prediction of cyclone track and intensity are very critical in assessing the precise consequences of storm surge. Thus, the organizers felt the need of this workshop. If the oceanic heat content (OHC) has to be estimated over larger temporal and spatial scales, satellite altimetry is the only solution. This workshop is also timely in the context of the launch of Altika onboard SARAL (Satellite with ARgoes and ALtika) in very near future. Altika is a ka-band altimeter with a foot print of ~8 km operating at 35.75 GHz. The smaller foot print can provide SSHA required to estimate the oceanic heat content closer to the coast (5km with a Ka-band as against 10 Km with Ku-band) enabling estimating the intensity of the cyclones just before crossing. G. Behera, Group Director, Oceanography and Water Resources Group welcomed the audience that has come from various national organizations, universities and the other academic institutions. In the inaugural speech Dr. P S Roy, Deputy Director (RS&GIS-AA), NRSC mentioned about the meteorological and oceanographic requirements for the CTIP. Dr. Gustavo J Goni, Director, Physical Oceanography Division, Atlantic

Oceanographic and Meteorological Laboratory (AOML), National Oceanic and Atmospheric Administration (NOAA) in his special address-emphasized the impact of altimeter derived SSHA in the cyclone predictions. He also mentioned how the incorporation of the altimeter derived tropical cyclone heat potential (TCPH) improved the statistical hurricane intensity prediction system (SHIPS) and the statistical typhoon intensity prediction system (STIPS) forecasts. Dr. Ajit Tyagi, Director General, India Meteorological Department (IMD) while delivering the key note address emphasized the importance of satellite observations in the operational weather forecasting and the need for improved CTIP.

INVITED SPECIAL TALKS SESSION:

The invited special talks **session** was chaired by Dr. S.C.Shenoy, Director, Indian National Centre for Ocean Information Services (INCOIS), Hyderabad with Dr.S.K. Sasmal as the rapporteur. The need for sustained ocean observation system for climate and weather studies, the challenges, being faced by the India Meteorological Department (IMD) and the efforts put by ISRO towards the ocean and the atmospheric programme are presented in this session. There were four presentations in this session. The first presentation was by Dr. Gustave Goni on sustained ocean observing system for cyclone forecasts. He discussed about the need for sustained ocean observations and compared the present network of ocean observations to the initial phase. He emphasized how the error in cyclone track and intensity prediction (CTIP) has reduced during 1985-2009 for 24 – 120 hours lead time forecast. He also discussed how to incorporate the SSHA into the statistical and numerical models improved the intensity and pressure forecasts. At the end he summarized the recommendations of the Ocean Observations 1999. Answering to a question, he mentioned that oceanographic data over convergence zones would help predicting the cyclogenesis accurately. The second presentation was by AVM (Dr) Ajit Tyagi, Director General, IMD on tropical cyclone prediction and challenges. In this presentation, he discussed about the present status of CTIP in India vis-a-vis the international standard and the requirements for an effective forecast over the north Indian Ocean. He summarized the various components of early cyclone warning,

monitoring and forecast. He emphasized the importance of initial positional and intensity accuracy for a better forecast. He also discussed on the factors effecting genesis. The role played by satellites in CTIP is presented in detail. He remarked that the information on subsurface thermal structure can improve the CTIP in the coupled ocean models. Prof. UC Mohanty presented on the impact of remote sensing data on the simulation of tropical cyclones with different initial and boundary conditions through WRF model for a few typical cyclones. The fourth presentation was on the ocean and atmospheric programme of ISRO by Dr. JV Thomas of ISRO, Bangalore. He covered the various ocean atmospheric studies carried out from the initial stages to the present. He briefed about the future Indian earth observation missions like INSAT-3D, Meghatropiques, Satellite with Argoes and Altika (SARAL) carrying a ka-band altimeter and the various utilization programmes of these payloads.

FIRST TECHNICAL SESSION:

The first technical session was chaired by Dr. Ajit Tyagi, DG, IMD with Dr. PV Nagamani as the rapporteur. This session had a lead talk followed by three invited talks. In the lead talk on cyclone prediction for satellite ISRO launch vehicles, Dr. G.V. Rama projected the requirement of the Satish Dhawan Space Centre for launching of the rockets. He emphasized the need for accurate cyclone track prediction to protect all technical facilities at various phases of the launch. The second talk was on whether ocean mean temperature can be a better parameter for cyclone track and intensity predictions by Dr. M M Ali. In this presentation he emphasized the need for better track and intensity prediction to accurately estimate the storm surge in view of the varying bathymetry of the Indian coast. He presented examples where sea surface height anomaly (SSHA) is proved to be a better parameter than SST through a statistical analysis for intensity prediction and through numerical model for track prediction. Operational cyclone predictions by IMD were presented by Dr. SK Roy Bhowmic in which he described the various track prediction numerical models. He described how the track errors have reduced by using multi model ensemble approach. He also presented the errors involved for different lead hours of forecast for the statistical intensity

prediction system. The fourth presentation was on the role of eddies on CTIP by Dr. Y Sadhuram of NIO. He observed that the storm tracks moved over the regions where TCHP is more and weakened or recurved when the cyclones encountered the low TCHP. The intensity of cyclone Aila enhanced by 43% after passing over the warm cover eddy.

SECOND TECHNICAL SESSION:

The second technical session was chaired by Dr. Gustavo Goni from NOAA, USA and the rapporteur was Dr. Neeraja Sharma. Dr. D. Sengupta of IISc, Bangalore delivered a lead talk on cooling of SST due to cyclones using model simulations. He remarked that the fresh water flow from rivers and rain inhibits mixing due to which the cooling of SST in the north Bay of Bengal is less in the post monsoon. He also dealt with the upper ocean heat budget by analyzing a few in-situ observations. The first invited presentation was on heat content from ocean circulation models by Dr. Gnanaseelan of IITM, Pune. He emphasized the importance of incorporating the vertical profiles in a cyclone forecast model. He compared the trends in model derived and altimeter observed SSHAs. He remarked that the model derived thermohaline heat content of the north Indian Ocean is increasing. The second invited talk was by Mr. Gharai of NRSC on the artificial neural network approach for the cyclone track prediction. He emphasized how critical is the estimation of CTIP, particularly over the Indian coasts due to its varying bathymetry that effects the storm surges. He compared the cyclone tracks predicted by the ANN approach with the actual tracks. The third invited presentation was by Dr. VV Gopalakrishna of NIO on the validation of satellite derived TCHP with in situ observations. He showed the requirement of estimation of TCHP from satellite observations by presenting the limited number of in situ measurements available in a month of an year. He concluded that the in situ and satellite derived estimations match well.

THIRD TECHNICAL SESSION:

The third technical session was chaired by Dr. YVN Krishna Murthy, NRSC with Mr. IV Ramana as the rapporteur. Dr. Gustavo Goni in his lead talk on “Upper ocean heat content from satellite altimetry” presented the importance of TCHP on cyclone intensity and pressure drops. He showed how the D26 and D2O isothermers and SSHa correlate well, particularly, in the tropical regions with special reference to the north Indian Ocean. After presenting the TCHP validation results, he dealt with the HYCOM-HWRF modeling efforts at AOML/NOAA and the non-secular trends of TCHP in the Arabian Sea and Bay of Bengal. Impact of global warming on cyclonic storms over the north Indian Ocean was presented by Dr. M.R.Ramesh Kumsr of NIO. He showed the trends in the heat content over Bay of Bengal over the pre and post monsoon seasons. He observed that the monsoon depressions are decreasing over the Bay of Bengal in the recent decades. “Estimation of mixed layer heat content using satellite data” was presented by Mr. M.V. Rao, NRSC. Since satellite derived TCHP values are available, he obtained a relation between the TCHP and the heat content of the mixed layer and extended this relation to infer the later parameter to study its temporal and spatial variations over a larger spatial and temporal extent. The next invited presentation was by Dr. Anitha Gera, INCOIS. She studied the influence of salinity and heat content on genesis and intensity of cyclones and concluded that low salinity in the upper layers increases its stability inhibiting the vertical mixing that in turn increases the mixed layer temperature. This condition could be favourable to the cyclone genesis. The last presentation of this session was on the “science and application plans of SARA-ALTIKA by Dr. R M Gairola, SAC. Altika ia a ka-band altimeter with the capability of providing SSHa closer to the coast that helps in assessing the heat potential available to the cyclones before the landfall. He described in detail about the payloads of the SARAL mission, ALTIKA Science and Application plans.

FOURTH TECHNICAL SESSION:

The fourth technical session of the workshop was chaired by Mr. LVG Rao, and the rapporteur was Dr. T. Anasuya . The lead talk was on “Prediction of tropical cyclones uses satellite data” by Dr. CM Kishtawal, SAC. After dealing with the key issues in the tropical monitoring and prediction, he presented how microwave observations help in reducing the geolocation errors. The criticality in the accuracy of the initial position error for the precise track prediction was also presented. He also showed the importance of scatterometer data in predicting the cyclogenesis. Estimation of cyclone intensity and wind structure using microwave data are other topics covered by him. The next presentation was by Mr. V. Bhanumurthy of NRSC. He presented the cyclone impact assessment using satellite data. He informed that as a part of the decision support center operational services, cyclone inundation maps, recession maps and damage assessment are provided to the central and state level agencies and the ministries. The role of space observations for impact assessment is stressed. Basing on the cyclone track predicted by the meteorological team at NRSC, DSC acquires and analyses the satellite data for impact assessment. He mentioned about a few success stories of a few cyclones like Aila and Nargis. He expressed the difficulties involved in acquiring the satellite data when the forecasting of the track position frequently changes. The third presentation on “Impact of cyclones on ocean productivity” by Mr. K.H.Rao discussed about the enhancement of chlorophyll and phytoplankton blooms after the passage of the cyclones. For a few examples of the cyclones he demonstrated how the chlorophyll, phytoplankton blooms and the mixed layer productivity, estimated using OCM data, increased due to the upwelling created by the cyclonic winds. AVHRR data were used to show the reduction in SST. Dr. P.N. Sridhar presented on cyclones and coastal vulnerability. He mentioned that historically east coast of India is more vulnerable than the west coast due to more number of cyclones in the Bay of Bengal than in the Arabian Sea. He described how wind, storm surge and the rain, the three destructive elements of the cyclones are responsible for the damage of the coastal regions.

CONCLUDING SESSION:

The concluding session was chaired by Dr. V. Jayaraman, Director, NRSC. He mentioned how the programmes of the Earth Observation System and Global Ocean Data Assimilation Experiment have given a momentum to the oceanographic activity. He also remarked that scatterometer onboard Oceansat is the only sensor available as on today that provides wind vector. The importance of SSHA from Altika was also stressed. The forecasting of cyclone intensity prediction that has not progressed as much as track prediction, needs a coordinated research by various research and academic institutions. He assured that the remote sensing data could be made available through Bhuvan, an ISRO's earth visualization portal. He questioned whether using the depth of 26°C isotherm (D26) as the reference for the TCHP is the right choice for the Indian Ocean conditions.

As a follow up of this workshop it is decided to develop a coordinated research program comprising of the research, academic and operational agencies to study the impact of OHC for cyclone track and intensity predictions. The reference depth suitable for the Indian Ocean cyclones will also be examined.

The extended abstracts including the one by Prof. Lynn Shay, who could not attend the workshop, are given in annexure-3 and presentations in annexure-4. The list of invitees and resource persons are in annexure-5. The members of the organizing committees are provided in annexure-6. Finally the workshop group photo is attached as annexure-7.

Annexure-1
Programme

**Program of the workshop
on
Utilisation of Satellite Derived Oceanic Heat
Content for Cyclone Studies
March 25-26, 2010**

First day: 25 March, 2010 Thursday

- Registration:** 09:15 -10:00hrs
- Inaugural Session:** 10:00 -11:00hrs
- Welcome Address:** Shri G. Behera, GD (WR&OG), NRSC
- Inauguration and Address:** Dr. P. S. Roy, DD (RS&GIS), NRSC
- Special Addresses:** Dr. Gustavo Goni, NOAA, USA
- Keynote Address:** Dr. Ajit Tyagi, DG, IMD, New Delhi
- Vote of Thanks:** Dr. MM Ali, NRSC
- Invited Special Talks:** 11:30 - 13:30hrs
- Chairman:** Dr S. C. Shenoi, INCOIS, Hyderabad
- Talk 1:** Sustained ocean observing system for climate and weather studies:
Dr. Gustavo Goni, NOAA
- Talk 2:** Tropical cyclone prediction: Challenges
Dr. Ajit Tyagi, DG, IMD, New Delhi
- Talk 3:** Impact of satellite data in tropical cyclone simulations:
Prof. U. C. Mohanty, IIT-D
- Talk 4:** Ocean and atmosphere program of ISRO:
Dr. V. S. Hegde, ISRO HQ

Venue: 100 seater conference hall

Technical Session I: 14:15 - 15:45hrs

Chairman: Dr. Ajit Tyagi, DG, IMD, New Delhi

Lead Talk: Cyclone prediction for satellite launch vehicle at Sriharikota:
Dr. G. V. Rama, SDSC/ISRO

Ocean mean temperature for cyclone studies:
Dr. M. M. Ali, NRSC

Operational cyclone predictions: Dr. Roy Bhowmic, IMD, Delhi

Role of eddies and heat content on cyclone track
& intensity from satellite data: Dr. Y. Sadhuram, NIO-RC, Waltair

Technical Session II: 16:00 - 17:30hrs

Chairman: Dr. Gustavo Goni, NOAA, USA

Lead Talk: Cooling of SST due to cyclones - Trough models:
Dr. D. Sengupta, IISc, Bangalore

Heat content from ocean circulation models:
Dr. C. Gnanaseelan, IITM, Pune

Cyclone track predictions - An ANN approach:
Mr. Biswadip Gharai, NRSC

Validation of satellite derived tropical cyclone heat potential :
Dr. V. V. Gopala Krishna, NIO

Cultural Programme: 18:00-19:00hrs

Second Day 26 March, 2010 Friday

Technical Session III: 09:30 - 11:00hrs

Chairman: Dr. Y. V. N. Krishna Murthy, DD (RRSC), NRSC

Lead Talk: Upper ocean heat content from satellite altimetry:
Dr. Gustavo Goni, NOAA

Role of climate change on cyclones in the North Indian Ocean:
Dr. M. R. Ramesh Kumar, NIO, Goa

Estimation of mixed layer heat content using satellite data:
Mr. M. V. Rao, NRSC

Operational generation of TCHP maps using ARGO data:
Dr. M. Ravichandran, INCOIS

Altica utilization programme : Dr. R. M. Gairola, SAC/ISRO

Technical Session IV: 11:30 - 13:00hrs

Chairman: Dr. L. V. G Rao, Dy. Director (Rtd), NIO

Lead Talk: Prediction of tropical cyclones using satellite data:
Dr. C. M. Kistawal, SAC/ISRO

Cyclone Impact Assessment using satellite data :
Mr. V. Bhanu Murthy, NRSC

Impact of cyclones on ocean productivity:
Mr. K. H. Rao, NRSC

Cyclone and coastal vulnerability:
Dr. P. N. Sridhar, NRSC

Panel Discussions and Recommendations: 14:00 – 16:00hrs

Annexure-2
List of participants

List of Participants

Sl. No.	Name of the participant	Designation	Institute
1	Patra S. K.	Scientist	ADRIN
2	Manga Rao B.	Scientist	APSRAC
3	Prasada Rao G.	Scientist	APSRAC
4	Rama Krishna Naga Raju A.	Scientist	APSRAC
5	Ramana Murty M. V.	Scientist	APSRAC
6	Ramana Murthy P. V.	Scientist	APSRAC
7	Lakshmi T. N.	Research Fellow	CSBoB
8	Suresh R. R. V.	Research Fellow	CSBoB
9	Smitha A.	Research Fellow	CUST, Kochi
10	Sravani N.	Research Fellow	HCU
11	Yunus Ali P.	Research Fellow	HCU
12	Krishna Kishore	Proj. Asst.	IIT, Delhi
13	Murty P. L. N.	Research Fellow	IIT-Delhi
14	Palas Sinha	Proj. Asst.	IIT, Delhi
15	Rahul S.	JRF	IITM
16	Rabindra Nayak	Scientist	IIRS
17	Satya Kumar M.	Director	IMD
18	Sudhkar Rao G.	Director	IMD
19	Thomar C. S.	Scientist	IMD
20	Anitha Gera	Scientist	INCOIS
21	Francis Pavanathara	Scientist	INCOIS

22	Girishkumar M. S.	Scientist	INCOIS
23	Harikumar R.	Scientist	INCOIS
24	Hasibur Rahaman	Scientist	INCOIS
25	Neethu Chako	Scientist	INCOIS
26	Prince	Scientist	INCOIS
27	Siva Reddy	Scientist	INCOIS
28	Sudheer Joseph	Scientist	INCOIS
29	Vimlesh Pant	Scientist	INCOIS
30	Uday Bhasker	Scientist	INCOIS
31	Yelluripati Ravi K.	Scientist	INCOIS
32	Babula Jena	Scientist	NCAOR
33	Akhil V.P.	JRF	NIO
34	Keerthi, M.G	Research Fellow	NIO
35	Pravin D. Kunte	Scientist	NIO
36	Somayajulu Y. K.	Scientist	NIO
37	Sumesh K. G	Research Fellow	NIO
38	Suneel Vasimalla	Research Fellow	NIO
39	Chakradhar V. N.	JRF	NIO-RC
40	Vara Prasad B. B. V. S.	JRF	NIO-RC
41	Steephen Paul Y.	JRF	NIO-RC
42	Anil Kumar	Research Fellow	NPOL
43	Jagadeesh P. S. V.	Research Fellow	NPOL
44	Aslam M.Y.	M.Tech student	NRSC

45	Mahalakshmi D.V.	JRF	NRSC
46	Raja Sekhar S. S.	Scientist	NRSC
47	Sivaprasad Reddy M.	M.Tech student	NRSC
48	Suguna C. P.	M. Tech Student	NRSC
49	Thamayanthi K. V.	M. Tech Student	NRSC
50	Vijaya Bhanu A.	Scientist	NRSC
51	Swain D.	Scientist	SPL, VSSC
52	Vijaya Bhaskara Rao D.	Professor	SVU, Tirupati

Annexure-3

Extended Abstracts

Surface Height Anomaly for Cyclone Predictions

MM Ali

Oceanography Division

National Remote Sensing Centre

Hyderabad 500625 (India)

Improvements in predicting the cyclone track and intensity has been a challenging problem for disaster management practices in order to reduce loss of life and the economical vulnerability due to the sudden and unexpected intensification. This problem is more critical when the coastal bathymetry varies significantly, like in the case of Indian coast, where even a slight error in the prediction of landfall point and the intensity can lead to a totally different storm surge height. While attempts are being made to improve the predictions through statistical and dynamical models, it is also worthwhile to attempt improving the input parameters and/or incorporating new parameters to the models. The present article suggest the use of sea surface height anomaly (SSHA) derivable from satellite altimeters in the atmospheric models, particularly, in the cyclone models, in place of sea surface temperature (SST).

Through numerical model Emanuel (1999) demonstrated that the evaluation of hurricane intensity depends mainly on three factors: the storm initial intensity, the thermodynamic state of the atmosphere through which it moves, and the heat exchange with the upper layer of the ocean under the core of the hurricane. In most of the cyclone models SST has been the only oceanographic input. The importance of SST, as a limiting factor, in the genesis of tropical cyclones has long been known. Palmen (1948) showed that hurricanes cannot form unless the SST is greater than 26°C, though this is not the only necessary condition. However, cyclones interact not only with the surface but with the deeper oceans, the depth depending upon the strength of the wind mixing. Thus the energy source through air sea flux for intensification comes from the oceans (Emanuel 1999). Hence, even if atmospheric conditions are favorable, cyclones cannot intensify without sufficient supply of heat flux from the oceans (Lin et al.2009). However, cyclones can never form just because the oceanic heat content is more unless the atmospheric factors are also favourable. Thus, cyclone formation and intensification is due to a

complex interactions between atmosphere, ocean and the cyclone structure (Emanuel 2000, 2006; Shay et al. 2000; Kaplan and De Maria 2003; Emanuel et al. 2004; Lin et al 2005; Pun et al 2007; Wu et.al.2007). The stronger the cyclone, the more intense the winds and deeper the ocean mixing (Price, 1981; Bender and Ginis, 2000 and Pun et al. 2007). Hence, it is necessary to consider the thermal structure of the upper ocean for cyclone studies. However, most of the cyclone intensity research focusses on the pre-storm SST, besides certain atmospheric properties, though it is well known that cyclones modify the surface temperature of the oceans over which they pass (Emanuel 1999). The latent heat release that fuels the system reduces SST due to the wind induced mixing even before the center of the cyclone passes a given area. Gallacher et al. (1989) through a coupled model reported that a mere 2.5K decrease in SST near the core of the storm is sufficient to shut down the entire energy production for the storm. This reduction in the surface temperature is intense if the background climatological warm layer is relatively shallow. On the other hand, the reduction in SST is negligible if the upper warm ocean is already deep as the background itself is sufficient to restrain the self induced cooling mechanism. Thus, SST does not always represent the subsurface thermal structure and hence the energy available to the storm. On the other hand, positive (negative) SSHAs represent more (less) oceanic heat content compared to the climatology.

Gopalakrishna et al. (2003), through their atlas, have documented that SSHAs represent the subsurface thermal structure better than SST alone. Namias and canyan (1981) has reported that patterns of lower atmospheric anomalies are more consistent with the upper ocean thermal structure variability than just with SSTs. Through a coupled ocean-atmospheric model, Mao et al. (2000) proved that the rate of intensification and final intensity of cyclones are sensitive to the initial spatial distribution of the mixed layer. The sudden unexpected intensification of Hurricane Opal from 965 to 916 hectopascals in the Gulf of Mexico over a 14-hour period (Shay et al. 2000) is a classical example of the influence of a warm core eddy on cyclone intensity. Ali et al. (2007a), Goni and Trainanes (2003) and Shay et al. (2000) demonstrated the impact of oceanic eddies on cyclone intensity. The rapid intensification of cyclone Nargis in the Bay of Bengal from category-1 to category-4 within 24 hours was attributed to the presence of a pre-existing warm SSHA evidenced by the in situ and altimeter observations. Without the presence of a warm core oceanic feature (that could be easily observed from satellite altimetry) the entropy would not have increased to support the rapid intensification of this cyclone (Lin et.al.2009). Goni et al.

(2009) have shown an almost one to one correspondence between the cyclone heat potential calculated using SSHA and the intensity of Katrina.

Ali et al. (2007a) analysed two cyclones (10-19 May 2003 and 15-22 December 2005) over the Bay of Bengal to study the impact of oceanic eddies/dynamic topography on the intensification and dissipation of cyclones. They observed almost a one to one correspondence between the SSHAs and the intensity of the two cyclones (Figure 1c). On the contrary, such a correspondence was not found by them between SST and the cyclone intensity. The latent heat release caused by the winds even at the periphery of the cyclone reduce SST representing the very thin layer of the ocean. While this negative feed back regime tends to decrease the storm intensity, pre-existing mesoscale features like warm core eddies or deeper mixed layer, obtainable from altimeter observations, provide the heat source for the intensification of the cyclones. Hence, a cyclone can intensify even if SST is less. Warm core features are more critical over the shallow oceanic regions (Lin et al. 2008) as the reduction in SST would not be as intense as it would have been under the climatological condition. The cyclone intensity has increased after the cyclone passed over a cooler SST region and decreased after passing over a warmer region (Figure 1d). Similarly, the 15-22 December 2005 Bay of Bengal cyclone dissipated after passing over a cold-core eddy with less OHC (Figure 1e)

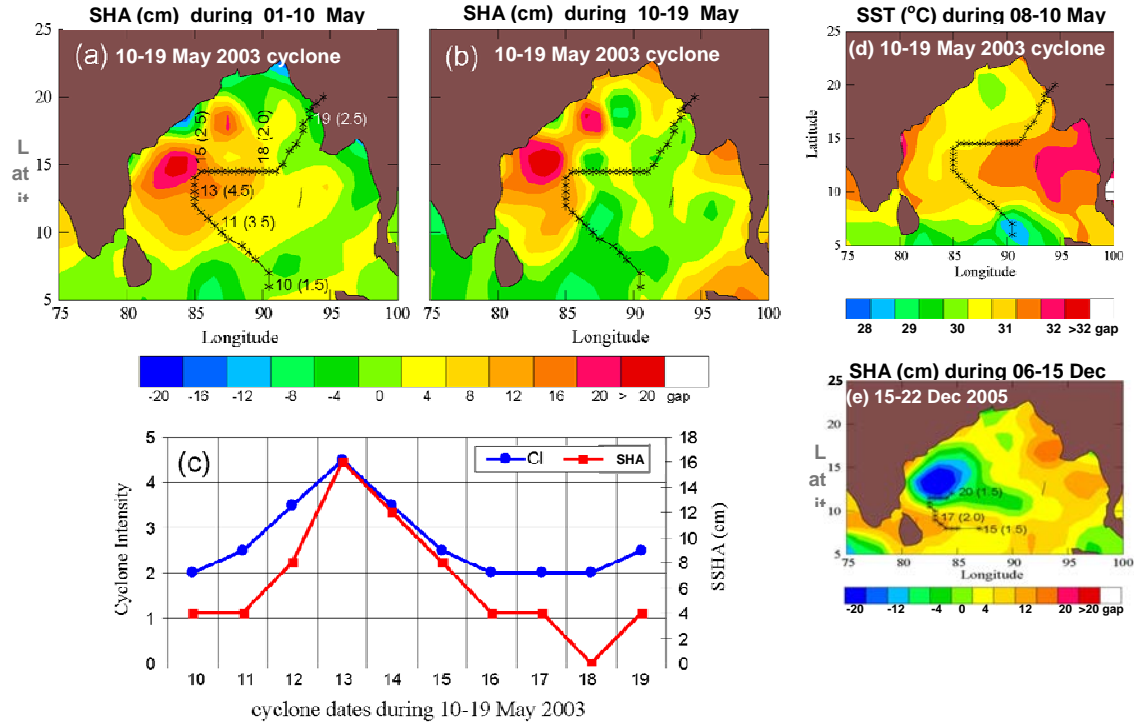


Figure 1: Impact of sea surface height anomaly (SSHA) and sea surface temperature (SST) on cyclone intensity (CI): (a) Bay of Bengal cyclone track during 10-19 May 2003 superimposed on the SSHA field during 1-10 May 2003 and (b) SSHA fields during 10-19 May 2003 for the same cyclone, (c) comparison of SSHA and CI of the same Bay of Bengal cyclone, (d) three day composite Tropical Rainfall Monitoring Mission Microwave Imager SST during 8-10 May 2003 and (e) cyclone track of 15-22 December 2005 superimposed on SSHA during 6-15 December 2005. Time of observations (intensity) at selected locations for both the cyclones are superimposed in Figure 5a and 5e. (Figures taken from Ali et al. (2007a))

The role upper ocean plays in the tropical cyclone intensification in various ocean basins and the use of ocean parameters in forecasting the cyclone intensities has been summarized by Goni et al. (2009).

While sufficient literature is available on the role of SSHA or the upper ocean heat content in modifying the cyclone intensity, very little investigations have been carried out in the direction for track predictions. Ali et al. (2007b) studied the impact of SSHAs on the unusual westward movement of the 6-11 May 2002 Arabian Sea cyclone (generally the cyclones originating in this

area during this period move northward) through fifth generation National Centre for Atmospheric Research Mesoscale Model (MM5). Since MM5 does not directly consider SSHAs as an input they linearly converted SSHAs to SST without considering the units of the two parameters. They compared the results obtained by using these converted SSTs with those obtained by using the SST from National Centre for Environmental Prediction final reanalyzed (NECEP-FNL) fields. Joint Typhoon Warning Centre (JTWC) best tracks were considered as the standard track for comparison. They observed that the mean displacement errors have reduced from 733 km to 419 km by using SSTs converted from SSHA.

From the references cited above, it can be concluded that SSHAs play a better role than SST alone in modifying the cyclone processes, provided other atmospheric factors remain same. Since most of the cyclone models do not consider SSHAs as an input, a method has to be evolved to convert SSHAs to SST. One such approach towards this could be (i) to estimate OHC using SSHAs and SST following Mainelli-Huber (2000) and the references therein, for example, and (ii) to obtain the ocean mean temperature (OMT) of the upper ocean by dividing OHC with the product of density and specific heat capacity of the ocean water. This new parameter could be of vital importance in other atmospheric processes and climate change studies also.

The focus of this article is to bring forth the importance of SSHAs available from altimeters that better represent the subsurface features compared to SST that some times may not be a representative of the upper ocean layer. It does not imply that other atmospheric factors like vertical wind shear or high level wind flow (Emanuel, 1999; Frank and Ritchie 2001) are not critical for intensification or movement. Secondly, this is a concept paper attempting to prove the relative importance of SSHA compared to SST, by considering the results already published. The suggestion to consider SSHA in place of or along with SST is significant considering the launch of a Ka-band altimeter in very near future by the Indian Space Research Organisation jointly with CNES. The SSHAs that can be obtained from this altimeter closer to the coast can improve the understanding of the role of SSHA/OHC/OMT on cyclone intensity/track predictions just before land falling.

Acknowledgement: The author acknowledges the support provided by the National Remote Sensing Centre to carry out this analysis.

References:

Ali, M. M., P.S.V. Jagadeesh and Sarika Jain (2007a). Effects of Eddies on Bay of Bengal Cyclone Intensity, Earth Observations System, Vol. 88, ps 93, 95.

Ali, M. M., Sinha, P., Jain, S. and Mohanty, U. C. (2007b). Impact of Sea Surface Height Anomalies on Cyclone Track, Nature Proceedings: doi: 10.1038/npre.2007.1001.1 : Posted 14 Sep 2007

Bender, M. A., and I Ginis (2000). Real-case simulations of hurricane-ocean interaction using a high-resolution coupled model: Effects on hurricane intensity, Mon. Wea. Rev., Vol. 128, pp 917-946.

Emanuel, K.A. (1986). Thermodynamic control of hurricane intensity, Nature, Vol. 401, pp 665-669.

Emanuel, K.A. (2000). A statistical analysis of tropical cyclone intensity. Mon. Wea. Rev. Vol. 128, pp 1139-1152.

Emanuel, K.A., C. DesAutels, C. Holloway and R. Korty (2004). Environmental control of tropical cyclone intensity. J. Atmos. Sci., Vol 61, pp 843-858.

Emanuel, K.A. (2006). Climate and tropical cyclone activity: A new model downscaling approach. J. Climate, Vol. 19, pp 4797-4802.

Gallacher, P.C., R. Rotunno and K. A. Emanuel (1989). Tropical cyclones in the coupled ocean-atmospheric model. Preprints, 18th conference on Hurricanes and Tropical Meteorology, San Diego, CA, Amer. Meteor. Soc., pp 121-122.

Frank, W. M., and E. A. Ritchie (2001), Effects of vertical wind shear on the intensity and structure of numerically simulated hurricanes, *Mon. Weather Rev.*, 129, 2249–2269.

Goni, G. J., and J. A. Trinanes (2003). Ocean thermal structure monitoring could aid in the intensity forecast of tropical cyclones, *Eos Trans. AGU*, 84(51), 573, 577–580.

Goni, G.J. M. DeMaria, J. Knaff, C. Sampson, I. Ginis, F. Bringas, A. Mavume, C. Lauer, I-I Lin, M. M. Ali, P. Sandery, S. Ramos-Buarque, K. Kang, A. Mehra, E. Chassignet, and G. Halliwell (2009). Applications of satellite-derived ocean measurements to tropical cyclone intensity forecasting, *GODAE Special Issue Feature, Oceanography*, Vol. 22, pp 190-197.

Gopalakrishna, V. V., M. M. Ali, N. Araligidad, S. Shenoy, C. K. Shum, and Y. Yi (2003), An atlas of XBT thermal structures and TOPEX/Poseidon sea surface heights in the north Indian Ocean, *Spec. Publ., NIO-NRSA-SP-01-03*, Natl. Inst. of Oceanogr., Goa, India.

Kaplan, J., and M. DeMaria, (2003). Large-scale characteristics of rapidly intensifying tropical cyclones in the North Atlantic basin. *Wea. Forecasting*, Vol. 18, pp 1093-1108.

Lin, I.-I., C.-C Wu, K. A. Emanuel, I.-H Lee, C.-R Wu and I.-F Pun (2005). The interaction of super typhoon Maemi (2003) with a warm ocean eddy, *Mon. Wea. Rev.*, Vol. 133, pp 2635-2648.

Lin, I.-I., C.-C Wu, I.-F Pun and D.-S. Ko (2008). Upper ocean thermal structure and the western North Pacific category-5 typhoons. Part I: Ocean features and category-5 typhoons interaction, *Mon. Wea. Rev.* Vol. 136, pp 3288-3306.

Lin, I.-I., C.-C. Chen, I.-F Pun, W. T. Liu and C.-C Wu (2009). Warm ocean anomaly, air sea fluxes, and the rapid intensification of tropical cyclone Nargis, *Geophys. Res. Lett.*, Vol. 36, L03817, doi:10.1029/2008GL035815.

Mainelli-Huber, M. (2000). On the role of the upper ocean in tropical cyclone intensity change. Masters Thesis, The University of Miami, FL, 73pp.

Mao, Q., S. W. Chang, and R. L. Pfeffer (2000), Influence of large-scale initial oceanic mixed layer depth on tropical cyclones, *Mon. Weather Rev.*, *128*, 4058–4070.

Namias, J., and D. R. Canyan (1981), Large air-sea interaction and short period climatic fluctuations, *Science*, *214*, 869–876.

Palmen, E. (1948), On the formation and structure of tropical cyclones, *Geophysics*, *3*, 26–38.

Price, J. F., R. A. Weller, and R. Pinkel (1986), Diurnal cycling: Observations and models of the upper ocean response to diurnal heating, cooling, and wind mixing, *J. Geophys. Res.*, *91*, 8411 – 8427.

Pun, I.-F., I.-I. Lin, C.-R. Wu, D.-S. Ko, and W. T. Liu (2007), Validation 315

and application of altimetry-derived upper ocean thermal structure in the 316

western North Pacific Ocean for typhoon intensity forecast, *IEEE Trans. 317, Geosci. Remote Sens.*, Vol. 45, pp 1616– 1630.

Shay, L. K., G. J. Goni, and P. G. Black (2000), Effects of a warm oceanic feature on Hurricane Opal, *Mon. Weather Rev.*, *128*, 1366–1383.

Wu, C.-C., C.-Y. Lee, and I.-I. Lin (2007), The effect of the ocean eddy on 328 tropical cyclone intensity, *J. Atmos. Sci.*, *64*, 3562–3578.

Global upper ocean heat content estimates from satellite altimetry.

Gustavo Jorge Goni¹, Pedro DiNezio^{2, 1}, Francis Bringas^{2, 1}, Joaquin Trinanes^{2,1}

- (1) National Oceanic and Atmospheric Administration, Atlantic Oceanographic and Meteorological Laboratory, Physical Oceanography Division, Miami, Florida, USA.
- (2) University of Miami, Rosenstiel School of Marine and Atmospheric Science, Cooperative Institute for Marine and Atmospheric Studies, Miami, Florida, USA.

Tropical cyclones occur in seven ocean basins: tropical Atlantic, northeast Pacific, northwest Pacific, southwest Indian, north Indian, southeast Indian, and south Pacific (Figure 1). The intensification of TCs includes very complex mechanisms, such as TC dynamics, upper ocean interaction, and atmosphere circulation. In general, the accuracy of TC intensity forecast has lagged behind the TC track because of the complexity of the problem and because many of the errors introduced in the track forecast are translated into the intensity forecast (DeMaria *et al.*, 2005). The importance of the ocean thermal structure in TC intensification was first recognized by Leipper and Volgenau (1972). While sea surface temperature (SST) plays a role in the genesis of TCs, the ocean heat content (OHC) contained between the sea surface and the depth of the 26°C isotherm (D26), also referred as Tropical Cyclone Heat Potential (TCHP), has been shown to play an important role in TC intensity changes (Shay *et al.*, 2000). The TCHP shows high spatial and temporal variability associated with oceanic mesoscale features. TC intensification has been linked with high values of TCHP contained in these mesoscale features, particularly warm ocean eddies, provided that atmospheric conditions are also favorable. Since sustained *in situ* ocean observations alone cannot resolve global mesoscale features and their vertical thermal structure, different indirect approaches and techniques are used to estimate the TCHP. Most of these techniques use sea surface height observations derived from satellite altimetry, a parameter that provides information on the upper ocean dynamics and vertical thermal structure.

This presentation highlights the importance of integrated data and, particularly, of satellite derived observations, by presenting different methodologies and approaches to compute the

ocean heat content in the ocean using altimetry-derived sea height anomalies as a proxy and with special emphasis on the upper ocean. Results will be presented on global ocean computations, including validation of estimates.

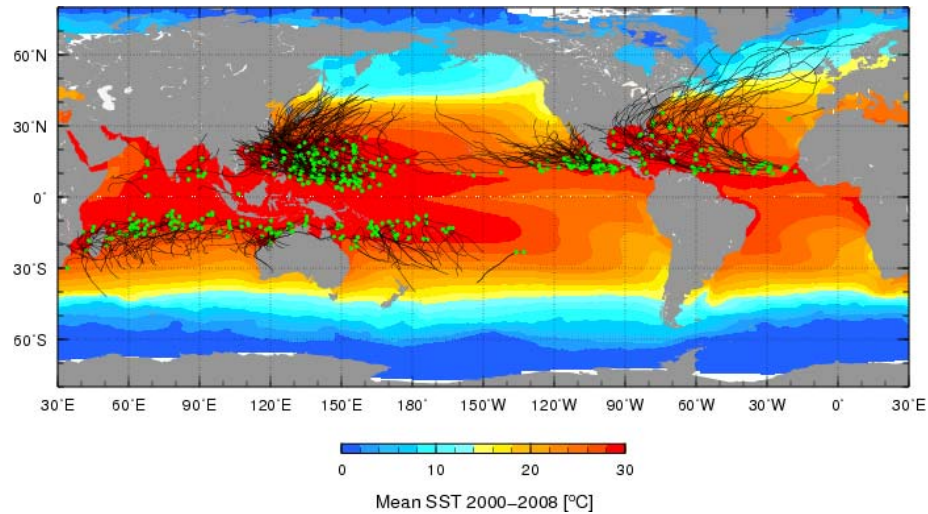


Figure. Global map showing the tracks of tropical cyclones (category 1 and above) during the period 2000-2008, with the green circles indicating the location of their formation. The background color is the satellite-derived mean sea surface temperature during the same years, for June through November in the Northern hemisphere and November through April in the Southern hemisphere.

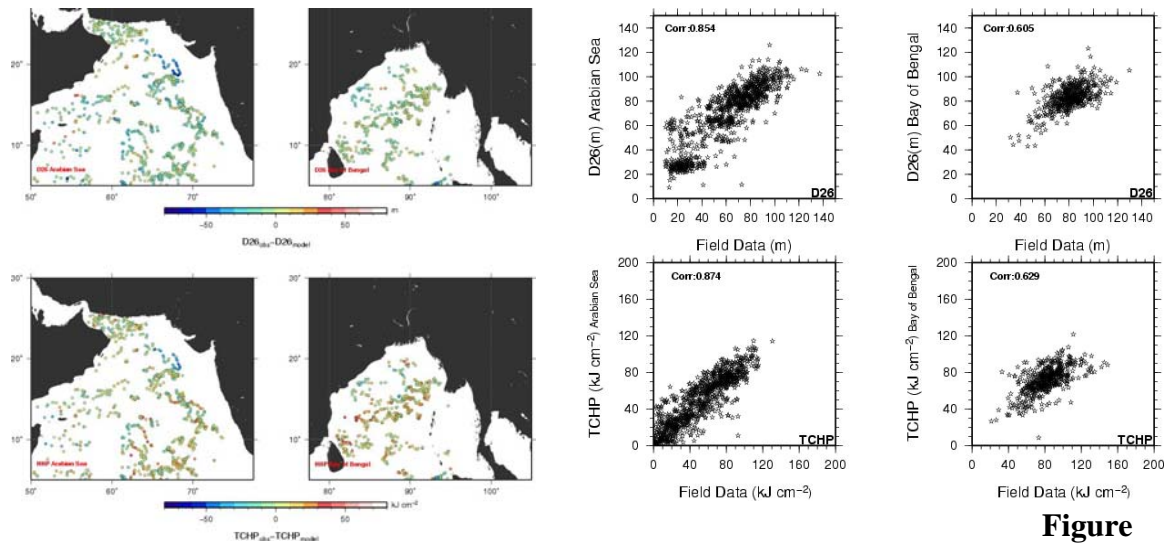
Monitoring the tropical cyclone heat potential in the Bay of Bengal and in the Arabian Sea.

Gustavo Jorge Goni ¹, Francis Bringas ^{2,1}, Joaquin Trinanes ^{2,1}, Pedro DiNezio ^{2,1}, M.M. Ali ³

- (1) National Oceanic and Atmospheric Administration, Atlantic Oceanographic and Meteorological Laboratory, Physical Oceanography Division, Miami, Florida, USA.
- (2) University of Miami, Rosenstiel School of Marine and Atmospheric Science, Cooperative Institute for Marine and Atmospheric Studies, Miami, Florida, USA.
- (3) Department of Space, National Remote Sensing Center, Hyderabad, India.

The link between tropical cyclone intensification and the upper ocean heat content or Tropical Cyclone Heat Potential (TCHP) has been identified in the north Indian Ocean, showing that TCs intensify (dissipate) after travelling over anticyclonic (cyclonic) eddies of high (low) TCHP values. The TCHP fields are estimated in the North Indian Ocean using synthetic temperature profiles, obtained from correlations between sea height anomaly fields (SHA) and in situ observations (XBTs, profiling floats, etc). These temperature profiles are integrated from the sea surface to the depth of the 26C isotherm. Estimates of TCHP fields are validated using in-situ observations (Figure 1).

Time series of estimates of TCHP in the Bay of Bengal and in the Arabian Sea since 1993 are examined and evaluated. Time trends of sea height in these two regions exhibit an increase, which are also observed in sea surface temperature and TCHP (Figure 2). These changes are not homogeneous but vary regionally. This presentation will show how the parameters associated with the upper ocean thermal conditions have changed since 1993.



(Maps) Locations of in-situ observations during 2008 used for (dispersion plots) the comparison of depth of the (top) 26°C isotherm using (left) historical relationships between altimetry and (right) in-situ and altimetry observations within a two-layer reduced-gravity approximation.

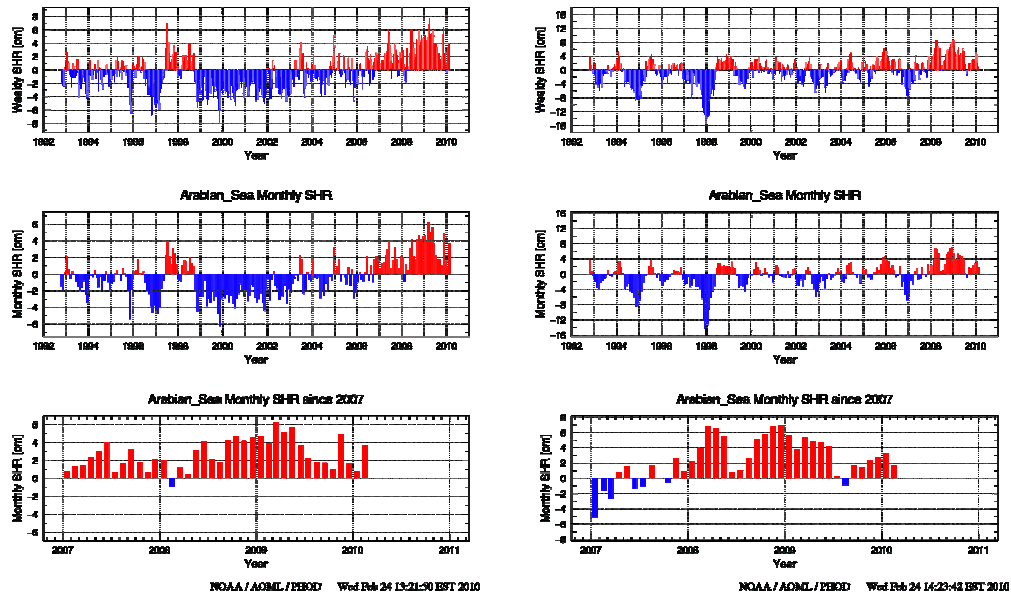


Figure 2. Time series of sea height residuals (sea height anomalies with seasonal cycle removed) since 1993 in the (left) Arabian Sea and (right) Bay of Bengal.

Oceanic heat content using satellite and insitu observations in the north Indian Ocean

V. V. Gopalakrishna, M. M. Ali, P.V. Nagamani, Nisha Kurian, Amit Naik, Gustavo Goni
and Pedrov

The primary objective of this study is to see whether satellite derived cyclone heat potential can be utilized to examine its spatio temporal variability on a basin scale. North Indian Ocean experiences formation of devastating tropical cyclones particularly in the Bay of Bengal and in the Arabian Sea. Formation of cyclonic storms are more in the Bay of Bengal when compared to the Arabian Sea. In fact Bay of Bengal is one of the region where a minimum of 4 to 5 severe cyclonic storms generate every year during pre and post monsoon seasons (Ganesan et al 1994).

Assuming the atmospheric parameters are same, the cyclone heat potential is the most important parameter for the genesis, intensification and movement of cyclonic storms. Cyclone heat potential can be estimated from in situ temperature profiles. We define cyclone heat potential as the heat content with respect to 26⁰C isotherm. In order to understand better its spatio temporal variability on basin scale, one need to have voluminous temperature data. However, the availability of vertical temperature profiles for the north Indian Ocean is relatively sparse when compared to other oceanic regions. In addition if one looks at the temperature data density for a particular season or a month, the data availability is much more sparse.

Here the importance of satellite derived cyclone heat potential comes handy it plays a significant role. We have pooled up all the available temperature profiles for the north Indian Ocean and computed the cyclone heat potential. Temperature data density used in the present study for computing the cyclone heat potential is shown in **Fig.1**. Black dots indicate temperature. We have used corresponding satellite derived cyclone heat potential values from Atlantic Oceanographic and meteorological Laboratory (AOML), NOAA.

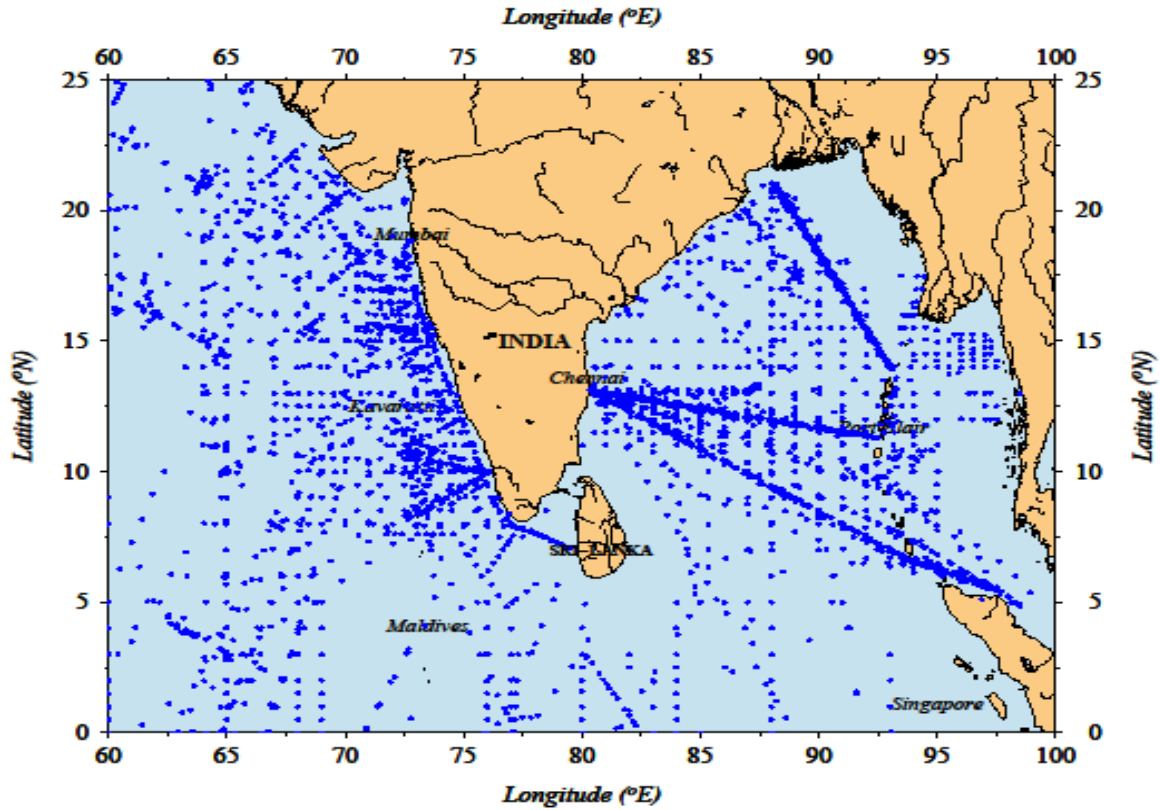


Fig:1: In situ observations over the North Indian Ocean

In order to examine how good the cyclone heat potential values obtained from satellite data match with the cyclone heat potential values computed using in situ data, we have prepared a scatter plot (Fig.2a). In general the match up is very good – except for some regions where higher in situ cyclone heat potential values are noticed for the same satellite derived cyclone heat potential value.

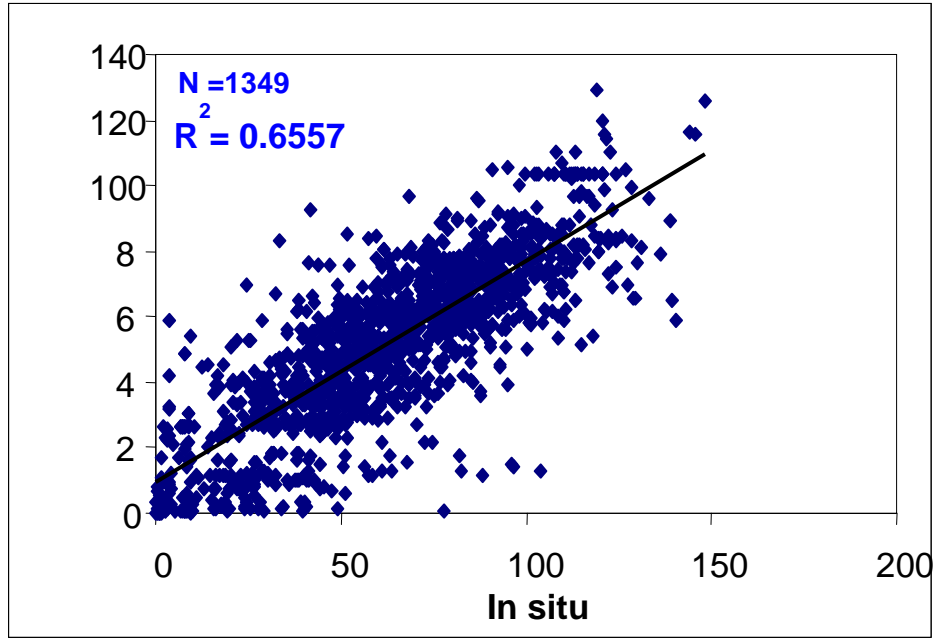


Fig. 2a: Comparison of satellite derived and in situ TCHP

Suspecting that, the mismatch is due to the temperature profiles collected close to the coastal regions, we have removed all the coastal stations data and re – examined the scatter between these parameters (Fig 2b). The match up is much better than with the coastal stations data. But still there are places where the scatter is much wider. We have separated the data pertaining to the Arabian Sea S and the Bay of Bengal and again re examined the scatter region wise. It is seen that that the match up is very good for the Arabian Sea when compared to the Bay of Bengal. Besides scatter plot, we have also prepared an XY plot with running means of satellite and in situ estimated cyclone heat potential. It once again showed a good one -to-one correspondence. Hence satellite derived cyclone heat potential can be used to study the basin scale variability. Since we got a good correlation between the cyclone heat potential computed using satellite data as well as in situ data we have also look at whether any relation exists between the annual frequency of tropical cyclones and the

cyclone heat potential. The cyclone frequency is very high when the cyclone heat potential is high and vice versa.

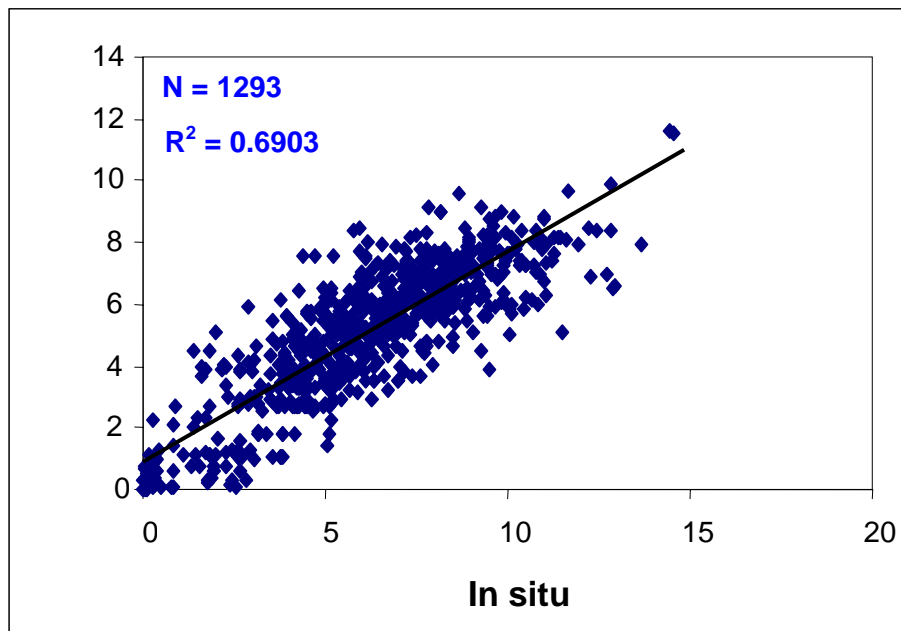


Fig : 2b Comparison of satellite derived and in situ TCHP (after removing the coastal stations)

Impact of Satellite Data in Simulation of Tropical cyclones over Indian seas

U C Mohanty, Sujata Pattanayak and Krishna Kishore Osuri

Centre for Atmospheric Sciences,
Indian Institute of Technology Delhi,
Hauz Khas, New Delhi – 110016, India
Correspondence to: ucmohanty@gmail.com

Abstract

Tropical cyclones are well known for their devastation mainly due to torrential rains, strong winds and associated storm surges which cause flooding, soil erosion and land slides, even far away from the landfall location, resulting in numerous human casualties and enormous property damage. These disasters are particularly severe over North Indian Ocean (NIO) comprising both Bay of Bengal (BOB) and Arabian Sea (AS) as their coastal areas are heavily populated. In the past 300 years, out of all recorded cases of very heavy loss of life (ranging from about 5000 to well over 300, 000) in the world due to tropical cyclones, more than 75% cases have been occurred in BOB and AS. In recent years, non-hydrostatic mesoscale models perform better simulation of track and intensity of tropical cyclones than global models due to improved model resolution, adequate physical parameterization etc.

Prediction of track and intensity of tropical cyclones over NIO remains a challenging problem mainly due to non-availability of adequate observations leading to inaccurate representation of the vortex in the initial values for the models. Hence, a study has been undertaken to assess the impact of assimilation of sea surface winds from Quick Scatterometer and Special Sensor for Microwave Imager on initial analyses and on simulation of track, intensity and structure of tropical cyclones. For this purpose, very severe cyclonic storm,

“Nargis” and super cyclonic storm “Gonu” over NIO are considered with 9 different initial conditions. Two sets of numerical experiments namely, CNTL (using global FNL analyses) and second sets of experiments using 3-Dimensional Variational (3DVAR) Data Assimilation System (with modified analysis by the assimilation of above mentioned satellite winds as initial values) are conducted using Weather Research Forecasting (WRF) system.

The inclusion of satellite derived winds through 3DVAR data assimilation system contributes to significant improvement in simulation of intensity, structure and track of the tropical cyclones. Out of 9 cases, the initial position of vortex improves in 7 cases by about 35 %. The 24-, 48-, 72- and 96-hrs mean track forecast improves by 22%, 31%, 41% and 47% respectively. The landfall prediction is significantly improved by 40% in 8 cases. The intensity prediction in terms of mean sea level pressure (MSLP) and 10-m maximum wind improves by 10-20 %. Kinematic and thermodynamic structures of tropical cyclones are better explained, as it could simulate heat and momentum exchange between sea surface and upper air. Due to better simulation of structure, intensity and track, the 24-hr accumulated rainfall intensity and distribution are also in better agreement with the TRMM observations compared to CNTL experiments.

Keywords: tropical cyclones, satellite derived wind, 3DVAR data assimilation system, track, intensity

IMD NWP based Objective Cyclone Forecast System

S. K. Roy Bhowmik and S.D. Kotal

India Meteorological Department

New Delhi

1. Introduction

Tropical cyclones are among the most deadly natural hazards as they are associated with very strong winds, heavy rain and storm surge. Due to the increasing human habitation near the coasts, accurate and timely forecasting of Tropical Cyclone has posed a challenging task to the operational forecasters. The synoptic methods have been the mainstay of tropical weather forecasting. Of late, NWP methods have acquired greater skills and are playing increasingly important role in delivering operational real time weather forecasts. However, limitations remain, particularly in the prediction of track and intensity of tropical cyclone. As such there has been an operational requirement to formulate an objective procedure to handle operational cyclone forecasting work in a more efficient and effective manner.

Various stages of cyclone forecasting are: (a) Genesis, (b) Track, (c) Intensity and (d) Decay after landfall. During 2008-09, IMD used an objective numerical method for the operational cyclone forecasting work. The method comprises of four forecast components, namely (a) cyclone genesis potential parameter (GPP), (b) Multi-model Ensemble (MME) technique for track prediction, (c) cyclone intensity prediction (SCIP) model and (d) predicting decaying intensity after the landfall.

Every year about one dozen low pressure areas form over the Indian Seas, but only a few of them intensify into a cyclonic storm. So from the operational point of view, it is very important to know at the initial stage the potentiality of a low pressure system to intensify into a

cyclonic storm. In a recent study, Roy Bhowmik (2003) proposed a genesis potential parameter on the basis of some dynamical parameters (such as low level divergence, vorticity and vertical wind shear between lower and upper troposphere), derived from the model analysis fields. This provides very useful information which has direct relevance to disaster management preparedness and other activities such as transportation, tourism, fishing etc. Kotal et al. (2009) further extended the work and suggested another genesis potential parameter (GPP) which takes into account both dynamical and thermodynamical factors.

A potential approach as emerged in recent studies (Krishnamurti *et al.*, 1999, Ebert, 2001; Arribas *et al.*, 2005; Roy Bhowmik and Durai, 2009) to address to the problem of weather forecasting is the Multi-Model Ensemble (MME) technique. In the MME approach, forecasts made with different models are combined into a single forecast to partially take into account the uncertainties in the model formulation and initial conditions. This type of ensemble is different from the ensemble forecast of the single model that utilizes a set of different initial conditions where the different initializations constitute the member models (Brooks and Doswell, 1999). In the context of cyclone track prediction, several studies Goerss, 2000; Mackey and Krishnamurti, 2001; Weber, 2003; Vijaya kumar et al. 2003; Williford et al., 2003) have shown that the application of the MME approach is very promising.

Towards this direction, a multimodel ensemble (MME) based track forecast technique has been attempted for the tropical cyclones over the Bay of Bengal (at 12-hour interval up to 72 hours) using the cyclone data of 2008.

In view of limitations of NWP models in the prediction of intensity of tropical cyclones (Elsberry et al, 2007; Houze et al, 2007), in a recent study, Kotal et al. (2008a) developed a statistical-dynamical cyclone intensity prediction (SCIP) model for prediction of intensity at 12-hour interval up to 72 hours to aid operational cyclone forecasting work over the Bay of Bengal. The maximum potential intensity (MPI) of a cyclone during life time of the system for the Bay of Bengal is also investigated in a recent study (Kotal et al., 2008b).

The forecast of inland wind after the landfall of a cyclone is of great concern to disaster management agencies. To address this problem, Roy Bhowmik et al. (2005) proposed an empirical decay model for predicting 6-hourly surface winds (intensity) valid till the system becomes a weak low-pressure area after the landfall over the Indian region

The aim of this work is to describe the objective cyclone forecast system and demonstrate the performance skill of the objective procedure during the Bay of Bengal severe cyclone Aila of November 2009.

2. Formulation of the objective cyclone forecast system

As stated above, various features of cyclone forecasting are: (a) Genesis, (b) Track, (c) Intensity and (d) Decay after landfall. The four forecasting components of tropical cyclone are described below.

2.1 Genesis Potential Parameter (GPP)

The process of initiation of a cyclonic disturbance over the Sea area is called cyclogenesis. To quantify the cyclogenesis, McBride et al (1981) proposed a Daily Genesis Potential parameter (DGP) on the basis of model analysis fields over the Atlantic and Pacific Ocean basin. In their study, DGP is defined as the difference of vorticity between 900 hPa and 200 hPa. The study showed that DGP is three times greater for developing systems than that of non-developing systems. An analysis of Cyclone Genesis Parameter for the Bay of Bengal, conducted by Roy Bhowmik (2003), showed that the procedure is capable of providing useful predictive signal. Kotal et al (2009) extended the work further by defining Genesis Potential Parameter (GPP) as:

$$GPP = \frac{\xi_{850} \times M \times I}{S} \quad \text{if } \xi_{850} > 0, M > 0 \text{ and } I > 0 \quad \dots(1)$$

$$= 0 \quad \text{if } \xi_{850} \leq 0, M \leq 0 \text{ or } I \leq 0$$

Where , ξ_{850} = Low level relative vorticity (at 850 hPa) in 10^{-5} s^{-1}

S = Vertical wind shear between 200 and 850 hPa (knots)

$$M = \frac{[RH-40]}{30} = \text{Middle troposphere relative humidity}$$

Where, RH is the mean relative humidity between 700 and 500 hPa

$I = (T_{850} - T_{500}) ^\circ\text{C}$ = Middle-tropospheric instability (Temperature difference between 850 hPa and 500 hPa). All the variables are estimated by averaging of all grid points over an area of radius 2.5° around the centre of cyclonic systems.

The study showed that GPP values are 3 to 5 times greater for the developing systems (T.No. > 2.5 ; maximum wind speed > 35 knots) than for non-developing systems (T.No. ≤ 2.5 ; maximum wind speed ≤ 35 knots) and is useful in differentiating between developing and non-developing systems at their early stages of development. They also showed that GPP values are equal and above 8.0 for developing systems and below 8.0 for non-developing systems in more than 85% of cases. GPP values for developing and non-developing systems as reported by Kotal et al (2009) are shown in Table 1.

Table 1. Genesis potential parameter (GPP) for Developing Systems and Non-Developing Systems.

GPP ($\times 10^{-5}$) \rightarrow					
T.No. \rightarrow	1.0	1.5	2.0	2.5	3.0
Developing	11.1	12.3	13.3	13.5	13.6
Non-Developing	3.4	4.2	4.6	2.7	-

Various thermo-dynamical parameters, which are used for real time analyzing Genesis Potential Parameter (GPP) for cyclonic storms over the Bay of Bengal during 2008-2009, are derived from the operational model analysis of the limited area model (LAM) of India Meteorological Department (IMD), New Delhi.

2.2 Track : Multimodel Ensemble (MME) Technique

India Meteorological Department operationally runs three regional models, Limited Area Model (LAM), MM5 model and Quasi-Lagrangian Model (QLM) for short-range prediction. The MM5 model is run at the horizontal resolution of 45 km with 23 sigma levels in the vertical and the integration is carried up to 72 hours over a single domain covering the area between lat. 30 ° S to 45 ° N long 25 ° E to 125 ° E. Initial and boundary conditions are obtained from the NCEP Global Forecast System (NCEP GFS) readily available on the Internet at the resolution of 1 ° x1 ° lat. /long. The boundary conditions are updated at every six hours interval. The LAM is integrated up to 48 hours at the horizontal resolution of 0.75 ° x0.75 ° lat/long with 16 sigma levels in the vertical over the same domain using the initial and boundary conditions of T-80 Global operational model run at NCMRWF. The model is also made flexible to run with NCEP GFS outputs as initial and boundary conditions. The QLM model is used for cyclone track prediction in case of cyclone situation in the Arabian Sea or Bay of Bengal. IMD also makes use of NWP products prepared by some other operational NWP Centres like, ECMWF (European Centre for Medium Range Weather Forecasting), GFS (NCEP), JMA (Japan Meteorological Agency) etc. The outputs at 12 hours forecast intervals of these models are first post- processed using GRIB decoder. The 12 hourly predicted cyclone tracks are then determined from the respective mean sea level pressure fields using a cyclone tracking software. In this report performance of these models during cyclone season of 2008 and pre-monsoon cyclone season of 2009 has been presented. The performance statistics of operational model QLM is shown in Table .2.

Table-2: QLM Model – Cyclone Track Error Statistics

Year	24-hour forecast (km)	36/48-hour forecast (km)	72-hour forecast (km)
1998	143	224	--
1999	119	248	--
2000	100	173	--
2001	106	183	--
2002	150	115	425
2003	187	251	280
2004	176	223	240
2005	174	306	345
2006	97	123	196
2007	136	252	408
2008	133	255	496
Mean Error (QLM)	138	214	341

A multimodel ensemble (MME) technique is developed using cyclone data of 2008. The technique is based on a linear statistical model. The predictors (shown in Table 3) selected for the ensemble technique are forecasts latitude and longitude position at 12-hour interval up to 72-hour of five operational models. In the MME forecasts, model-forecast latitude position and longitude position of the member models are linearly regressed against the observed latitude position and longitude position respectively for each forecast time at 12-hours intervals for the

forecast up to 72-hour. Multiple linear regression technique is used to generate weights (regression coefficients) for each model for each forecast hour (12hr, 24hr, 36 hr, 48hr, 60hr, 72hr). These coefficients are then used as weights for ensemble forecasts.

12-hourly forecast latitude (LAT^f) and longitude (LON^f) positions by multiple linear regression technique is defined as:

$$\left. \begin{aligned} LAT_t^f &= a_0 + a_1 ECMWF_t^{lat} + a_2 NCEP_t^{lat} + a_3 JMA_t^{lat} + a_4 MM5_t^{lat} + a_5 QLM_t^{lat} \\ LON_t^f &= a'_0 + a'_1 ECMWF_t^{lon} + a'_2 NCEP_t^{lon} + a'_3 JMA_t^{lon} + a'_4 MM5_t^{lon} + a'_5 QLM_t^{lon} \end{aligned} \right\} \text{----(2)}$$

for t = forecast hour 12, 24, 36, 48, 60 and 72

The dependent variable latitude (LAT^f) in °N and longitude (LON^f) in °E.

The detailed of model predictors are given in Table 3. The constant term a_0 and coefficients a_1, a_2, \dots, a_5 for 12 hourly forecast intervals for latitude and a'_0 and coefficients a'_1, a'_2, \dots, a'_5 for longitude are given in Table 4 and Table 5 respectively.

Table 3. *Model Parameters*

S.No.	Member models	Symbol of Predictors	
		Latitude position	Longitude position
1.	European Centre for Medium-Range Weather Forecasts (ECMWF),	ECMWF ^{lat}	ECMWF ^{lon}
2.	GFS of National Centers for Environmental Prediction (NCEP)	NCEP ^{lat}	NCEP ^{lon}
3.	Japan Meteorological Agency (JMA)	JMA ^{lat}	JMA ^{lon}
4.	MM5 Model	MM5 ^{lat}	MM5 ^{lon}
5.	Quasi-Lagrangian model (QLM)	QLM ^{lat}	QLM ^{lon}

Table 4. *Regression coefficients for latitude position for different forecasts hours*

Forecast hours	a_0	a_1	a_2	a_3	a_4	a_5
12 hr	1.46633	0.48327	0.08762	0.0474	-0.06954	0.34208
24 hr	0.75662	0.76242	-0.08543	-0.17727	-0.02354	0.45521
36 hr	1.28923	0.61778	-0.05394	0.04076	0.12614	0.17496
48 hr	0.60173	1.35212	0.30361	-0.3094	-0.00463	-0.27553
60 hr	0.36611	1.12986	-0.15616	0.1433	-0.11323	0.03574
72 hr	2.49751	0.37663	-0.37158	0.90057	-0.21182	0.14239

Table 5. *Regression coefficients for longitude position for different forecasts hours*

Forecast hours	a'_0	a'_1	a'_2	a'_3	a'_4	a'_5
12 hr	2.12692	0.33632	0.07031	0.10898	-0.04351	0.49902
24 hr	1.04316	0.85076	-0.14555	-0.07929	0.16159	0.19624
36 hr	5.82346	0.32571	-0.10423	0.34342	-0.05668	0.42152
48 hr	0.29452	0.36666	-0.04239	0.08226	0.18461	0.40281
60 hr	1.63954	0.24631	0.03642	0.23184	-0.12901	0.59908
72 hr	6.21043	0.28419	0.04475	0.48297	-0.01591	0.13165

2.3 Intensity

Roy Bhowmik et al (2007) proposed a simple empirical model for predicting cyclone intensity over the Bay of Bengal. The study is based on the assumption that tropical cyclone intensifies exponentially, where the intensification factor is determined using past 12 hours intensity changes. A major limitation of this empirical model (Roy Bhowmik et al 2007) is that it does not include parameters to take into account the physical and dynamical processes involved. The study warranted further investigation in a more general manner incorporating other synoptic and thermodynamical factors, which play important role for intensification of storms. In order to overcome these shortcomings, Kotal et al (2008a) developed a Statistical Cyclone Intensity Prediction (SCIP) model for the Bay of Bengal for predicting 12 hourly cyclone intensity (up to 72 hours), applying multiple linear regression technique using various dynamical and physical parameters as predictors. The model equation (Kotal et al 2008a) is given as:

$$dv_t = a_0 + a_1 IC12 + a_2 SMS + a_3 VWS + a_4 D200 + a_5 V850 + a_6 ISL + a_7 SST + a_8 ISI$$

for t= forecast hour 12, 24, 36, 48, 60 and 72 ------(3)

dv_t = Intensity change during the time interval t

The detailed of model predictors are given in Table 6. The constant term a_0 and coefficients a_1, a_2, \dots, a_8 for a 12 hourly forecast interval are given in Table 7.

Table 6 Model parameters

S.No.	Predictors	Symbol of Predictors	Unit
1.	Intensity change during last 12 hours	IC12	Knots
2.	Vorticity at 850 hPa	V850	$\times 10^5 \text{ s}^{-1}$
3.	Storm motion speed	SMS	ms^{-1}
4.	Divergence at 200 hPa	D200	$\times 10^5 \text{ s}^{-1}$
5.	Initial Storm intensity	ISI	Knots
6.	Initial Storm latitude position	ISL	$^{\circ}\text{N}$
7.	Sea surface temperature	SST	$^{\circ}\text{C}$
8.	Vertical wind shear	VWS	Knots

Table 7 Regression coefficients for different forecasts hours

Forecast hours	a ₀	a ₁	a ₂	a ₃	a ₄	a ₅	a ₆	a ₇	a ₈
12	-9.54983	0.31517	0.6749	-0.18668	0.865	0.75918	0.16853	0.24186	0.04103
24	-14.66671	0.58485	1.42963	-0.54507	1.58903	1.46658	0.5017	0.36094	0.14683
36	-7.61006	0.57747	3.03779	-0.8867	2.51223	2.28032	1.02698	-0.072297	0.22346
48	4.4943	0.54152	5.0484	-1.18528	3.29409	2.63681	1.66914	-0.71783	0.3127
60	18.75396	0.37624	6.66114	-1.33578	3.14652	2.85734	1.95777	-1.08646	0.1684
72	24.58879	0.19425	7.87951	-1.31717	5.09006	2.49177	2.22359	-1.30808	0.10789

The thermodynamic parameters used as predictors for the Statistical Cyclone Intensity Prediction (SCIP) model are derived from the forecast fields of ECMWF (European Center for Medium Range Weather Forecast) model and Sea Surface Temperature (SST) analysis at 1°

latitude-longitude grid interval from NCEP (National Center for Environmental Prediction) is used in real time forecasting.

2.4 Decay of intensity after the Landfall

The forecast of inland wind after the landfall of a cyclone is of great concern to disaster management agencies. To address this problem, Roy Bhowmik et al. (2005) proposed an empirical model for predicting 6-hourly maximum sustained surface winds (intensity) that is valid till the system becomes a weak low pressure area after the landfall over the Indian region. According to the decay equation (Roy Bhowmik et al., 2005), the maximum sustained surface wind speed (MSSW) after the landfall at time t is given by:

$$V_{t+6} = V_b + (V_t - V_b) * R_1, \text{ for } t=0 \text{ ----- (4)}$$

$$= V_b + (V_t - V_b) * R_2, \text{ for } t=6, 12, 18 \text{ and } 24 \text{ ---- (5)}$$

Where, reduction factors

$$R_1 = \exp(-a_1 * 6.0) \text{ ----- (6)}$$

$$\text{and, } R_2 = \exp(-a_2 * 6.0) \text{ ----- (7)}$$

Decay constant a_1 for the first six hours after the landfall (for $t=0$ to 6) is given by:

$$a_1 = [\ln \{(V_o - V_b) / (V_6 - V_b)\}] / 6 \text{ ----- (8)}$$

The decay constant a_2 for the remaining 12 hours (for $t=6$ to 18 hours) is taken as:

$$a_2 = [\ln \{(V_6 - V_b) / (V_{18} - V_b)\}] / 12 \text{ ----- (9)}$$

Regression equation relating R_1 and R_2 as given below:

$$R_2 = 0.982 * R_1 - 0.081 \text{ ----- (10)}$$

Where, V_0 is the maximum sustained surface wind speed at the time of landfall, V_t is the wind speed at time t after the landfall and V_b is the background wind speed. After landfall, tropical cyclone decays to some background wind speed. The background wind speed V_b and the reduction factors R_1 & R_2 as determined (Table 8) in the decay model (Roy Bhowmik et al, 2005) are used in this study.

The steps suggested by Roy Bhowmik et al (2005) for the operational forecasting are:

- (i) At the time of landfall (at $t=0$), employ the observed landfall intensity V_0 and the values of R_1 , R_2 and V_b , that are obtained based upon the sample average decay rate (Table 1.2.8), to make a six hourly prediction of V_t using equation (1.2.4).
- (ii) Six hours after the landfall (at $t=6$), use V_0 and V_6 from observation and V_b from Table 1.2.8 to compute actual R_1 from equations 1.2.6 and 1.2.8. Then get new R_2 from equation 1.2.10 and use equation (1.2.5) to revise the forecast for 12 hours after the landfall and later times.
- (iii) Twelve hours after the landfall (at 12), employ observed V_{12} to make a six hourly prediction using equation 1.2.5.
- (iv) Eighteen hours after the landfall, employ observed values of V_0 , V_{18} to calculate actual R_2 from equations 1.2.7 and 1.2.9 and revise the forecast for 24 hours and beyond using equation 1.2.5.
- (v) Twenty four hours after the landfall, use observed V_{24} to make a final forecast for V_{30} .

Table 8 Decay parameters of mean curve

MSSW (knots)	a_1 (h^{-1})	R_1 (6 h) $^{-1}$	a_2 (h^{-1})	R_2 (6 h) $^{-1}$	V_b (knots)
< 65	0.099	0.552	0.149	0.408	19.0
≥ 65	0.154	0.339	0.194	0.311	21.0

3. Bay of Bengal Severe Cyclonic storm “AILA ” of May 2009

Under the influence of the cyclonic circulation, a low-pressure area formed over the southeast Bay of Bengal on 22 May. It concentrated into a depression at 0600 UTC of 23 May and lay centered near Lat. 16.5° N/Long 88.0° E. The depression moved mainly in a northerly direction and intensified into a deep depression at 0300 UTC of 24 May and lay centred near Lat. 18.0°N/Long 88.5°E. It further intensified into a cyclonic storm ‘ALIA’ at 1200 UTC of 24 May and lay centred near Lat. 18.5°N/Long 88.5°E. It continued to move in northerly direction and intensified into a severe cyclonic storm at 0600 UTC of 25 May and lay over northwest Bay of Bengal near 21.5°N/Long 88.0°E. The system crossed West Bengal coast close to the east of Sagar Island between 0800 UTC to 0900 UTC as speed of landfall, and lay near Kolkata. The system maintained its intensity of cyclonic storm till 0000 UTC of 26 May. Moving northerly direction, it further weakened into a deep depression and lay centred at 0300 UTC of 26th May near Malda. It weakened into a depression and lay centred at 0600 UTC of 26 May over the same region. It weakened into a well marked low pressure area over Sub-Himalayan West Bengal at 0900 UTC of 26 May and became less marked on 27 May. The observed track of the system is shown in Figure 1.

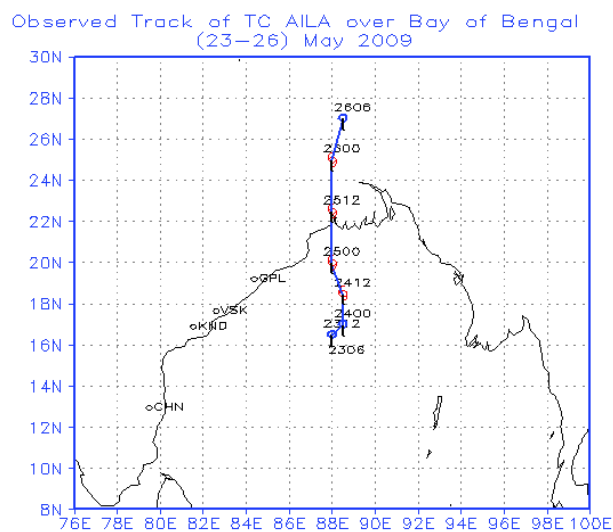


Figure 1

3.1. Analysis of GPP

GPP values computed for this cyclone “AILA” on the basis of real time model analysis fields along with the GPP values for Developing Systems and Non-Developing Systems are shown in

Table 9. The higher GPP values (> 8.0 , the threshold value) at early stages of development (T.No. 1.0, 1.5) have clearly indicated that the cyclone “AILA” had enough potential to intensify into a developing system (>35 knots).

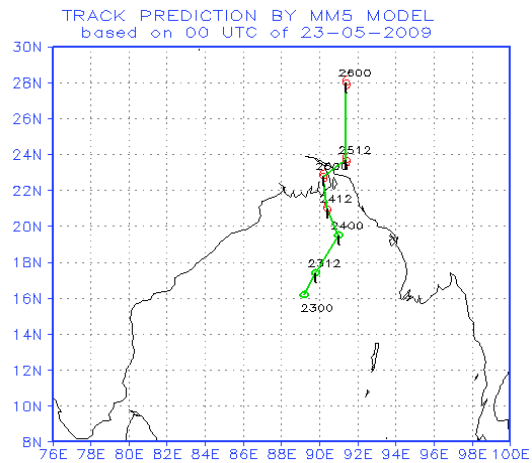
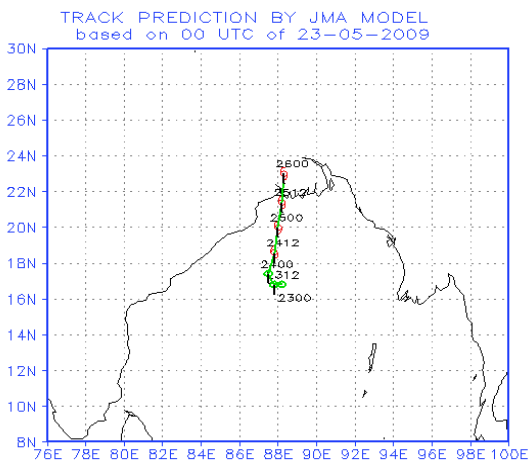
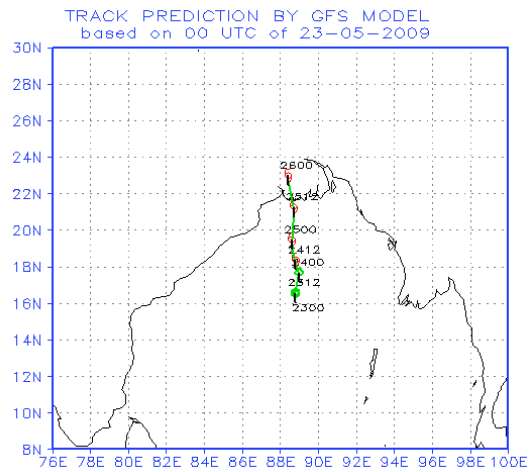
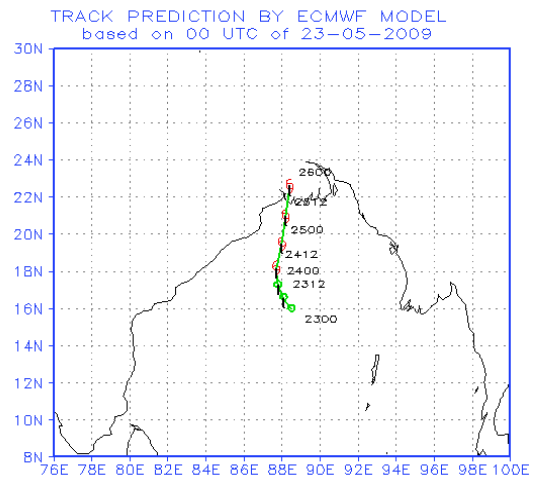
Table 9 Genesis potential parameter (GPP) for Developing System, Non-Developing System and Cyclone “AILA”

GPP ($\times 10^{-5}$) \rightarrow					
T.No. \rightarrow	1.0	1.0	1.0	1.0	1.5
Developing	11.1	11.1	11.1	11.1	12.3
Non-Developing	3.4	3.4	3.4	3.4	4.2
Cyclone “AILA”	20.0 (00UTC /22.05.2009)	20.0 (1200UTC /22.05.2009)	14.3 (0000UTC /23.05.2009)	14.9 (1200UTC /23.05.2009)	16.3 (00UTC /24.05.2009)

3.2 Track prediction by NWP models

Figure 2-4 display the forecast track positions of the cyclone AILA by various NWP models (ECMWF, GFS (NCEP), JMA, MM5, QLM) and multimodel ensemble (MME) with the initial conditions of 0000 UTC of 23 May, 24 May and 25 May 2009 respectively. All the NWP models consistently indicated that the cyclonic storm AILA was going to move northerly direction and crossed Indo-Bangla border. Although the QLM model based on 0000 UTC of 23.05.2009 showed northwesterly recurvature and crossed Orissa coast and MM5 model showed southeast Bangladesh coast, but during subsequent forecast hours it showed crossing of Indo-Bangla border.

The forecast errors of member models based on different initial conditions and the corresponding consensus forecasts (MME) are summarized in Table 10.-12. The tables show that consensus forecasts could provide useful guidance under the circumstances of wide variations of individual models (e.g. QLM, MM5 based on 00 UTC of 23.05.2009).



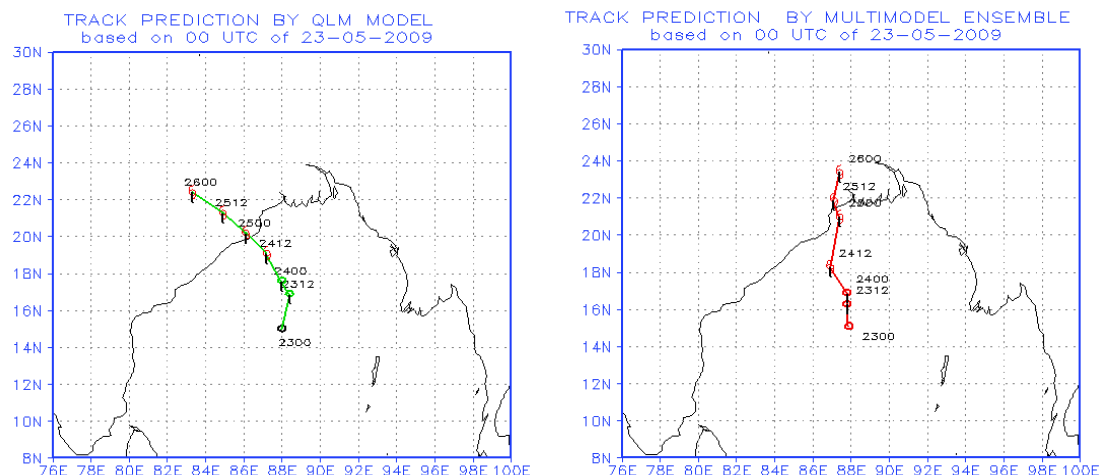


Figure 2: Forecast track of multimodel ensemble and its member models based on 0000 UTC of 23.5.2009

Table 10: Track forecast error (km) of multi-model ensemble and its member models based on 0000 UTC/23.5.2009

HOUR	ECMWF	GFS	JMA	MM5	QLM	MME
0	123	187	201	185	0	15
12	15	86	40	216	61	31
24	81	94	115	383	85	75
36	91	33	75	341	115	67
48	50	76	0	303	199	127
60	168	152	124	372	346	114
72	270	226	224	475	559	295
LF	20 km	62 km	40 km	227 km	275 km	83 km
ERROR	10 hr delay	8 hr delay	6 hr delay	8 hr early	11 hr delay	2 hr delay

Table 11: Track forecast error (km) of multimodel ensemble and its member models based on 0000 UTC/24.5.2009

HOUR	ECMWF	GFS	JMA	MM5	QLM	MME
0	70	113	98	116	0	31
12	0	46	54	120	61	49
24	20	70	59	77	156	70
36	102	20	56	146	132	145
48	120	60	180	82	78	129
LF	10km	23km	10km	124km	175km	20km
ERROR	5h delay	1h delay	1h delay	4h delay	8h early	7h delay

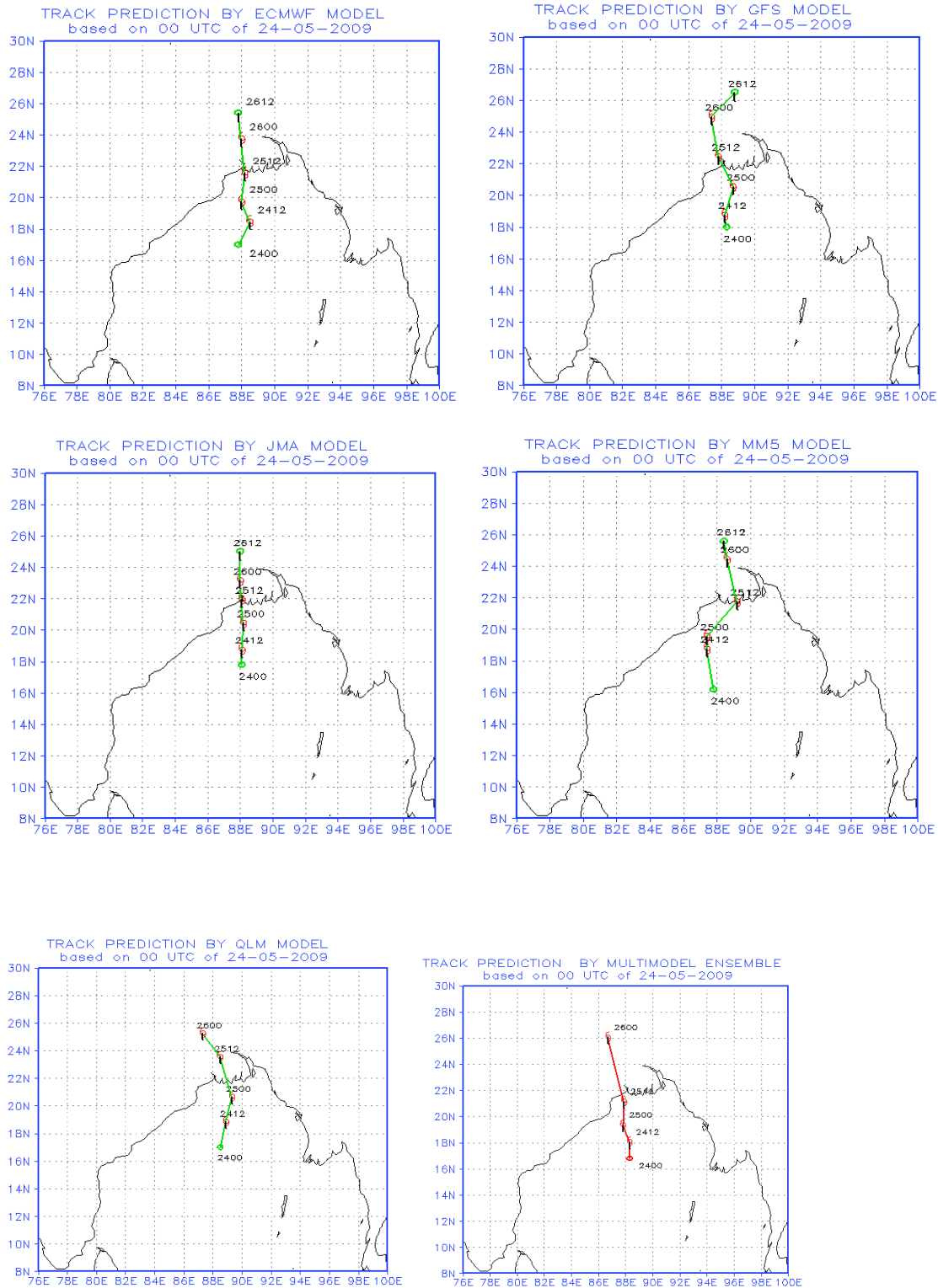


Figure 3: Forecast track of multi-model ensemble and its member models based on 0000 UTC of 24.5.2009

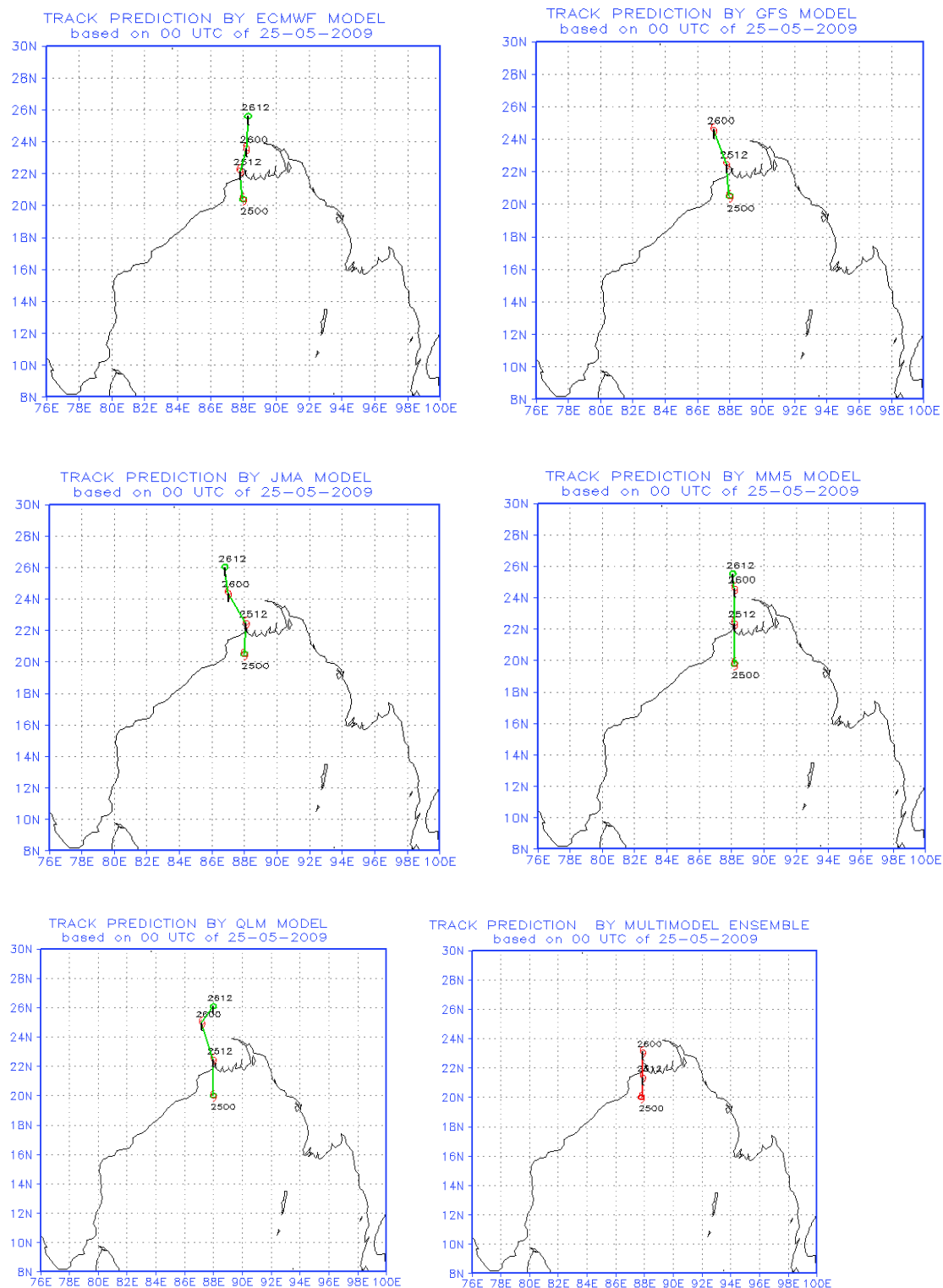


Figure 4: Forecasts track of multi-model ensemble and its member models based on 0000 UTC of 25.5.2009

Table 12 Track forecast error (km) of multimodel ensemble and its member models based on 0000 UTC/25.5.2009

HOUR	ECMWF	GFS	JMA	MM5	QLM	MME
0	40	50	50	30	0	20
12	39	20	10	23	0	15
24	157	110	121	59	80	100
LF ERROR	10 km Close to LF time	15 km Close to LF time	15 km Close to LF time	20 km 2hr delay	10 km 2hr delay	15 km 2hr delay

4. Intensity prediction by SCIP model

Based on 0000 UTC of 23 May 2009:

The cyclone “AILA” intensified gradually from its depression stage and maintained its intensification till landfall. The cyclone reached to its severe cyclonic stage at 0600 UTC of 25 May 2009. The 12 hourly intensity forecast (based on 0000 UTC of 23 May 2009) valid up to 60 hours (Table 13) shows that the model could predict intensity with reasonable success with a maximum error of 10 knots at 48 hours.

Table 13. Model (SCIP) performance based on 0000 UTC of 23 May 2009

Forecasts hours →	00 hr	12 hr	24 hr	36 hr	48 hr	60 hr
Observed (knots)	20	25	25	35	40	50
Forecasts (knots)	20	25	31	43	50	55
Error (knots)	-	0	+6	+8	+10	+5

The updated forecasts based on 0000 UTC of 24 May and 0000 UTC of 25 May show improvement of error at all forecasts hour (Table 14-15).

Table 14 Model (SCIP) performance based on 0000UTC of 24 May 2009

Forecasts hours →	00 hr	12 hr	24 hr	36 hr
Observed (knots)	25	35	40	50
Forecasts (knots)	25	32	38	49
Error (knots)	-	-3	-2	-1

Table 15 Model (SCIP) performance based on 0000 UTC of 25 May 2009

Forecasts hours →	00 hr	12 hr
Observed (knots)	40	50
Forecasts (knots)	40	48
Error (knots)	-	+2

5. Decay of AILA after landfall

The cyclone “AILA” maintained its intensity of cyclonic storm till 15 hours after landfall and depression stage for next 6 hour. Figure 5 shows the decay curves on the basis of observations (line with solid squares), 6-hourly forecast intensity (using equation 4) up to 18 hours after the landfall (line with open circles) and six hour after landfall, the updated forecast intensity (using equation 5) up to 12 hours (line with solid circles). The 6 hourly decay forecast (based on 0900 UTC of 25 May 2009, at the time of landfall) valid up to 18 hours (Table 16) shows that the decay model could predict intensity with reasonable success with a maximum error of 6 knots (under estimation) at 12 hours. The updated forecast (6 hour after landfall) valid up to 12 hours (Table 17) shows improvement of forecast error.

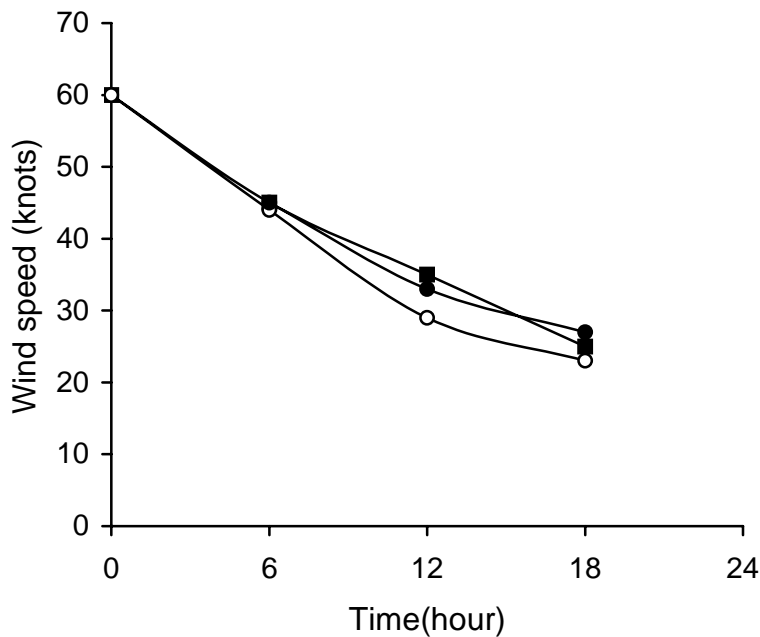


Figure 5: Decay of intensity of AILA after landfall

Table 16. Decay model performance (at the time of landfall)

Forecasts hours →	00 hr	6 hr	12 hr	18 hr
Observed (knots)	60	45	35	25
Forecasts (knots)	60	44	29	23
Error (knots)	--	-1	-6	-2

Table 17 Updated Decay forecast (6 hr after landfall)

Forecasts hours →	00 hr	6 hr	12 hr
Observed (knots)	45	35	25
Forecasts (knots)	45	33	27
Error (knots)	--	-2	+2

6. Concluding Remarks

During 2008-09, IMD experimented this objective numerical method for the operational cyclone forecasting work. The method comprising of four forecast components, namely (a) Cyclone genesis potential parameter (GPP), (b) Multi-model Ensemble (MME) technique for cyclone track prediction, (c) Cyclone intensity prediction (SCIP) model and (d) Predicting decaying intensity after the landfall. This paper describes the development of objective cyclone forecast system and documents the performance skill during the Bay of Bengal Severe Cyclone Aila of November 2009. The study shows that the GPP analysis at early stages of development (T.No. 1.0, 1.5, 2.0) could indicate the potential of the systems for intensification. The 12-hourly track forecast by MME technique and intensity forecasts by SCIP model valid up to 72 hours and subsequent updated forecasts are found to be consistent and useful to the operational forecasters.

The error statistics of the decay model shows that the model could predict the decaying intensity after landfall with reasonable success.

The new approach was found very useful for delivering improved operational cyclone forecast and warning.

Acknowledgment: Authors are grateful to Dr. (AVM) Ajit Tyagi, Director General of Meteorology, India Meteorological Department for his keen interest, encouragement, constant support and providing all facilities to carry out this work.

REFERENCES

Arribas, A, Robertson, K.B., Mylne, K.R., (2005): Test of a Poor Man's Ensemble Prediction System for short range probability forecasting. *Monthly Weather Review* , **133**, 1825-1839

Brooks H.E. and Doswell C.A., (1999): New technology and numerical weather prediction. *Weather* **48**: 173-177.

Ebert E.E., (2001): Ability of a poor man's ensemble to predict the probability and distribution of precipitation, *Monthly Weather Review* , **129**, 2461-2479

Elsberry, R.L., Lambert, T.D.B. and Boothe, M.A., (2007): Accuracy of Atlantic and eastern North Pacific tropical cyclone intensity forecast guidance, *Wea. Forecasting*, **22**:747-762.

Goerss, J. S., (2000): Tropical cyclone track forecasts using an ensemble of dynamical models. *Mon. Wea. Rev.*, **128**, 1187–1193.

Houze, R.A., Chen, S.S., Smull, B.F., Lee, W.C. and Bell, M.M. (2007): Hurricane intensity and eyewall replacement, *Science*, **315**:1235-1238.

Kotal, S.D., Kundu, P.K. and Roy Bhowmik, S.K. (2009): Analysis of cyclogenesis parameter for developing and non-developing low pressure systems over the Indian Sea, *Nat. Hazards*, **50**:389-402

Kotal, S.D., Roy Bhowmik, S.K. and Kundu, P.K. and Das, A.K. (2008a): A Statistical Cyclone Intensity Prediction (SCIP) Model for Bay of Bengal, *J. Earth. Sys. Sci.* **117**:157-168.

Kotal, S.D., Kundu, P.K. and Roy Bhowmik S.K., (2008b). An analysis of Sea Surface Temperature and Maximum Potential Intensity of Tropical Cyclones over the Bay of Bengal between 1981 to 2000. *Meteorological Applications* **16**:169-177

Krishnamurti T.N., Kishtawal C.M., Larow T., Bachiochi D., Zhang Z., Willford E.C., Gadgil S. and Surendran S., (1999): Improved weather and seasonal climate forecasts from multimodel super ensemble. *Science* **285**: 1548-1550.

McBride, J.L. and Zehr, R.M. (1981): Observational analysis of tropical cyclone formation. Part II: Comparison of non-developing versus developing systems, *J. Atmos. Sci.*, **38**:1132–1151.

Mackey, B. P. and . Krishnamurti, T.N. (2001): Ensemble Forecast of a Typhoon Flood Event. *Wea. and Forecasting* , **16**, 399-415

Roy Bhowmik, S.K. (2003): An evaluation of cyclone genesis parameter over the Bay of Bengal using model analysis, *Mausam*, **54**:351-358.

Roy Bhowmik, S.K., Kotal, S.D. and Kalsi, S.R. (2007): Operational tropical cyclone intensity prediction—an empirical technique. *Nat. Hazards*, **41**:447-455.

Roy Bhowmik S.K., Kotal, S.D. and Kalsi S.R, (2005). An empirical model for predicting decaying rate of tropical cyclone wind speed after landfall over Indian region, *Journal of Applied Meteorology*, **44**:179-185.

Roy Bhowmik S.K. and Durai V.R., (2010): Application of multi-model ensemble technique for real-time district level forecasts over Indian region in short range time scale, *Meteorol. Atmos. Phy.*, **106**, 19-35

Vijaya kumar T. S. V., T. N. Krishnamurti, M. Fiorino and M. Nagata, (2003): Multimodel superensemble Forecasting of Tropical Cyclones in the Pacific. *Mon. Wea. Rev.*, **131**, 574–583.

Weber, H.C. (2003): Hurricane Track Prediction Using a Statistical Ensemble of Numerical Models. *Mon. Wea. Rev.*, **131**, 749–770.

Williford, C. E., Krishnamurti, t.n., Ricardo Correa Torres, Steven Cocke, Zaphiris Christidis, and Vijaya Kumar, T.S., (2003): Real-Time Multimodel Superensemble Forecasts of Atlantic Tropical Systems of 1999. *Mon. Wea. Rev.*, **131**, 1878–1894.

Cyclone Prediction for Satellite Launch Vehicles at Sriharikota

G V Rama, Meteorology Facility, Sriharikota – 524 124

Email: gvrma@shar.gov.in

Satish Dhavan Space Centre, SRIHARIKOTA (SDSC SHAR) is the prestigious satellite launch station of India, located over east coast of southern peninsular India. It is a tropical coastal island, sandwiched between Pulicat Lake and Bay of Bengal. It is prone to severe tropical cyclones in May and October to December that developed in Bay of Bengal. The station experienced a very severe cyclonic weather on 13th – 14th, November 1984 for 36 hours with gale speeds of the order 220 kmph and very heavy rain (approximately 100 cm). The connecting road to main land was partly breached. It caused lot of damage to installations and inconvenience to people living in island. The station is well equipped with tall structures and technical facilities. Weather critical technical operations are generally going on daily. Hence, there is a specific demand on tropical cyclone forecast which comes within 500 km of SDSC SHAR (warning zone) with a lead time of 2 to 9 days to safeguard launch pad facilities, to schedule day to day weather critical launch operations and to schedule satellite launch.

To meet this requirement, Meteorology Facility, SDSC SHAR is well equipped with a *net work of* an upper air, Boundary layer, Surface observatories with data acquisition systems connected through a Local Area Network (LAN) to a centralised computing facilities. In addition to these, data from national meteorological agency i.e., India Meteorological Department (IMD) and Global data (GFS) is also being received through internet and used. Data validation, processing, analysis and Numerical Weather Prediction (NWP) is being carried out using high speed computers. Generally forecast expressed in probabilistic terms is being provided so that user can easily use the information to make decisions.

Data application may be mentioned as, Climatological extremes are used while designing technical facilities and tall structures. Although, ideally, a space vehicle design should accommodate all expected operational atmospheric conditions, it is neither economically nor technically may be feasible to design them to withstand all weather conditions such as squally

weather associated with cyclones and thunderstorms, triggered lightning discharges, strong ground wind and upper wind velocities associated with large vertical wind shears, heavy rain etc., . For this reason, consideration is given to protect space vehicles from extreme weather conditions by suitable design, at least for ninety-five percentiles of weather conditions. Avoiding weather critical operations and rocket launch during the remaining five percent unfavourable weather conditions for which vehicle is not designed is an ultimate solution. To meet this demand, numerical Weather predictions and conventional techniques are used to provide Medium range / Short Range predictions valid for the next 5 days to 1 day, up dated at 12 / 24 hour interval during assembly phase of the vehicle. Nowcasting techniques are used for day to day operations and from T-2 hours on launch day where 'T' is launch time. The over all requirement of weather prediction and prediction methodology is briefly presented below.

- T-9 days General out look to move launch vehicle to launch pad for making vehicle ready for launch. Global models & Regional models are used updated daily at 12 hourly intervals.
- T-3 days (72 hours), Very time specific and location specific short range forecast in steps of 6 hours is issued and updated at 12 hour interval. Global , Regional and Synoptic models are used for this purpose.
- On launch day, weather parameters are predicted based on Regional models and Real time observations for launch window with reference to Launch Weather Commit Criteria (LCC) on critical weather parameters.
- From T-2 Hr, close weather watch is maintained with frequent balloon ascents at 20 minute interval at SHAR and MST radar observations at Gadanki on upper wind variations with time to implement Day of Launch Wind Biasing (DOL-WB). Satellite cloud imageries, DWR products, AWS & Fieldmill net work data of SHAR is used for local weather prediction up to launch window.
- At T-30 minutes, Weather briefing is provided to confirm whether predicted values of all Launch Commit criteria parameters are within specified limits. Close weather watch is continued for significant changes if any and shall be informed to launch authorities for taking go / no-go decision with launch operations.

Case studies like predictions on Cyclone “Nargis” which was at about 600 km east of SHAR on PSLV – C9 launch day (28-4-2008) and predictions made on cyclones namely Rashmi, Khai- Mukh and Nisha are presented and discussed.

Role of eddies and upper ocean heat content in the intensity and movement of cyclones from Satellite data.

K.Maneesha and Y.Sadhuram*

National Institute of Oceanography, Regional Centre,

176, Lawson's Bay Colony, Visakhapatnam

*E-mail:sadhuram@nio.org

Abstract

Bay of Bengal is well known for meso scale eddies .These eddies highly influence the vertical thermal structure of the top 200m and the Upper Ocean Heat Content (UOHC).From a few in situ CTD profiles, it is found that the UOHC is almost three times higher in anti cyclonic eddy (ACE) compared with that in a cyclonic eddy (CE).This large variability plays a vital role in the intensification /weakening of storms if they encountered with the eddies. It is found that the models which incorporate the role of eddies and UOHC in the north west Pacific Ocean showed better results than using only SST. Such studies are not attempted for Bay of Bengal.

The cyclone “Aila “ during 22-24th May ,2009 encountered with a warm core ACE over the central Bay of Bengal. The intensity of the storm enhanced by 43 % due to this eddy which is well comparable with the estimated (34%) from the best fit line (developed for north west Pacific Ocean) . UOHC in the eddy region was about 300% higher than the climatological value. This high UOHC opposes cooling induced by the storm and provides large enthalpy flux (latent+sensible) which supports the intensification of the storm. The translation speed of the storms (Sidr & Nargis) estimated using UOHC and the depth of 26 °C isotherm (D26) are well comparable with the observed values. A simple method to compute UOHC from Sea Surface Height Anomalies (SSHA) had been developed using the time series data of RAMA buoys in the Bay of Bengal during pre-monsoon (April-May) and post-monsoon (Oct-Nov) seasons for the period, 2007-2009.

It is suggested that the mesoscale eddies and UOHC may be considered in the intensity and track prediction of cyclones in the Bay of Bengal.

Heat Content from ocean circulation models

C. Gnanaseelan*, B. Thompson, S. Rahul and C. Soumi

Indian Institute of Tropical Meteorology, Pashan, Pune 411008, India

*Email: seelan@tropmet.res.in

Abstract

The long term variability in the temperature and sea level over the north Indian Ocean during the period 1958-2000 has been investigated in this study. A comprehensive assessment of the recently developed Modular Ocean Model version 4 using the sea level observations from tide-gauges, Topex/Poseidon (T/P) satellite, in situ temperature profile observations from WHOI moored buoy and sea surface temperature (SST) observations from DS1, DS3 and DS4 moored buoys has also been performed for the available periods. Long (6-8 years) warming episodes in the SST over the north Indian Ocean are followed by short episodes (2-3 years) of cooling. The model temperature and sea level anomaly over the north Indian Ocean show an increasing trend in the study period. The model thermocline heat content per unit area shows a linear increasing trend (from 1958-2000) at the rate of $0.0018 \times 10^{11} \text{ J/m}^2$ per year for north Indian Ocean. North Indian Ocean sea level anomaly (thermosteric component) also shows a linear increasing trend of 0.31 mm/year during 1958-2000.

1. Introduction

The oceans largely remain a data sparse region despite their importance in modifying the weather and climate. Even though atmospheric data over the oceans are also sparse (as compared to land), it has improved in the recent years with the advent of satellite observations. However the remote sensing techniques can only measure a few oceanic variables at the surface such as sea surface temperature (SST) and sea surface height. However the relative abundance of atmospheric data can be imposed in a state-of-the-art Ocean General Circulation Model (OGCM) framework and more realistic simulation of oceanic geophysical parameters can be obtained in surface and subsurface of the oceans. In this scenario three dimensional OGCMs provide the most reliable estimate of variables in the surface and interior of oceans. The availability of high performance computing systems gave the model developers the freedom to reduce unrealistic approximations and employ more realistic parametrisation of unresolved processes. This in fact has helped to reduce the inaccuracies in the model simulations to a great extent (Griffies *et al* 2003).

Oceans are a major component of the global climate; covering roughly 72% of the planet's surface, they have thermal inertia and heat capacity to help maintain and restructure climate variability. Recent observations of global ocean temperature changes have shown substantial warming in the upper 1000 m, averaging about 0.1°C between 1955 and 1995 (Levitus *et al* 2000). However the warming rate varies considerably among different ocean basins. Levitus *et al* (2001) suggested that the observed increase in ocean heat content is largely due to the increase of anthropogenic gases in earth's atmosphere. One of the immediate responses of the ocean warming is the increase in sea level. The sea level rise can be contributed by various factors like changes in thermal and haline structure of the oceans (steric change), melting of continental ice and filling of continental reservoirs (mass change), and geologic changes due to the vertical crustal movement of tide gauges (Carton *et al* 2005). The thermosteric term is known to be a significant contributor to the global average sea level rise at a rate of 0.42 ± 0.12 mm/year (during 1961-2003, IPCC Report, 2007). According to IPCC Report (2007) the global average sea level rose at an average rate of 1.8 mm/year over 1961-2003. The other terms contributing to the

sea level rise are melting of ice caps and ice sheets (glaciers and ice cap ~ 0.5 mm/year, Greenland ice sheet ~ 0.19 mm/year) and individual climatic contributions (~ 1.1 mm/year). Meanwhile, the rate of sea level rise was faster over the period 1993-2003. Satellite altimetry shows that the global sea level rose at a rate 3.1 ± 0.7 mm/year over this period (IPCC Report, 2007). The linear increasing trend in the global sea level from 1950 are reported by many authors (Antonov *et al* 2002; Church *et al* 2004 and 2006)

The above factors motivated us to carry out the present study on ocean thermal structure, heat content and sea level using a regional ocean model forced with interannually varying surface forcing. The model simulations are compared with in situ temperature and sea level anomaly (SLA) derived from satellite and tide gauges. The warming and sea level variability over the north Indian Ocean (NIO) during the period 1958-2000 is examined in the present study. The temperature and sea level variability over AS, BoB and Equatorial Indian Ocean (EIO) are discussed in detail in this paper.

2. Model and Methodology

The OGCM used for this study is the Geophysical Fluid Dynamics Laboratory (GFDL) Modular Ocean Model Version 4 (MOM4p0) (Griffies *et al* 2003). MOM4p0 is a z-coordinate (3 dimensional) numerical representation of hydrostatic primitive equations with Boussinesq approximation and explicit free surface. Prognostic variables include the two active tracers of temperature and salinity, the horizontal velocity components and passive tracer field, the height of free ocean surface. The time stepping scheme is based on a predictor-corrector method, which is more stable than the leapfrog scheme. The model tracer field, the baroclinic velocity and free surface height are computed every 9600 seconds. Since the tracer and baroclinic time steps are equal, total tracer is conserved in the model, except for time discretisation errors arising from the use of a time filtered surface height. The barotropic fields have a time step of 120 seconds. The equation of state is based on the formulation described by McDougall *et al* (2003), which is more accurate than the linearised equation of state. The vertical mixing in the model is handled through the

K-Profile Parameterisation Scheme (Large *et al* 1994) using local and non-local mixing with Bryan-Lewis Background Diffusivity (Bryan and Lewis, 1979). The heating due to penetrative shortwave radiation is attenuated by the inclusion of chlorophyll data.

The model region is 30°E to 120°E and 40°S to 25°N with 30 vertical levels. The upper ocean mixed layer and thermocline zones are well resolved in the model with 15 vertical levels within a depth of 150 m. The vertical resolution gradually changes from 10 m to a maximum of 712 m at 5600 m. The model has been provided with a realistic topography of 0.5° resolution. Model has a constant zonal resolution of 1° and meridional resolution varying from 0.3353° at equator to 0.7° at 25°N and 1.5° at 40°S. Solid walls are assumed at the eastern and southern boundaries and no slip conditions are assumed for momentum. For temperature and salt no flux boundary conditions are assumed. Additionally, the southern and eastern boundaries are provided with a sponge layer of 4° width, where the temperature and salinity are restored to monthly climatologies of Levitus (1998) with a timescale of 5 days. The model was initialized with annual climatologies of temperature and salinity from Levitus (1998) and forced by climatological downwelling shortwave and longwave radiation, 10m surface wind fields, specific humidity, air temperature, surface pressure and surface precipitation from NCAR climatology (Large and Yeager 2004). Chlorophyll-a climatology computed from SeaWiFS satellite for the period 1999-2001 is used for the shortwave penetration scheme. After 20 years of spin up the model has been integrated from 1958-2000 with NCAR corrected interannual datasets (Large and Yeager 2004) of daily downwelling shortwave and longwave radiation, 6-hourly 10 m surface wind fields, specific humidity, air temperature, surface pressure and monthly precipitation.

3. Data Used

The in situ data used for the model validation are the Woods Hole Oceanographic Institution (WHOI) mooring observations at 61.5°E, 15.5°N from 15-October-1994 to 20-October-1995, National Institute of Ocean Technology (NIOT) moorings DS1 at 69.3°E, 15.3°N from 1-February-1998 to 31-December-1998, DS3 at

87°E, 13°N from 1-Jan-1998 to 10-June-1998 and DS4 at 89°E, 19°N from 1-Jan-1998 to 31-12-1998. The temperature observations at the surface and subsurface down to 250 m observed from WHOI mooring are used for comparison with model simulations. The details of instruments and observations used in the WHOI moorings are discussed in Weller *et al* (1998 and 2002). The SST measured from DS1, DS3 and DS4 buoys are also compared with model SST. The accuracy of the DS1, DS3 and DS4 buoy data were given in Premkumar *et al* (2000). The temperature in the first layer (0-5 m) of the model is taken as the model SST and the temperature observations are averaged in the same layer is averaged to obtain the observed SST.

The T/P altimeter provides sea surface height with a repeat cycle of 10 days with the accuracy of approximately 2 cm (Tapley *et al* 1994; Cheney *et al* 1994). The SLA derived from T/P observations are extensively used for studying interannual sea level variations in the Indian Ocean (Vinayachandran *et al* 1999; Chambers *et al* 1999). The SLA from T/P is monthly averaged for the period 1993-2000 and compared to model SLA for the period 1993 to 2000. The tide-gauge observations of monthly sea level from the data archive of Permanent Service for Mean Sea Level (Woodworth and Player, 2003) are used for the comparison of model sea level. The Revised Local Reference (RLR) data are analysed here. In the north Indian Ocean (north of 10°N) not many island tide-gauge observations are available also the time period of observations is shorter. Meanwhile the coastal tide-gauges provide sea level observations of longer record lengths. Unnikrishnan *et al* (2006) used tide-gauge observations along the Indian coast for studying the sea level changes over the region. Their estimates of mean sea level rise at selected stations along the coast of India indicate a rise of slightly less than 1 mm/year. The coastal tide-gauge observations from Marmagoa (73.48°E, 15.25°N, 1969-2000), Cochin (76.16°E, 9.8°N, 1958-2000), Palau Langkawi (99.46°E, 6.26°N, 1986-2000) and island tide-gauge observation from Male-B (Hulule) (73.32°E, 4.11°N, 1991-2000) are compared with model SLA. The model SLA is averaged in a 2° x 2° box over the observation point. The locations of the mooring and tide-gauge observations used in the study are shown in figure 1.

HadISST v.1.1 and the Simple Ocean Data Assimilation (version SODA_1.4.2) dataset are also used for the model calibration and analysis of model simulated temperature fields. In situ sea surface observations and satellite estimates at the sea surface are included in the HadISST Global Ocean Surface Temperature analysis (Rayner *et al* 2003). SODA is a University of Maryland reanalysis product using an eddy-permitting global model based initially on POP_1.3 numerics and SODA procedure (Carton *et al* 2005; Carton and Giese 2006).

4. Results and Discussions

4.1 Model Temperature - Validation

The model temperature simulations are validated with the in situ observations before doing more analysis on its variability. The continuous mooring observations by WHOI, DS1, DS3 and DS4 buoys provided an opportunity for the validation of model simulated temperature. The correlation and rms difference between model and in situ observations are given in table 1. Figure 2a shows the time series of daily SST from model and WHOI mooring off the coast of Oman (61.5°E 15.5°N). The rms difference between WHOI and model SST is 0.45°C. Even though a cold bias is observed in the model SST, the SST variability is very well correlated (0.95). Cooling of the AS in the boreal winter (January-February) and during monsoon (July-August) seasons and warming in pre-monsoon (May) and post-monsoon (October) are well reproduced by the model. Maximum difference (~1°C) between model and observations is seen during July-August, where the model underestimated the SST cooling. The vertical section of temperature from WHOI and model at the mooring point is shown in figure 3. The figure shows that the convective cooling during winter season and pre-monsoon warming are well reproduced by the model. The vertical extent of pre-monsoon warming is smaller than observed in the model. Also the monsoonal cooling (due to momentum flux and surface heat fluxes) is not well simulated by the model.

The model SST and DS1 buoy observation are compared in figure 2b. As seen in figure 2a, the cold bias in the model SST is observed in DS1 mooring location

also. The DS1 buoy is located in the eastern AS region (69.3°E, 15.3°N). The pre-monsoon warming and monsoonal cooling of SST over this region is well reproduced by the model. The steep fall in SST seen in buoy observation in early June was due to the presence of a severe cyclonic storm in the AS during June 3-9 (Premkumar *et al* 2000). Such a steep fall is not seen in the model SST. This could be due to the inaccuracy and the coarseness of the forcing fields (ie, wind and precipitation fields), since no well-marked cyclonic condition is seen in the forcing fields. The intermediate model resolution may also be a possible reason for this discrepancy. The SST comparison at DS3 and DS4 buoy locations is shown in figure 2c and 2d. The DS3 and DS4 buoys are located in the central BoB. These areas are prone to intraseasonal oscillation (Sengupta and Ravichandran 2001). The time series at DS4 location (figure 2d) shows the intra seasonal oscillation in the observations during the summer monsoon, which is also reproduced by the model SST.

4.2 Model Sea Level Anomalies - Validation

The correlation between T/P observed SLA and model SLA shows that the model is in good agreement with the observations (figure 4a) except over the western BoB, western AS and eastern Indian Ocean south of 10°S. Over 65% of the basin is found to have correlation above 95% confidence level. Correlation above 0.9 is seen in the southeastern AS. The correlation is observed to be above 0.80 in the regions where strong interannual variability is observed (e.g. eastern EIO). The root mean square (rms) difference between model and T/P anomalies is shown in figure 4b. Over the tropical Indian Ocean region between 10°S and 10°N, most of the AS and southern BoB, the rms differences are observed to be less than 4 cm, which represents less than 35% of standard deviation of T/P SLA (figure 4d). Inconsistency between model and T/P SLA are seen in the western AS, western BoB and in the Indian Ocean south of 10°S, where the correlation is also less.

The basin wide average of SLA for the period 1993 to 2000 over the North Indian Ocean [45°E to 110°E, 10°S to 25°N], Arabian Sea [45°E to 80°E, 5°N to 25°N], Bay of Bengal [80°E to 100°E, 5°N to 20°N] and Equatorial Indian Ocean [40°E to 110°E, 10°S to 5°N] are drawn in figures 5a, 5b, 5c and 5d respectively. It is

important to note that the deseasonalised time series are shown. The seasonal signal was computed considering the 8 years average of each month and the difference between total and seasonal signal is considered as the deseasonalised signal. The correlation and rms difference between model and T/P SLA observation is shown in table 2. Over NIO the correlation of 0.6 is seen between model and T/P, while the rms difference is 0.78 cm, which is a less than 20% peak-to-peak variation in T/P SLA. Notable difference between the model SLA and observed SLA is seen in the BoB region. The rms difference is observed to be relatively higher (1.9 cm) in BoB, which represents 15% of variability in T/P SLA.

The SLA from tide-gauge observations at Cochin, Marmagoa, Male-B (Hulule) and Palau Langkawi are plotted against the model SLA in figure 6. The time series are detrended by removing their linear trends. In these tide-gauges long period records are available only for Cochin and Marmagoa. There are some long gaps in data available for the Marmagoa station, from 1979-1986 and 1994-1998. The figure shows that good agreement is found between model and observations. The correlation between model and tide-gauge SLA are 0.71, 0.71, 0.78 and 0.83 respectively.

4.3 Warming Trend in the North Indian Ocean and Decadal Variability of Temperature and Sea level

The ocean heat content is a dominant component of the variability of earth heat balance (Rossby 1959; Levitus *et al* 2001). The ocean temperature variability in multi year/decadal timescales is significant in this warming scenario. There are many studies available in the literature, which documented the warming of the world ocean in the recent decades (Levitus *et al* 2000 and 2005). The SST averaged over the NIO, AS, BoB and EIO from HadISST (observation), model and SODA are shown in figures 7a, 7b, 7c and 7d respectively. The model SST is seen to be 0.2-0.4°C higher than observations in all these basins. However the SODA temperature is about 0.8-0.9 °C greater than observations. The NIO shows a warming of about 0.4 °C in the model SST as well as HadISST during the last 40 years. A similar pattern is also seen in SODA SST data. The warming tendency is clearly seen in the time series of SST averaged over the individual basins AS, BoB and EIO

(figure 7b-d). One interesting feature observed in the SST variability over NIO is the quasi-decadal time scale oscillation. It is observed that the long warming episodes (6-8 years) are followed by short episodes (2-3 years) of SST cooling. A Similar pattern of variability is seen in all the basins.

The warming is not only confined to the surface, the warming trend is observed well below the thermocline depth also. The depth of 20°C isotherm is taken as a proxy for tropical oceanic thermocline. The linear trend of thermocline heat content (HCd20) from 1958-2000 is illustrated in figure 8a. The trend of HCd20 is not uniformly distributed in space. The highest positive trend is found in the AS north of 12°N, western BoB and between equator and 5°S. The negative linear trend is seemed to be concentrated over the Somali coast and the region south of 5°S and west of 80°E. The HCd20 for unit area calculated for the NIO, AS, BoB and EIO regions are shown in figure 9. The linear trend line for the corresponding time series is also drawn in the figure. Similar to the SST warming observed in these basins, the HCd20 also showed an increasing trend. The HCd20 values in AS is higher than BoB and EIO basins. This is due to the existence of deeper thermocline in AS. The thermocline in the AS shows a deepening of 10 m (125 to 135 m) in the last 40 years, meanwhile the BoB and EIO shows deepening of 10 m (105 to 115 m) and 5 m (110 to 115 m) respectively. The pattern of variability in the 20°C isothermal surface is also similar to that of HCd20 (figure not shown). For the NIO the linear trend of thermocline heat content increase (from 1958-2000) is $0.0018 \times 10^{11} \text{ J/m}^2$ per year, representing a heat content increase of $0.079 \times 10^{11} \text{ J/m}^2$ for unit area. For AS, BoB and EIO regions the rate of heat content increase (linear trend) is 0.0020, 0.0025 and $0.0017 \times 10^{11} \text{ J/m}^2$ per year, which corresponds to heat content increase of 0.086, 0.107 and $0.072 \times 10^{11} \text{ J/m}^2$ for unit area respectively. The warming tendency is seen about 300 m depth. The warming trend of the oceanic subsurface, even below the thermocline depth illustrates the role ocean dynamics in the warming process. In the subsurface below 100 m, the magnitude of warming slowly decreases and beyond 400 m slight cooling ($\sim 0.1^\circ\text{C}$) is seen in the model simulation (figure not shown).

Similar to warming trend in temperature, the model SLA also shows an increasing trend in the NIO in the last four decades. The linear trend of model SLA is

shown in figure 8b. The rise in sea level trend appears to be well related to the HCd20 trend over most of the regions. The correlation between these two is found to be 0.87 over the NIO. It highlights the contribution of thermosteric term in the sea level rise over NIO. The analysis of model SLA shows that in the NIO, the sea level rise is minimum in the AS and maximum in the BoB (figure 10). The SLA exhibits an increasing trend in the mid 1960s and late 1970s. In the NIO the SLA shows a linear increasing trend of 0.31 mm/year, which signify sea level rise of 13.22 mm during 1958-2000 (figure 10). Since the OGCM used for the study is closed in the eastern and southern boundaries, the possible contribution of melting of ice caps and ice sheets and other climatic contributions towards this sea level rise are not accounted. So the linear trend in the model SLA can be attributed by the thermosteric effect. The linear trend of model SLA (0.31 mm/year) is close to the observed global thermosteric contribution (0.42 ± 0.12 mm/year). During 1993-2000 the T/P observation shows a global average sea level rise of about 3 mm/year. However the rate of sea level rise over the NIO is observed to be less than one third of global average sea level rise, showing a linear increasing trend of 0.96 mm/year. The model SLA over the period 1993-2000 shows a rise of 0.8 mm/year. Over AS, BoB and EIO regions, the model SLA shows a linear trend of 0.12, 0.76 and 0.30 mm/year over the period 1958-2000.

4.4 Heat budget of the ocean from model and observations

The ocean thermal structure simulated by the model is comparable with the observed thermal structure. The depth of 20°C isotherms are shown in Figure 11. The left panels are based on the model climatology (annual, March to May, June to September, December to February is shown from top panel to bottom panel respectively). The respective climatologies from the WOA observations are shown in the right panels. Both the model and observations show deeper thermocline in the Arabian Sea and shallow thermocline in the Bay of Bengal. Moreover the southwest equatorial Indian Ocean shows a very shallow thermocline and is called the thermocline ridge region in the Indian Ocean. The heat budget analysis (figure not shown) revealed that the atmospheric heat flux dominate the SST evolution process in all the basins, whereas the role of advection is considerable in the equatorial region.

5. Summary

The Ocean General circulation models form an integral part of the dynamical and thermodynamical process studies of the oceans. The models need to be validated with observations before applying the model for complex oceanographic process studies. The comparison of model simulations with observations from WHOI, DS1, DS3 and DS4 moored buoys shows that model is able to reproduce the seasonal evolution of temperature structure in the AS and BoB. The analysis showed that good quantitative as well as qualitative agreement exists between the anomalies of sea level observed from tide-gauges and T/P during 1993-2000 and those calculated from model. The correlation between model and T/P is better in NIO and poor correlation is seen in the western AS and western BoB. The key regions of interannual variability in the tropical Indian Ocean are southeast AS and eastern EIO, the correlations over these regions are found to be larger than 0.8 with maxima in the southeastern AS. The NIO shows SST warming of about 0.4 °C during 1958-2000. The linear trend of thermocline heat content increase for the NIO is $0.0018 \times 10^{11} \text{ J/m}^2$ per year. In the NIO the model SLA shows a linear increasing trend of 0.31 mm/year over 1958-2000. This is very close to the contribution of thermosteric term to the observed global average sea level rise. The model and T/P observations show that the sea level rise over NIO is only about one third of global average sea level rise. The model temperature shows slight cooling in the subsurface (~ 400 m). The subsurface cooling in the tropical Indian Ocean is further discussed by Alory *et al* (2007), which suggest that it is due to the shallowing of thermocline transmitted from the Pacific Ocean by the throughflow, and by Han *et al* (2006), which suggest that the cooling is linked to local wind forcing and associated upward Ekman pumping velocity. But the model thermocline heat content shows the signature of subsurface cooling south of 5°S, even without the inclusion of Indonesian throughflow in the model. This result implies that the thermodynamical processes responsible for the subsurface cooling need to be investigated further. Also the role of subsurface cooling in the upper ocean warming requires further modeling studies.

Acknowledgments. We acknowledge the financial support of INCOIS, Hyderabad

and support of Director, I.I.T.M. Acknowledgments are also due to GFDL, Princeton for making the MOM4 code available, PSMSL, AVISO, NCAR, UMD, and UK met office for datasets. Most of the contents of this paper are adopted from Thompson et al. 2008.

References

- Alory G, Wijffels S and Meyers G 2007 Observed temperature trends in the Indian Ocean over 1960–1999 and associated mechanisms; *Geophys. Res. Lett.*, **34** L02606 doi:10.1029/2006GL028044.
- Antonov J I, Levitus S and Boyer T P 2002 Steric sea level variations during 1957–1994: Importance of salinity; *J. Geophys. Res.* **107** doi:10.1029/2001JC000964.
- Bryan K and Lewis L J 1979 A water mass model of the world ocean; *J. Geophys. Res.* **84** 2503–2517.
- Carton J A, Giese B S and Grodsky S A 2005 Sea level rise and the warming of the oceans in the Simple Ocean Data Assimilation (SODA) ocean reanalysis; *J. Geophys. Res.* **110** C09006 doi:10.1029/2004JC002817.
- Carton J A and Giese B S 2006 SODA: A reanalysis of ocean climate; *Mon. Wea. Rev.* (submitted).
- Chambers D P, Tapley B D and Stewart R H 1999 Anomalous warming in the Indian Ocean coincident with ElNino; *J. Geophys. Res.* **104** 3035–3047.
- Cheney R E, Miller L, Agreen R, Doyle N and Lillibridge J 1994 Topex/Poseidon: The 2-cm solution; *J. Geophys. Res.* **99** 24553–24563.
- Church J A, White N J, Coleman R, Lambeck K and Mitrovica J X 2004 Estimates of the regional distribution of sea-level rise over the 1950 to 2000 period; *J. Clim.* **17** 2609–2625.
- Church J A, White N J and Hunter J R 2006 Sea-level Rise at tropical Pacific and Indian Ocean islands; *Global and Planetary Change* **53** 155–168.
- Griffies S M, Harrison M J, Pacnowski R C and Rosati A 2003 A Technical Guide to MOM4; GFDL Ocean Group Technical Report No. 5, Princeton, NJ: NOAA/Geophysical Fluid Dynamics Laboratory.
- Han W, Meehl G A, and Hu A 2006 Interpretation of tropical thermocline cooling in the Indian and Pacific oceans during recent decades; *Geophys. Res. Lett.*, **33** L23615 doi:10.1029/2006GL027982.

- Large W G, McWilliams J C and Doney S C 1994 Oceanic vertical mixing: A review and a model with a nonlocal boundary layer parameterization; *Reviews of Geophysics* **32** 363–403.
- Large WG and Yeager S G 2004 Diurnal to decadal global forcing for ocean and sea-ice models: the data sets and flux climatologies; NCAR, Technical Note NCAR/TN-460+STR, 111 pp.
- Levitun S 1998 Climatological atlas of the world ocean; Tech. Rep., NOAA, Rockville, Md.
- Levitus S, Antonov J and Boyer T P 2000 Warming of the world ocean; *Science* **287** 2225-2229.
- Levitus S, Antonov J L, Wang J, Delworth T L, Dixon K W and Broccoli A J 2001 Anthropogenic warming of Earth's climate system; *Science* **292** 267-270.
- Levitus S, Antonov J and Boyer T P 2005 Warming of the world ocean, 1955-2003; *Geophys. Res. Lett.* **32** doi:10.1029/2004GL021592.
- McDougall T J, Jacket D R, Wright D G and Feistel R 2003 Accurate and computationally efficient algorithms for potential temperature and density of seawater; *J. Atm. Ocean. Tech.* **20** 730-741.
- PremKumar K, Ravichandran M, Kalsi S R, Sengupta D and Gadgil S 2000 First results from new observational system over the Indian Seas; *Curr. Sci.* **78** 323-330.
- Rayner N A, Parker D E, Horton E B, Folland C K, Alexander L V, Rowell D P, Kent E C and Kaplan A 2003 Global analysis of sea surface temperature, sea ice, and night marine air temperature since the late nineteenth century; *J. Geophys. Res.* **108** doi:10.1029/2002JD002670.
- Rossby C 1959 Current problems in meteorology, in *The Atmosphere and Sea in Motion*; Rockefeller Inst. Press, New York, pp. 9–50.
- Sengupta D and Ravichandran M 2001 Oscillations of Bay of Bengal sea surface temperature during the 1998 summer monsoon; *Geophys. Res. Lett.* **28** 2033-2036.
- Tapley B D, Chambers D P, Shum C K, Eanes R J and Ries J C 1994 Accuracy assessment of large scale dynamic topography from TOPEX/POSEIDON altimetry; *J. Geophys. Res.* **99** 24605-24617.

- Thompson B, Gnanaseelan C and Salvekar P S 2005 Indian Ocean Dipole Simulation using Modular Ocean Model; I. I. T. M. Research Report, No RR-108.
- Thompson B, Gnanaseelan C, Parekh A and Salvekar P S 2008 North Indian Ocean warming and sea level rise in an OGCM; *J. Earth. Sys. Sci.* 117(2), 169-178.
- Unnikrishnan A S, Kumar K R, Fernandes S E, Michael G S, and Patwardhan S K 2006 Sea level changes along the Indian coast: Observations and projections; *Current Science* **90** 362-368.
- Vinayachandran P N, Saji N H and Yamagata T 1999 Response of the equatorial Indian Ocean to unusual wind event during 1994; *Geophys. Res. Lett.* **26** 1613-1616.
- Weller R A, Baumgartner M F, Josey S A, Fischer A S and Kindle J C 1998 Atmospheric forcing in the Arabian Sea during 1994-1995: observations and comparisons with climatology and models; *Deep-Sea Res. Part II* **45** 1961-1999.
- Weller R A, Fischer A S, Rudnick D L, Eriksen C C, Dickey T D, Marra J, Fox C and Leben R 2002 Moored observations of upper-ocean response to the monsoons in the Arabian Sea during 1994-1995; *Deep Sea Res. Part II*, **49** 2195- 2230.

Table 1. The correlation and rms difference of SST between model and moored observations.

Mooring	Location	Correlation	rms difference ($^{\circ}\text{C}$)
WHOI	15.5 $^{\circ}$ N, 61.5 $^{\circ}$ E	0.95	0.45
DS1	15.3 $^{\circ}$ N, 69.3 $^{\circ}$ E	0.94	0.29
DS3	87 $^{\circ}$ E, 13 $^{\circ}$ N	0.96	0.4
DS4	89 $^{\circ}$ E, 19 $^{\circ}$ N	0.95	0.56

Table 2. The correlation and rms differences of SLA between model and T/P.

Region	Correlation	rms difference (cm)
NIO	0.6	0.78
AS	0.75	1.2
BoB	0.73	1.9
EIO	0.87	0.7

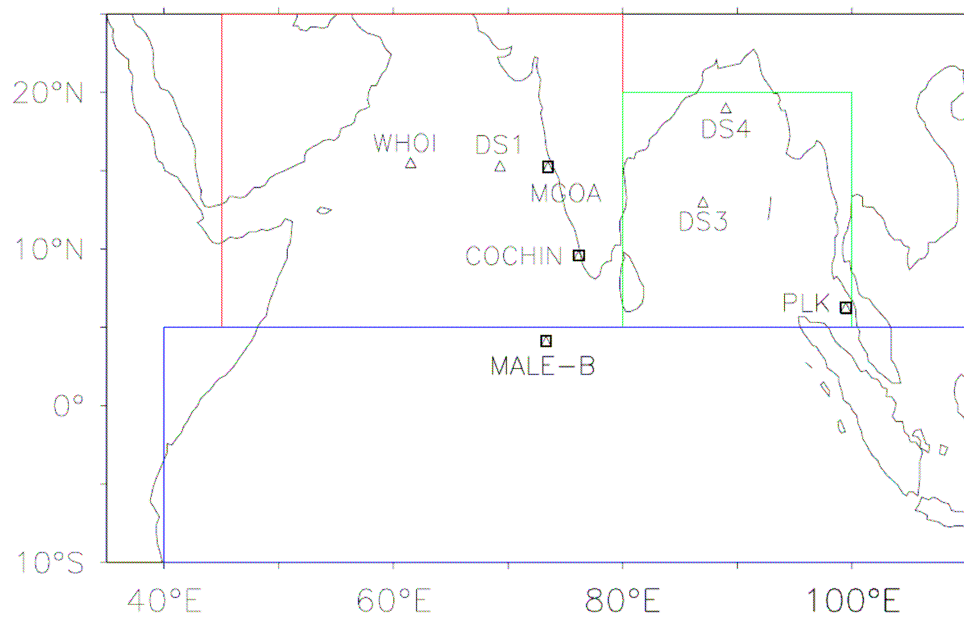


Figure 1. Map showing the location of mooring buoys WHOI, DS1, DS3, DS4 and tide-gauges at Marmagoa (MGOA), Cochin, Male-B and Palau Langkawi (PLK).

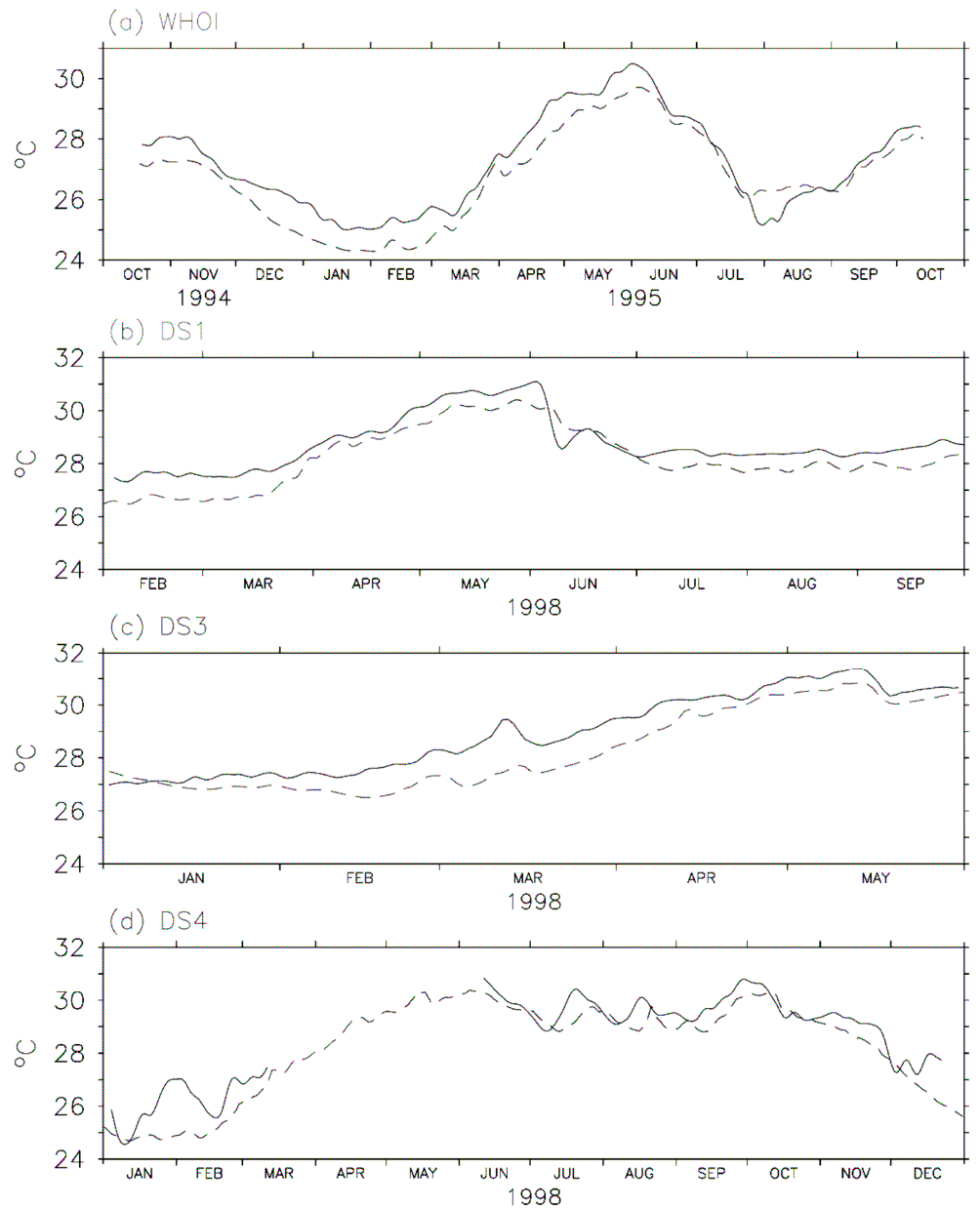


Figure 2. The SST comparison from mooring observation (continuous line) (a) WHOI (61.5°E, 15.5°N), (b) DS1 (69.3°E, 15.3°N), (c) DS3 (87°E, 13°N) and (d) DS4 (89°E, 19°N). The model SST corresponding to the mooring locations is shown as dashed line.

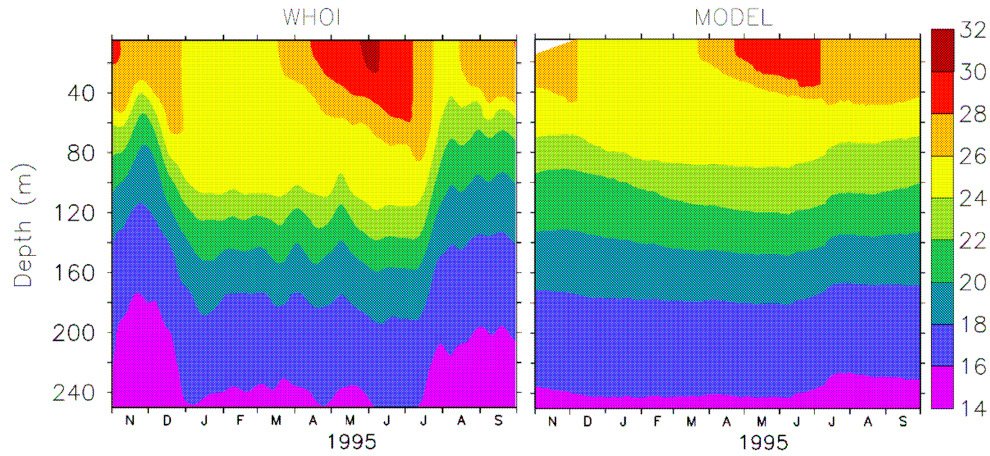


Figure 3. The vertical section of temperature at 61.5°E, 15.5°N from WHOI observation and model.

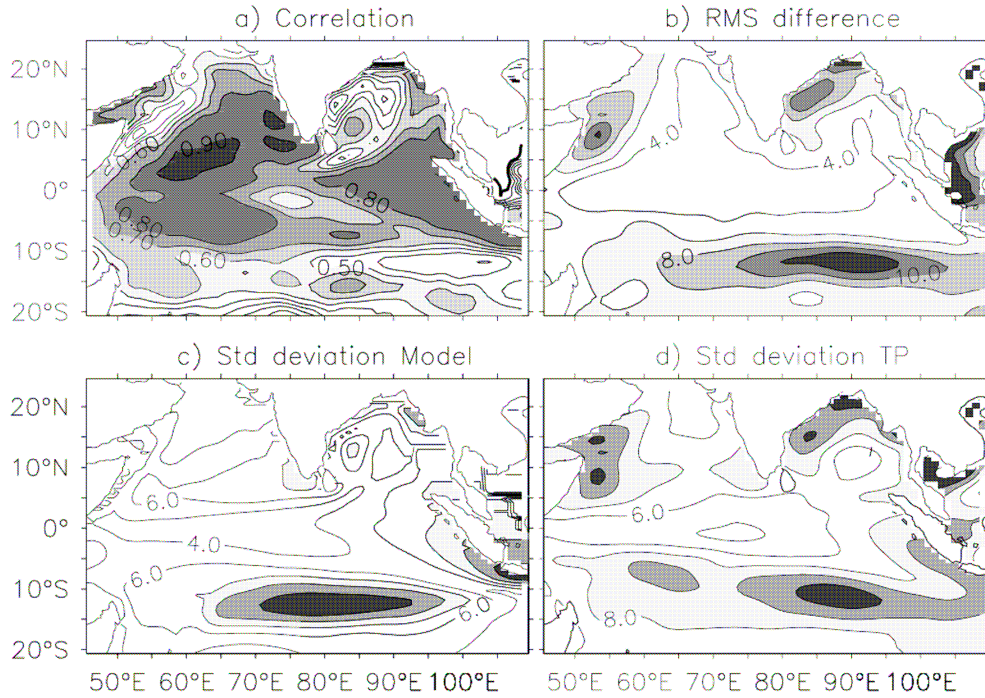


Figure 4. (a) The correlation between sea surface height anomalies from Topex and model (correlation above 0.5 shaded). (b) rms difference between sea surface height anomalies from Topex and model (rms difference above 6 cm shaded). (c) Model sea surface height anomaly standard deviation. (d) Topex surface height anomaly standard deviation. For figures 3c and 3d standard deviation above 8 cm shaded.

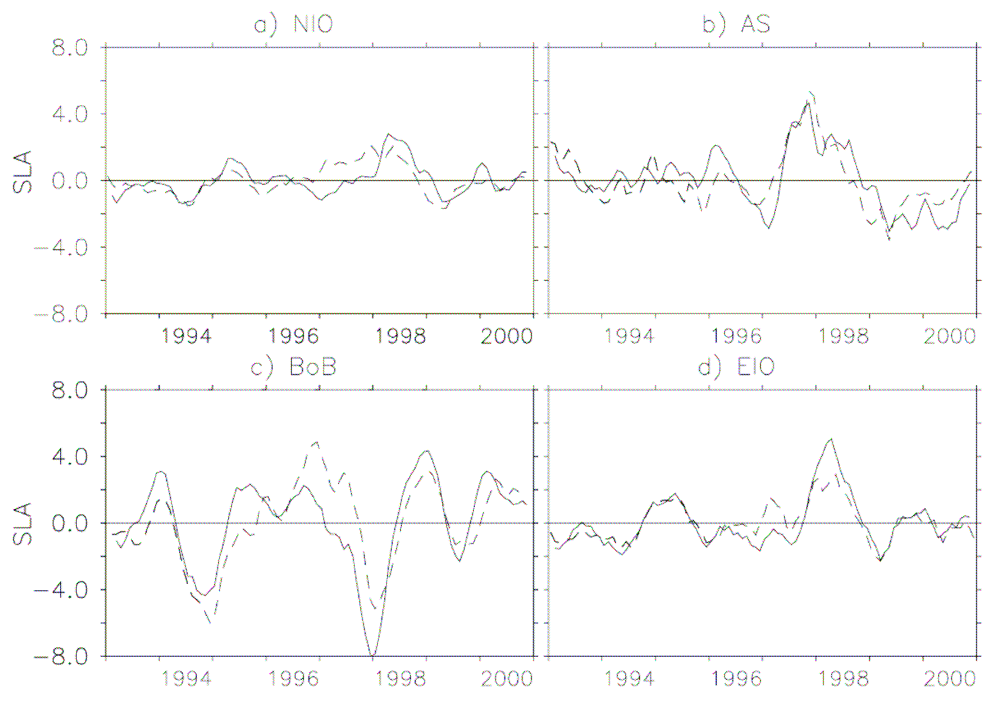


Figure 5. Deseasonalised sea level anomalies (cm) averaged over (a) Northern Indian Ocean (45°E to 110°E , 10°S to 25°N), (b) Arabian Sea (45°E to 80°E , 5°N to 25°N), (c) Bay of Bengal (80°E to 100°E , 5°N to 20°N) and (d) Equatorial Indian Ocean (40°E to 110°E , 5°N to 10°S). Continuous line represents Topex and dash represents model SLA.

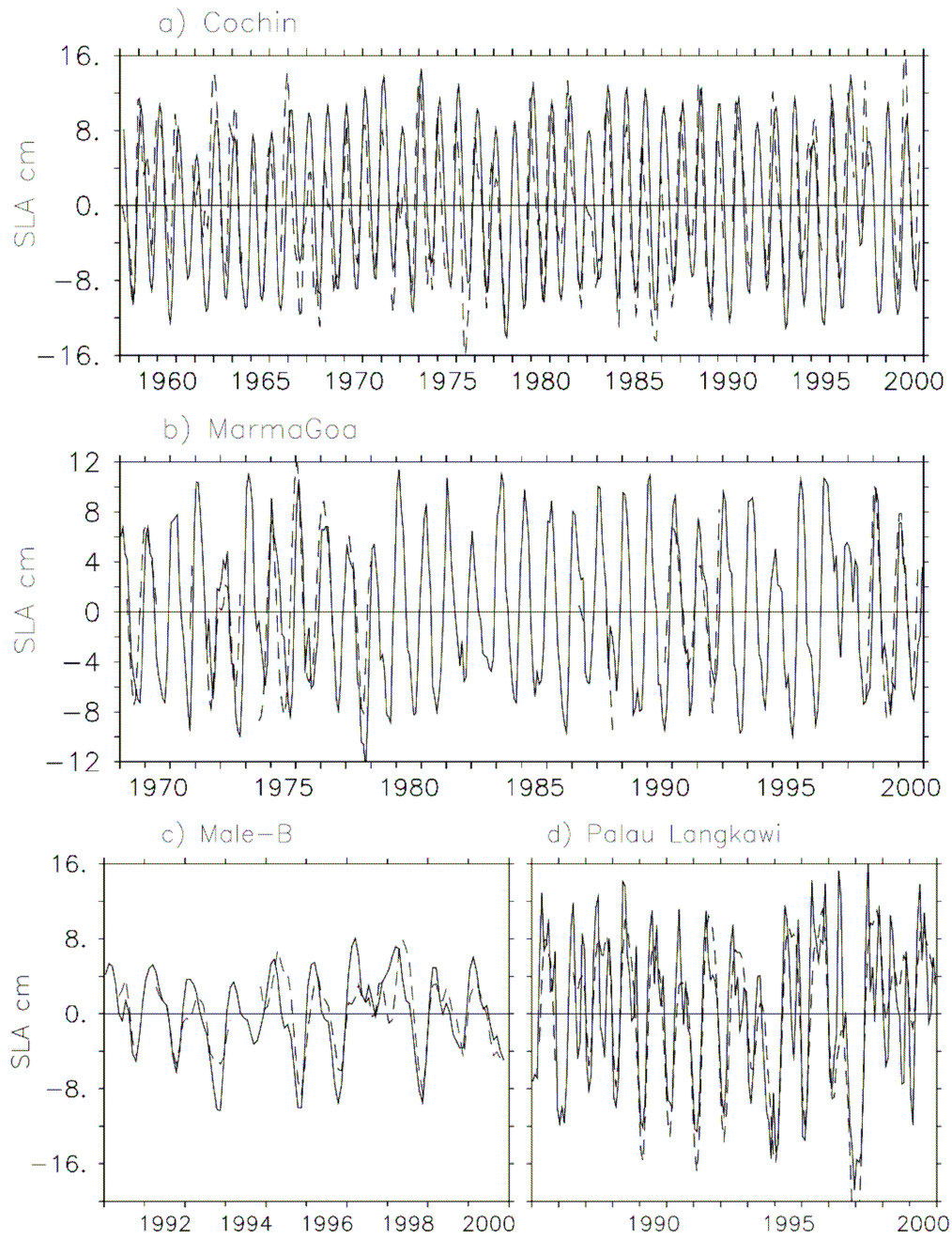


Figure 6. The time series of SLA from tide-gauge observations (dashed line) and Model (continuous line) at (a) Cochin, (b) Marmagao, (c) Male and (d) Palu Langkawi. The time series are detrended by removing their linear trends.

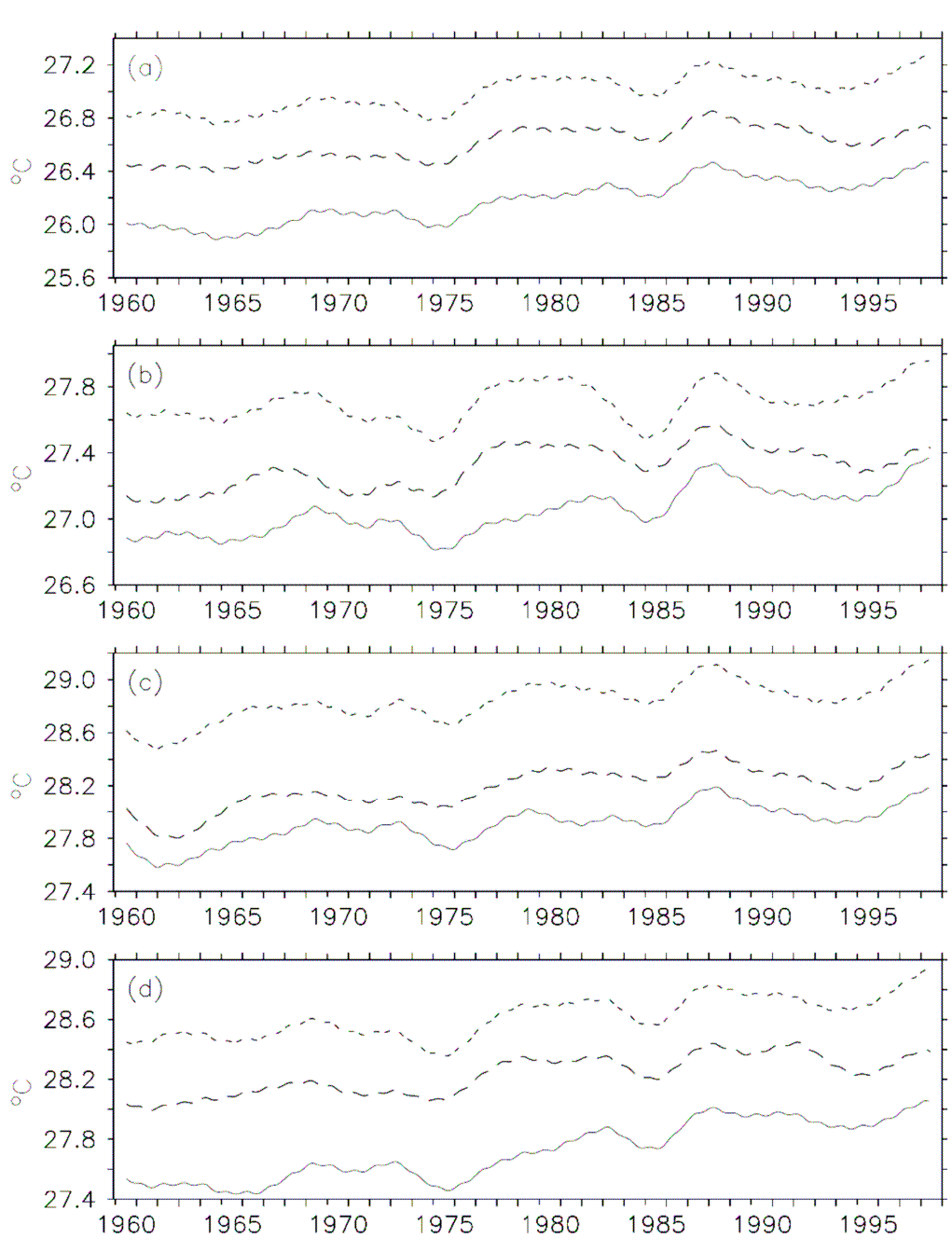


Figure 7. Sea surface temperature averaged over (a) north Indian Ocean, (b) Arabian Sea, (c) Bay of Bengal and (d) equatorial Indian Ocean. Continuous line represents Had ISST, dashed line represent model and dotted line denotes SODA. The time series low-pass filtered with a 5-year running filter.

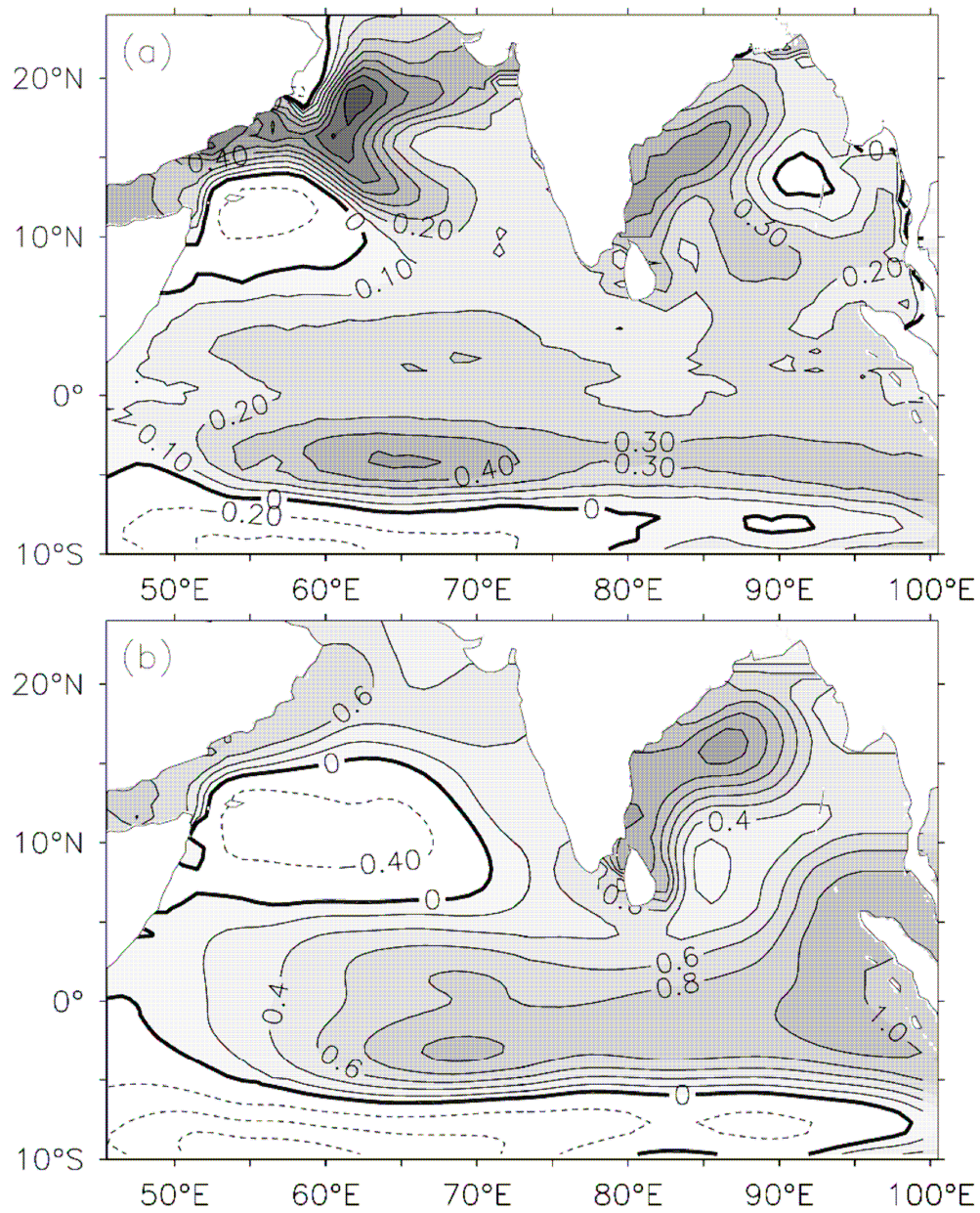


Figure 8. Linear trends for 1958-2000 (a) model thermocline heat content in 10^9 J/m^2 per year and (b) model sea level anomaly in mm per year.

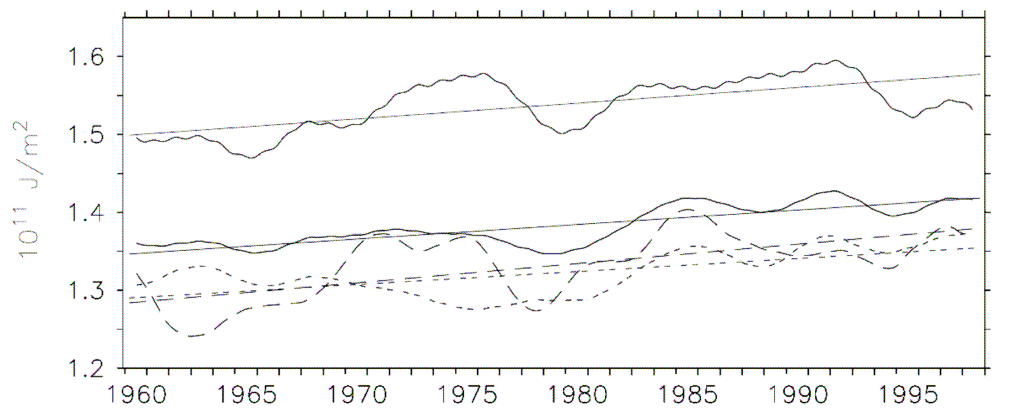


Figure 9. The thermocline heat content per unit area calculated from model for the north Indian Ocean (continuous thick line), Arabian Sea (continuous thin line), Bay of Bengal (dashed line) and equatorial Indian Ocean (dotted line). The corresponding linear trend of each time series is also shown. The time series low-pass filtered with a 5-year running filter.

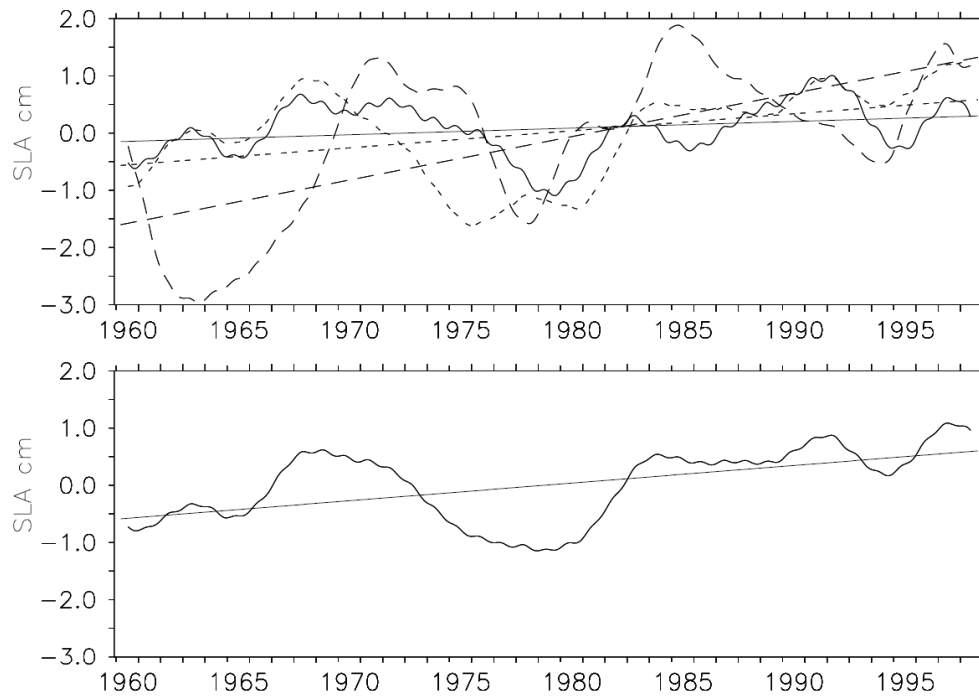


Figure 10. The SLA from model. In the top panel, Arabian Sea (continuous line), Bay of Bengal (dashed line), equatorial Indian Ocean (dotted line) and the bottom panel represents SLA over north Indian Ocean. The corresponding linear trend lines are also shown. The time series low-pass filtered with a 5-year running filter.

Model Climatology

WOA Climatology

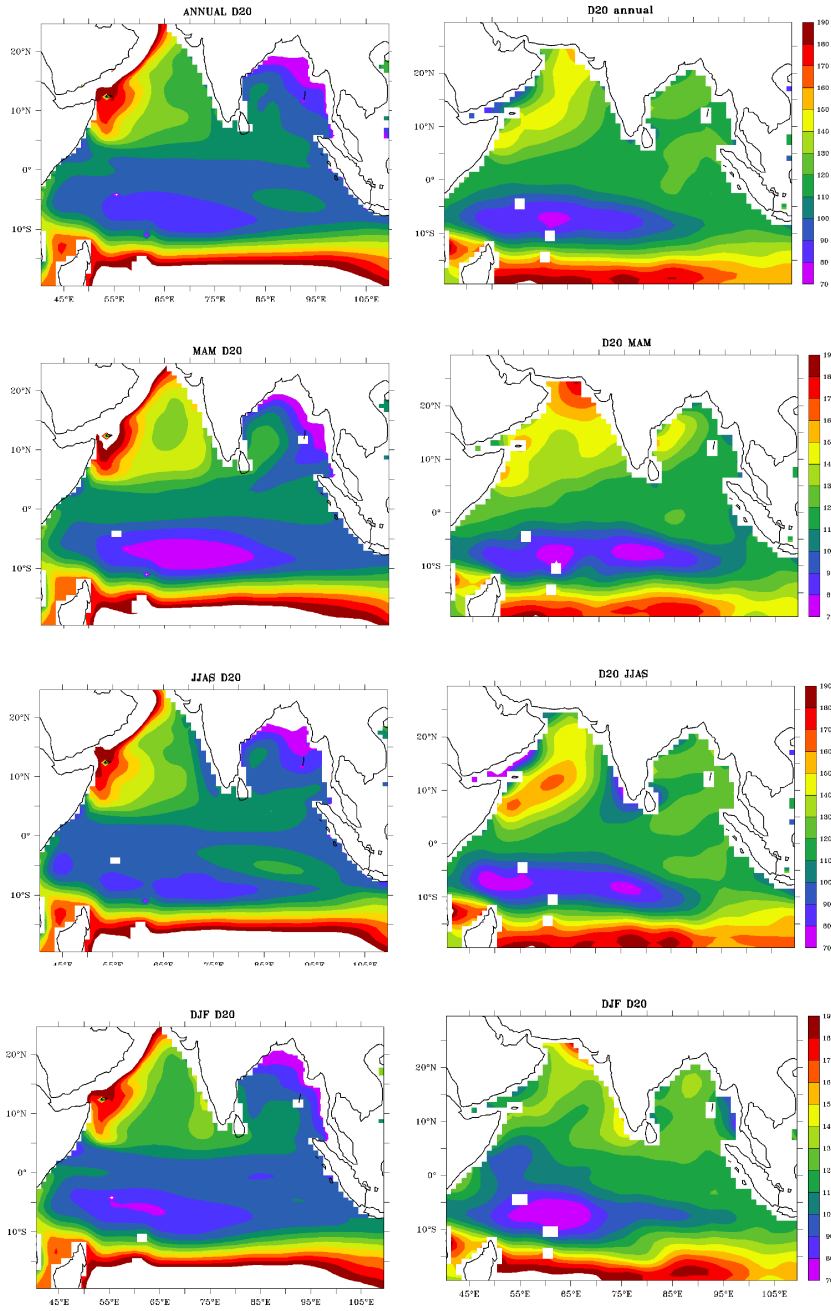


Figure 11: The model versus observed climatological depth of the 20°C isotherms, the left panels are model climatology and the right panels are WOA climatology.

OCEAN-ATMOSPHERE INTERACTIONS DURING TROPICAL CYCLONES

Lynn K. Shay

Rosestiel School of Marine and Atmospheric Science

University of Miami

Miami, Florida, 33157, U.S.A.

nshay@rsmas.miami.edu

1. Background

In this global context, significant progress has been made in the area of upper ocean response and air-sea interactions during TC passage. Here, we will review progress in this topical area as described in Shay (2009) over the past two decades since Ginis (1995). Upper ocean thermal structure in the western parts of the world's ocean basins are often encountered by tropical cyclones (TCs). As these storms move over highly energetic oceanic regimes occupied by western boundary currents (Fig. 1), and warm and cold core eddies (WCEs and CCEs), horizontal thermal gradients tighten over distances of $O(10 \text{ km})$. Observational evidence indicates that, under neutral or favorable atmospheric conditions, deep oceanic mixed layers (OML), large heat content (relative to the 26°C isotherm depth), and reduced OML cooling response in warm oceanic features contributes to TC intensification (Shay *et al.* 2000; Jacob and Shay 2003; Lin *et al.* 2005, 2009; Scharroo *et al.* 2005; Sun *et al.* 2006; Shay 2006, 2009; Shay and Uhlhorn 2008; Jaimes and Shay 2009). Numerical models have generally shown that deeper, warmer OMLs have had less negative feedback on the TC due in part to the reduced levels of mixed layer cooling (Schade and Emanuel 1999; Bender and Ginis 2000; Hong *et al.* 2000; Lin *et al.* 2005; Wu *et al.* 2004). By contrast, shallow OMLs that cool quickly (e.g., cold oceanic features) could contribute to TC weakening (Walker *et al.* 2005; Halliwell *et al.* 2008; Shay 2006; Jaimes and Shay 2009). Thus, understanding the contrasting OML thermal response to wind stress over mesoscale oceanic features is important not only for predicting accurate oceanic response, but also TC intensity changes and the level of negative feedback mechanisms to atmospheric boundary layers.

One theme that has resurfaced is the idea of integrated thermal structure on TC intensity. Leipper and Volgenau (1972) demonstrated that the 26°C isotherm depth and the upper ocean's thermal structure, known as oceanic heat content (OHC), has important implications on TC intensity variations:

$$\text{OHC} = c_p \int_0^{D26} \rho [T(z) - 26] dz,$$

where c_p is specific heat at constant pressure, $D26$ is the 26°C isotherm depth, and OHC is zero when SST decrease to less than 26°C . While their ship-based measurements were not acquired under directly forced TC conditions, post-pre OHC differences demonstrated the importance of this integrated oceanic thermal energy.

The most apparent effect of TC passage is the marked SST cooling, and by proxy the OML temperature response, of typically 1 to 6°C occurring to the right (left) of the storm track by 1-2 radii of maximum winds (R_{max}) in the northern (southern) hemispheres. These larger *biases* of the maximum SST decreases and OML depth increases of 20 to 40 m are usually due to entrainment mixing of the cooler thermocline water with the warmer OML (see Fig. 2) associated with vertical shear of the horizontal currents across the OML base. Ocean mixing and cooling are principally a function of wind-forced currents and their associated shears ($\partial v / \partial z = S$). These wind-forced currents are often associated with near-inertial response (periods close to f^{-1} , where f is the local Coriolis parameter). While the forced current structures have large vertical scales, near-inertial shears across the OML base tend to be associated with shorter vertical wavelengths (e.g., higher order baroclinic modes) that reduce the Richardson numbers (defined as the ratio of buoyancy frequency (N^2) and (S^2)) to below critical threshold values (Price

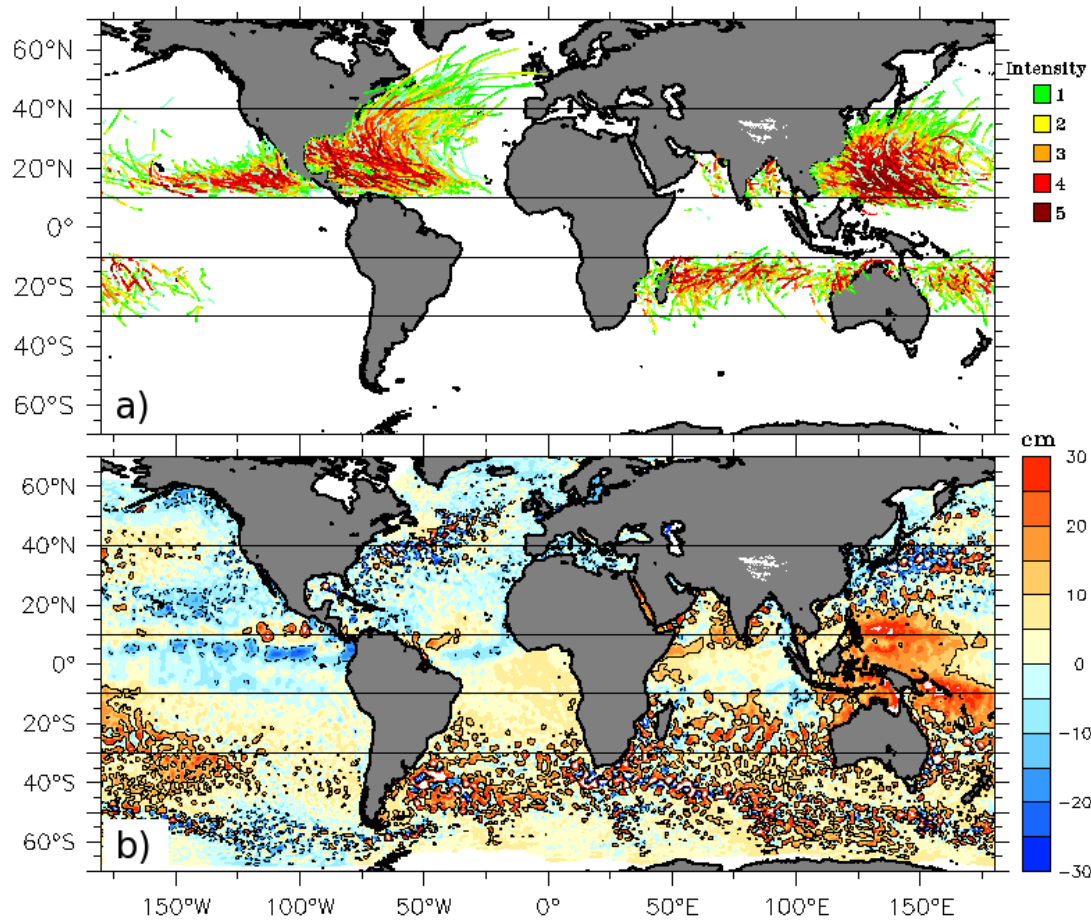


Figure 1. (a) Distribution of all tropical cyclone trajectories on record (hurricane intensity level), from the National Hurricane Center and Joint Typhoon Warning Center databases. (b) Global distribution of sea surface height anomalies (SHA) from a daily composite of the AVISO product. Blue (red) shades are for cyclonic (anticyclonic) ocean eddies.

et al. 1994; Shay *et al.* 1998; Sanford *et al.* 2005; Jacob *et al.* 2003; Shay 2009). Other physical processes are associated with the OML heat budget through surface enthalpy flux (sensible and latent heat : Q_o); upwelling (w) of the isotherms; and, horizontal advection by the current field by background and forced flows.

Parameterizations of momentum, heat and moisture transfers are further complicated by sea state, sea spray and the complexities of the upper ocean. There is a level of mutual dependence of the air-sea transfer processes of heat, moisture and momentum as suggested in idealized model simulations (Emanuel 1995) that intensity is sensitive to the ratio of enthalpy and drag coefficients ($c_k c_d^{-1}$, where c_k is the bulk enthalpy coefficient and c_d is the surface drag coefficient). The conclusion that this quantity probably lies within a rather limited range (≤ 1.5) is commensurate with the observation that most TCs do not usually reach their maximum potential intensity (MPI).

2: Oceanic States

Coupled models to predict hurricane intensity change are being used to issue forecasts to the public who increasingly rely on the most advanced weather forecasting systems to prepare for landfall (Marks and Shay 1998). Oceanic models will have to include realistic initial conditions to simulate not only the oceanic response to

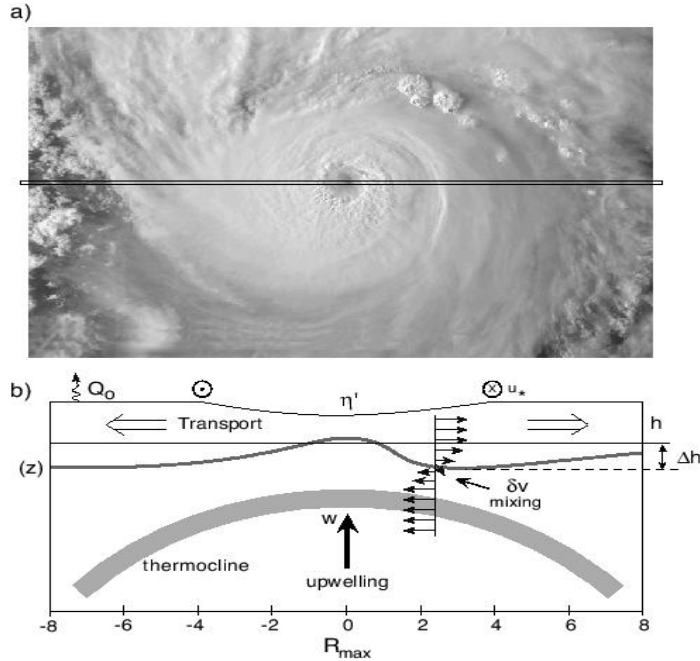


Figure 2: a) TC image and b) a cartoon depiction of basic physical processes forced by hurricane winds such as shear-induced mixing and OML deepening, upwelling due to transport away from the center, and surface heat fluxes from the ocean to the atmosphere, all of which may contribute to ocean cooling during TC passage (from Shay 2009).

TC forcing (Sanford *et al.* 2007; Price *et al.* 1994; D'Asaro 2003; Jacob and Shay 2003; Black *et al.* 2007; Shay and Uhlhorn 2008; Jaimes and Shay 2009, 2010), but also to simulate the atmospheric response to oceanic forcing (Bender and Ginis 2000; Bao *et al.* 2000; Shay *et al.* 2000; Hong *et al.* 2000; Walker *et al.* 2005; Lin *et al.* 2005, 2009; Wu *et al.* 2007; Ali *et al.* 2007; Manielli *et al.* 2008; Shay and Brewster 2010). The atmospheric response is related to the level of feedback from the oceanic responses.

Assimilative ocean modeling efforts and feature based model initialization are effective methods for providing initial boundary conditions to the oceanic and coupled TC prediction models (Falkovich *et al.* 2005; Halliwell *et al.* 2008; 2010). It is now fairly clear that the ocean model used in forecasting must be initialized so that altimetry-derived surface height anomaly (SHA) features are in the correct locations with consistent temperature and salinity profiles, and hence the OHC and OML depths are realistic. As shown in Figure 3, oceanic forecast systems based on Hybrid Coordinate Ocean Model (HYCOM) were evaluated in the northwest Caribbean Sea and Gulf of Mexico (GOM) for Sept 2002 prior to TCs Isidore and Lili, and for Sept 2004 prior to TC Ivan (Halliwell *et al.* 2008). In the NW Caribbean Sea, for example, the thermal structure hindcast followed the September climatology but does not reproduce the larger OHC values found in the observed profiles (Shay and Uhlhorn 2008).

The OML heat budget and ensuing air-sea fluxes are influenced by the choice of entrainment mixing parameterizations across the OML base. Contrasting viewpoints on this entrainment mixing topic have been focused on documenting the differences between 1-D and 3-D responses to TC passage (Jacob *et al.* 2000; Jacob and Shay 2003; Yablonsky and Ginis 2009; Halliwell *et al.* 2008, 2010). Away from strong oceanic fronts, the 1-D approach seems to be valid in that advective tendencies by weak background currents are considered to be nonessential in modeling efforts especially for moderate to fast moving TCs (Price *et al.* 1994; Schade and Emanuel 1999). The modified 1-D column approach follows from this approach except that the domain is initialized with differing thermal structure. In the horizontal plane, temperature (and hence density) gradients have to geostrophically adjust prior to turning on the TC forcing. If the ocean is not in geostrophic balance, simulations (i.e. levels of SST cooling) will be unrealistic due to a mass field imbalance. The adjusted, steady-state ocean currents are small compared to a translation speed of most TCs (e.g., Froude number). In regimes where strong

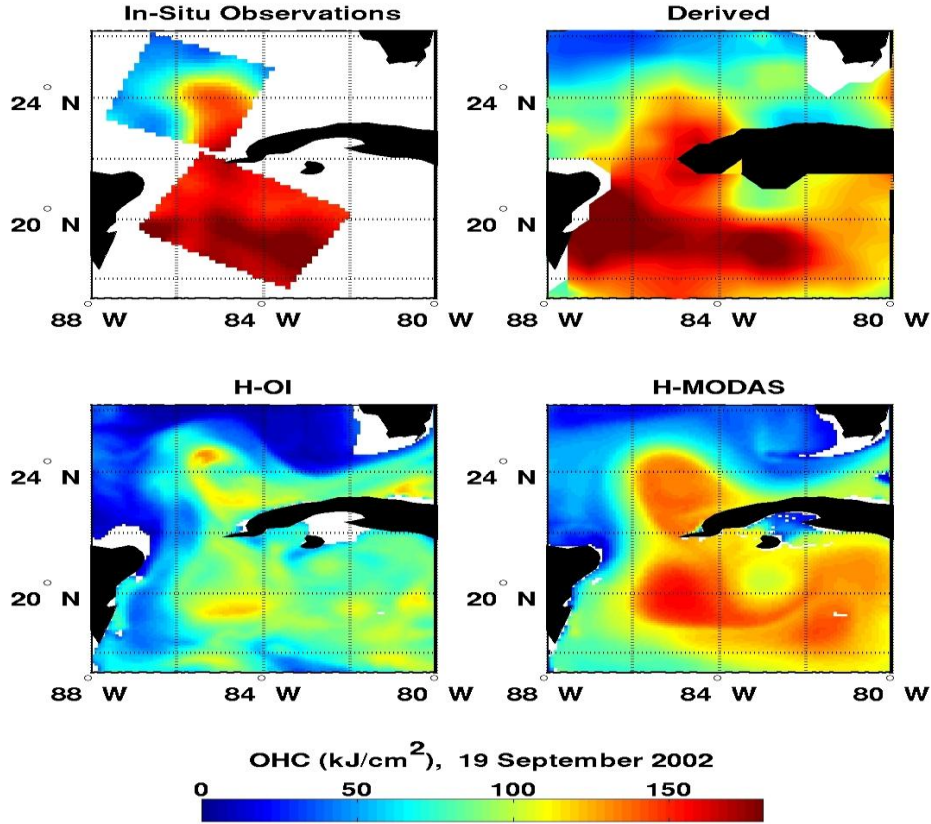


Figure 3: OHC (kJ cm^{-2}) in the northwest Caribbean Sea and southeast GOM from an objective analysis of in situ observations, altimetry from the hurricane season climatology of Mainelli (2000), HYCOM OI, and HYCOM-MODAS on 19 September 2002 prior to hurricane Isidore (From Halliwell *et al.* 2008). Notice the marked agreement between the in situ data and that derived from the altimetry in the upper panels.

pressure gradients exist, the bulk Richardson number instability, which is at the core of the “1-D assumption”, remains at critical levels only for a short period (Uhlhorn 2008) that limits SST cooling and OML deepening. In a 3-D ocean model with realistic ocean conditions for the Gilbert case, Jacob and Shay (2003) simulated OML temperatures and compared with observed profile data and found that the three higher-order turbulent mixing schemes lead to a more accurate ocean response simulation with a WCR present. However, in most basins, strong fronts and currents are often located very close to the coast (Kuroshio, Gulf Stream, etc) and must be accounted for in forecasting landfalling TCs as they represent an additional TC energy source (Marks and Shay 1998).

3: Oceanic Response

During TC Gilbert (1988), the sampling strategy was designed to measure the momentum and thermal structural variations from pre, during and two cold-wake experiments in a quiescent area of the western GOM (Shay *et al.* 1998). As shown in Figure 4, temperatures and OML depths revealed that Gilbert induced an SST decrease of 3.5°C to the right of the storm track associated with deeper OML of up to 70 m. The spatial evolution of the response indicated a near-inertial, wave-like pattern. Jacob *et al.* (2000) assessed the various contributions to the observed OML heat and mass budgets during and subsequent to Gilbert’s passage. Advection of temperatures by the background currents accounted for 5% of the heat budget near the track and up to 15% of the budget in the WCR, whereas the wind-forced current advection was much weaker. Estimated surface fluxes contributed 10% to the heat balance between the track and $3 R_{\text{max}}$. In this quiescent ocean, cooling in the wake was dominated by

entrainment heat flux induced by the shear at the OML base by forced near-inertial currents behind the eye. In front of the storm, the wind stress accounted for a similar fraction of cooling for the asymmetric based on Powell and Houston (1996) winds. More recently, measurements from TC Frances revealed an SST decrease of 2.3°C based on drifter and float measurement deployed during the CBLAST experiment (Black *et al.* 2007).

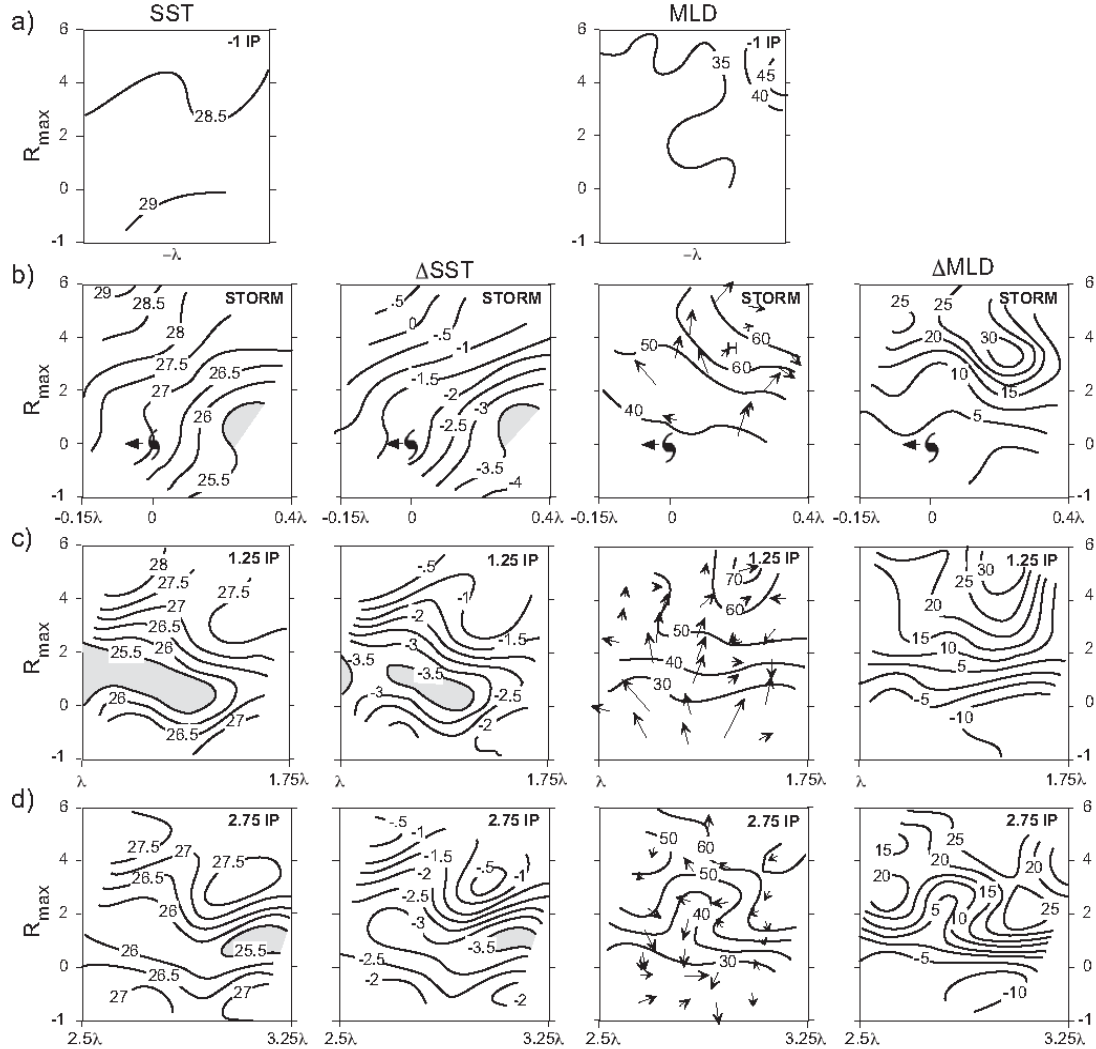


Figure 4: A sequence of analyses observed during TC Gilbert (1988) for SST ($^{\circ}\text{C}$) and MLD (m) for a) Pre (- IP : 15 Sept) , b) During (TC: 16 Sept) , c) Wake 1 (1.25 IP: 17 Sept), and d) Wake 2 (2.75IP: 19 Sept) in a TC coordinate system where cross-track ($R_{\text{max}} = 60 \text{ km}$) and along-track is scaled in inertial wavelengths ($\Lambda = \text{IP} \times U_h$: 580 km where $U_h \sim 5.6 \text{ m s}^{-1}$ and $\text{IP} \sim 30 \text{ h}$). In the SST images, the maximum cooling is shaded in gray and the mean mixed layer currents (arrows) and MLD are contoured at 10 m intervals and ΔMLD is contoured at 5 m intervals (from Shay *et al.* 1992).

The ocean's momentum response is classified into two regimes: the directly-forced or near-field; and the evolving 3-dimensional wake or far-field. In the near-field, the cyclonically-rotating wind stress field of a TC causes OML currents of about $1 \text{ to } 1.5 \text{ m s}^{-1}$ to diverge from the storm track starting within one-quarter of an inertial wavelength (Λ) which is the product of the storm translation speed (U_h) and the local inertial period (IP) as noted above. This current divergence causes the upwelling of cooler water underneath the storm track, thereby decreasing the OML depth. Over the next half of the inertial cycle, OML currents converge towards the storm

track, causing an increase in the OML depth as warmer water is downwelled into the thermocline. This alternating cycle of upwelling and downwelling of the isotherms (and isopycnals) occurs over distances of Λ and establishes horizontal pressure gradients that couple the OML to the thermocline as part of a spreading 3-dimensional wake (Price *et al.* 1994; Shay *et al.* 1998, 1992; Zedler *et al.* 2001; D'Asaro 2003; Sanford *et al.* 2007). In this context, the near-inertial wake response has been fairly well observed and modeled during TC passage. Observations of the ocean current response to TC passage have been generally sparse over the global oceans as the community has had to rely on fortuitous encounters with buoys and moorings deployed in support of other experiments or ships crossing TC wakes (Teague *et al.* 2007, Zedler *et al.* 2001). Surface currents have also been shown to impact the direction of the surface wind stress which may be important in high wind conditions (Drennan and Shay 2006) and affect the wind-forced surface waves (Sanford *et al.* 2007).

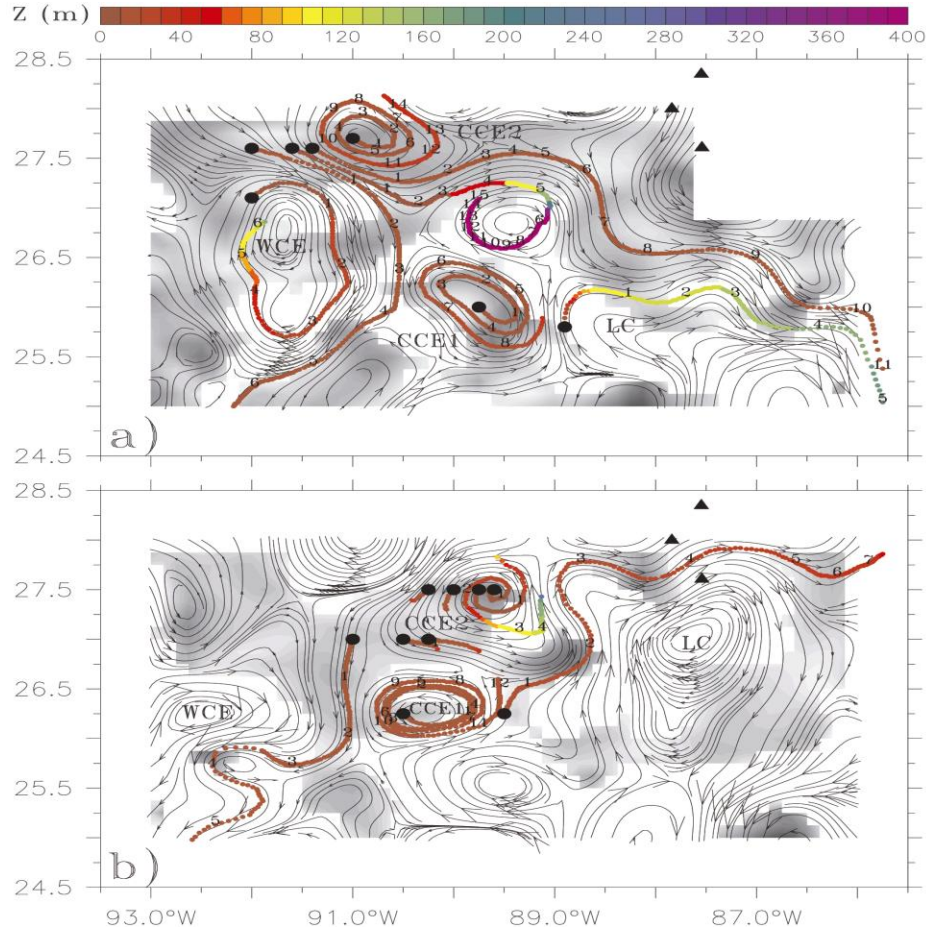


Fig. 5: Near-inertial wave ray-tracing for (a) Katrina and (b) Rita. Numbers along wave rays indicate inertial periods (IP ~ 25.5 hr), dots are hourly positions, color is the ray's depth level, and flow lines are from geostrophic flow fields derived from (a) post Katrina (15 Sept) and (b) post Rita (26 Sept) airborne-based data. Gray shades represent regions where geostrophic straining can be neglected (Jaimes and Shay 2010).

For forced near-inertial motions in the 3-dimensional wave wake, currents rotate anticyclonically with depth in the northern hemisphere in time as energy propagates downward into the thermocline while the phase propagates upward. This has been observed in current profilers in Gilbert (Shay *et al.* 1998), moored ADCP measurements in Ivan (Teague *et al.* 2007), and EM/APEX floats deployed in Frances during CBLAST (Sanford *et al.* 2005, 2007). Gilbert current profiles revealed a predominance of the anticyclonic-rotating energy where the average ratio of the anticyclonic to cyclonic energies was 3.6 (e.g., preference for downward energy propagation from the

OML). The corresponding vertical energy flux indicated an average value of $\sim 2 \text{ ergs cm}^{-2} \text{ s}^{-1}$ (Shay and Jacob 2006). That said, the near-inertial response in the vicinity of oceanic fronts and western boundary currents do not necessarily reveal such a clear energetic response (Jaimes and Shay 2010).

Understanding this contrasting OML thermal and momentum response to wind stress in mesoscale oceanic features is central for predicting accurate TC intensity changes. During the directly forced stage, underlying geostrophic circulations affect the wind-driven horizontal current divergence underneath the eye. Upwelling (downwelling) regimes predominantly develop where the wind stress vector is with (against) the geostrophic OML velocity vector. Moreover, direct measurements and ray-tracing techniques in realistic geostrophic flow indicate that, during the relaxation stage, TC-forced OML near-inertial oscillations are horizontally trapped in regions of negative geostrophic vorticity (warm features), where they rapidly propagate downward into the thermocline (Figure 5). These anticyclonic-rotating regimes coincided with distribution of reduced OML cooling, as rapid downward dispersion of near-inertial energy reduced the amount of kinetic energy available to increase vertical shears at the OML base. By contrast, TC-forced OML near-inertial oscillations were stalled in OMLs of cyclonic circulations (cold features), which strengthened vertical shears and entrainment cooling at the layer's base. To improve the prediction of TC-induced OML cooling, models must capture geostrophic features; and models and turbulence closures must represent near-inertial wave processes such as dispersion and breaking (turbulent mixing) between the OML base and the seasonal thermocline (Jaimes and Shay 2010)..

4: Global Ocean Monitoring:

As shown in Figure 2, the thermal structure is directly affected by the momentum response during TC passage. However, the level of ocean cooling depends crucially on the initial OML and the 26°C isotherm depths and the strength of the stratification (N) across the base of the OML as noted. In many basins, the 26°C isotherm depth is located near the OML base. Integrated thermal energy values reflect the vertical distribution of the thermal energy in the OHC estimation (e.g., Shay and Brewster 2010). Since the amount of work done on the OML scales as the surface friction velocity (u_*^3), the deeper the layer (e.g., 26°C isotherm), the higher the stress-induced turbulent mixing is needed to redistribute OML properties through shear-induced instabilities. In this framework, high OHC (100 kJ cm^{-2}) values, strong buoyancy frequencies ($N \sim 20 \text{ cph}$), and lower latitudes (10 to 20°) affect the thermal structure and that decrease the negative feedback during TC passage. This is one reason why no cold wakes are apparent in the Eastern Pacific warm pool regime.

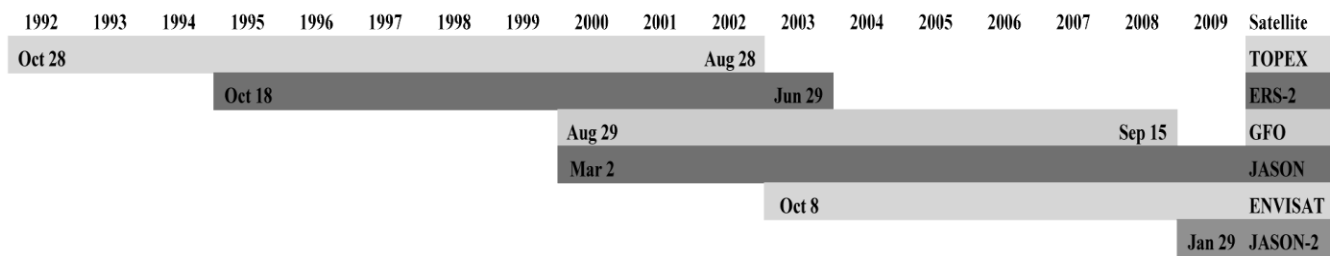


Figure 6: Bar chart showing time line of available SHA field from various altimetry platforms.

Global ocean monitoring for isotherm depths, thermal structure and OHC given the relative paucity of *in situ* profiler measurements with perhaps the exception of the global ARGO float network. Thus, satellite remote sensing using satellite altimetry (Figure 6) offers the optimal approach to infer isotherm depths and OHC variations. That is, measurements from radar altimeter missions of the SHA field from NASA TOPEX, Jason-1 and 2, U.S. Navy Geosat Follow-On-Mission (GFO), Envisat and ERS-2 (Cheney *et al.* 1994; Scharroo *et al.* 2005) and SSTs are used in a reduced gravity model (e.g., Goni *et al.* 1996) with hurricane season climatology (Mainelli 2000). Since mesoscale ocean features only move a few km d^{-1} , altimeter-derived SHA locates warm (cold) features that are usually identified as positive (negative) values as observed during TC's Opal (Shay *et al.*

2000), Ivan (Walker *et al.* 2005; Halliwell *et al.* 2008), Katrina and Rita in the Gulf of Mexico (Mainelli *et al.* 2008 ; Shay 2009), Maemi (Lin *et al.* 2005, Wu *et al.* 2007), Chaba and Songda (Wada and Usui 2007) in the western Pacific Ocean basin, and cyclones in the Bay of Bengal (Jena *et al.* 2006; Ali *et al.* 2007).

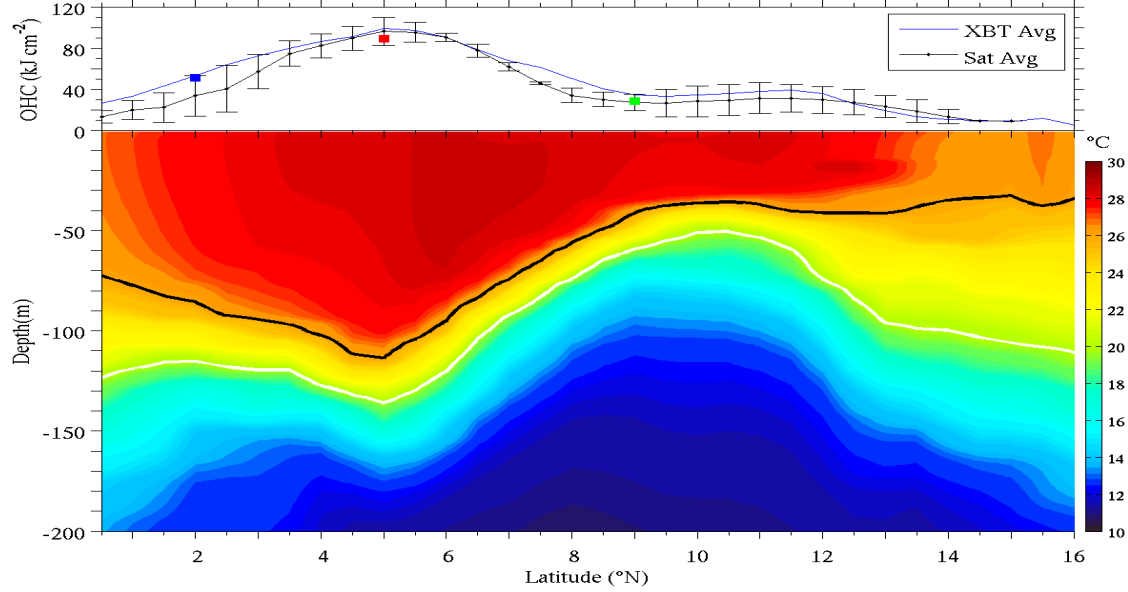


Figure 7: Average OHC (upper panel: kJ cm^{-2}) from repeat XBT transects in the eastern Pacific Ocean basin (blue line), TAO moorings at 2, 5 and 8°N (140°W: colored boxes) and the corresponding satellite-derived values (black line) with $\pm 2\sigma$ and the corresponding vertical temperature structure from the XBTs (lower panel) where the depth of the 20°C isotherm (white line) and the 26°C (black line). Data are averaged from the months of July from 2000 to 2005 (From Shay and Brewster 2010).

Given the availability of the satellite-derived values of OHC derived from radar altimetry, it is very important to assess these values relative to available *in situ* data profiles. From measurements acquired during pre and post-Rita research flights (including satellite tracked drifters), satellite-inferred and *in situ* isotherm depths and OHC values were correlated at levels of 0.9. Regression slope for the OHC is 0.9 with a bias of 1.3 kJ cm^{-2} in the WCE. For the 26°C isotherm depths, the slope was about 1.1 with a 9.3 m bias where the altimeter-derived value was larger than that from the profiler data. This larger bias was due to the advection of the CCE between the LC and WCE from the post-Rita data set (Jaimes and Shay 2009). These estimates were also consistent with those derived from drifter-based measurements. While the bias in the depth is large, the result suggests this is roughly a 10 to 15% uncertainty in the signals where isotherm depths ranged from 90 to 105 m in the WCR. Several sets of profiler measurements have suggested that the OHC scales as $\sim 1 \text{ kJ cm}^{-2} \text{ m}^{-1}$ in the LC and WCR structures.

To further illustrate the validity of this OHC approach from altimetry under non-forcing conditions, satellite-derived values were compared to *in situ* XBT transect data (see <http://noaa.aoml.gov/phod>) in the eastern Pacific Ocean basin (Shay and Brewster 2010). Five years of data along a repeated XBT transect is used to determine OHC and compare it to the five-year average from satellite-inferred values along the same transect as well as the closest moorings (Figure 7). There is marked agreement between the XBT, mooring and satellite-derived OHC values. In addition, there are no significant differences between the two *in situ* and the remotely sensed values at 95% confidence. Over a broader spatial scale from 2000 to 2008 during the EPAC basin hurricane season, OHC value statistics from 6,420 *in-situ* data points revealed RMS OHC differences were 13 to 20 kJ cm^{-2} or up to 15% of the maximum values. The slope of regression line for OHC values is 0.9 with an RMS difference of 17 kJ cm^{-2}

where the dynamic range lies between 113 to 190 kJ cm⁻² (not shown). This latter value is a maximum rather than an average. Thus, estimating the 26°C isotherm depth using satellite altimetry in a reduced gravity model (Goni *et al.* 1996) allows one to determine OHC for use with Statistical Hurricane Intensity Prediction Scheme (SHIPS: DeMaria *et al.* 2005; Mainelli *et al.* 2008).

An important aspect of this problem is the considerable variability in OHC estimates between basins due to the different temperature and salinity characteristics, and more importantly the strength of the thermocline and halocline. Temperatures and salinities vary in response to incoming radiation and precipitation (ITCZ) as well as the air-sea fluxes (Gill 1982), which impact the buoyancy frequency profile ($N(z)$). The maximum buoyancy frequency (N_{max}) occurs at the base of the OML. For example, in the Eastern Pacific Ocean (EPAC), N_{max} is ≈ 20 cycles per hour (cph) due to the sharpness of the thermocline and halocline (pycnocline) located at the OML base (i.e. 30 to 35 m). Beneath this maximum, $N \geq 3$ cph are concentrated in the seasonal thermocline over an approximate thermocline scale of 200 m and exponentially decay with depth approaching 0.1 cph. Such behavior has important implications for shear-instability and vertical mixing processes. In the EPAC, this implies that for large N , wind-forced shears have to be significantly larger for mixing to occur. Given a large N , and lower latitudes (12°N) where the inertial period is long in the EPAC warm pool, SST cooling and OML deepening will be much less than in the GOM as observed during hurricane Juliette in Sept 2001 (Shay and Jacob 2006; Shay and Brewster 2010). This is precisely why few cold wakes are found in the EPAC warm pool regime. By contrast, significant SST cooling of more than 5°C occurred when Juliette moved northwest where N_{max} decreased to about 14 cph at higher latitudes (18 to 20°N). While for the same hurricane in the GOM, similar levels of SST cooling would be observed in the GCW, but not in the LC water mass because the 26°C isotherm depth is three to four times deeper. These regional to basin-scale variations in oceanic structure and the resultant stratification represent a paradox for hurricane forecasters, which is the rationale underlying the use of satellite radar altimetry in mapping isotherm depths and estimating OHC from SHA and assimilating them into oceanic and coupled models.

To place these differing variations into context, a stratification parameter is introduced that allows us to understand such differences. This parameter (s) is given by $\sqrt{N_{max}/N_o}$ where N_{max} represents the maximum buoyancy frequency located across the OML base and N_o is the reference buoyancy frequency for a given reference density (temperature, salinity). The stratification parameter (s) has a maximum value in the EPAC warm pool where N_{max} ranged between 20 to 24 cph observed during the Eastern Pacific Investigation of Climate (EPIC: Raymond *et al.* 2004). Thus, this ratio is approximately 2.8 to 3 in the warm pool compared to values of about 1.5 to 2 on the periphery of the warm pool and the northern tier of the hurricane-prone domain. Further west, s ranges increases to 2.6 to 2.8 between 8 to 12°N and between 130 to 145°W. However, the stratification parameter decreases to values less than 1.8 west of this patch of higher values.

The stratification parameter is determined empirically from in situ measurements and climatology keeping in mind the strength of the stratification at the OML base is an important parameter in vertical mixing processes through the Richardson number (Price 1981; Sanford *et al.* 1987; Shay *et al.* 1992). Here we then introduce equivalent OHC given by:

$$OHC_E = OHC \times \sqrt{N_{max}/N_o},$$

where OHC is the vertically integrated thermal structure from the surface to the depth of the 26°C isotherm as above. This expression allows us to compare OHC values in differing basins or regions. For example, OHC in Sept 2001 in the warm pool ranged between 38 to 43 kJ cm⁻² as noted above. However given the strength of the stratification ($s \sim 3$), OHC_E ranges from 114 to 129 kJ cm⁻², respectively (Figure 8) which means the highly stratified water will act as a barrier to strong shear-induced mixing until such time that vertical shears develop to lower the Richardson number to below critical values. At these low latitudes from 10 to 14°N, more OHC is available during hurricane passage through the air-sea fluxes as mixing will be suppressed for a long period of

time. In general, entrainment mixing is what forces 65 to 80% of the cooling and layer deepening during hurricane passage (Price 1981; Jacob *et al.* 2000).

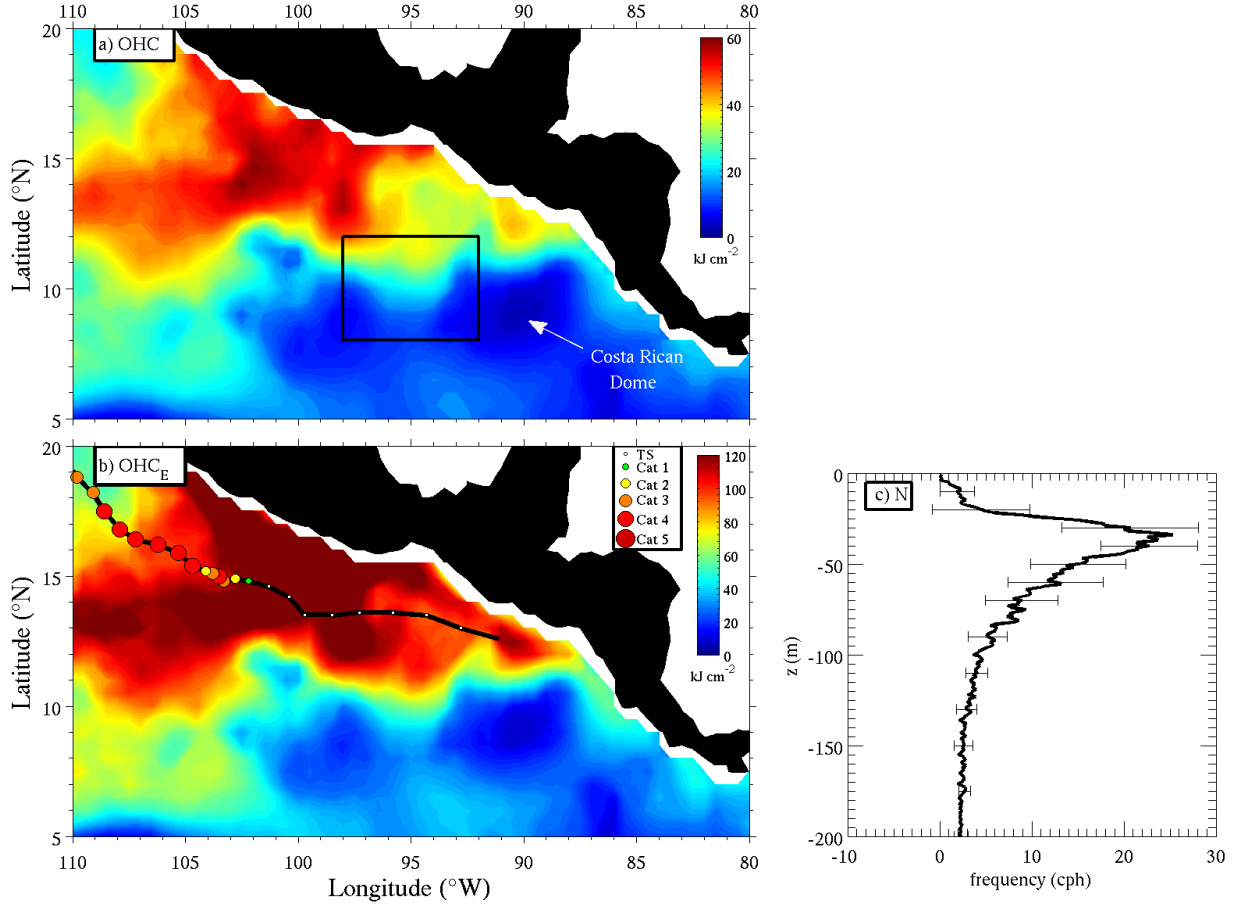


Figure 8: Averaged a) OHC and b) OHC_E (kJ cm^{-2}) during Sept 2001 during the EPIC field program (black box in panel a) and the track and intensity of Juliette (23 Sept to 3 Oct). Panel c is the buoyancy frequency (cph) from 19 days of CTD measurements from the NOAA *R/V Brown* at 95°N and 10°W where the maximum buoyancy frequency was about 22 cph consistent with AXCTDs deployed from the NOAA aircraft. Notice the OHC maps clearly delineate the Costa Rican Dome just east of the EPIC domain and the warm pool.

During hurricane Juliette's passage in Sept 01 (Shay and Jacob 2006), and the subsequent intensification to category 4 status, the SST cooling was less than 1°C in the regime with strong vertical gradients (~ 20 to 24 cph: cycles per hour) (Wijesekera *et al.* 2005). Wind-driven ocean current shear tends to be insufficient to significantly cool the upper ocean through shear instability until Juliette moved into an area with weaker stratification (~ 10 cph) where SST cooling was 4 to 5°C . Entrainment mixing across the OML base due to ocean current shear did not lower the bulk Richardson number to below criticality. Hence, a larger fraction of OHC was available for Juliette through air-sea fluxes during the rapid intensification phase over less than 24 hours (Raymond *et al.* 2004).

Secondly, these levels of OHC_E are nearly equivalent to those observed in the western Atlantic basin. That is, OHC values in the NW Caribbean Sea have values of 120 to 150 kJ cm^{-2} with a corresponding equivalent OHC value since $s \sim 1$ in that regime. Similar values of OHC_E are found in the subtropical water (e.g., LC). In the western Pacific Ocean, s ranges from 1.2 to 1.4 . Thus, the relative import of this simple empirical relationship is

that it allows forecasters to understand not only spatial variability in OHC levels, but provides perhaps a simplified means of assessing these processes in differing basins based on stratification which is in the numerator of the Richardson number.

5. Air-Sea Interface:

Due to limited observations at the air-sea interface in high-wind conditions, the understanding has not progressed nearly enough to significantly improve the parameterization of momentum and energy transfers between the two fluids. The relationships of the transfer processes of small-scale roughness (Charnock 1955) and stability are understood under moderate-wind conditions (Large and Pond 1981), but additional phenomena not typically observed such as the sea state maturity (Donelan et al. 2004; Moon *et al.* 2004a,b) and sea spray (Wang *et al.* 2001; Andreas and Emanuel 2001) have been shown to modulate the heat and momentum exchange.

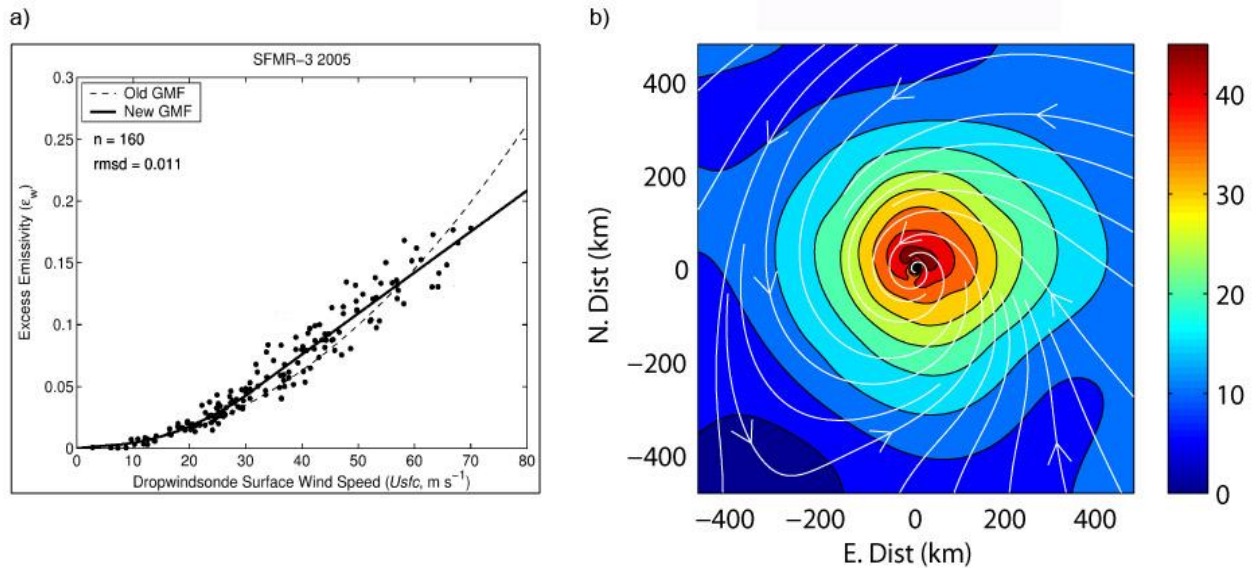


Figure 9: a) Excess emissivity from SFMR compared to 10-m surface winds measured from GPS dropsondes. The total number of samples is 160 and the RMS difference between the SFMR model function was 0.011 (left panel) and b) example of an HWIND wind field (Powell and Houston 1996) and streamlines relative to the TC center (0,0) when SFMR data are included into the analysis from TC Frances (2004) where the color bar is in $m s^{-1}$ (from Uhlhorn *et al.* 2007).

As shown in Figure 9, surface winds in TC's have been estimated remotely using the Stepped-Frequency Microwave Radiometer (SFMR) from aircraft (Uhlhorn *et al.* 2007). They developed a new emissivity and wind speed model function based on comparisons with direct measurements of surface winds in hurricanes by GPS dropwindsondes. This function eliminates a previously-documented high bias in moderate SFMR-measured wind speeds (10 to 50 $m s^{-1}$), and additionally corrects an extreme wind speed ($>60 m s^{-1}$) systematic underestimate in the past cases. The model function behaves differently below and above the hurricane wind speed threshold (32 $m s^{-1}$).

Enthalpy (heat and moisture) fluxes across the interface and into the atmospheric boundary layer are critical elements to TC's (Emanuel 1995). Momentum transfer between the two fluids is characterized by the variations of wind with height and a c_d that is a function of wind speed and surface roughness. Using GPS sondes (Hock and Franklin 1999) deployed in the TC boundary layer, Powell *et al.* (2003) found a logarithmic variation of mean wind speed in the lowest 200 m, a maximum speed at 500 m, and a gradual weakening with height to 3 km. From these estimates, the surface stress, roughness length, and neutral stability drag coefficient determined by the

profile method suggest a leveling of the surface momentum flux as winds increase above hurricane-force with a decrease of the drag coefficient with increasing winds.

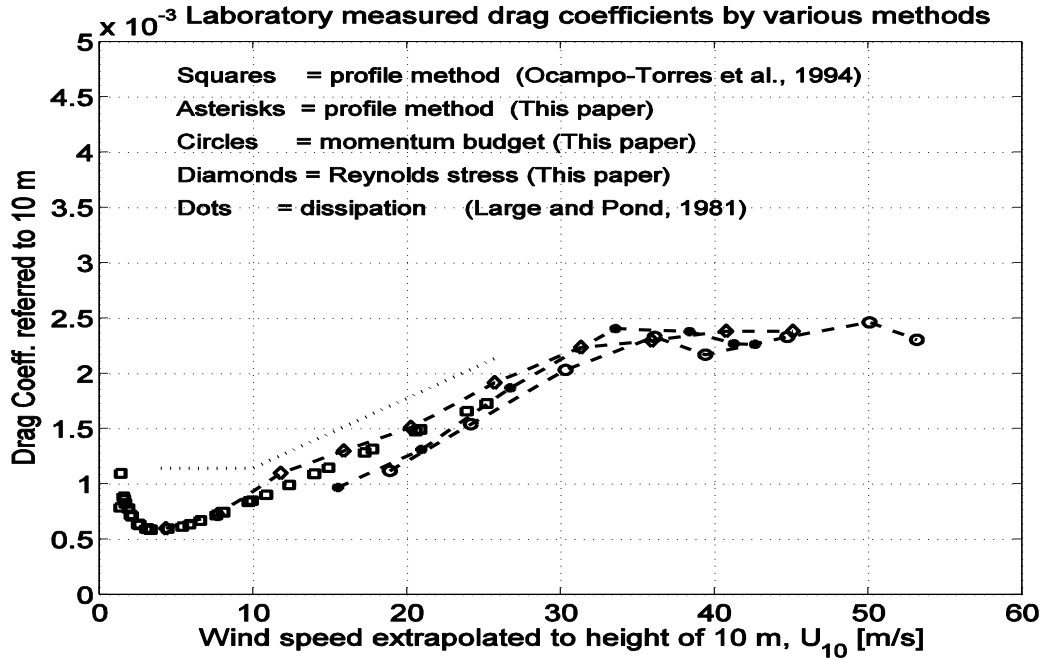


Figure 10: Laboratory measurements of the neutral stability drag coefficient ($\times 10^{-3}$) by profile, eddy correlation (“Reynolds”), and momentum budget methods. The drag coefficient refers to the wind speed measured at the standard anemometer height of 10 m. The drag coefficient formula of Large and Pond (1981) is also shown along with values from Ocampo-Torres et al (1994) derived from field measurements (from Donelan *et al.* 2004)

Donelan *et al.* (2004) described a series of tank experiments and found a “saturation” of the drag coefficient does appear once the wind speed is $\sim 33 \text{ m s}^{-1}$ (Figure 10). Beyond this speed, the surface does not become any rougher. The saturation level for c_d is ~ 0.0025 , corresponding to a roughness length of 3.35 mm from the laboratory results. Powell *et al.* (2003) found a “saturation” of the drag coefficient at 0.0026 at about 35 m s^{-1} that decreased at higher wind speeds using wind profiles normalized by a mean boundary layer wind. Shay and Jacob (2006) found a “saturation” wind speed at 30 m s^{-1} of 0.0034 where c_d began to leveled off at surface wind speeds up to 38 m s^{-1} . A similar approach was used from the TC Ivan data set (Teague *et al.* 2007). Jarosz *et al.* (2007). found a peak value of 0.0026 at 32 m s^{-1} before decreasing. Sanford *et al.* (2007) estimated the volume transport per unit of width based on velocity profiles in TC Frances using surface drag coefficients of Powell *et al.* (2003) and Large and Pond (1981) formulations. Numerical simulations from a mixing model embedded in the 3-D ocean model (Price *et al.* 1994) indicated consistent results for the volume transport and SST cooling values at two of the three floats to the right of the storm track. Along the track, however, differences differed by about 15 to 20%. As Sanford *et al.* (2007) point out, an azimuthal dependence in the surface drag coefficient due to surface waves (Wright *et al.* 2001) must be included in the models.

As shown in Figure 11, the momentum flux is parameterized with a non-dimensional surface roughness (Charnock’s equation) and the stability correction based on similarity theory. Moon *et al.* (2004a,b) investigated the Charnock coefficient under TC conditions using a coupled wind-wave (CWW) model. In the CWW model, the surface wave directional frequency spectrum near the spectral peak is calculated using the WAVEWATCH III (Tolman 2002) model and the high frequency part of the spectrum was parameterized using the theoretical model of Hara and Belcher (2002). The wave spectrum is then introduced to the wave boundary layer model of Hara and Belcher (2004) to estimate the Charnock coefficient at differing wave evolution stages. The regression lines

between the wave age and the Charnock coefficient have a negative slope at low wind speeds but have a positive slope at higher wind speeds. This slope change occurs between 25 and 35 m s⁻¹ consistent with these saturation estimates above.

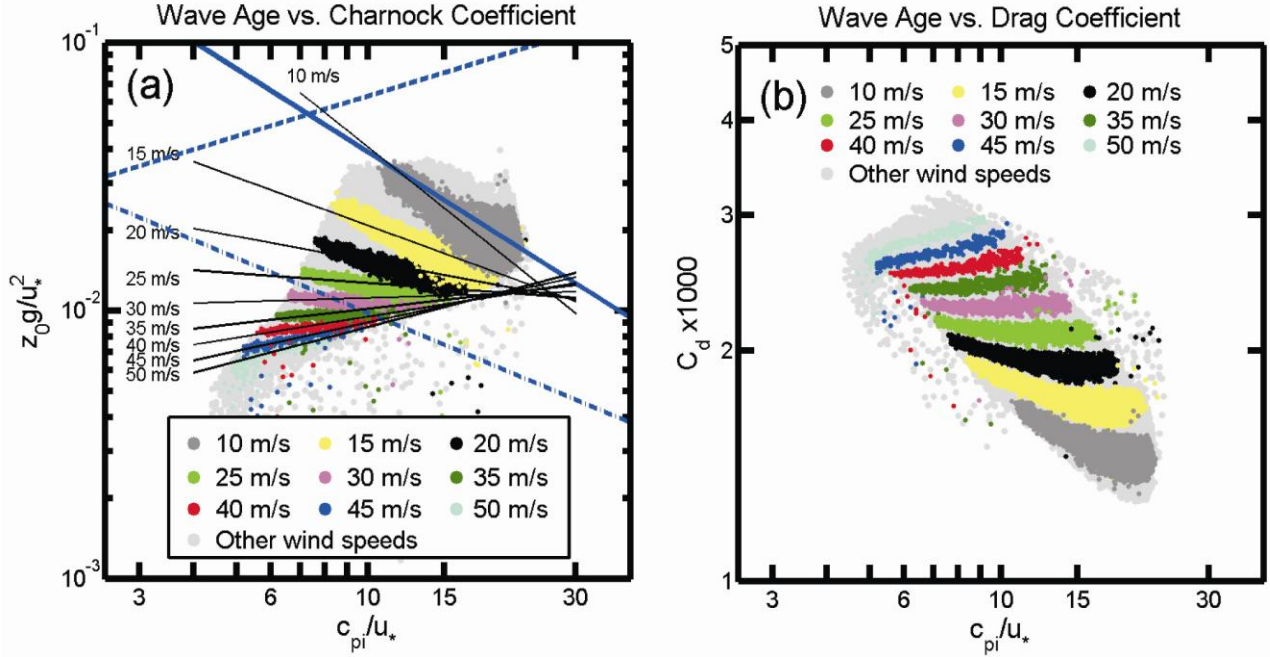


Figure 11: Scatterplots of the a) Charnok Coefficient (z_{ch}) and b) drag coefficients (c_d) as a function of the wave age (cp / u_*) for several TCs in the Atlantic Ocean. Differing colors represent 5-m s⁻¹ intervals for surface winds for z_{ch} and c_d . are the best fits for each wind speed group. In panel a, blue solid line and dash-dot represent empirical estimates for ocean and laboratory experiments (Donelan 1990). Dotted line is the formula of Toba et al. (1990) (Figure from Moon *et al.* 2004a).

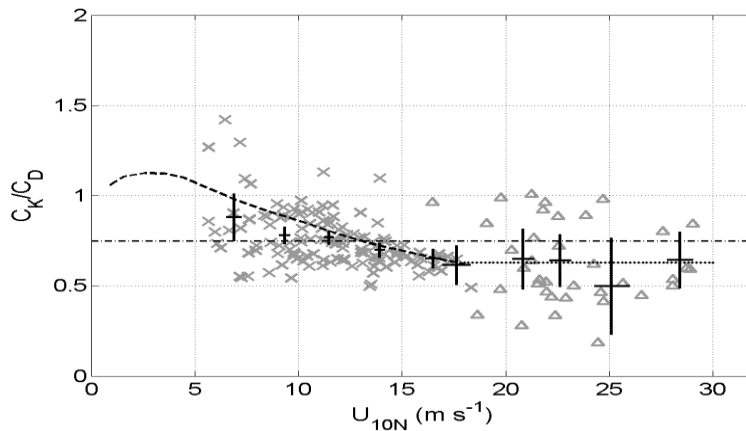


Figure 12: The ratio of c_k / c_d as a function of 10-m neutral wind speed. Data from CBLAST (Δ), and HEXOS (\times) are shown. Solid black lines show the mean and 95% confidence intervals of the combined HEXOS and CBLAST field data after binning average by wind speed. The dotted black line shows the mean of the CBLAST data. The ratio based on COARE 3.0 bulk flux algorithm is shown as the dashed line. The threshold value of 0.75 suggested by Emanuel is also shown as the dash-dotted line (from Zhang 2007).

As shown in Figure 12, direct turbulent flux measurements were carried out in the hurricane boundary layers using a research aircraft instrumented with fast-response turbulence sensors (Black *et al.* 2007). The wind speed range for momentum and enthalpy fluxes and exchange coefficients has been extended by over 50% compared to that in previous studies. The drag coefficient (c_d) increase linearly with 10 m wind speed up to 22 m s^{-1} then level off at higher wind speed (French *et al.* 2007). The Dalton number (c_E) is nearly constant with 10 m wind speed up to 30 m s^{-1} (Drennan *et al.* 2007). Combining the sensible and latent heat flux measurements, Zhang (2007) derived the enthalpy flux and the exchange coefficient for enthalpy transfer (c_k) showing that there is no evidence of an increase of c_k with wind speed, in good agreement with the Humidity Exchange over the Sea (HEXOS) result (DeCosmo *et al.* 1996). The ratio of c_k/c_d versus wind speed for the flux runs with both momentum and enthalpy flux measurements. The average of the c_k/c_d values is 0.63 well below the 0.75 threshold for TC development (Emanuel 1995).

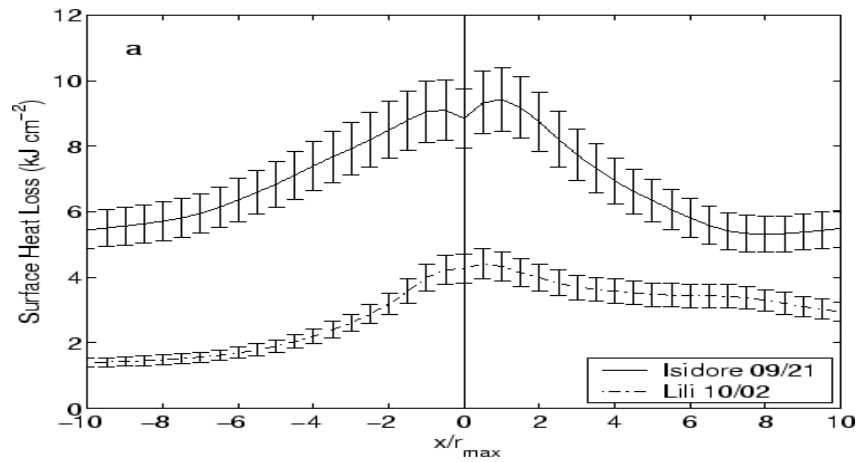


Figure13: Integrated along-track variations in the normalized cross-track direction of the surface heat loss (upper curve) observed during TC's Isidore (solid) and Lili (dashed) with the uncertainties based on observed ocean and atmospheric data (from Shay and Uhlhorn 2008).

Fluxes of heat and moisture are central to the TC intensity question and are usually determined from bulk aerodynamic formulae that utilize near-surface atmospheric observations and upper-ocean temperature data measured by ocean profiles. Estimates of enthalpy fluxes during TC's Isidore and Lili were sensitive to the storm translation speed. In Isidore, peak enthalpy flux $\sim 1.7 \text{ kW m}^{-2}$ is in the right-rear quadrant of the storm due to the high SSTs ($\sim 30^\circ\text{C}$) as there was a negligible decrease from pre-storm SST conditions, especially over the warm LC where ocean cooling was minimal (Shay and Uhlhorn 2008). Although the maximum momentum flux (7 Pa) is in the right-front quadrant, TC Isidore's wind stress field was symmetric as it moved at only 4 m s^{-1} . Estimated maximum surface enthalpy fluxes in Lili were about 1.4 kW m^{-2} due in part to the marked asymmetry associated with the faster storm translation speed (7 m s^{-1}) and smaller SSTs by about 1°C . This result highlights how modest SST differences alter the surface heat fluxes during extreme winds (Cione and Uhlhorn 2003).

Enthalpy fluxes were integrated along the track to obtain the cross-track (radial) distributions of net sea surface heat loss (Figure 13). The estimated surface heat loss in Isidore ($\sim 9 \text{ kJ cm}^{-2}$) is almost a factor of two larger than in Lili ($\sim 4.5 \text{ kJ cm}^{-2}$) due to the enhanced enthalpy fluxes, slower storm speed, and larger horizontal SST gradients along the western side of the Yucatan Strait. These inferred surface heat losses reflect the lack of the oceanic response of the LC observed during both TC's. For example, Cione and Uhlhorn (2003) argue that it is only inner-core SSTs that the storm responds to if the OHC was held constant. However, OHC is not

remaining constant underneath a eyewall as SSTs decrease. Since SSTs represent the boundary condition for OHC estimates from the data, any SST decrease has to be reflected in the estimation procedure.

6. Summary

Significant progress has been made in understanding the basic oceanic and atmospheric processes that occur during TC passage (Ginis 1995). There is a continuing need to isolate fundamental physical processes involved in the coupled interactions through detailed process studies using experimental, empirical, theoretical, and numerical approaches with data assimilation methods. As suggested from new observations, these approaches are needed to improve predictions of tropical cyclone intensity and structure.

Considerable ocean-atmosphere variability occurs over the storm scales that include fundamental length scales such as the radius of maximum winds and radius to gale-force winds. Here, the fundamental science questions are how the two fluids are coupled through oceanic and atmospheric boundary layer processes, and what are the primary time scales of this coupling? These questions are not easily answered as the interactions occur over a broad range of time and space scales. One school of thought is that the only important process with respect to the ocean is underneath the eyewall where ocean cooling has occurred. While it is at the eyewall where the maximum momentum and enthalpy fluxes occur, the broad surface circulation over the warm OML also has non-zero fluxes that contribute heat and moisture to the TC. The deeper the OML (and 26°C isotherm depth), more heat (OHC) is available to the storm through the enthalpy fluxes. It is not just the magnitude of the OHC, since the depth of the warm water is important to sustaining surface enthalpy fluxes. Process studies need to begin to examine these multiple scale aspects associated with the atmospheric response to ocean forcing.

To understand the coupling with the upper ocean, measurements must be made prior to the TC arrival over an oceanographic area to resolve background flows and the associated thermodynamics. Such data are needed not only to initialize ocean models (e.g., Loop Current, Kuroshio, Gulf Stream), but these data are required during the TC to examine vertical mixing processes on the upper ocean momentum and thermal response. In addition to aircraft-based sampling by AXCPs and AXCTDs and new profiling floats such as the EM/APEX and drifters, efforts along the southeastern United States are underway to deploy high frequency radars to map the surface currents to 200 km from the coast as part of an integrated ocean observing system. Such measurements would not only be invaluable to map the wind-driven surface currents during high winds, but also to map the directional wave spectra over the domain. These measurements could then be used to not only examine air-sea interactions and evaluate the coupled models, but also assess the relative importance of surface wave-current interactions in surge models.

To place the OHC into context with other basins, an empirical stratification parameter, based on the maximum buoyancy and a reference buoyancy frequencies, provides a normalization based on the strength of the stratification observed at the OML base where shear-induced mixing occurs. These mixing events are driven by vigorous near-inertial motions forced by the wind stress and its curl (Shay *et al.* 1989). Thus, this empirical approach then allows us to compare values and assess the threshold values currently used in SHIPS of 60 kJ cm⁻² in the Atlantic Ocean basin (DeMaria *et al.* 2005; Mainelli *et al.* 2008). There is observational evidence that this threshold is fairly large compared to the coupled measurements acquired during Isidore and Lili (Shay and Uhlhorn 2008) where surface heat losses were more on the O (10 kJ cm⁻²) with surface heat fluxes of 1.4 to 1.7 kW m⁻². This is an important issue that needs to be resolved in coupled models aimed at forecasting intensity change.

Surface drag coefficient variations has received attention over the last five years largely through highly specialized experiments. Several treatments have come to the conclusion that there is a leveling off or saturation values of $\approx 30 \text{ m s}^{-1} \pm 3 \text{ m s}^{-1}$. The ratio of the enthalpy coefficient and the drag coefficient is central to air-sea fluxes impacting the TC boundary layer. In this context, the relationship between the coupled processes such as wave breaking and the generation of sea spray and how this is linked to air-sea fluxes remains a fertile research

area. A key element of this topic is how the atmosphere responds to the oceanic forcing where there seems to be contrasting viewpoints. One argument is that the air-sea interactions are occurring over surface wave (wind-wave) time and space scales and induce intensity changes of more than a category. Yet empirical studies suggest the drag coefficients range between 1 and 4×10^{-3} depending on the quadrant where the surface waves change direction relative to the 10-m winds (M. Powell, personal communication, 2007). In recent coupled model studies, the partitioning of the wind energy into the current and waves remains an important research question. There should be more in depth experimental and empirical studies where surface waves are measured along with upper ocean currents and surface winds. Surface waves are essentially submesoscale phenomena that affect the enthalpy fluxes in differing quadrants, however, first-order balances are primarily between the atmospheric and oceanic boundary layers that constrain and impact the sea surface processes.

Acknowledgments: This workshop paper represents excerpts from the WMO IWTC-VI Proceedings in Costa Rica (edited by Hugh Willoughby) and a recent chapter entitled Air-Sea Interactions in Tropical Cyclones for the second volume of the Global Perspectives of Tropical Cyclones book edited by Professors J. C. Chan, C. P. Chang and Dr. J. Kepert. The author gratefully acknowledges support from the NSF through grants *ATM-01-08218*, *04-44525*, NASA Hurricane Science Program and NOAA Joint Hurricane Testbed program. I continue to be grateful to the NOAA Aircraft Operation Center (Dr. Jim McFadden) who make it possible to acquire high quality data during hurricanes. Mr. Bill Teague (NRL-Stennis) and Drs. Rick Lumpkin, Peter Black, Eric Uhlhorn, Jun Zhang, Mark Powell, George Halliwell (NOAA-AOML), Mark Donelan, Brian Haus, Will Drennan (all at RSMAS), S. Daniel Jacob (University of Maryland-Baltimore County), Tom Sanford (Applied Physics Laboratory, University of Washington), Nan Walker (Louisiana State University), Isaac Ginis (University of Rhode Island), I.-I. Lin (National Taiwan University), Y. Yoshikawa (Kyushu University) and I.-J. Moon (Cheju National University) shared material used herein. Dr. Russell Elsberry made editorial comments on the original version of this chapter for the IWTC-VI workshop edited by Dr. Hugh Willoughby. Without the cooperation of these contributing scientists these chapters would not be possible. Ms. Jodi Brewster, Dr. Benjamin Jaimes and Mr. Pat Myers assisted with some of the graphics.

References:

- Ali, M. M., P. S. V. Jagadeesh, and S. Jain, 2007: Effects of eddies on Bay of Bengal cyclone intensity, *EOS*, **88**, 93,95.
- Andreas, E. and K. A. Emanuel, 2001: Effects of sea spray on tropical cyclone intensity. *J. Atmos. Sci.*, **58**, 3741-3751.
- Bao, J.-W., J. M. Wilczak, J. K. Choi, and L. H. Kantha, 2000: Numerical simulations of air-sea interaction under high wind conditions using a coupled model: A study of hurricane development. *Mon. Wea. Rev.*, **128**, 2190-2210.
- Bender, M. and I. Ginis, 2000: Real-time simulation of hurricane-ocean interaction. *Mon. Wea. Rev.*, **128**, 917-946.
- Black, P. G., E. A. D'Asaro, W. Drennan, J. R. French, P. P. Niiler, T. B. Sanford, E. J. Terrill, E. J. Walsh, and J. Zhang, 2007: Air-sea exchange in hurricanes: synthesis of observations from the Coupled Boundary Layer Air-Sea Transfer experiment. *BAMS*, **88**, 357-384.
- Bosart, L., C.S. Veldon, W.E. Bracken, J. Molinari, and P.G. Black, 2000: Environmental influences on the rapid intensification of hurricane Opal (1995) over the Gulf of Mexico. *Mon. Wea. Rev.*, **128**, 322-352.
- Braun, S. A. and W.-K. Tao, 2000: Sensitivity of high resolution simulations of hurricane Bob (1991) to planetary boundary layer parameterizations. *Mon. Wea. Rev.*, **128**, 3941-3961.

- Chen, S., J. F. Price, W. Zhao, M. Donelan, and E. J. Walsh, 2007: The CBLAST Hurricane program and the next generation fully coupled atmosphere-wave-ocean models for hurricane research and prediction., *BAMS*, **88**, 311-317.
- Cione, J.J., P. G. Black, S. H. Houston, 2000: Surface observations in the hurricane environment. *Mon. Wea. Rev.* **128**, 1550-1561.
- Cione, J.J., and E.W. Uhlhorn, 2003: Sea surface temperature variability in hurricanes: Implications with respect to intensity change. *Mon. Wea. Rev.*, **131**, 1783-1796.
- D'Asaro, E. A., 2003: The ocean boundary layer under hurricane Dennis. *J. Phys. Oceanogr.*, **33**, 561-579.
- DeCosmo, J. B., K. B. Katsaros, S. D. Smith, R. J. Anderson, W. A. Oost, K. Bumke, and H. Chadwick, 1996: Air-sea exchange of water vapor and sensible heat: The Humidity Exchange over the Sea (HEXOS) results. *J. Geophys. Res.*, **101**, 12,001-12,016.
- DeMaria, M., M. Mainelli, L. K. Shay, J. Knaff, and J. Kaplan, 2005: Further improvements to the statistical hurricane intensity prediction scheme. *Wea and Forecasting*, **20**, 531-543.
- Donelan, M A., 1990: Air-sea interaction. The Sea, B. LeMehaute and D. Hanes, Eds, *Ocean Engineering Science*, **9**, John Wiley and Sons, 239-292.
- Donelan, M. A., B. K. Haus, N. Reul, W. J. Plant, M. Stiassine, H. Graber, O. Brown, and E. Saltzman, 2004: On the limiting aerodynamic roughness of the ocean in very strong winds. *Geophys. Res. Letters*, **31**, L18306, doi:10.29/2004GRL019460.
- Drennan, W. M. and L. K. Shay. 2006: On the variability of the fluxes of momentum and sensible heat. *Bound. Layer Meteor.*, **119**(1), 81-107.
- Drennan, W. M., J. A. Zhang, J. R. French, C. McCormick, and P. G. Black, 2007: Turbulent fluxes in the hurricane boundary layer, Part II: Latent heat flux. *J. Atmos. Sci.*, **64**, 1103- 1115.
- Emanuel, K A., 1986: An air-sea interaction theory for tropical cyclones Part 1: Steady-State maintenance. *J. Atmos. Sci.*, **43**, 585-605.
- Emanuel, K A., 1995: Sensitivity of tropical cyclones to surface exchange and a revised steady-state model incorporating eye dynamics. *J. Atmos. Sci.* , **52**, 3969-3976.
- Falkovich, A., I. Ginis, and S. Lord, 2005: Implementation of data assimilation and ocean initialization for the coupled GFDL/URI hurricane prediction system. *J. Atmos. and Ocean. Tech.*, **22**, 1918–1932.
- French, J. R., W. M. Drennan, J. A. Zhang, and P. G. Black, 2007: Turbulent fluxes in the hurricane boundary layer. Part 1: Momentum flux. *J. Atmos. Sci.*, **64**, 1089-1102.
- Gill, A. E., 1984: On the behavior of internal waves in the wakes of storms. *J. Phys. Oceanogr.*, **14**, 1129-1151.
- Ginis, I., 1995: Interaction of tropical cyclones with the ocean. In *Global Perspective of Tropical Cyclones*, Chapter 5, Ed. R. L. Elsberry, **Tech. Document WMO/TD 693**, World Meteorological Organization, Geneva, Switzerland, 198-260.

- Goni, G. J., and J. Trinanes, 2003: Ocean thermal structure monitoring could aid in the intensity forecast of tropical cyclones. *EOS, Trans. Amer. Geophys. Union*, **85**, 179.
- Goni, G. J., S. Kamholz, S. L. Garzoli, and D. B. Olson, 1996: Dynamics of the Brazil/Malvinas confluence based on inverted echo sounders and altimetry. *J. Geophys. Res.*, **95**, 22103-22120.
- Halliwel, G., L. K. Shay, S. D. Jacob, O. Smedstad, and E. Uhlhorn, 2008: Improving ocean model initialization for coupled tropical cyclone forecast models using GODAE nowcasts. *Mon Wea Rev*, **136** (7), 2576–2591.
- Halliwel, G., L. K. Shay, J. Brewster, and W. Teague, 2009: Evaluation and sensitivity analysis of an ocean model to hurricane Ivan in the northern Gulf of Mexico. *Mon. Wea. Rev.* (**Accepted , resubmitted**)
- Hara, T., and S. E. Belcher, 2004: Wind profile and drag coefficient over mature ocean surface wave spectra. *J. Phys. Oceanogr.*, **34**, 2345-2358.
- Hock, T. J., and J. L. Franklin, 1999: The NCAR GPS dropwindsonde. *BAMS*, **80**, 407-420.
- Hong, X., S. W. Chang, S. Raman, L. K. Shay, and R. Hodur, 2000: The interaction of hurricane Opal (1995) and a warm core ring in the Gulf of Mexico. *Mon. Wea. Rev.*, **128**, 1347-1365.
- Jacob, D. S., L. K. Shay, A. J. Mariano, and P. G. Black, 2000: The three-dimensional mixed layer heat balance during hurricane Gilbert. *J. Phys. Oceanogr.*, **30**, 1407-1429.
- Jacob, S. D., and L. K. Shay, 2003: The role of oceanic mesoscale features on the tropical cyclone- induced mixed layer response. *J. Phys. Oceanogr.*, **33**, 649-676.
- Jaimes, B. and L. K. Shay. 2009: Mixed layer cooling in mesoscale eddies during Katrina and Rita. *Mon. Wea. Rev.*, **137** (12), 4188-4207.
- Jaimes, B. and L. K. Shay. 2010: Near-inertial wave wake of hurricanes Katrina and Rita in mesoscale eddies. *J. Phys. Oceanogr.* (In Press)
- Jaimes, B., L. K. Shay and G. H. Halliwel, 2010: On the response to tropical cyclones in quasi-geostrophic oceanic vortices. *J. Phys. Oceanogr.* (In Preparation)
- Jarosz, E., D.A. Mitchell, D.W. Wang, and W.J. Teague, 2007: Bottom-up determination of air-sea momentum exchange under a major tropical cyclone. *Science*, **315**, 1707.
- Jena, B., M. V. Rao and B. K. Sahu, 2006: TRMM-derived sea surface temperature in the wake of a cyclonic storm over the central Bay of Bengal. *Inter. J. of Rem. Sens.*, **27**(14), 3065-3072.
- Large, W.G., and S. Pond, 1981: Open ocean momentum flux measurements in moderate to strong winds. *J. Phys. Oceanogr.*, **11**, 324-336, 1981
- Leipper, D., and D. Volgenau, 1972: Hurricane heat potential of the Gulf of Mexico. *J. Phys. Oceanogr.*, **2**, 218-224.
- Lin, I.-I., C.-C. Wu, K. A. Emanuel, I.-H. Lee, C.-R. Wu, and I.-F. Pun, 2005: The interaction of supertyphoon Maemi (2003) with a warm ocean eddy. *Mon Wea. Rev.*, **133**, 2635-2649.

- Lin, I.-I., I.-F. Pun and C.-C. Wu, 2009: Upper ocean thermal structure and the western north Pacific Category 5 typhoons. Part II: Dependence on translation speed. *Mon. Wea. Rev.*, **137**, (In Press).
- Mainelli, M., 2000: On the role of the upper ocean in tropical cyclone intensity change. M.S. Thesis, RSMAS, University of Miami, Miami, FL, 73 pp.
- Mainelli, M., M. DeMaria, L. K. Shay and G. Goni, 2008: Application of oceanic heat content estimation to operational forecasting of recent category 5 hurricanes. *Wea. and Forecast*, **23**, 3-16.
- Marks, F., and L.K. Shay, 1998: Landfalling tropical cyclones: Forecast problems and associated research opportunities: Report of the 5th Prospectus Development Team to the U.S. Weather Research Program, *BAMS*, **79**, 305-323.
- Moon, I., I. Ginis, and T. Hara, 2004a: Effect of surface waves on Charnock coefficient under tropical cyclones. *Geophys. Res. Lett.*, **31**, L20302.
- Moon I.-J., I. Ginis, and T. Hara, 2004b: Effect of surface waves on air-sea momentum exchange. II: Behavior of drag coefficient under tropical cyclones. *J. Atmos. Sci.*, **61**, 2334-2348.
- Park, J., K.-A. Park, K. Kim, and Y.-H. Youn, 2005: Statistical analysis of upper ocean temperature response to typhoons from ARGO floats and satellite data. *IEEE*, 2564-2567.
- Perlroth, I, 1969: Effects of oceanographic media on equatorial Atlantic hurricanes. *Tellus*, **21**, 230-244.
- Powell, M. D., and S. Houston, 1996: Hurricane Andrew's landfall in South Florida. Part II: surface wind fields. *Wea and Forecasting*, **11**, 329-349.
- Powell, M.D., P.J. Vickery, and T.A. Reinhold, 2003: Reduced drag coefficient for high wind speeds in tropical cyclones. *Nature*, **422**, 279-283.
- Price, J. F., R. A. Weller, and R. Pinkel, 1986: Diurnal cycling: Observations and models of the upper ocean response to diurnal heating, cooling and wind-mixing. *J. Geophys. Res.*, **7**, 8411-8427.
- Price, J. F., T. B. Sanford, and G.Z. Forristall, 1994: Observations and simulations of the forced response to moving hurricanes. *J. Phys. Oceanogr.*, **24**, 233-260.
- Sanford, T.B., P.G. Black, J. Haustein, J.W. Feeney, G. Z. Forristall, and J.F. Price, 1987: Ocean response to a hurricane. Part I: Observations. *J. Phys. Oceanogr.*, **17**, 2065-2083.
- Sanford, T.B., J.H. Dunlap, J.A. Carlson, D.C. Webb and J. B. Girton, 2005: Autonomous velocity and density profiler: EM-APEX. Proceedings of the IEEE/OES 8th Working Conference on Current Measurement Technology, IEEE Cat No. 05CH37650, ISBN: 0-7803-8989-1, 152-156.
- Sanford, T B., J. F. Price, J. Girton, and D. C. Webb, 2007: Highly resolved observations and simulations of the oceanic response to a hurricane. *Geophys. Res. Lett.*, **34**, L13604, 5 pp.
- Schade, L., and K. Emanuel, 1999: The ocean's effect on the intensity of tropical cyclones: Results from a simple ocean-atmosphere model. *J. Atmos. Sci.*, **56**, 642-651.
- Scharroo, R., W.H. Smith, and J.L. Lillibridge, 2005: Satellite altimetry and the intensification of Hurricane Katrina. *EOS*, **86**, 366-367.

- Shay, L. K., 2006: Air-sea interface and oceanic influences (Chapter 1.3). Topic Chairman and Rapporteurs Report For Tropical Cyclone Structure and Structure Change of the 6th WMO International Workshop on Tropical Cyclones (IWTC-6) 20 Nov - 30 Nov 2006 in San Jose, Costa Rica, *World Meteorological Organization Tropical Meteorology Research Series*, **WMO TMRP 72**, Ed. Hugh Willoughby, Geneva, Switzerland, 120-150.
- Shay, L.K., 2009: Upper Ocean Structure: Response to Strong Forcing Events. In: *Encyclopedia of Ocean Sciences*, 2nd Edition, ed. John Steele, S.A. Thorpe, Karl Turekian and R. A. Weller, Elsevier Press International, Oxford, UK, 4619-4637, doi: 10.1016/B978-012374473-9.00628-7.
- Shay, L. K., 2010: Air-Sea Interactions in Tropical Cyclones (Chapter 3). In *Global Perspectives of Tropical Cyclones*, 2nd Edition, Eds. Johnny C. L. Chan and C. P. Chang, *World Scientific Publishing Company: Earth System Science Publication Series*, London, UK, 99-131 (In Press).
- Shay, L.K., R.L. Elsberry and P.G. Black, 1989: Vertical structure of the ocean current response to a hurricane. *J. Phys. Oceanogr.*, **19**, 1249 - 1269.
- Shay, L.K., P.G. Black, A.J. Mariano, J.D. Hawkins and R.L. Elsberry, 1992: Upper ocean response to hurricane Gilbert. *J. Geophys. Res.*, **97**, 20,227 - 20,248.
- Shay, L.K. and S.W. Chang. 1997: Free surface effects on the near-inertial ocean current response to a hurricane: A revisit. *J. Phys. Oceanogr.*, **27(1)**, 23 - 39.
- Shay, L.K., A.J. Mariano, S.D. Jacob, and E.H. Ryan, 1998: Mean and near-inertial ocean current response to hurricane Gilbert. *J. Phys. Oceanogr.*, **28**, 858 – 889, 1998.
- Shay, L. K., G. J. Goni, and P. G. Black, 2000: Effects of a warm oceanic feature on hurricane Opal. *Mon. Wea. Rev.*, **128**, 1366-1383.
- Shay, L. K, and S. D. Jacob, 2006: Relationship between oceanic energy fluxes and surface winds during tropical cyclone passage (Chapter 5). Atmosphere-Ocean Interactions II, *Advances in Fluid Mechanics*. Ed. W. Perrie, WIT Press, Southampton, UK, 115-142.
- Shay, L. K., and E. W. Uhlhorn, 2008: Loop Current response to Hurricanes Isidore and Lili. *Mon Wea. Rev.*, **136**, 3248-3274
- Shay, L. K., and J. Brewster. 2010: Eastern Pacific oceanic heat content estimation for hurricane forecasting. *Mon. Wea. Rev.*, 138, (**In Press**).
- Teague, W.J., E. Jarosz, D.W. Wang, and D.A. Mitchell, 2007: Observed oceanic response over the upper continental slope and outer shelf during Hurricane Ivan. *J. Phys. Oceanogr.*, **37**, 2181-2206.
- Tolman, H. L., 2002: User manual and system documentation of WAVEWATCH-III version 2.22. NOAA/NWS/NCEP/OMB Tech. Note 222, 133 pp.
- Uhlhorn, E. W., P. G. Black, J. L. Franklin, M. Goodberlet, J. Carswell and A. S. Goldstein, 2007: Hurricane surface wind measurements from an operational stepped frequency microwave radiometer. *Mon. Wea. Rev.*, **135**, 3070-3085.
- Uhlhorn, E. W., 2008: Gulf of Mexico Loop Current mechanical energy and vorticity response to a tropical cyclone. *PhD Dissertation*. RSMAS, University of Miami, Miami, FL 33149, 148 pp.

- Wada, A., and N. Usui, 2007: Importance of tropical cyclone heat potential for tropical cyclone intensity and intensification in the western north Pacific. *J. of Oceanography*, **63**, 427-447.
- Walker, N., R. R. Leben, and S. Balasubramanian 2005: Hurricane forced upwelling and chlorophyll a enhancement within cold core cyclones in the Gulf of Mexico. *Geophys. Res. Letter*, **32**, L18610, doi: 10.1029/2005GL023716, 1-5.
- Wang, D.W., D.A. Mitchell, W.J. Teague, E. Jarosz, and M.S. Hulbert, 2005: Extreme waves under Hurricane Ivan. *Science*, **309**, 896.
- Wang, Y., J. D. Kepert, and G. J. Holland, 2001: The effect of sea spray evaporation on tropical cyclone boundary layer structure and intensity. *Mon. Wea. Rev.*, **129**, 2481-2500.
- Wright, C. W., E. J. Walsh, D. Vandemark, W. B. Krabill, A. W. Garcia, S. Houston, M. Powell, P. Black, and F. D. Marks, 2001: Hurricane directional wave spectrum spatial variations in the open ocean. *J. Phys. Oceanogr.*, **31**, 2472-2488.
- Wu, C.-C., C.-Y. Lee, and I-I Lin, 2007: The effect of the ocean eddy on tropical cyclone intensity. *J. Atmos. Sci.*, **64**(10), 3562-3578.
- Yablonsky, R. M, and I. Ginis, 2009: Limitation of one-dimensional ocean models for coupled hurricane-ocean forecasts. *Mon. Wea. Rev.*, DOI 10.1175/2009MWR2863
- Yin, X., Z. Wang, Y. Liu, and Y. Xu., 2007: Ocean response to typhoon Ketsana traveling over the northwest Pacific and a numerical model approach. *Geophys. Res. Lett.*, **34**, doi:10.1029/3007GL031477.
- Zedler, S., T. Dickey, S. Doney, J. Price, X. Yu, and G. Mellor, 2001: Analyses and simulations of the upper ocean's response to hurricane Felix at the Bermuda Testbed Mooring site: 13-23 August 1995. *J. Geophys. Res.*, **107**, 3232.
- Zhang, J. A., 2007: An airborne investigation of the atmospheric boundary layer structure in the hurricane force wind regime. *Ph.D.Dissertation*, RSMAS, University of Miami, Miami, FL 33149, 60pp.

Annexure-4

Power Point Presentations

Can Ocean Mean Temperature be a better parameter for Cyclone Track and Intensity Predictions ?

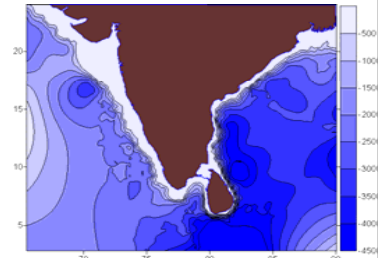
MM Ali, G. Goni, D. Pedro, PV Nagamani, VV Gopalakrishna, DV Bhaskara Rao

**Oceanography Division
National Remote Sensing Centre
Hyderabad**

The Need:

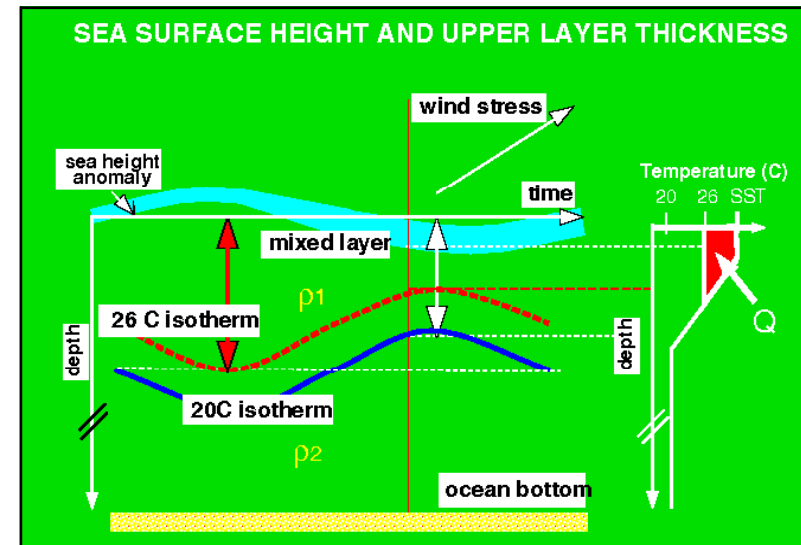
- Storm surge that depends upon the coastal bathymetry is the most devastating element of the TC impact
- Indian coast has varying coastal bathymetry
- A minor deviation of the landfall point and intensity may generate altogether different peak surge heights.
- Forecast with minimal positional errors required for effective warnings for disaster management practices
- Also, the warned region is 3 times larger than the region of actual damage – proving more expensive

In this presentation
Impact of SSHA



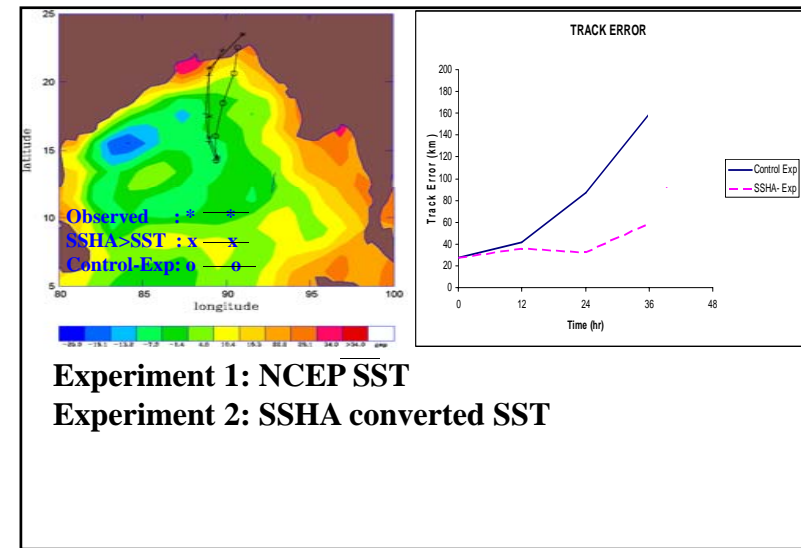
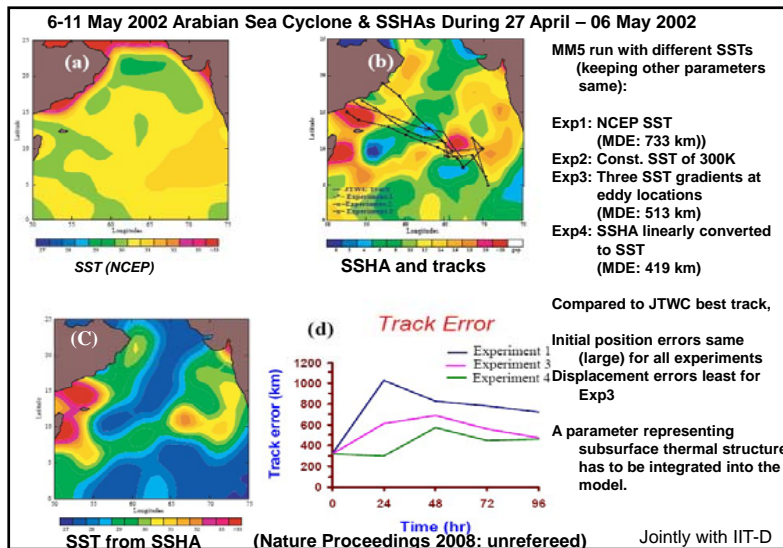
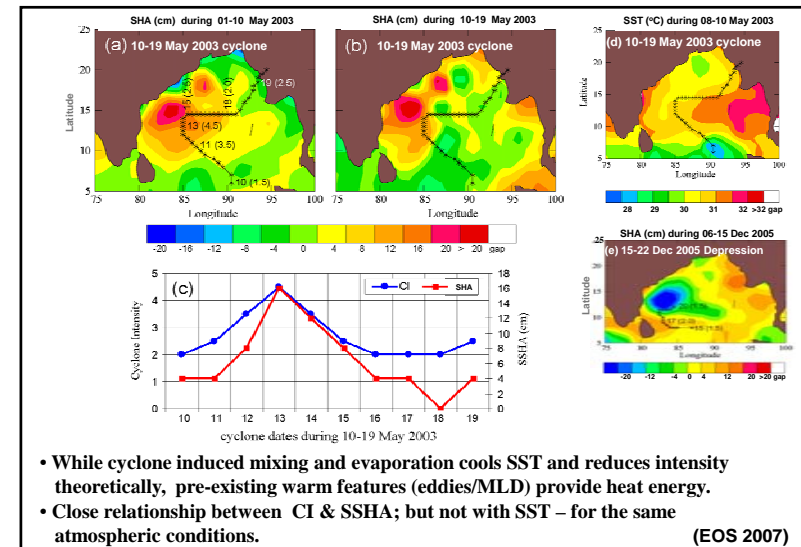
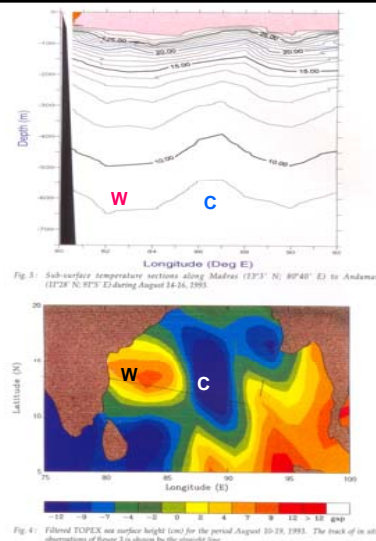
Impact of SSHA:

- SST is a critical parameter in the genesis
- OHC plays more prominent role in intensity and track changes
- SST has been the oceanographic input to the cyclone models.
- Patterns of lower atmospheric anomalies are more consistent with the upper ocean thermal structure than with SST (Namias and Canyan, 1981)
- SSHAs represent the upper ocean thermal structure.
- Cyclone induced mixing cools SST reducing storm intensity
- Pre-existing mesoscale features (warm core eddies & deeper mixed layer) provide the heat source



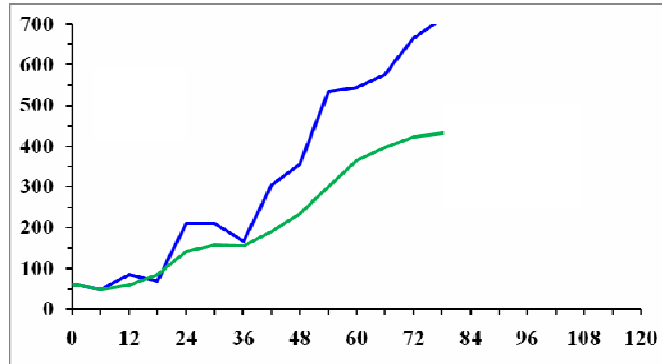
SSHA a better parameter than SST??

- Patterns of subsurface thermal structure (eddies/MLD) are reflected in SSHAs – not in SST sometimes (Baroclinic conditions: SST & SSHA correlate)



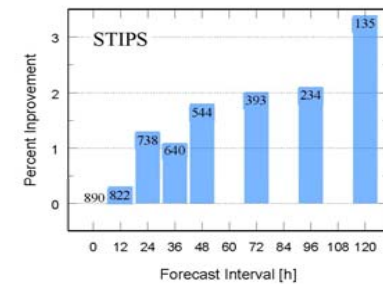
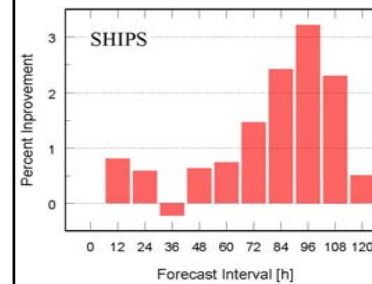
Impact of Ocean Mean Temperature on Cyclone Tracks: Nargis

The Vector Track errors (km): Nargis



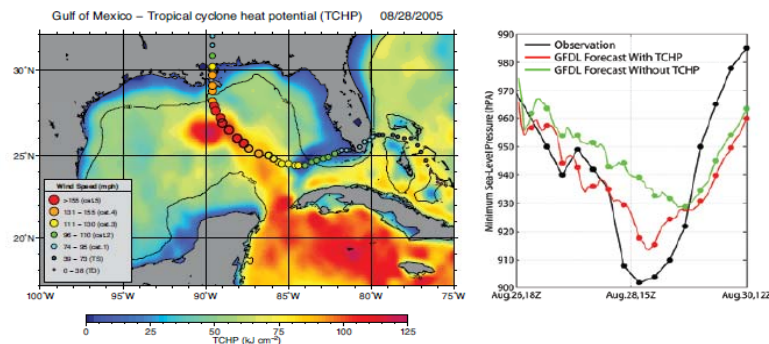
- Track error reduced by using OMT in place of NCEP SST
- Impact more for large lead hours

Percentage improvement of 2004-07 operational Ships (Atlantic) and STIPS (Pacific) forecasts by the inclusion of altimeter derived TCHP



Goni et al. 2009: Oceanography

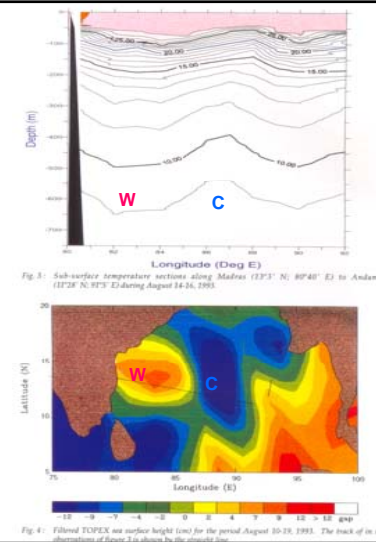
Katrina: Impact of TCHP on Sea Level Pressure



Goni et al. 2009, Oceanography

SSHA a better parameter than SST??

- Patterns of subsurface thermal structure (eddies/MLD) are reflected in SSHAs – not in SST sometimes
- (Baroclinic conditions: SST & SSHA correlate)
- Having a priori information on subsurface thermal structure and SSHAs OHC can be estimated
- How to incorporate these features into the atmospheric cyclone numerical models?









Cyclone Impact Assessment using Satellite Data

V Bhanumurthy
National Remote Sensing Centre, ISRO
Hyderabad
bhanumurthy_v@nrsdc.gov.in

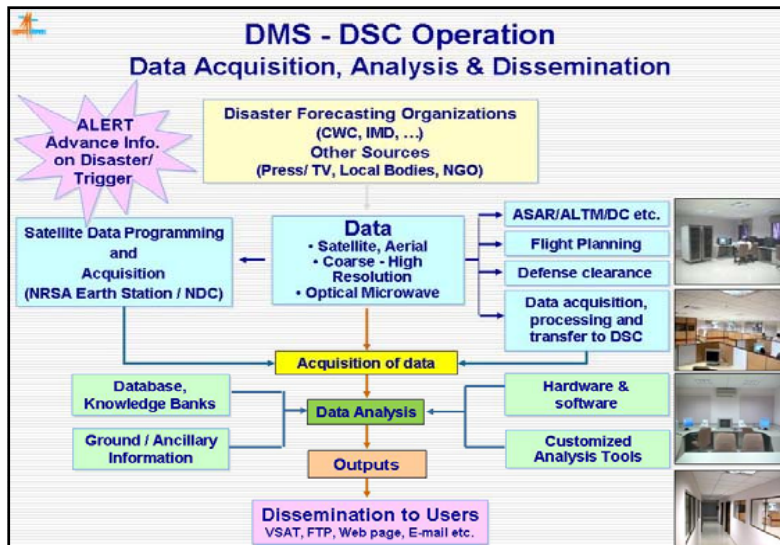
workshop on
Utilization of satellite derived oceanic heat content for cyclone studies
25-26 March, 2010
NRSC, Hyderabad

Decision Support Centre

Operational Services provided currently

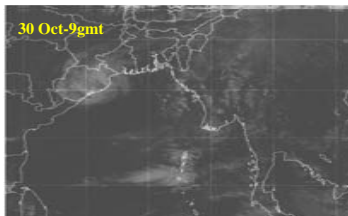
Floods  <ul style="list-style-type: none"> • Flood Inundation Maps • Damage Assessment • Hazard Zonation • Bank Erosion Studies 	Earthquake  <ul style="list-style-type: none"> • Damage Assessment
Cyclone  <ul style="list-style-type: none"> • Inundation Maps • Recession Maps • Damage Assessment 	Landslide  <ul style="list-style-type: none"> • Damage Assessment • Hazard zonation
Drought  <ul style="list-style-type: none"> • Monthly Agril. Drought Report • End-of-the-Season Agril. Drought Report 	Forest Fire  <ul style="list-style-type: none"> • Active Fire Detection • Damage Assessment

Information Dissemination
Central: MHA, CWC, Min. of Agri, GSI, IMD, MOEF
State: Relief Commr., DM, Agri, Forest, other concerned Line Depts.

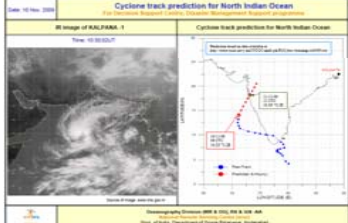


Role of Space Technology In Cyclone Disaster Management


- Monitoring & Tracking
- Dissemination of Warning
- Emergency Communication
- Impact Assessment
- Hazard Zonation



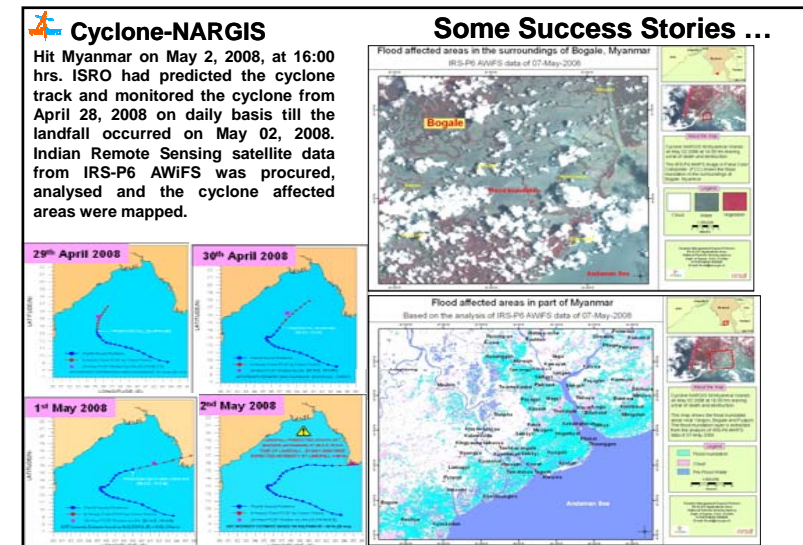
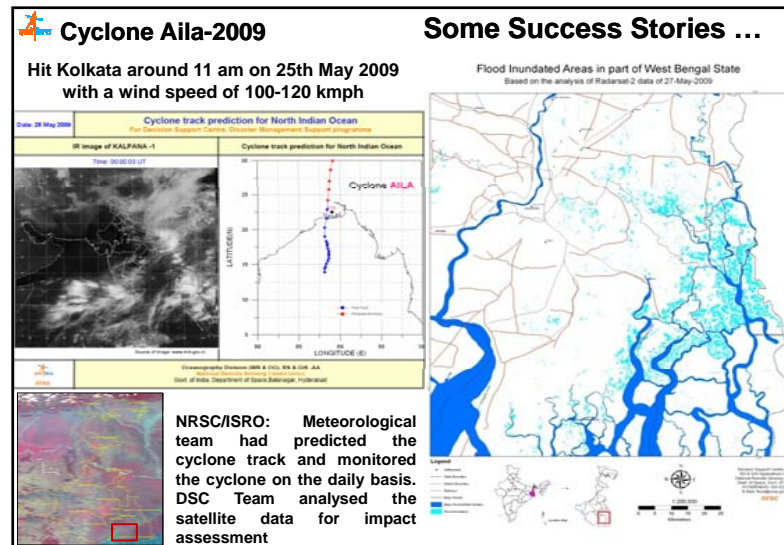
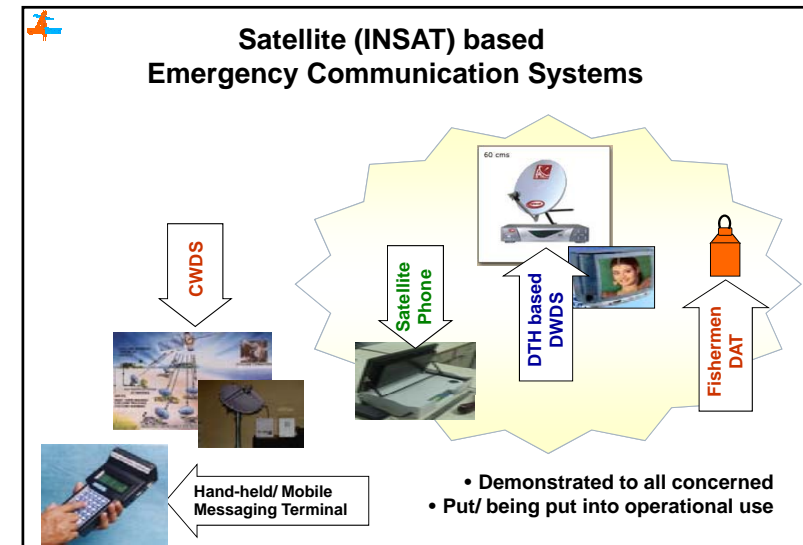
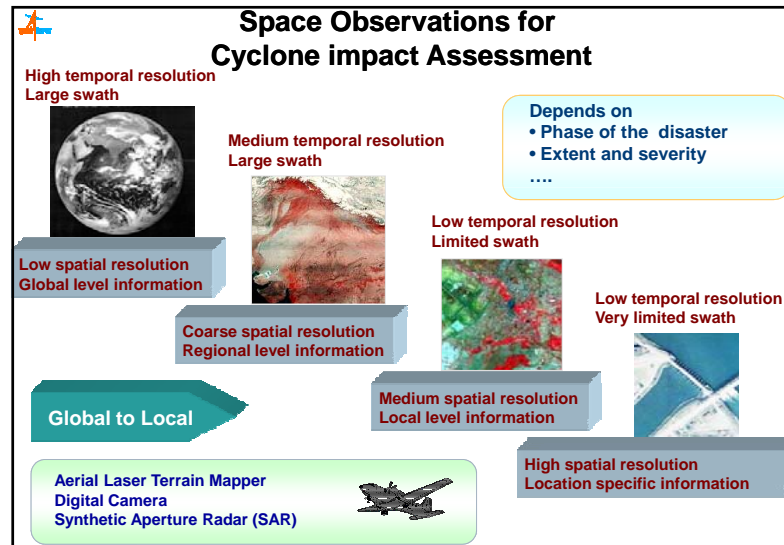
30 Oct-9gmt

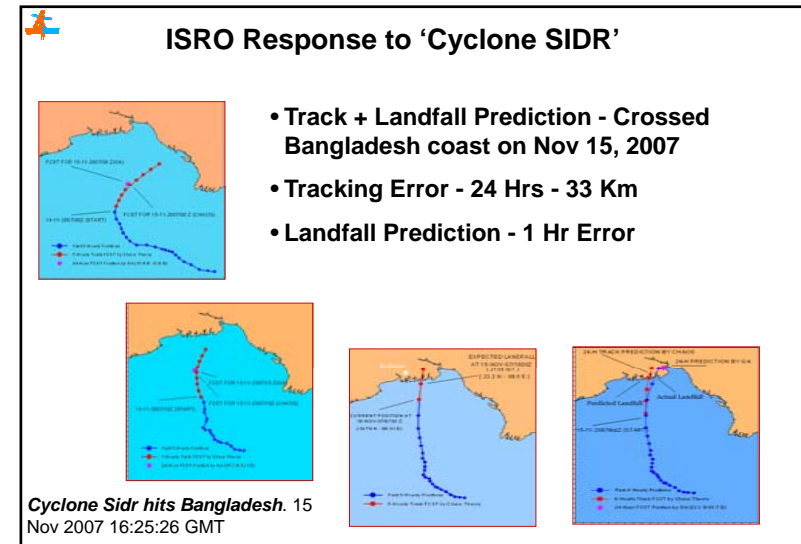
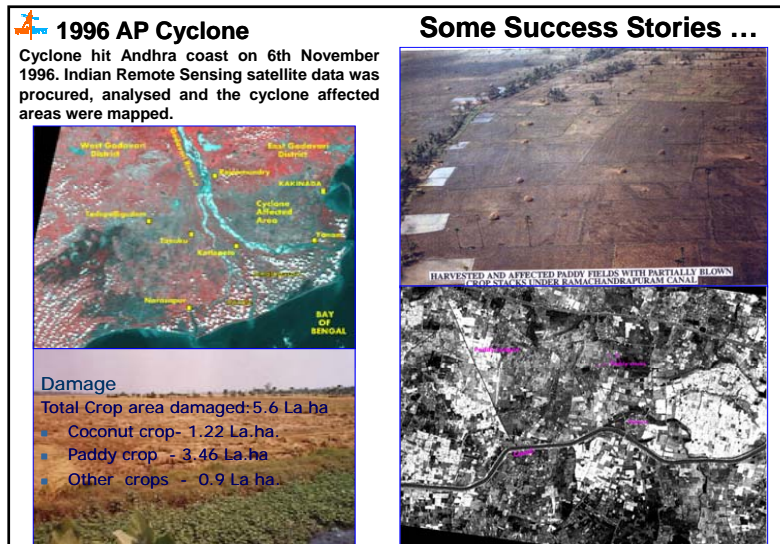
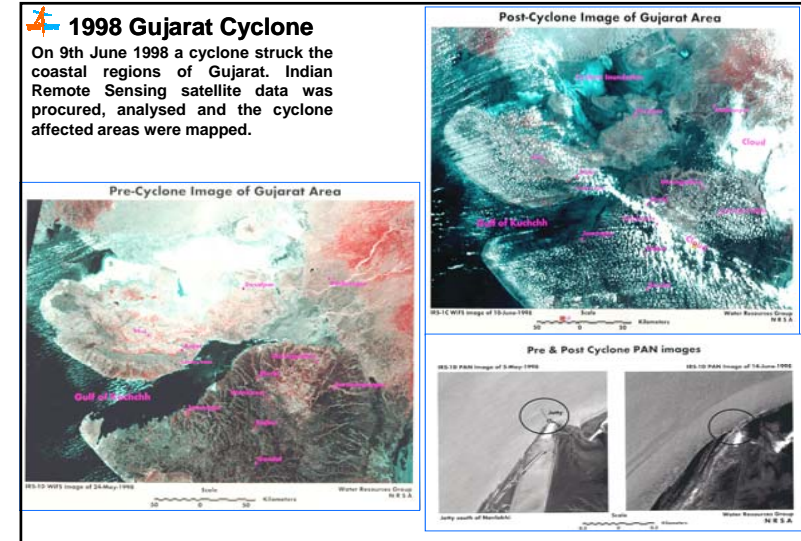
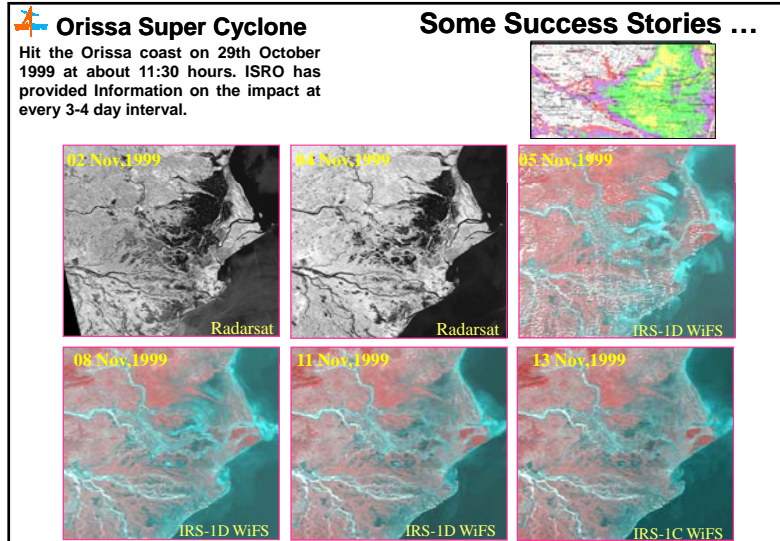


Cyclone track prediction for North Indian Ocean
 Prepared by: Disaster Management Support Programme
 Date: 10 Nov 2009



Cyclone Warning Dissemination Network





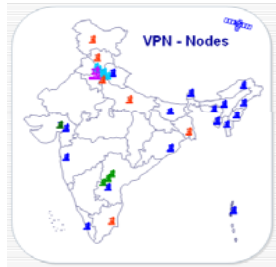


Some Lessons learnt

Detailed Database for multi-hazard prone districts

Information Dissemination

Non-availability of satellite data



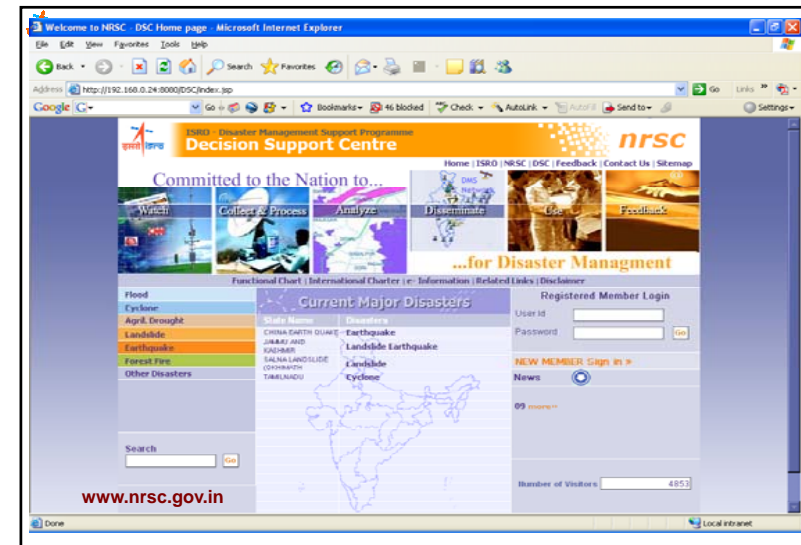
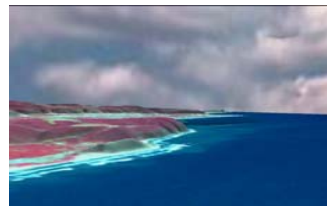
Remedial Action

Database generation for multi-hazard prone districts

Cartosat Carto DEM for Indian Coast

Establishment of VPN Network

Strengthening of Airborne Services



Concerns...

Planning Satellite data acquisition esp where track is frequently changed

Automatic info extraction (from RS data) tools for quick damage assessment

Customized warnings thro' Mobiles

Establishment of ground infrastructure

Awareness and capacity building at community level

Cyclone resistant structures in coastal district



Right TIP to Disaster Management

Right Time

Minutes
To
Days

Right Information

Simple Text Msg
To
Large – spatial Info

Right Person

Top Administrator
To
Common Man

Cyclone Track Prediction : An ANN Approach

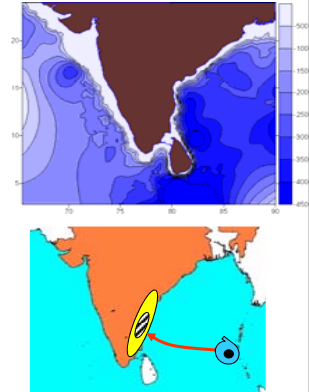
Biswadip Gharai, Dr. M.M.Ali

6/1/2010

1

Need of Cyclone Track Prediction

- Storm surge that depends upon the coastal bathymetry is the most devastating element of the TC impact.
- A minor deviation in the forecasting of the landfall point and intensity may generate altogether different peak surge heights.
- Forecast with minimal positional errors required for effective warnings for disaster management practices
- Also, the warned region is 3 times larger than the region of actual damage – proving more expensive



6/1/2010

2

Cyclone Track Prediction- different approach

Best Approach:

To model the dynamic system from first principles using equations of motion

To integrate these equations forward to predict

In absence of such a perfect physical model:

Use statistical approaches governing physical processes (eg. Climatology and persistence / CLIPER)

Assumption:

Random cyclone movement can be modelled from chaotic nature of a non linear and deterministic dynamics

In this study Artificial Neural Network (ANN) approach is used.

6/1/2010

3

Artificial Neural Network Analysis- Concepts

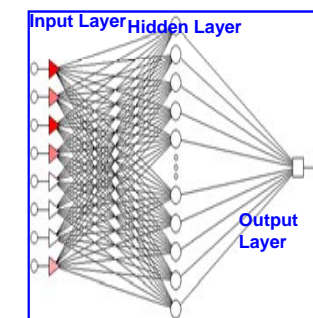
Conceptually, ANN is based upon the human brain's structure.

Consists of interconnected processing elements (neurons)

Has the ability to learn one or more target variables from a set of input variables

Learns by minimizing the error between the desired and network output.

ANN can learn through non-linear interactions that are difficult with regression schemes



6/1/2010

4

Data used

Data:
Best track cyclone positions from the analysis of Joint Typhoon Warning Centre (JTWC)

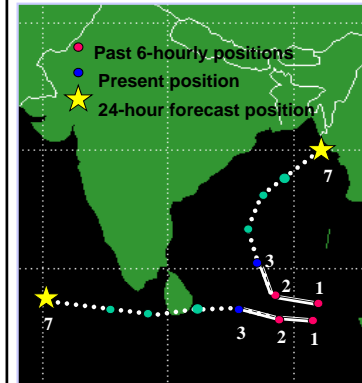
India Meteorological Department

Region:
North Indian Ocean (40-110oE & 5-25oN)

Period: 1971-2002 (JTWC) and 2008-09

6/1/2010

5

Approach- ANN for Cyclone Track Prediction

Individual tracks divided into track segments consisting of

Predictors :

Past two six-hourly positions (Lat & Lon) and present position

Predictand :

One 24 hours in advance position (12, 24, 36, 48)

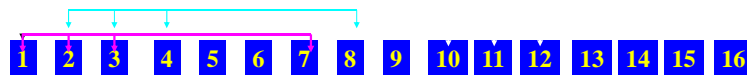
Analysis :

All together 3463 track segments (230 cyclones) analysed

One ANN algorithm developed for Arabian Sea and Bay of Bengal

6/1/2010

6

Approach- ANN for Cyclone Track Prediction

Segment	Predictors	Predictant
1	1,2,3	7
2	2,3,4	8
3	3,4,5	9
4	4,5,6	10
5	5,6,7	11
.....		
10	10,11,12	16

6/1/2010

7

Approach- ANN for Cyclone Track Prediction

ANN model needs three sets of data:

Out of 3463 track segments during 1971-2002,

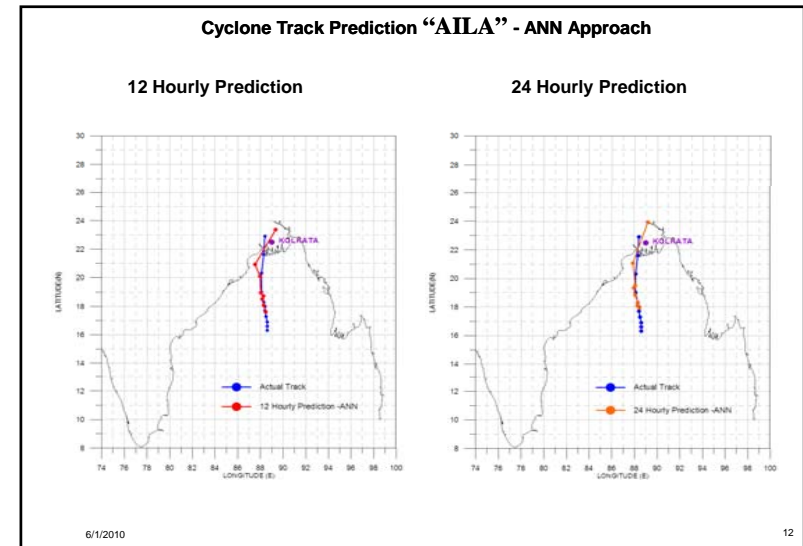
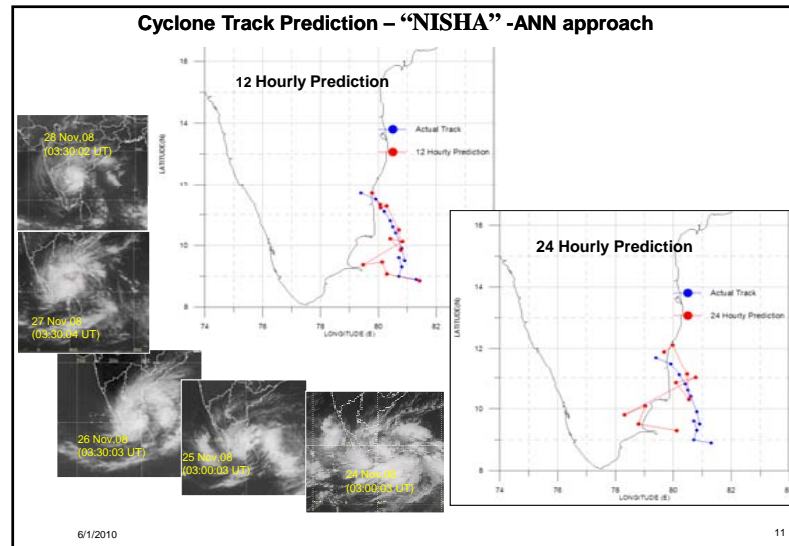
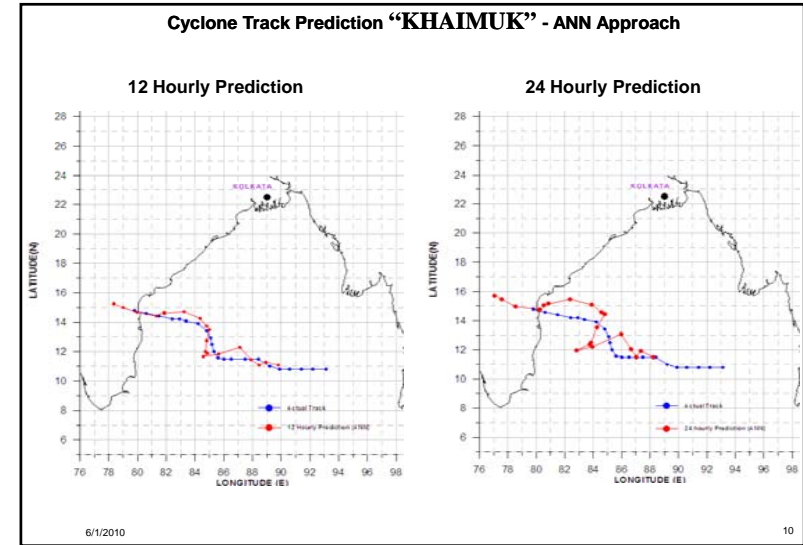
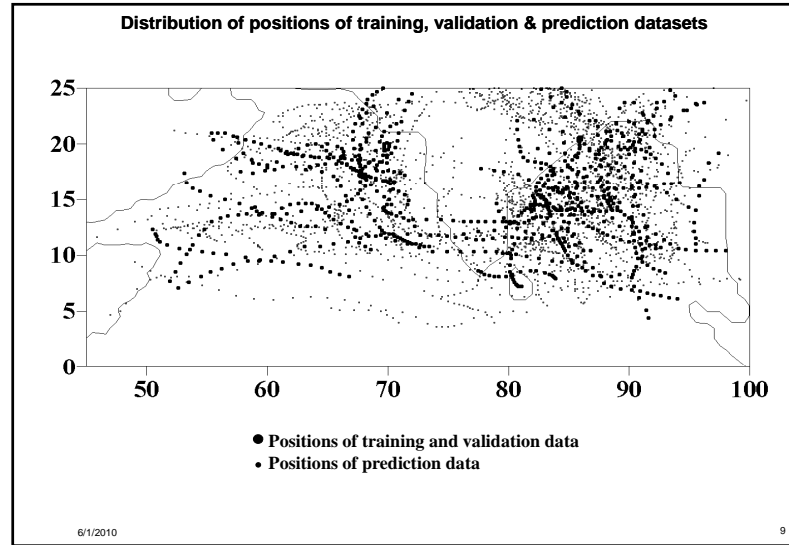
Training (1971-1982): 1713 (49.46%) segments (131 cyclones)

Validation (1983-1994): 920 (26.56%) segments (58 cyclones)

Prediction (1995-2002): 830 (23.96%) segments (41 cyclones)

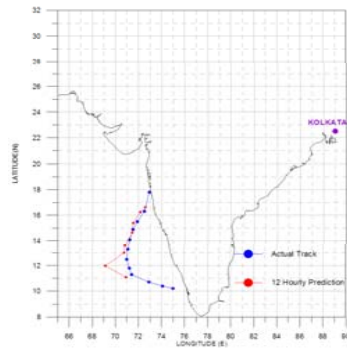
6/1/2010

8



Cyclone Track Prediction “PHYAN” - ANN Approach

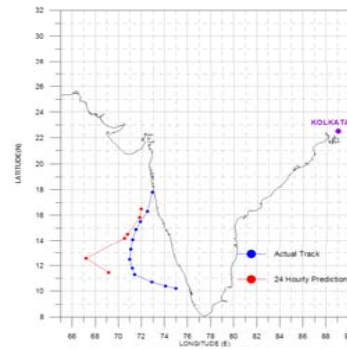
12 Hourly Prediction



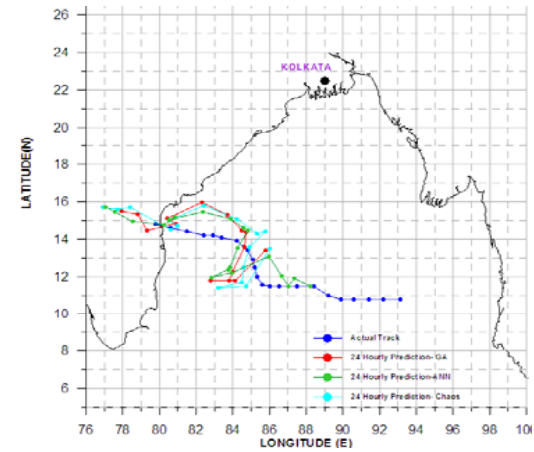
6/1/2010

13

24 Hourly Prediction



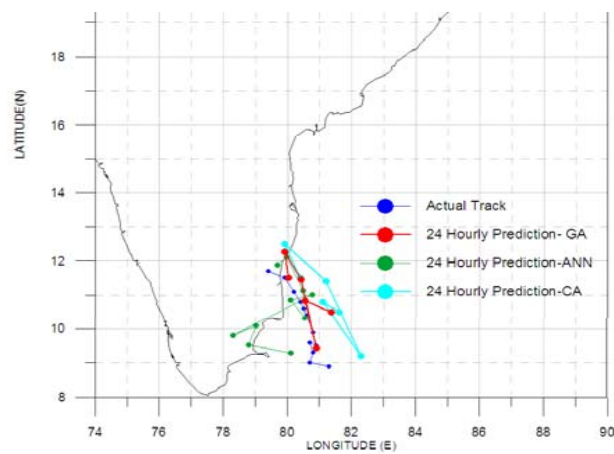
Comparison of 24 Hourly Cyclone Track Prediction- KHAIMUK



6/1/2010

14

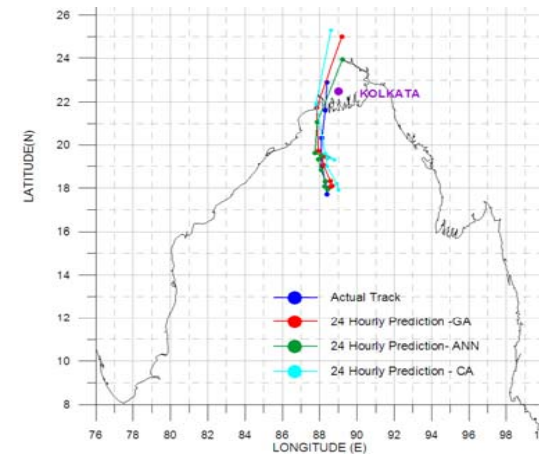
Comparison of 24 Hourly Cyclone Track Prediction- “NISHA”



6/1/2010

15

Comparison of 24 Hourly Cyclone Track Prediction- “AILA”



6/1/2010

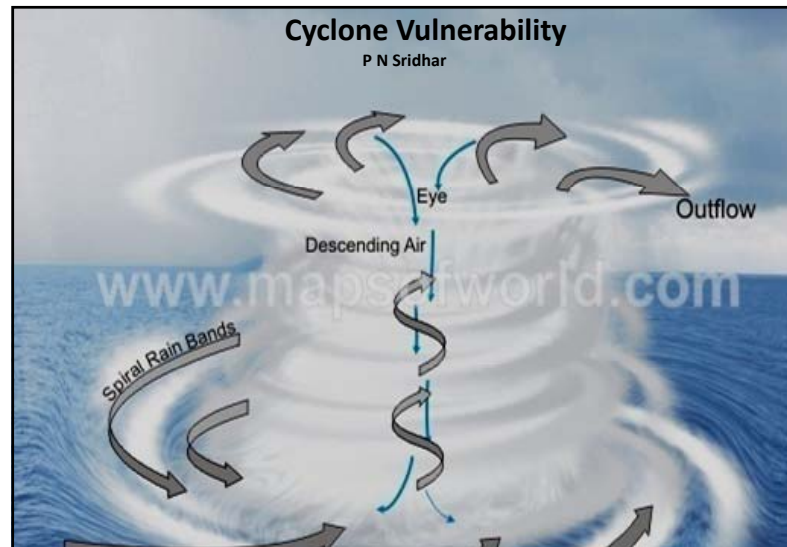
16

Comparison of 24 hourly Mean Distance Error by Different Approaches

Cyclone Name	Formation date	Mean Distance Error (MDE) in km		
		Chaos Algorithm	Genetic Algorithm	ANN Algorithm
KHAIMUK	10-Nov-08	165.06	157.13	148.45
NISHA	23-Nov-08	131.55	78.77	52.42
AILA	21-May-09	143.88	124.32	100.33
PHYAN	5-Sep-09	68.20	155.34	133.56

Future Plan:
Inclusion of oceanographic inputs like

- (i) cyclonic heat potential
- (ii) locations of eddies
- (iii) sea surface height



Vulnerability is a relative term with the following conception

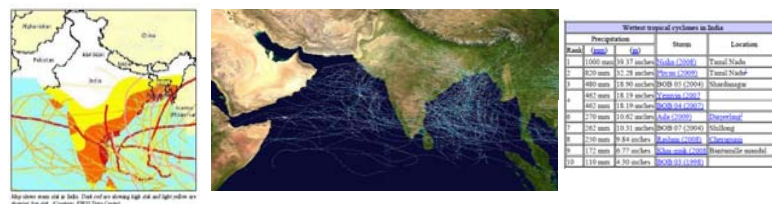
- ❑ a geographic area is at various degree of risks to threat, depending on its characteristics,
- ❑ in a geographic area the community, structure, service are likely to be affected, damaged or disrupted by the impacts of a hazard that depend on the nature, duration and proximity to the hazard.
- ❑ accordingly the areas is designated as susceptible (at the lower degree of risk) or vulnerable (at the higher degree of risk).
- ❑ The distinction between vulnerability and susceptibility marks the difference and awareness of this difference should give additional force ...in research ethics. It follows that 1) being fragile and liable to compound additional harm is susceptible and 2) being intact but fragile is vulnerable (Michael H kottow, University of Chile).
- ❑ Hence, a vulnerability assessment leads to calculation of social and economic ability to withstand or resist a particular hazard, so a risk management could lead to social and economic ability to cope with the disruption or loss.

40% of total population lives within 100 km ocean coast.

Indian subcontinent has experienced several cyclone which not only affected only coastal plain but also high altitudes especially with unprecedented rainfall and gale.

However, historical data reveals that east coast is more vulnerable than west coast to cyclones

A GIS based analysis, by Sheikh M. Nazmul Hossain and Ashbindu Singh of the USGS EROS Data Center shows that an estimated 54 million people in 20 Indian states extremely vulnerable to cyclone. However, quantitative assessment of vulnerability is random and arbitrary .



There are three elements that cause destruction, associated with a cyclone:
wind, storm surge, and rain

The main features of a cyclone that cause death and destruction are:

- ❑ Storm surge, a rapid increase in sea level along the coast, primarily caused by the strong surface wind field of the cyclone as it approaches the coast,
- ❑ the violent sustained wind and wind gusts or cyclonic gale with dense rainfall and
- ❑ the heavy rain and consequent flooding.

Where, when and how ?

Of those reported killed by natural disasters, 83 percent lived in Asia, while 67 percent lived in the nations with low human development indicators (IFRC, 2001).

Accounts for almost 38 percent of hydrological and meteorological disasters which occurred during the period 1991-2000 all over the world.

Cause and Effect:

Heavy and prolonged rains due to cyclones results rivers flood and inundation of low lying areas, pollute drinking water sources causing outbreak of epidemics.

Causes loss of life and property due to strong wind and gale

Short term Impact:

Cyclonic wind and rain during harvest time causes loss of standing crops and paralyse the livelihood of farmers and agriculture economy.

Long term impact :

Most of the farmland are non-cutivable due to sand deposition , Loss of livestock and artisans implements.

•Historical cyclone data reveals that Indian sub continent especially coast zone is extremely vulnerable to cyclone, however, extreme events of cyclone effects are recorded in the interior regions too. As per the IMD data West coast has 11 events

1	Oct 19-24, 1975	Crossed Saurashtra coast about 15 km to the northwest of Porbandar at 0930 UTC of October 22.the storm maintained its severe intensity inland up to Jamnagar Rajkot area. Maximum wind speeds were 160-180 (86-97 kts) 85 people died. The cyclone caused considerable damage to property (estimated to be about Rs. 75 crores.)
2	May 31-June 5, 1976	The storm crossed Saurashtra coast on the morning of June 3.Maximum wind speed of 167KM/h (90 kt) was reported by the Ship HAAKON MAGNUS. People killed 70-51 villages were affected badly:25,000 Houses were damaged : 4500 Cattle heads perished. The total damaged was estimated to be Rs. 3 crores.
3	Nov 15-23, 1977	Crossed near Honavar, Karnataka and Kerala coast affected. Tidal waves were reported to have damaged 620 Fishing vessels.
4	Oct 28 to Nov 2, 1981	Crossed Saurashtra coast close to and west of Mangrol shortly after mid-night of November 1 and moved closed to Porbandar in the early morning of November 2nd . then moving northeastwards as a severe cyclone upto Jamnagar, it weakened into a depression and lay near Radhanpur at 1200 UTC. About 5700 houses and about an equal number of huts were partially or fully damaged in Junagarh, Jamnagar districts.
5	Nov 4 to 9, 1982	Crossed south Gujarat coasts 5 km west of Kodinagar (Veraval) 511 persons lost their lives. 12624 Pucca and 54549 Kutchha houses destroyed. Damage to crop to the tune of Rs. 127.23 crores.
6	Oct 1-3, 1992	Crossed Oman coast on 3rd October morning and weakened rapidly into a low pressure area over Saudi Arabia by the morning of October 5th . the system did not cause any rainfall or damage to India.
7	Nov12 -15, 1993	Disipated off Gujarat -Sind coast on 16th early morning. No loss of life or damage to property on the Indian territory as the system weakened over the sea itself.
8	Nov15-20, 1994	Crossed north somalia coast on the early morning of November 20. As the system hit the sparsely populated region north of Somalia, the death toll reportedd to be 30 only.
9	June 17-20, 1996	Crossed near Diu between 2200 and 2300 UTC of 18th June. 33 people died and near about 2082 Cattle and 2472 people were affected in Maharashtra. 14 persons died and 1611 houses damaged
10	June 5-9, 1998	The cyclone crossed Gujarat coast north of Porbandar at 0200 UTC of June 9. The system maintained its intensity till noon when it lay over Gulf of Kutch port. Thence onwards, it moved north -east wards and weakened gradually. Total lives lost 1173 and 1774 persons were missing. Losses incurred due to storm were of the tune of Rs.1865 crores.
11	May 16-22, 1999	Crossed Pakistan coast to International Border in the afternoon of May 20. The system caused severe damage in Kutch and Jamnagar districts. Loss of life:453: Loss of property : Rs. 80 crores. Partial damage: 5153. In Rajasthan loss of life is one. Cattle heads perished :5104. Houses completely damaged : 50. Partially damaged: 5153.

Reference: NIO Publications & IMD

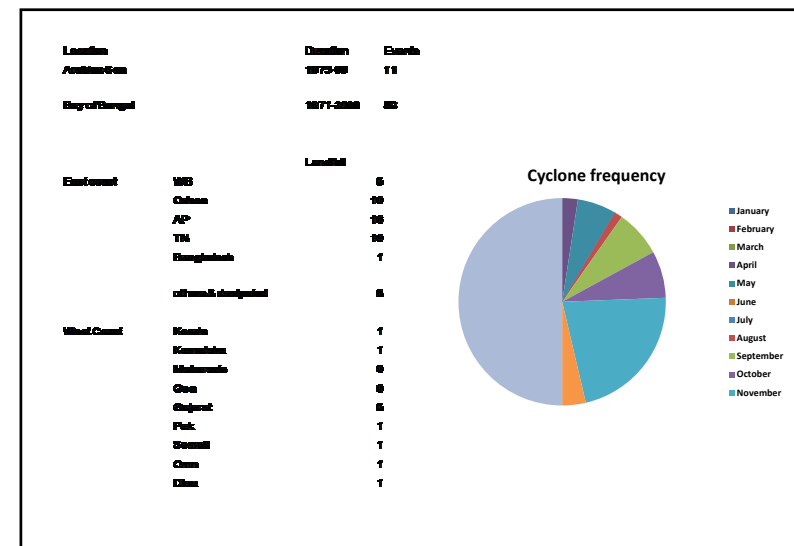
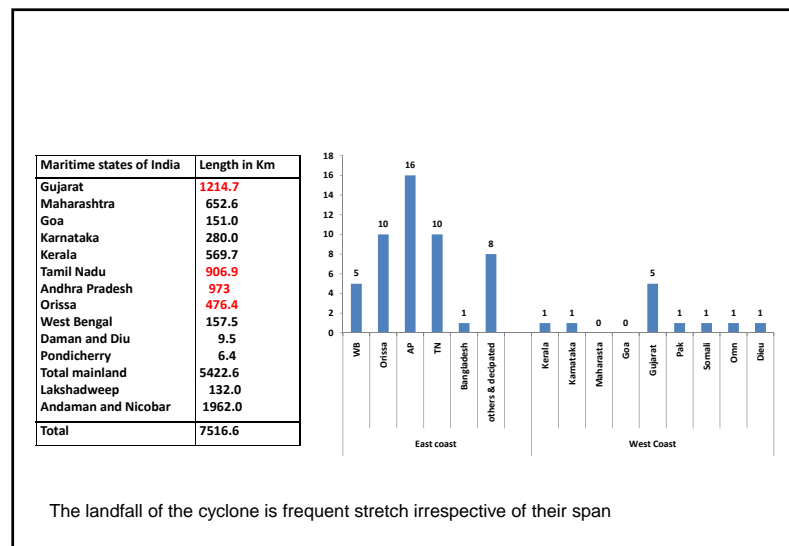
East Coast of India has		
1	Sept 7-14, 1971	Crossed south Orissa coast adjoining Northern Andhra on 10 th and killed 90 people and 8000 cattles
2	Sept 20-25, 1971	Crossed south Orissa coast on 22 nd and Damaged crops and houses due to flood in Vamsadhura of Koraput district
3	Sept 27-Oct 1, 1971	Crossed west Bengal coast near Sundarban on Oct, 1 killed 60 people and damaged 1000s of houses
4	Oct 26-30, 1971	Crossed Orissa near Paradip early October 30, max speed 150-74 kph (80-90 kts) 10000 died, home less a million, 50,000 cattle perished, 8, 00,000 houses damaged.
5	Sept 7-14, 1972	Crossed north AP near Baruva on 10 th , 100 people died and 8000 cattle lost. 2-lakh people affected
6	Nov 15-23, 1972	Crossed Southern AP at Sriharikotta on 22 nd with max wind of 111 -167 km/h .
7	Dec 1-8, 1972	Crossed Tamilnadu coast north of Cuddalore, Killed 80 people and homeless 30, 000 in Chennai, Loss Rs. 40 lakhs
8	Nov 3-9, 1973	Crossed Orissa Coast near Paradip,
9	Aug 13-20, 1974	Crossed WB near Contai at 139 KM/h (75kt)
10	Sept 6-19 1976	Crossed near Contai and reached SE MP on 13 th with max wind speed of 160km/h, 40 died and 4000 cattle perished. EL Rs 1.25lakhs
11	Nov 3-6 1976	Crossed Machillipatinam, AP, killed 25, 25, 000 huts damaged, 13 fishermen
12	Nov 15-17, 1976	Crossed Kavali, Nellore Dt on 16 th with 222-259 km/h , 30 people died and 10,000 homeless EL: Rs 4 Cr
13	Oct 27-Nov 1, 1977	Crossed at Kavalli, Nellore Dt, on 31 st

14	Nov 8-12, 1977	Crossed TN coast within 10 km to south of Nagapattinam early in the morning of 12th with 120 KMPH (65kt)560 people died and 10 lakh people rendered homeless. 23,000 Cattle heads perished. Total damage Rs. 155 crores.
15	Nov 14-19.1977	Crossed near Chirala in A.P On 19th Nov and weakened into a low on the evening of 20th. It dissipated over Southeast M.P Loss of human lives reported as 10,000. 27,000 Cattle head perished. Damage to the crops
16	Nov 19-24, 1978	Crossed between Kilakkarai and Ramanatharam District of TN.on 24th.evening as a severe storm and emerged into the Arabian Sea off Kerala. Max wind speed northerly 145 KMPH (78 kt). In India 5,000 huts damaged, EL in Rs. 5 cr. In SriLanka, 915 people died and one million people affected One lakh Houses were damaged in SriLanka.
17	May 10-13 1979	Crossed near Ongole in A.P on13 th May 1979.Nellore reported maximum wind speed of 100-160 KMPH (51-86 kt) 700 People killed and 3 Lakh cattle heads perished . Near about 40 Lakh people affected. House damaged 7 Lakh.
18	Nov .24-28. 1981	Crossed Orissa coast near Puri on September 26 and weakened into a depression on that evening over interior Orissa and adjoining MP.
19	Dec 4-11. 1981	Crossed West Bengal Coast near Sagar Island on December 10 and weakened into a depression on 11 th . 200 people died in 24- Parganas district of West Bengal One Million people affect in the districts of 24- Parganas.
20	May 31 to June 5 th 1982	Crossed on 3rd June near Paradip, caused heavy damage in the coastal districts of Puri , Cuttack and Balasore.
21.	Oct 11-17 , 1982	Crossed A.P. coast and adjoining Telengana as a low on 17 th morning. Heavy rainfall caused damage to roads.
22	Oct9-4.1984	Crossed North Orissa coast near Chandbali on14th
23	Nov 9-14, 1984	Crossed between Sriharikota and Durgarajupatnam on14th and the village, 54 lives in Tamil Nadu,1 lakh livestock perished and 3,20,000 houses destroyed in AP.

24	Nov 27-30, 1984	Crossed south Tamilnadu coast near Nagapattinam on December 1 near Karaikal. About 35,000 people were affected Tamilnadu. 50,000 acres of land.
24	Sept. 17-21, 1985	Crossed on 20 th close to Puri Orissa.
25	Oct, 13-17, 1985	Crossed near Balasore. High tidal Crossed near Balasore.
26	Oct, 31-3 Nov. 1987	Crossed north of Nellore (A.P.) 50 People died in .A.P. 50 people died and 25,800 live stocks A.P. 68,000. Houses damaged.
27	Nov, 23-30, 1988	crossed 20 Indo-Bangladesh border on 30 th , 2000 People killed. 6000, people reported missing in Bangladesh.
28	May 23-27, 1989	crossed 40 Km northwest of Balasore 61 persons died in Orissa and West Bengal 1000 Cattle heads perished in West Bengal.
29	Nov 01-09, 1989	Crossed near Kavali (A.P.). 69 people died and 7100 cattleheads perished. Loss of property estimated to be Rs. 14 Crores.
30	May 04-09, 1990	Crossed 40 Km SW of Machilipatnam 967 people died. 3.6 million livestock perished. 14.3 lakh houses damaged.
31	April 24-30, 1991	crossed Chittagong (Bangladesh) across Sandweep Island. 13200 people died Sandweep Island. 13200 people died. Colossal loss of property. One among The most devastating cyclones affected. The most devastating cyclones affected Bangladesh.
32	Nov, 11-15, 1991	Crossed Tamil Nadu Coast north of Karaikal 185 people died and 540 cattle perished 16 people died in A. P. History of Past Cyclones.
35	Nov, 11-17, 1992	Crossed near Tuticorin (Tamil Nadu), 175 people died and 160 reported missing Damage to standing crops due to flood Reported.
36	Dec 01-04 1993	Crossed on 4th Nov. 30 Km north of Karaikal. 100 People died in Tamil Nadu.
37	April 29-May 02 1994	Crossed near Bangladesh on May 2. Loss of life was limited to 188 due to timely and adequate cyclone warning issued by Bangladesh Met.
38	Nov. 07-10, 1995	Crossed North A.P. Coast south of Ichchapuram, 05 Persons and 81 boats were affected. 2631 houses damaged. 153 fishermen were reported to be missing.
39	Nov 05-07 1996	Crossed A.P. Coast 50 Km south of Kakinada around on 6th Nov. 978 Persons died. 1375 Persons reported to be missing. 1300 Villages affected in A.P. 6464 boats lost in sea.
40	Nov. 28-06 Dec 1996	Crossed near Chennai on 6th Dec. 1996. The cyclone persisted for 9 days which is reported to be very long life compared to any cyclone in the Indian Ocean. It caused severe damage to life and property.
41	Nov 15, 1999	Super cyclone, Orissa that crossed Orissa coast caused havoc and huge loss of life and resource.

Wettest tropical cyclones in India				
Rank	Precipitation		Storm	Location
	(mm)	(in)		
1	1000 mm	39.37 inches	Nisha (2008)	Tamil Nadu
2	820 mm	32.28 inches	Phyan (2009)	Tamil Nadu
3	480 mm	18.90 inches	BOB 05 (2004)	Shardanagar
4	462 mm	18.19 inches	Yemyin (2007)	
	462 mm	18.19 inches	BOB 04 (2007)	
6	270 mm	10.62 inches	Aila (2009)	Darjeeling
7	262 mm	10.31 inches	BOB 07 (2004)	Shillong
8	250 mm	9.84 inches	Rashmi (2008)	Cherapunji
9	172 mm	6.77 inches	Khair-muk (2008)	Bantumille mandal
10	110 mm	4.30 inches	BOB 03 (1998)	

http://en.wikipedia.org/wiki/List_of_wettest_tropical_cyclones_by_country



Vulnerability to storm surges is not uniform along Indian coasts. The following segments of the east coast of India are most vulnerable to high surges

i) North Orissa, and West Bengal coasts.

ii) Andhra Pradesh coast between Ongole and Machilipatnam.

iii) Tamil Nadu coast, south of Nagapatnam.

The West coast of India is less vulnerable to storm surges than the east coast of India in terms of both the height of storm surge as well as frequency of occurrence. However, the following segments are vulnerable to significant surges :

i) Maharashtra coast, north of Harnai and adjoining south Gujarat coast and the coastal belt around the Gulf of Bombay.

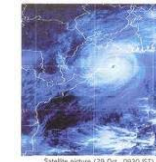
ii) The coastal belt around the Gulf of Kutch.

IMD-Mumbai

- To explain this, I have taken to events of Bay of Bengal cyclones both are destructive both economically and socially.....

- Super Cyclone - 25th-30th October 1999,
- Nisha - 25th -29th November 2008, Respectively affected Orissa and TN.

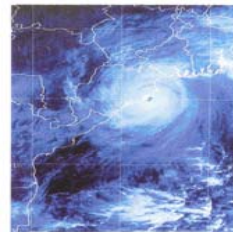
The cyclone (severe) struck Orissa coast with a max wind speed of 300 km per hours (162 kts) accompanied with 7 meter high storm surges.



Satellite picture (29 Oct., 0930 IST) of 1999 Orissa Super Cyclone.

India Meteorological Department Tropical Cyclone Intensity Scale	
Category	Sustained winds (3-min average)
LOW or N/A:	
Category 1:	Category 3:
Category 2:	Category 4:
	Category 5:
Super Cyclonic Storm	>130 kts >222 km/h
Very Severe Cyclonic Storm	64-119 kts 118-221 km/h
Severe Cyclonic Storm	48-63 kts 88-117 km/h
Cyclonic Storm	34-47 kts 62-87 km/h
Deep Depression	28-33 kts 52-61 km/h
Depression	≤27 kts ≤51 km/h

The average annual rainfall is about 1300 mm (51 inches), Chennai average maximum Wind Speed during normal days : 12 mph



Satellite picture (29 Oct., 0930 IST) of 1999 Orissa Super Cyclone



There was a down pour of 447 mm to 955 mm in coastal and central Orissa.



275,000 homes were destroyed, leaving 1.67 million people homeless. 19.5 million people were affected by the super cyclone. A total of 9,803 people officially died from the storm, with 40 others missing, 3,312 people were injured. 2,043 out of 5,700, or 36% of the residents of Padmapur perished. The number of domestic animals fatalities was around 2.5 million and number of livestock that perished in the cyclone amounted to only 406,000. The high number of domestic animal deaths may have possibly had to do with around 5 million farmers losing their livelihood. The damage across fourteen districts in India^[2] resulted from the storm was approximately \$4.5 billion (1999 USD, \$5.1 billion 2005 USD).^[3]



Super Cyclone Oct 29-31, 1999

Affected area	46 municipalities and 17,993 villages in 14 districts	
Affected population	19 million	
Killed	8,479	
Homeless	8.26 million	
Houses damaged	2.06 million	
Crop damaged	2.1 million Ha (mainly Paddy/Rice) worth INR 18 billion (USD 391 million)	
Livestock killed	2.479 million heads	
Total Damage	INR 62.2759 billion	USD 1.3538 billion



Source: ARCHDIOCESE OF CUTTACK

Out of total number of 30 Districts, 11 coastal districts were heavily affected leading to a death toll of more than 10,000 people.

The heavy rainfall resulted in flooding and devastated large tracts of central and northern districts. The two cyclones, with attendant rains and tidal waves left over thirteen million people affected. Incessant rain affect high and low topography Inundation and flood submerge habitations.

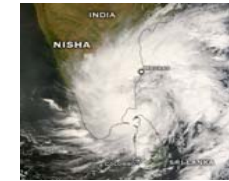
In the recorded history of cyclones, more than a million lives have been lost in India and Bangladesh in 21 cyclones in Bay of Bengal. In October 1999 two cyclones struck the state of Orissa, in the east coast of India, within a gap of fifteen days.

The relative vulnerability of coastal districts of India using an integrated vulnerability index that takes into account *impact*- induces by present day and future climate pressures, as well as the *adaptive capacity* of the districts characterized by a range of physical, economic, social and demographic parameters.

A rough estimate by FAO (1999) indicates that in the past three decades Andhra Pradesh lost 40 percent of its mangroves to shrimp farming, while the corresponding loss in Orissa, Tamil Nadu and West Bengal are 26 percent, 26 percent and 1.25 percent, respectively. It may be noted that majority of the highly vulnerable districts as per the estimations in this study are located in these four states.

Madras School of Economics says that, Cyclone associated scenario aggravates with rise in sea-level is likely to be a gradual process numerous adaptation problems-

27 Nov 2008 ... Chennai: Cyclone 'Nisha', with wind speed of 75 km, moved slightly northwards and crossed the Tamil Nadu coast close to north of Karaikal



Tropical Cyclone 2008 North Indian Ocean Nisha		
Formed	November 25, 2008	Duration
Dissipated	November 29, 2008	4 days
Highest wind speed	85 Km/hour (3minutes sustained) 100 km/hour (1 minutes sustained)	
Lowest pressure	996 hPa (mbar)	
Fatalities	204	
Estimated loss	\$ 800 million (USD)	
Regions affected	India and Sri Lanka	

Chennai: Cyclone Nisha, with wind speed of 50-75 km/hr, Thanjavur – 53 cm, Vedaranyam (Nagapattinam district) – 42 cm, Adirampattinam (Thanjavur) – 33 cm, Muthupet (Tiruvallur dt) – 30 cm and Kumbakonam (Thanjavur) – 26 cm.

It broke the 65-year record of the highest rainfall registered in 24 hours in the State. In two days, Orathanadu registered 99 cm.

Compilation of historic cyclone data show that

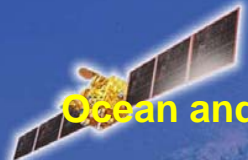
- 1) Intensity (wind and rainfall) is unpredictable,
- 2) Uncertain land fall and sustainability over land
- 3) Inherently coastal regions is low lying and prone to inundation due to its drainage characteristics,
- 4) Natural drainages are distorted and man made flood channels are not maintained
- 5) Death, damage and loss estimates are impure
- 6) Most of the flooded areas are not suitable for habitation but occupied or allotted
- 7) Loss other than cyclone also accounted for cyclone
- 8) Damaged dwelling are hutments and not suitable under adverse weather conditions
- 9) Most of the natural storage tanks, lakes and soil top are modified
- 10) Coastal community is not aware of veracity of the hazard
- 11) Timely assessment of the damage, mobilization and rehabilitations are not practiced or reaching the deserved.

□Require prediction well in advance for Agriculture and forming

Cyclone Risk Mitigation

- Construction of cyclone shelters,
- Protection by Shelter belt plantations,
- Mangrove regeneration,
- Construction of embankments to stop sea water inundation,
- Improve the lake and tank capacity
- Construction of missing road links,
- flood channels desilting

Require prediction well in advance for Agriculture and



Ocean and Atmospheric Programme

Earth Observation System ISRO HQ

Workshop on
Utilisation of Oceanic Heat Content
for Cyclone Studies
March 25-26, 2010
National Remote Sensing Centre,
Hyderabad

Ocean & Atmospheric Studies – Early Experiences

SEASAT
SAR (L-band)
Altimeter
Scatterometer
SMMR
VIS/IR Radiometer


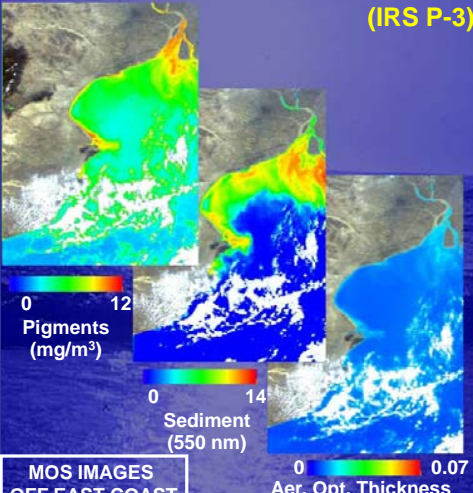
1963 SOUNDING ROCKETS
Atmospheric profiles upto 80 - 100kms
Atmospheric dynamics during Monsoon onset
Stratospheric warming and impact on monsoon

1978 NIMBUS - 7
Coastal Zone Color Scanner (CZCS)
SMMR

1979 BHASKARA - 1
TV CAMERA
SAMIR

FIRST OCEAN IRS MISSION (IRS P-3)

1996

MOS IMAGES OFF EAST COAST

- Pigments (mg/m³)**: 0 to 12
- Sediment (550 nm)**: 0 to 14
- Aer. Opt. Thickness (750 nm)**: 0 to 0.07

Joint ISRO-DLR Ocean Mission

Major Observations:

- MOS A – 4 Bands: Aerosol Characterization
- MOS B – 13 Bands: Ocean Colour Studies
- MOS C – 1 Band: Snow & Vegetation Studies

Ocean Applications:

- Algorithm for Ocean Color
- Chlorophyll-a Mapping
- Experiments for Color-temp Relationship for Fisheries; Water Clarity Maps
- Preparatory Phase For IRS-P4 Applications

OCEANSAT-1: GLOBAL OCEAN OBSERVATION MISSION (IRS P-4)

1999

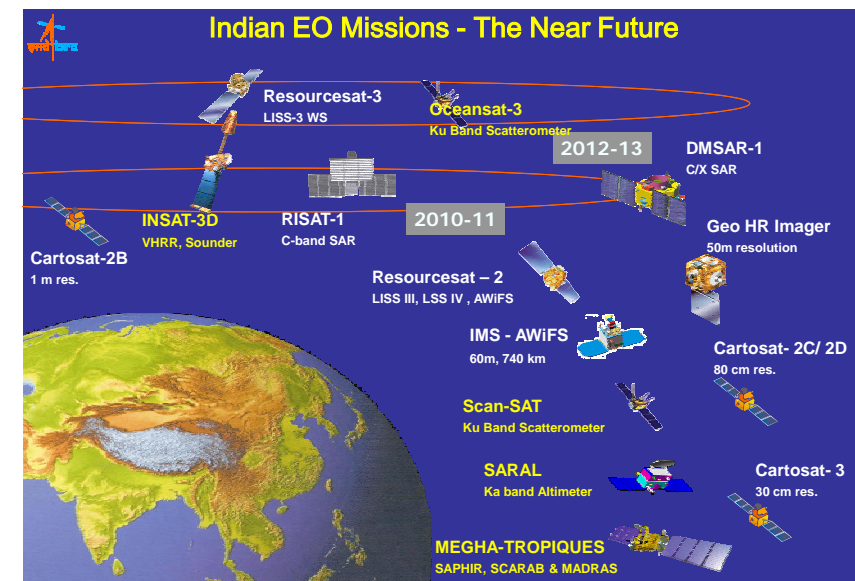
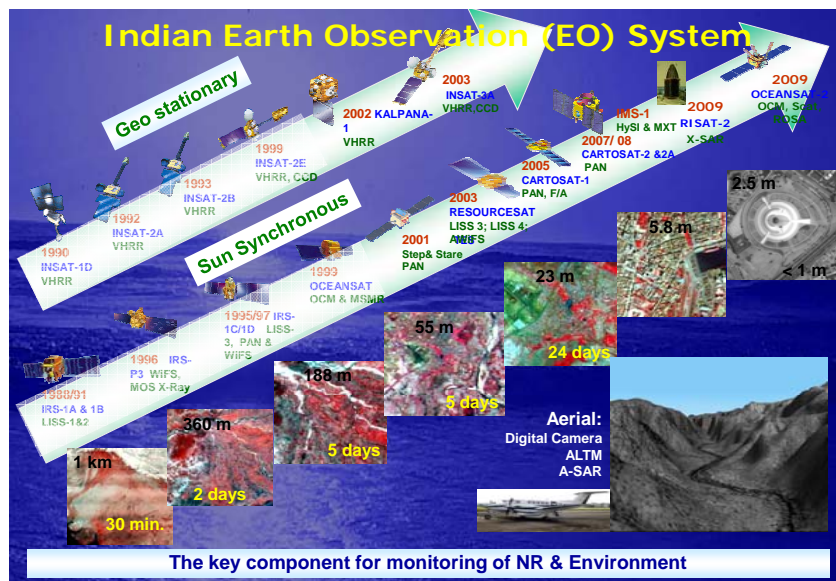
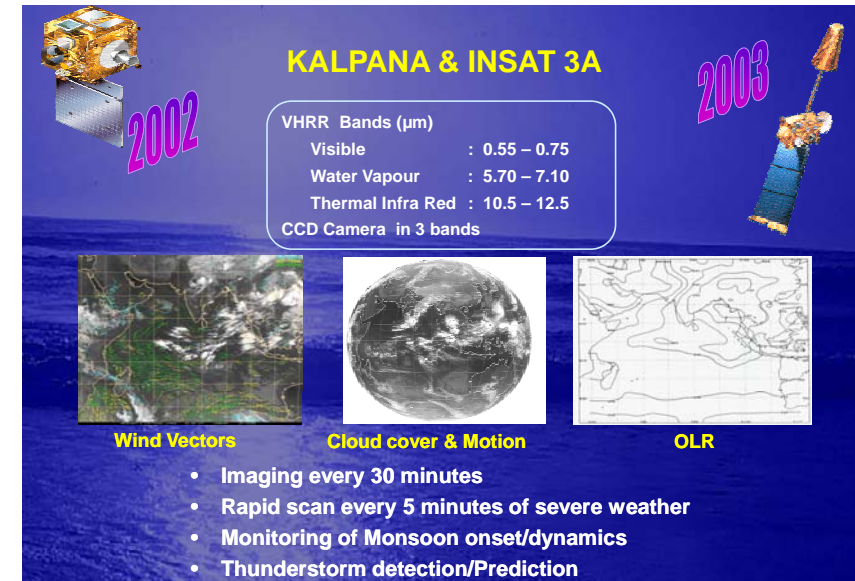
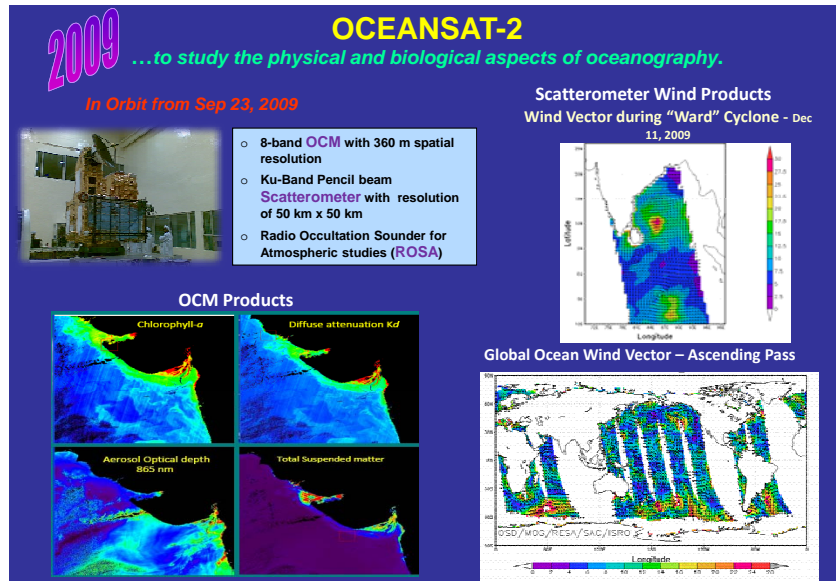



OCM

- 8 Spectral Bands
- ~ 360 M Resolution
- 2 Day Repetivity
- Water-leaving Radiances
- Diffuse Attenuation Coefficient
- Chlorophyll-a, Yellow Substance & Suspended Sediment Concentrations
- Aerosol Optical Thickness

MSMR

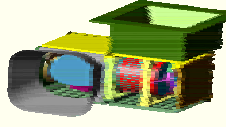
- 4 Freq. Dual Polarisation MW Radiometer
- Global Coverage, 2 Day Repetivity
- Antenna Temperature Data (ATD)
- Brightness Temperature Data (BTD)
- Geophysical Parameter – Wind, SST, Humidity
- Monthly Average Product (MAP)





INSAT - 3D

Improved Understanding of Meso-scale Systems



6 Channel IMAGER

- Spectral Bands (μm)

Visible	: 0.55	- 0.75
Short Wave Infra Red	: 1.55	- 1.70
Mid Wave Infra Red	: 3.70	- 3.95
Water Vapour	: 6.50	- 7.10
Thermal Infra Red - 1	: 10.30	- 11.30
Thermal Infra Red - 2	: 11.30	- 12.50
- Resolution

: 1 km for Vis & SWIR
4 km for MIR & TIR
8 km for WV

19 Channel SOUNDER

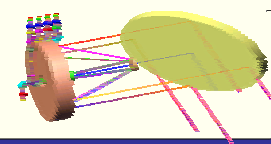
- Spectral Bands (μm)


Short Wave Infra Red	: Six bands
Mid Wave Infra Red	: Five Bands
Long Wave Infra Red	: Seven Bands
Visible	: One Band
- Resolution (km)

: 10 X 10 for all bands

- No of simultaneous

: 4 sounding per band





Megha Tropiques - A Joint ISRO-CNES Mission

For studying water cycle and energy exchanges to better understand the life cycles of the tropical convective system

Observations of tropics

- Water vapour
- Clouds
- Cloud condensed water
- Precipitation
- Evaporation

+ GPS RO

Contributing to Global Precipitation Mission (GPM)

SAPHIR

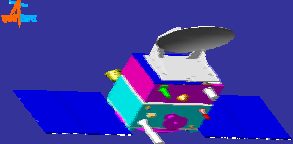
- Water vapour profile
- Six atmospheric layers upto 12 km height
- 10 km Horizontal Resolution

SCARAB

- Outgoing fluxes at TOA
- 40 km Horizontal Resolution

MADRAS

- Precipitation and Cloud properties
- 89 & 157 GHz : ice particles in cloud tops
- 18 & 37 GHz: Cloud Liquid Water and precipitation; Sea Surface Wind speed
- 24 GHz : Integrated water vapour



SARAL

Satellite with ARGOS and AltiKa
- Joint ISRO-CNES Mission

Polar - sun-synchronous; Inclination of 98.38 Deg;
Altitude ~800 km; Repeat cycle of 35 days

ALTIKA - Ka-band Altimeter

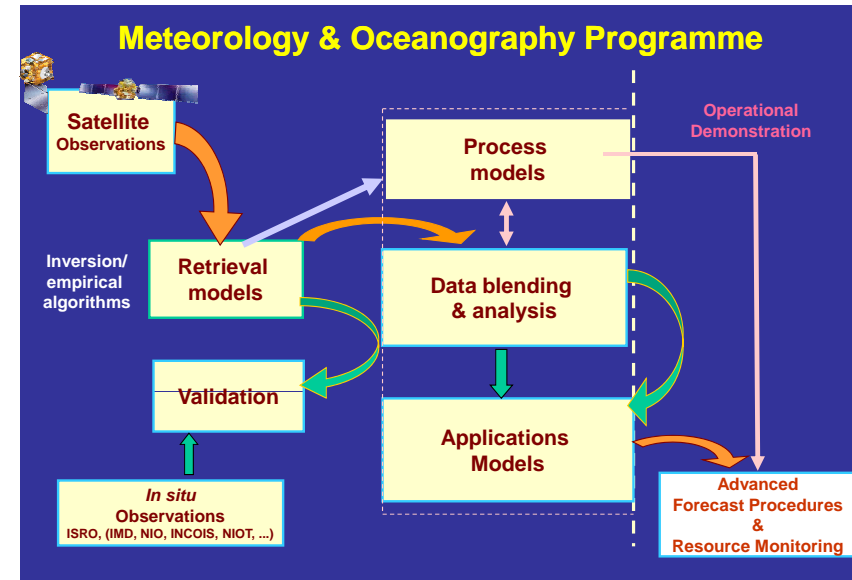
- A complement to JASON-1, and gap-filler for ENVISAT Altimetry
- Payload includes:
 - Ka-band Altimeter (~35.5GHz)
 - Dual frequency Radiometer (23.8/36.8 GHz)
 - A DORIS receiver
 - Laser Retro-reflector Array

For precise orbit determination

Data Utilisation and Application Programmes.....

Utilisation Programmes

- Well planned data Utilisation Programmes (UP) are launched with each mission
- Currently, UPs on Oceansat-2, Megha Tropiques and SARAL are on.
- Participation from all the relevant Institutes and Universities are ensured.
- The programme aims at improved parameter retrieval, calibration & validation and advanced applications.
- Through Announcement of Opportunity International participation is sought and being carried out.
- Oceansat-2, SARAL and MT being global missions, availability of NRT data within 180 minutes to modelers, Cal/val in globally distributed sites, distribution through ftp/ websites are being planned through bilateral cooperations with international agencies.



Weather & Ocean Information retrieval under MOP

- Temperature & humidity distribution in atmosphere (MODIS, INSAT-3D)
- Sea surface & land surface temperature (MODIS, INSAT-3D)
- Winds in atmosphere at selected levels (INSAT, METEOSAT)
- Ocean surface winds and waves (QSCAT, OS-II, RISAT, JASON, SARAL)
- Sea-level anomalies (JASON, SARAL)
- Radiation components at ocean surface and top of atmosphere (MT)
- Atmospheric ozone, aerosols and dust (MODIS, OCM)
- Distribution of clouds and rain (INSAT, MT, METEOSAT, TRMM)
- Total water vapour, liquid water, ocean surface winds (TRMM, MT, SSM/I)
- Distribution of chlorophyll, sediments and CDOM (OCM)
- Soil Moisture and ocean surface salinity (MSMR, TRMM, SMOS)

Geophysical Parameter Retrieval

KALPANA & INSAT 3A

AMV, OLR, UTH, Rain, SST

INSAT 3D

AMV, OLR, UTH, SST, QPE, Snow, Smoke/Aerosol, Ozone, NDVI,

Megha Tropiques

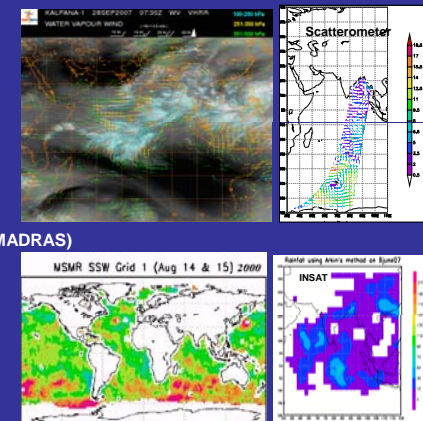
Rainfall, Total Precipitable Water, Cloud Liquid Water, Sea Surface Winds (MADRAS)
Humidity Profile (SAPHIR)
Radiation Fluxes (SCARAB)

OCEANSAT-II

Surface winds from scatterometer
Chlorophyll, sediments, CDOM

SARAL

SSH, SWH



Meteorological Applications

• CYCLONE

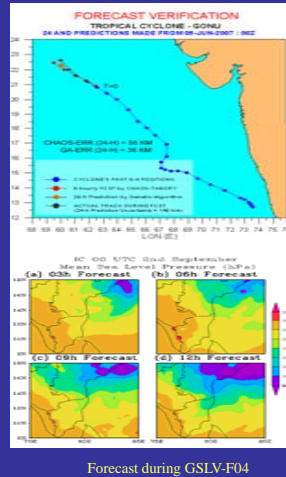
- Tracks of 4 tropical cyclones during 2009 predicted in real time.
- The average landfall accuracy (24-H lead time) for all the cyclones that reached the coast was better than 50 km

• MONSOON

- Seasonal Prediction: JJAS rainfall for 2009 was predicted as 94% of normal.

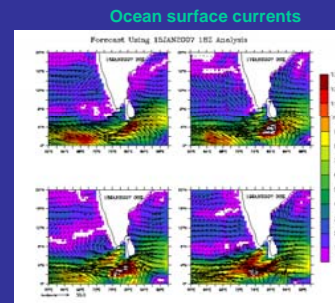
• Assimilation of INSAT & PRWONAM data for prediction during launch :

- Real-time meso-scale predictions over SHAR region (with assimilation of INSAT/KALPANA products and PRWONAM data) for the launches.

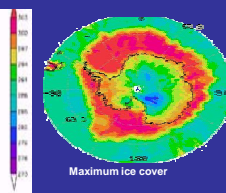
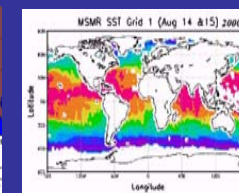
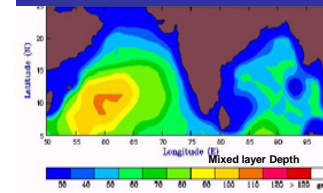


Physical Oceanographic Applications

- Ocean State forecast of Wave height, MLD, salinity, surface current and SST
- Data assimilation in ocean models
- Optimum ship routing using Satellite Data
- Polar ice and climate change

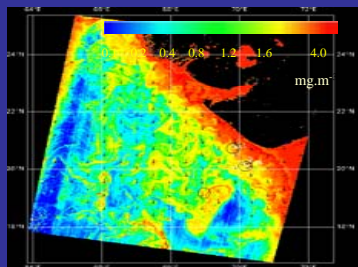
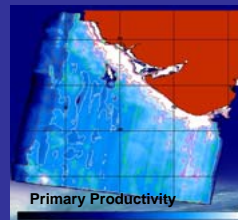


Mixed layer Depth



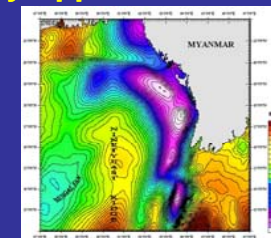
Biological Oceanography Applications

- Potential Fishery Zone Forecast (integration of Chl, SST, winds)
- Primary productivity modeling
- Deep water productivity (Tuna)
- Bio-geo-chemical analysis for nitrate & carbon cycle

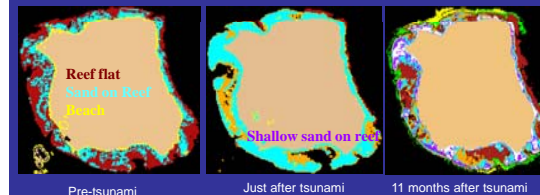


Coastal & geological Oceanography Applications

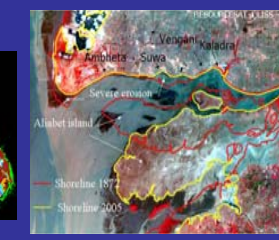
- Coastal habitat
- Coastal processes
- Satellite Geoid/Gravity Modelling for Lithospheric Studies



Coral Reef Monitoring (Andaman Reef)



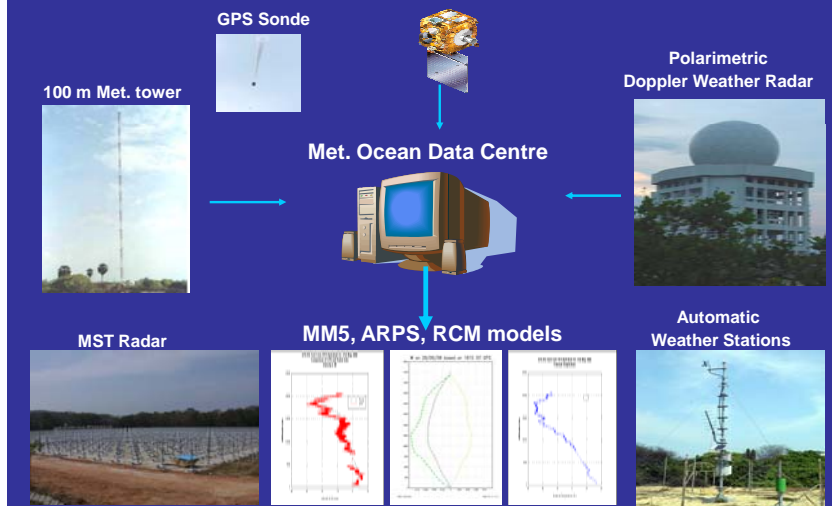
Marine lithosphere (Altimeter)



Shoreline Changes



Integration of Space & Ground Observations

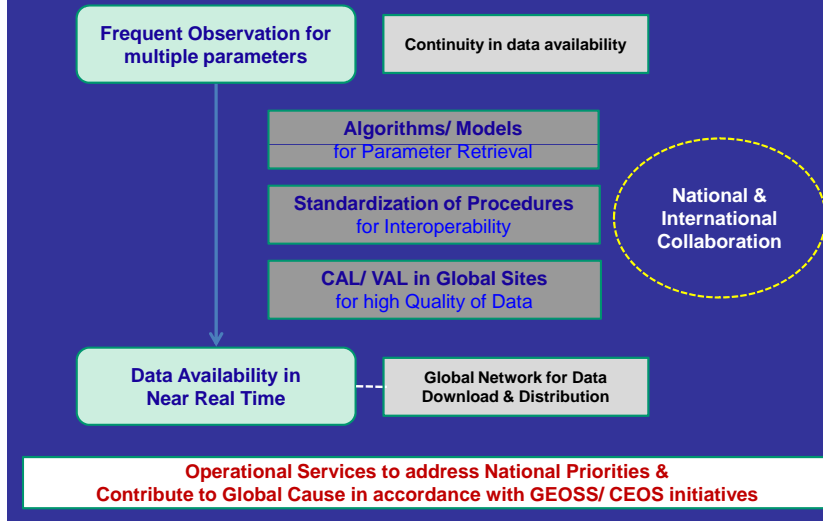


CAL-VAL Site at Kavaratti

- Operationalized reference CAL-VAL site at Kavaratti in Lakshadweep and demonstrated for OCEANSAT-II/ OCM-II vicarious calibration/validation
- Daily every hourly in-situ data collection, transmission and reception at SAC and INCOIS
- Site augmented with Automatic Weather Station, Disdrometer, and being augmented with Micro-rain radar, Dr.Pisharoty Radiosonde, etc.
- Useful for Oceansat-II, Megha-Tropiques, INSAT-3D and future MOP projects for product validation
- Identified for joint ISRO-NASA-NOAA and India-Australia efforts for OCM-II Calibration/validation



EO Strategy for Ocean and Atmosphere



Thank you....

Sustained Ocean Observing System for Tropical Cyclone forecasts and Studies

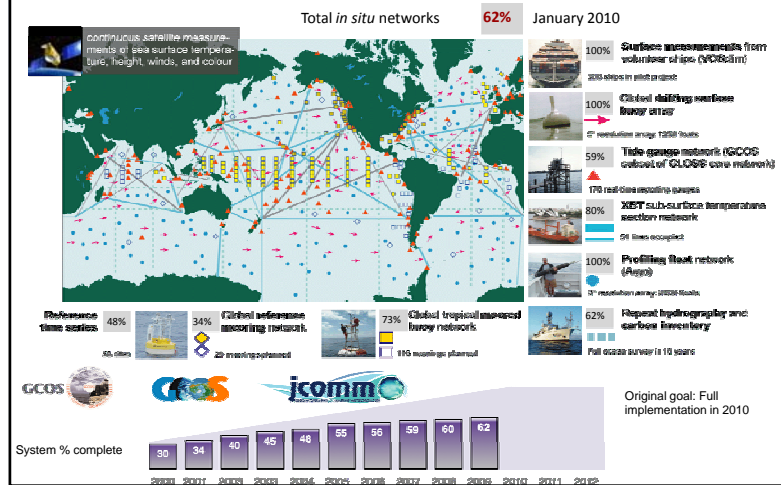
Gustavo Jorge Goni (NOAA/AOML)
gustavo.goni@noaa.gov



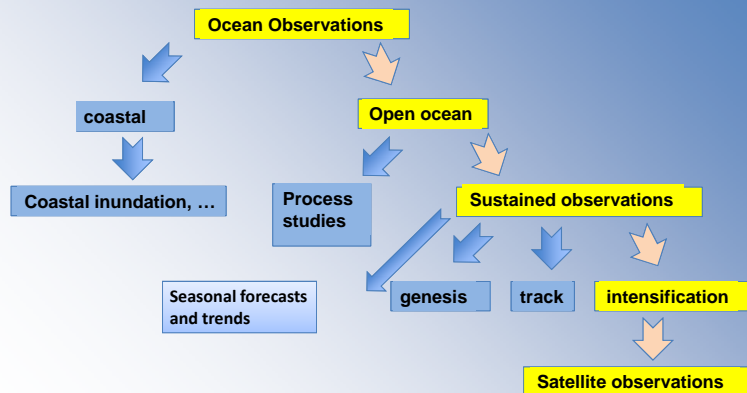
Workshop on
Utilization of Satellite Derived Oceanic Heat Content
for Cyclone Studies

Hyderabad, India, March 25-26, 2010

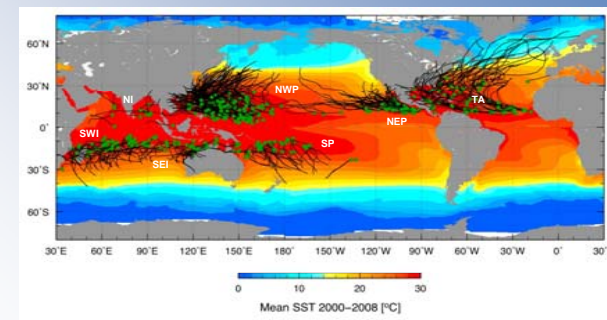
Initial Global Ocean Observing System for Climate Status against the GCOS Implementation Plan and JCOMM targets



Ocean observations for tropical cyclone studies and forecasts

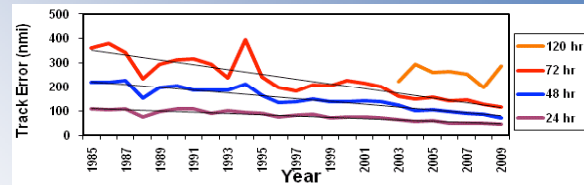


Tropical cyclone basins genesis and SSTs

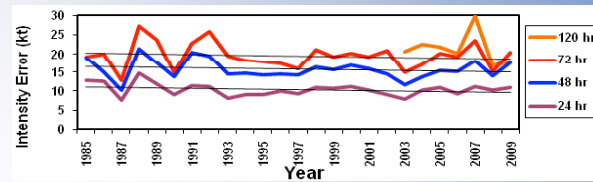


Goni et al 2009

Error reduction in TC track and intensity forecast Tropical Atlantic Ocean



48 hr track – 3.7 improvement per year

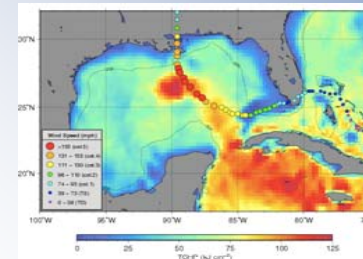


48 hr intensity 0.6% improvement per year

DeMaria, 2010



What studies in the tropical Atlantic have taught us Mesoscale features and upper ocean thermal structure



Mainelli et al, 2008
Goni et al, 2009

→ Realistic detection of mesoscale features

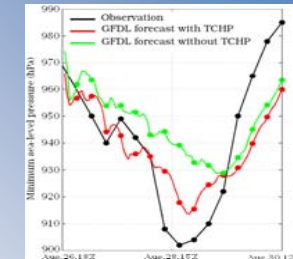
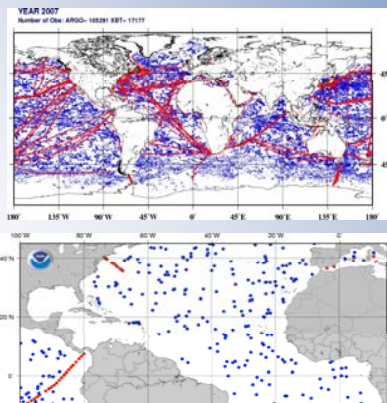


Figure by I. Ginis
Goni et al, 2009

→ Realistic monitoring of vertical thermal structure



Sustained ocean observations: Argo floats and XBTs



→ Cannot resolve mesoscale features

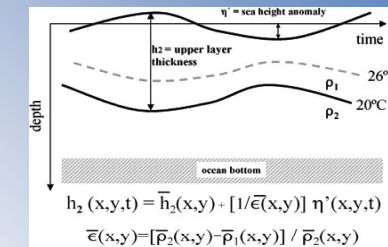
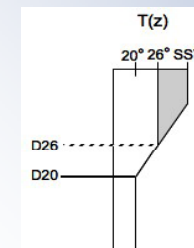


Tropical Cyclone Heat Potential (TCHP)

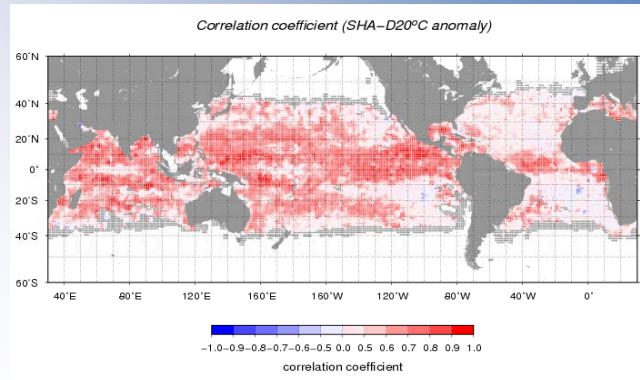
Hurricane Heat Potential (HHP), Ocean Heat Content (OHC)

www.aoml.noaa.gov/phod/cyclone

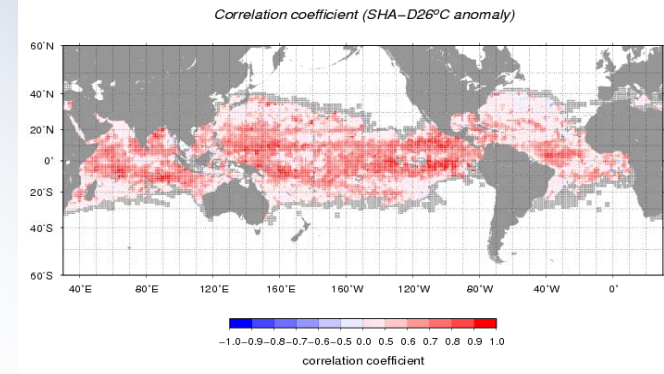
$$\text{OHC} = c_p \int_0^{D26} \rho [T(z) - 26] dz,$$



Depth of 20°C isotherm and sea height



Depth of 26°C isotherm and sea height



Tropical Cyclone Heat Potential (TCHP)

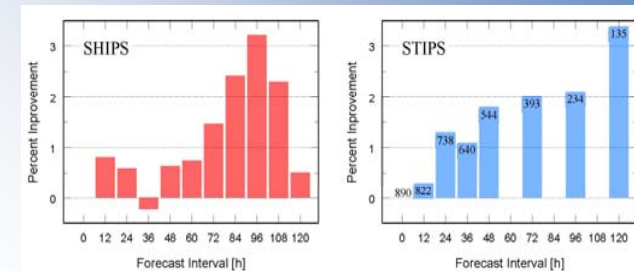
Hurricane Heat Potential (HHP), Ocean Heat Content (OHC)

Data distribution:
www.aoml.noaa.gov/phod/cyclone



Upper ocean thermal structure in individual TC forecasts:

Mean results for the Atlantic (SHIPS) and the NE Pacific (STIPS)

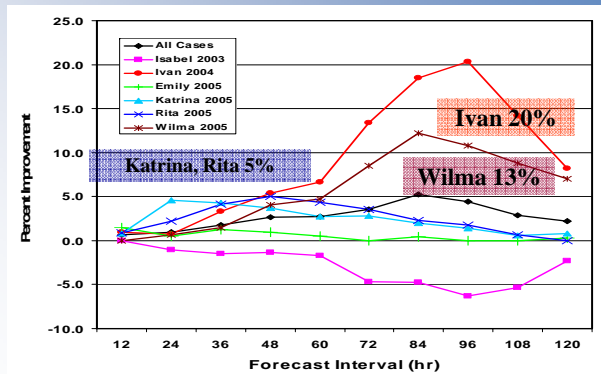


Goni et al, 2009

Is this really a good improvement ?



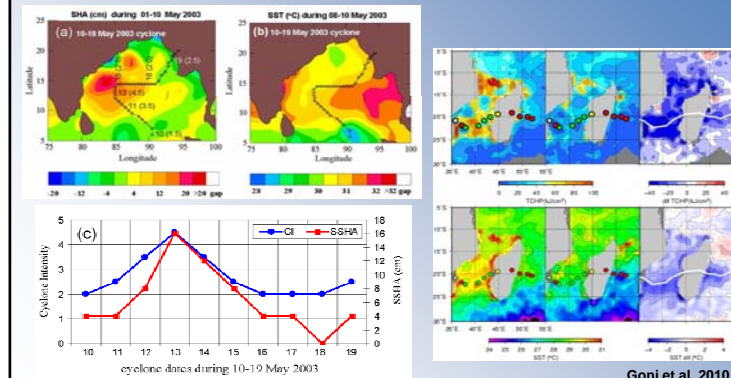
Upper ocean thermal structure And individual TC forecasts



Mainelli et al, 2008



Upper ocean thermal structure in individual TCs Indian Ocean

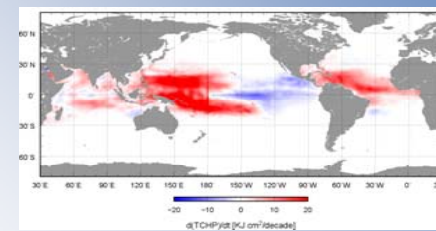
Figure by M.M. Ali
Goni et al, 2009

Current efforts in different basins

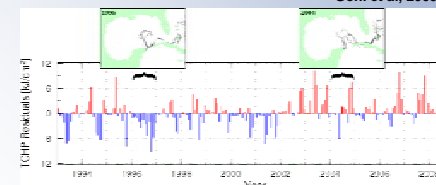
basin	agency	effort	mode
Atlantic	NOAA/NWS	SHIPS (statistical)	operational/research
	NOAA/GFDL	HYCOM + HWRF	research
	NOAA/NCEP	HYCOM + HWRF	operational
	U Miami and NOAA	HYCOM + HWRF	research
	NOAA	Ocean TCHP	To operational/analysis
	Mercator	Global upper ocean forecast	operational
NW Pac.	Nat. Taiwan Univ.	Ocean TCHP	Research/analysis
NE Pac.	US Navy and NOAA	STIPS (statistical)	operational
N Indian	Nat. Remote Sensing Center	Upper ocean monitoring	research/analysis
SW Pac.	BOM	CLAM/blue Link	Operational Ocean
SW Indian		TCLAPS	Research/analysis
SE Indian	UCP and NOAA	TCHP	research/analysis

Adapted from a more complete
table from Goni et al, 2010; some current
efforts may be incomplete and/or missing

Tropical Cyclone Heat Potential (non-secular) Trends (1993-2008)



Goni et al, 2009



Goni et al, 2009



Sustained *global* ocean observing system for TC intensification studies and forecasts

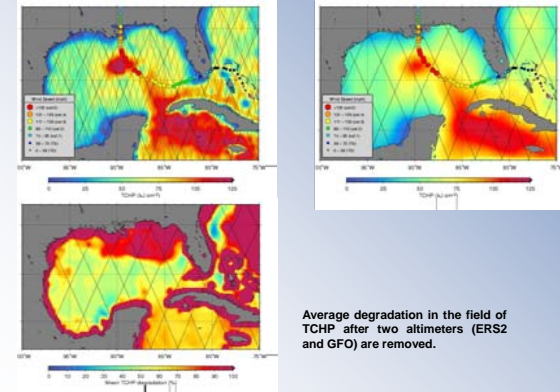
The current system was not designed for this type of studies.

- 1) An ocean observing system able to resolve mesoscale features
 - 2) An ocean observing system able to resolve their vertical thermal structure.
- * Implementing such a system could be impossible.
- 3) From what is already in place, satellite altimetry appears to be the most adequate tool, since resolve mesoscale and since the parameter that measures is linked to the upper ocean thermal structure.
- * In situ systems continue to play a critical role in process studies, to assimilate in numerical models, and to validate model outputs.

→ Is TCHP this the right ocean parameter ?



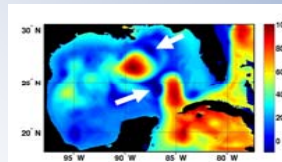
Ocean Observations: Satellite Altimetry, TCHP estimates degradation



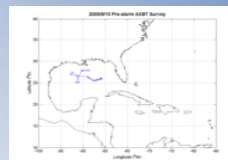
Average degradation in the field of TCHP after two altimeters (ERS2 and GFO) are removed.



One modeling effort (HYCOM-HWRF) NOAA/AOML and NCEP

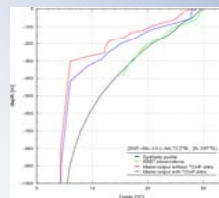
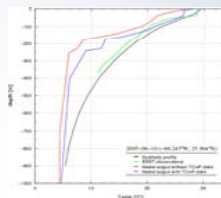


The features are approximately right, but the vertical thermal structure needs improvement.



AXBT survey pre-hurricane Rita (AUG 2005)

Goni et al, 2009



Green = AXBT
Black = altimetry
Red and blue = HYCOM

HYCOM has a colder ocean in the GOM.

Figures by Avichal Mehra



Ocean Obs'99 Recommendations

THE OCEAN OBSERVING SYSTEM FOR TROPICAL CYCLONE INTENSIFICATION FORECASTS AND STUDIES

Gustavo Goni⁽¹⁾, Mark DeMaria⁽²⁾, John Knaff⁽³⁾, Charles Sampson⁽³⁾, James Price⁽⁴⁾, Avichal Mehra⁽⁵⁾, Isaac Ginis⁽⁶⁾, I-I Lin⁽⁷⁾, Paul Sandery⁽⁸⁾, Silvana Ramos-Buarque⁽⁹⁾, M. M. Ali⁽¹⁰⁾, Francis Bringas⁽¹¹⁾, Sim Aberson⁽¹¹⁾, Rick Lumpkin⁽¹¹⁾, George Halliwell⁽¹¹⁾, Chris Lauer⁽¹²⁾, Eric Chassignet⁽¹³⁾, Alberto Mavume⁽¹⁴⁾, K. Kang⁽¹⁵⁾

- 1) Continue and support the international efforts to evaluate the role that the ocean plays in tropical cyclone intensification,
- 2) Support the creation and maintenance of an in-situ component of the ocean observing system, which is a complement to the current system, able to resolve mesoscale features and their upper ocean thermal structure for tropical cyclone intensification studies,
- 3) Support operational altimetry with a suit of satellites able to resolve mesoscale features,
- 4) Carry out upper ocean observations from airborne platforms, such as AXBTs and AXCTDs, before and after the passage of tropical cyclones,



Ocean Obs'99 Recommendations

- 6) Support new observations of other ocean parameters, such as salinity, to improve estimates of mixed layer depth properties,
- 7) Encourage the transmission of all observations into real-time data bases to allow immediate access to these data,
- 8) Support the validation efforts and improvement of ocean models that are used in TC studies,
- 9) Initiate an ocean Observing System Simulation Experiment, to optimize the observations made for TC studies and forecasts, and
- 10) Continue the strong presence of scientific presentations at international meetings and workshops.



Take Home Message

- Some sustained ocean observations performed for climate are adequate to investigate the link of TC intensification and the ocean.
- The only current *global* observations useful for TC intensity forecasts come from satellites, mainly altimetry.
- For TC intensity studies there is a wide range of observations available for process studies, including process studies using AXBTs, dropsondes, etc.
- Improvement in our understanding the physics of air-sea interaction in extreme weather events will be critical.
- International collaboration is key to advance in our understanding of the problematic in each region where TCs occur



Upper Ocean Heat Content from Satellite Altimetry Global estimates and the Arabian Sea and Bay of Bengal

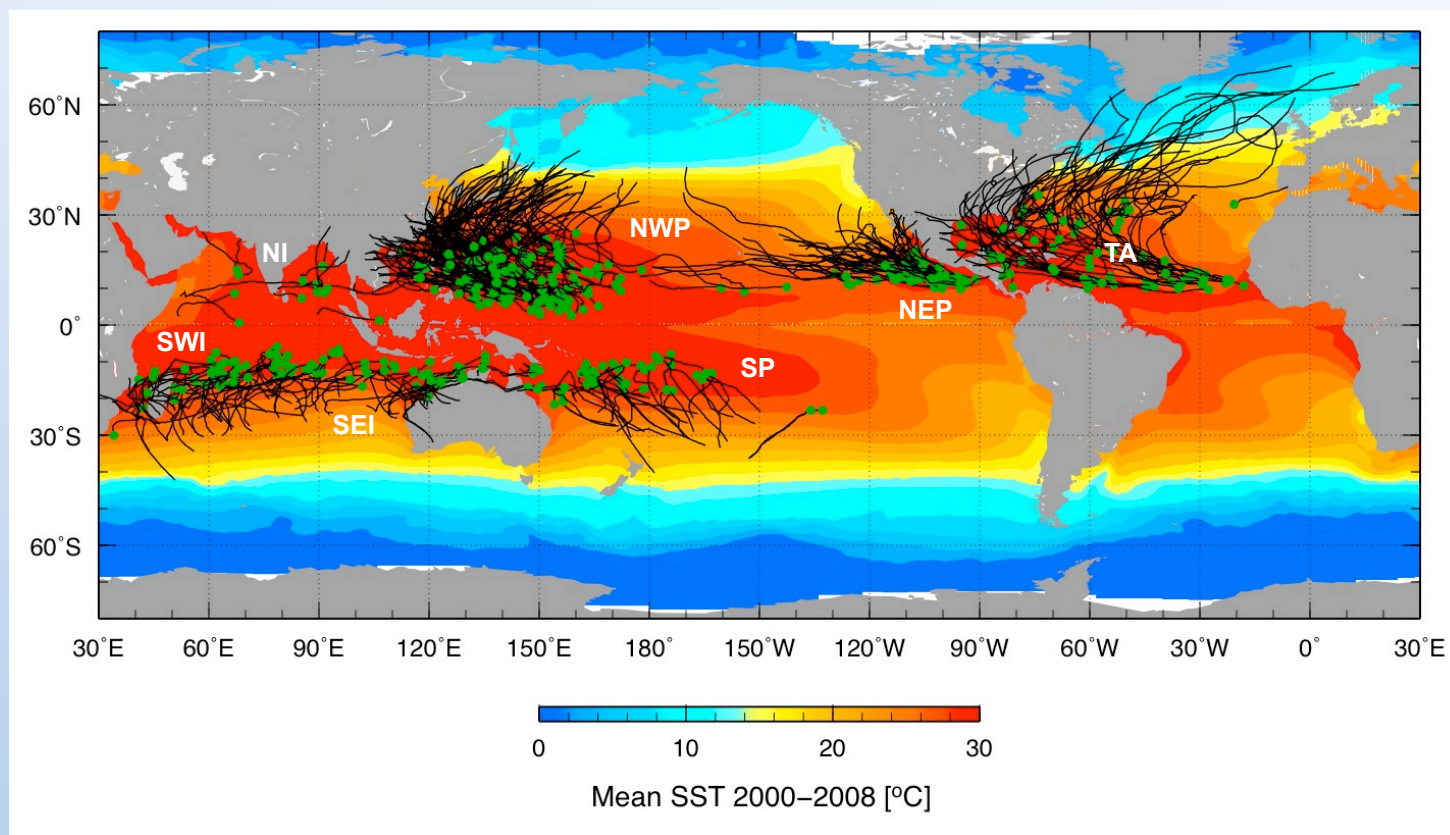
Gustavo Jorge Goni (NOAA/AOML)



**Workshop on
Utilization of Satellite Derived Oceanic Heat Content
for Cyclone Studies**

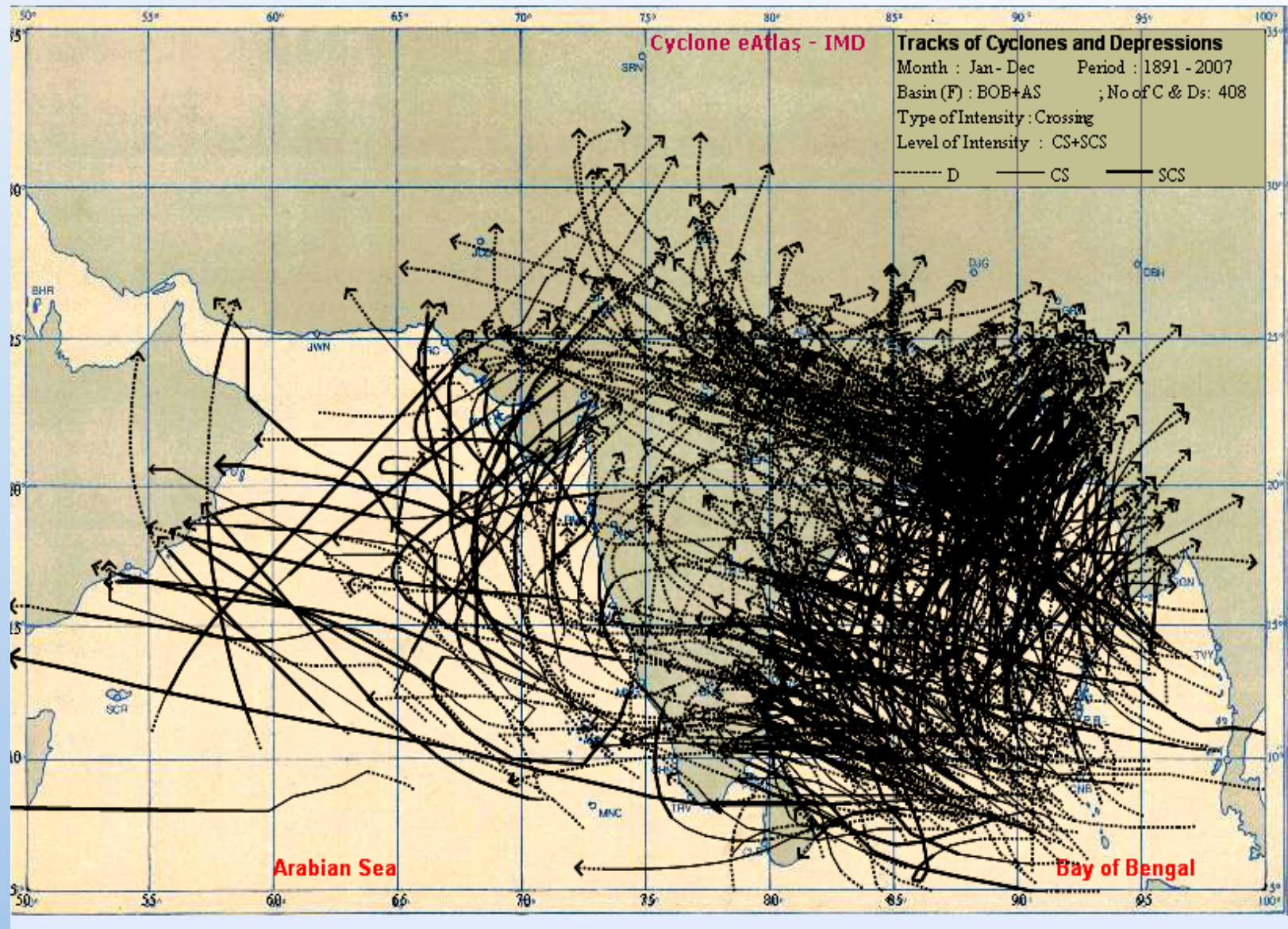
Hyderabad, India, March 25-26, 2010

Tropical cyclone basins and genesis



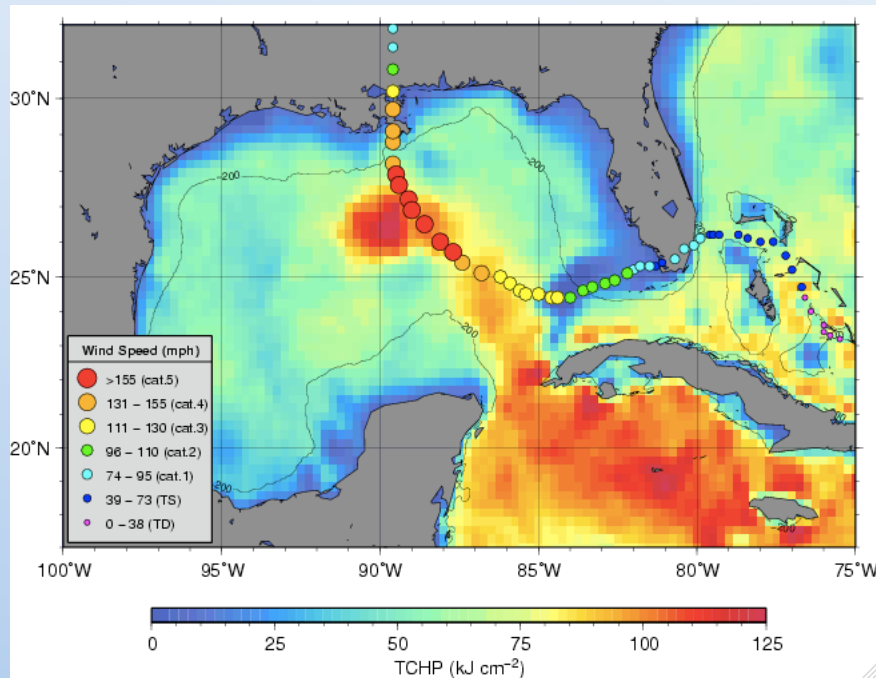
Goni et al 2009

Tropical cyclones in the BoB and AS.

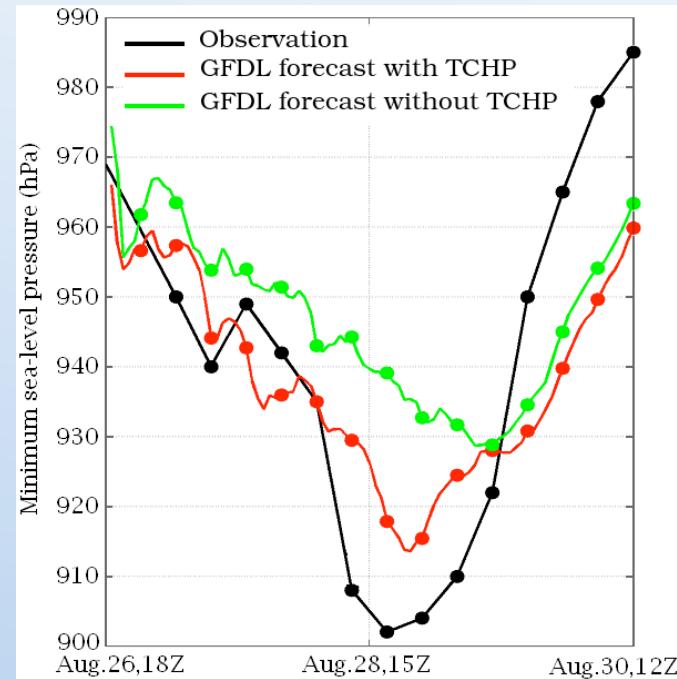


Lessons from the Gulf of Mexico

Hurricane Katrina

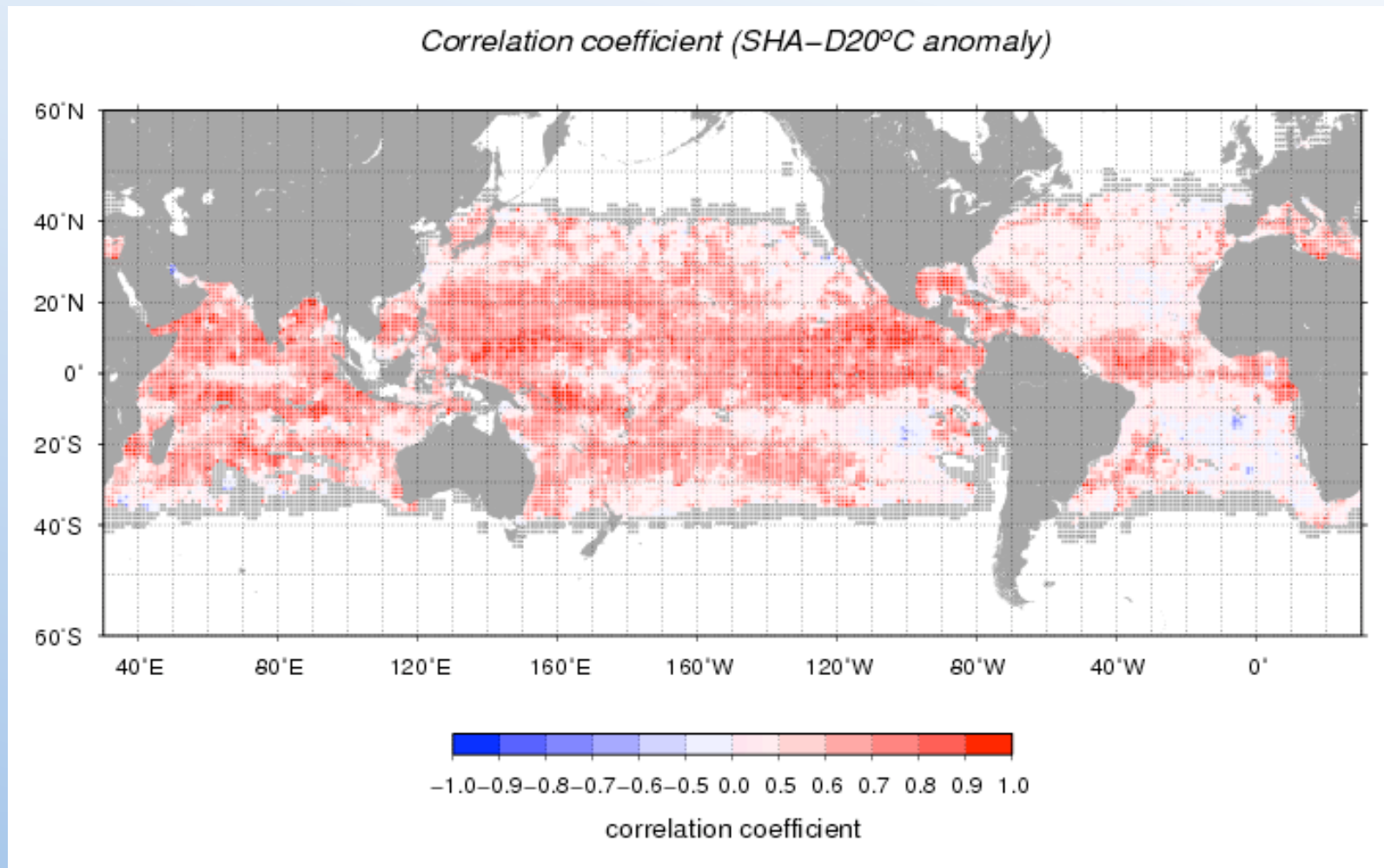


Goni et al, 2009

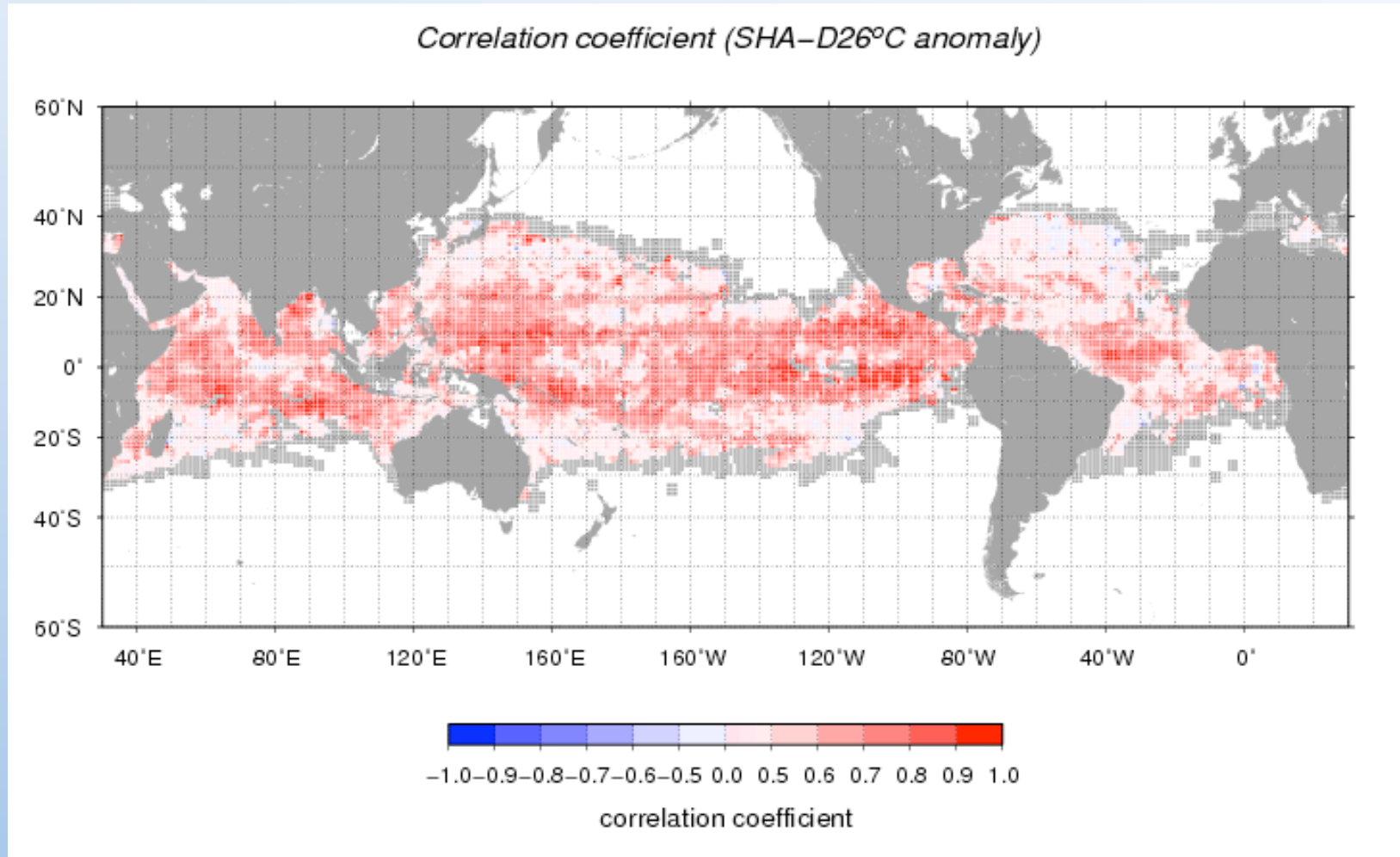


Goni et al, 2009;
Figure by Isaac Ginis (URI)

Isotherm depths and sea height

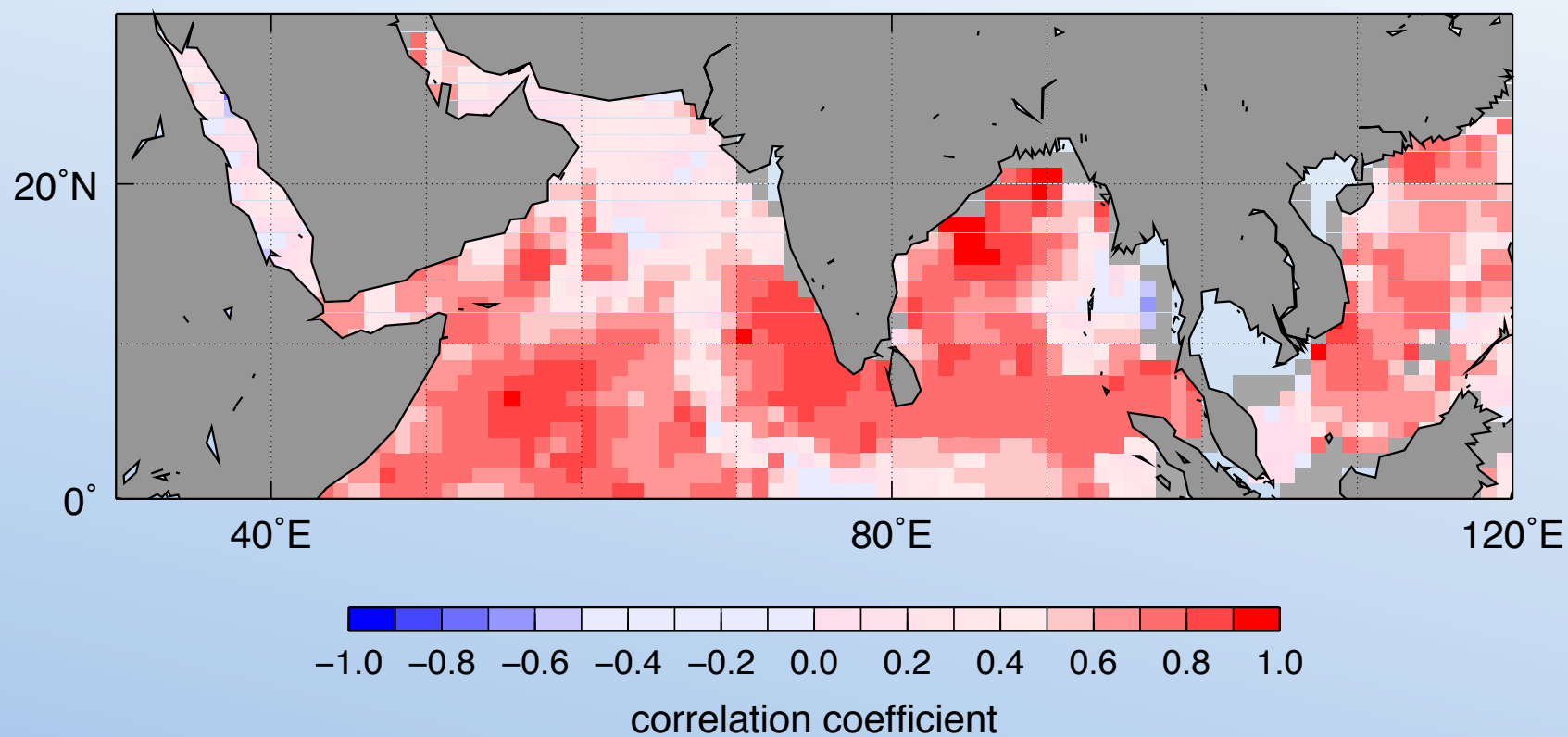


Isotherm depths and sea height



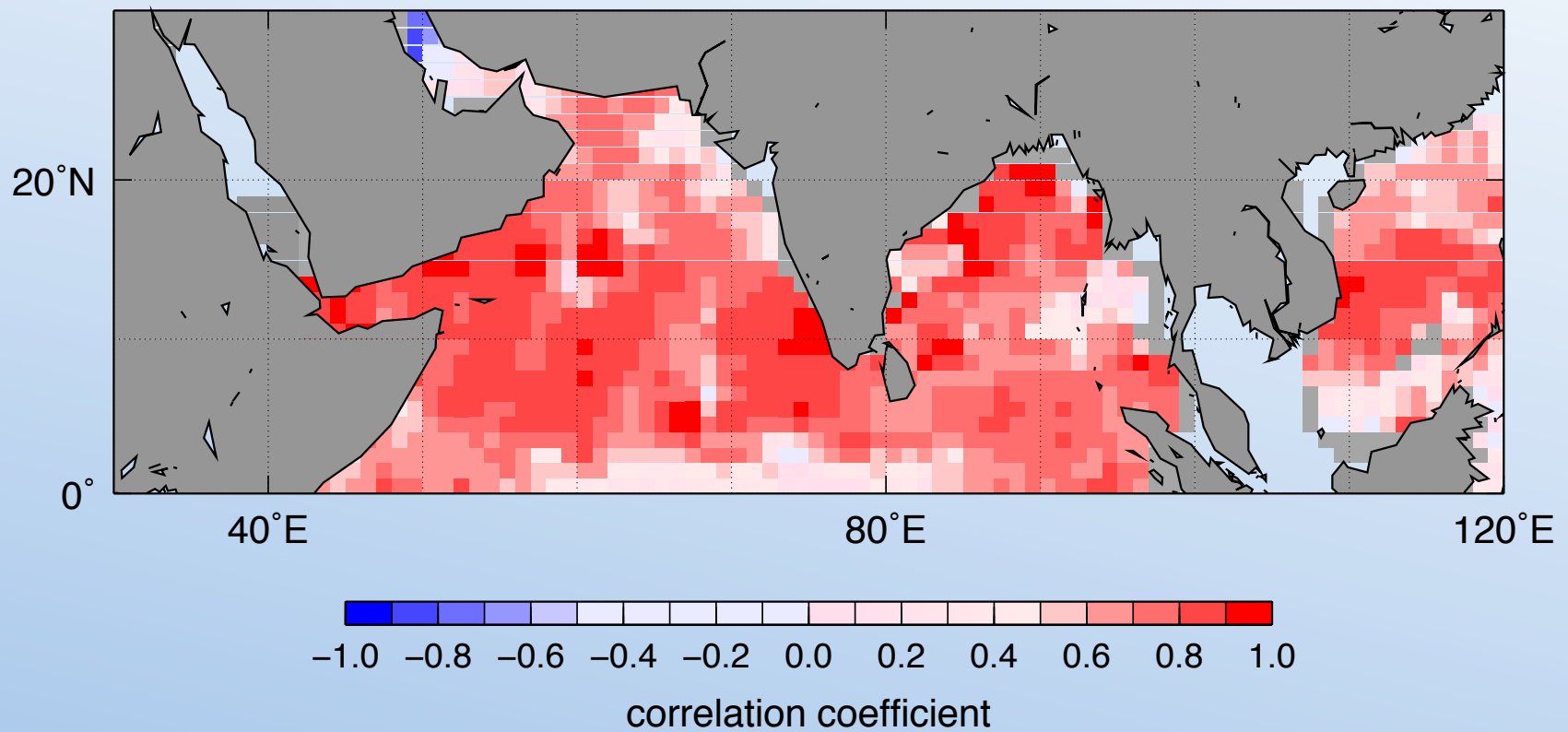
Isotherm depths and sea height

Correlation coefficient (SHA-D26°C anomaly)

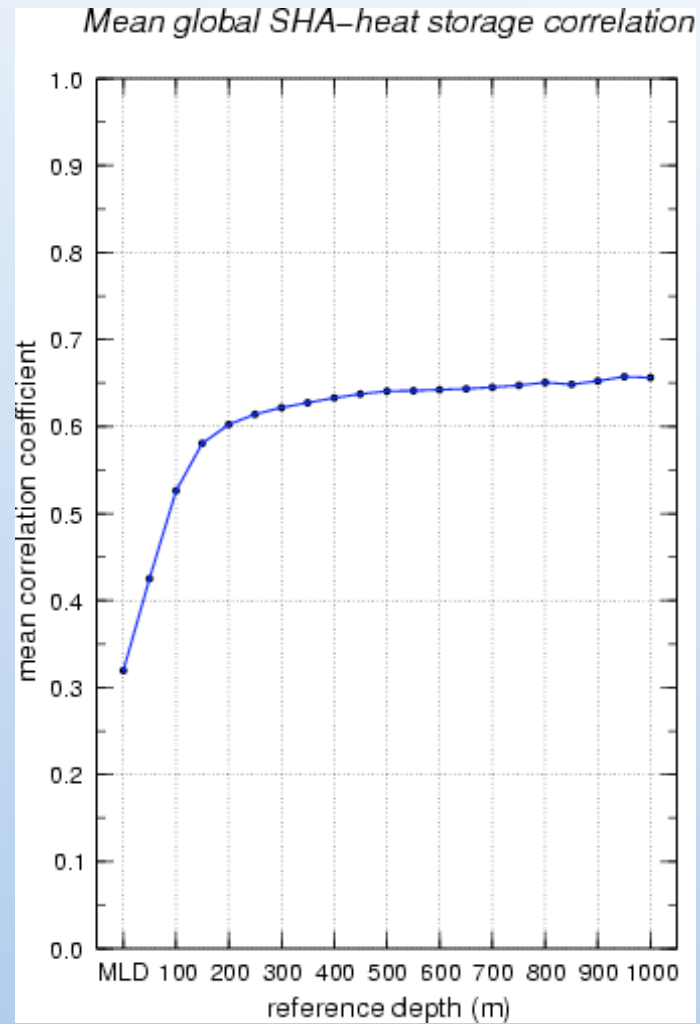


Isotherm depths and sea height

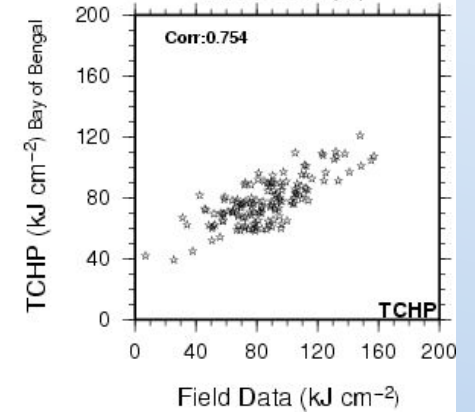
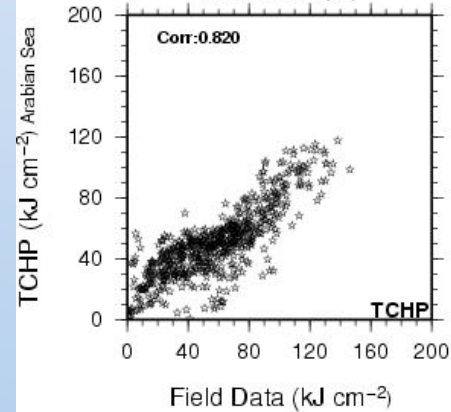
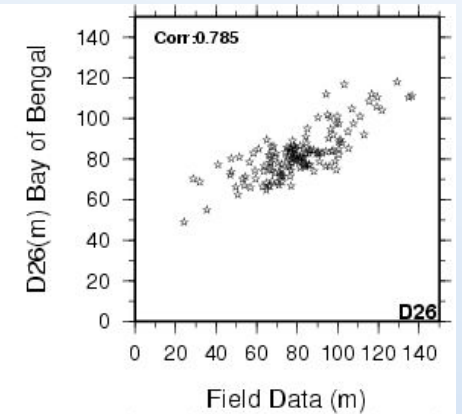
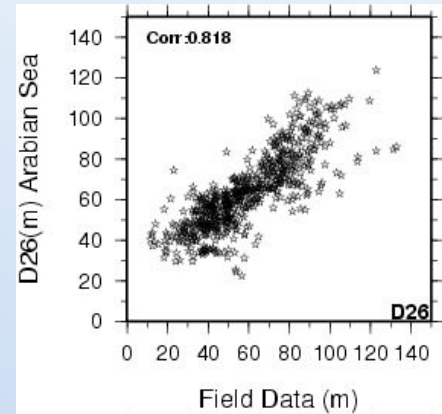
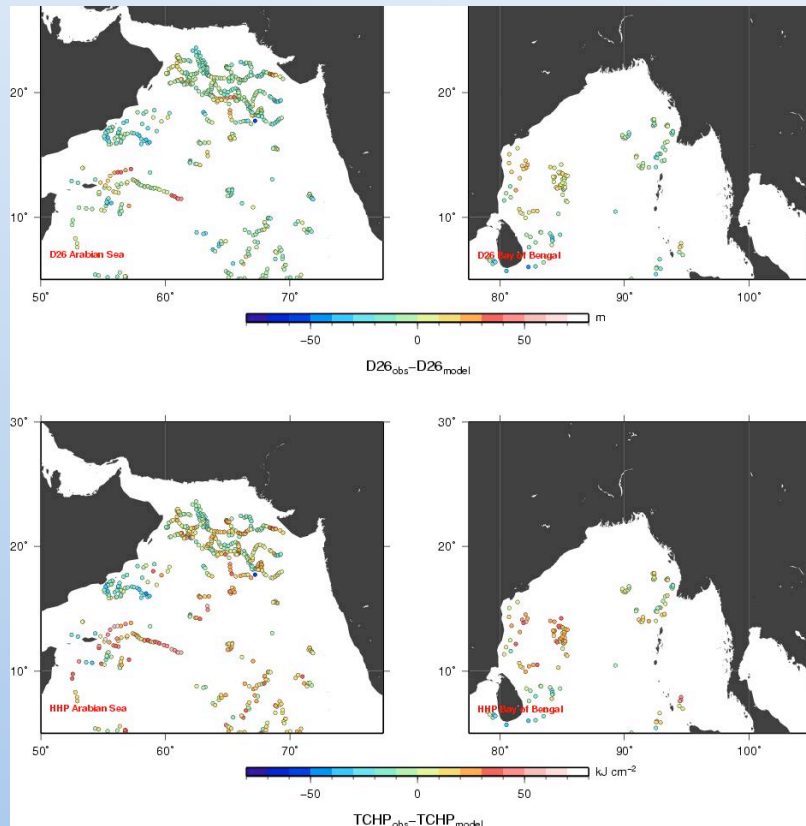
Correlation coefficient (SHA-D20°C anomaly)



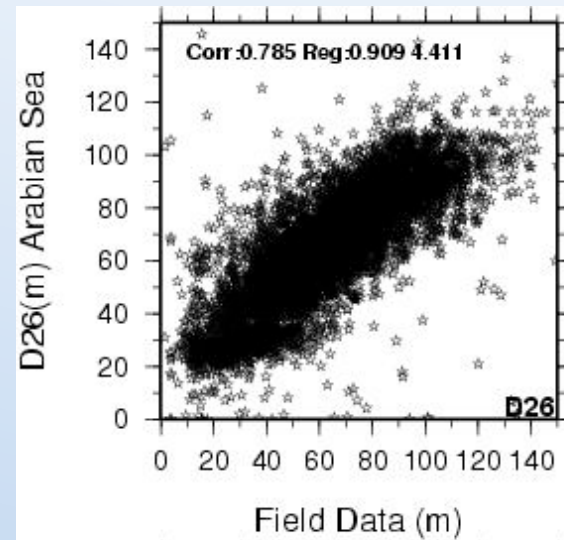
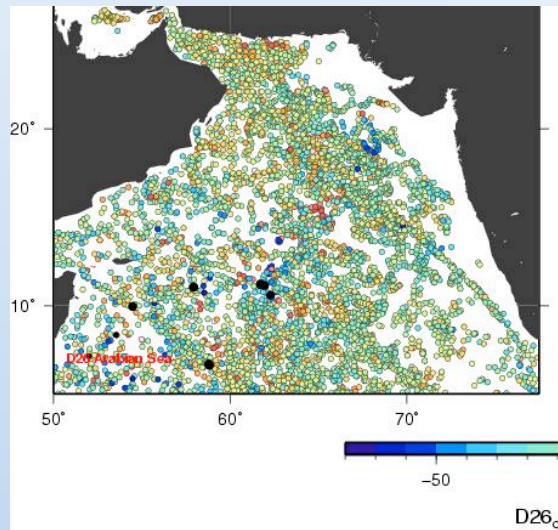
Isotherm depths and sea height



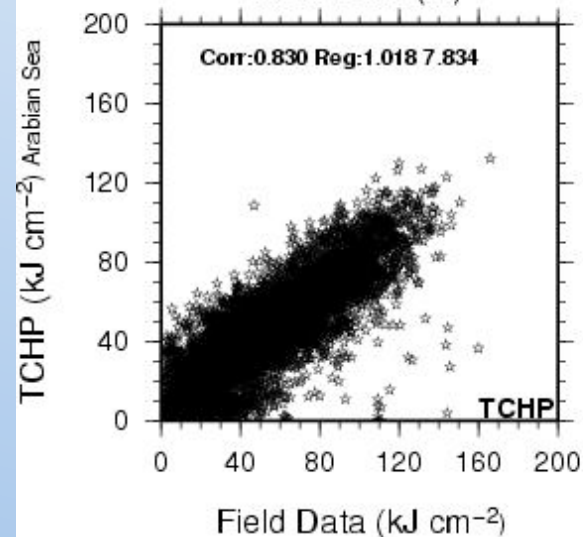
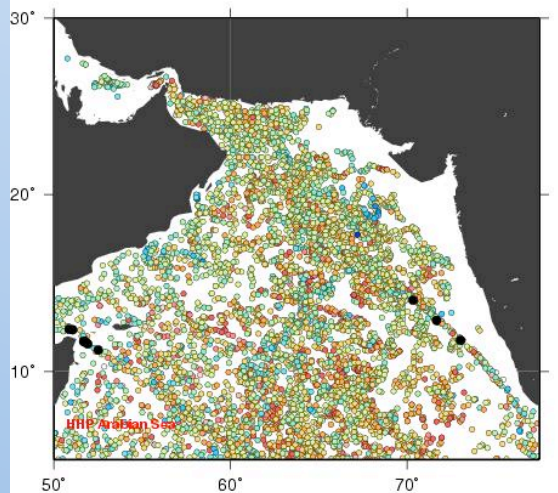
Validation of TCHP fields



Validation of TCHP fields

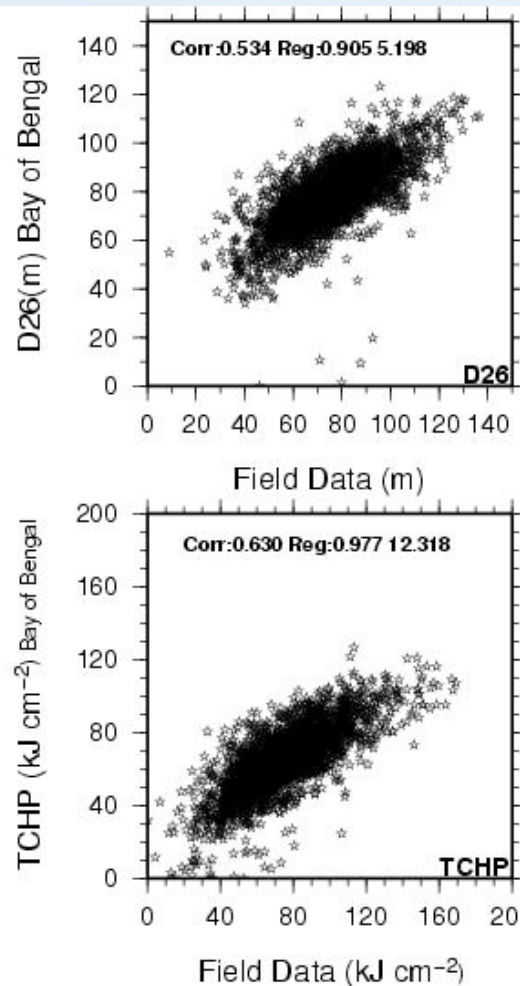
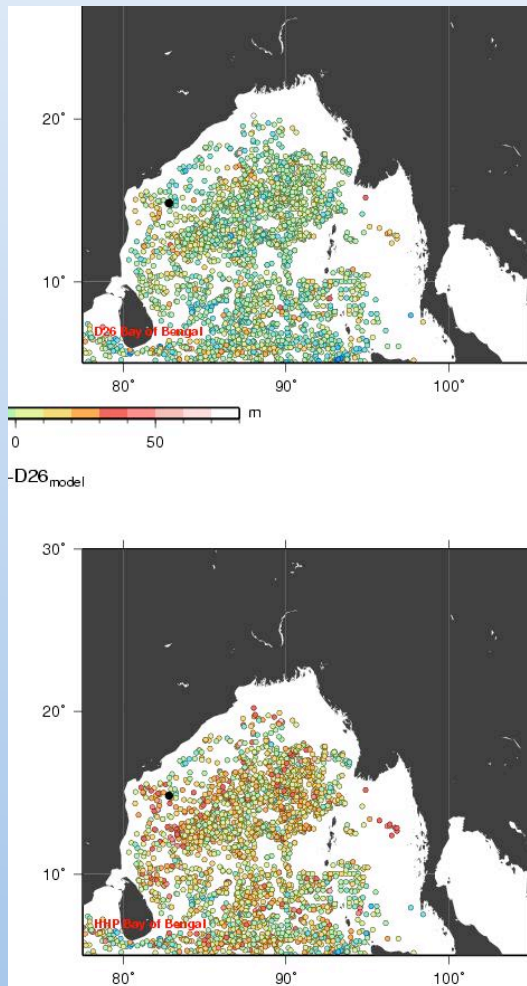


$$\text{D26 est} = 0.90 \text{ D26 obs} + 4\text{m}$$



$$\text{TCHP est} = 1.01 \text{ TCHP obs} + 7 \text{ kJ/cm}^2$$

Validation of TCHP fields

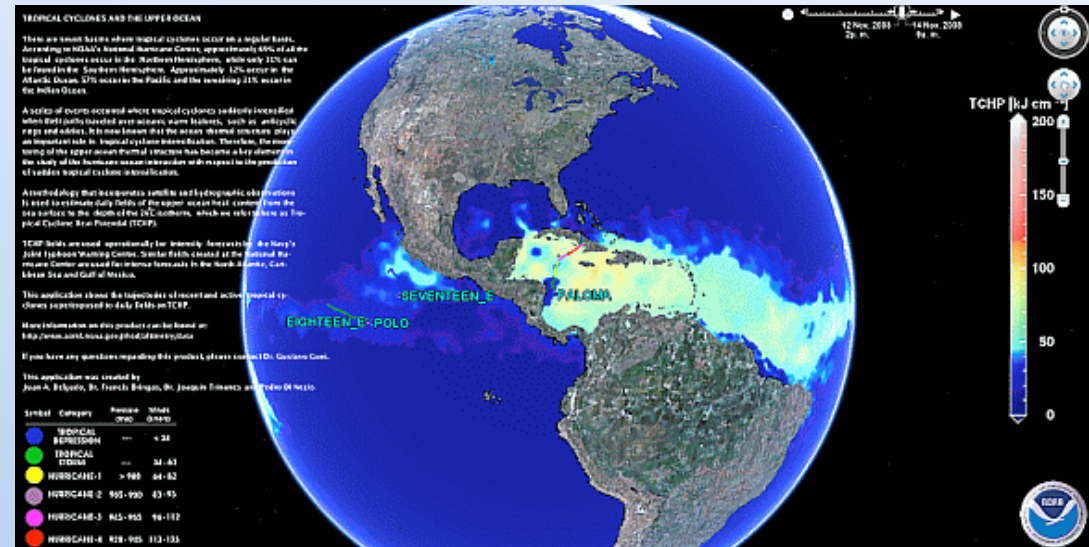
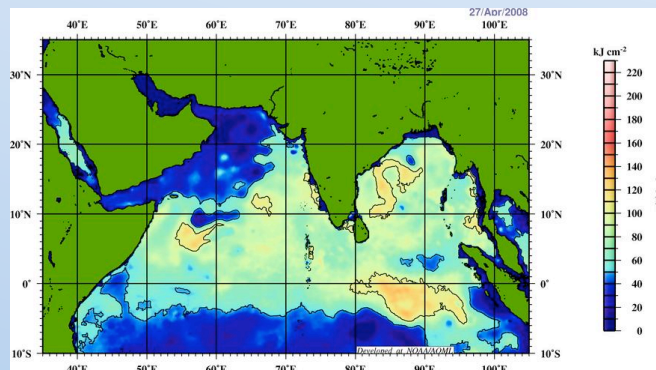


$$\text{D26 est} = 0.95 \text{ D26 obs} + 5\text{m}$$

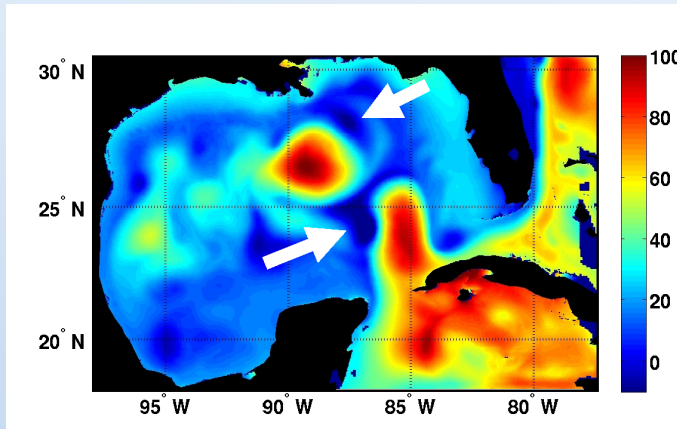
$$\text{TCHP est} = 0.97 \text{ TCHP obs} + 12 \text{ kJ/cm}^2$$

Tropical Cyclone Heat Potential data distribution

<http://www.aoml.noaa.gov/phod/cyclone/data/>

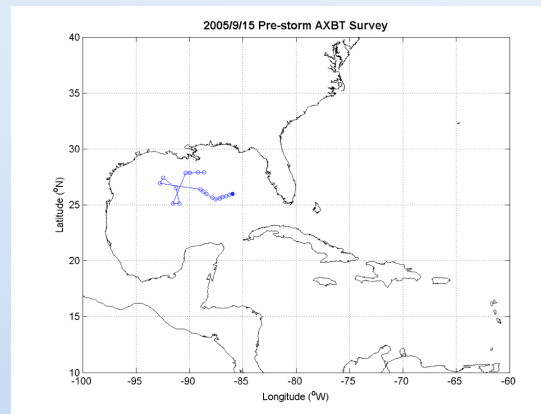


HYCOM-HWRF modeling effort AOML and NCEP

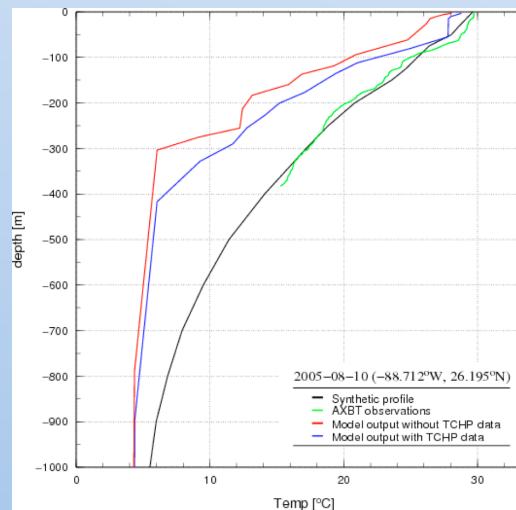
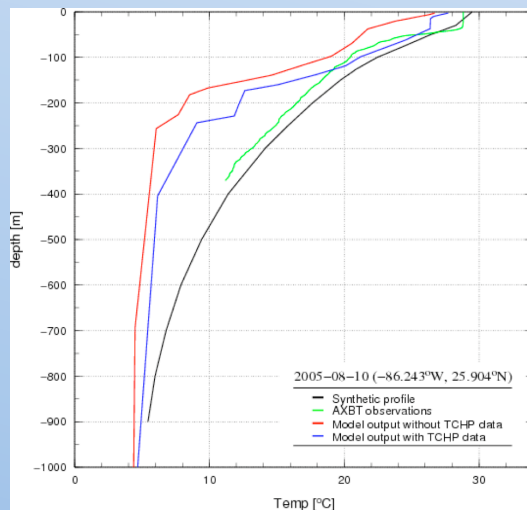


Goni et al, 2009
Figure by G. Halliwell

The features are more or less right, but the vertical thermal structure needs improvement.



AXBT survey pre-
hurricane Rita (AUG
2005)

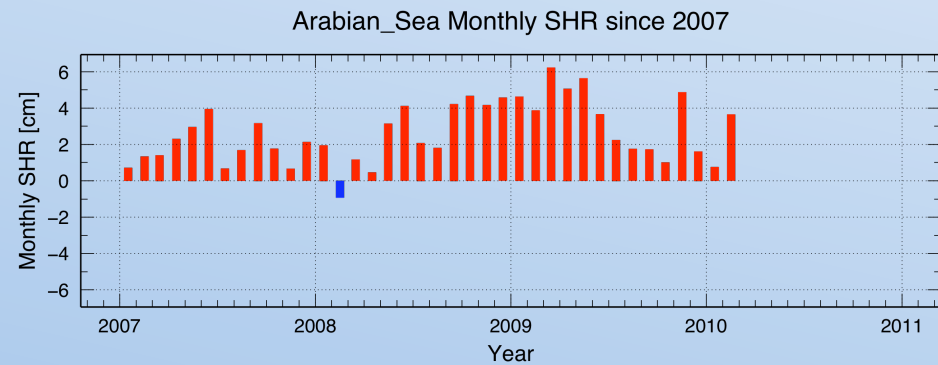
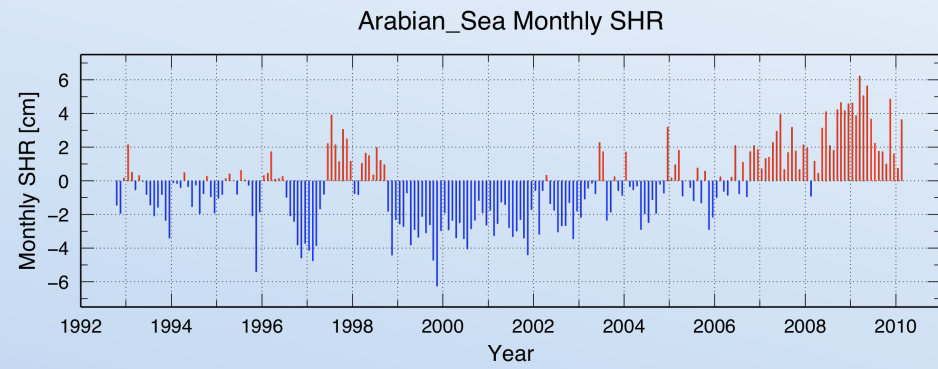
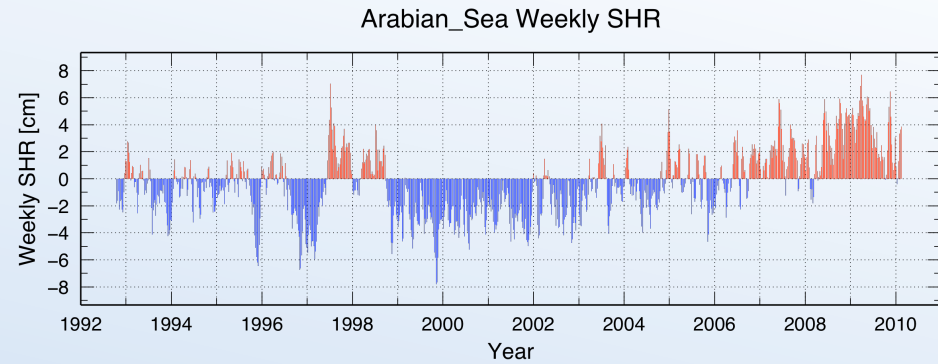
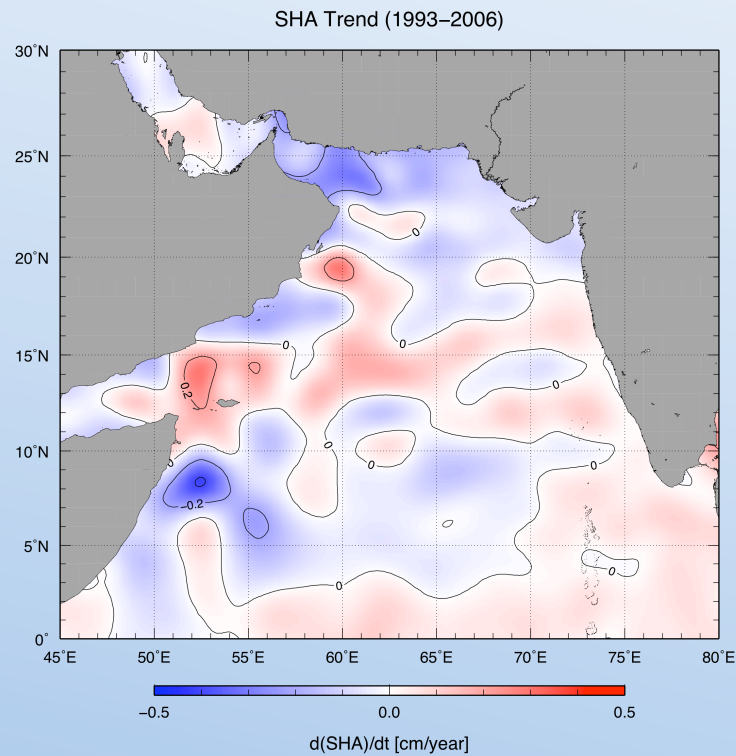


Green = AXBT
Black = altimetry
Red and blue = HYCOM

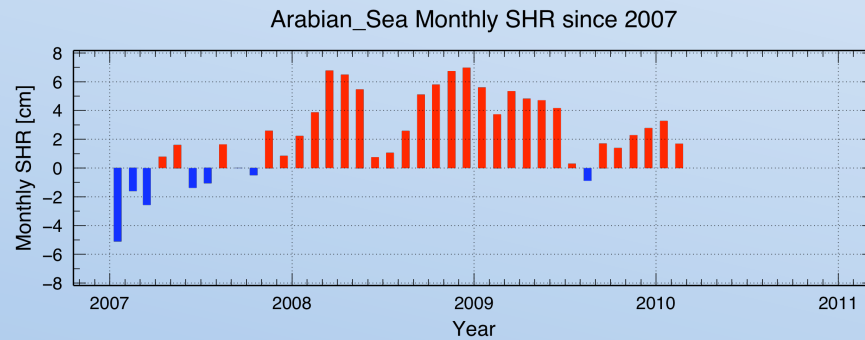
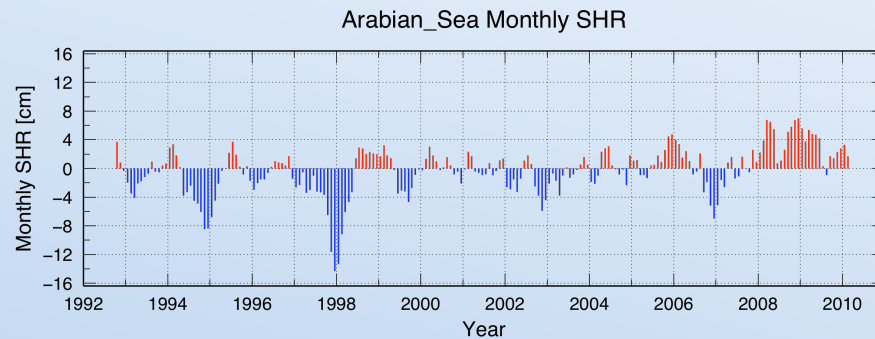
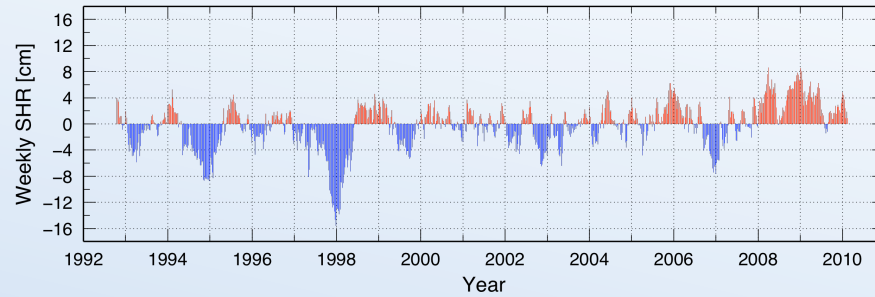
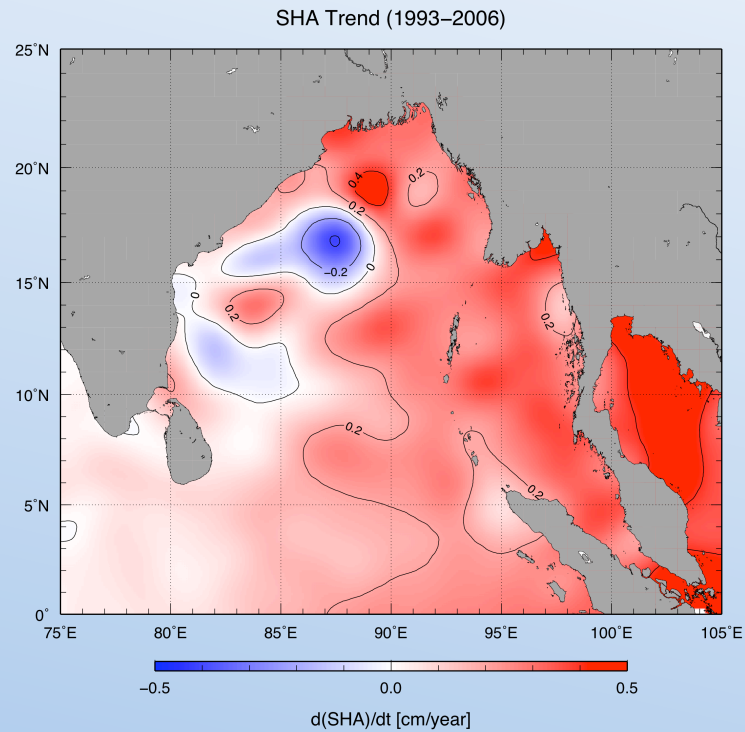
Figures by A. Mehra



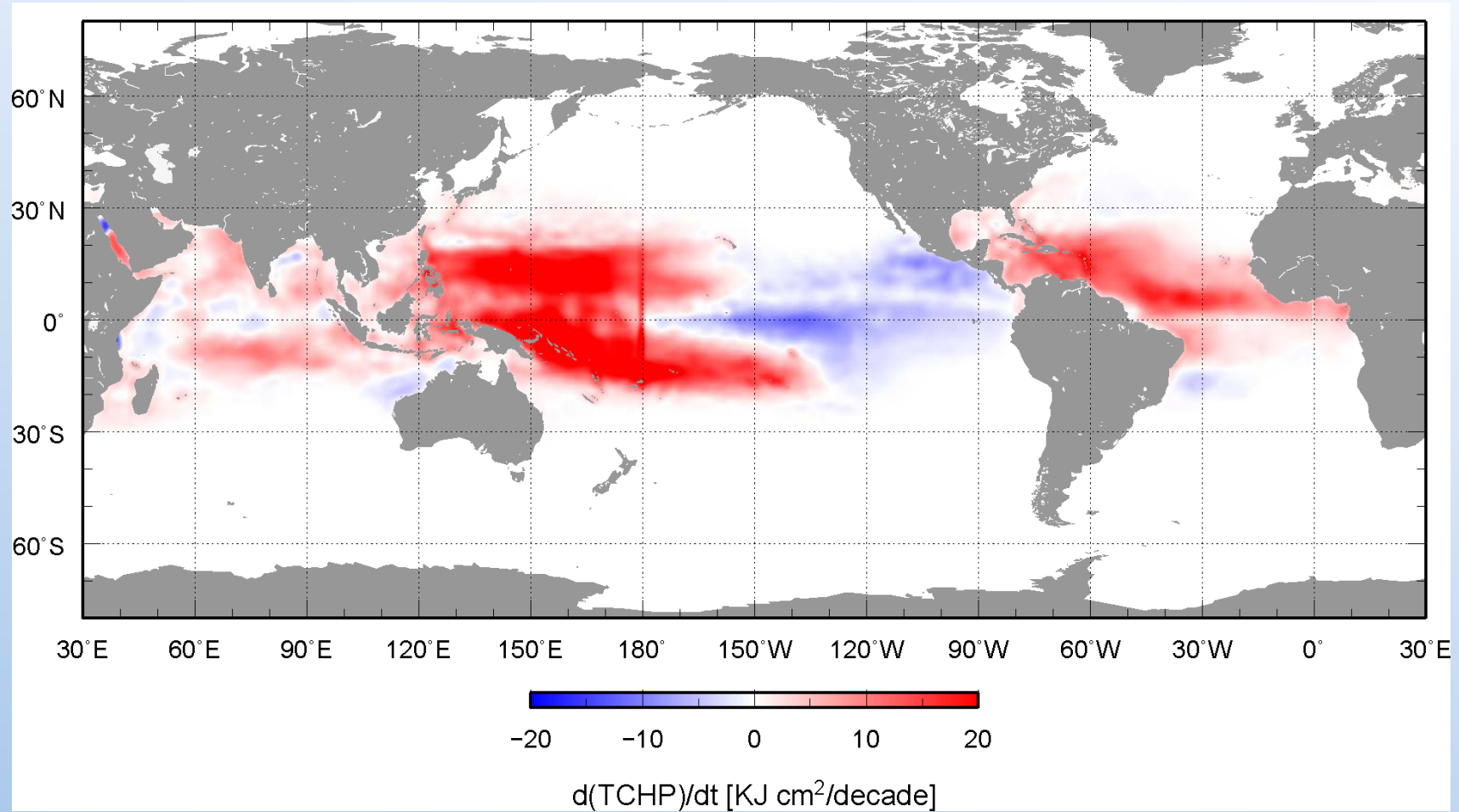
Arabian Sea, sea height (non-secular) trends



Bay of Bengal (non-secular) sea height trends



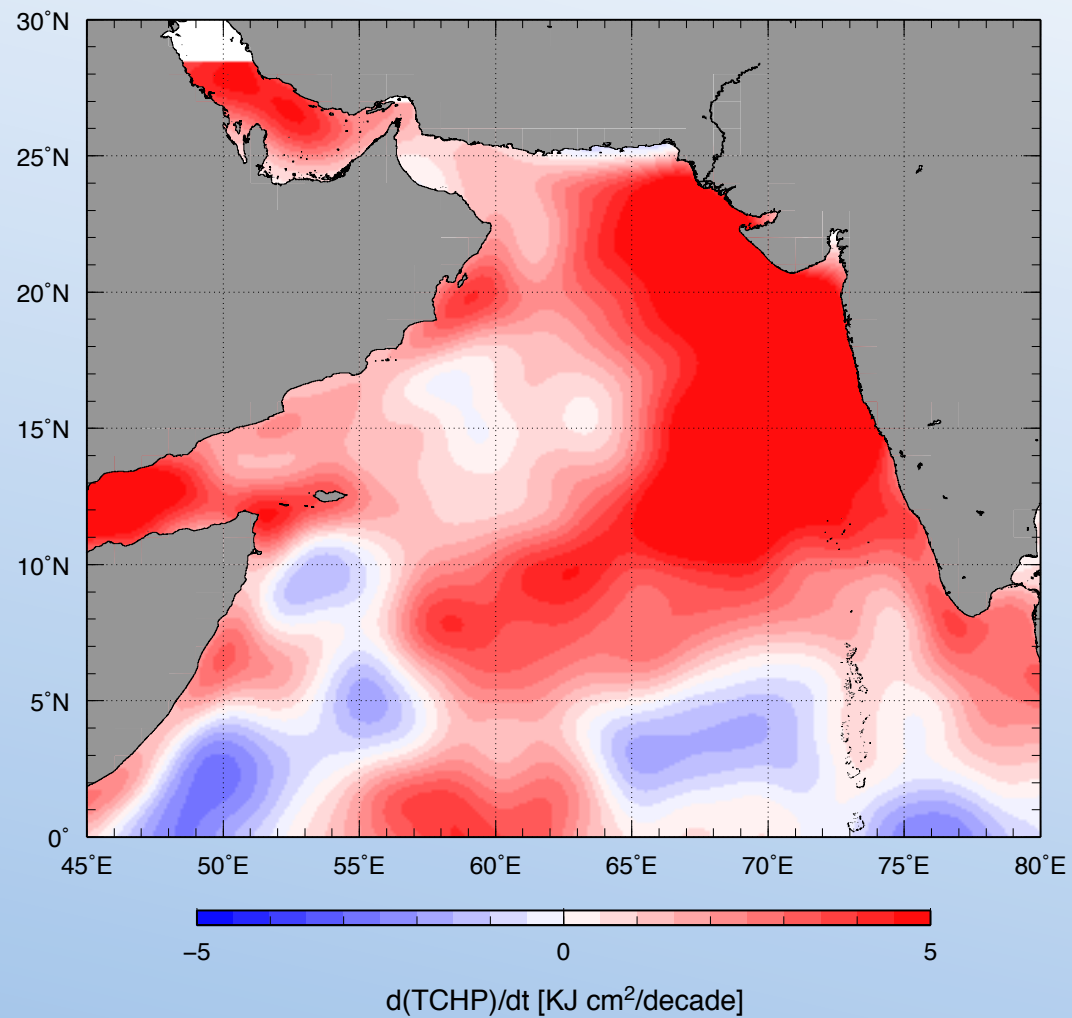
Tropical Cyclone Heat Potential (non-secular) Trends (1993-2008)



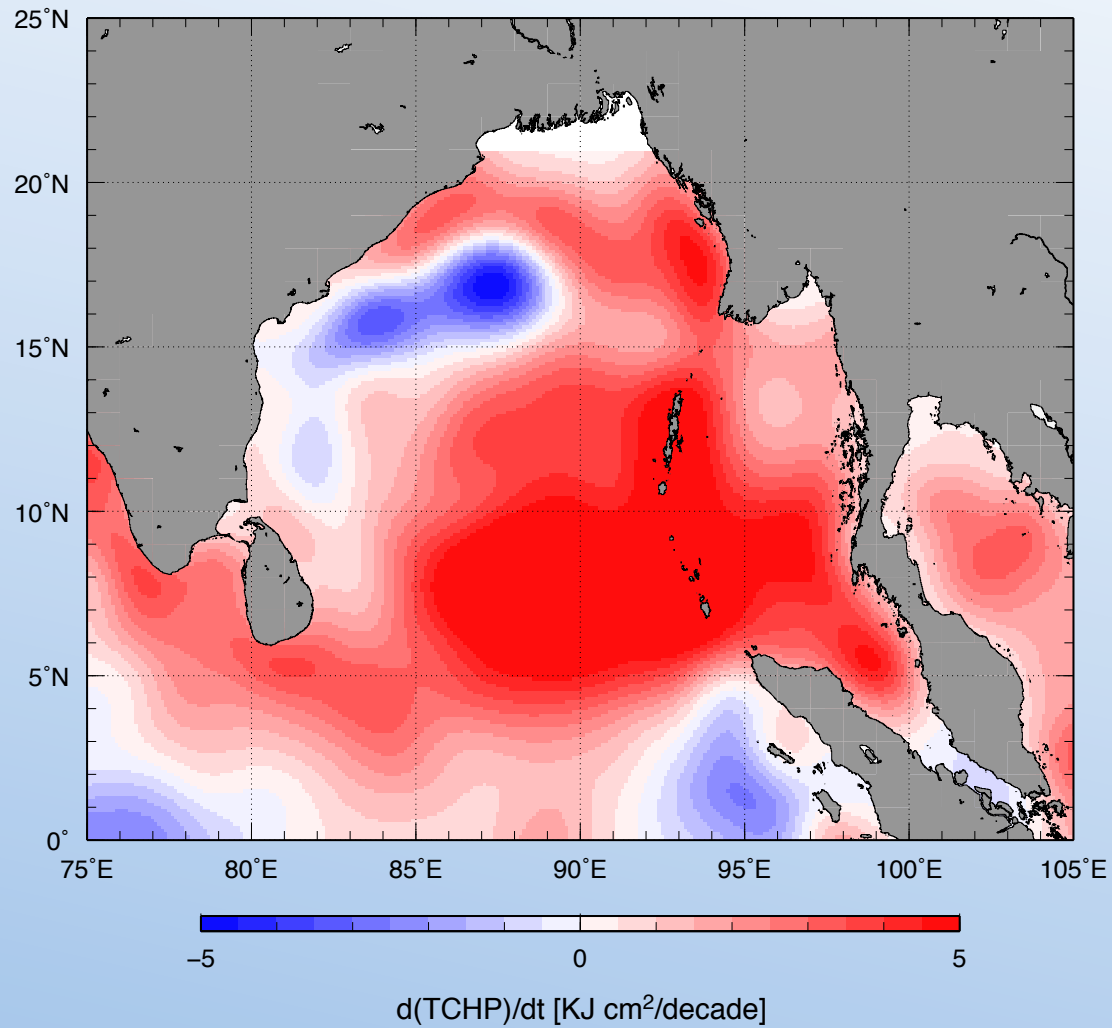
Goni et al, 2009



Arabian Sea TCHP (non-secular) trends (1993-2007)



Bay of Bengal TCHP (non-secular) trends (1993-2007)



Work ahead

- 1) Assess the role of the upper ocean thermal structure in the Arabian Sea and in the Bay of Bengal. Is TCHP the right parameter ?
- 2) Assess and validate temperature profiles of ocean numerical models, not just at the surface but also at the subsurface. For this we need ocean observations.
- 3) Assess temperature profiles obtained from purely statistical methods.
- 4) Support an ocean observing system for cyclone intensification studies, with satellite altimetry as the main platform for sustained observations.
- 5) Investigate if there is a link between TCHP trends and TC activity and TC intensification.
- 6) Exchange of data, products, and knowledge.
- 7) Collaboration, workshops, scientific publications.

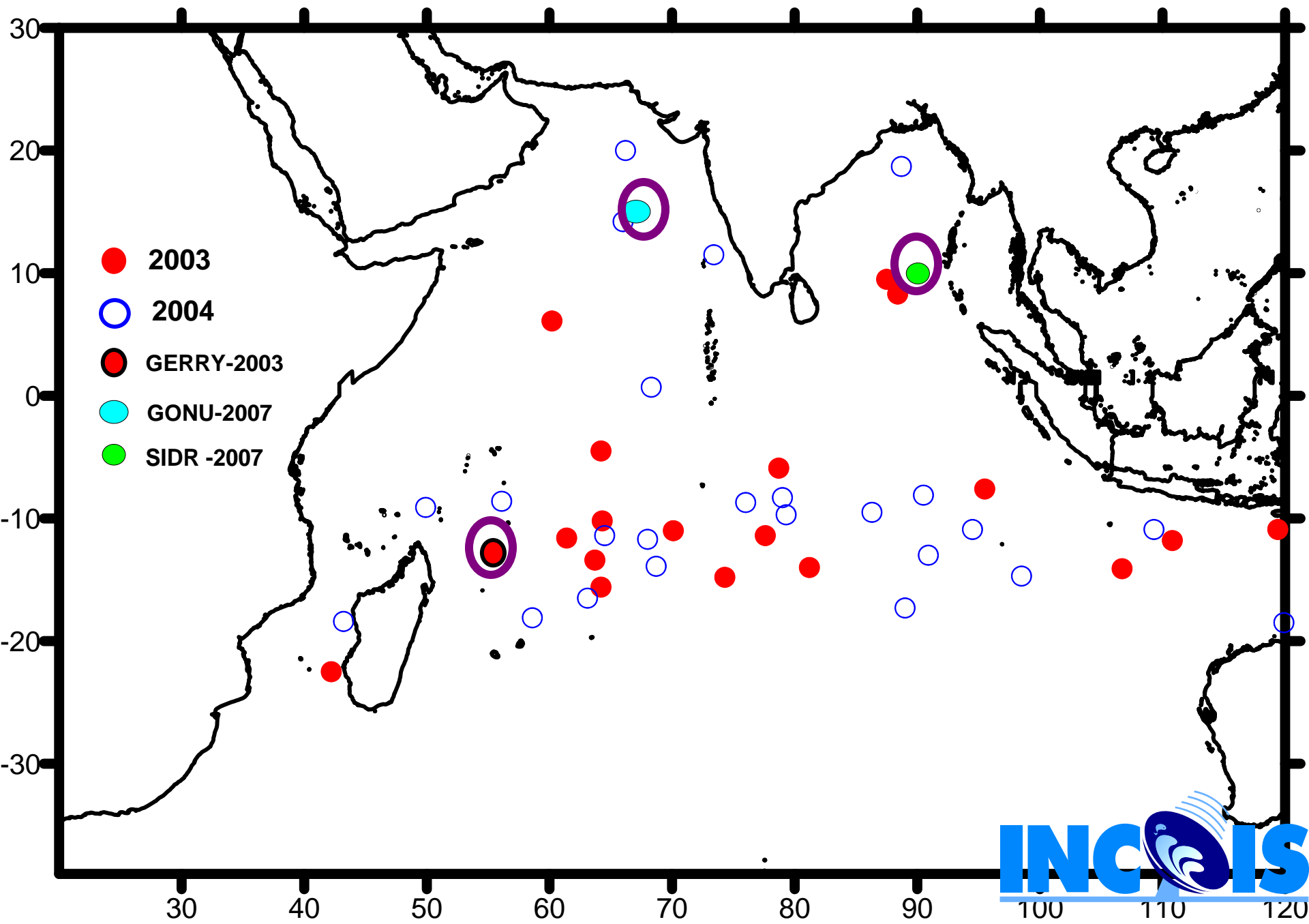




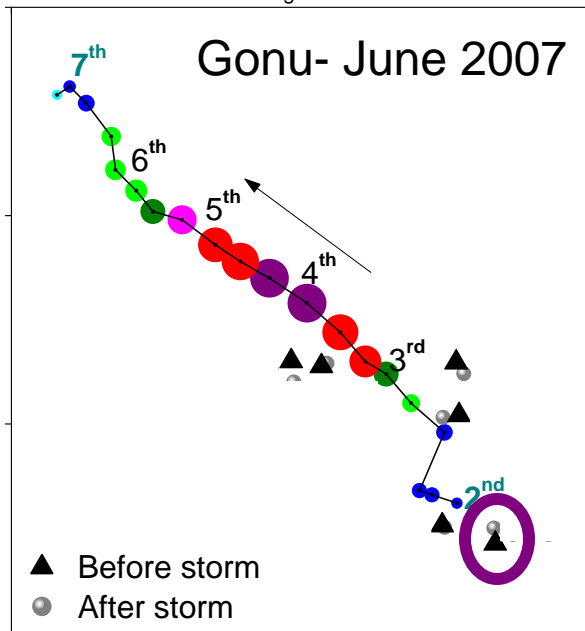
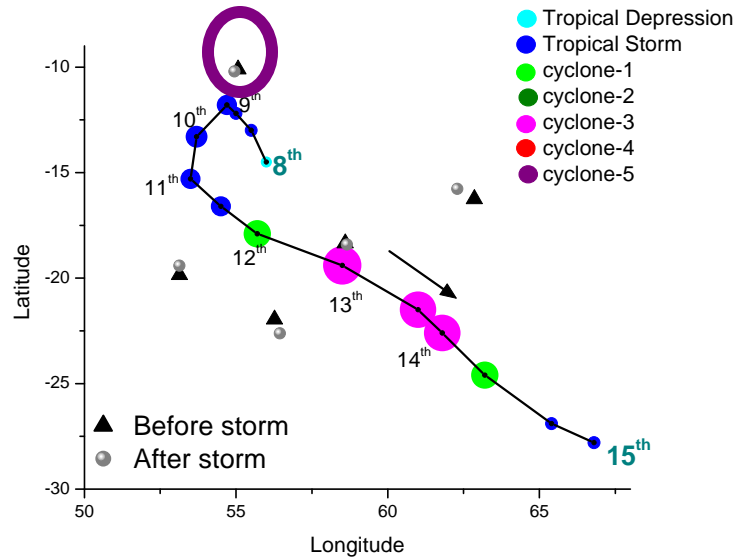
Influence of Salinity and Heat Content on Genesis and Intensity of a Cyclone

Ravichandran M and Anitha Gera

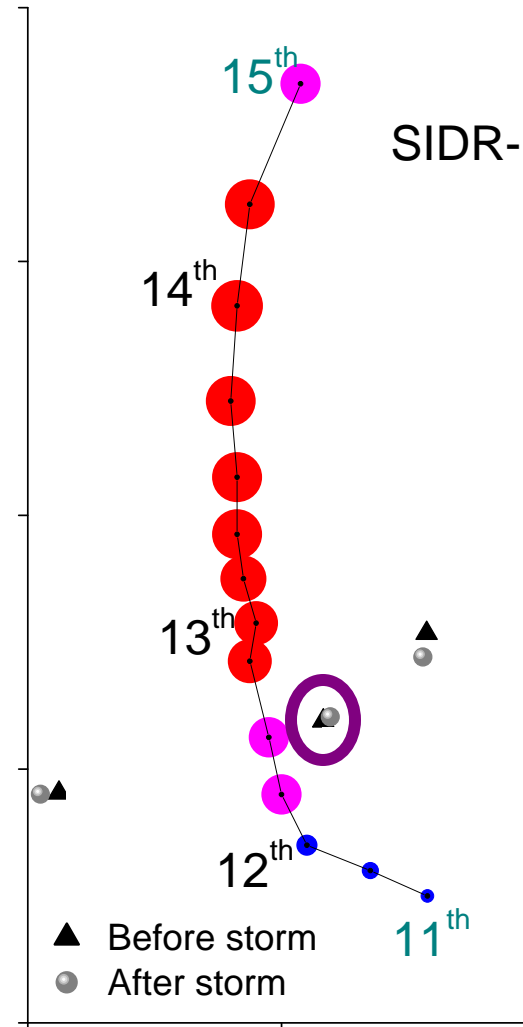
Indian National Centre for Ocean Information Services

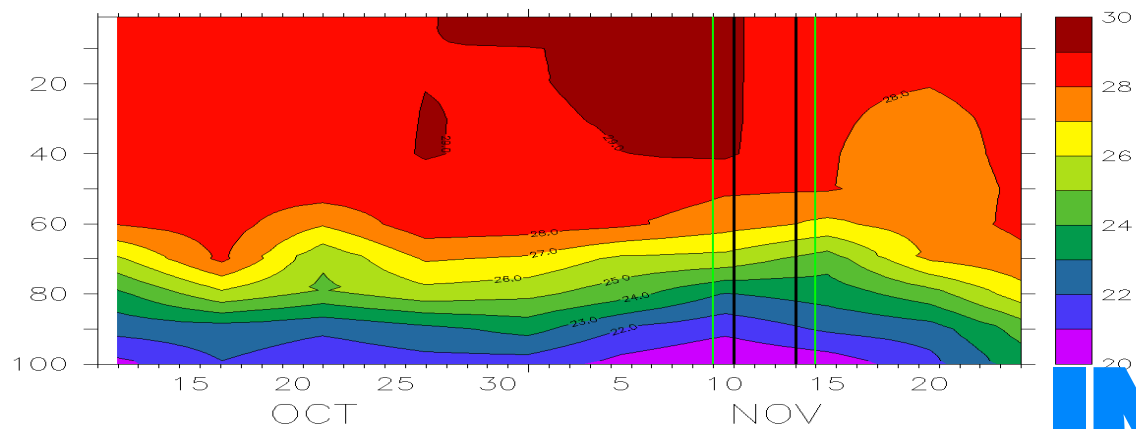
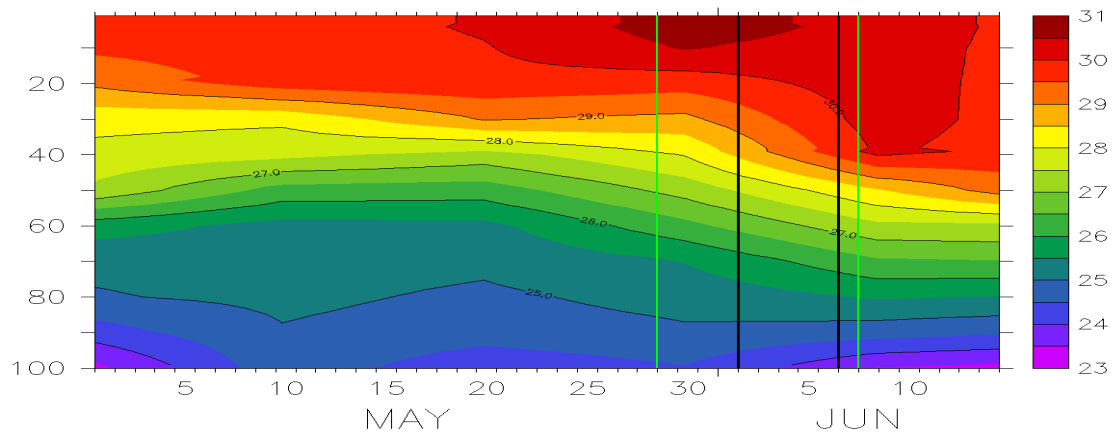
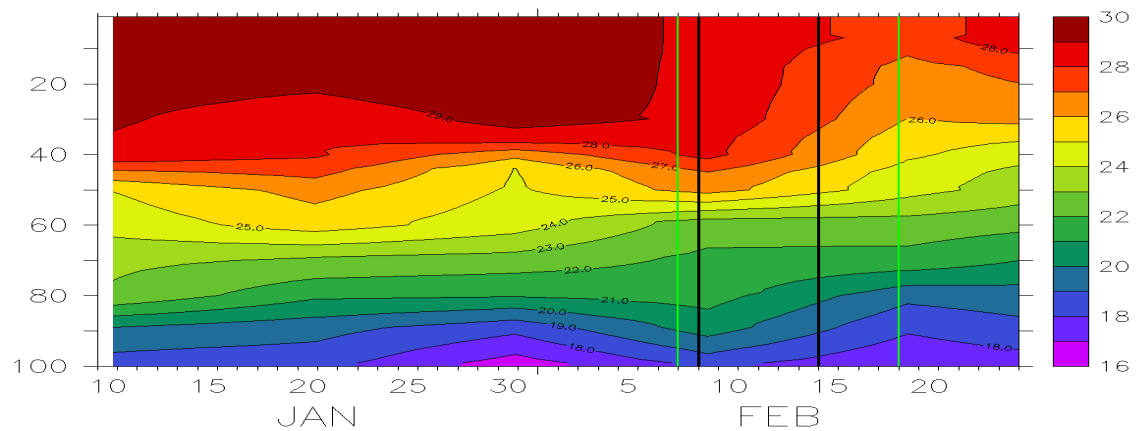


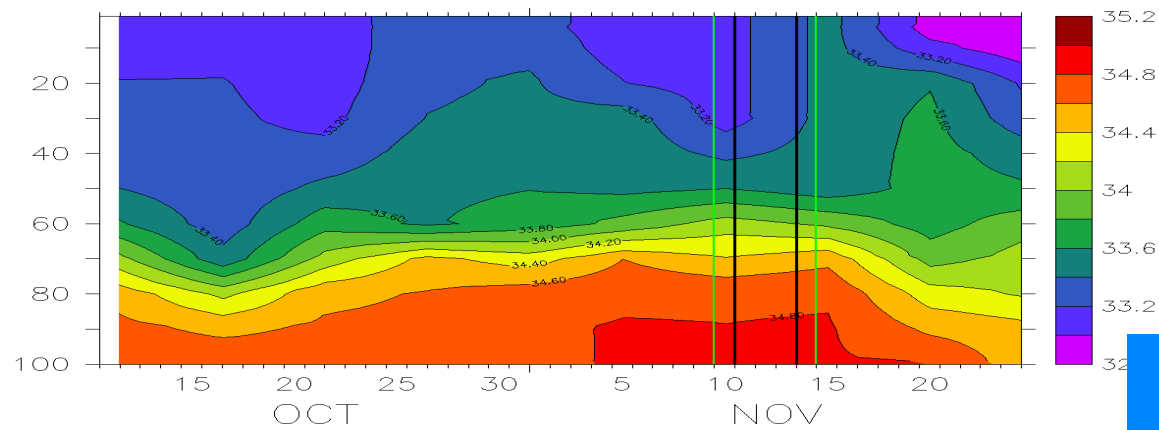
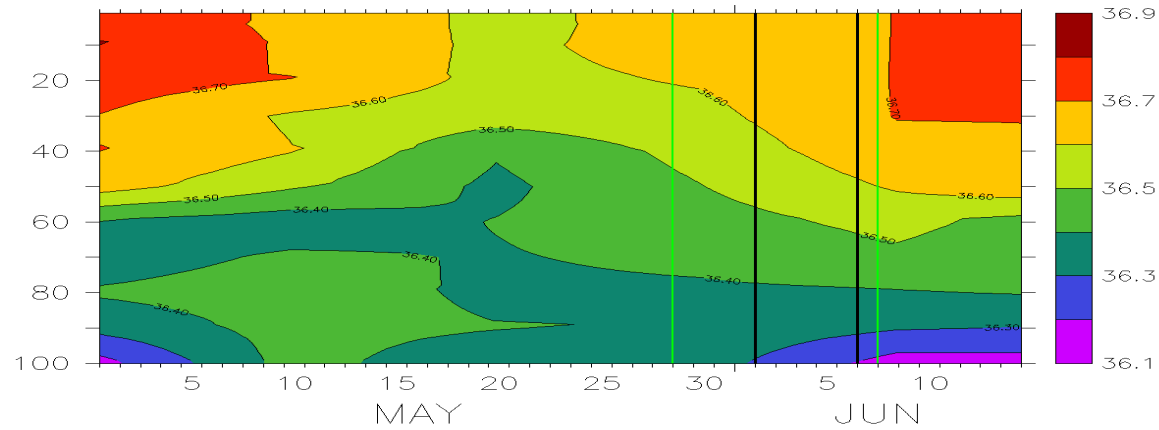
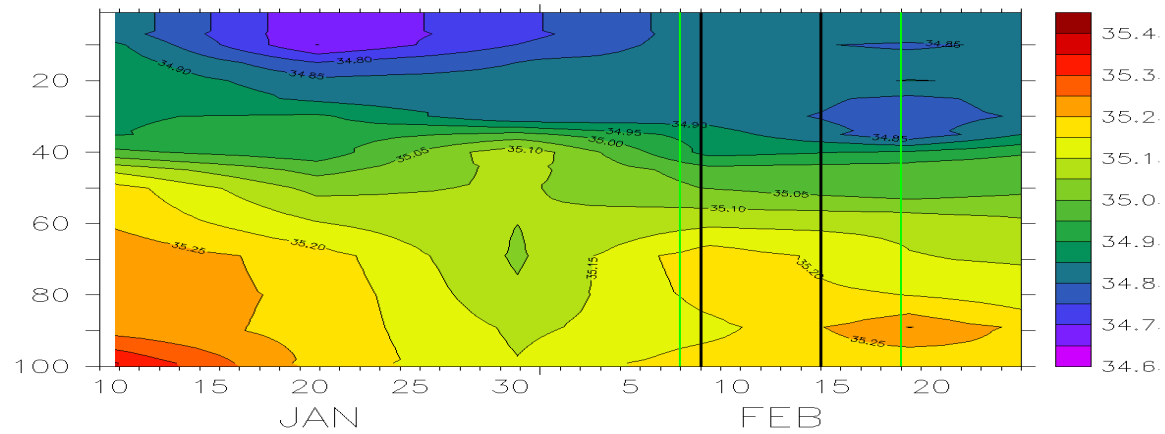
Gerry- Feb 2003

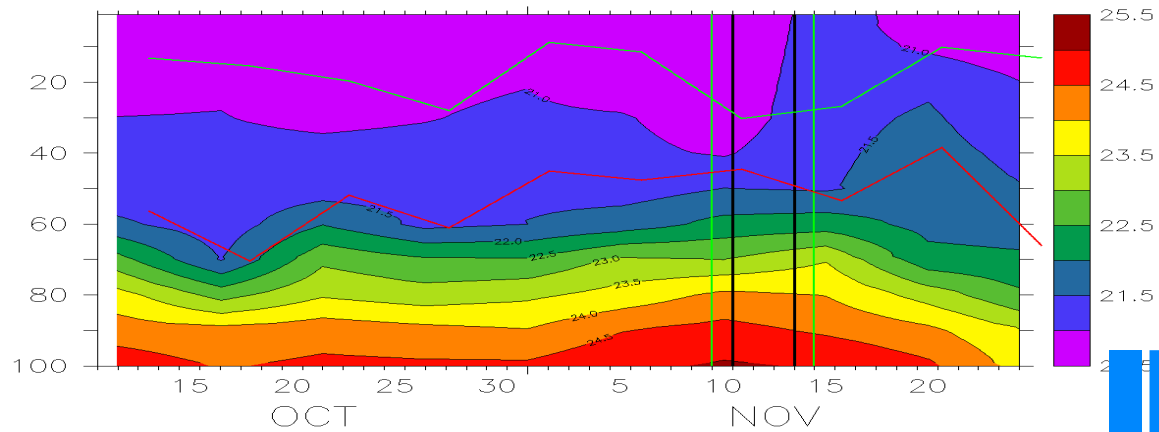
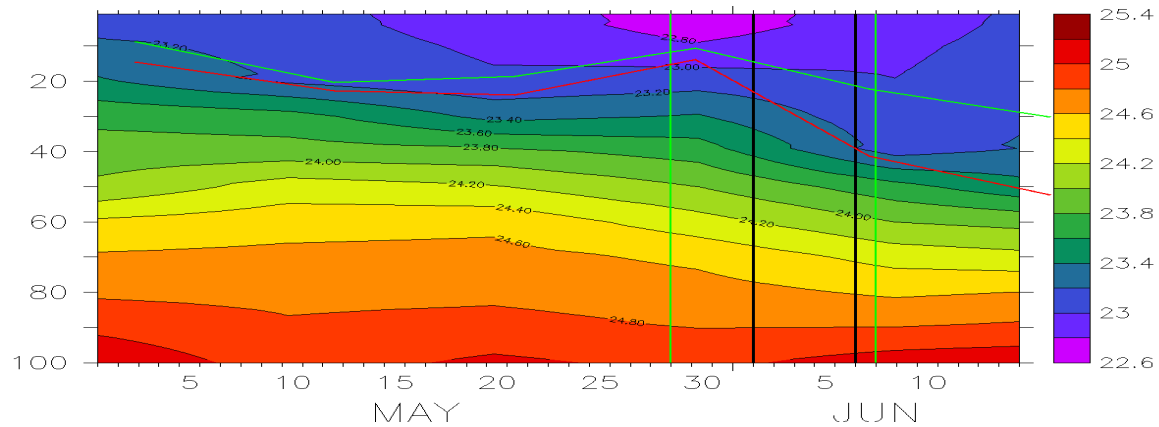
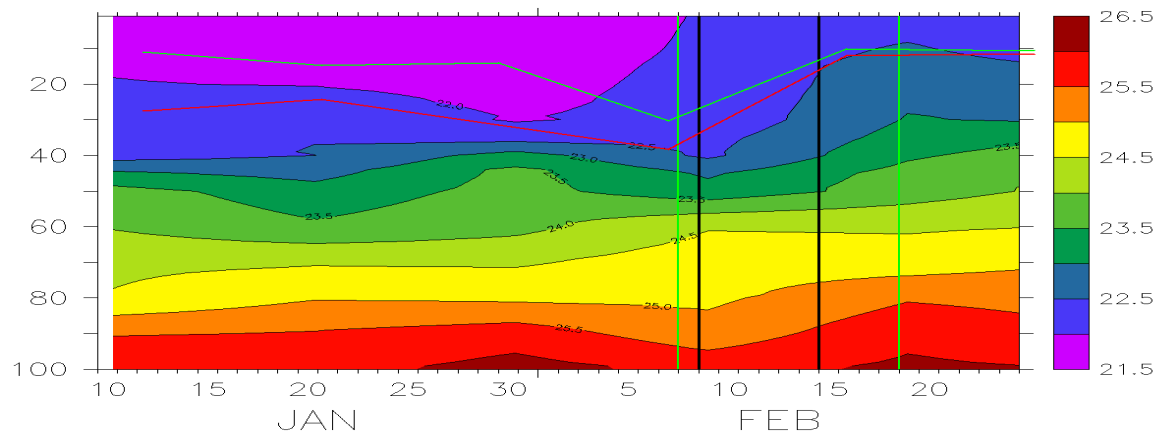


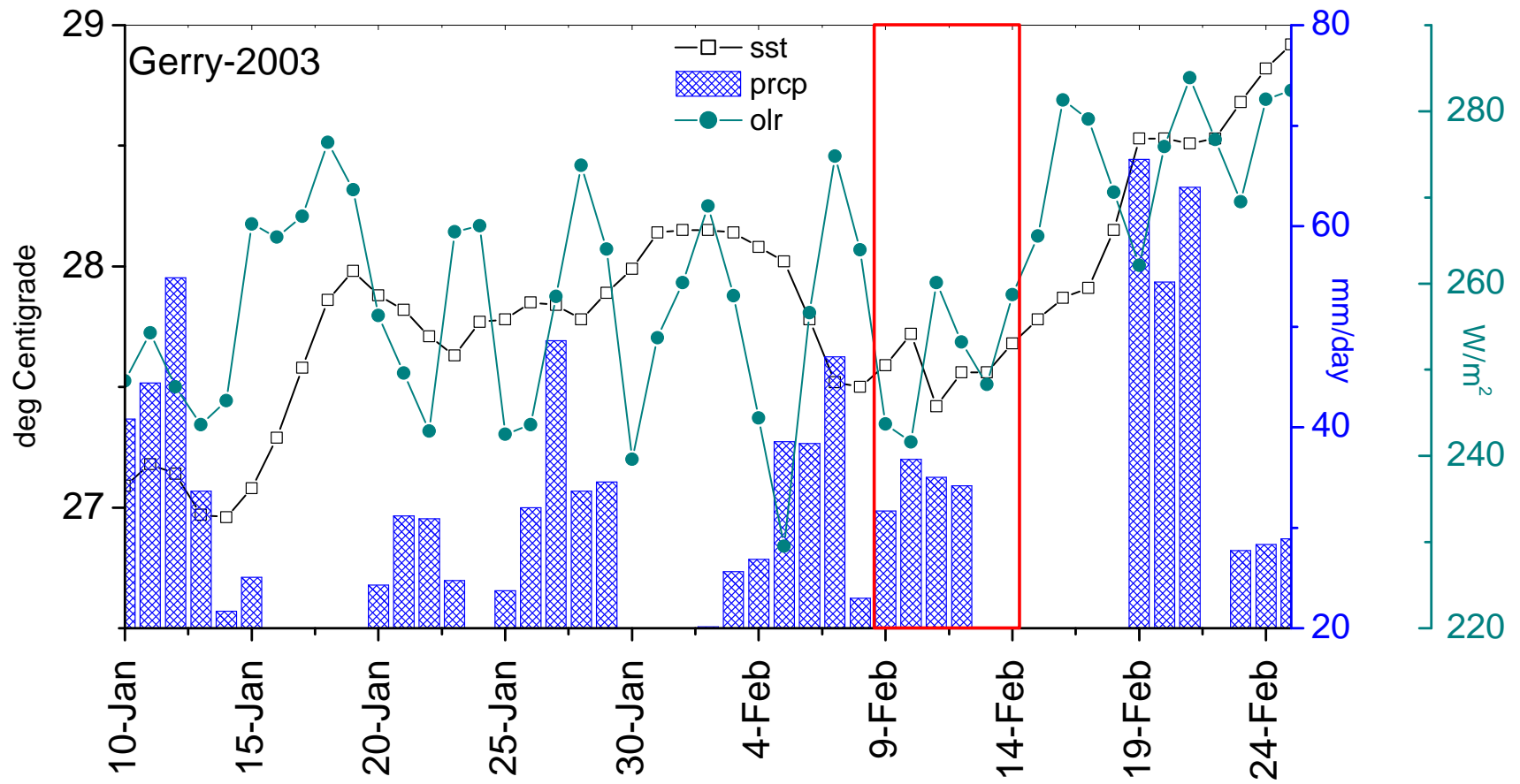
SIDR- Nov 2007

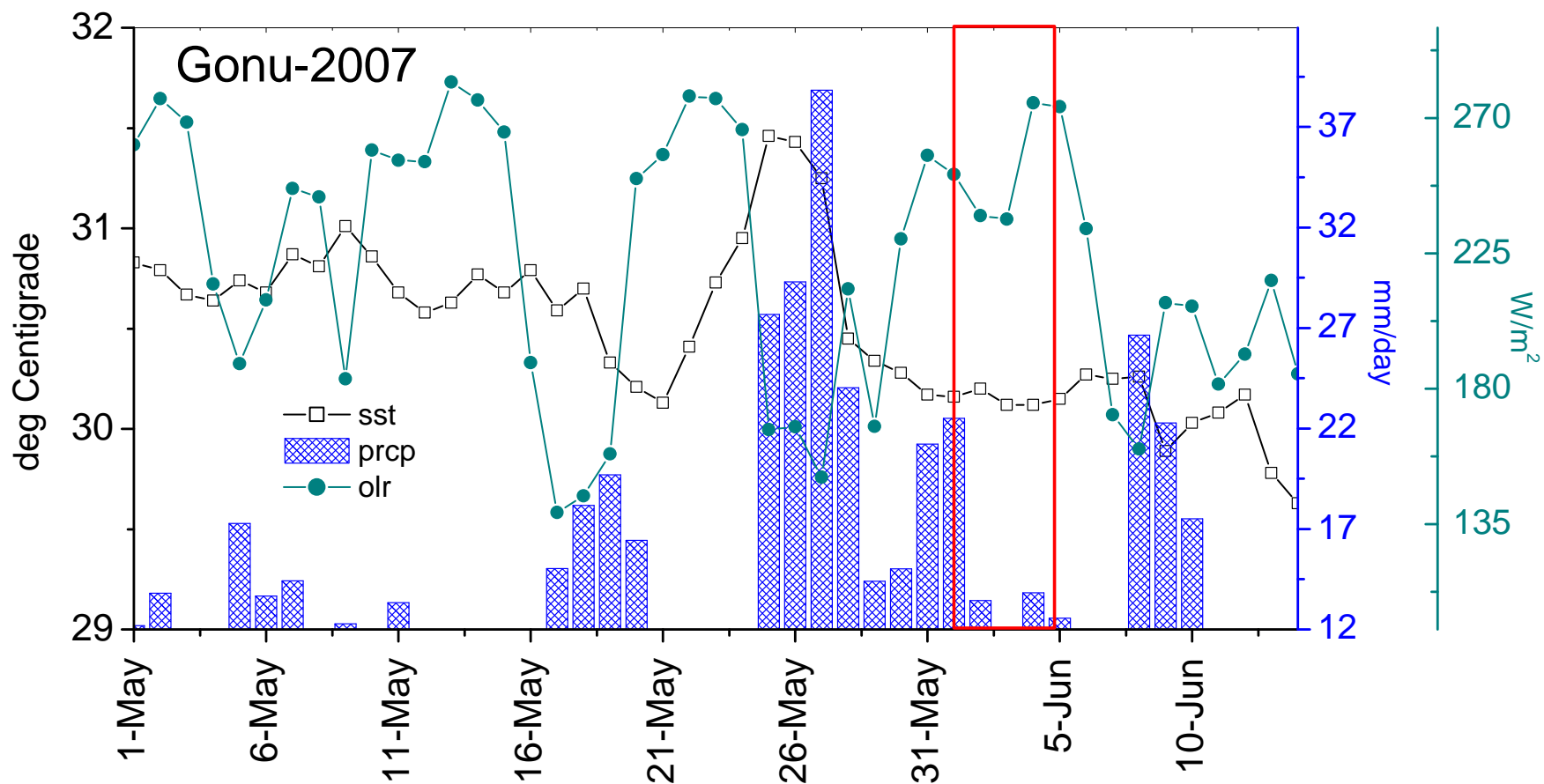


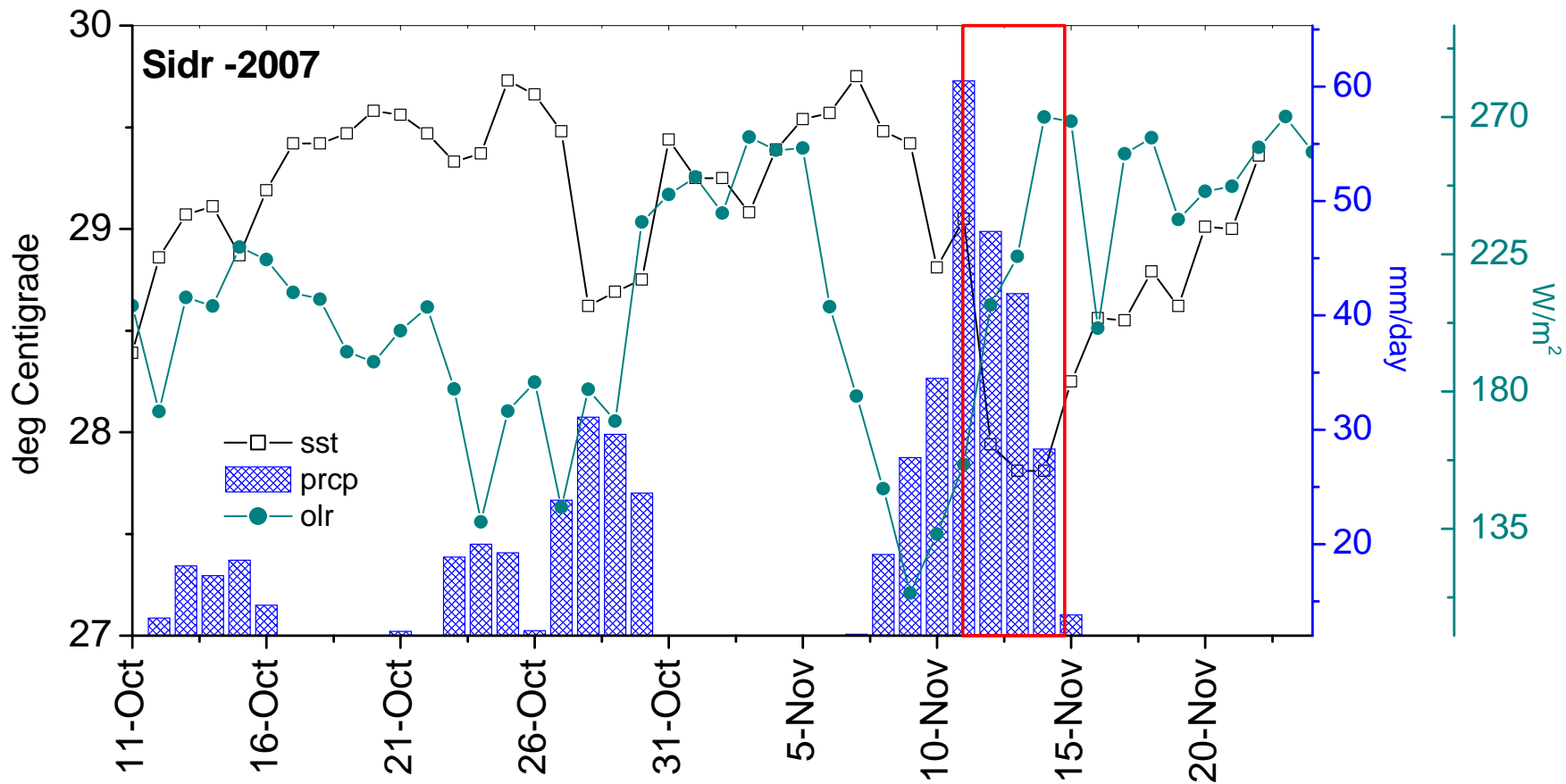


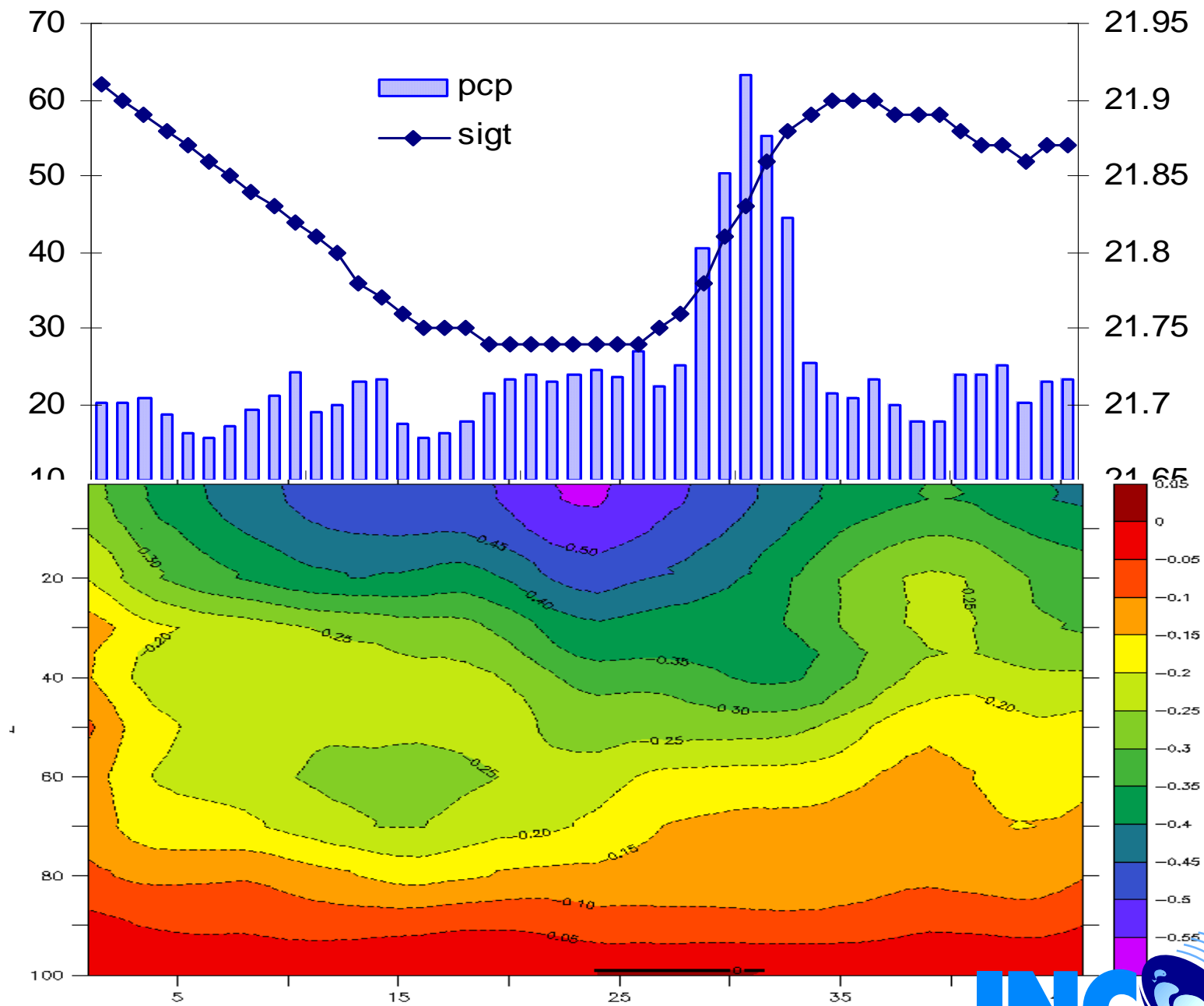


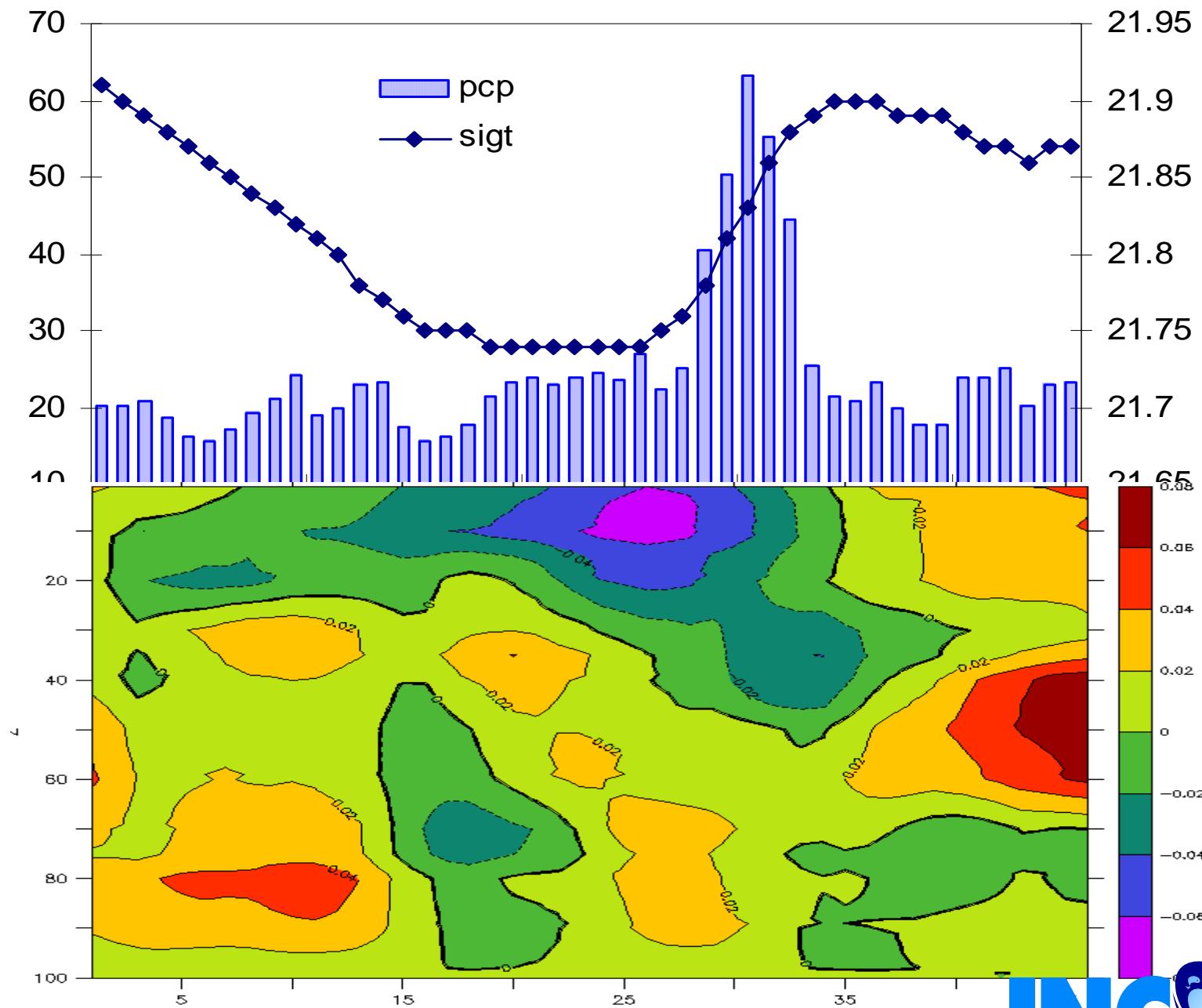




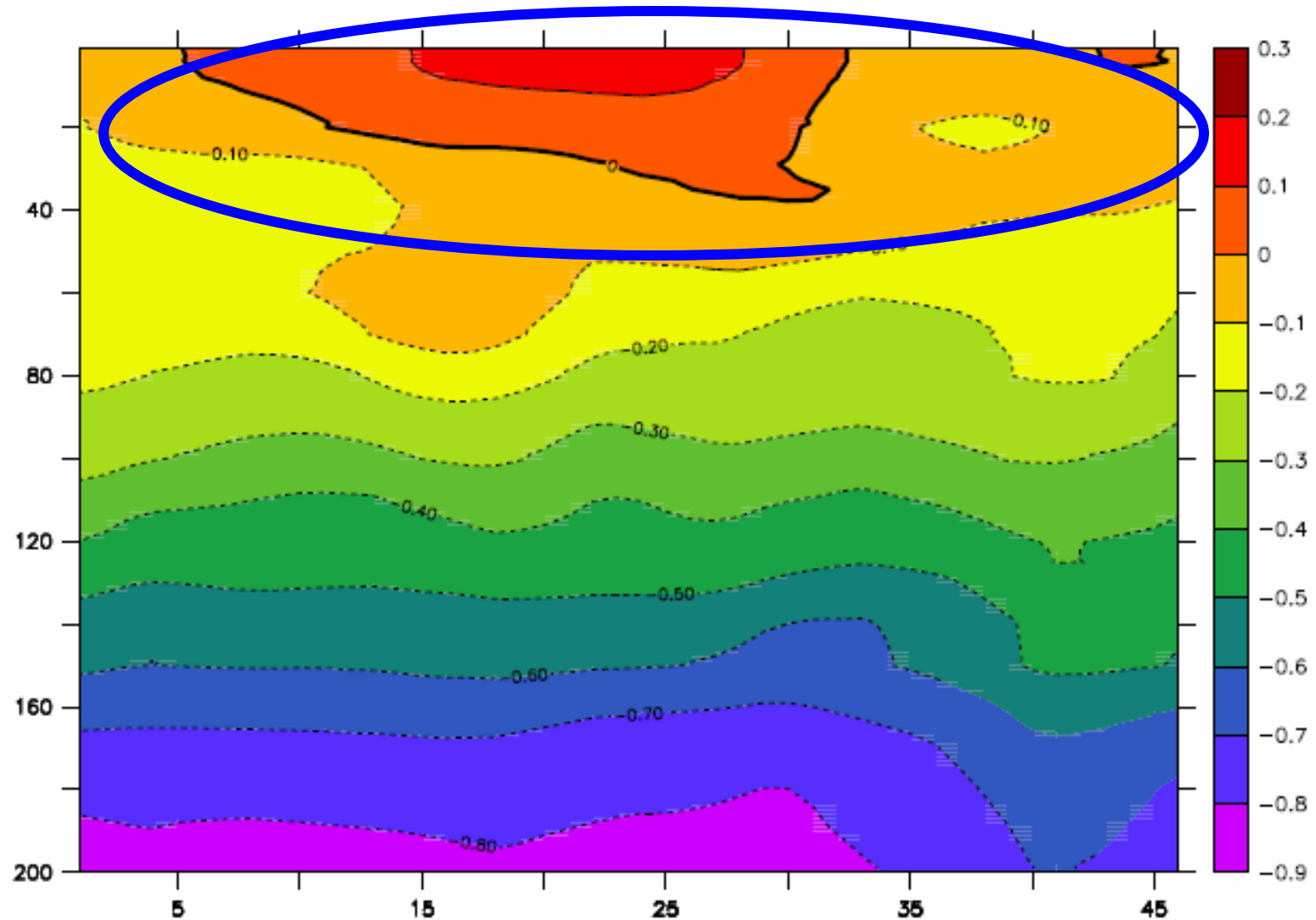




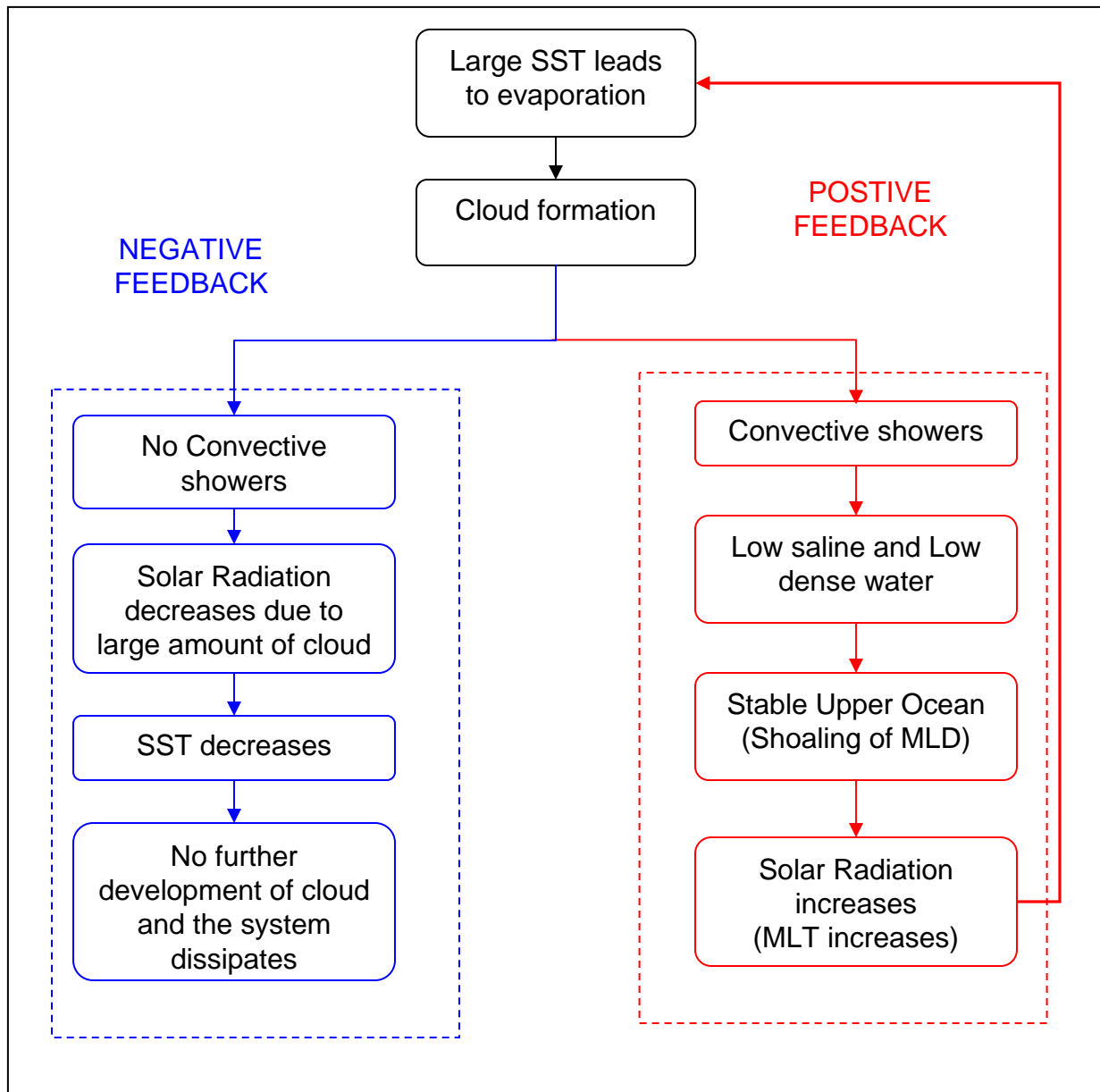


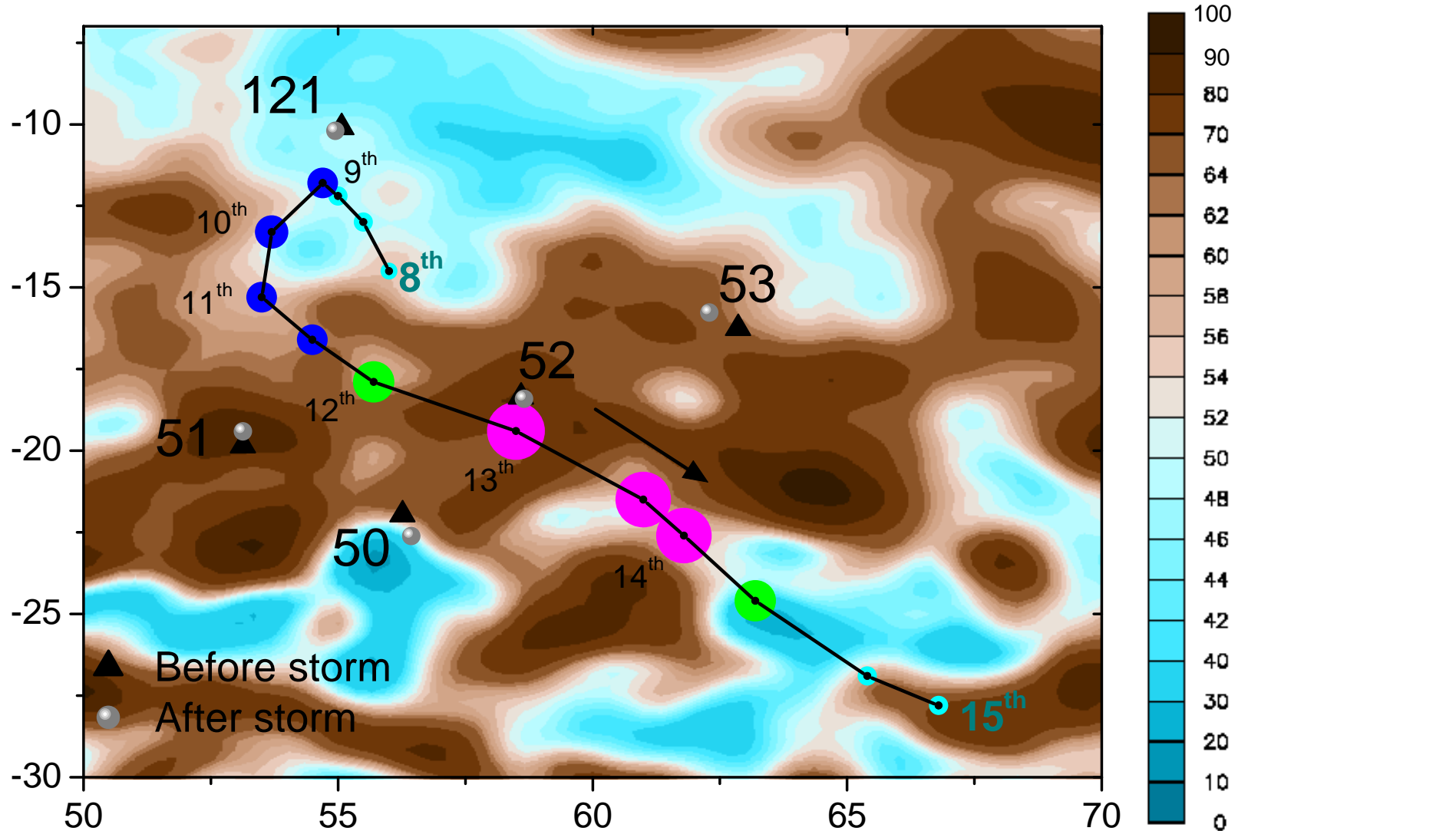


Density anomaly minus std dev of density

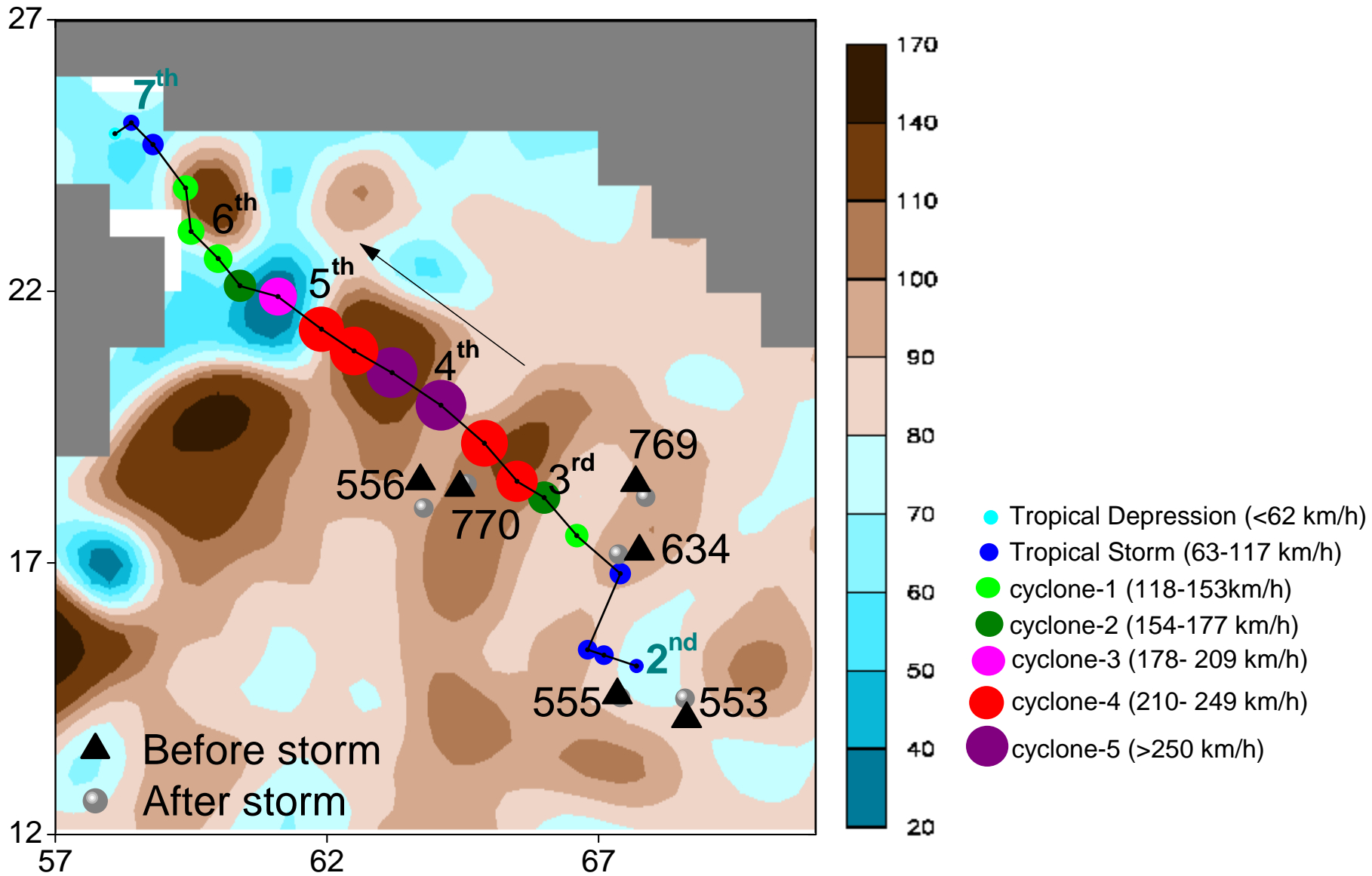


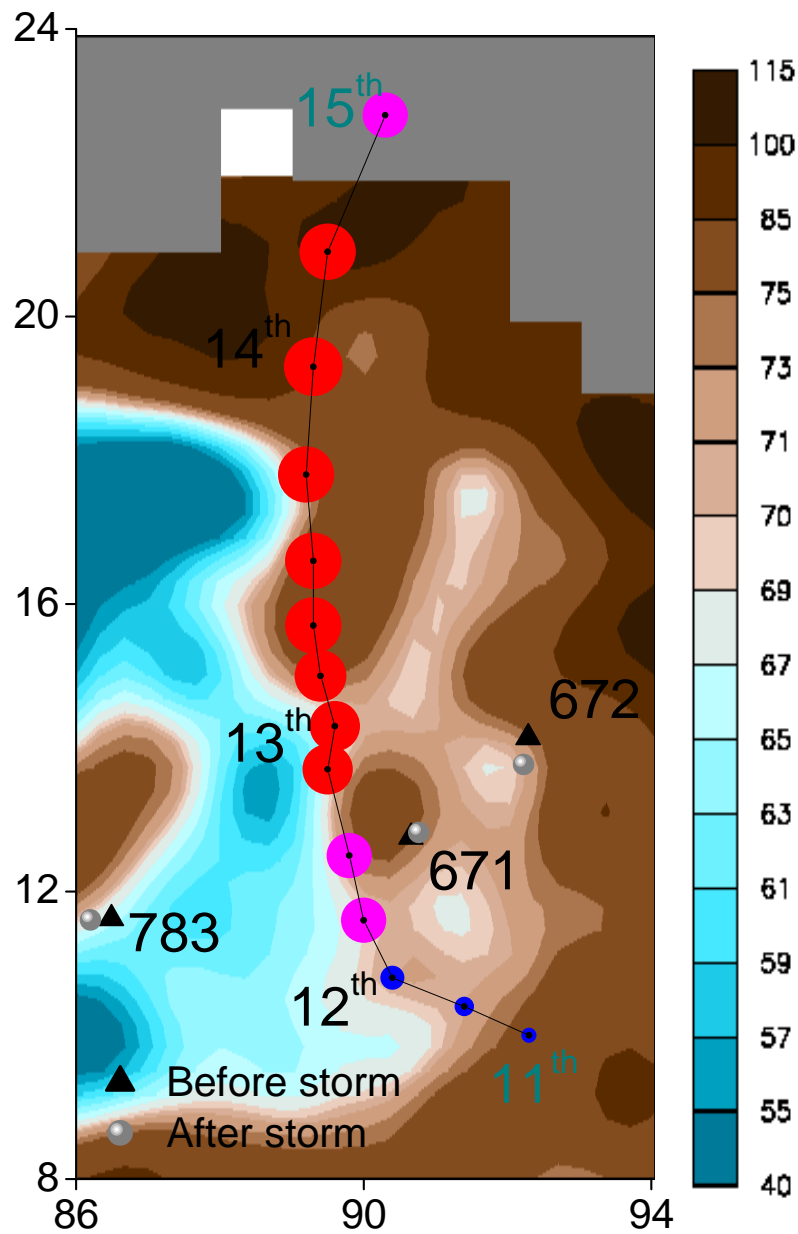
Density anomaly = woa density – argo density

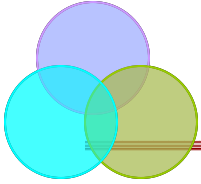




- Tropical Depression (<62 km/h)
- Tropical Storm (63-117 km/h)
- cyclone-1 (118-153km/h)
- cyclone-2 (154-177 km/h)
- cyclone-3 (178- 209 km/h)
- cyclone-4 (210- 249 km/h)
- cyclone-5 (>250 km/h)







Summary

- **Low salinity/density**
 - stabilize the upper ocean and inhibit vertical mixing , increasing MLT
 - enhances cloud formation and thereby genesis
- **More Heat Content**
 - Intensity increases

Thank You



Tropical Cyclone Studies by Satellite Observations

Chandra Mohan Kishtawal
ASD/MCC
Space Applications Centre



Key Issues in Tropical Cyclone Monitoring & Prediction

Correct Geolocation



Correct Intensity Estimation



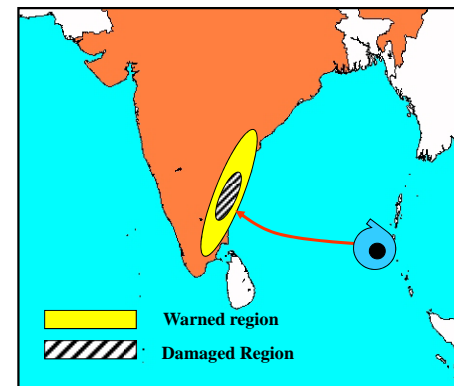
Correct Intensity Change Detection



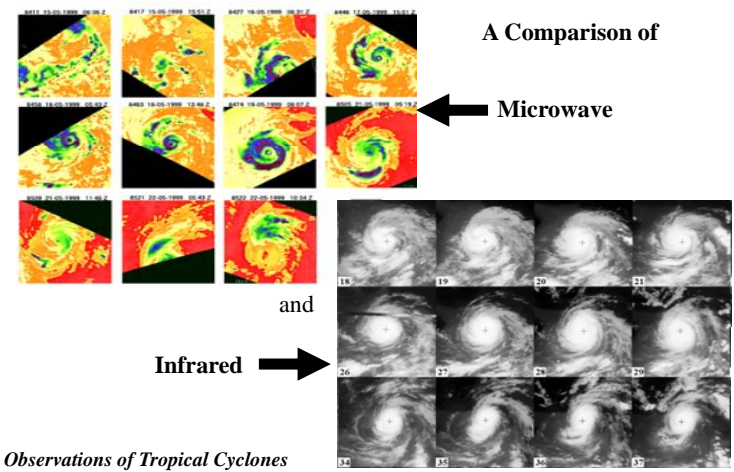
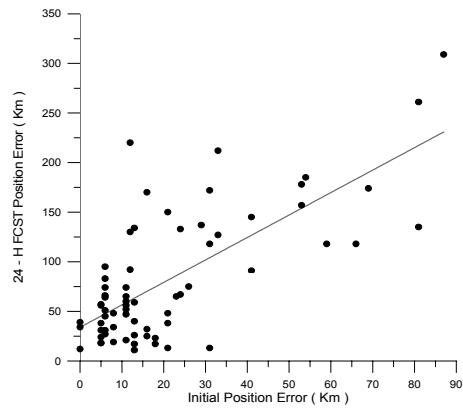
Correct Track Change Detection



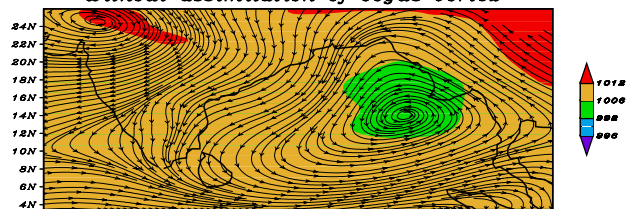
Cyclone Geolocation Using Microwave Observations



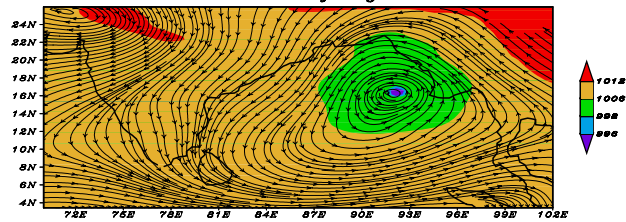
Impact of Initial Position Error on Track Forecast



(a) initial SLP(mb) and wind field (m/s) at 850 hpa, valid at 00 GMT of 27th October 1999 without assimilation of bogus vortex

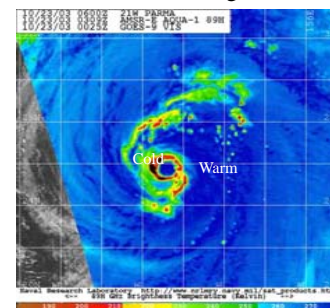


(b) initial SLP (mb) and wind field (m/s) at 850 hpa, valid at 00 GMT of 27th October 1999 with assimilation of bogus vortex

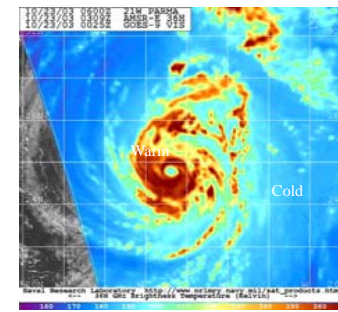


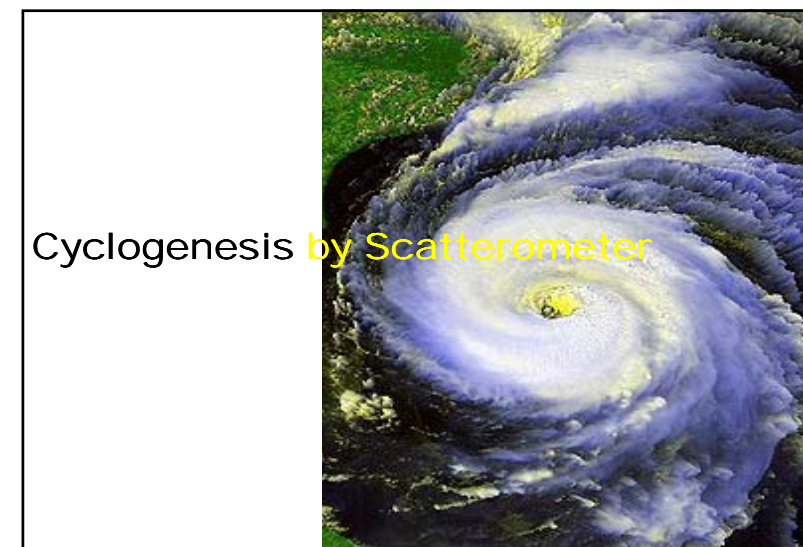
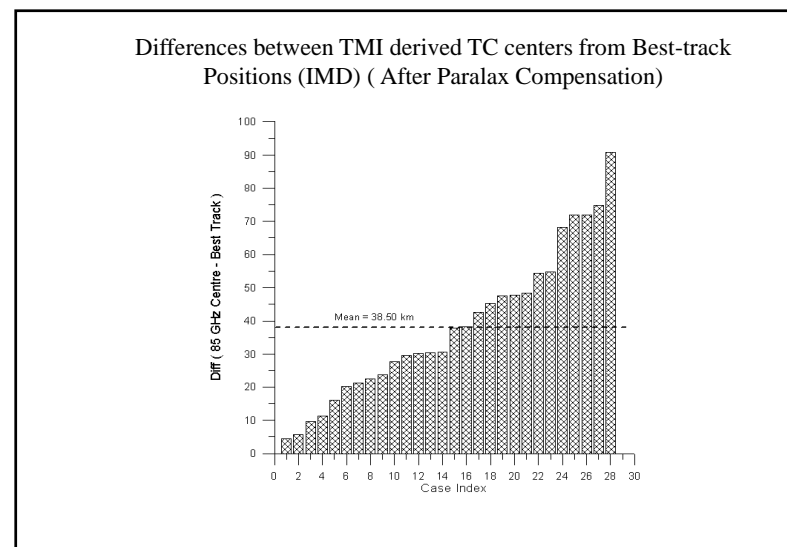
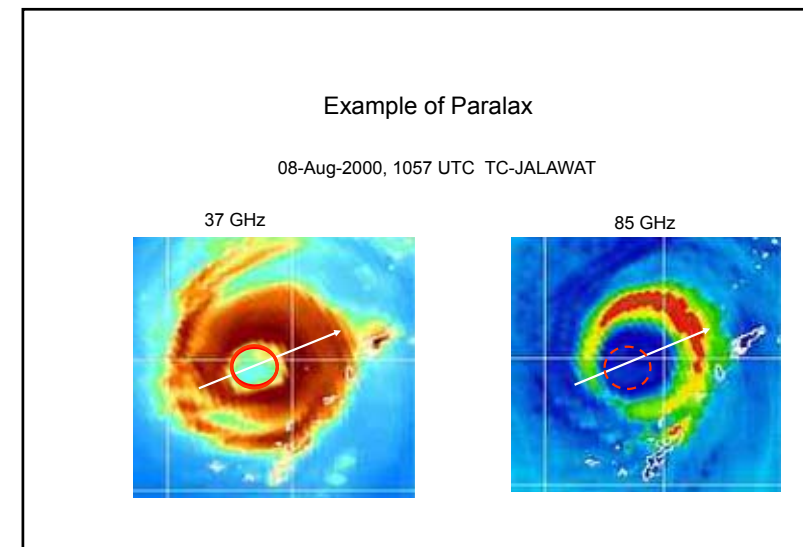
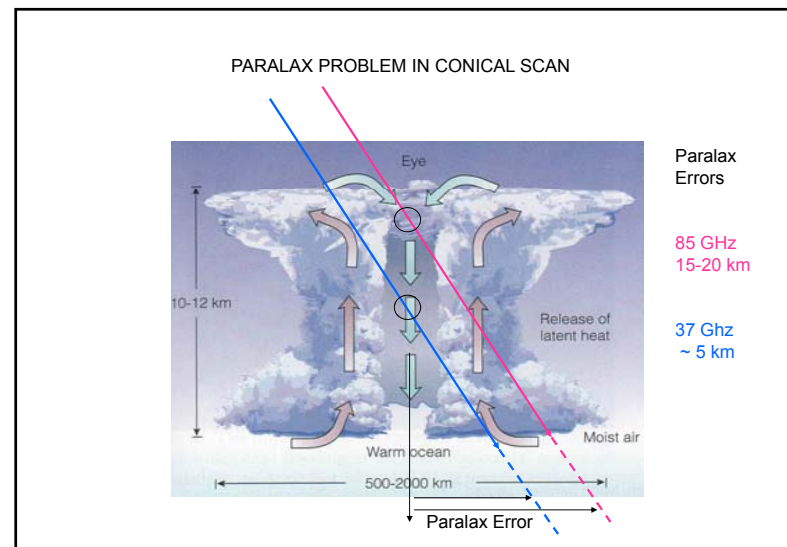
Two Main Microwave Sensing Channels for TC's

85 GHz
"Cold" Precipitation
Against Warmer
Ocean Background

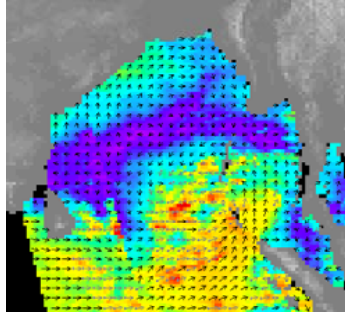


37 GHz
"Warm" Precipitation
Against Colder
Ocean Background



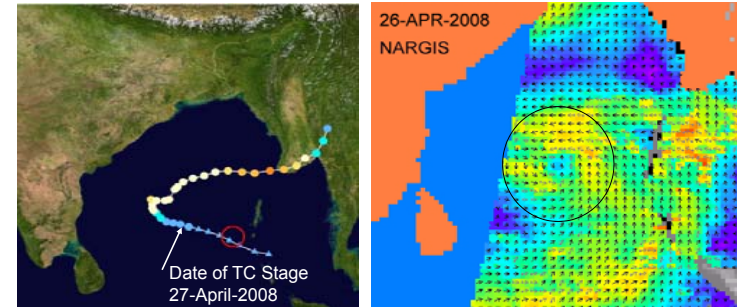


**TROPICAL CYCLOGENESIS
PREDICTION
USING
SCATTEROMETER DATA**



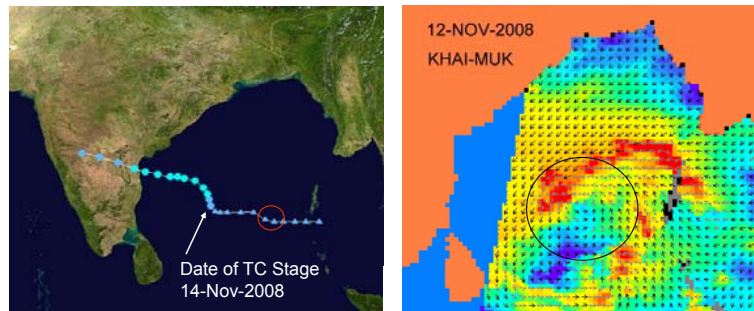
- Microwave scatterometers provide ideal measurements to detect early signals of tropical cyclogenesis.
- Vorticity-threshold based methods have been tried earlier (Bourassa et al.)
- Partial coverage of scenes by scatterometers, and also the inaccuracies in wind speed and direction pose problems in determination of reliable vorticity values, leading to false alarms.

Tropical Cyclone NARGIS (27-APR-01-MAY 2008)



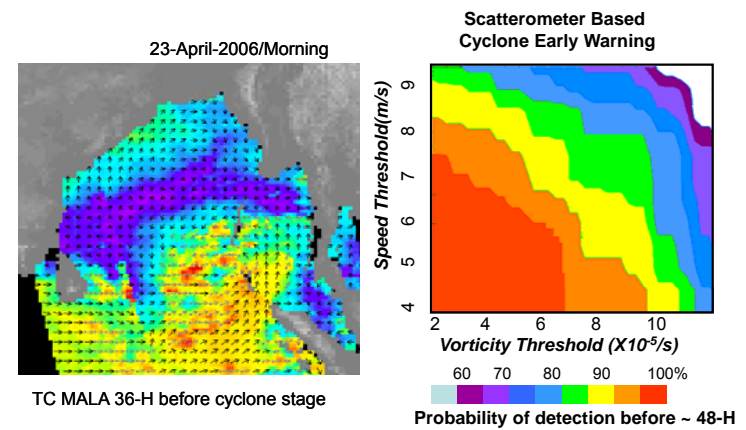
Vorticity-Based Cyclogenesis Detection Lead Time = 24 Hours

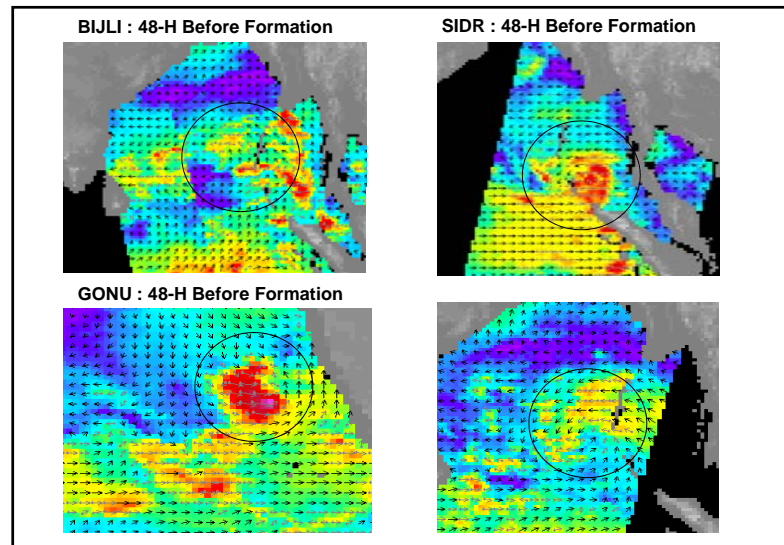
Tropical Cyclone KHAI-MUK (14-16 Nov-2008)



Vorticity-Based Cyclogenesis Detection Lead Time = 48 Hours

**New Starts : Tropical CYCLOGENESIS using
Satellite Measurements**





Data-Mining (DM) Techniques for Cyclogenesis Prediction Using Scatterometer data

BASIS :

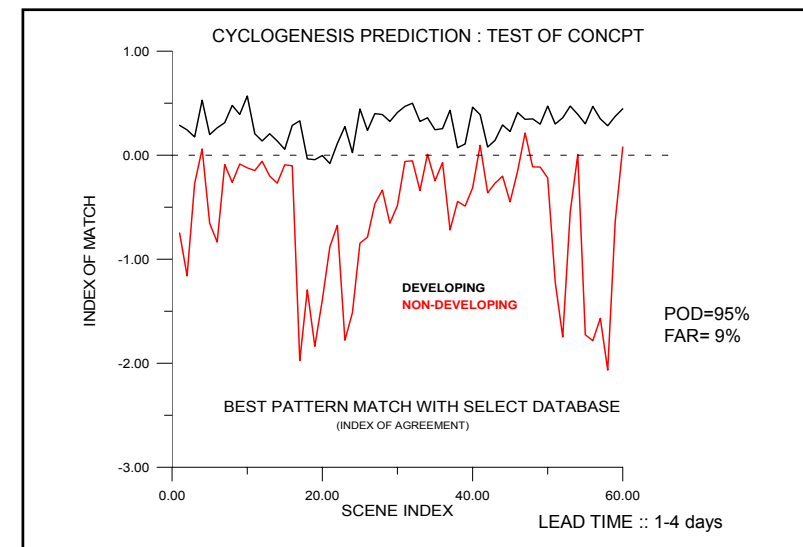
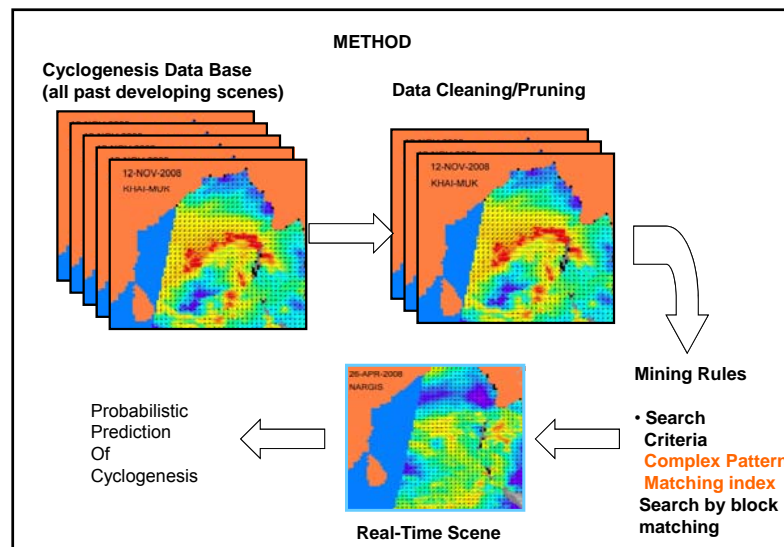
A large archive of Quikscat winds provide adequate sample to make data-based queries for cyclogenesis forecasting.

PROS :

- The DM techniques rely on “pattern matching”, and not on the derived parameters like vorticity and their thresholds. So statistically DM technique has higher robustness.
- DM techniques can make use of partial information like those from swaths of polar orbiting satellites.

CONS (or questions)

- Does the data-base contains all possible realizations of pre-storm wind patterns ?

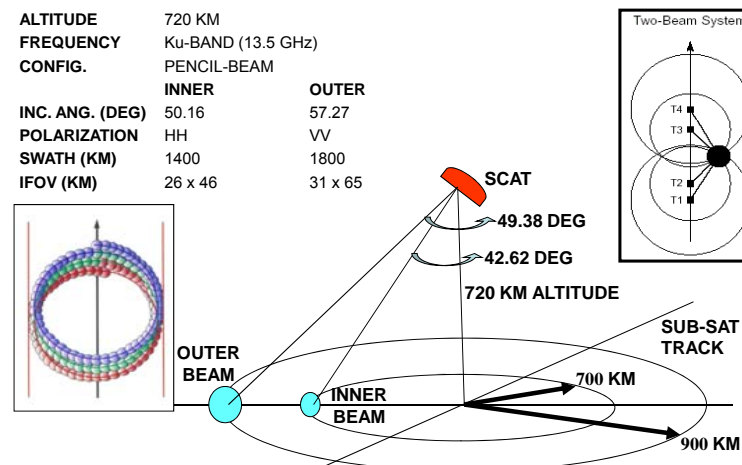


SCATTEROMETER

Parameter	Inner Beam	Outer Beam
Altitude (km)	720	
Frequency (GHz)	13.515	
Wind speed range (m/s)	4 - 24	
Wind speed accuracy	Better than 20% (rms)	
Wind Direction accuracy	20 Deg (rms)	
Resolution(km)	50 X 50	
Antenna offset (wrt +yaw)	46 degrees	
Polarisation	HH	VV
Scanning circle radius(km)	700	900
Elevation angle	42.6°	49.38°
Oneway 3DB Footprint(km)	26 X 46	31 X 65
Scanning rate	20.5 rpm	

Data availability: www.nrsa.gov.in (as per AO-PI)

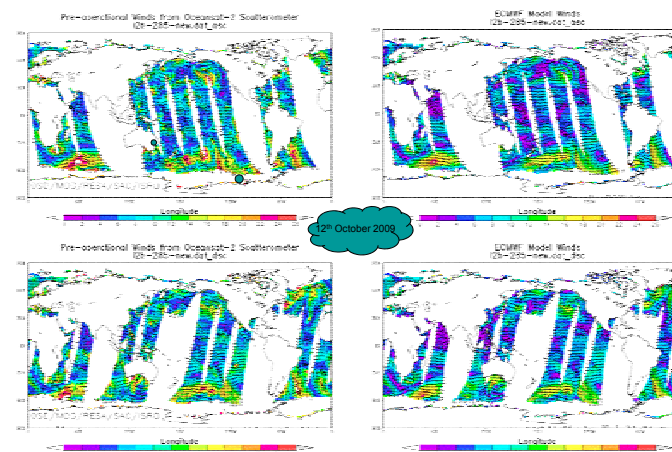
OCEANSAT-2 /SCATTEROMETER



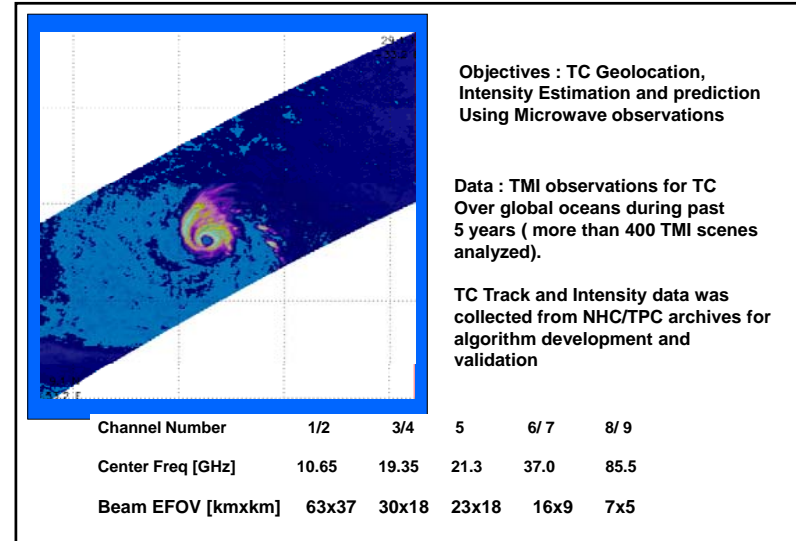
Features of Quikscat & Oceansat-2 Scatterometers

Specifications	Quikscat	Oceansat-2
Altitude (km)	803	720
Frequency (GHz)	13.4	13.5
Nadir Angle (H)	~40°	~44°
Nadir Angle (V)	~46°	~49°
Inc. Angle (H) (nom.)	~46°	~50°
Inc. Angle (V) (nom.)	~54°	~57°
Size of WVC (km)	25	50
Swath (km)	~1800	~1800
Other ancillary data for surface & rain flags	SSM/I	ECMWF
Applicable GMF	QSCAT-1	TBD

Pre-operational Ocean Surface Winds from Oceansat-2 Scatterometer

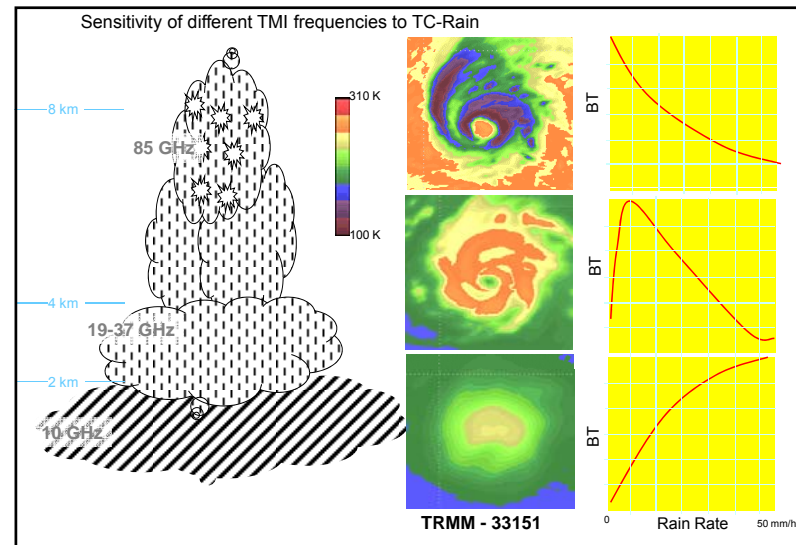


Cyclone Intensity Estimation



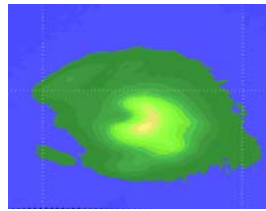
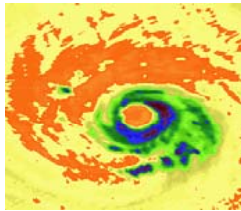
Operational Centers worldwide still depend on Dvorak's technique for TC intensity estimates that uses manual/automated pattern-analysis of VIS/IR images. In operational set-up it proves slow.

We developed an automatic technique for TC intensity assessment, that is quick, and reliable.

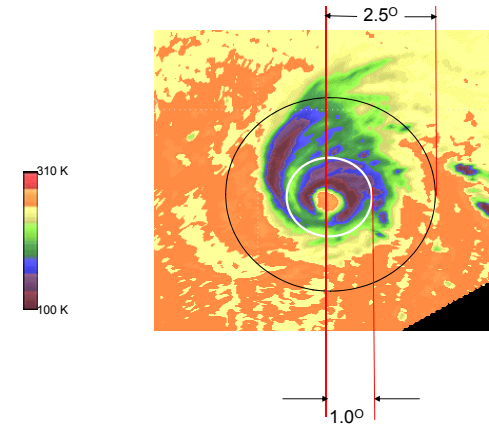
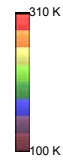
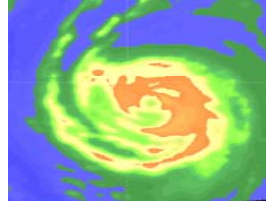
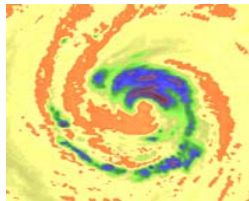


CONVECTIVE ORGANIZATION WITHIN STORMS

15582



33108

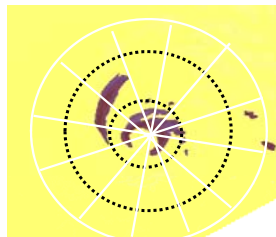


Quantifying Isotropy of Convection

$$ISO = \sum i \varnothing_i / ((n-1) * \bar{A}), n=12 \quad (5)$$

$$\varnothing_i = (\text{Loge}(N_i+1) - \bar{A}) \text{ if } \text{Loge}(N_i+1) \geq \bar{A}, \text{ otherwise } \varnothing_i = 0$$

N_i = No of TMI pixels with PCT < 240 K



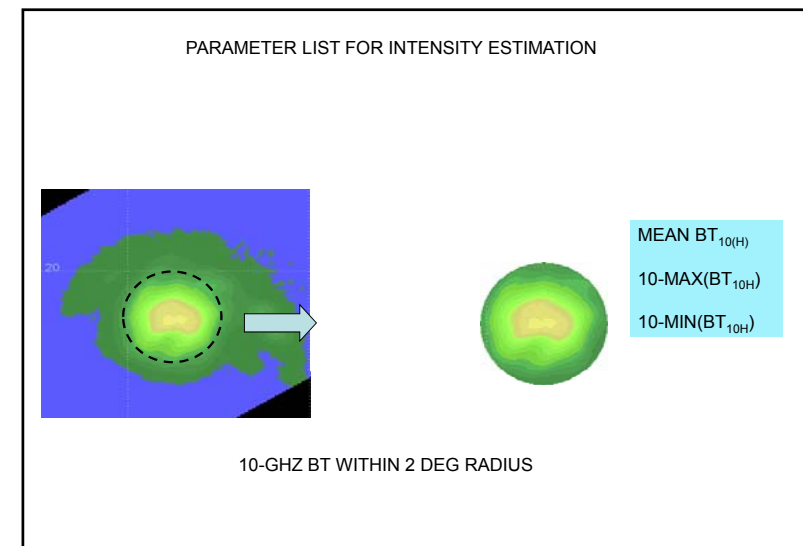
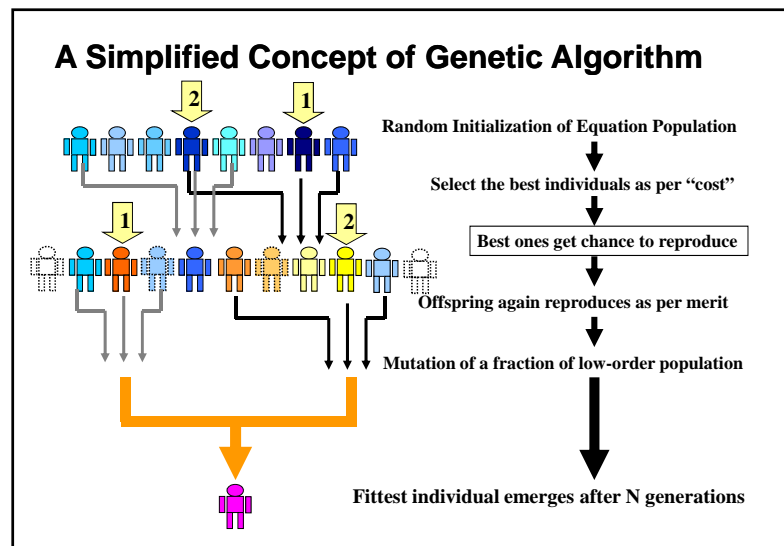
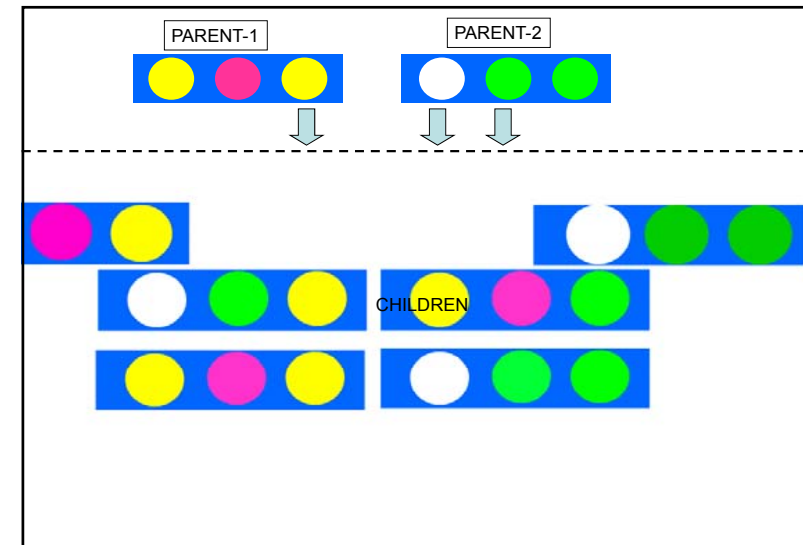
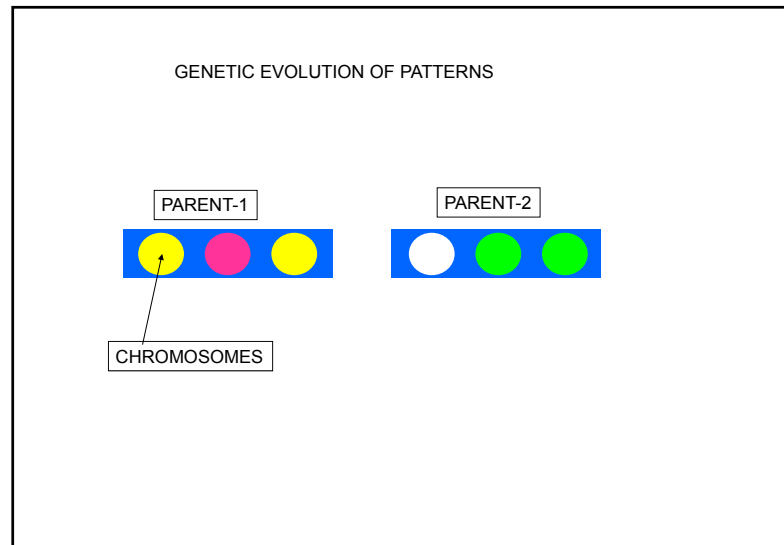
$ISO_{IN} = 0.621$
 $ISO_{OUT} = 0.234$

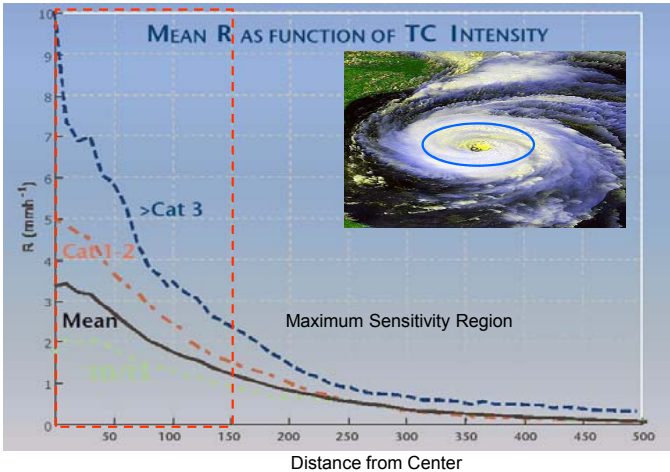


$ISO_{IN} = 0.832$
 $ISO_{OUT} = 0.523$

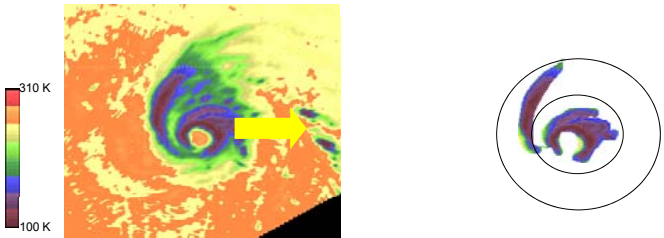
ALGORITHM DEVELOPMENT BY GENETIC ALGORITHMS

Randomized search and optimization technique
 guided by the principle of natural genetic systems.





CONVECTIVE ISOTROPY
(SYMETRY OF THE REGION DEFINED BY PCT < 240 K)



$$ISO = \sum_i \emptyset_i / ((n-1) \cdot \bar{A}), n=12 \quad (5)$$
$$\emptyset_i = (\text{Loge}(N_i+1) - \bar{A}) \text{ if } \text{Loge}(N_i+1) \geq \bar{A}, \text{ otherwise } \emptyset_i = 0$$

N_i = No of TMI pixels with PCT < 240 K

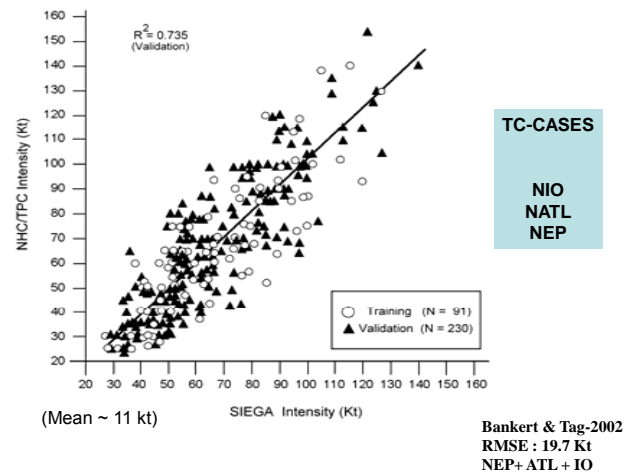
$$MSW(kt) = \frac{a-d/(i-7.09)+(e+f-d)/((-52.15+c/b-f/(h-75.75))^*(-21.96))+b-168.17}{((-52.15+c/b-f/(h-75.75))^*(-21.96))+b-168.17}$$

Term	Expression
a	Mean of 10-H for $r < 1^\circ$
b	Convective Isotropy for $r < 1^\circ$
c	Convective Isotropy for $1^\circ < r < 2.5^\circ$
d	Mean of cold 10-V pixels ($r < 1^\circ$)
e	Sum of 11 warmest 10-H ($r < 1^\circ$)
f	Sum of 11 coldest 10-H ($r < 1^\circ$)
g	Mean (37-V – 37-H) ($r < 1^\circ$)

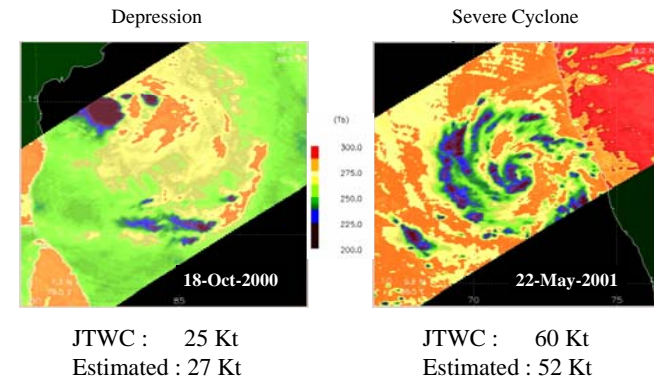
SENSITIVITY OF DIFFERENT TERMS

No	Parameter	Low Intensity Storms (MSW < 64 Kt)	High Intensity storms (MSW > 64kt)
1	Mean BT _{10-h} in R < 1 deg	1.33	1.33
2	Mean of coldest 10 pix	0.54	0.69
3	Isotropy (inner)	0.02	0.73
4	Isotropy (outer)	0.04	0.24

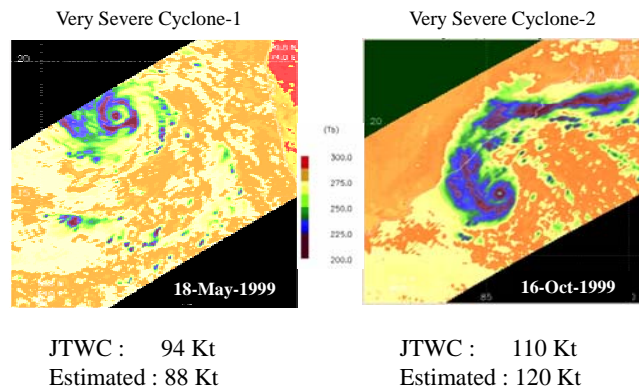
Automatic Intensity Estimation : Skill for Global TCs



Automatic Intensity Estimation : Case Studies



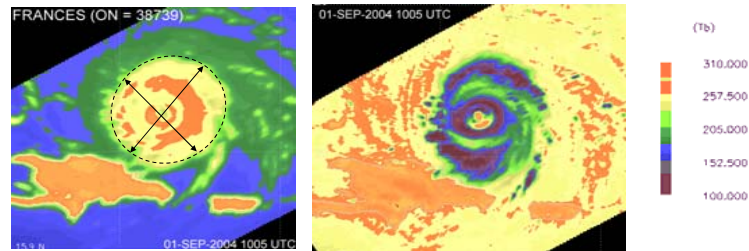
Automatic Intensity Estimation : Case Studies



Tropical Cyclone wind structure



Can Passive MW Observations Reveal Wind Structure ?



- Information of wind asymmetry is very crucial for model initial conditions, as well as for damage assessment due to cyclones.
- Passive microwave observations, particularly those at 37-GHz can reveal asymmetries in cyclone structure, that can be associated with wind structure.

THE PATH OF HURRICANE IKE



Asymmetry decides which side damage would occur

METHODOLOGY

Radial profile of wind can be approximated as (Chan and Williams (1987))

$$V(r) = V_{max} * (r/R_{max}) * \exp((1 - (r/R_{max})^b) / b) \quad (1)$$

While the shape parameter B is approximated as :

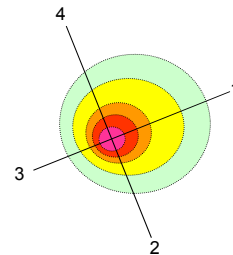
$$B_0 = \frac{V_{max}^2 \rho_a e}{P_n - P_c}$$

Step-1 : Solve (1) iteratively to get Rmax, if V(r) are known.

Step-2 : Use this Rmax to solve (1) again iteratively to get Vmax as a function of angle.

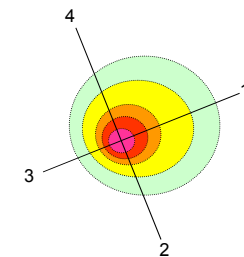
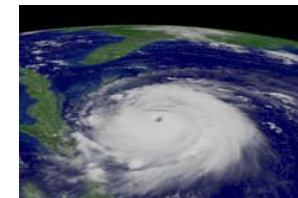
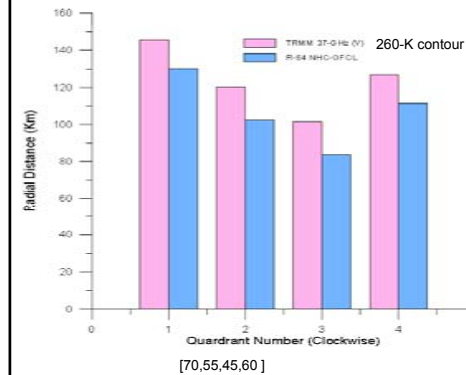
Step-3 : Use angle dependent Vmax to get full wind profile.

- Questions :
- Can we get Pmin from Vmax ? → YES
 - Can we get, say, R-64 kt, or, R-50 kt from TMI → Possible (very critical)
 - How closely we can know Pn → Reasonably well (within 2 mb)

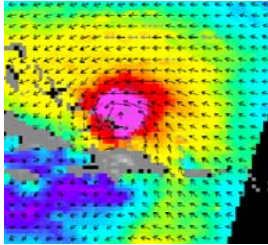


Hurricane FRANCES : 01-SEP-2004/1000 UTC

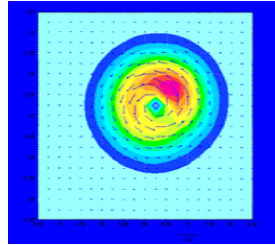
Comparison b/w NHC-Official 64-Kt wind radii and radii of 260 K contour of TMI-37 GHz (V)



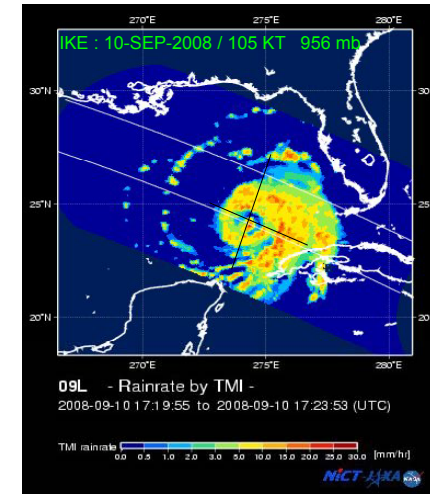
FRANCES : 01-SEP-2004 120-KT 936 mb



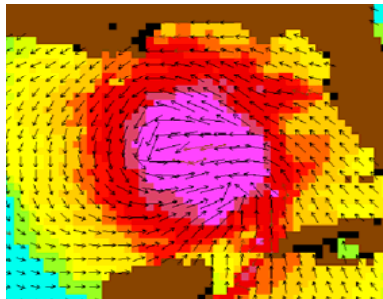
QuikScat



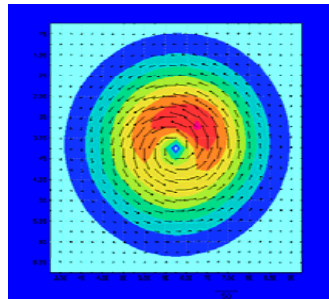
TMI-Reconstruction



IKE : 10-SEP-2008 / 105 KT 956 mb



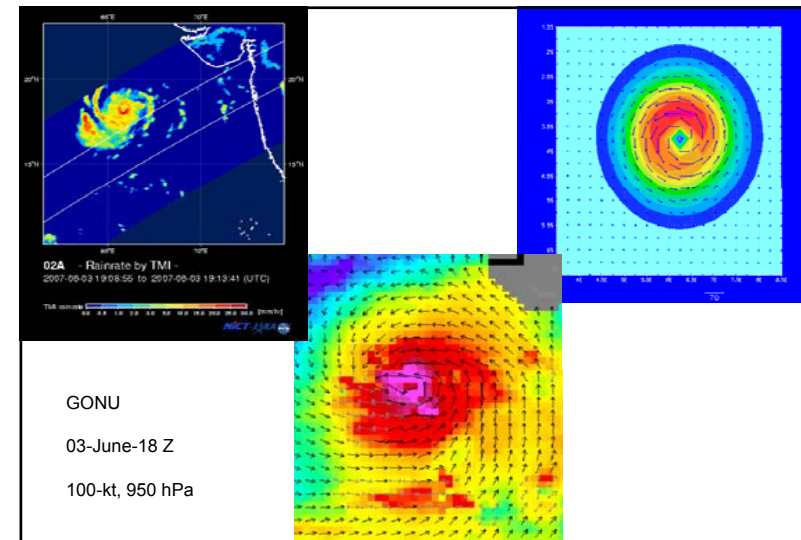
QuikScat



TMI-Reconstruction

Rmax (NHC) = 110 km

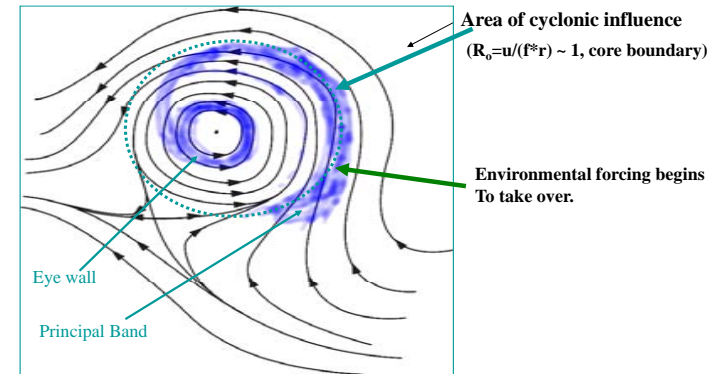
Rmax (TMI) = 106 km



Cyclone Intensity Prediction

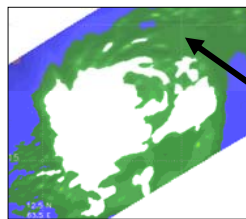


OBSERVATION-1 : Intensification Process Of Weak Cyclones (Msw < 64 Kt) is very much different from that of strong cyclones (MSW > 64 kt)



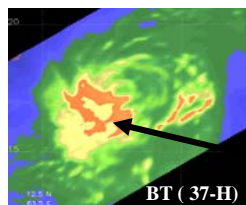
- The outward edge of bands respond earliest to environmental flow
- Convective bands transport large cloud mass upward, much larger than eye-wall

Intensity Change Predictors For Normal Intensity Cyclones



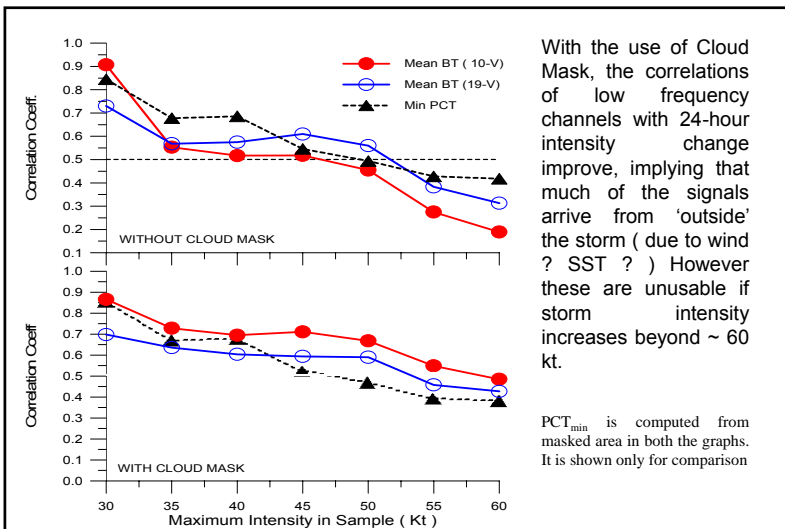
Mean of 5 low frequency channels over the un-masked region

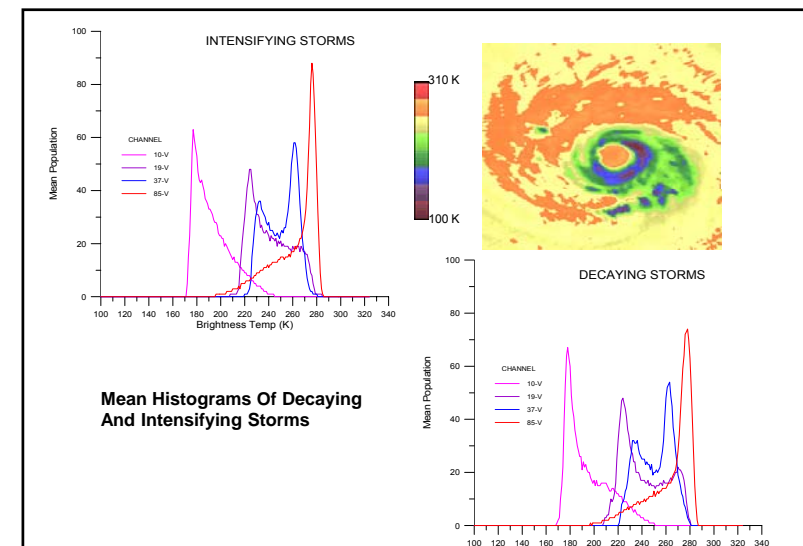
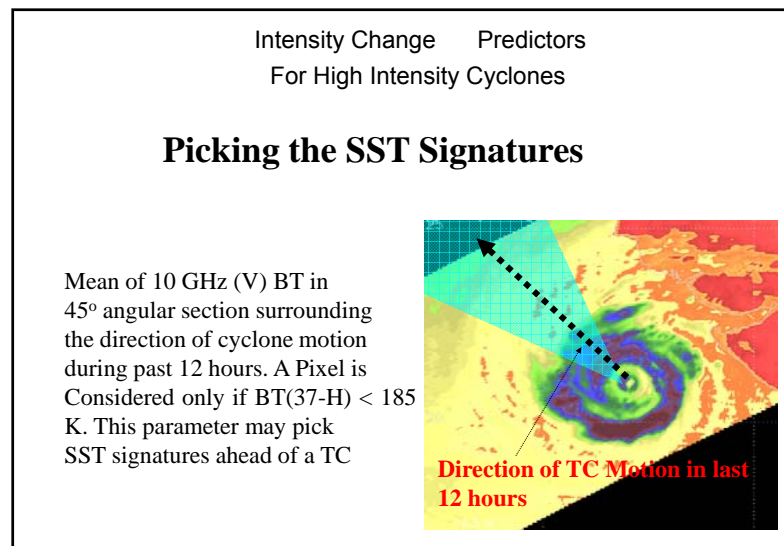
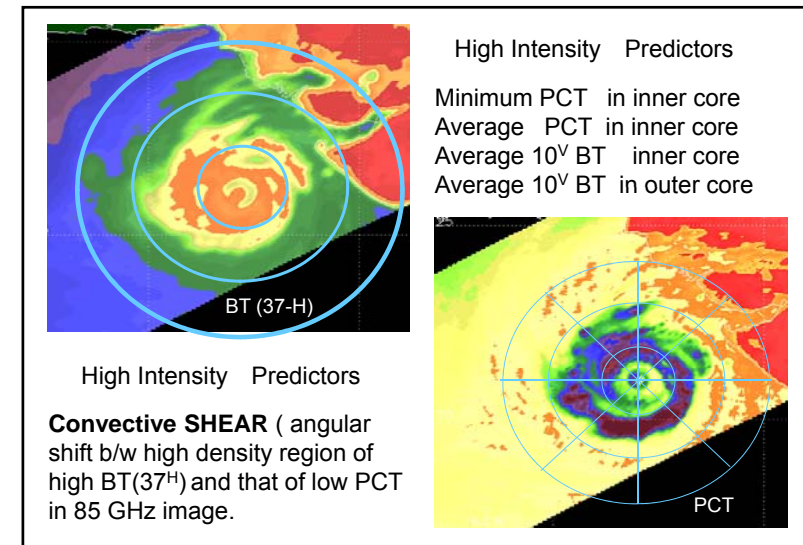
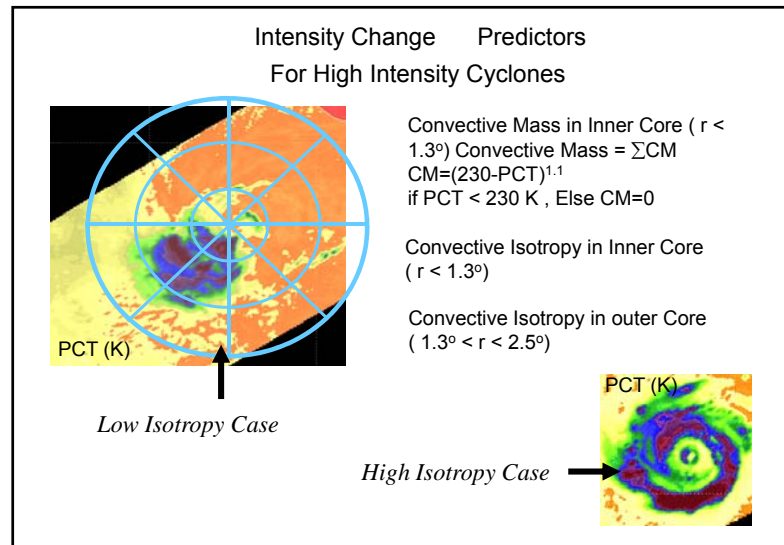
Convective Mass in high CLW region (BT-37^H > 240 K)
Convective Mass = ΣCM
 $CM = (240 - PCT)^{1.1}$
if $PCT < 240 K$, Else $CM = 0$

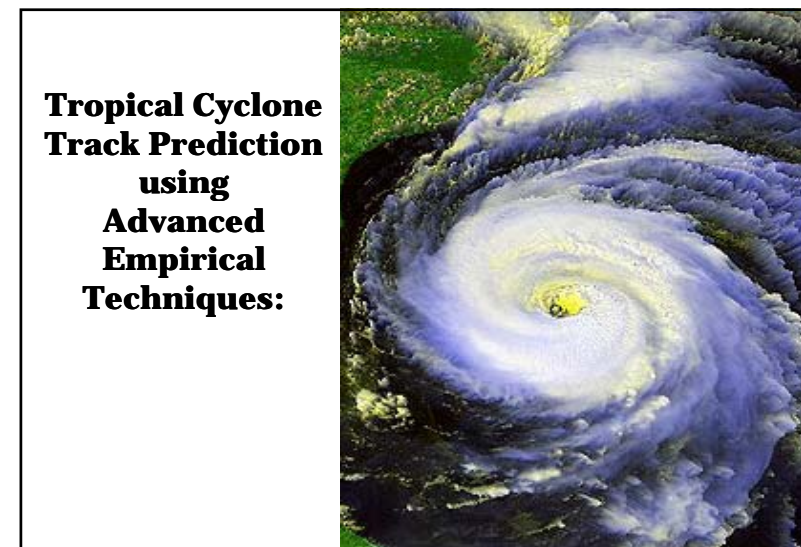
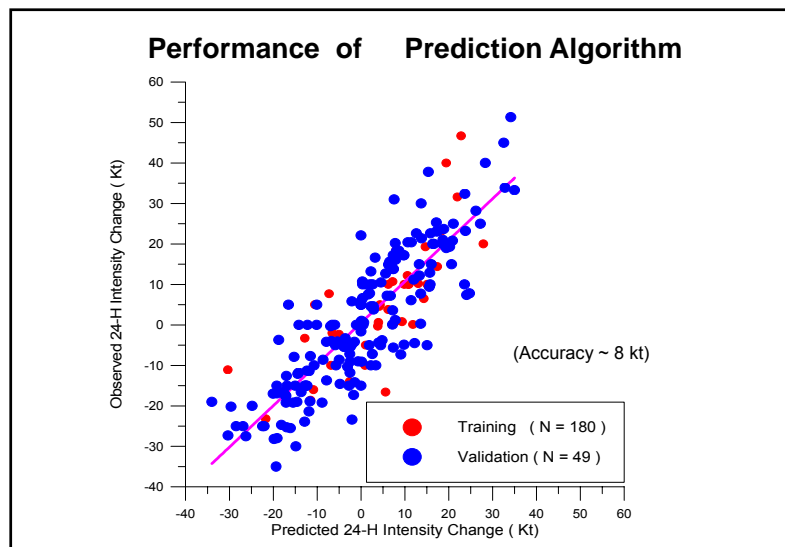
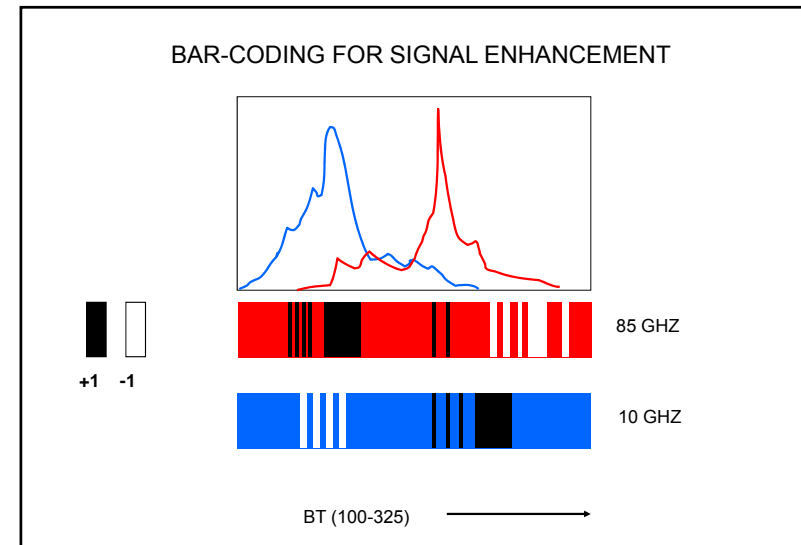
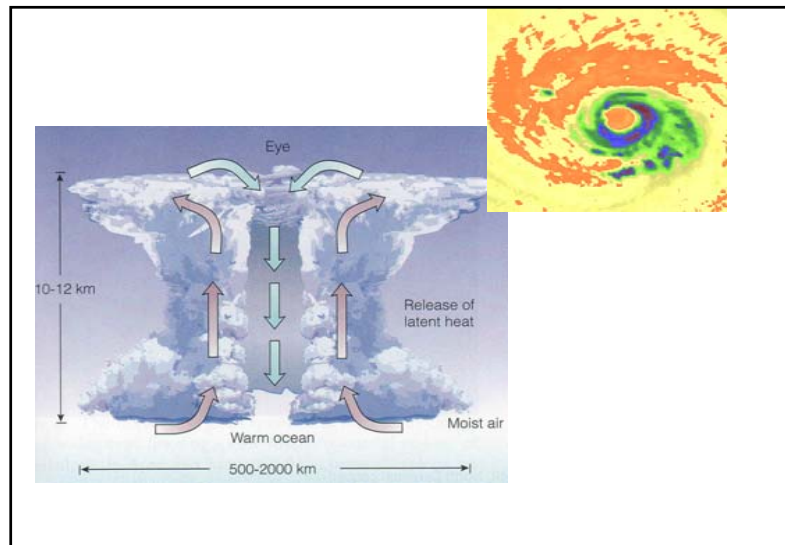


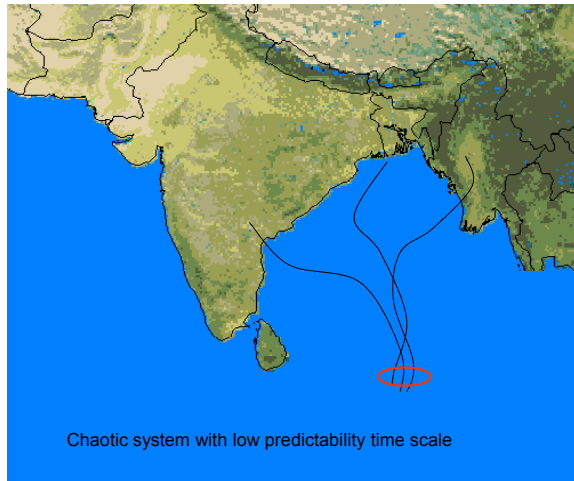
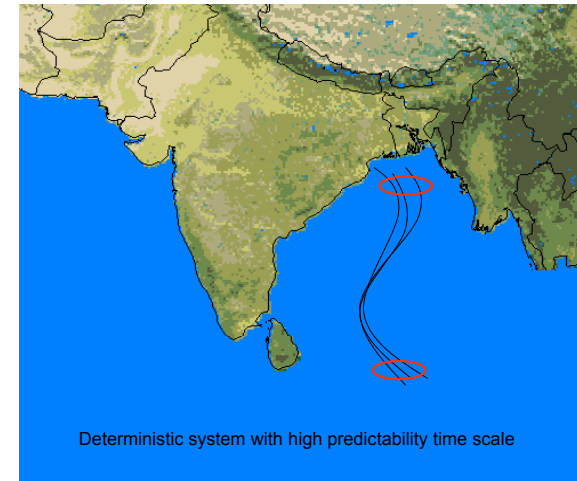
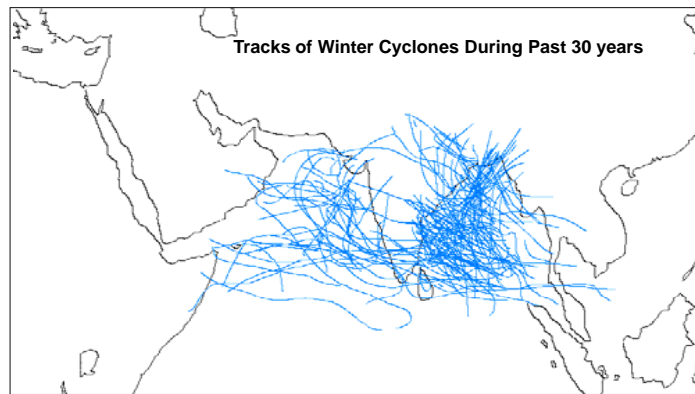
Minimum PCT in high CLW region

High CLW region









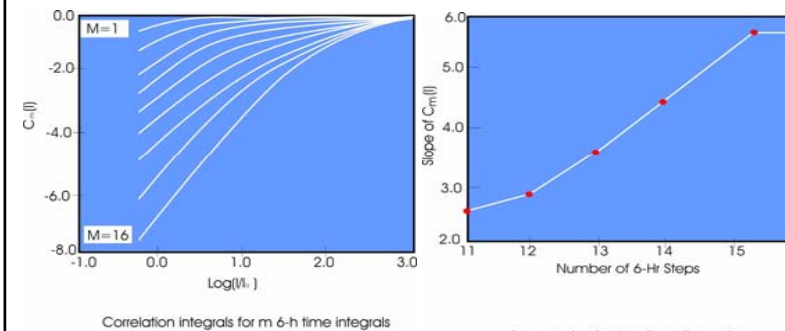
$$X_m(t_i) = \{X(t_i), \dots, X[t_i + (m-1)\Delta t]\},$$

$$C_m(l) = N_m(l) / (N_m - 1)^2,$$

$$K_2 = (1/l) \exp[C_m(l) / C_{m+1}(l)]$$

Correlation Integral
Kolmogorov-Sinai entropy of order 2

As $m \rightarrow \infty$ and $l \rightarrow 0$, $C_m(l) \sim l^d$



Background

✚ **Takens' theorem (Takens, 1981)** : Given a deterministic time series $\{x(t_k)\}$, $t_k = k\Delta t$, $k=1, \dots, N$, there exists a smooth mapping function P satisfying :

$$x(t) = P[x(t-\Delta t), x(t-2\Delta t), \dots, x(t-m\Delta t)] \quad (1)$$

where m is called the embedding dimension obtained from a state-space reconstruction of the time series (Abarbanel et al., 1993).

✚ **A Genetic Algorithm** tries to obtain the function $P[.]$ in Eq. (1) that best represents the amplitude function of a time series, which can then be used to predict the future state of the system.

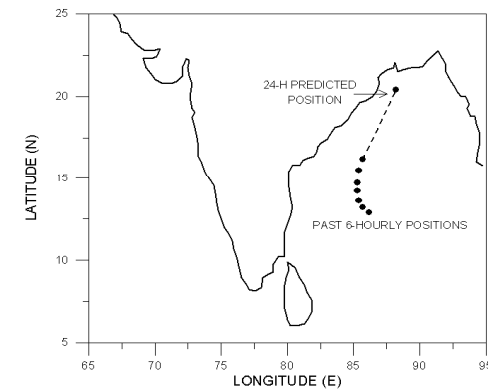
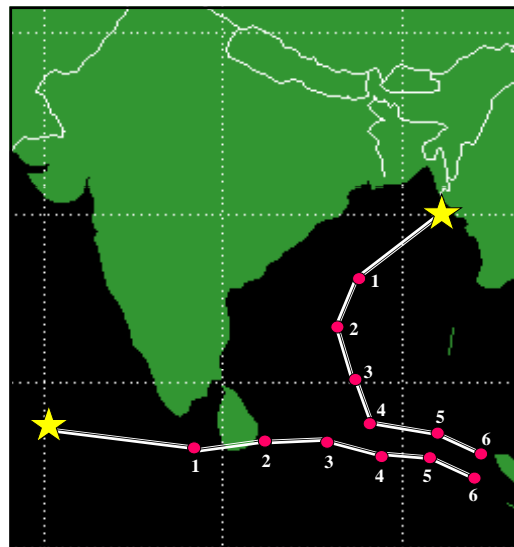


Figure-1 : An example of a track segment. 2567 such segments were used for the development of the track prediction algorithm.



Predictor Set

For 24-hour track prediction from any point $[x,y]$, the past six 6-hourly positions were used as the predictor set.

Every track point was represented as a complex number

e.g. $P = \text{Cmplx}[x,y]$

and we tried to obtain a unified prediction equation for both Lat and Longitude positions using Genetic Algorithm

Application of GA in Defining Empirical Equation for Prediction

An equation for predicting the TC position, 24-hours ahead of from any given time T was obtained as

$$P(T+24h) = f[P(T), P(T-6h), P(T-12h), P(T-24h), P(T-30h), P(T-36h)]$$

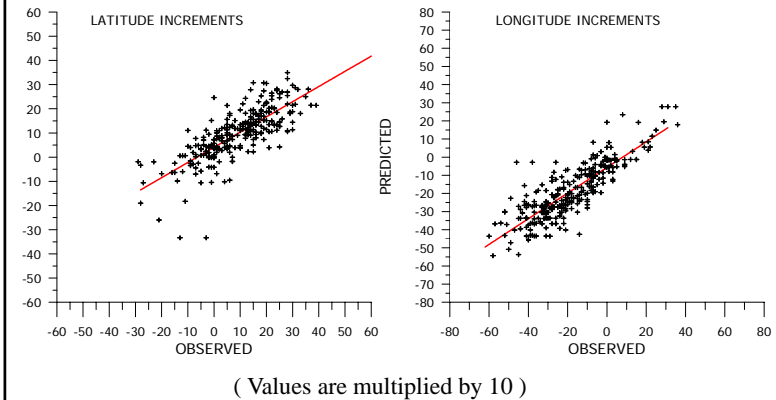
Where $P = \text{Complex}[Lat, Lon]$ at any given time.

We tried to obtain the form of function $f[.]$ using GA.

Our technique is not an alternative to dynamic models, but is an attempt to build a “CLIPPER” type quick track guidance system that is based on more accurate empirical modeling of track dynamics of Indian Ocean cyclones

Track Prediction using an Genetic Algorithm

24-HOUR PREDICTION
(RMS VECTOR DIFF = 1.23 DEG)



Error Histogram : Training + Validation

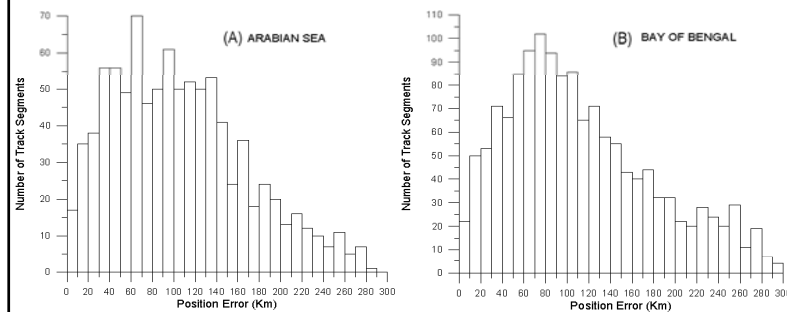
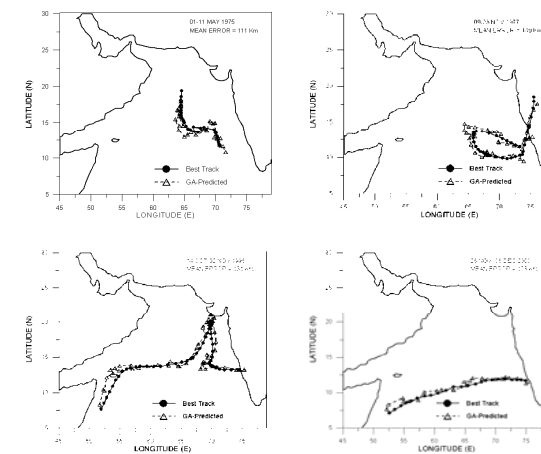


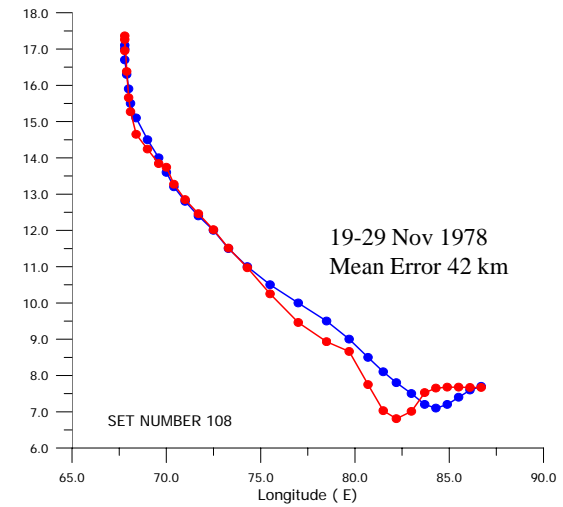
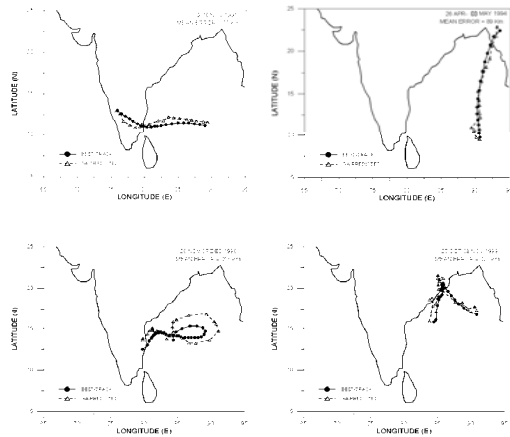
Fig. 2 : Histogram of position errors (Km) for (a) Arabian Sea and (b) Bay of Bengal

Mean vector error (BoB + AS) = 142 km for 24-H prediction for validation

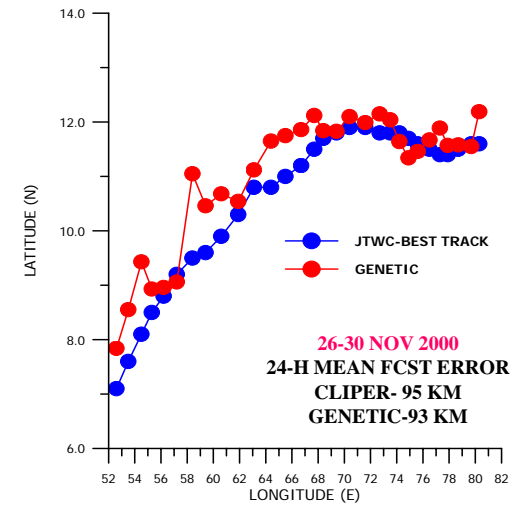
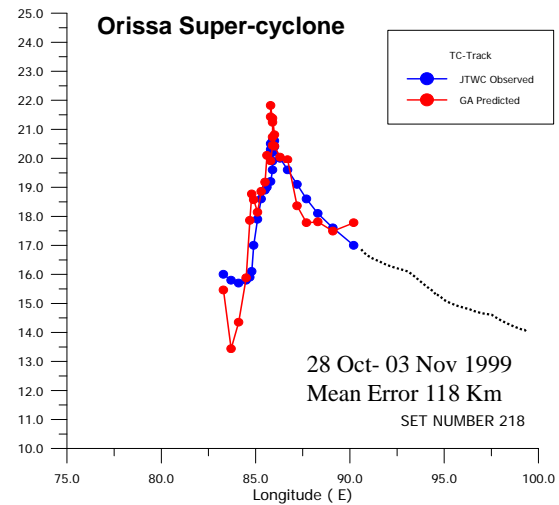
Some Non-Typical Validation Cases : Arabian Sea

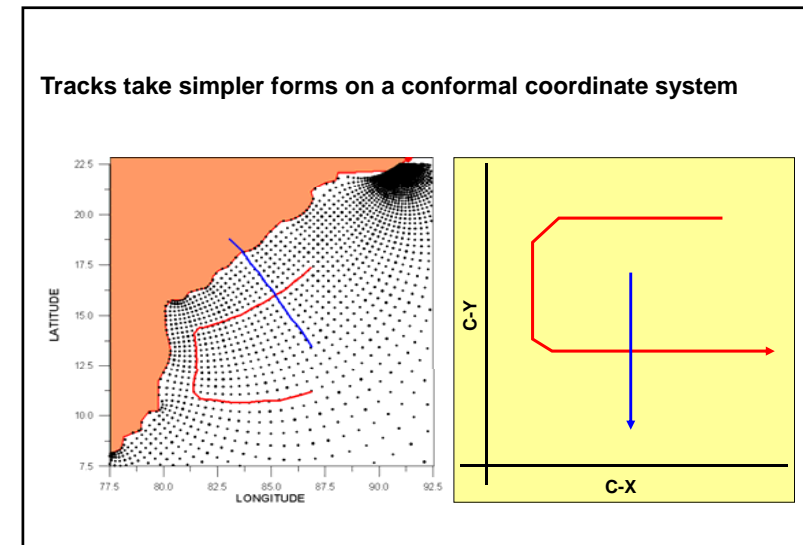
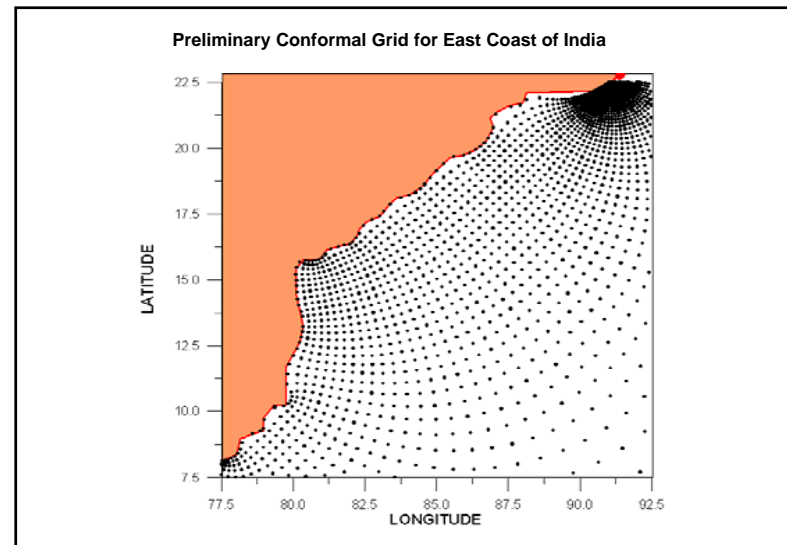
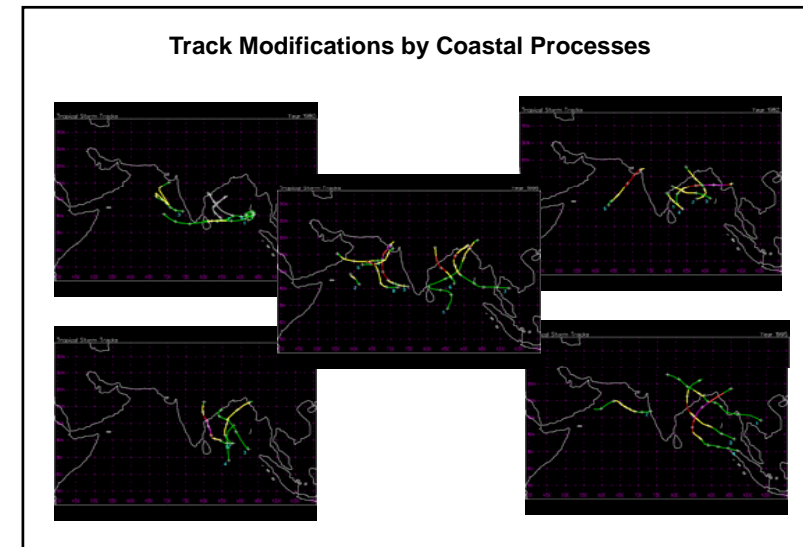
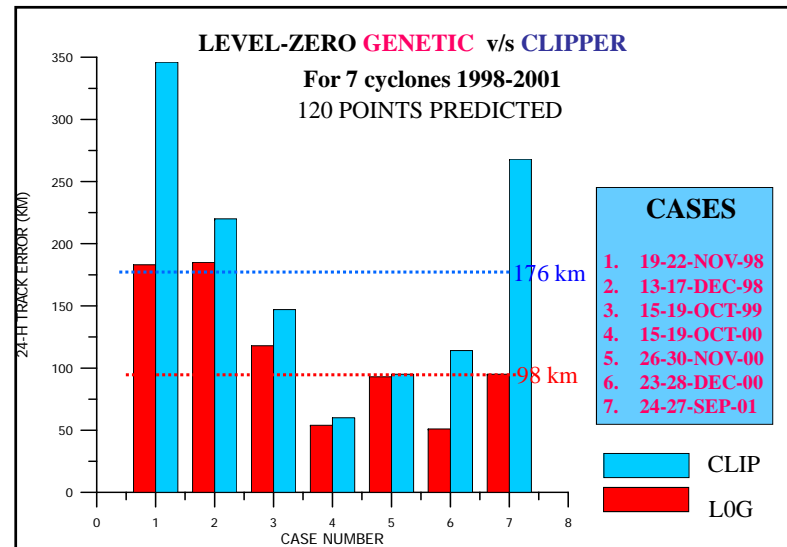


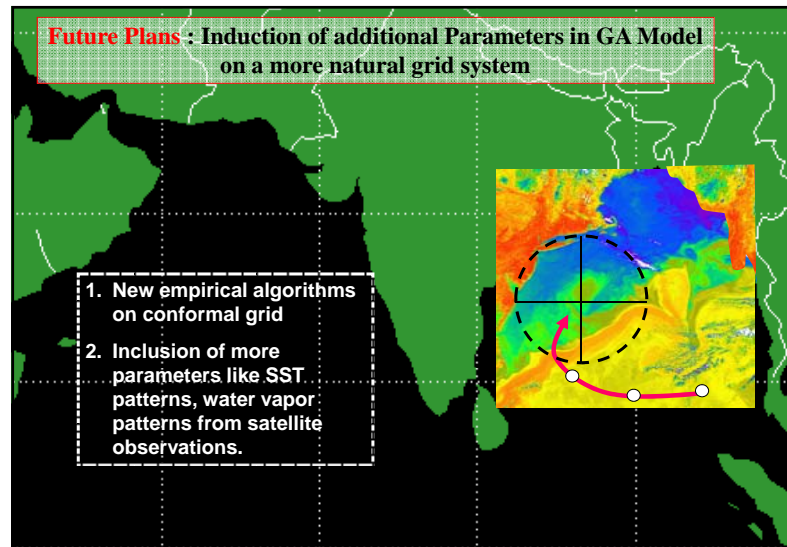
Some Non-Typical Validation Cases : Bay of Bengal



Orissa Super-cyclone

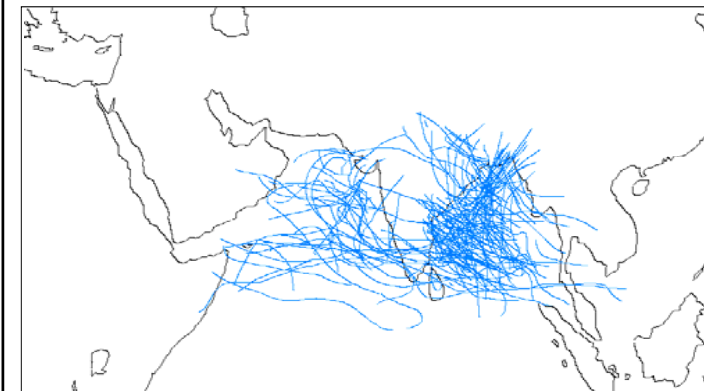
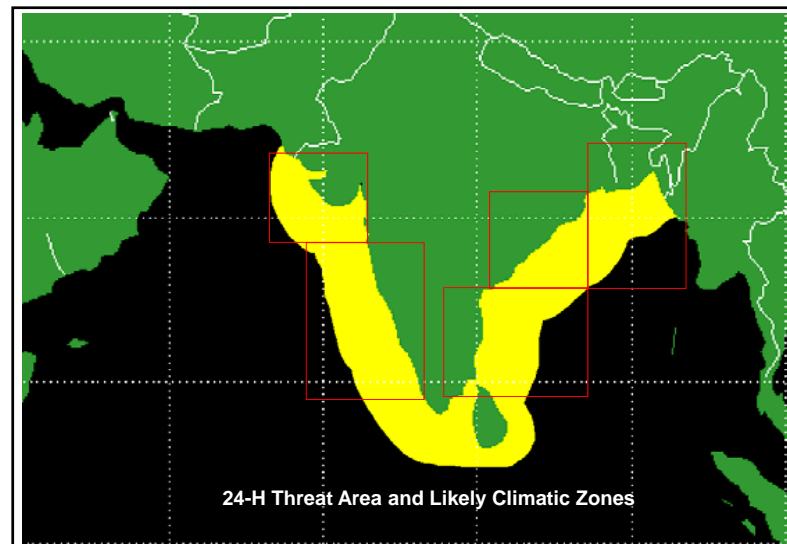






Few thoughts for the future of track prediction

1. Building a separate class of location-specific track-prediction algorithms for land-falling cyclones.
2. Put stress on GIS technology to provide value-added predictions using existing track prediction algorithms.
3. Combine current track and intensity prediction techniques with storm-surge models and GIS for possible forecasting applications.
4. Stress on the use of micro-scale features like topography and coastal geometry in track prediction algorithms.



$$X_m(t_i) = \{X(t_i), \dots, X[t_i + (m-1)\Delta t]\},$$

$$C_m(l) = N_m(l) / (N_m - 1)^2,$$

$$K_2 = (1/l) \exp[C_m(l) / C_{m+1}(l)]$$

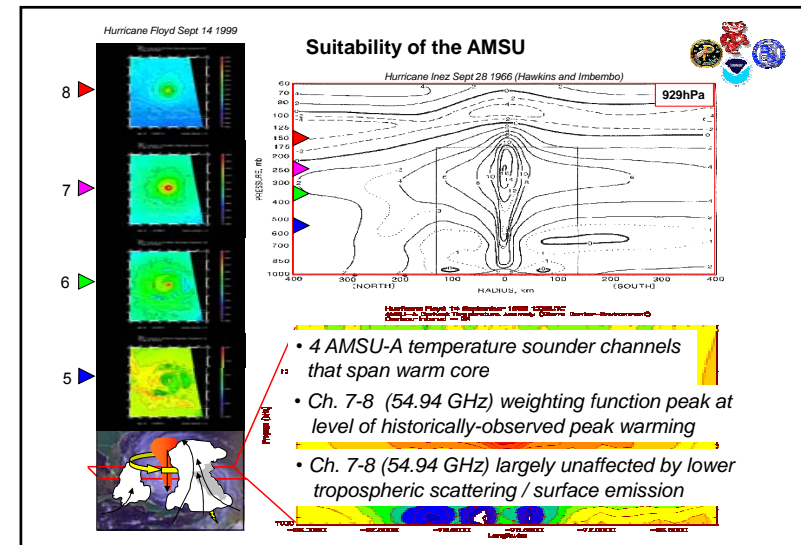
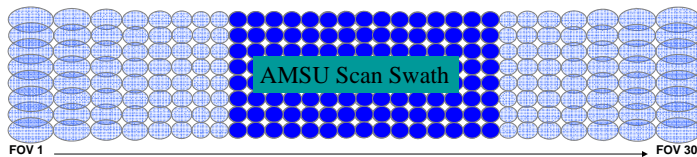
Correlation Integral

Kolmogorov-Sinai entropy of order 2

AMSU Background



- AMSU-A passive microwave radiometer
- Flown on NOAA-15/16/17 and Aqua polar orbiting satellites
- Senses upwelling terrestrial radiation near 55GHz region
 - Transparent to clouds
- **Challenges**
 - Scattering in lower channels prohibits hydrostatic integration
 - Variability in peak warming altitude
 - Variable horizontal resolution



Tropical Cyclone Prediction : Challenges



AVM (DR) AJIT TYAGI

India Meteorological Department
Mausam Bhavan, Lodi Road, New Delhi-1100 03.
E-Mail : ajit.tyagi@gmail.com



भारत मौसम विज्ञान विभाग
INDIA METEOROLOGICAL DEPARTMENT



Presentation Lay out

- ❖ Introduction
- ❖ Cyclone prediction
 - Present status in India
 - Present status in the world
 - Needs and requirements over North Indian Ocean
 - Future Plans
- ❖ Conclusion



भारत मौसम विज्ञान विभाग
INDIA METEOROLOGICAL DEPARTMENT



Components in the Cyclone Management

- ❖ Hazard Analysis
- ❖ Vulnerability Analysis
- ❖ Preparedness and Planning
- ❖ Prediction and Warning
- ❖ Prevention and Mitigation



भारत मौसम विज्ञान विभाग
INDIA METEOROLOGICAL DEPARTMENT



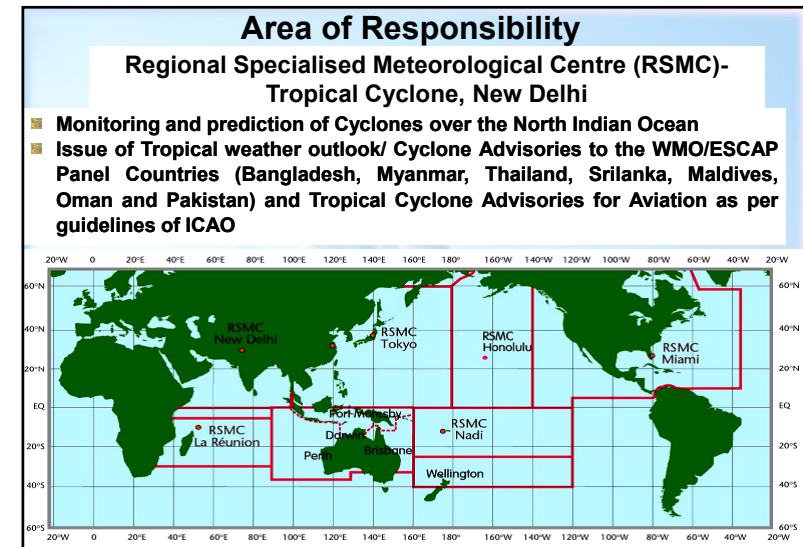
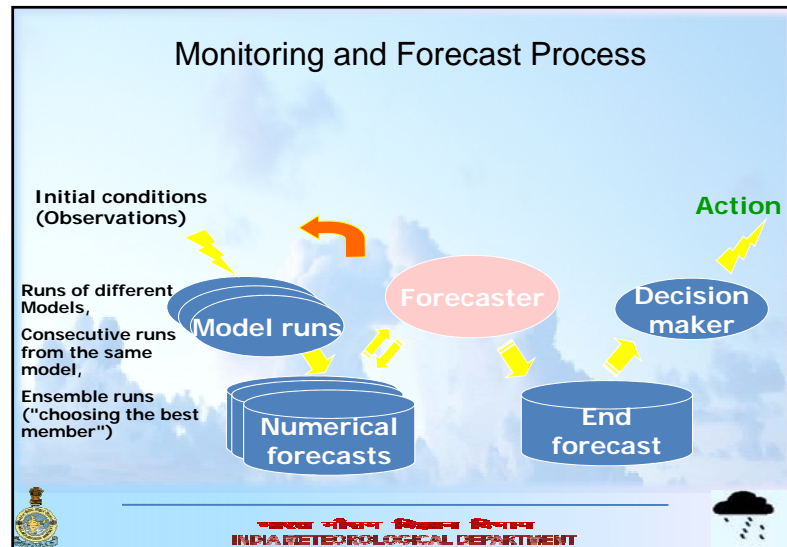
Components of Early Warning System of Cyclone

- Analysis and Prediction
- Warning Generation
- Warning products presentation
- Warning dissemination
- Coordination with emergency response units
- The post-event review
- Public education and reaching out



भारत मौसम विज्ञान विभाग
INDIA METEOROLOGICAL DEPARTMENT





CHALLENGES.....

- Genesis
- Location
- Intensity
- Track
- Landfall

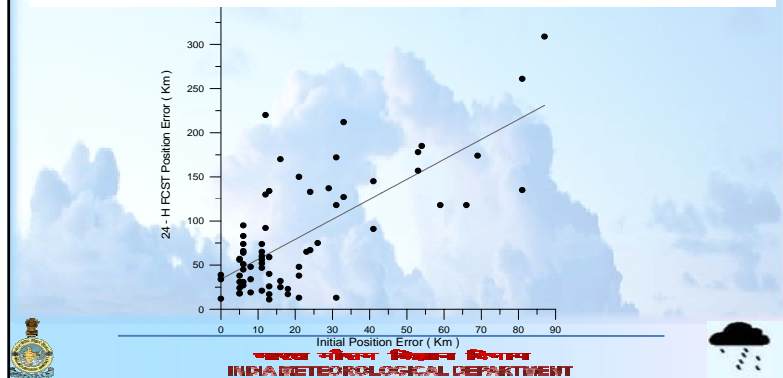


OBSERVATIONS

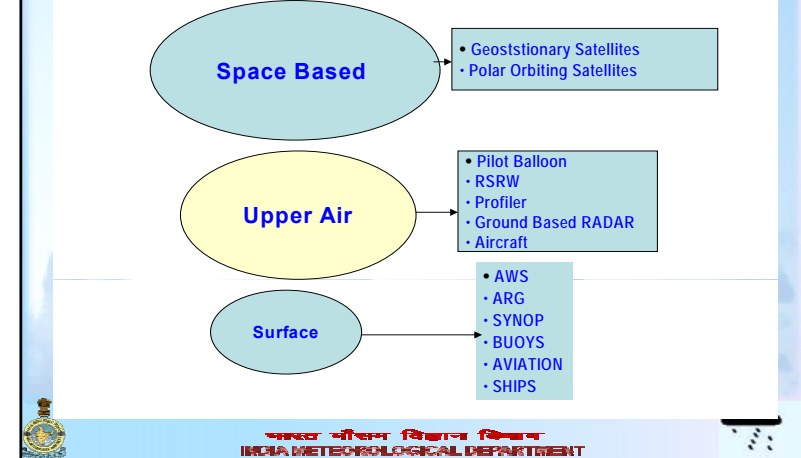


Cyclone monitoring (Need for good observational system)

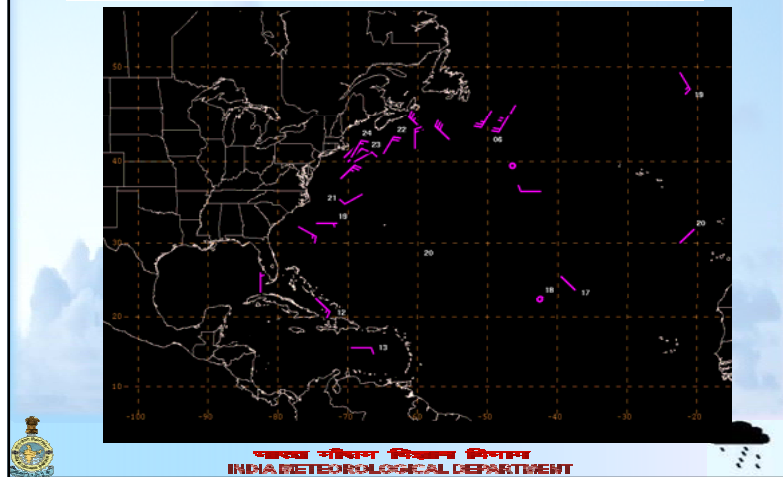
Correct estimation of location and intensity of cyclonic disturbances is as important as cyclone track and intensity forecasting. The initial error in location and intensity of the system can lead to exponential increase in forecast error. Hence there is a need for good observational system.



Broad Classification of Observations

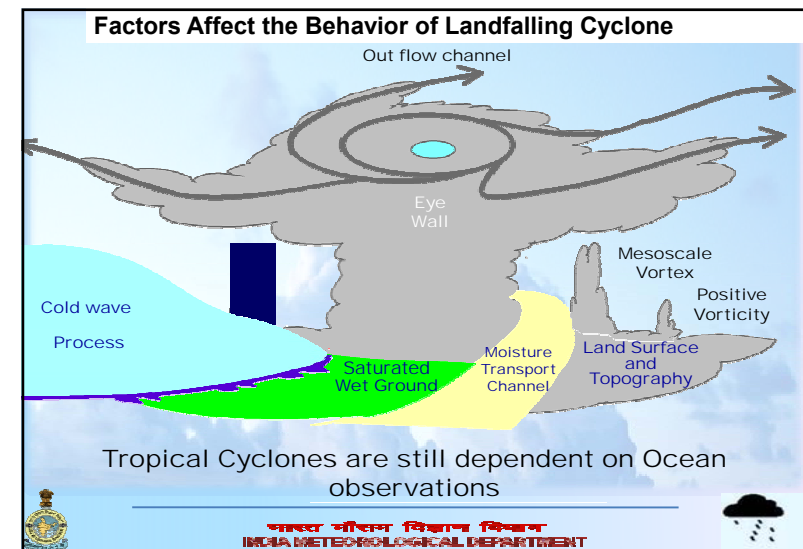
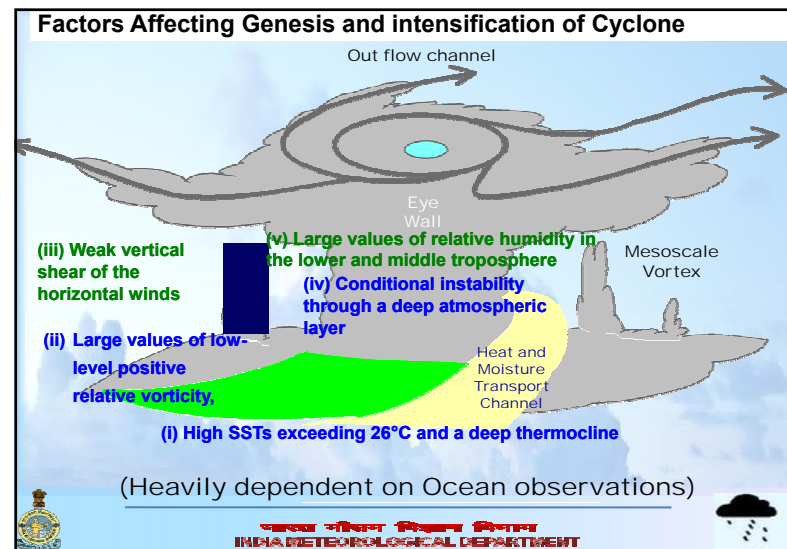
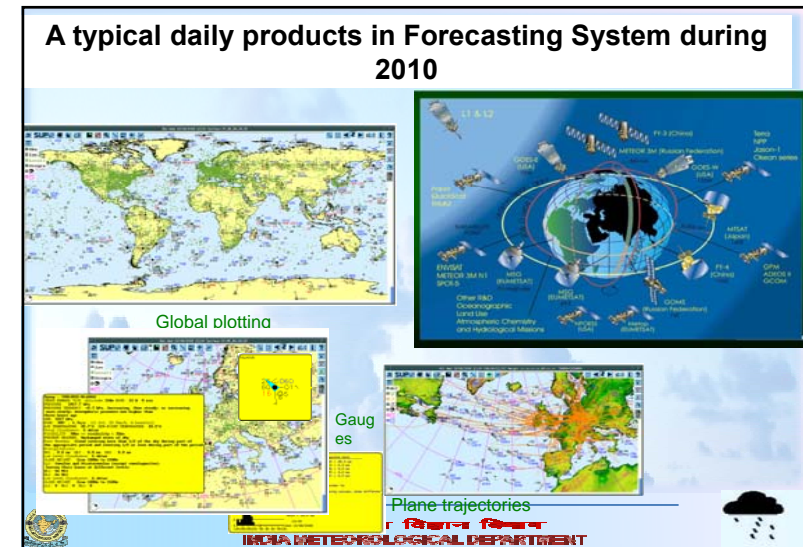
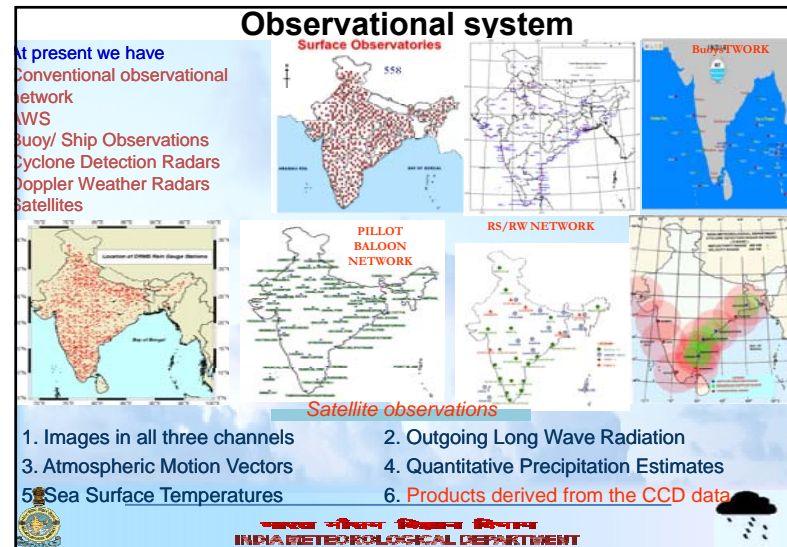


A Typical Day in 1910 – over the most developed region of North Atlantic Ocean



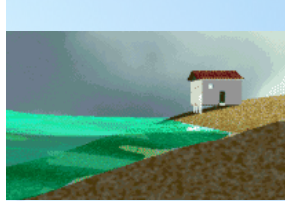
Issues related to cyclone studies during pre-satellite era

- ❖ Missing Cyclones
- ❖ Under-estimation of intensity over the sea
- ❖ Over estimation of intensity, especially short lived cyclones



Methods for Estimating Intensity

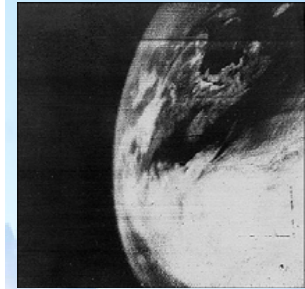
- ❖ Beaufort Scale (0-12: Calm to hurricane)
- ❖ Anemometers – Biases in Early Instruments
- ❖ Pressure-Wind Relationships
- ❖ Utilizing Size (Radius of Maximum Wind) Information
- ❖ Storm Surge/SLOSH runs
- ❖ Wind-caused Structural Damage
- ❖ Inland Wind/Pressure Decay Models
- ❖ Satellite (polar – 1960, Dvorak technique 1974, INSAT 1982)
- ❖ Buoys
- ❖ Aircraft Reconnaissance (?)



भारत मौसम विज्ञान विभाग
INDIA METEOROLOGICAL DEPARTMENT

History of Satellite Meteorology

- ❖ Satellites with meteorological instrumentation were first launched in the late 1950's.
- ❖ The first satellite completely dedicated to satellite meteorology was launched on 1 April 1960.
- ❖ It was called the TIROS (Television and Infrared Observational Satellite).
- ❖ The life span of this satellite was 79 days.
- ❖ The images, however, generated much excitement in the meteorological community.
- ❖ Nine additional TIROS satellites were subsequently launched through 1965.



भारत मौसम विज्ञान विभाग
INDIA METEOROLOGICAL DEPARTMENT

History of Satellite Meteorology

- ❖ Then came the Nimbus series, Nimbus 1 was launched on 28 August, 1964.
- ❖ Six more Nimbus satellites were subsequently launched and provided continuous coverage of the earth for the first time.
- ❖ This meant that tropical storms could be closely monitored for the first time.
- ❖ The last Nimbus satellite was launched in 1978.
- ❖ The current NOAA polar orbiting satellites are descendants of the original Nimbus satellites.
- ❖ 16 September, 1966 marked the launch of the first DMSP (Defense Meteorological Satellite Program) satellite.
- ❖ 7 December, 1966 marked the launch of the first Applications Technology Satellite (ATS 1).
- ❖ GOES 1 (Geostationary Operational Environmental Satellite) was launched on 16 October 1975.



भारत मौसम विज्ञान विभाग
INDIA METEOROLOGICAL DEPARTMENT

Current Indian Meteorological Satellites

Geostationary Satellites

1. INSAT Series
2. Kalpana Series



भारत मौसम विज्ञान विभाग
INDIA METEOROLOGICAL DEPARTMENT

Geo-Stationary Satellite

The first & second series of INSAT have only two channels – IR channel (10.5-12.5 micro meter) and Visible channel (5.5 - 0.75 micro meter)

INSAT	1A	1B	1C	1D
SSP	74°E	74°E	93°E	83°E
Date of launch	10-4-82	30-8-83	22-7-88	12-6-90
Date of operation	6-9-82	15-10-83	Lost on 22-11-89	17-7-90

Service	--	10yrs	---	12 yrs (approx)
INSAT	II-A	II-B	II-E	
SSP	74°E	93.5°E	*83°E	
Date of Launch	10-7-92	27-7-93		
Date of Operation	Aug 92	Aug 93	1999	

INSAT II-C & II-D are only for communication purpose meteorological payload is not available.



भारत मौसम विज्ञान विभाग
INDIA METEOROLOGICAL DEPARTMENT

Indian satellites - Present

Satellites	Met Payload	Channels	Spectral Range (µm)	Resolution
KALPANA-1(Sep'02)	VHRR	VIS	0.55-0.75	2
		WV	5.7-7.1	8
		IR	10.5-12.5	8
INSAT-3A (Apr'03)	VHRR	VIS	0.55-0.75	2
		WV	5.7-7.1	8
		IR	10.5-12.5	8
	CCD	VIS	0.62-0.68	1
		NIR	0.77-0.86	1
		SWIR	1.55-1.69	1



भारत मौसम विज्ञान विभाग
INDIA METEOROLOGICAL DEPARTMENT

Met. Satellites of special relevance to TC analysis over NIO

- ❖ VIS and IR images from polar orbiting satellites have been in use in IMD since 1960s for TC analysis
- ❖ Dvorak's technique for intensity classification is used for north Indian Ocean since 1974.



भारत मौसम विज्ञान विभाग
INDIA METEOROLOGICAL DEPARTMENT

Basic Geostationary Imagery for Cyclone Monitoring

- ❖ Visible
 - Tracking (locating the centre)
 - For intensity analysis by Dvorak Technique
- ❖ Infra-Red
 - Tracking (locating the centre)
 - For structure analysis
 - For intensity analysis
- ❖ Water Vapour
 - For synoptic assessment of the storm environment




भारत मौसम विज्ञान विभाग
INDIA METEOROLOGICAL DEPARTMENT

Satellite Products for cyclones.

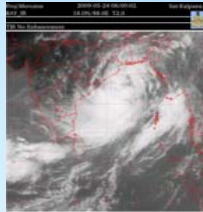
❖ Indian Satellite Images:-

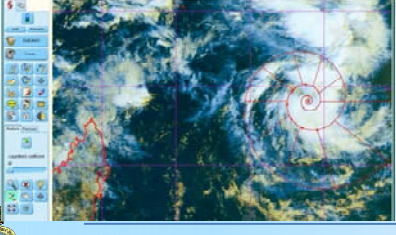
- (a). IR
- (b). VIS
- (c). WV.

Visible imagery of AILA




IR imagery of AILA





Water Vapour imagery of AILA



भारत मौसम विज्ञान विभाग
INDIA METEOROLOGICAL DEPARTMENT

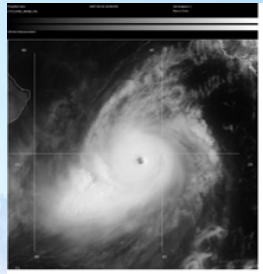
Visible imagery for cyclone monitoring

Helps better in monitoring the centre and intensity of cyclone, as

- It filters out the high clouds
- It has better resolution (2 km) compared to IR (8 km)

Limitations

- It is available only during day time
- It can not measure convection quantitatively



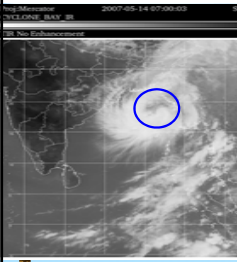
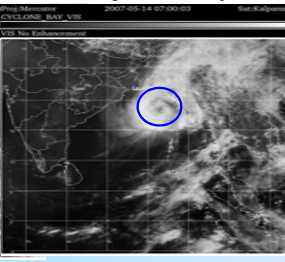
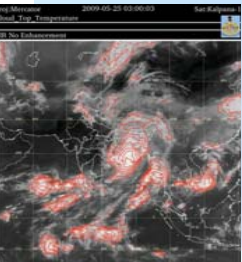
SUPER CYCLONE GONU
DATE: 04062007
INTENSITY T6.0
CENTRE 19.6N/64.3E

भारत मौसम विज्ञान विभाग
INDIA METEOROLOGICAL DEPARTMENT

IR imagery for cyclone monitoring

- IR imagery is available for continuous monitoring round the clock
- It is essential to compare the IR imagery with Visible imagery for better understanding of cyclone

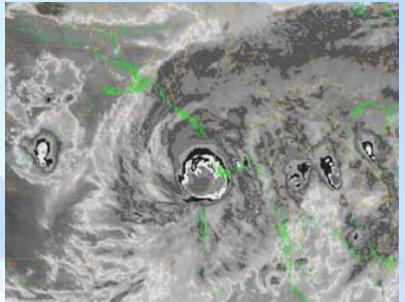
IR imagery clear shows that the cyclone is of curved band pattern VIS gives a false signature of Eye IR with CTT

भारत मौसम विज्ञान विभाग
INDIA METEOROLOGICAL DEPARTMENT

Enhanced IR Imagery for cyclone monitoring

- Based on cloud top temperature ranges in different shades
- Helps in better identification of location and intensity
- Enhanced IR imagerys are used in Dvorak Technique



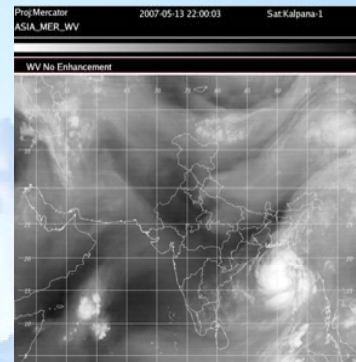
04Z EIR imagery of TC Mala (28-04-06)

भारत मौसम विज्ञान विभाग
INDIA METEOROLOGICAL DEPARTMENT

Water Vapour imagery for cyclone monitoring

- Water vapour imagery mainly helps in the following
- Movement of cyclone with
 - Location of westerly trough
 - outflow
 - Ridge
- Middle and upper tropospheric humidity

Role of westerly trough in Akash

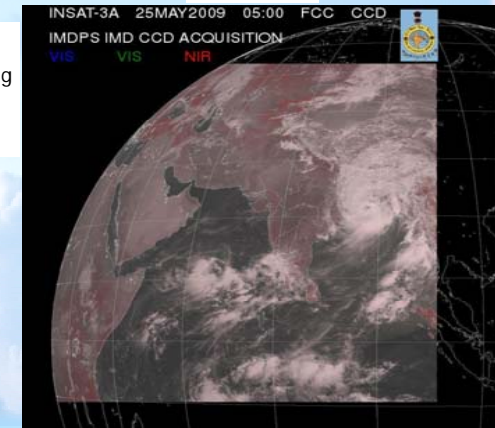


भारत मौसम विज्ञान विभाग
INDIA METEOROLOGICAL DEPARTMENT

CCD imagery for cyclone monitoring :

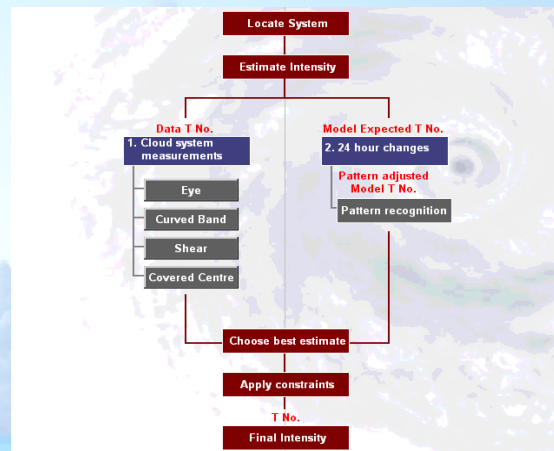
AILA Cyclone

- Resolution : 1 km
- Available every hour during day time



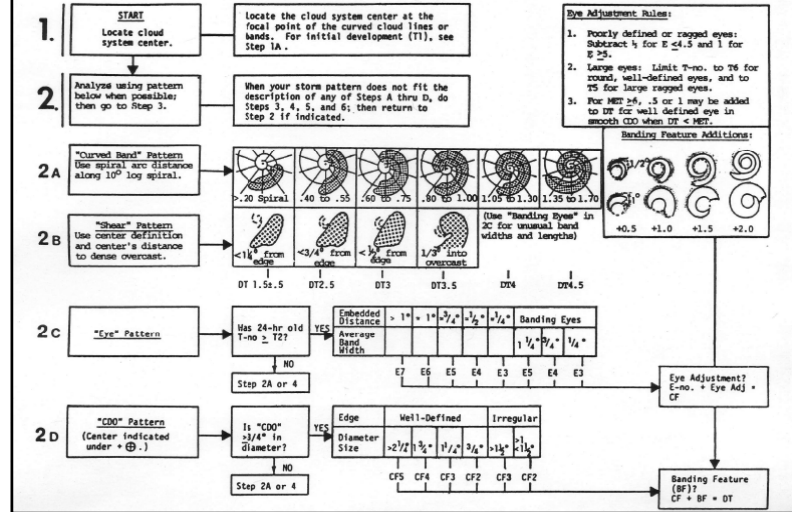
भारत मौसम विज्ञान विभाग
INDIA METEOROLOGICAL DEPARTMENT

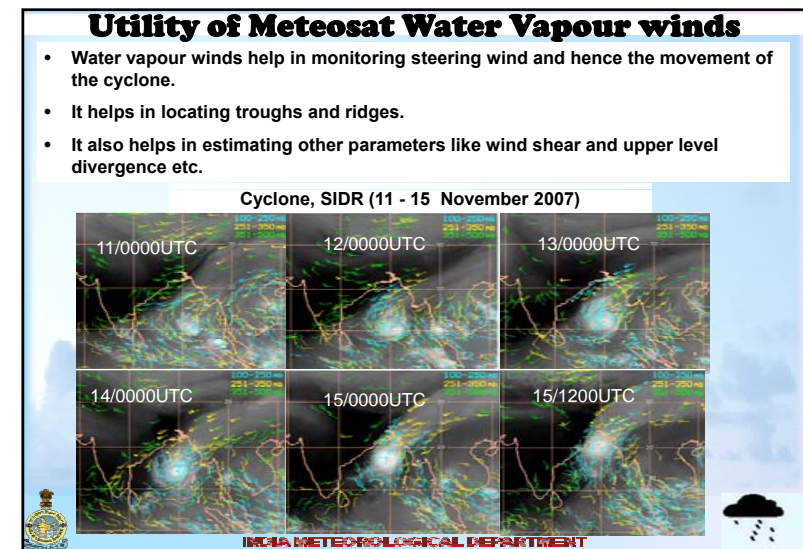
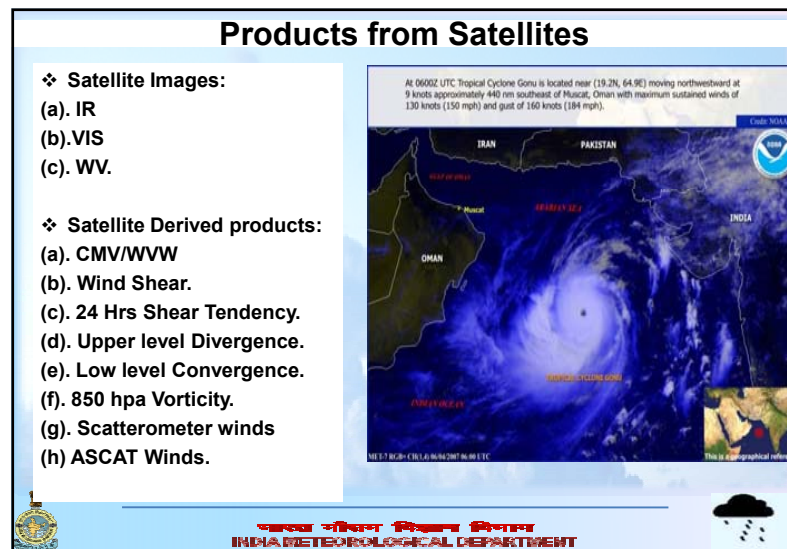
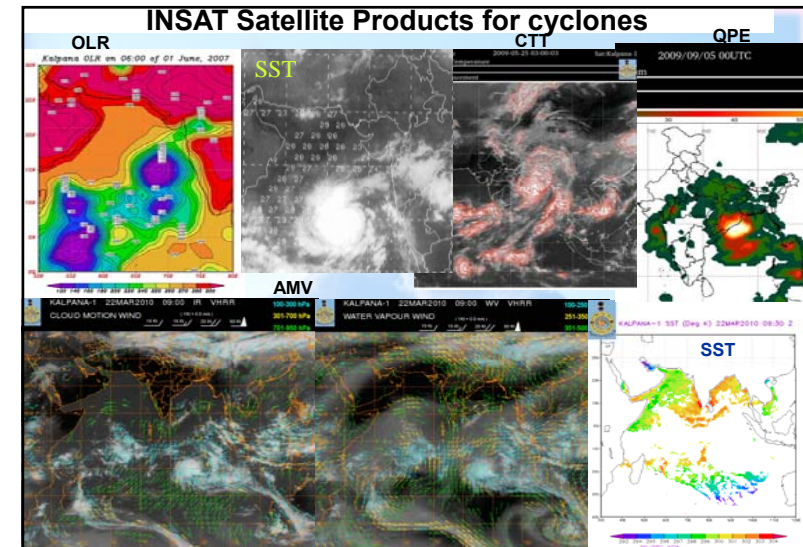
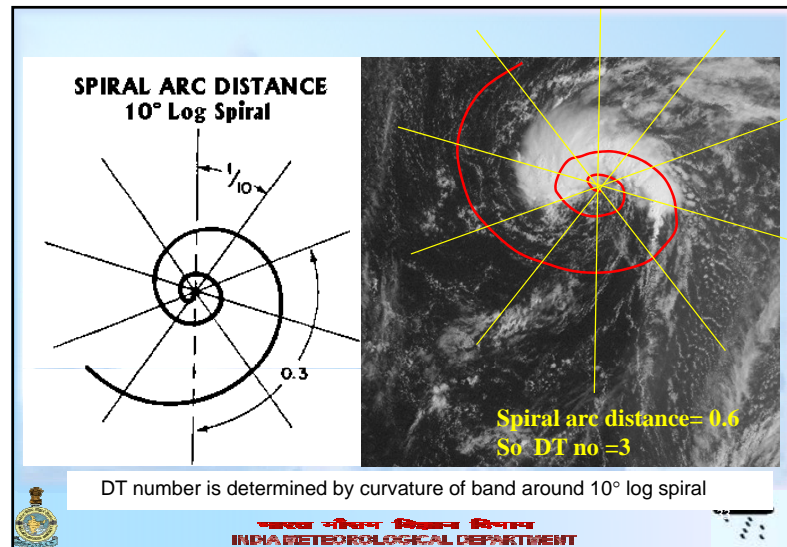
Intensity estimation : Dvorak Technique(Manual)



भारत मौसम विज्ञान विभाग
INDIA METEOROLOGICAL DEPARTMENT

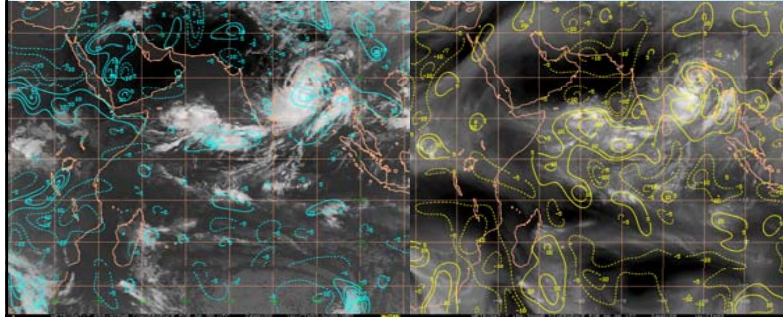
VIS Analysis Diagram-1





Meteosat 7 Satellite

Low Level Convergence and Upper Level Divergence for "Aila"



Convergence within the layer 850-925mb. Positive values are given by solid lines, with negative values by dashed lines.

Divergence within the layer 150-300mb. Positive values are given by solid lines, with negative values by dashed lines.

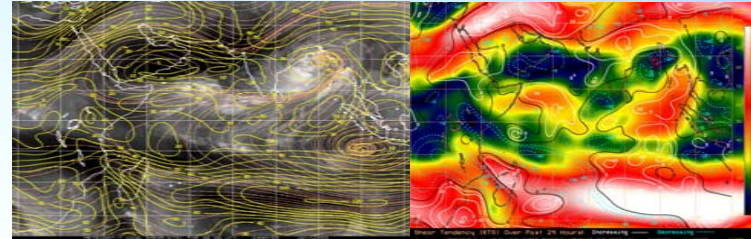


भारत मौसम विज्ञान विभाग
INDIA METEOROLOGICAL DEPARTMENT



Derived Products Meteosat 7 satellite.

Vertical wind shear and Wind Shear Tendency for "Aila"



Vertical wind shear as calculated by subtracting the low-level layer-averaged flow (925-700mb) from the upper-level layer-averaged flow (150-300mb). The brown streamline contours indicate the direction of the shear. The yellow contours show the magnitude of the shear (kt).

Shear tendency over past 24 hours
White solid lines for increasing trend.
Blue dotted lines for decreasing trend.
Black lines for no change in shear.

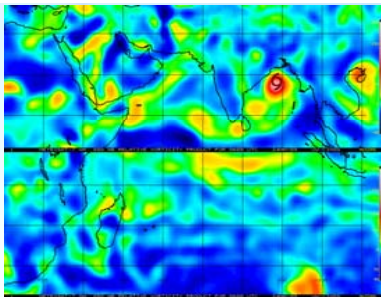


भारत मौसम विज्ञान विभाग
INDIA METEOROLOGICAL DEPARTMENT



Derived Products of Meteosat 7 satellites

Relative vorticity and Atmospheric Motion Vectors for "Aila"



Relative vorticity at 850 hPa level

All these products are available on CIMSS website.



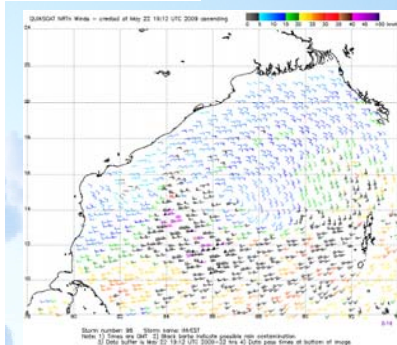
भारत मौसम विज्ञान विभाग
INDIA METEOROLOGICAL DEPARTMENT



Derived products of other satellites

Scatterometer data

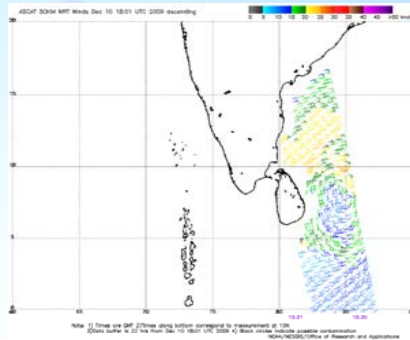
- Useful tool to locate the surface-wind circulation centre.
- Gives an idea of surface wind distributions and vortex structure.
- The maximum wind speeds in a TC observed in Quikscat data can be useful in assessing its intensity.
- The QuikSCAT nominal mission ended on November 23, 2009.
- QuikSCAT was launched in 1999 and Oceansat-II has been launched on 23rd Sept, 2009



भारत मौसम विज्ञान विभाग
INDIA METEOROLOGICAL DEPARTMENT



Derived products of other satellites



- ASCAT wind data can also be utilized to locate the centre of a weak system.
- Rain contamination of winds are less in ASCAT compared to Quikscat
- Its swath is less (550 km) compared to 1800 km of Q-Scat
- As Q-Scat is not available, AScat is only alternative at present



भारत मौसम विज्ञान विभाग
INDIA METEOROLOGICAL DEPARTMENT



Cyclone monitoring from Space World wide status

Microwave Radiometer SSM/I, TMI, AMSR-E

Estimate the following Parameters from TB

Rainrate, TPW, Surface Wind Speed, SST,
CLW, Salinity

MW Scatterometer QuikSCAT, ASCAT

Estimate Sea Surface Wind from Backscattering

MW Rain Radar TRMM/PR

Estimate Rainrate from Backscattering of Raindrops

MW Sounder AMSU

Estimate Temperature/Moisture Profile from

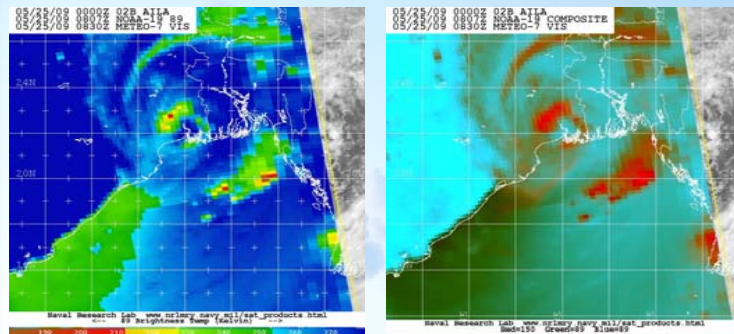
Atmospheric TB using Absorption Bands



भारत मौसम विज्ञान विभाग
INDIA METEOROLOGICAL DEPARTMENT



Utility of superimposed image of NOAA 19 and Meteosat7



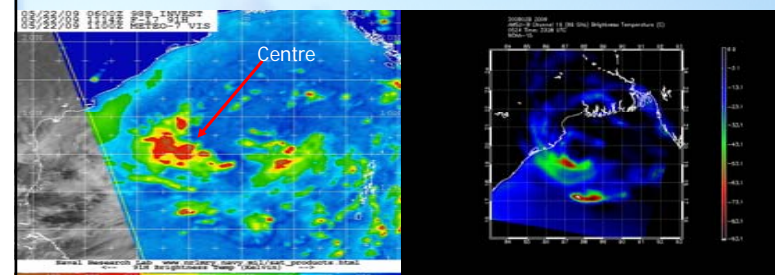
- These images are helpful to locate the centre of system



भारत मौसम विज्ञान विभाग
INDIA METEOROLOGICAL DEPARTMENT



Utility of brightness temperature for cyclone monitoring



- These images are helpful to locate the centre in the initial stage
- The product is extensively available in US Navy site



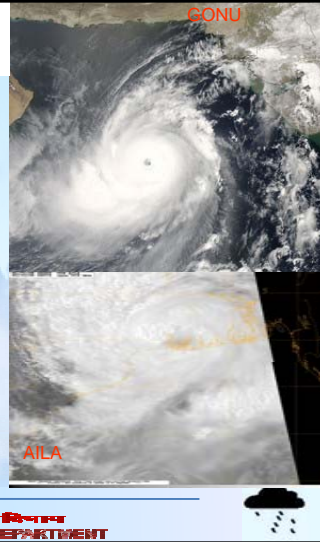
भारत मौसम विज्ञान विभाग
INDIA METEOROLOGICAL DEPARTMENT



➤ MODIS (Moderate Resolution Imaging Spectroradiometer)

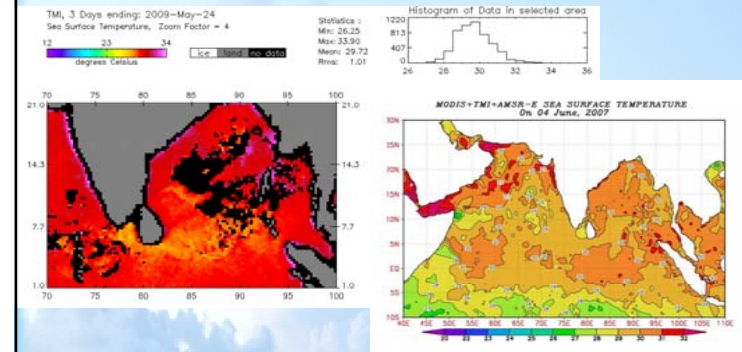
- On board: TERA & AQUA
- Waveband: Visible-TIR: 36 bands in range 0.4-14.4μm
- Spatial resolution: 250m (day) and 1000m (night)

It helps in locating meso-scale vortices and pre-cyclone squall lines



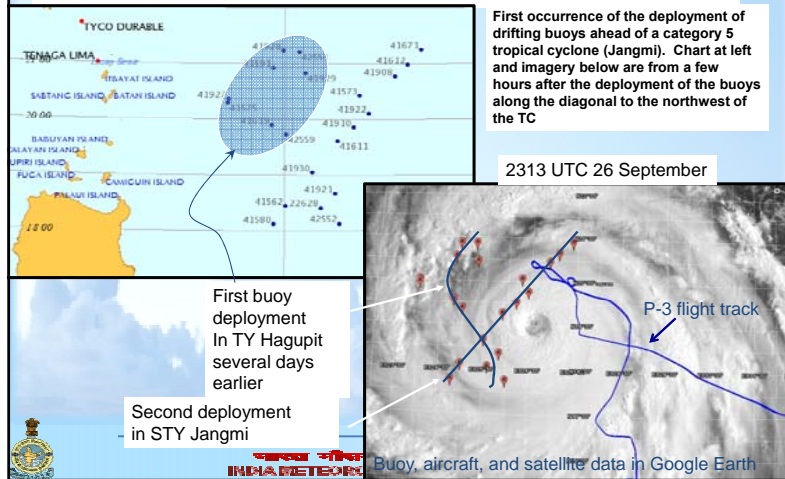
भारत मौसम विभाग
INDIA METEOROLOGICAL DEPARTMENT

TMI SST



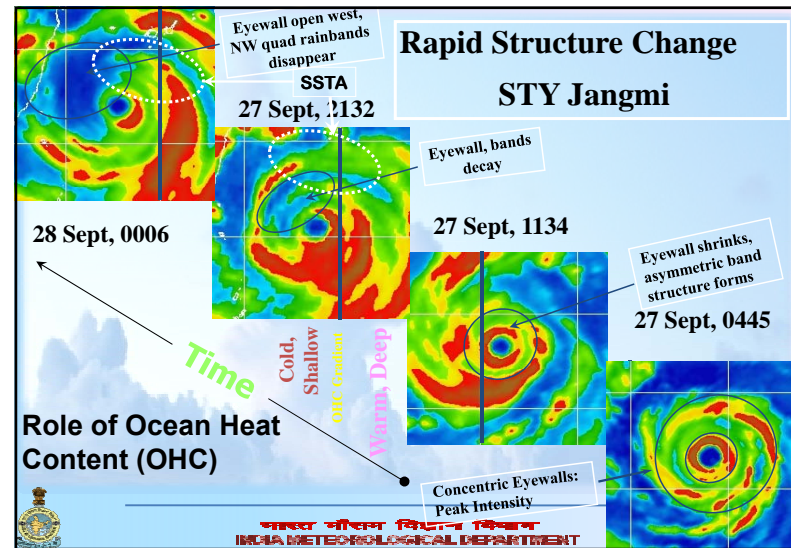
भारत मौसम विभाग
INDIA METEOROLOGICAL DEPARTMENT

Aircraft – Buoy Deployment

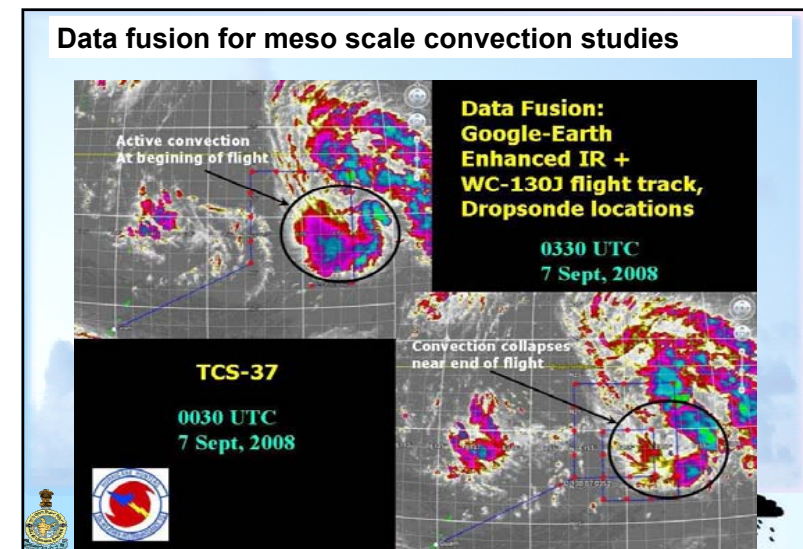
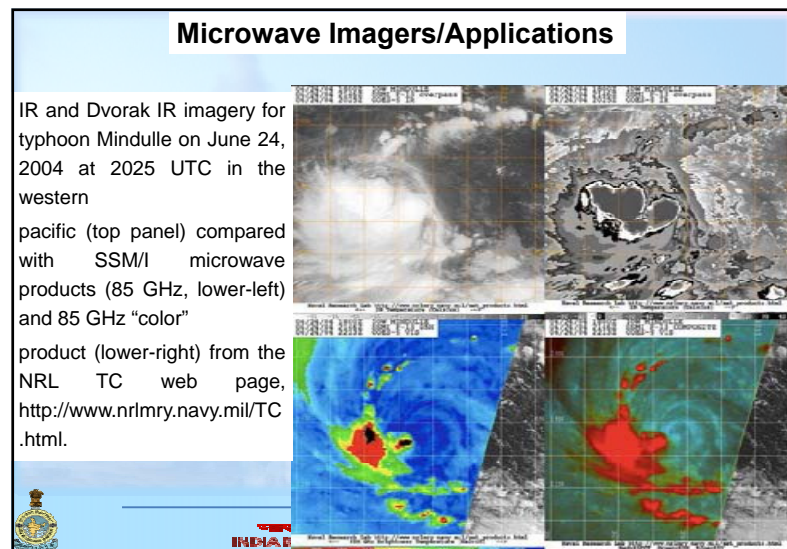
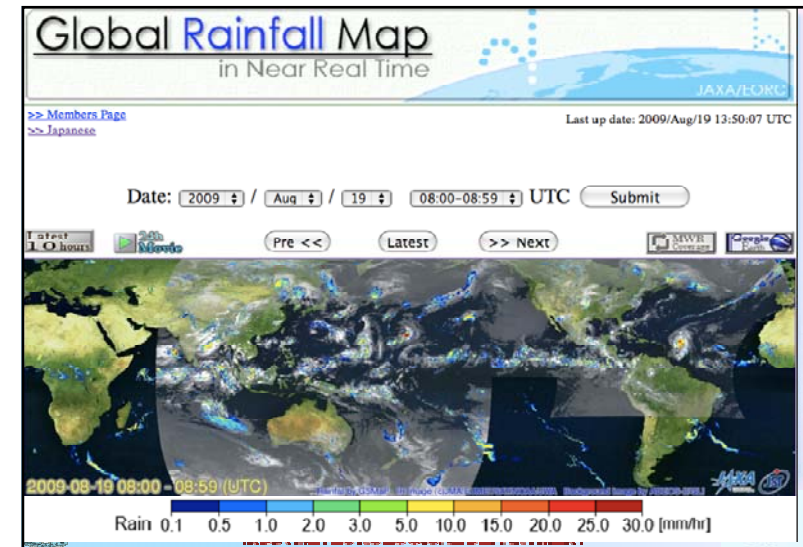
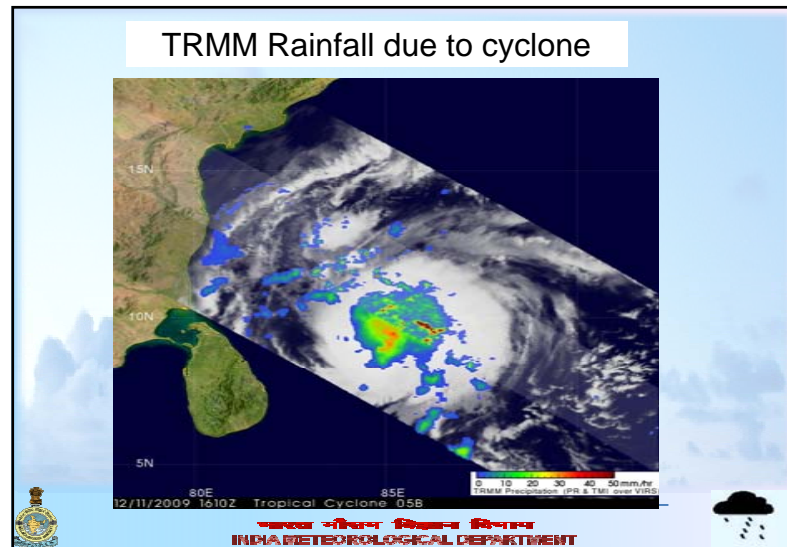


भारत मौसम विभाग
INDIA METEOROLOGICAL DEPARTMENT

Rapid Structure Change STY Jangmi



भारत मौसम विभाग
INDIA METEOROLOGICAL DEPARTMENT



Challenges : Intensity and track estimation

- Lack of observational data over the oceanic region leading to uncertainty in location of the system. The mean best track error may be considered as 50 km.
- In the absence of the observations over the north Indian Ocean, the best track of the cyclone is mostly estimated with the satellite imagery interpretation with the help of Dvorak's technique.
- However, this technique, which has been developed for north Atlantic Ocean basin needs to be validated for north Indian Ocean. Further automated Dvorak's technique has to be validated/developed for north Indian Ocean to minimize the human error based on aircraft reconnaissance.

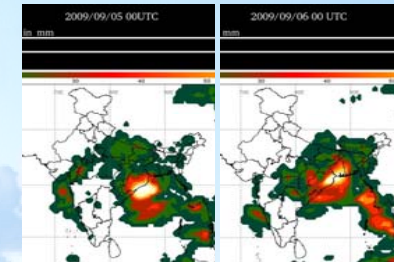


भारत मौसम विज्ञान विभाग
INDIA METEOROLOGICAL DEPARTMENT



Challenges : Heavy Rainfall monitoring and prediction

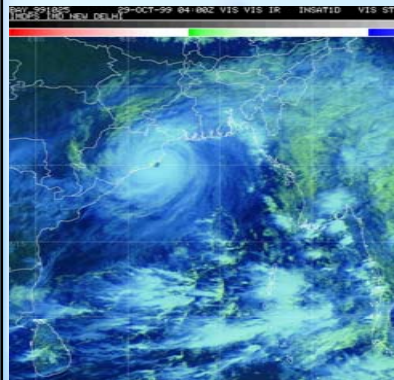
- QPE is an underestimate of heavy rainfall, though it can estimate the pattern
- Need of the hour : Location specific heavy rainfall estimate and precipitation apart from river catchment rainfall



भारत मौसम विज्ञान विभाग
INDIA METEOROLOGICAL DEPARTMENT



Challenges: Tropical Cyclone structure Forecasting



- Structure
 - Eye,
 - Eye wall/ Wall cloud region
 - Spiral bands
 - Outermost layer
- Objective :
 - Prediction of wind distribution in the cyclone
- Utility :
 - Needed for bogussing in the NWP Model
 - Sea and coastal weather forecasting
 - Storm Surge prediction

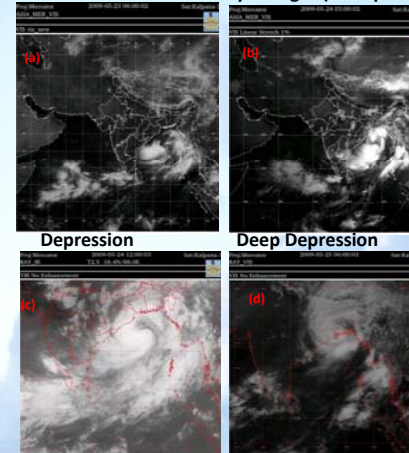
Methodology:
Surface pressure and wind can be derived from the brightness temperature measured by microwave sounders in satellite like that in AMSU B



भारत मौसम विज्ञान विभाग
INDIA METEOROLOGICAL DEPARTMENT



Prediction of Intensity changes (Example : Cyclone AILA)



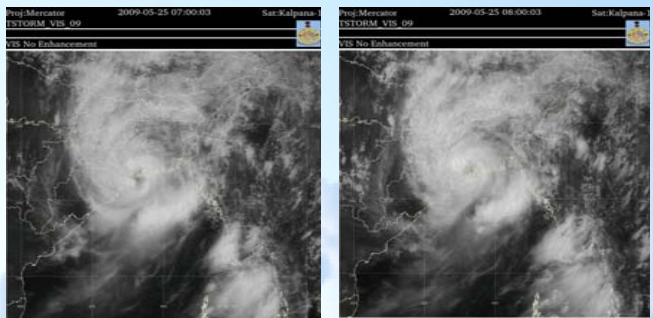
- Current Status
- Intensity monitored by Dvorak's Technique
- Shear pattern at depression stage
- Curved band pattern thereafter till landfall
- Rapid intensification/Weakening
- Cyclone sometimes rapidly intensifies before landfall like AILA
- Intensity change at night is not possible in present technique
- It can be possible with microwave sensors



भारत मौसम विज्ञान विभाग
INDIA METEOROLOGICAL DEPARTMENT



Challenges : Tropical cyclone landfall processes



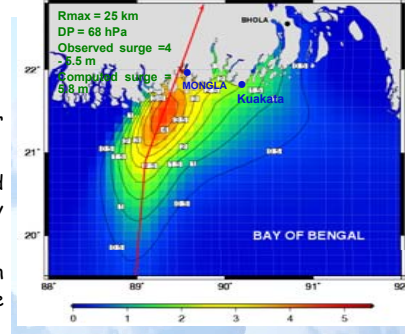
- Structure changes during landfall
- Accordingly rainfall, pressure and wind distribution changes
- These features can not be studied more accurately in the present satellite due to low resolution to detect the embedded mesoscale convective vortices which leads to structural changes.

भारत मौसम विज्ञान विभाग
INDIA METEOROLOGICAL DEPARTMENT

Tropical cyclone landfall processes : Storm Surge

Meteorological inputs for storm surge prediction

- ❖ Pressure drop
- ❖ Radius of Max. winds
- ❖ Vector motion of the cyclone
- ❖ Bathymetry of the coast line near landfall point
- ❖ Hence, proper monitoring and prediction of cyclone is very essential
- ❖ At present satellite has limitation of about 50 km to detect the centre of cyclone
- ❖ Similarly there is intensity error



भारत मौसम विज्ञान विभाग
INDIA METEOROLOGICAL DEPARTMENT

Payloads on the future INSAT-3D satellite

- It has a 6-channel.
- It has a 19 –channel Sounder.
- It has a Data Relay Transponder (DRT) similar to Kalpana-1 and INSAT-3A.
- Resolution : VIS : 1 km and IR : 4 km and WV : 8 km

Expected improvements in cyclone analysis and forecasting

- Detection of center & estimation of intensity of tropical cyclone is expected to improve as higher resolution imageries will be available for analysis.
- Many new meteorological/geophysical parameters will be evaluated in addition to the improvement of current available products obtained from Kalpana-1/INSAT-3A as mentioned below.

भारत मौसम विज्ञान विभाग
INDIA METEOROLOGICAL DEPARTMENT

Derived Products from INSAT 3D : QPE

Parameters	Present	INSAT-3D
Method	Arkin's Tech	Hydro-Estimate
Advantage		Convective & non-convective clusters are identified and different rainfall, temperature relationship are applied.
Improvements	1° x 1°	0.5° x 0.5° Limitaion of 72mm/3hr removed.

भारत मौसम विज्ञान विभाग
INDIA METEOROLOGICAL DEPARTMENT

Derived Products from INSAT 3D : OLR

	Present	INSAT-3D
Method	SBDART (Santa Barbara DISORT Atmosphere Radiative Transfer model)	Same algorithm but now there are three input channels viz. TR ₁ , TR ₂ & WV.
Improvements		Accuracy upto 3 % Resolution 1°x1°



भारत मौसम विज्ञान विभाग
INDIA METEOROLOGICAL DEPARTMENT



Derived Products from INSAT 3D : SST

	Present	INSAT-3D
Method	Mean Estimate Histogram technique (using single channel only)	Multiple channel (SWIR, TIR -1, TIR -2, MIR) MODTRAN will be used.
Advantage		Using multiple channel ensure more accuracy.
Improvements		Accuracy: 1-2K (day); >1K (night) Resolution: 0.5° x 0.5°



भारत मौसम विज्ञान विभाग
INDIA METEOROLOGICAL DEPARTMENT



Derived Products from INSAT 3D : CMV

	Present	INSAT-3D
Method	1. In Kalpana-1 IR, VIS band and in INSAT-3A only IR band was used 2. Pattern matching by cross-correlation. 3. IR-Window intercept techniques. 4. H ₂ O intercept technique recently introduced.	1. TIR ₁ , TIR ₂ & WV Band will be used. 2. Pattern matching by Genetic algorithm . 3. H ₂ O plus IR-Window intercept technique
Advantage		More reliable pattern matching and height assignment techniques.



भारत मौसम विज्ञान विभाग
INDIA METEOROLOGICAL DEPARTMENT



Derived Products from INSAT 3D : WVVV

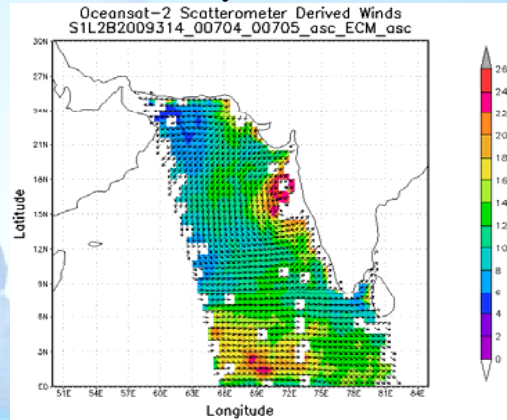
	Present	INSAT-3D
Method	Recently WV winds are derived by using WV band from Kalpana-1 only in INSAT-2E system.	WV Band from INSAT-3D. Pattern matching by Genetic algorithm .
Advantage		More reliable pattern matching and height assignment techniques.
Improvements		Accuracy 5m/sec Resolution 0.5-2.5°C



भारत मौसम विज्ञान विभाग
INDIA METEOROLOGICAL DEPARTMENT



Derived Products from OCEANSAT-2 during Phyan cyclone



भारत मौसम विज्ञान विभाग
INDIA METEOROLOGICAL DEPARTMENT

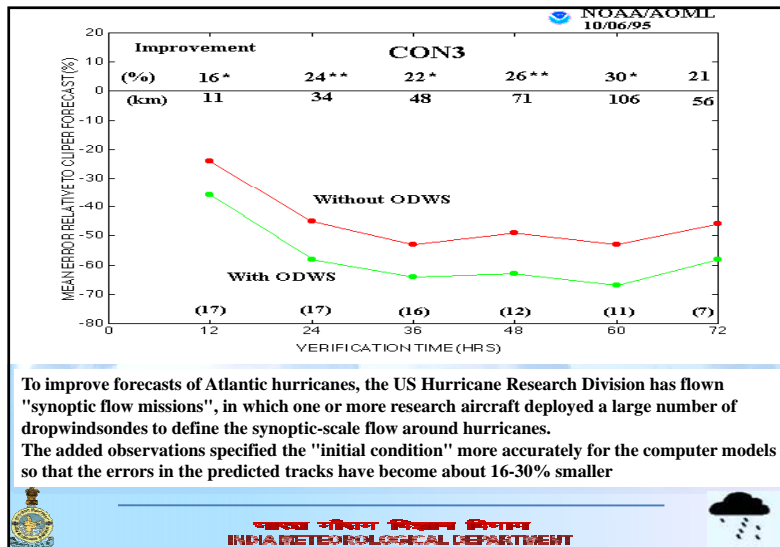


Automated Dvorak Technique (ADT)

- ❖ ADT software (version 7.2.1) was installed in SATMET unit in Oct'08.
- ❖ Latest version (7.2.2) was again installed in Nov'08.
- ❖ The Advanced Dvorak Technique (ADT) utilizes longwave-infrared, temperature measurements from geostationary satellites to estimate tropical cyclone (TC) intensity.



भारत मौसम विज्ञान विभाग
INDIA METEOROLOGICAL DEPARTMENT



भारत मौसम विज्ञान विभाग
INDIA METEOROLOGICAL DEPARTMENT



PROSPECTS : FORECAST DEMONSTRATION PROJECT ON LANDFALLING CYCLONES

- ❖ OBJECTIVE :
COLLECT OBSERVATIONS IN THE TC CORE ENVIRONMENT USING RESEARCH AIRCRAFT AND UNMANNED AERIAL VEHICLE (UAV).
DEMONSTRATE THE USE OF THE DROP SOUNDINGS AND UAV DATA IN PROVIDING IMPROVED NUMERICAL GUIDANCE FOR GENESIS, TRACK AND INTENSITY PREDICTION OF THE BAY OF BENGAL TROPICAL CYCLONE
- ❖ PROJECT SCHEDULE :
PRE-PILOT PHASE : 15 OCT - 30 NOV 2008, 2009
PILOT PHASE : 15 OCT - 30 NOV 2010
MAIN EXP. PHASE : 15 OCT - 30 NOV 2011
- ❖ REGION OF STUDY : BAY OF BENGAL
- ❖ MULTI-INSTITUTIONAL PROJECT



भारत मौसम विज्ञान विभाग
INDIA METEOROLOGICAL DEPARTMENT



Deliverables

- ❖ ADVANCED OPERATIONAL TROPICAL CYCLONE DATA ASSIMILATION – FORECAST FRAMEWORK FOR GENERATING IMPROVED TRACK, INTENSITY AND LANDFALL OF BAY OF BENGAL CYCLONES
- ❖ DEVELOPMENT OF HIGHLY SKILLED POOL OF PROFESSIONALS TO EXPAND AND INSTITUTIONALIZE TROPICAL CYCLONE SPECIFIC OBSERVATIONAL (CYCLONE PROBING AIRCRAFT/UAV), R & D AND OPERATIONAL FACILITIES IN INDIA



भारत मौसम विज्ञान विभाग
INDIA METEOROLOGICAL DEPARTMENT



Future Requirements

- Microwave Radiometer
 - Estimate the following Parameters
 - Rainrate, Surface Wind Speed, SST, Salinity etc
- MW Scatterometer
 - Estimate Sea Surface Wind from Backscattering
- MW Rain Radar
 - Estimate Rainrate from Backscattering of Raindrops
- MW Sounder
 - Estimate Temperature/Moisture Profile from Atmospheric TB using Absorption Bands



भारत मौसम विज्ञान विभाग
INDIA METEOROLOGICAL DEPARTMENT



Summary and conclusions

- ❖ Satellite is the only *reliable and consistently available* data platform for TC analysis when it is over the ocean.
- ❖ Depending on the tropical cyclone initial position satellite imagery can be used for short-term forecast.
- ❖ Provides input for numerical weather prediction models.
- ❖ Direct Readout is critical for accurate position/intensity analysis



भारत मौसम विज्ञान विभाग
INDIA METEOROLOGICAL DEPARTMENT



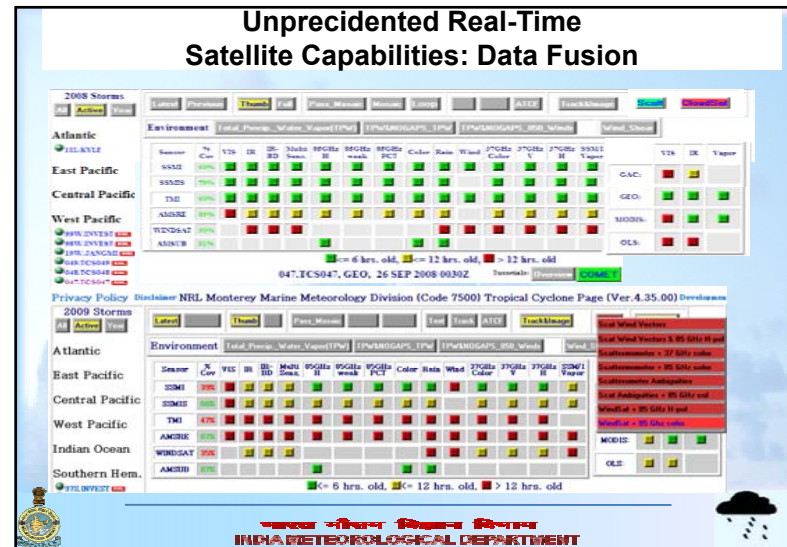
FINAL COMMENT

- We are at an historic turning point in history for improving cyclone intensity and location observation and forecasting
- The capability to observe the TC surface and mid-level wind domain concurrent with subsurface ocean thermal structure matches the improved coupled model capabilities to assimilate and model the total TC environment.
- This alignment should provide the next best opportunity for improving cyclone intensity and structure forecasting.



भारत मौसम विज्ञान विभाग
INDIA METEOROLOGICAL DEPARTMENT





Future prospects Modernisation programme of IMD

1. Forecasting and PWS
2. Satellite products
3. Doppler Weather Radars
4. Automatic Weather Stations (AWS)
5. Automatic Rain gauges (ARG)
6. Airport Modernization
7. Real Time Communication
8. High power computing system
9. Location specific forecast and now-casting

INDIA METEOROLOGICAL DEPARTMENT

ENHANCED CHLOROPHYLL/PHYTOPLANKTON BLOOMS DUE TO TROPICAL CYCLONES IN THE NORTH INDIAN OCEAN: USING IRS-P4 OCM, MODIS and SCATTEROMETER WIND FIELD MODEL DATA PRODUCTS

¹K. H. Rao, ²A. Smitha, ³N. Srinivasa Rao, ⁴D.Sengupta,¹ M. M. Ali
and ⁵M. Ravichandran

¹ Oceanography Division, National Remote Sensing Centre\ISRO, Hyderabad-500625

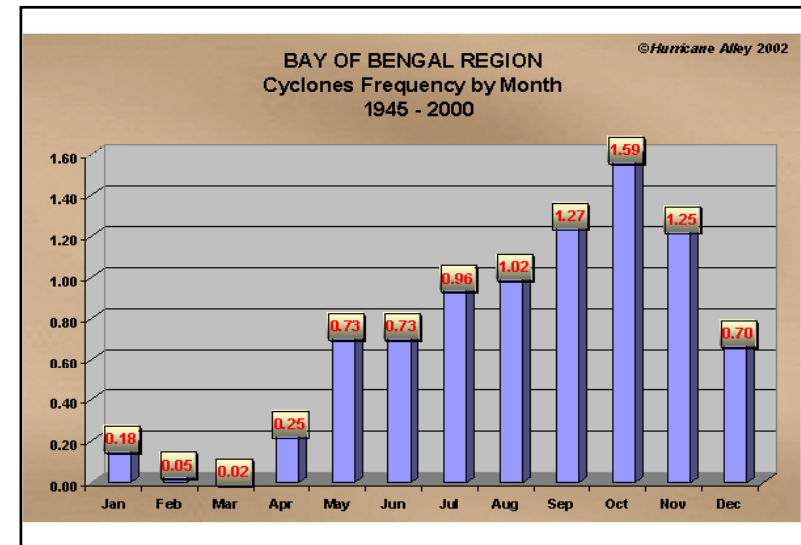
² Department of Atmospheric Science, , Cochin University of Science and Technology, Kochi-682016,

³ Centre for Earth Atmosphere&Weather Modification Technologies,(CEA&WMT) ,JNTUH, Hyderabad -500085

⁴ Centre for Atmospheric and Oceanic Sciences (CAOS),IISC, Bangalore-560012

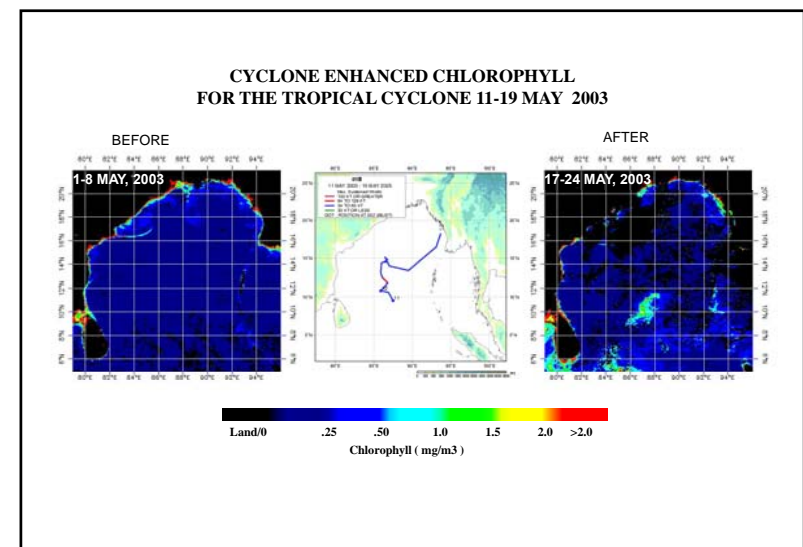
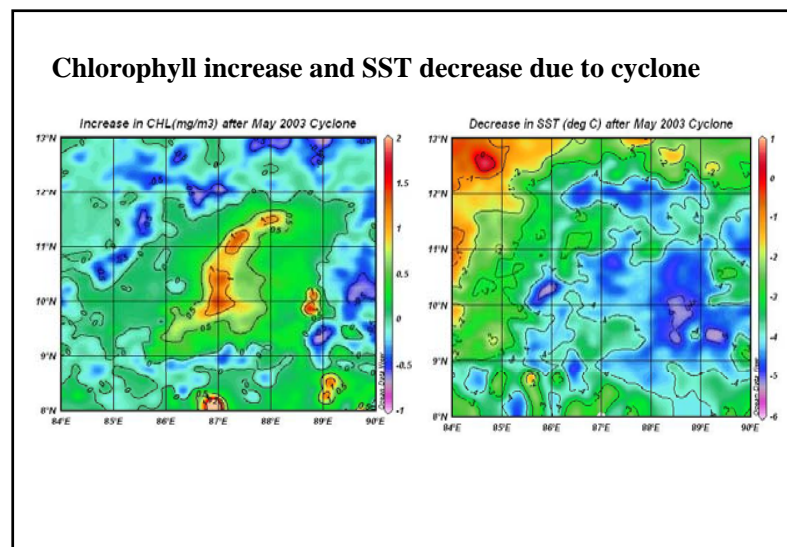
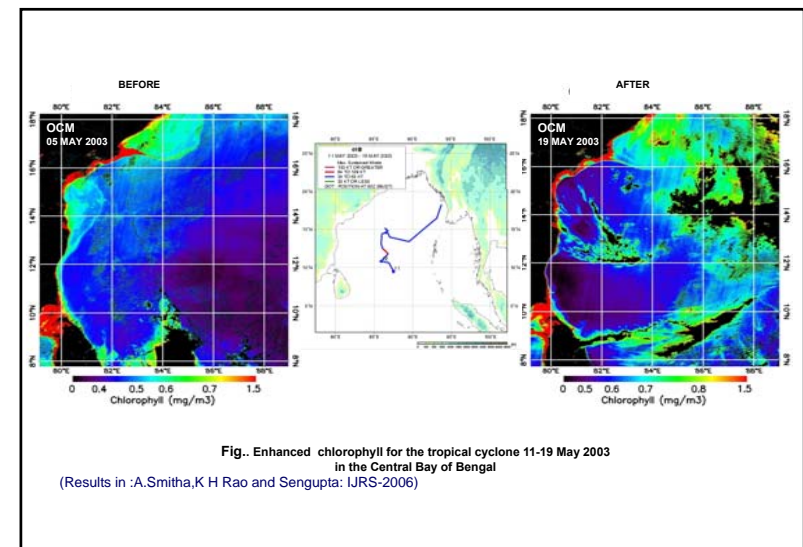
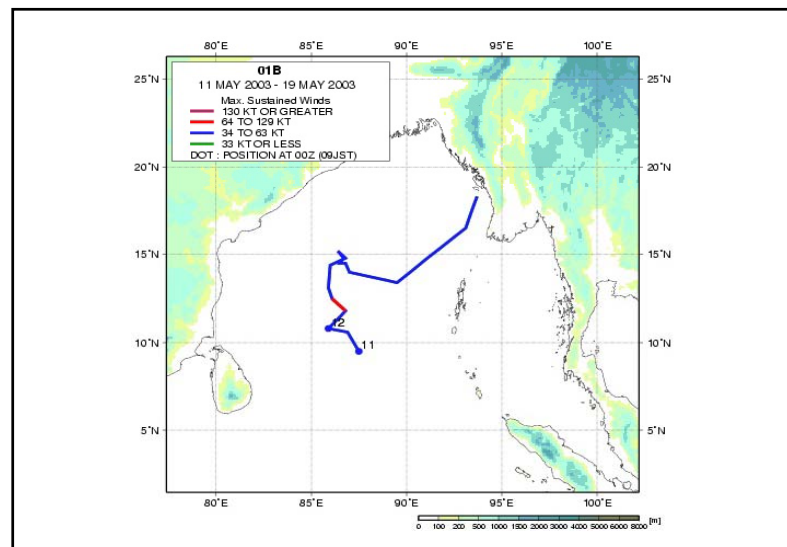
⁵ Indian National Centre for Ocean Information Services (INCOIS),Hyderabad-500055

- Tropical cyclones are a major hazard in tropical coastal regions, both in terms of loss of life and economic damage.
- The effect of the tropical cyclone to the cooling of Sea Surface Temperature (SST) is widely known, where its effect on the distribution of phytoplankton and chlorophyll in the open waters is yet to be documented.
- In the open sea, tropical cyclones may deepen the mixed layer by 20-30 m. The nutrients injected to the well-lit euphotic zone in such events trigger the growth of the plankton.
- Shortly after a cyclone event an increase in phytoplankton biomass and productivity is observed using OCM/MODIS data in the north Indian ocean.
- Ocean-color for chlorophyll concentrations is a new approach for understanding the influence of tropical cyclones on biology, such as phytoplankton blooms, and oceanic physical processes, such as eddies.



DATA USED

- OCM and MODIS L-1B passes covering the north Indian ocean (One week before, during and after the cyclones)
- SST (TMI/AVHRR/MODIS)
- Scatterometer backscatter cross section mean values
- Derived wind vectors/ wind stress
- Modeled MLD(NRL 3 day)
- Weekly averaged PP(VGPM and Mixed layer)
- SSHA (Altimeters)



CYCLONE ENHANCED MIXED LAYER PRIMARY PRODUCTIVITY FOR THE TROPICAL CYCLONE 11-19 MAY 2003

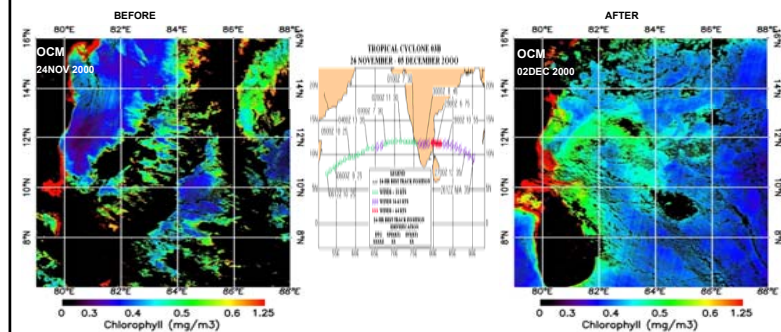
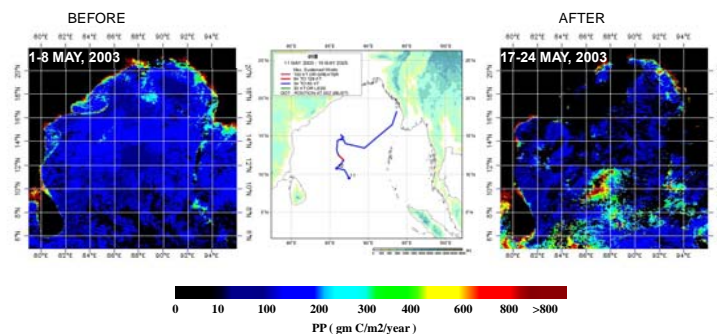
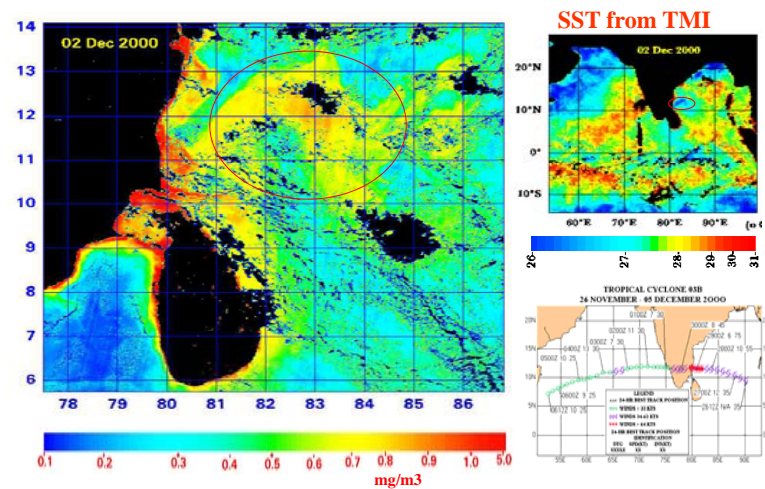
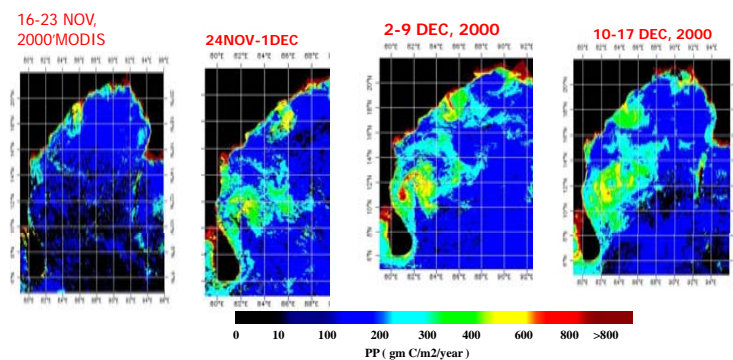
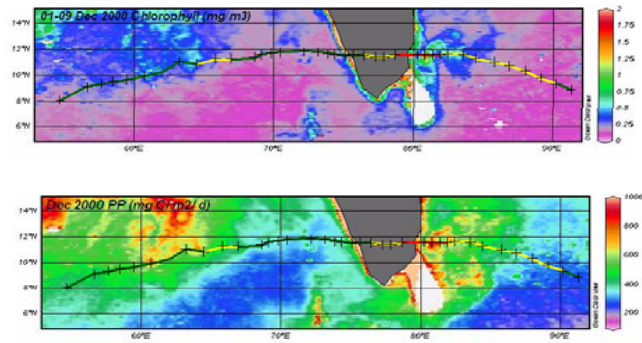


Fig. Enhanced chlorophyll for the tropical cyclone 24 Nov- 5 Dec 2000
in the south-western Bay of Bengal
(K H Rao, Smitha and MM Ali 2007,IJMS- June 2007)

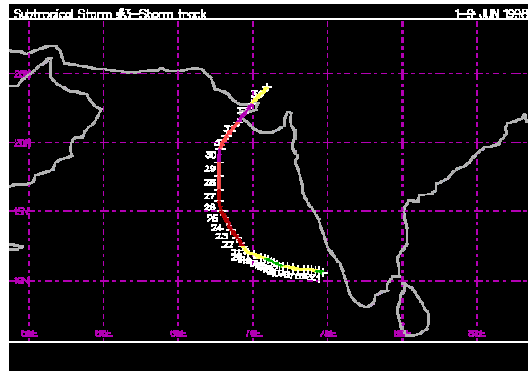


WEEKLY COMPOSITE PRIMARY PRODUCTIVITY (HOWARD-YODER-RYAN MODEL)



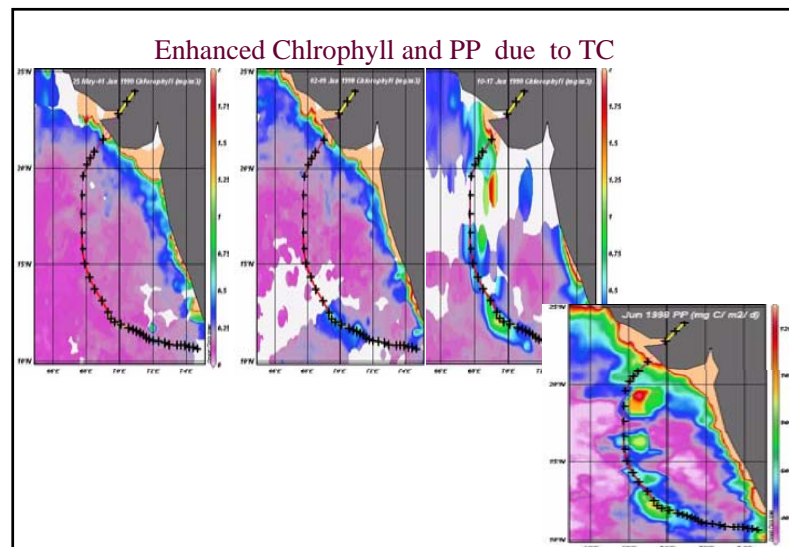


Tropical cyclone track during 1st 9th June, 1998 in the eastern Arabian Sea

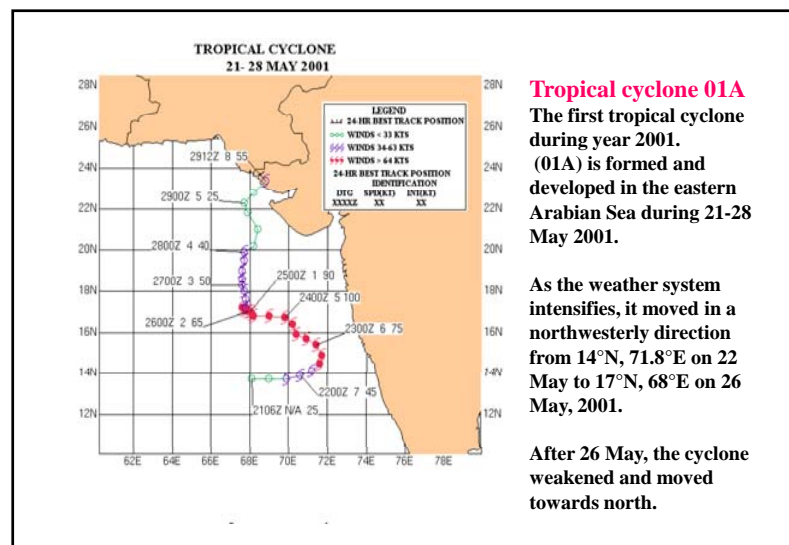


Tropical Cyclone 03A, the most intense tropical cyclone to strike India in 25 years, formed off the southwest tip of India early in June. The storm tracked westward over the Arabian Sea, then turned north and moved inland near Porbandar, India. Attained a maximum intensity of 105 kt, just prior to making landfall.

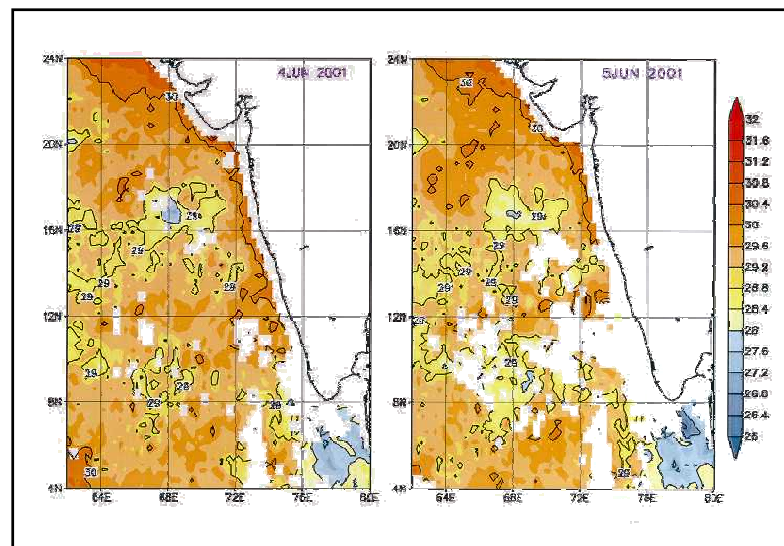
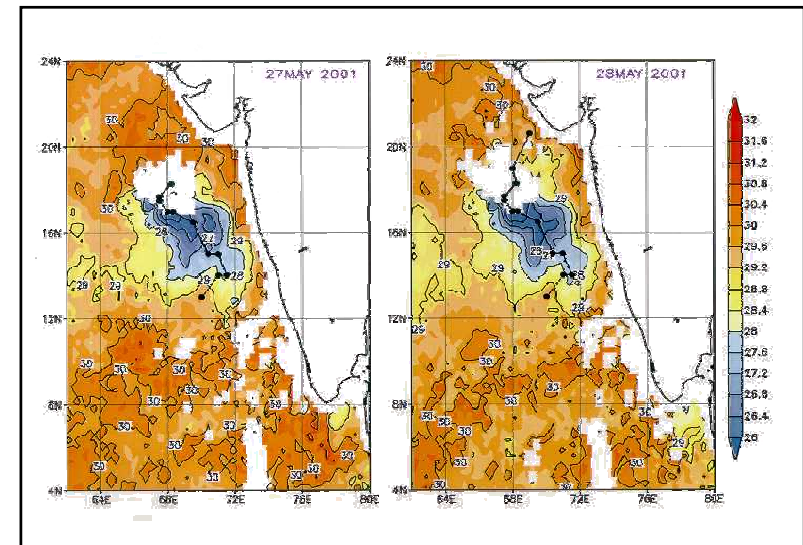
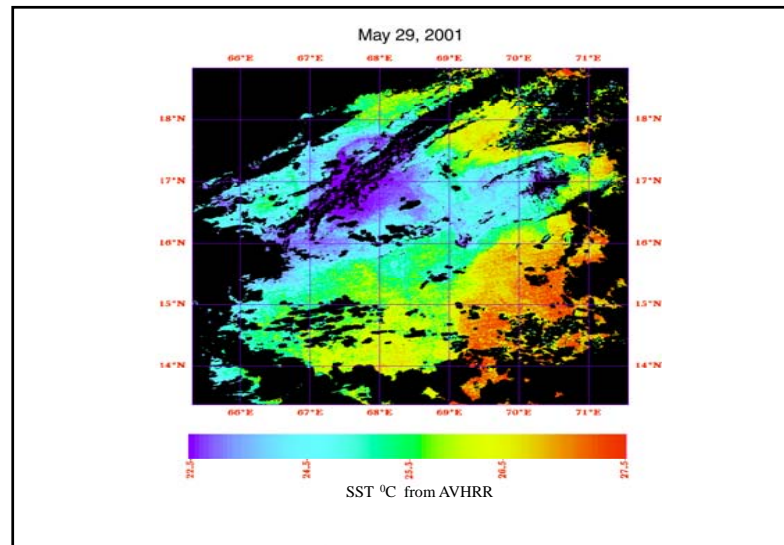
ADV	LAT	LOE	TIME	WIND	STAT
1	10.6	74.7	06/01/06Z	25	TROPICAL DEPRESSION
2	10.7	74.4	06/01/12Z	30	TROPICAL DEPRESSION
3	10.7	74.2	06/01/18Z	35	TROPICAL STORM
4	10.8	73.9	06/02/00Z	35	TROPICAL STORM
5	10.8	73.7	06/02/06Z	35	TROPICAL STORM
6	10.8	73.4	06/02/12Z	35	TROPICAL STORM
7	10.8	73	06/02/18Z	35	TROPICAL STORM
8	10.9	72.7	06/03/00Z	35	TROPICAL STORM
9	11	72.3	06/03/06Z	35	TROPICAL STORM
10	11	72	06/03/12Z	30	TROPICAL DEPRESSION
11	11.1	71.8	06/03/18Z	30	TROPICAL DEPRESSION
12	11.2	71.6	06/04/00Z	30	TROPICAL DEPRESSION
13	11.3	71.4	06/04/06Z	30	TROPICAL DEPRESSION
14	11.4	71.2	06/04/12Z	30	TROPICAL DEPRESSION
15	11.5	71	06/04/18Z	30	TROPICAL DEPRESSION
16	11.6	70.8	06/05/00Z	35	TROPICAL STORM
17	11.7	70.5	06/05/06Z	40	TROPICAL STORM
18	11.9	70.1	06/05/12Z	50	TROPICAL STORM
19	12	69.7	06/05/18Z	50	TROPICAL STORM
20	12.2	69.5	06/06/00Z	55	TROPICAL STORM
21	12.5	69.3	06/06/06Z	70	CYCLONE-1
22	13.1	68.9	06/06/12Z	70	CYCLONE-1
23	13.7	68.5	06/06/18Z	70	CYCLONE-1
24	14.3	68.2	06/07/00Z	75	CYCLONE-1
25	15	67.9	06/07/06Z	75	CYCLONE-1
26	15.8	67.7	06/07/12Z	80	CYCLONE-1
27	16.6	67.7	06/07/18Z	90	CYCLONE-2
28	17.6	67.7	06/08/00Z	95	CYCLONE-2
29	18.6	67.7	06/08/06Z	100	CYCLONE-3
30	19.6	67.8	06/08/12Z	95	CYCLONE-2
31	20.5	68.2	06/08/18Z	95	CYCLONE-2
32	21.5	69	06/09/00Z	105	CYCLONE-3
33	22.8	69.9	06/09/06Z	80	CYCLONE-1
34	24	70.9	06/09/12Z	60	TROPICAL STORM



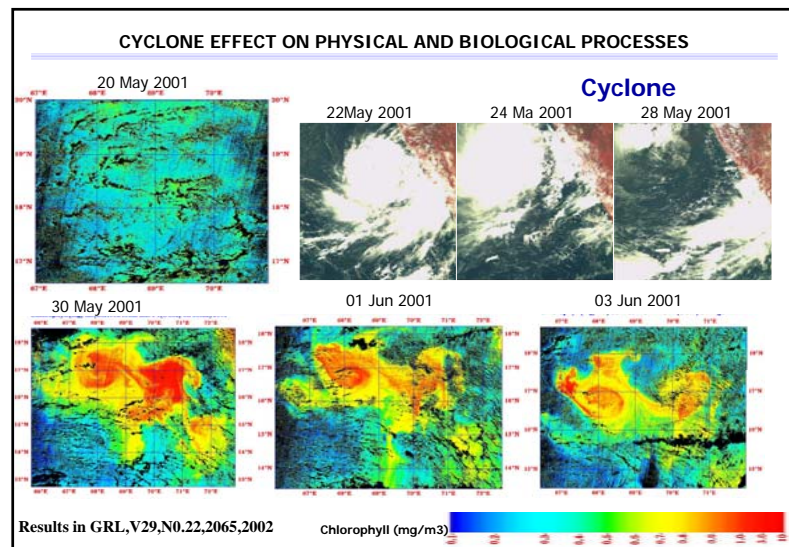
Tropical cyclone track during 21-28 May, 2001 in the eastern Arabian Sea



Sea Surface Temperature (°C) from NOAA /AVHRR on May 29, 2001 in the Arabian Sea.
Around 4°C cooling in the Core of the Cyclone.
SST from TMI from 12st May 5th June 2001

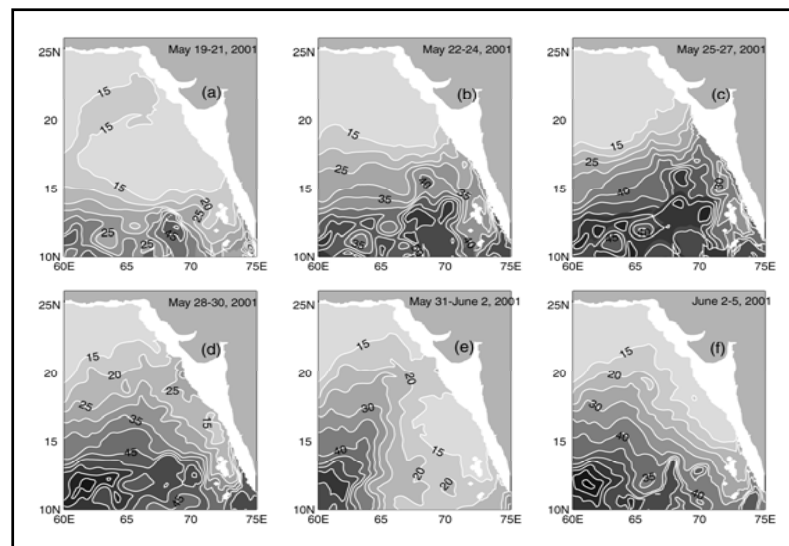


Chlorophyll-a concentrations (mg. m^{-3}) from OCEANSAT-1 Ocean Color Monitor at various stages of cyclone (a) prior to its formation on May 20 and after it was intensified and weakened towards north on May 30, June 1, June 3, 2001 in the Arabian Sea.



NRL model simulated 3.05 day averaged mixed layer depth (m)

During various stages of cyclone (a) 19-21 May, (b) 22-24 May, (c) 25-27 May, (d) 28-30 May, (e) 31 May – 2 June, and (f) 3-5 June 2001.



Tropical Cyclone , 06B SIDR, 11-15 November 2007

- Started as a tropical storm on 11th Nov 2007
- Intensified into a Category-3 with wind speed of 105 kts on 12th Nov 2007
- Further intensified into Category-4 cyclone with wind speed of 115 kts on 13th Nov
- Intensity decreased and became category-3 cyclone on 15th Nov 2007
- Became a tropical storm by 16th Nov 2007

Data used

•Satellite data products

- Quiksat (wind vectors)
- MODIS-Aqua(SST and Chlorophyll)
- TMI(temperature)

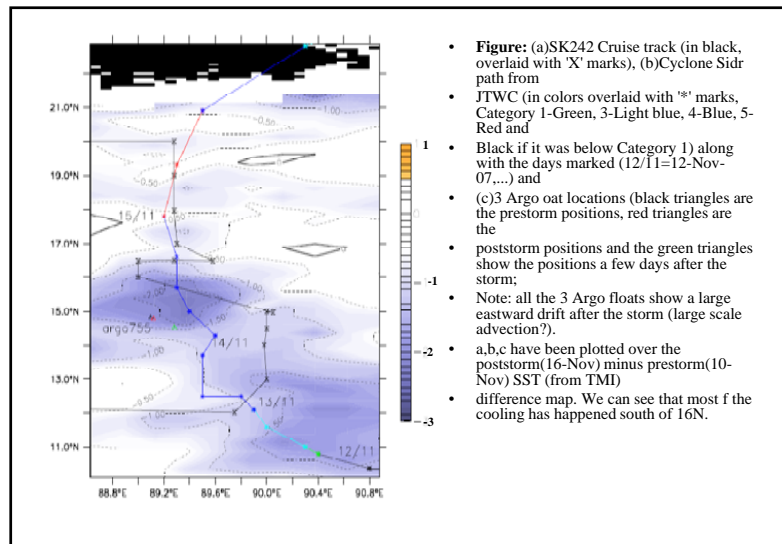
•In-situ profiles(CTD) salinity and Temperature

- Sagra kanya Cruise (SK-242)(INCOIS and IISc)
- Argo Floats profiles

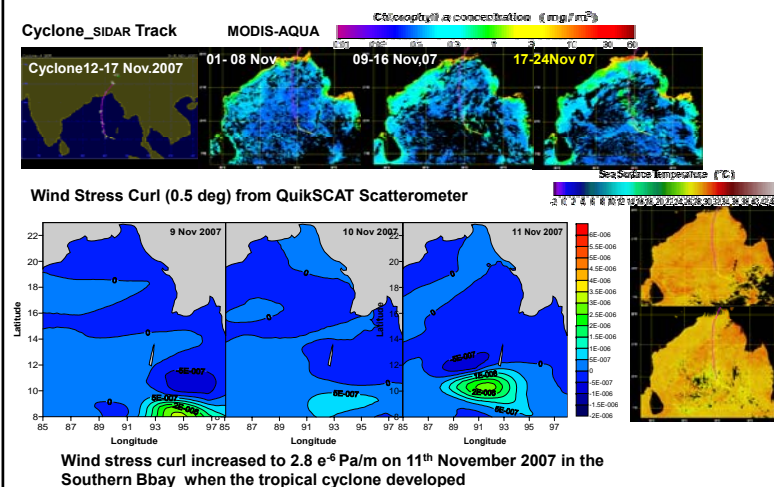
• Model

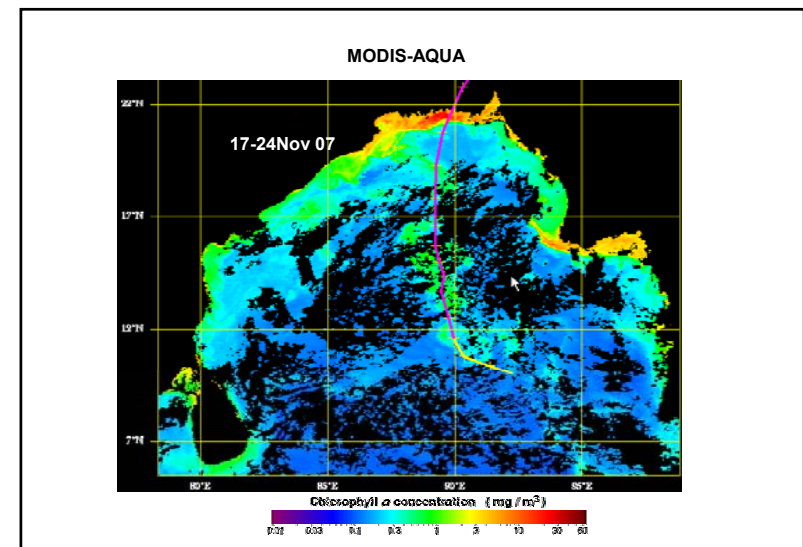
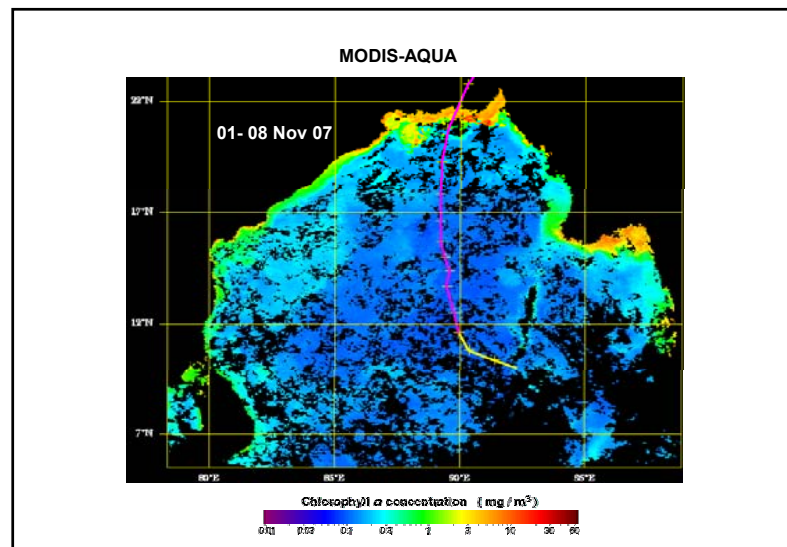
1-D Mixing model (IISC_Bangalore)

Cyclone - SIDR



Upper ocean response to SIDAR Cyclone





Location	Season	cyclone Period	wind speed m/s		Transit time(h)	Transit Distance (km)	Transit Speed (km/h)	radius maximum winds, Km		Chl- <i>a</i> (mg/m ³)		SST (°C)	
			Max	Mean				tropical storm force	Cyclone Force	Before	After	Before	After
AS	SW	01-09 Jun 1998	53.97	43.48	72	1252	17.38	280	78	0.25	1.8	31.8	24.75
AS	NE	11-17 Dec 1998	33.41	28.48	66	957	14.5	316	156	0.188	2.88	27.6	20.55
BOB	NE	13-16 Nov 1998	43.69	37.52	24	398	16.6	275	105	0.15	0.4	29.25	25.5
BOB	NE	16-23 Nov 1998	38.55	30.84	54	770	14.26	250	142	0.2	0.58	28.2	26.55
BOB	FALL	15-18 Oct 1999	61.68	51.91	24	260	10.8	148	75	0.39	5.96	30	24.3
BOB	FALL	25 Oct-03 Nov 1999	71.96	65.54	30	399	13.3	185	55	0.33	3.55	28.95	24.9
AS	Spring	15-21 May 1999	56.54	49.86	66	1045	15.8	194	79	0.36	0.8	29.25	22.95
BOB	NE	26 Nov-06 Dec 2000	33.41	33.41	18	175	9.72	144	63	0.18	1.8	29.1	25.2
AS	Spring	21-29 May 2001	56.54	44.20	84	576	6.86	292	79	0.12	3.1	30.75	22.2
BOB	Spring	08-19 May 2003	30.84	28.78	48	492	10.25	222	105	0.1	0.3	31.5	25.35
AS	NE	10-18 Nov2003	41.12	36.49	30	316	10.53	190	73	0.19	0.89	28.65	25.65
AS	NE	28 Nov-03 Dec 2004	33.41	33.41	42	1275	30.75	271	64	0.11	0.8	28.95	23.7
BOB	NE	06-10 DEC 2005	33.41	25.98	48	965	20.1	204	83	0.24	1.55	27.9	24.15
BOB	Spring	24-29 APR 2006	59.11	30.84	48	1343	28	186	78	0.112	0.7	31.2	22.05

Cyclone physical characteristics with Satellite derived SST and Chl-*a* response

Location	Season	cyclone Period	Lat	Coriolis Frequency f°(10-4)s-1	Inertial periodTf hours	Transit speed Uh(Km/h)
AS	SW	01-09 Jun 1998	17.77	0.444	39.319	17.38
AS	NE	11-17 Dec 1998	17.23	0.431	40.512	14.5
BOB	NE	13-16 Nov 1998	14.14	0.355	49.122	16.6
BOB	NE	16-23 Nov 1998	16.89	0.423	41.303	14.26
BOB	FALL	15-18 Oct 1999	17.97	0.449	38.895	10.8
BOB	FALL	25 Oct-03 Nov 1999	19.61	0.488	35.755	13.3
AS	Spring	15-21 May 1999	21	0.521	33.485	15.8
BOB	NE	26 Nov-06 Dec 2000	11.49	0.29	60.242	9.72
AS	Spring	21-29 May 2001	14.22	0.357	48.851	6.86
BOB	Spring	08-19 May 2003	10.64	0.269	64.992	10.25
AS	NE	10-18 Nov2003	6.1	0.155	112.926	10.53
AS	NE	28 Nov-03 Dec 2004	5.43	0.138	126.81	30.75
BOB	NE	06-10 DEC 2005	10	0.253	69.105	20.1
BOB	Spring	24-29 APR 2006	16.53	0.414	42.177	28

Cyclonically rotating cyclone winds cause the oceanic mixed layer currents to diverge from the storm track starting within one-quarter of an inertial wave length behind the eye, where the inertial wave length (λ) is defined as the product of the storm translation speed (Uh) and the inertial period (IP= 12/ sin Φ hr) at that latitude Φ . SST decreases in this directly forced regime are due to surface fluxes of latent and sensible heat to the atmosphere (20%) and vertical mixing at the base of the oceanic mixed layer (80%) induced by wind stress and strong vertical shears. Over the next half inertial cycle (i.e. up to 0.75 λ), mixed layer currents converge toward the storm track, causing an increase in the mixed layer depth. This alternating cycle of upwelling and downwelling occurs over distances of λ or inertial periods and establish a horizontal pressure gradient that excites baroclinic near-inertial motions in the thermocline.

Estimation of mixed layer heat content using satellite data

M. V. Rao
Oceanography Division, NRSC

Workshop on Utilisation of Satellite Derived Oceanic Heat Content for Cyclone Studies during March 25-26, 2010 *nrsc*

Introduction:

- North Indian Ocean (NIO) is an ideal place for oceanographers to work with, because it has complimented with extraordinary phenomena such as Somali current, the equatorial jets, the western boundary current or east India current, etc.
- Oceanic mixed layer acts as a heat reservoir that provides the sensible and latent heat energies to the atmosphere.
- Tropical cyclones (TCs) rely, for the formation, intensification and maintenance, of the latent and sensible heat releases that fuel the system.
- Thus the information on MLD and its heat content Over NIO is required for a better understanding of the cyclogenesis, intensification and movement.

nrsc

Objectives

To estimate mixed layer heat content of the North Indian Ocean using satellite data

Data Sets used :

In situ temperature and salinity profiles from ARGO data, Tropical Cyclone Heat Potential from satellite data and Model

nrsc

Methodology

The heat content (HC) of Upper ocean/Mixed layer is estimated conventionally using the following equation

$$HC = \rho C_p \int_0^Z (\bar{T} - T_{mix}) dz$$

Where ρ is density of sea water ($1.026 \times 10^3 \text{ Kg/m}^3$)

C_p is specific heat of air at constant pressure ($4.014 \times 10^3 \text{ J Kg}^{-1} \text{ } ^\circ\text{C}^{-1}$)

\bar{T} is average water temperature of that layer dz

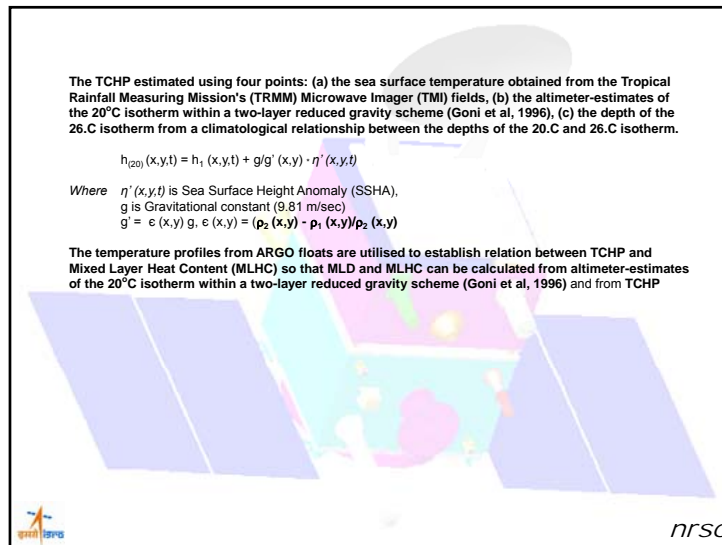
T_{mix} is Temperature at MLD and Z is the depth of the mixed layer

The heat content of mixed layer (HC) and Tropical Cyclone Heat Potential (TCHP) are estimated using ARGO temperature profiles

$$TCHP = \rho C_p \int_0^Z (T - 26) dz$$

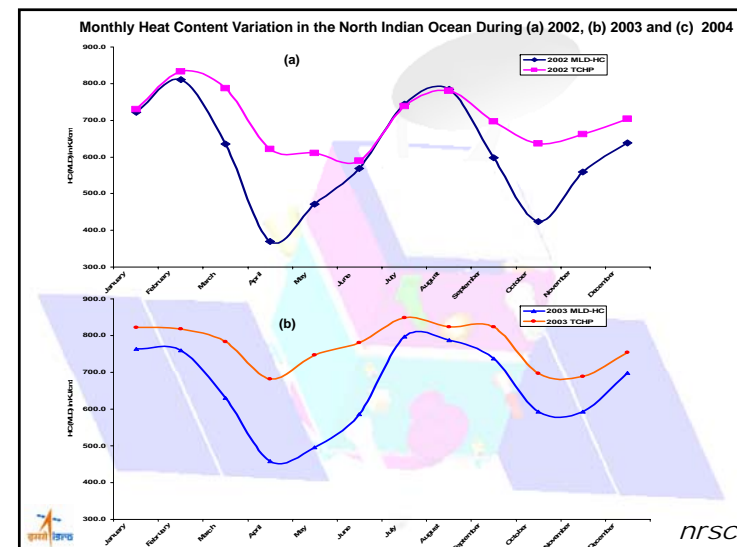
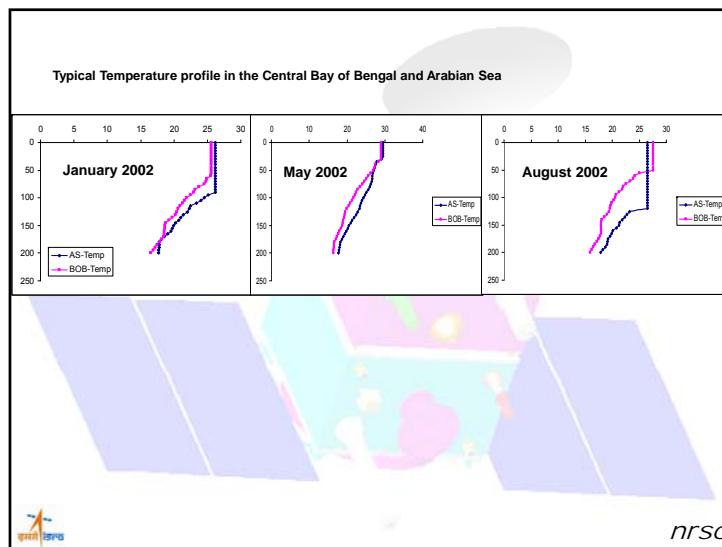
Where Z is the depth of 26°C contour

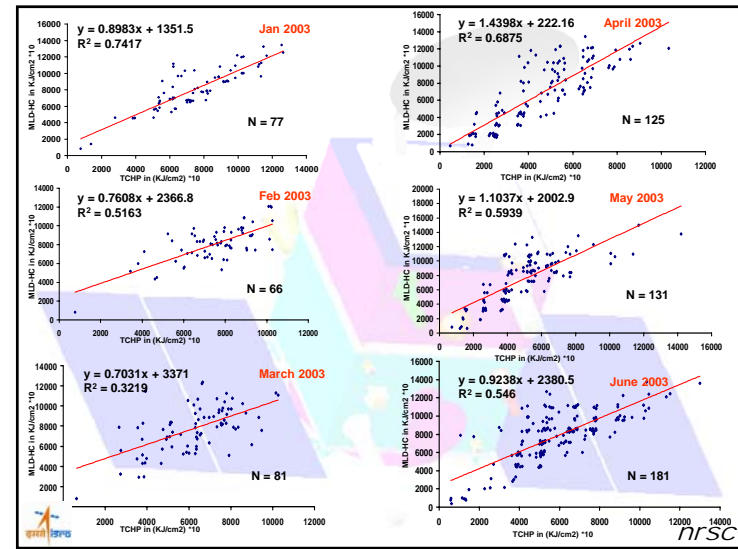
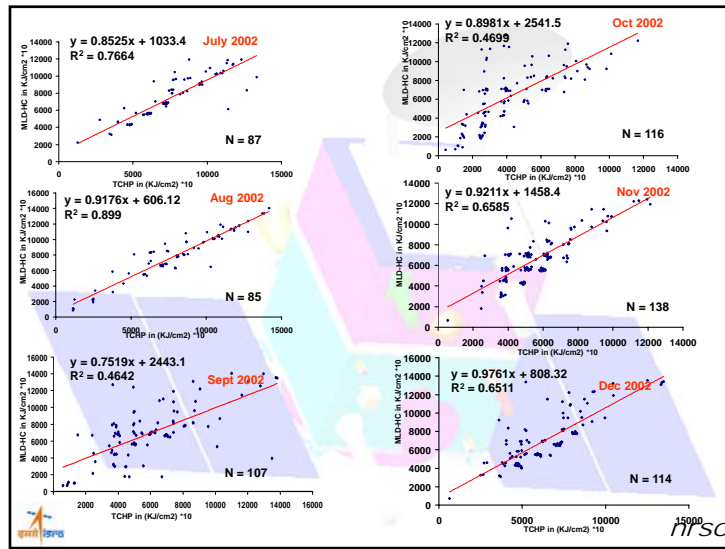
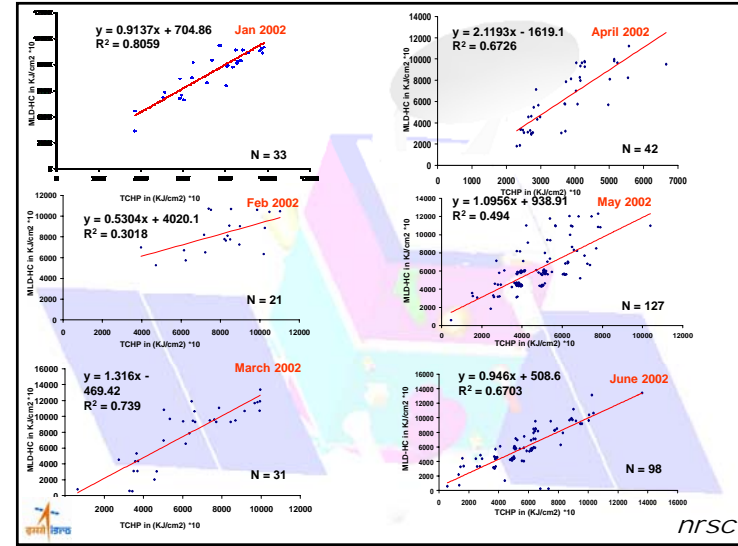
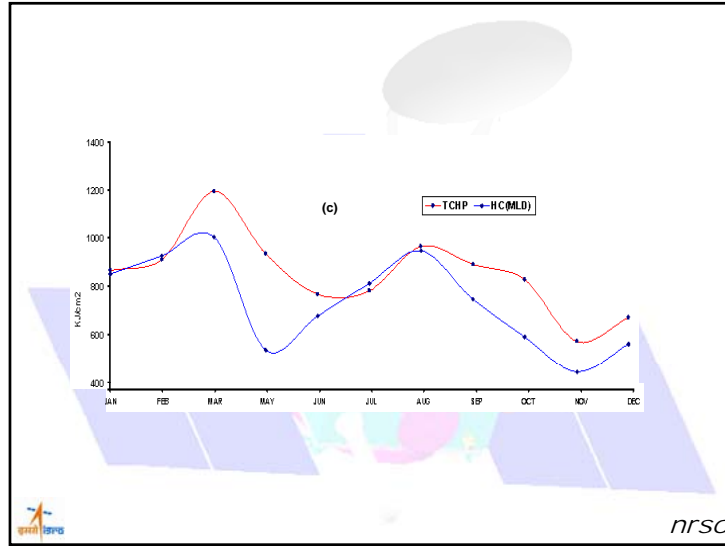
nrsc

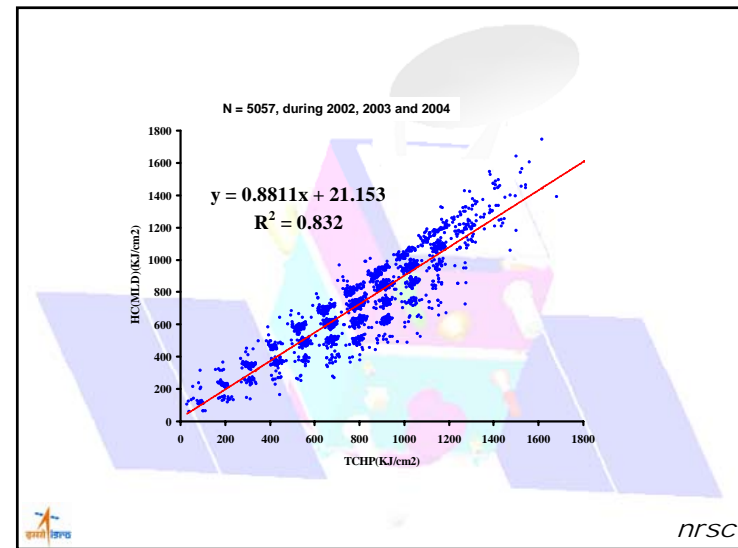
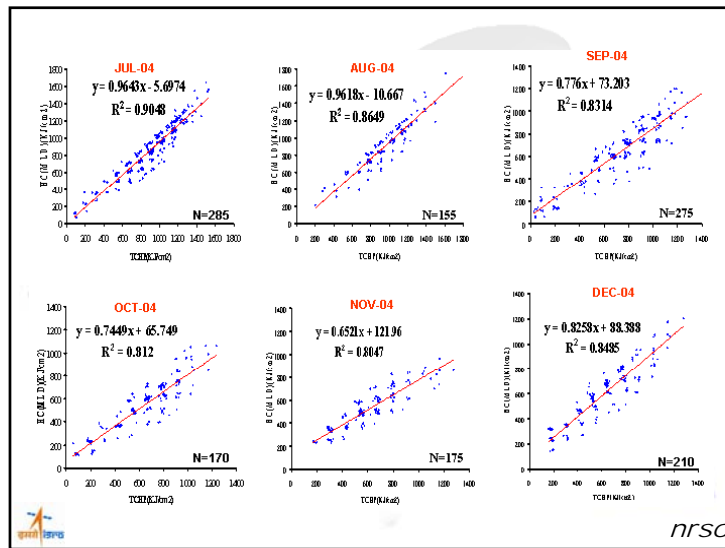
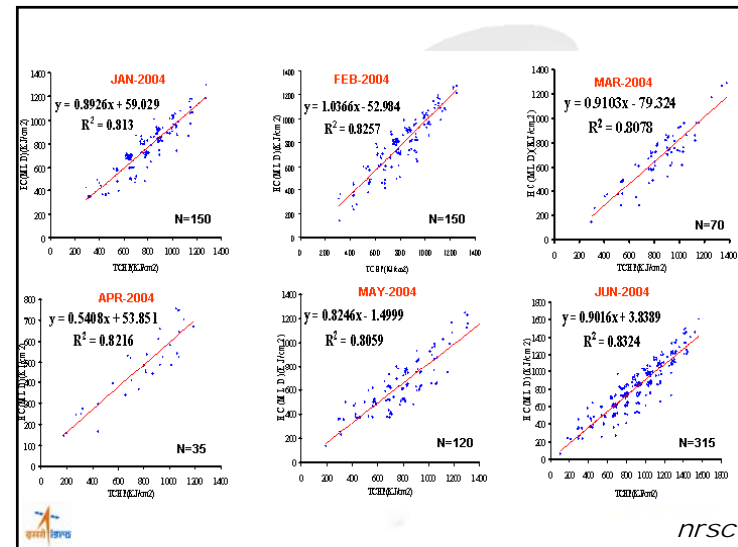
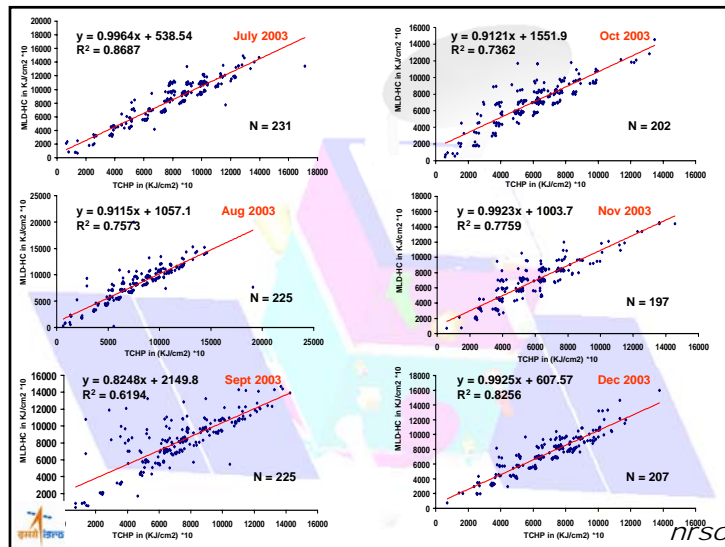


Analysis of Argo Floats:

- More than 5000 Argo floats data analysed
 - Heat content (HC) of the Mixed Layer (ML) and Tropical Cyclone Heat Potential (TCHP), (HC up to 26°C) estimated
 - Relation between HC of the ML and TCHP obtained
 - This relation is used to estimate the HC of ML from TCHP
-
- nrsc

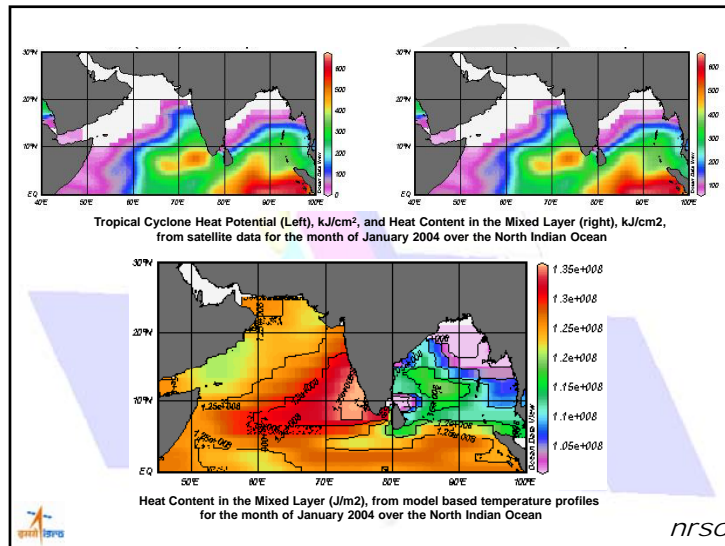
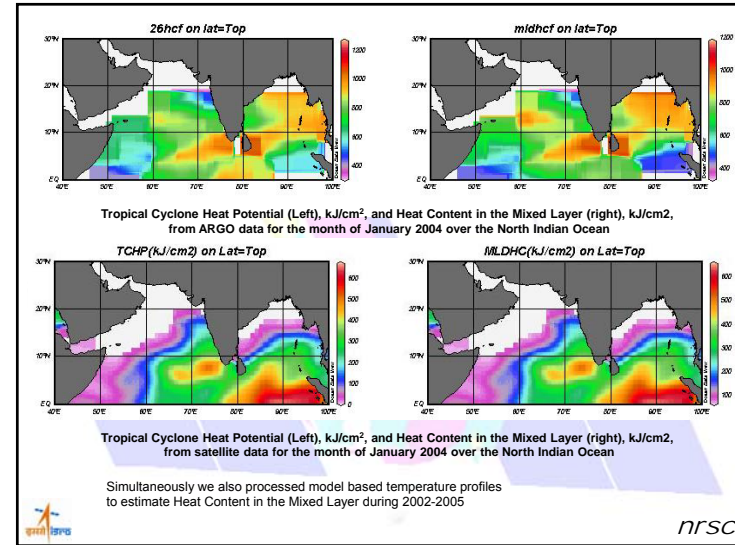






	2002	2003	2004
Determinant	of	Coefficient (R^2)	
January	0.806(033)	0.742(077)	0.813(150)
February	0.302(021)	0.516(066)	0.826(150)
March	0.739(031)	0.322(081)	0.808(070)
April	0.673(042)	0.688(125)	0.822(035)
May	0.494(127)	0.594(131)	0.806(120)
June	0.670(098)	0.546(181)	0.832(315)
July	0.766(087)	0.869(231)	0.905(285)
August	0.899(085)	0.757(225)	0.865(155)
September	0.464(107)	0.619(225)	0.831(275)
October	0.470(116)	0.736(202)	0.812(170)
November	0.659(138)	0.776(197)	0.805(175)
December	0.651(114)	0.826(207)	0.849(210)
For all three years	0.832(5057)		

nrsc



Highlights of results

- More than 5000 temperature profiles from Argo floats were analysed over the north Indian Ocean to study the heat content variability during 2002-2004, since heat content of the upper/mixed layer is a critical information in strengthening of cyclones as well as Indian Summer monsoon activity.
 - Strong relation exist between TCHP and the MLHC ($R^2 = 0.83$)
 - Using the linear relationship, the MLHC for the month of January 2004 have been computed from satellite based TCHP and the results are encouraging
 - Hence both the MLD and MLHC can be computed using depth of 260 C isotherm and CHP with a reasonable accuracy
- nrsc

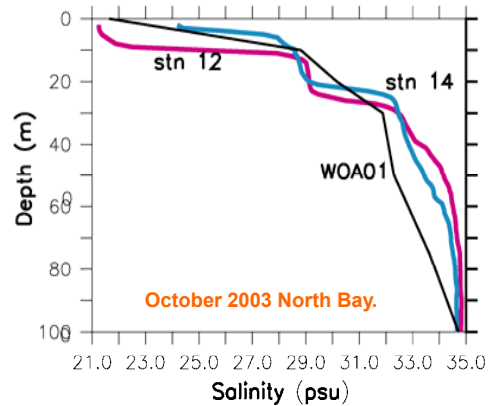
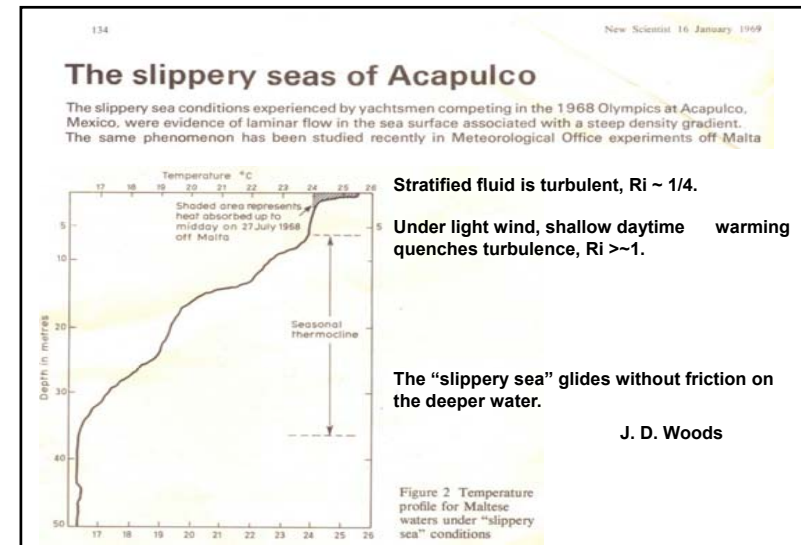
Cyclones and Bay of Bengal cooling



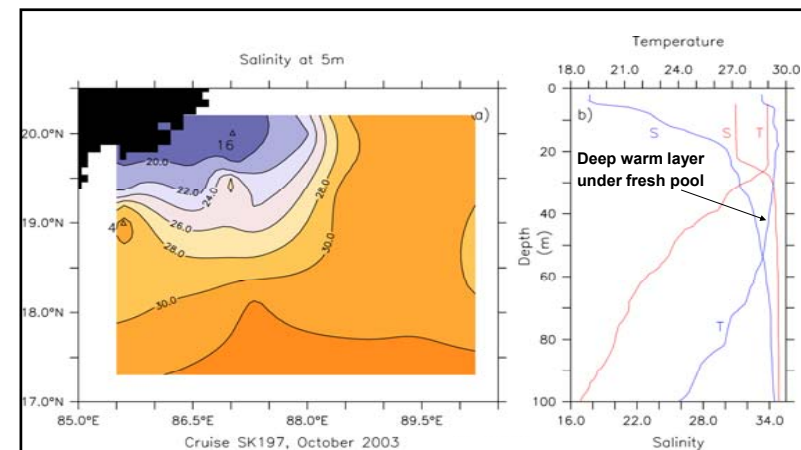
ORV Sagar Kanya

Debasis Sengupta

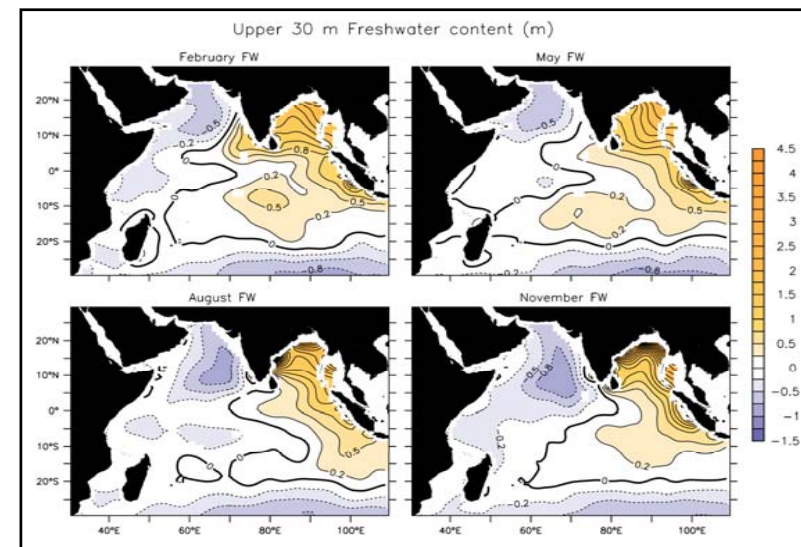
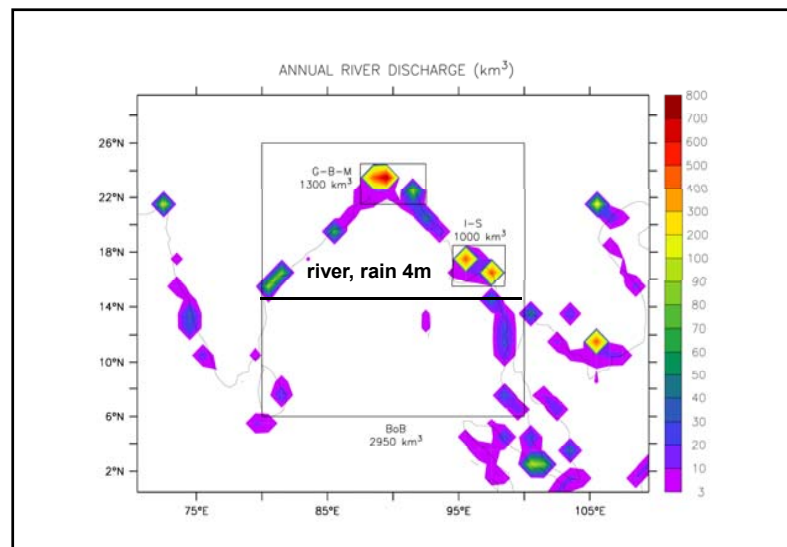
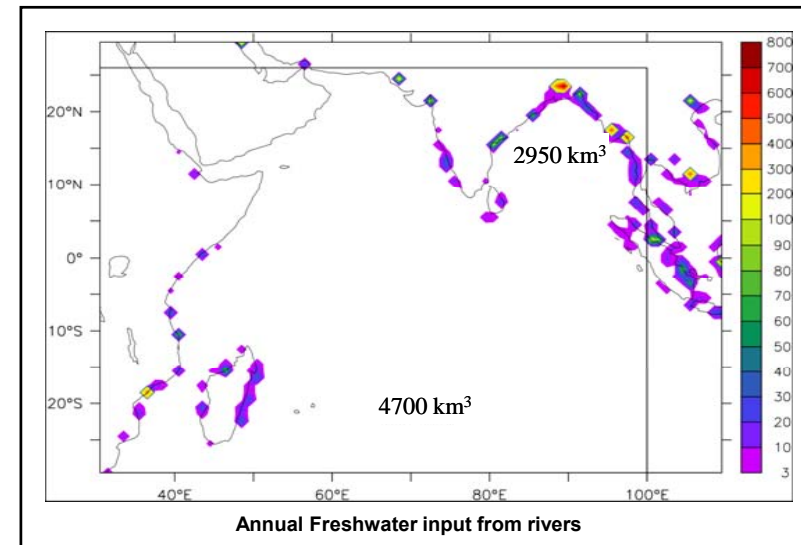
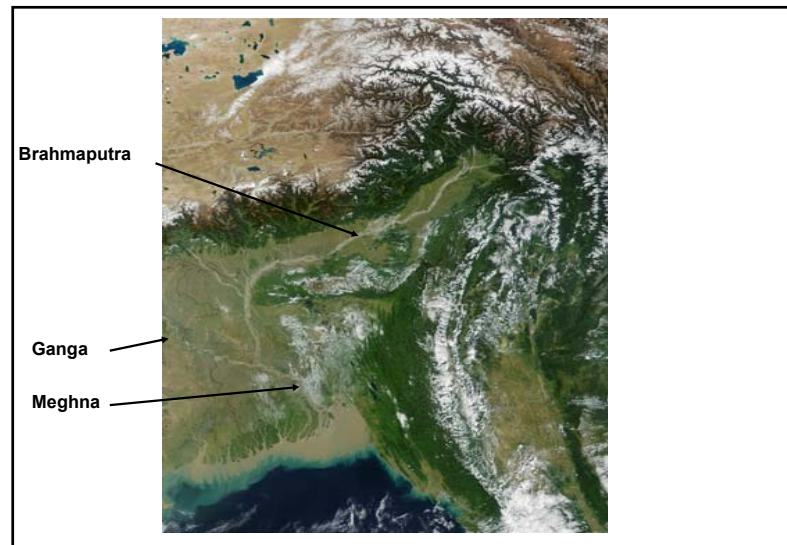
Centre for Atmospheric and Oceanic Sciences
Indian Institute of Science Bangalore

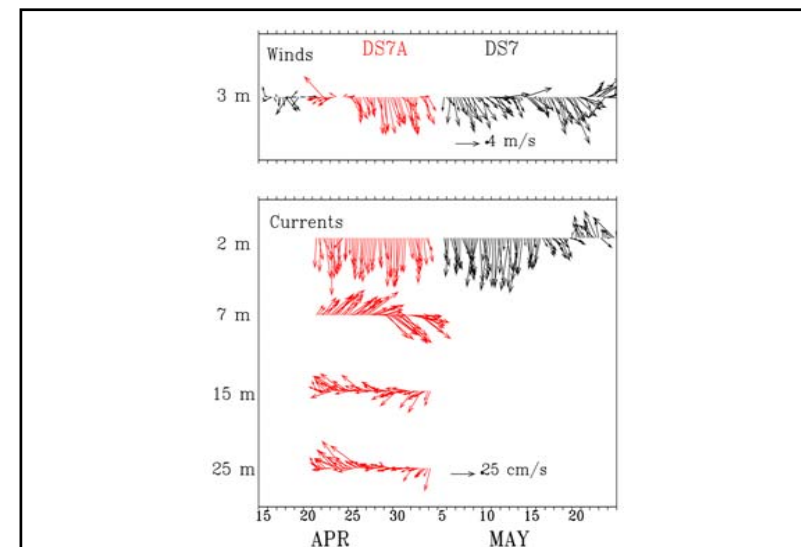
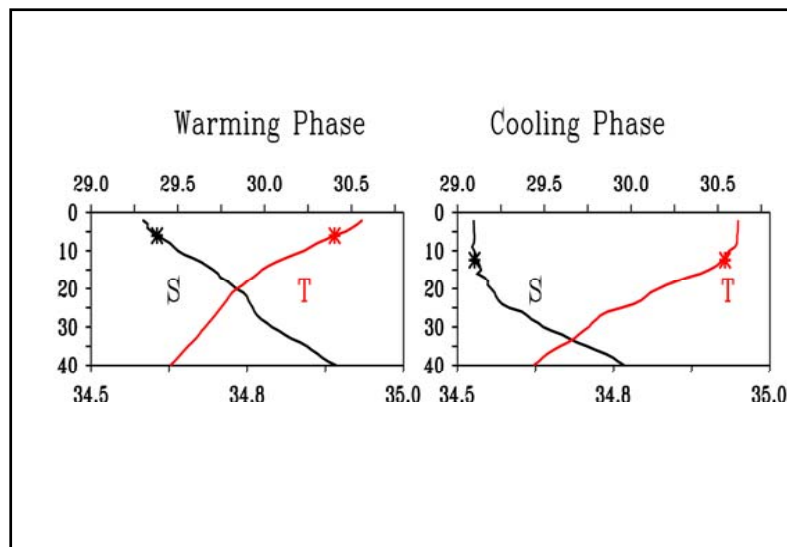
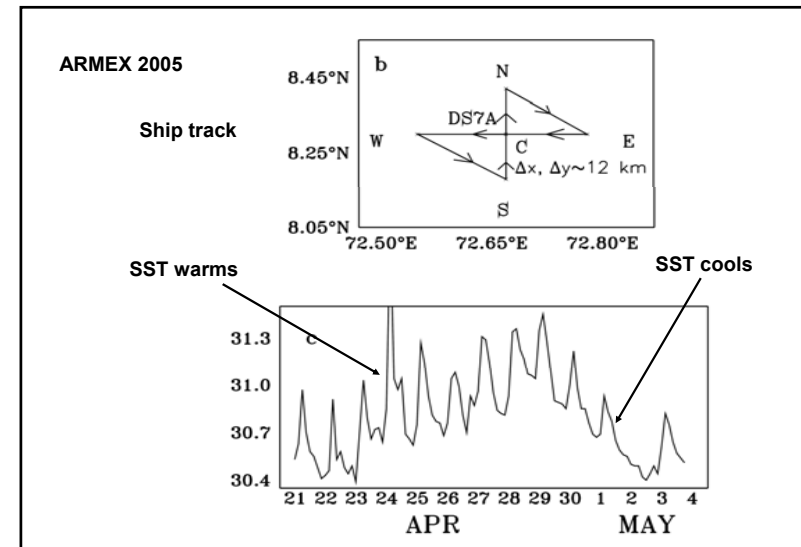
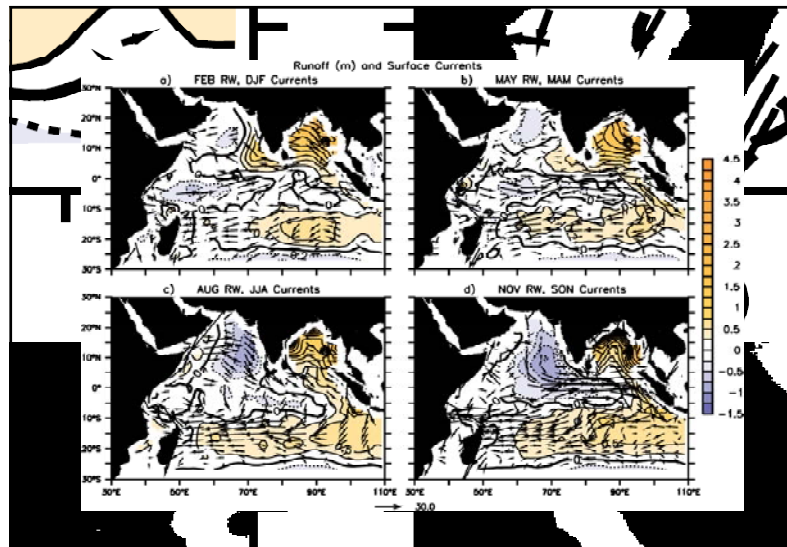


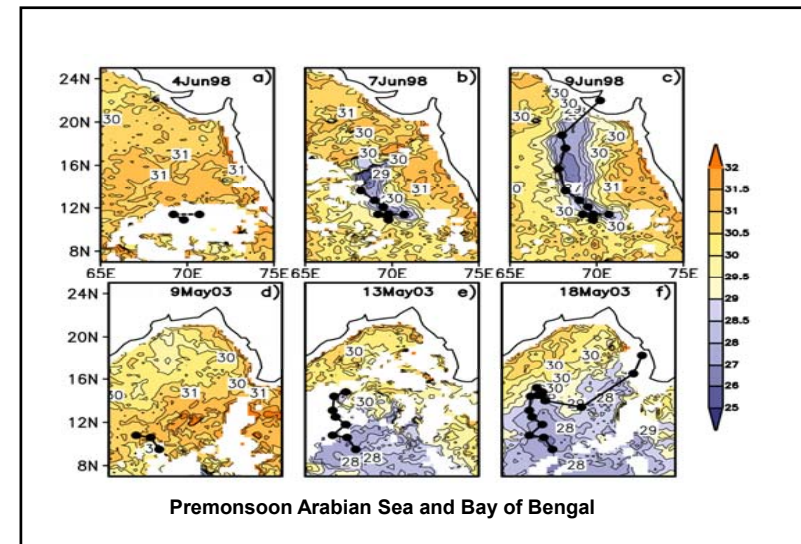
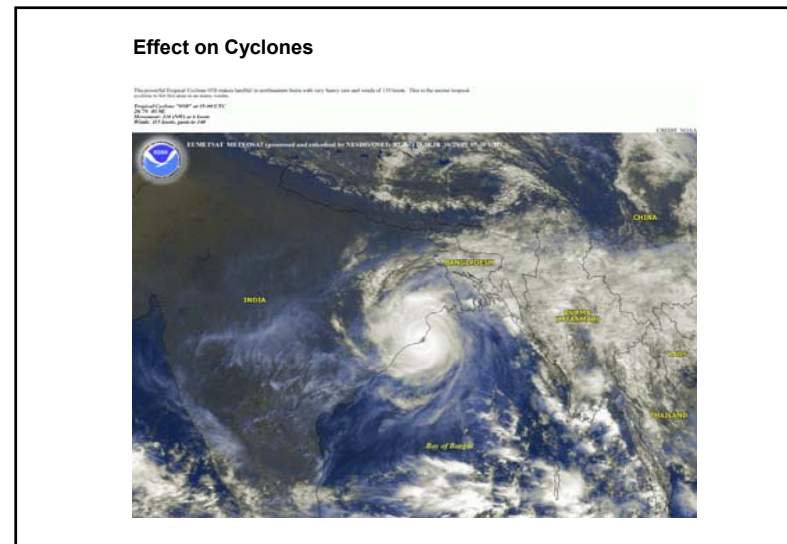
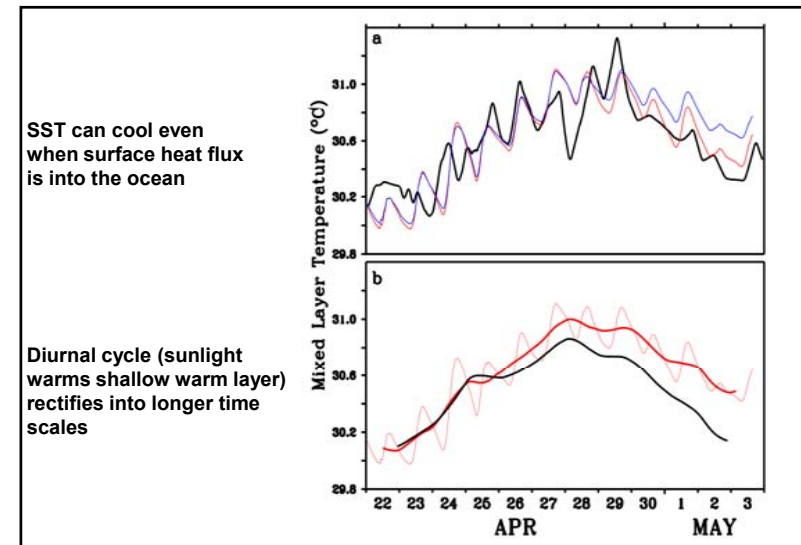
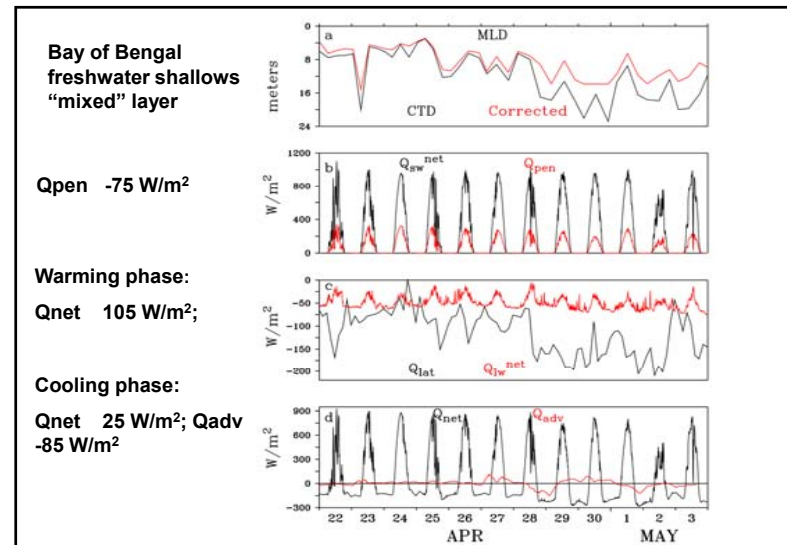
Does the fresh water "glide" without friction ?
Stratification quenches turbulence, reduces mixing ?

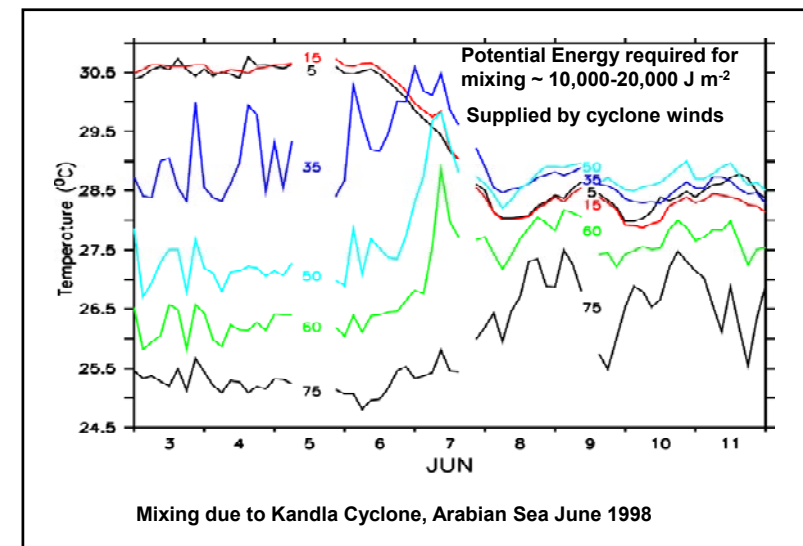
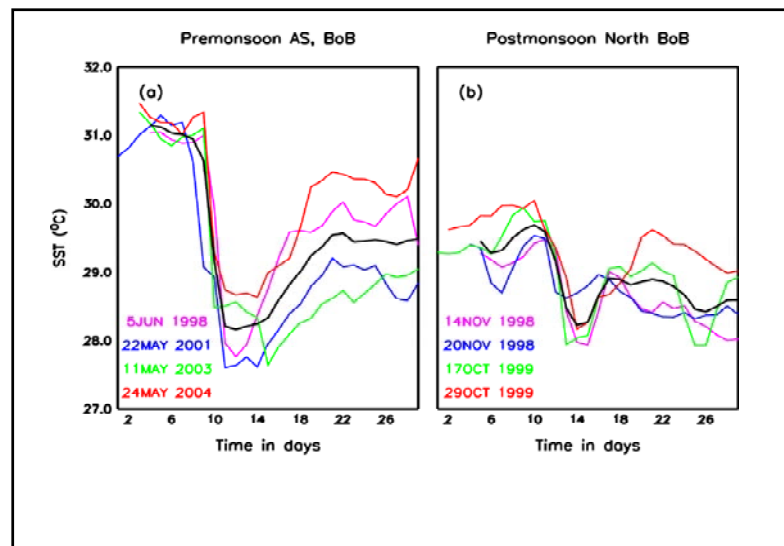
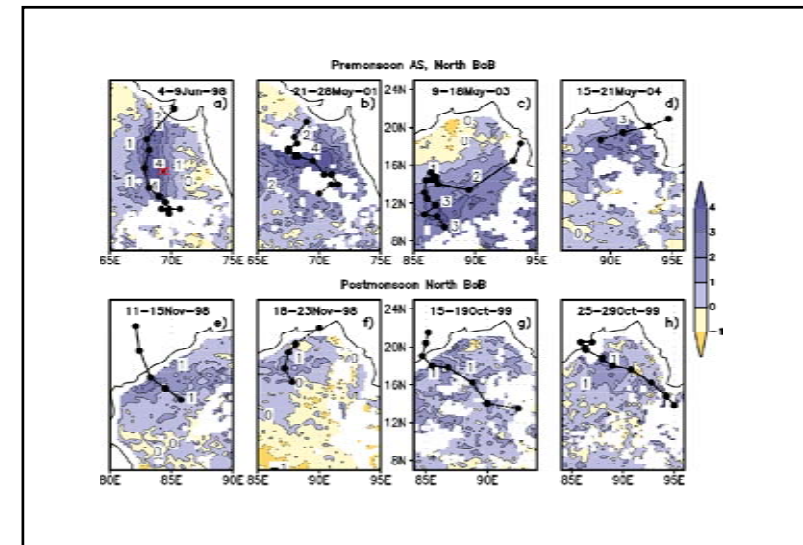
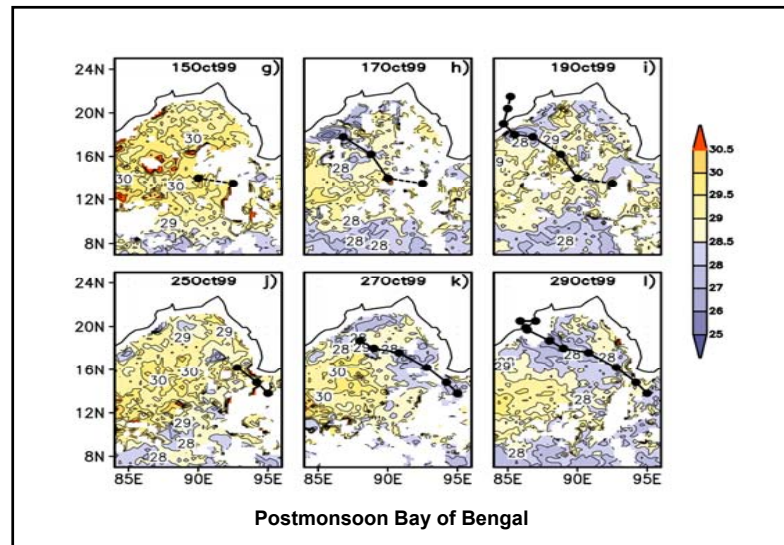


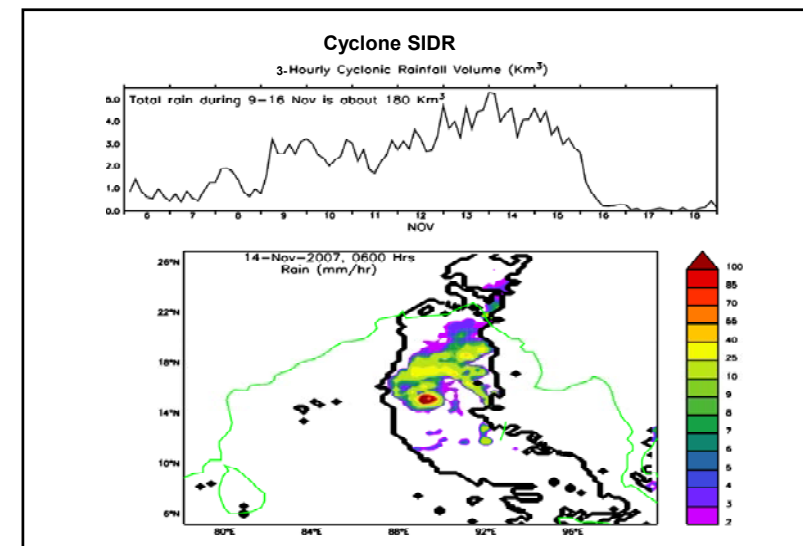
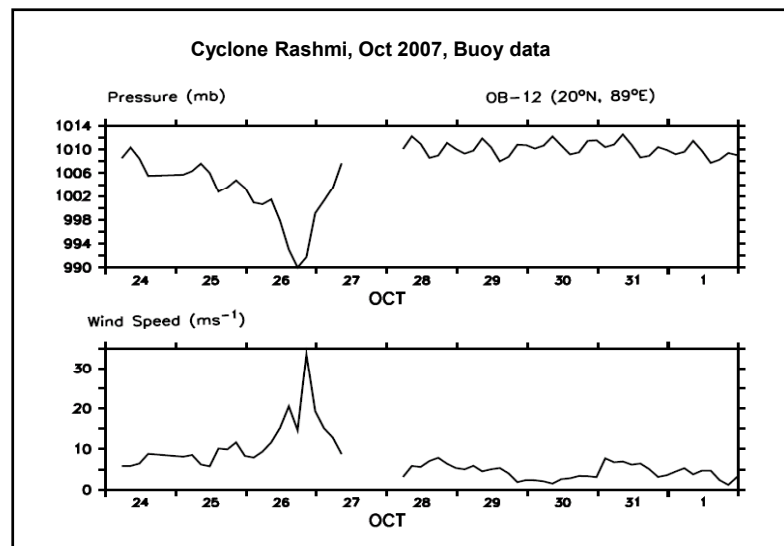
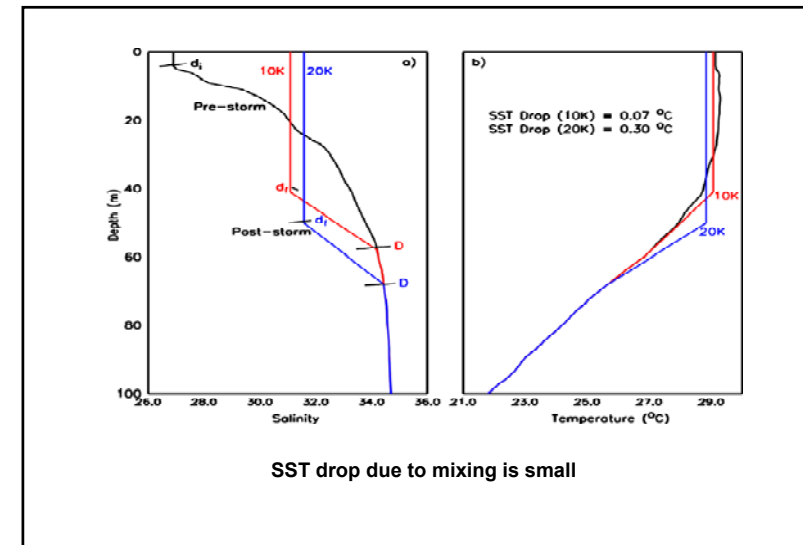
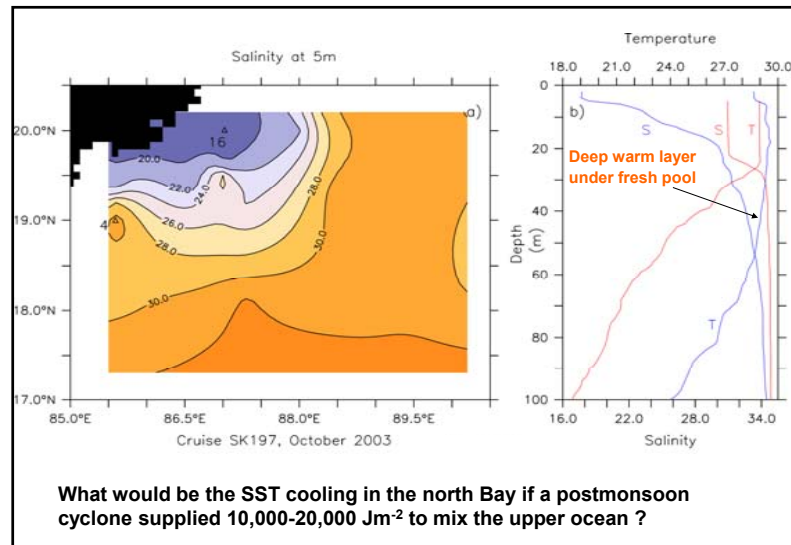
How much does SST cool due to a postmonsoon cyclone ?

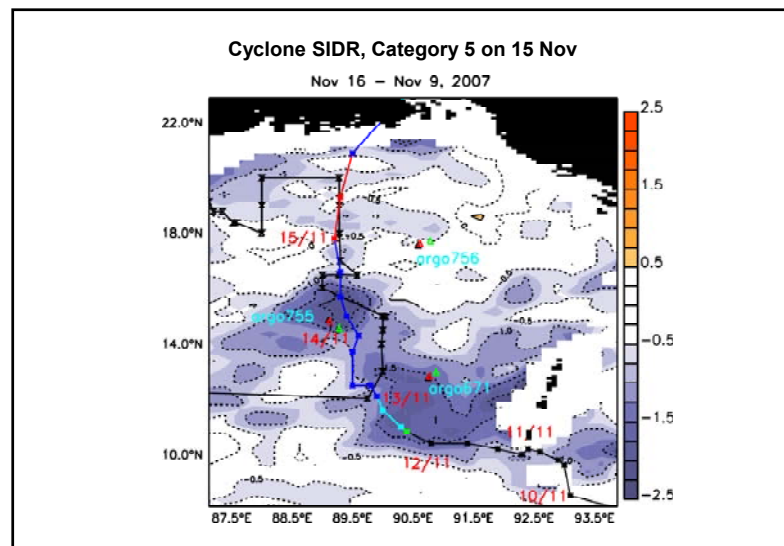
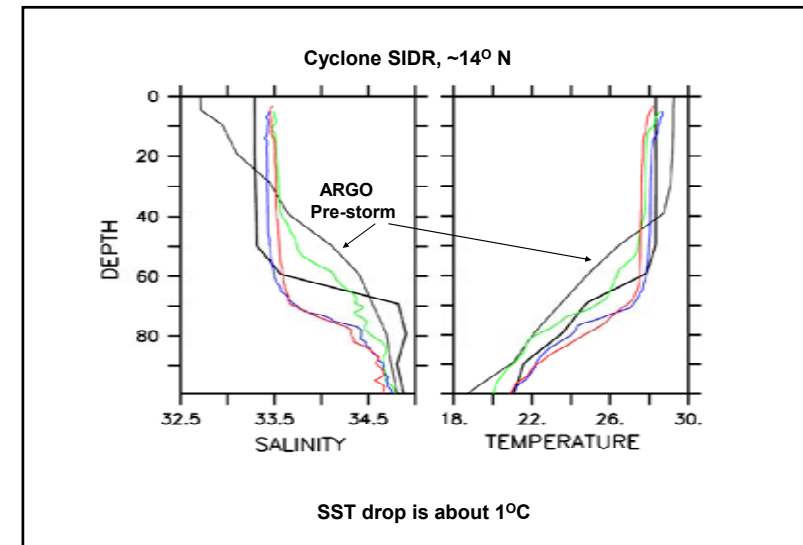
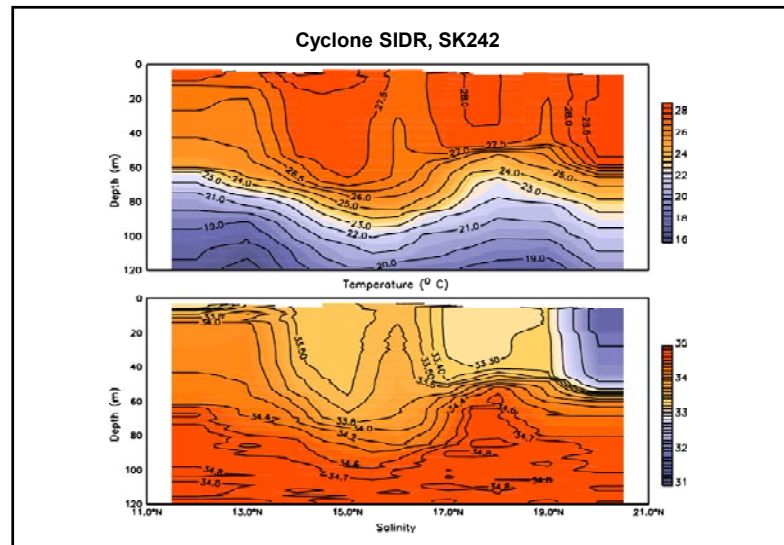












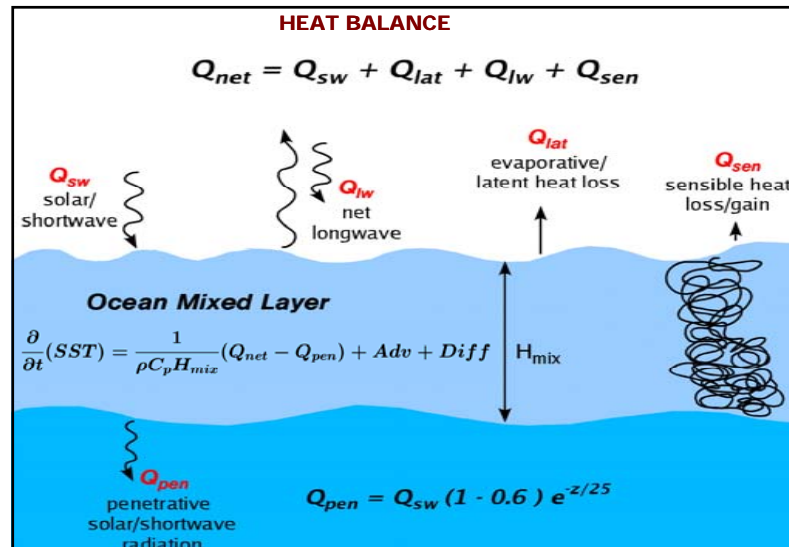
Conclusions

Freshwater from rivers and rain inhibits mixing

Subsurface warm water layer is deep

North Bay of Bengal SST cooling due to postmonsoon cyclones is small

Does this influence cyclone intensity ?



Thermodynamics (heat budget) of upper “mixed” layer :

$$\frac{\partial T}{\partial t} = \frac{Q_{NET} - Q_{PEN}}{\rho C_p H_{MIX}} - (u \frac{\partial T}{\partial x} + v \frac{\partial T}{\partial y} + w \frac{\partial T}{\partial z}) + \text{Turbulent Mixing} + \text{Diffusion}$$

usually no measurements

Net heat flux into ocean surface :

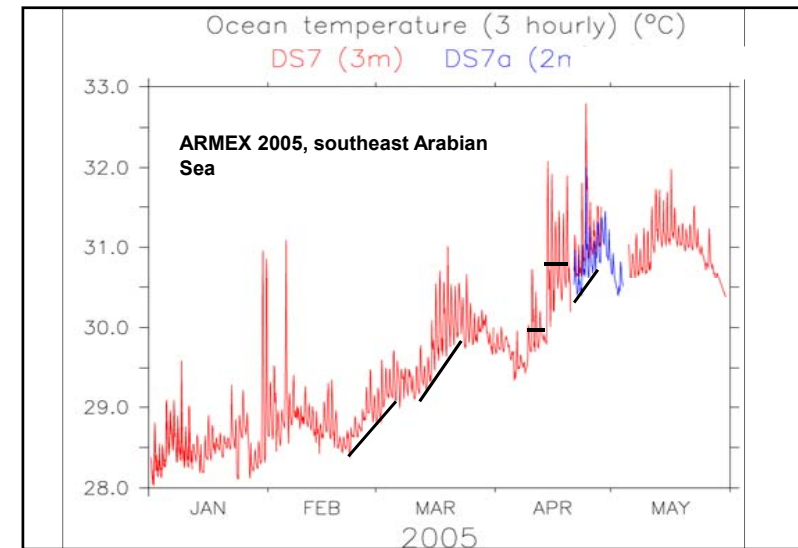
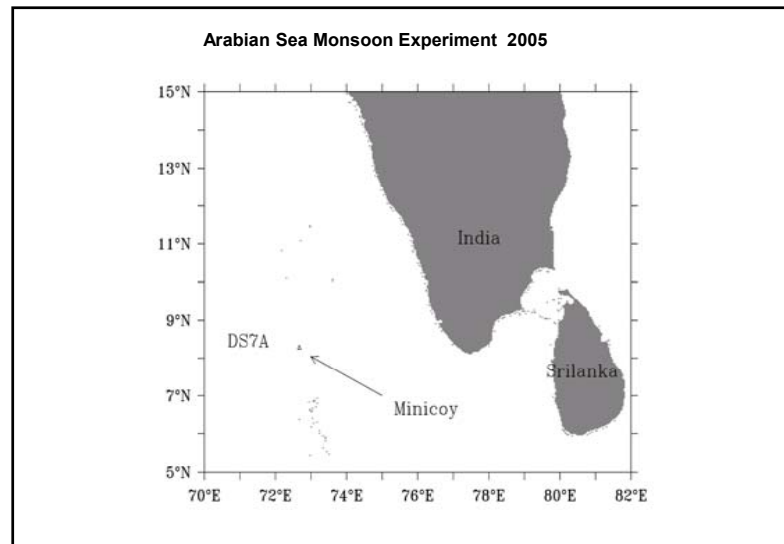
$$Q_{NET} = Q_{SW}^{net} - Q_{LW}^{net} - [L_E C_E U (q_s - q_a)] - [C_P C_E U (T_s - T_a)]$$

Penetrative Radiation :

$$Q_{PEN} = Q_{SW}^{net} (1 - \mathfrak{D}) \exp \{-H_{MIX} / z_o\}, \quad \mathfrak{D} = 0.58; \quad z_o \text{ is attenuation depth}$$

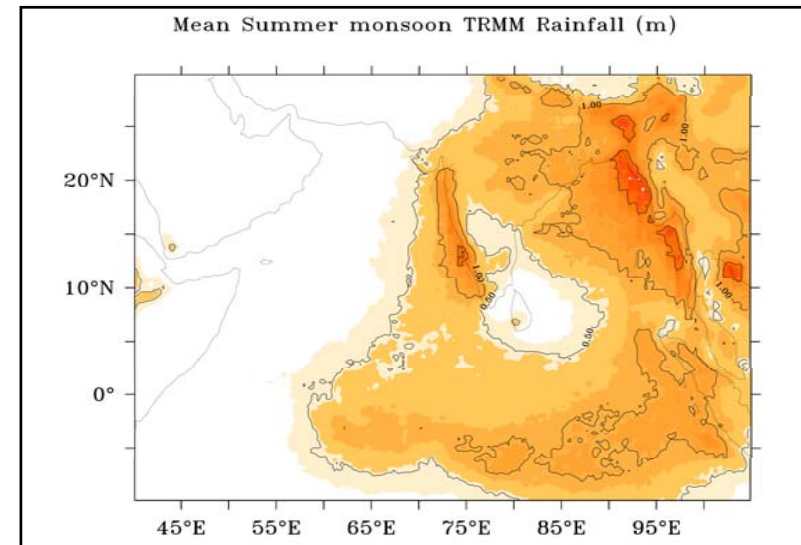
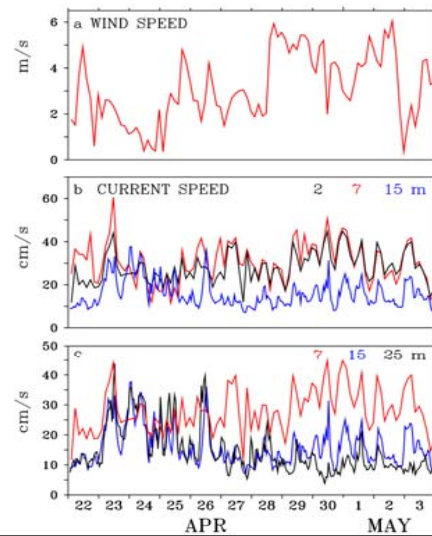
“Mixed” Layer Depth (H_{MIX}) :


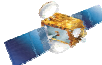
$$\rho_{MLD} = \rho_{Surface} + 0.125 \text{ kg/m}^3$$




ARMEX 2005

Upper layer glides

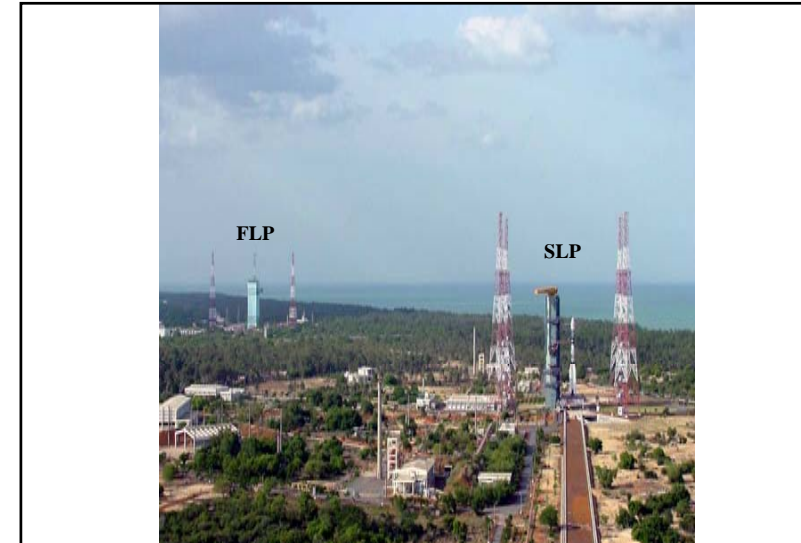


 **Cyclone Monitoring & Prediction at**
SATISH DHAWAN SPACE CENTRE SHAR 

Dr G V Rama
 Email: gvrana@shar.gov.in



INDIAN SPACE RESEARCH ORGANISATION



Scope of Presentation

- **Cilmatology of cyclones over and around SHAR**
- **Requirements for Launch Centre**
- **Launch Commit Criteria**
- **Net-work of MET Data Systems**
- **Synoptic forecast & NWP – Modeling**
- **Case studies**
- **Expected precision & Limitations in forecast**
- **Future Requirements & Research towards improvements in forecast**

Cilmatology of cyclones over and around SHAR

- 9 Cyclones crossed within 200 km of SHAR since 1974.
- SHAR experienced a very severe cyclone on 12th – 13th, November 1984. Cyclonic weather prevailed for 36 hours.
- Estimated gale wind speed was 220 kmph, and rain ~ 100 cm.

Daily forecast for Operational Requirements

- Cyclone Track prediction and warning to protect all technical facilities
- Daily weather prediction for weather concern technical operations

Requirements during Design Phase

- Climatology (Statistical estimates) to design
- Ground Facilities, Tall structures and Buildings
- Satellite launch vehicles & Embedded control systems (Wind magnitude & Vertical Shear)

Requirements during Assembly Phase

- Assembly phase goes for about 2 to 3 months
- Movement of launch vehicle modules
- Electrical and electronic checks, fuel filling trials at launch complex.
- Global checks & Rehearsal

Forecast

- Cyclone forecast for 2 to 3 days
- Thunderstorm & Lightning, Rain & Ground wind prediction (2-6 hrs)

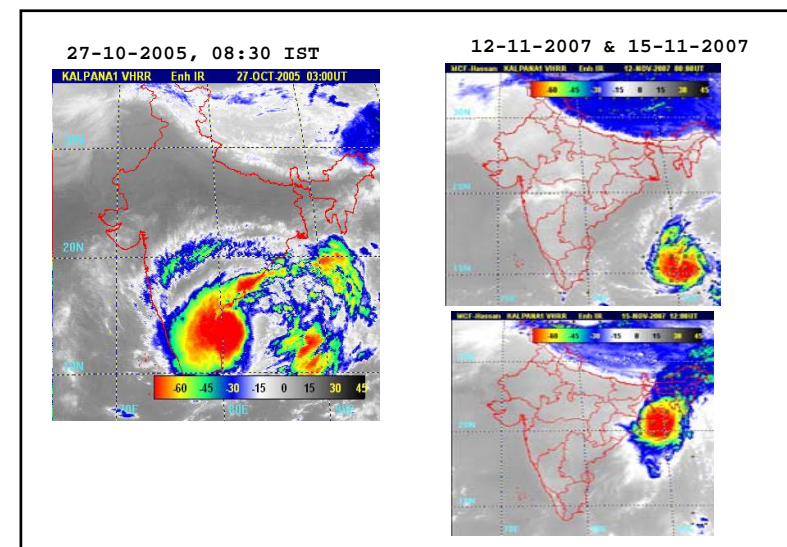
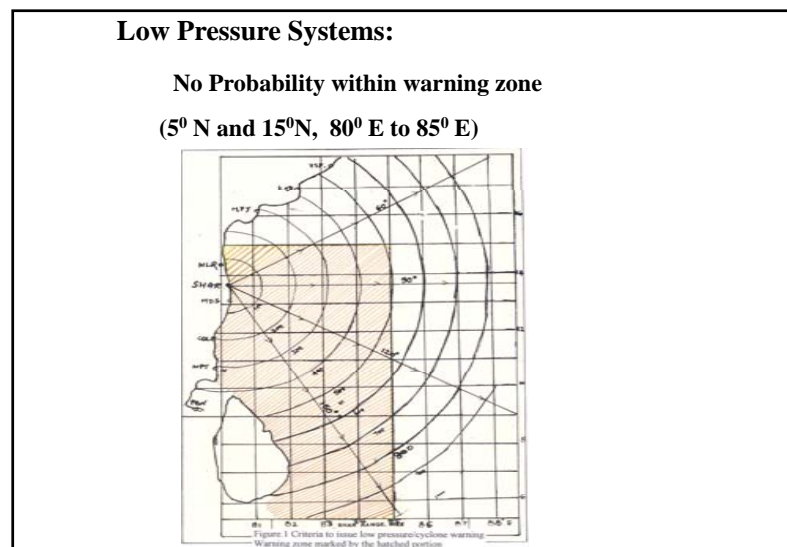
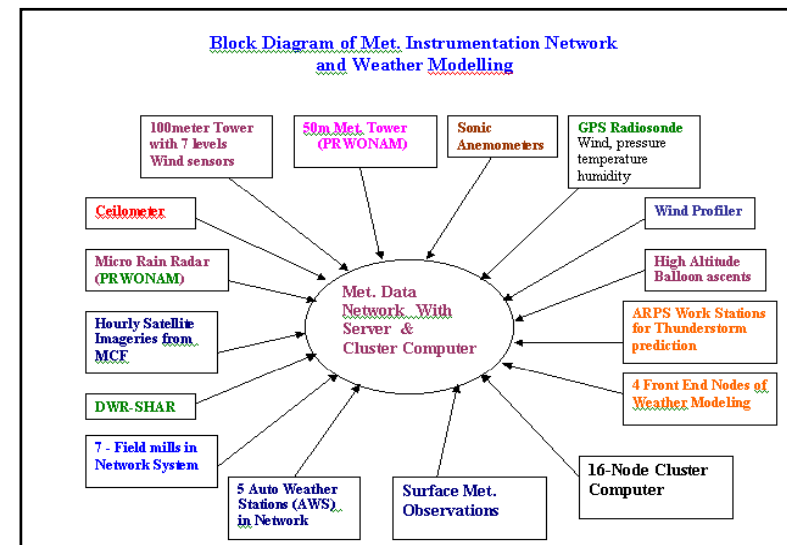
Requirements for Scheduling Launch to Take off

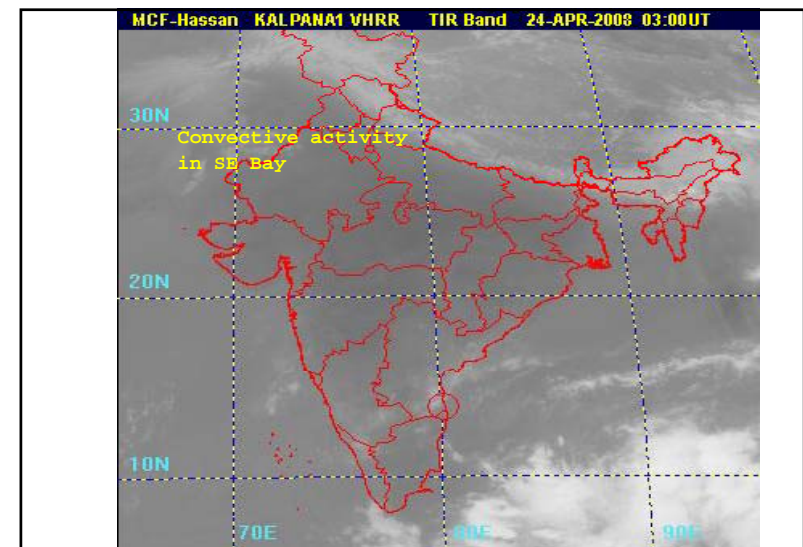
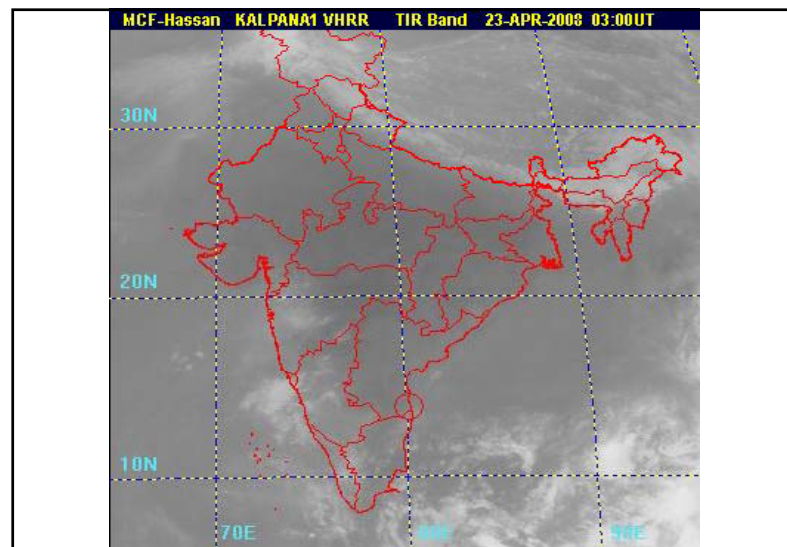
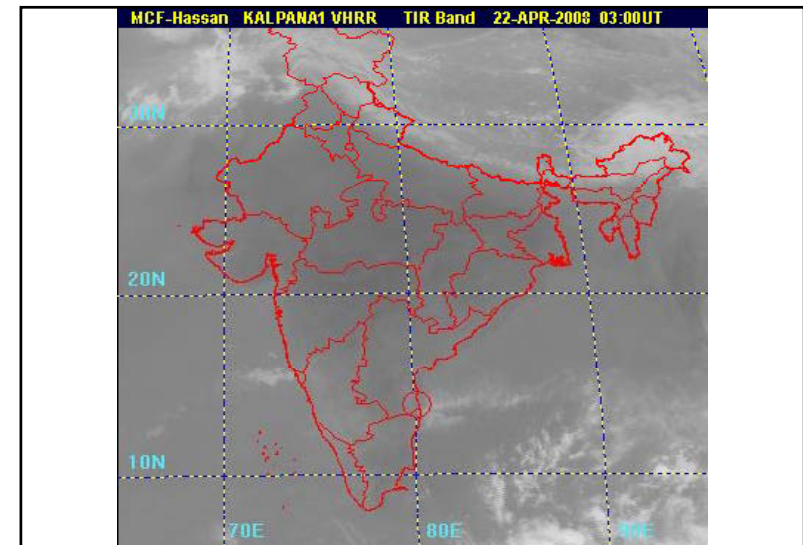
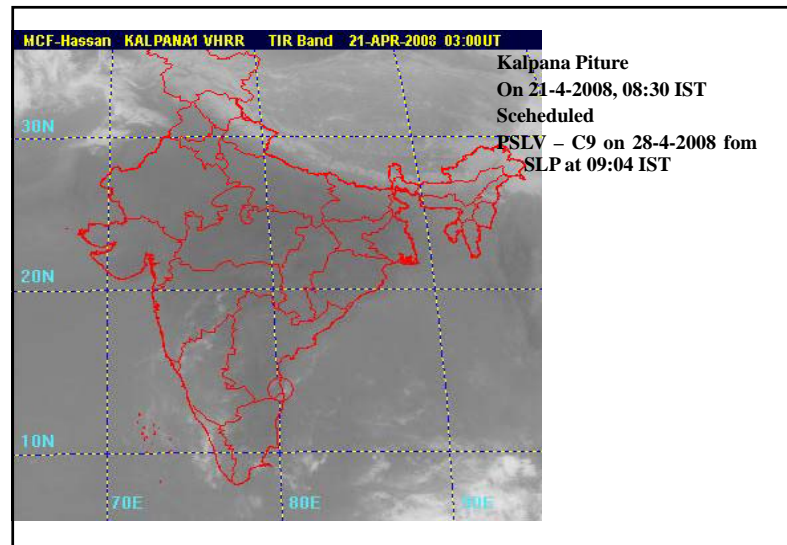
- 9 days before launch vehicle moves to launch pad
- 3 days before scheduling launch & count down starts
- Launch day vehicle takes off

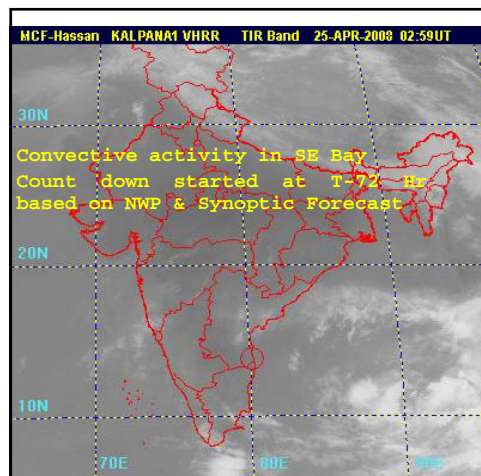
Forecast

- Cyclone (2 –3 days), Thunderstorm & Triggered lightning , Rain
- Boundary layer winds (up to 100m ht) for Launch standing wind and lift off.
- Upper wind variations for implementing Day of Launch Wind Biasing (DOL-WB)

Launch Commit Criteria (an example)			
Weather	Limit / Criteria	Predicted	Status
Low pressure system from T-3 days	No System within 500 km of SHAR	Nil	Green
Thunder storm from T - 30 min.	Within 20km mainly in flight path direction	Nil	Green
Field values from T-15 min	< 1000 v/m in 5 km radius	~ 300 v /m	Green
Tower winds At take off time up to 100m Ht	20 to 25 m/s from 10m to 100m	Avg : 4 to 8 m/s Gust: 6 to 10 m/s	Green
Upper wind profiles & Variations	To be cleared through simulation studies by project	Variations are generally 2 – 4 m/s	Cleared
Vertical Visibility	Up to 1 km ht.	Very good	Green

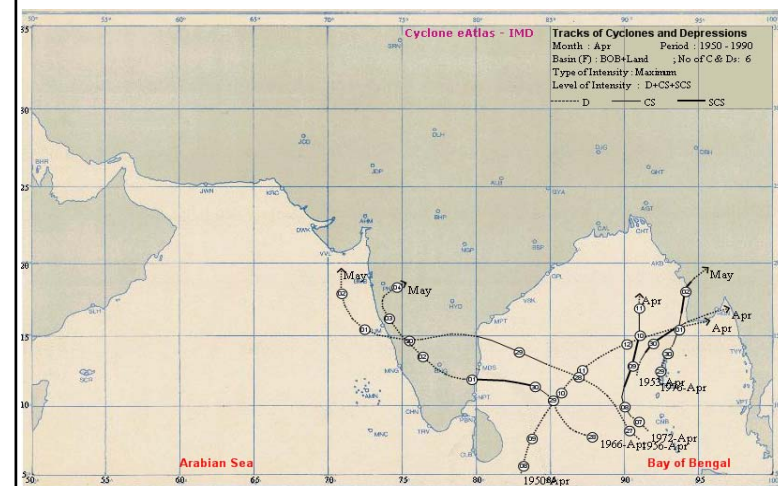




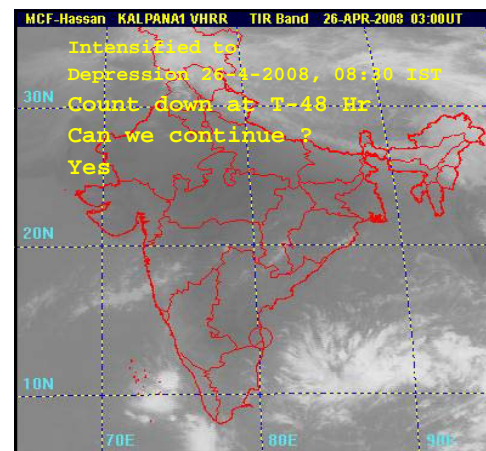
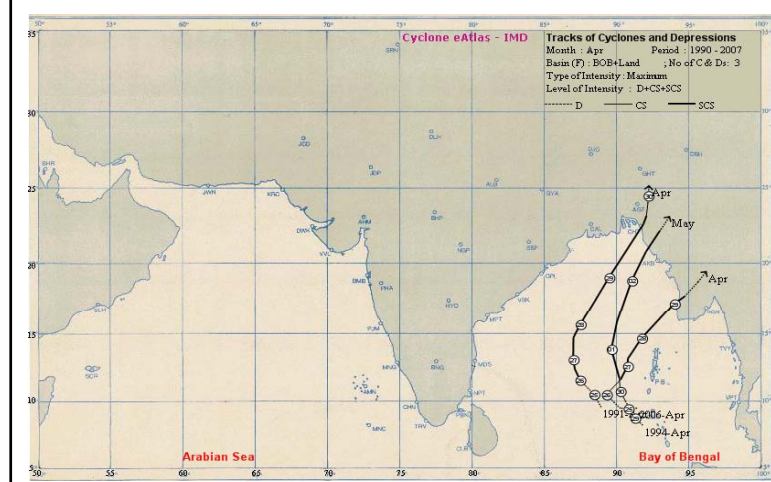


On 25-4-2008, 09 00 IST
Scheduled PSLV – C9 launch
on 28-4-2008

Low Pressure Systems in Bay of Bengal in April (1950-1990)



Low Pressure Systems in Bay of Bengal in April (1990-2007)



Model Prediction,
with 26th, 00 UTC

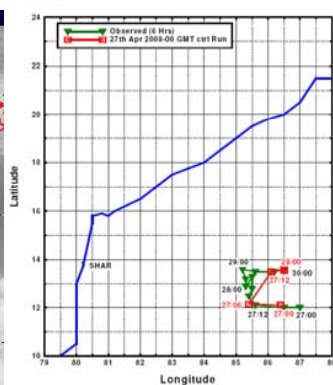
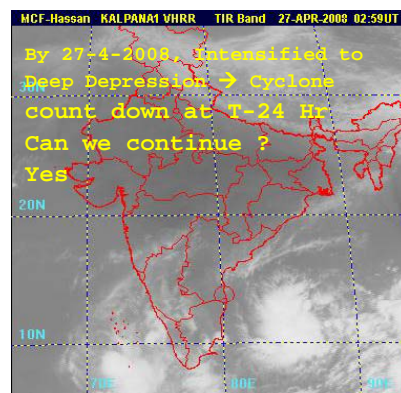
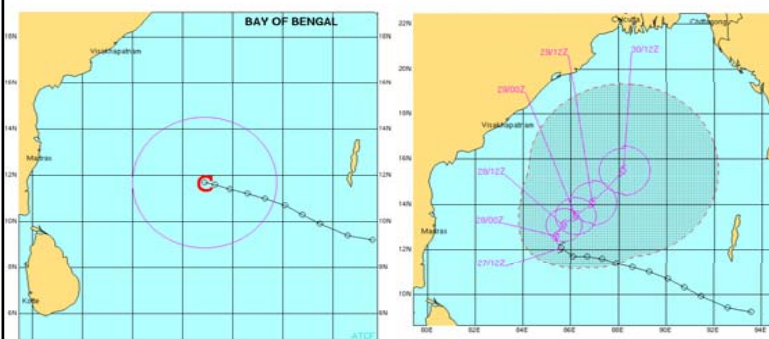
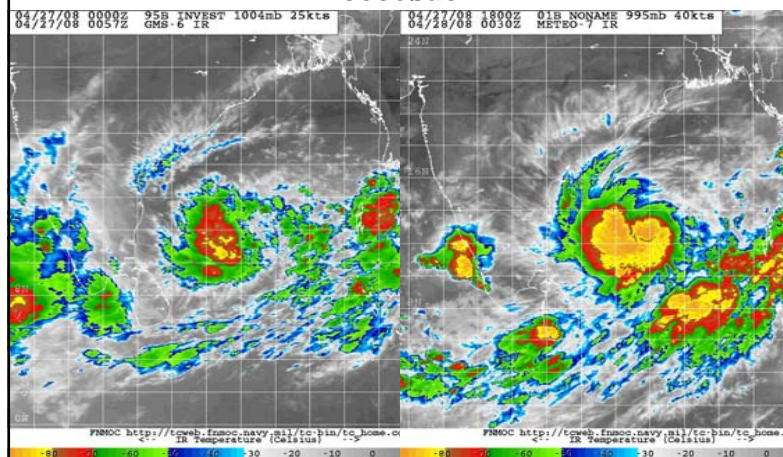


Fig.1 Cyclone track prediction on 27th April 2008 00UTC. Green: Assimilation run, Red: Observed

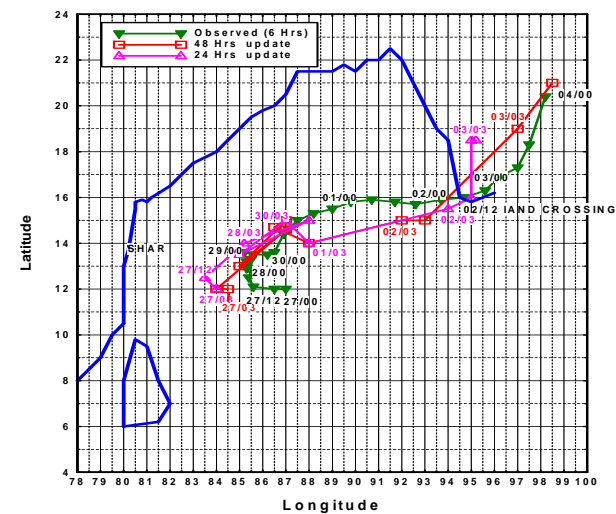
JTWC Nargis Tracks

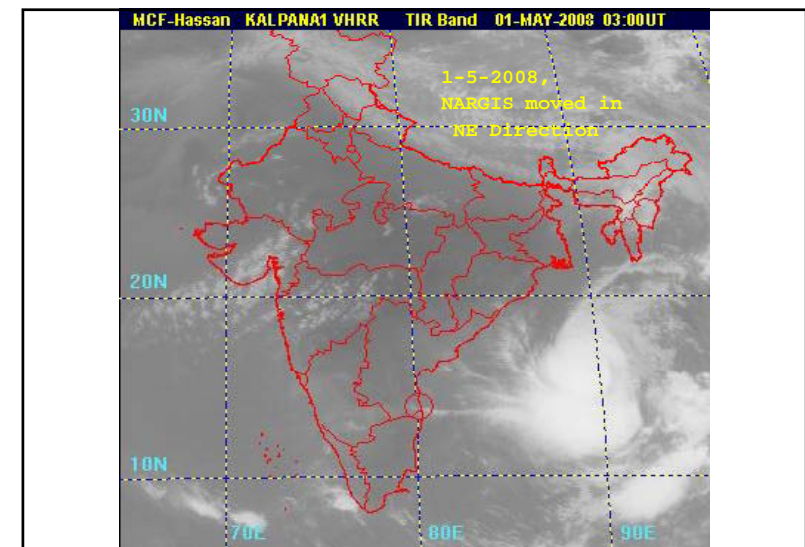
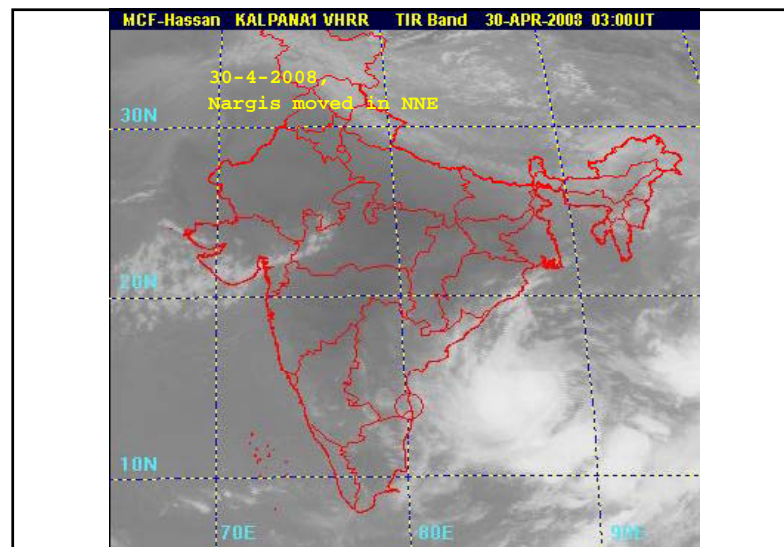
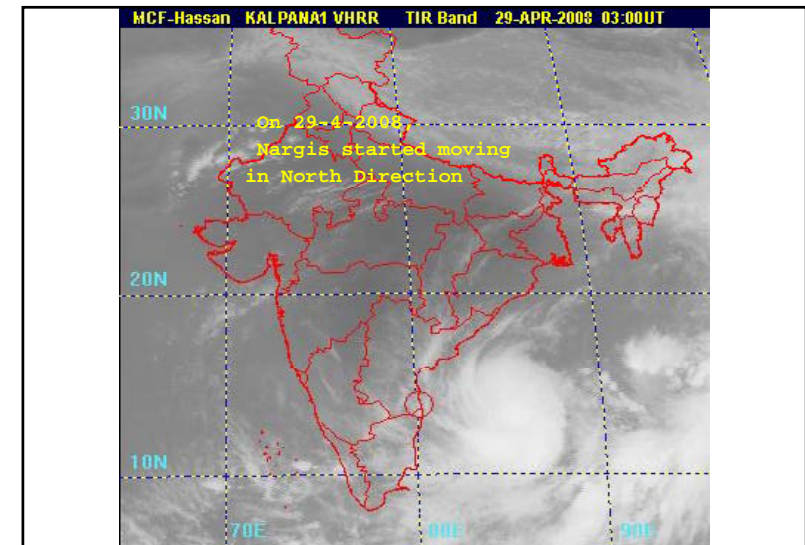
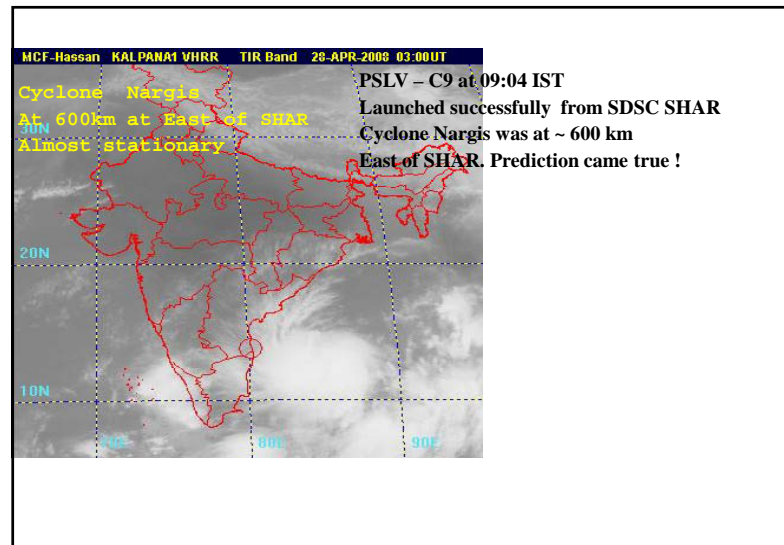


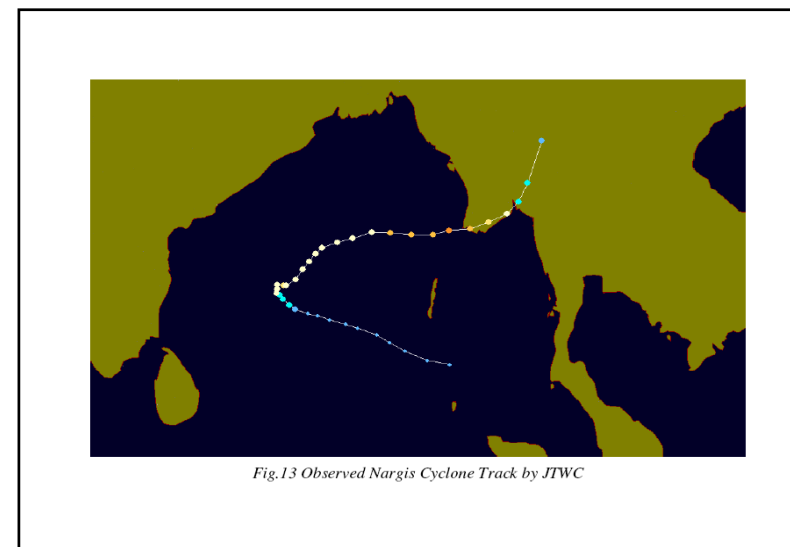
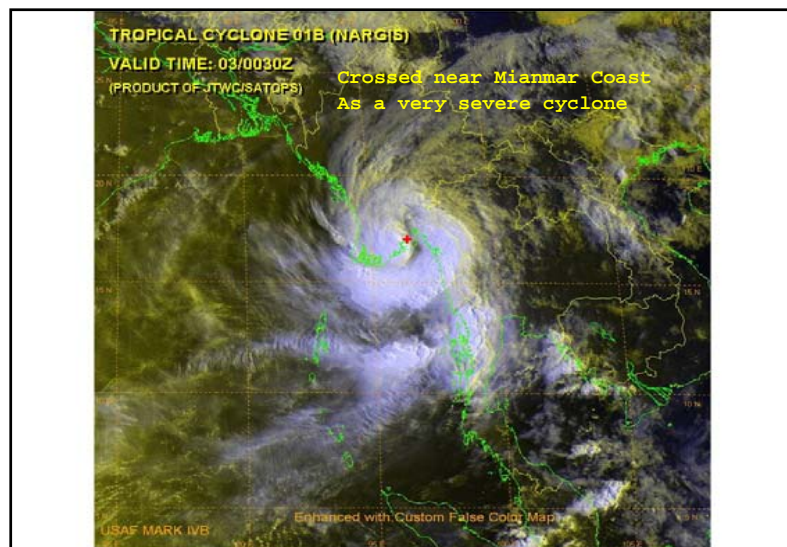
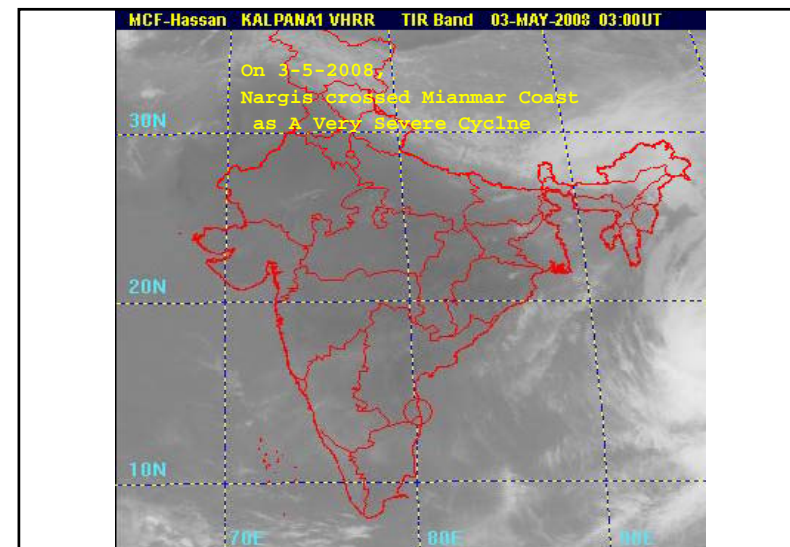
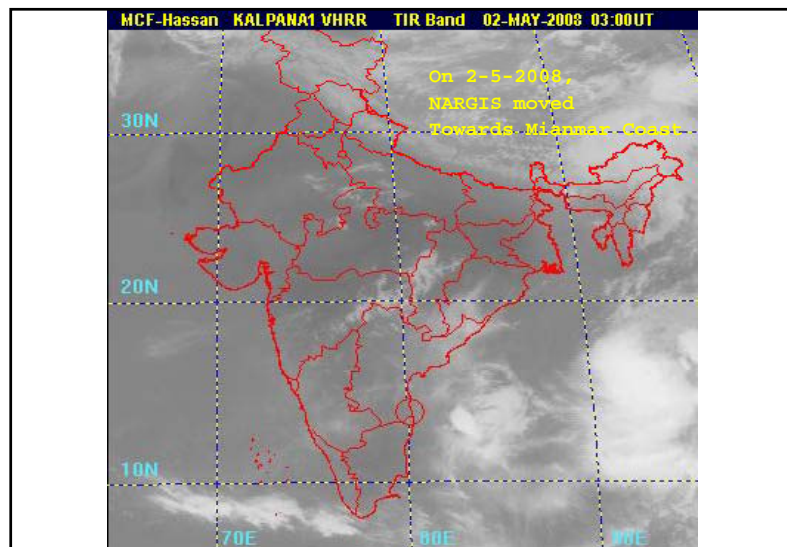
Meteosat-7

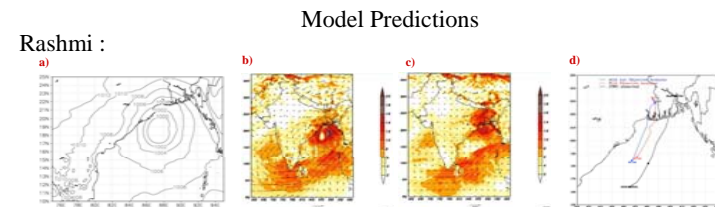
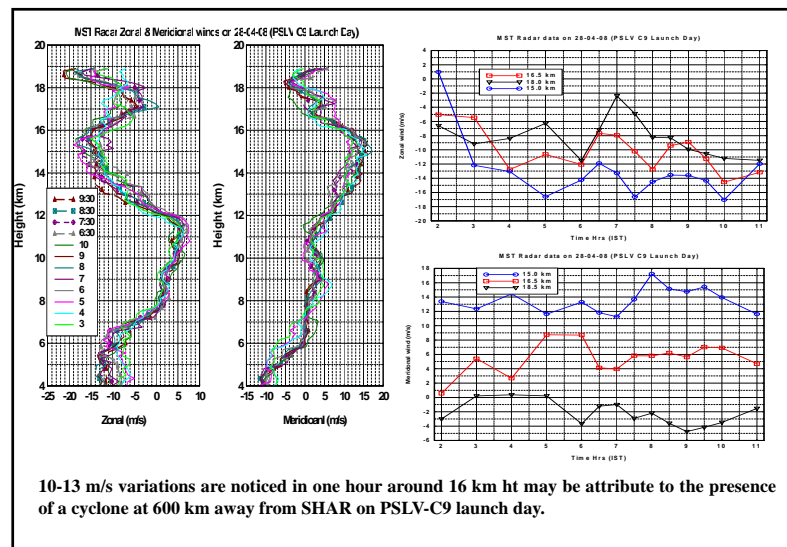


Nargis track comparison between SHAR MM5 & observation









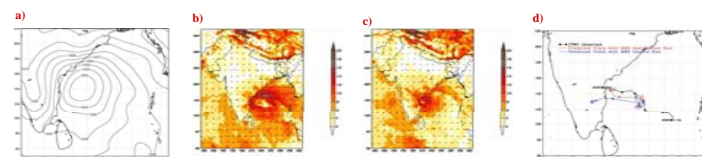
(a) MSLP on 26th 00 UTC
(b,c) Surface winds predicted by the model based on 25th 00UTC Initiz on 26th (b) and 27th (c) 00UTC
(d) Comparison of Predicted and JTWC Observed Cyclone track of Rashmi based on 25th 12UTC

➤The predictions based on the four initial conditions indicate a minimum central pressure of 994 hpa at 18 UTC on 26th October against the IMD observed least central pressure of 984 hpa at 21 UTC of 26th October.

➤All the four simulations predicted the maximum surface winds of intensity 25-30 m/s between 15 – 18 UTC of 26th October against the observed at 21 UTC with an intensity of 23 m/s.

➤Model clearly indicated the landfall between 26th 18 UTC to 27th 00 UTC, which is in agreement with the observed landfall at 2230 UTC of 26th

Khai-Mukh :



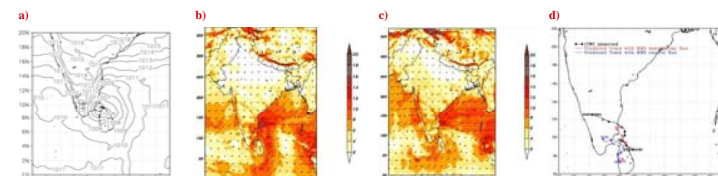
a)MSLP on 14th 00 UTC c)850 hpa circulation on 14th 00 UTC
b,c) Surface winds predicted by the model based on 14th 00UTC Initiz on 15th (b) and 16th (c) 00UTC
d) Comparison of Predicted and JTWC Observed Cyclone track of khaimuk based on 14th 00UTC

➤The weakening of the system into deep depression before landfall was predicted by the model with maximum prevailing surface winds of intensity 17m/s with a lead time of 30 hours.

➤All the four simulations show that the track predicted by the model with objective data analysis has less error compared to the track predicted without objective data analysis.

➤ The 24 hr and 48 hr predictions based on all the initial conditions show the maximum prevailing wind in the northern sector, which is in agreement with the IMD observed winds.

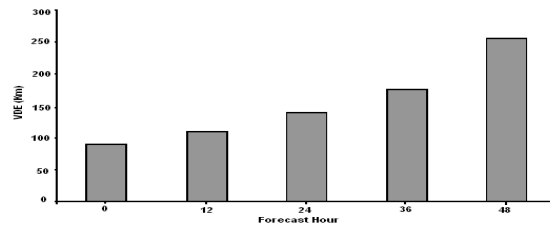
Nisha :



a)MSLP on 26th 00 UTC
b,c) Surface winds predicted by the model based on 25th 00UTC Initiz on 26th (b) and 27th (c) 00UTC
d) Comparison of Predicted and JTWC Observed Cyclone track of Nisha based on 25th 00UTC

Analysis of the vertical structure of the system show that the circulation extends upto 300 hpa level. So the winds above this level (200 hpa), which have a weak northeasterly flow, acted as steering current, leading to the quasi-stationary northward movement of the system which is an important feature of this cyclone.

Vector Displacement Error



Mean Vector Displacement Error for all 12 Initial Conditions for the three cyclones

The mean track prediction error of the cyclone:

Before 24 Hours : 100-150 Km

Before 48 Hrs : 200-250 Km.

Experiments in Progress at SDSC SHAR based on NWP towards improving predictions

- By updating Topography, Vegetation data and by assimilating data from Satellite, DWR, GPS-RS, AWS net work into models.
- To minimise model running time using faster computing facilities
- Sensitivity of movement and Intensity of a Tropical cyclone to the Physical processes in the model with Convection, Planetary Boundary Layer & Micro Physical processes.

- *Simulations with 3D Var*

FAQ - Low Pressure system ?

- Low Pressure system within 72 hours?
- Whether it will come within 200km of SHAR (before launch)?
- What will be it's intensity (in terms of wind velocity & rain) & duration?
- Will there be significant change in upper wind field?
- Enroot forecast for RLV
- **Limitation : Error in Track prediction, intensity & land fall time with 72, 48 & 24 Hour lead time**

FAQ – Thunder storm ?

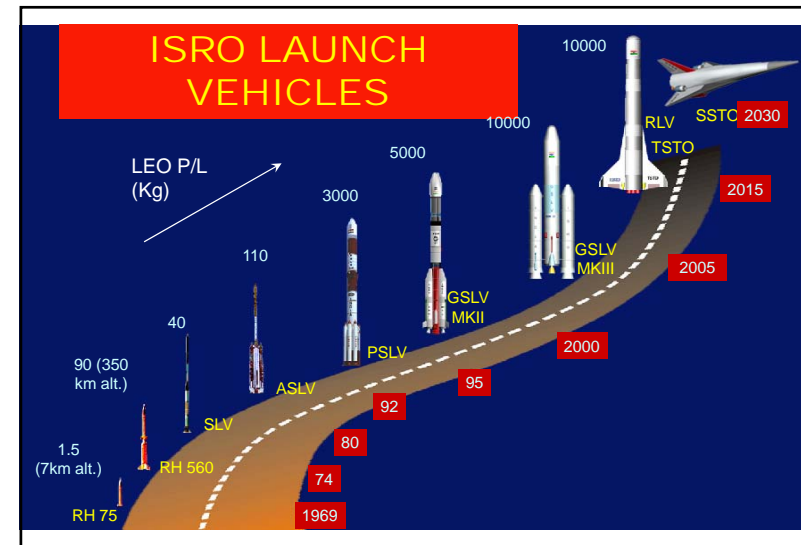
- Requires six hours prediction for 20 km radius of Launch facilities during assembly phase to launch phase.
- On launch day, prediction on Natural & Triggered lightning in 5 km radius from T-15 minutes to launch window.

Limitation : Now casting techniques based n Satellite, DWR, Fieldmill net work & AWS data are being used to predict for the next 2 hours with good confidence.

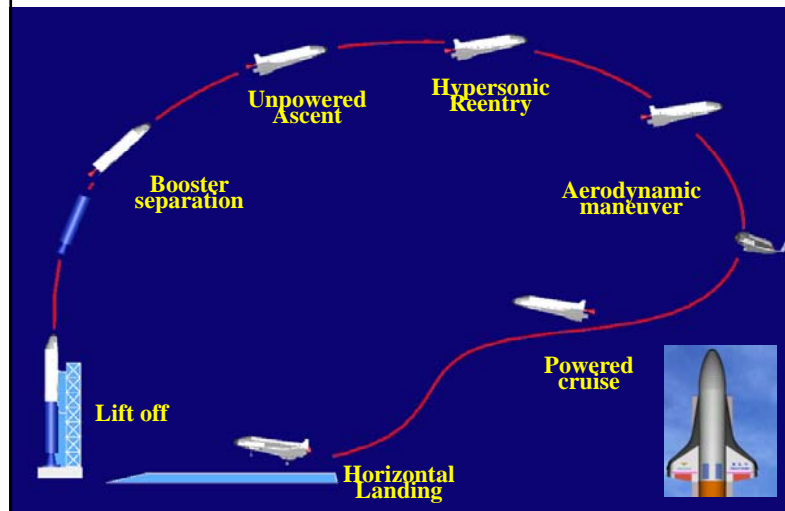
ARPS model is used to predict for the next 6 hours.

FAQ – Upper wind variations

- Upper wind variations due to presence of a distant low pressure system and Passage of convective cloud over the region from T-2 hours for implementing for DOL-WB.
- Limitation : Prediction of wind field variations with time over the launch station with distance and intensity of the prevailing system.



RLV TECHNOLOGY DEMONSTRATOR FLIGHT PROFILE



Future Requirements

- Reentry Launch Vehicle (RLV) as aircraft needs enroute Prediction from reentry to landing including Clear Air Turbulence (CAT) in the flight path direction.

Conclusions:

- The intensity predictions of the cyclones are also in good agreement with the observations.
- Analysis of vertical wind shear clearly indicated the weakening of the cyclonic storm Khai-muk before landfall with a lead-time of about 30 hours.
- The quasi-stationary movement of the cyclone Nisha, which is the special feature of this cyclone, could be captured based on the vertical structure of the system along with the environmental flow.
- But the movement of the cyclone Nisha could not be predicted accurately after the landfall compared to other two cyclones, which may be due to the complex terrain and the frictional force effect.

- The mean VDE, calculated at every 12-hour interval indicate that the system could be well tracked after it attained into deep depression stage.
- Positive impact of objective analysis is well proved in the prediction of cyclone movement.

Impact of Global Warming on Cyclonic Storms Over North Indian Ocean

M.R.Ramesh Kumar,

Scientist

National Institute of Oceanography

Dona Paula, Goa – 403004

Email: kramesh@nio.org



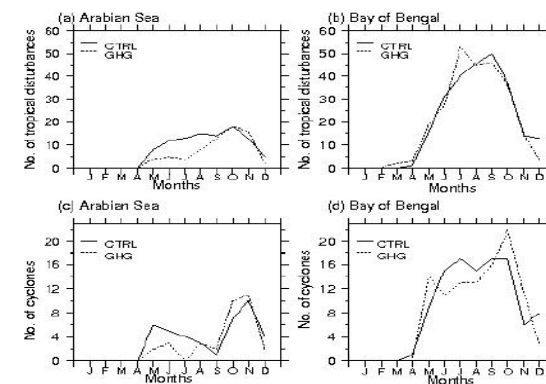
Motivation

- There is a growing concern that the global warming may be affecting extreme weather events such as tropical cyclone frequency, duration and their intensity.
- Previous studies based on global circulation and modeling suggest that increases may occur in tropical cyclone frequency.

Classification of Systems over the Indian Seas

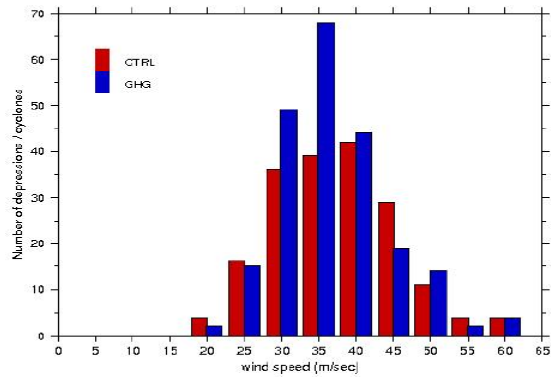
	Maximum sustained winds	
Low	< 17 knots	< 31 kmph
Depression	17 – 27 kts	31 – 51 kmph
Deep Depression	28 – 33 kts	52 – 62 kmph
Cyclone	34 – 47 kts	63 – 87 kmph
Severe Cyclone	48 – 63 kts	88 – 117 kmph
Very Severe Cyclone	64 – 119 kts	118 – 221 kmph
Super Cyclone	120 kts & above	222 kmph & above

HadRM2 for CTRL run (1990, solid) and in increased GHG run (2050, dashed).



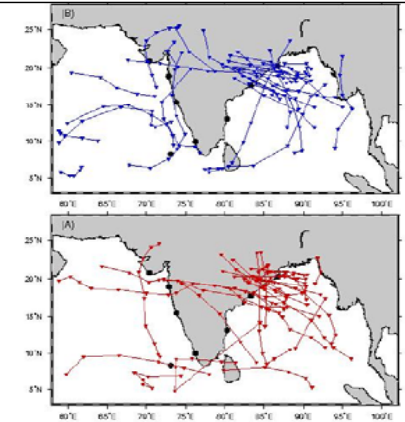
Unnikrishnan et al., (2006)

HadRM2 for CTRL run (1990, red) and in increased GHG run (2050, blue).



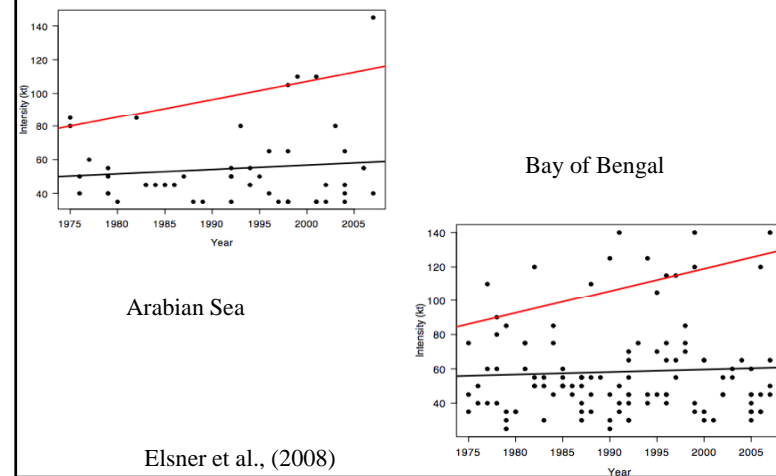
Unnikrishnan et al., (2006)

HadRM2 for CTRL run (1990, red) and in increased GHG run (2050, blue).



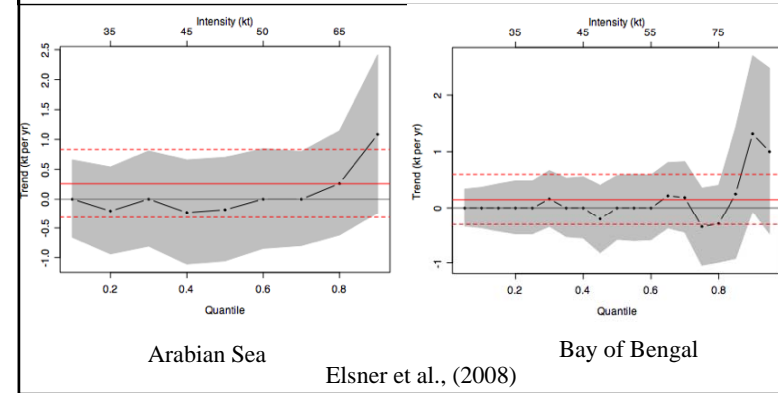
Unnikrishnan et al., (2006)

Analysis and model results of TC lifetime MWS. Trends lines are shown for the median, 0.75 quantile and 1.5 times the quantile range.



Elsner et al., (2008)

Trends in satellite derived TC MWS by quantile, from 0.1 to 0.9 in increments of 0.1 AS. Trends are estimated coefficients from quantile regression in units of m/s/y. The point wise 90% confidence band is shown in grey, under the assumption that the errors are independent and identically distributed. The solid red line is the trend from a least squares regression of wind speed as a function of year and the dashed red lines delineate the 90% point wise confidence band about this trend.



Elsner et al., (2008)

Questions to be addressed

- Will there be a change in frequency and intensity of SCS over the AS and BB in a global warming scenario ?
- Will the SCS impact the same coastal areas or will they be different ?
- Will genesis of these SCS occur in new places than the current places and will they form in different months or seasons ?

Cyclogenesis Parameters

- ✧ Low level Relative Vorticity
- ✧ Inverse of the Vertical shear of the horizontal wind between lower and upper troposphere.
- ✧ Ocean thermal energy , SST > 26°C upto a depth of 60 m
- ✧ MTRH (500 hPa).

Data

- NCEP/NCAR Reanalysis
- Tracks of storms from e Atlas of IMD
- Extended Reconstruction Sea Surface Temperature (ERSST)
- IMD data of coastal stations

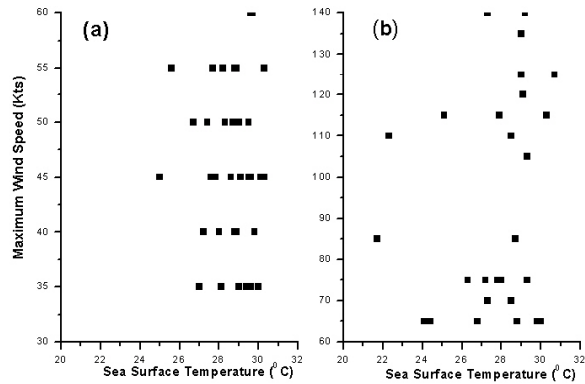
Methodology

The data for the study period 1951-2007 have been further subdivided into two epochs a) 1951-1978 and b) 1979-2007 to bring out the role satellite data in the identification of storms.

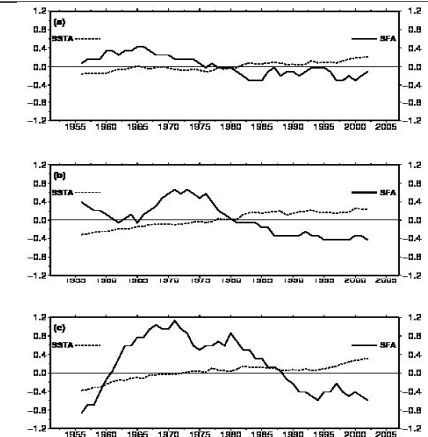
We have partitioned Bay of Bengal into three regions

- S.B.B : 5 N – 11 N ; 80 E – 100 E
- C.B.B : 11 N – 17 N ; 80 E – 100 E
- N.B.B : 17 N – 23 N ; 80 E – 100 E

Scatter diagram of SST a) CS b) SCS in Bay of Bengal.



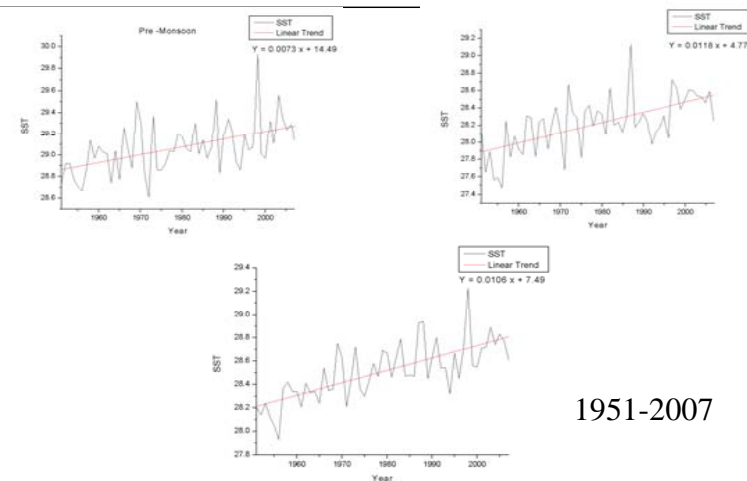
SSTA and SFA over BoB for a) Pre Monsoon b) Monsoon and c) post monsoon seasons for the period 1951-2007 .



The occurrence of the CS and SCS over BB for different SST

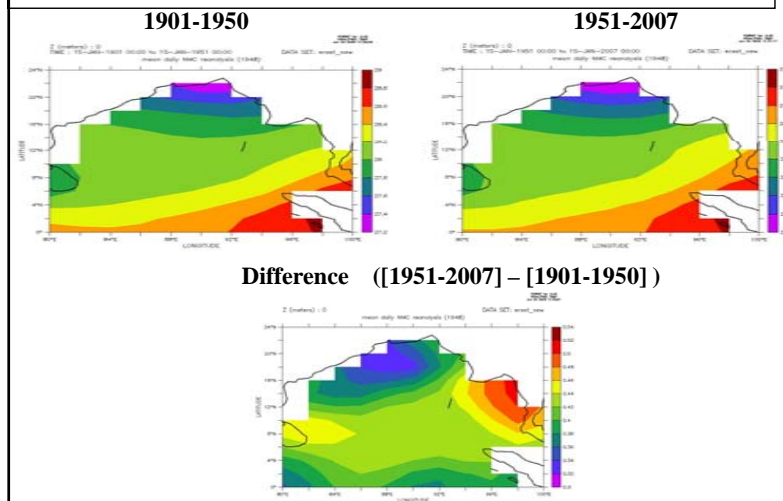
SST (° C)	Cyclonic Storms	Severe Cyclonic Storms	Total systems	% of SCS
25.0 – 25.9	2	1	3	33.3
26.0 – 26.9	1	2	3	66.7
27.0 – 27.9	7	6	13	46.2
28.0 – 28.9	11	5	16	31.3
29.0 – 29.9	13	8	21	38.1
30.0 – 30.9	4	3	7	42.9

Trend in SST over BB for different seasons.



1951-2007

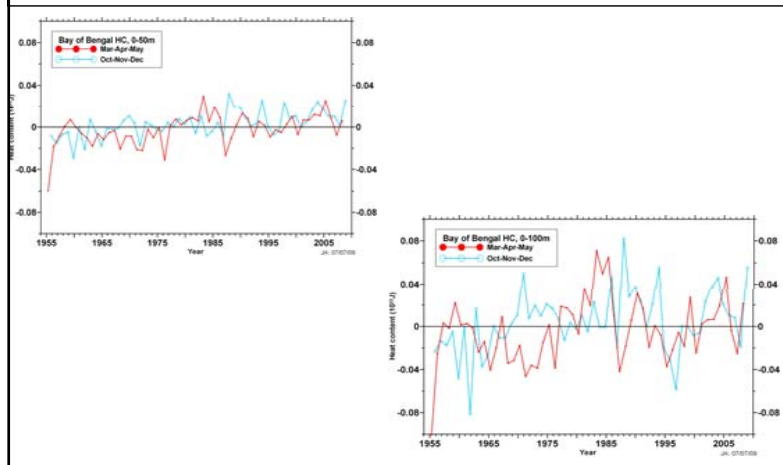
Spatial Distribution of SST over BB.



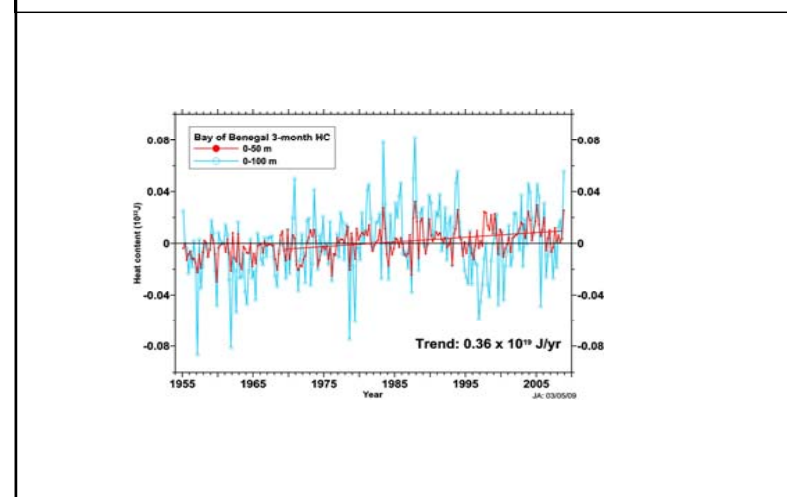
Mean value of SST for two epochs for different regions of BB

Season	North Bay		Central Bay		Southern Bay	
	1951-1978	1979-2007	1951-1978	1979-2007	1951-1978	1979-2007
Winter	25.42	25.73	26.88	27.22	27.74	28.11
Pre Monsoon	28.22	28.41	29.12	29.30	29.33	29.58
Monsoon	28.83	29.11	28.55	28.91	28.38	28.76
Post Monsoon	27.66	27.93	28.17	28.48	28.23	28.57

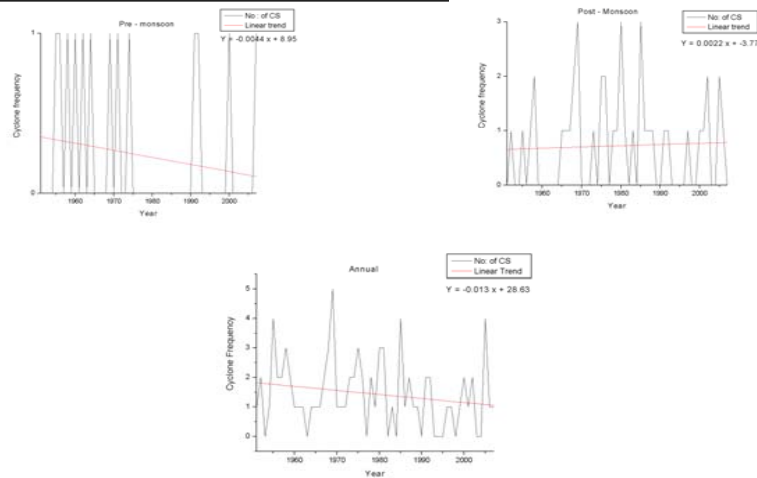
Trend in HC over BB for Pre Monsoon and Post Monsoon seasons from 0-50 m and 0-100 m



Trend in HC over BB for recent years JJA



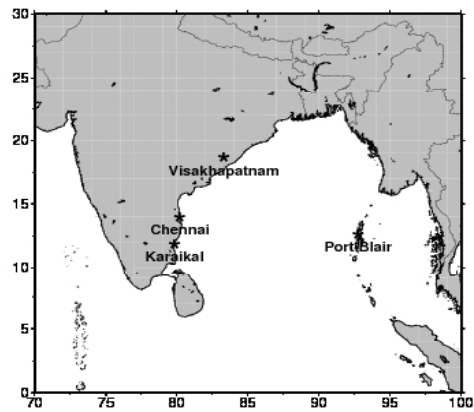
Trend of CS in BB for 1951- 2007.



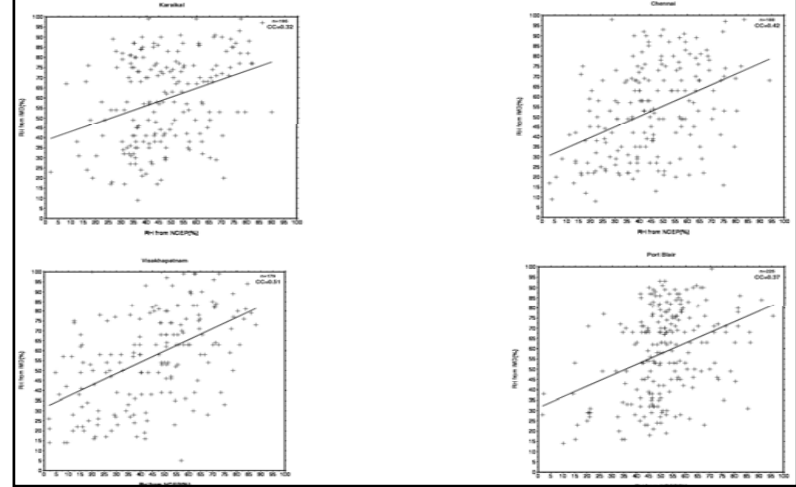
Changes of CS and SCS in BB for different epochs

Period	North Bay		Central Bay		Southern Bay	
	Storm	Severe Storm	Storm	Severe Storm	Storm	Severe Storm
1951-1978	25	25	12	12	12	12
1979-2007	7	7	11	12	10	10

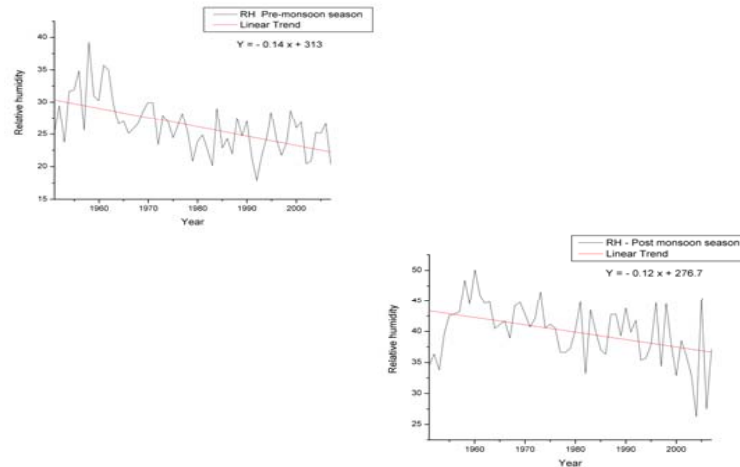
Map showing the stations used for validation.



Validation of RH at 500 hPa for BB.



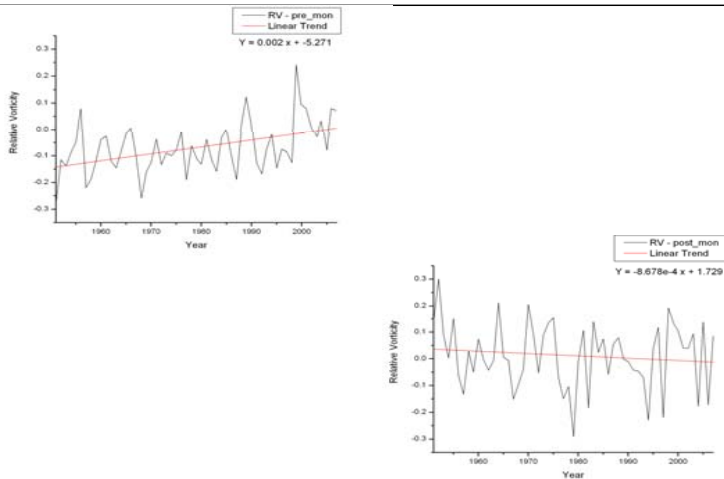
Trend of MTRH over BB for different seasons.



Trend of MTRH over BB for different seasons.

Season	North Bay		Central Bay		Southern Bay	
	1951-1978	1979-2007	1951-1978	1979-2007	1951-1978	1979-2007
Winter	19.36	16.44	25.28	20.70	41.55	37.60
Pre Monsoon	22.63	19.07	29.65	23.91	44.70	37.84
Monsoon	62.95	58.5	62.72	57.13	57.83	54.72
Post Monsoon	35.73	31.2	45.55	42.36	55.07	53.86

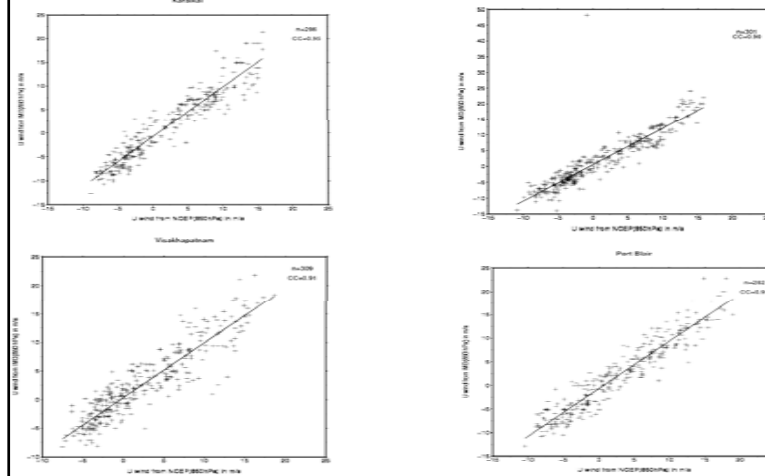
Trend of RV over BB for different seasons.



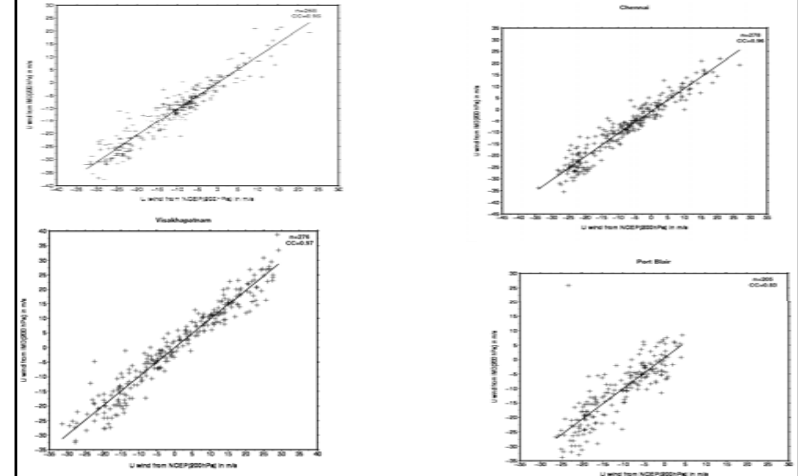
Trend of MTRH over BB for different seasons.

Season	North Bay		Central Bay		Southern Bay	
	1951-1978	1979-2007	1951-1978	1979-2007	1951-1978	1979-2007
Winter	19.36	16.44	25.28	20.70	41.55	37.60
Pre Monsoon	22.63	19.07	29.65	23.91	44.70	37.84
Monsoon	62.95	58.5	62.72	57.13	57.83	54.72
Post Monsoon	35.73	31.2	45.55	42.36	55.07	53.86

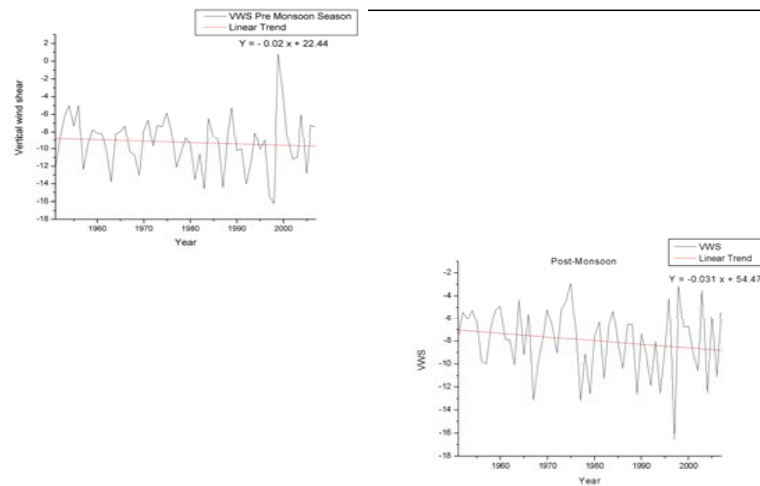
Validation of Zonal wind speed at 850 hPa for BB.



Validation of Zonal wind speed at 200 hPa for BB.



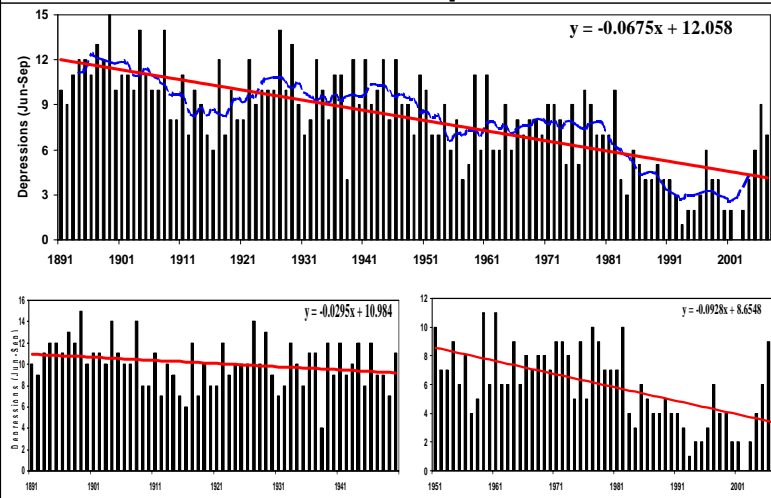
Trend of VVS over BB for Pre Monsoon 1951-2007.



Trend of VVS over BB for Pre Monsoon 1951-2007.

Season	North Bay		Central Bay		Southern Bay	
	1951-1978	1979-2007	1951-1978	1979-2007	1951-1978	1979-2007
Winter	-27.98	-28.46	-13.21	-0.55	-2.21	-3.02
Pre Monsoon	-14.93	-4.28	-4.28	0.16	5.27	4.79
Monsoon	16.49	24.81	24.81	0.41	28.72	28.2
Post Monsoon	-14.60	-1.48	0.02	-1.48	8.97	6.9

Trends of Monsoon Depression in BoB



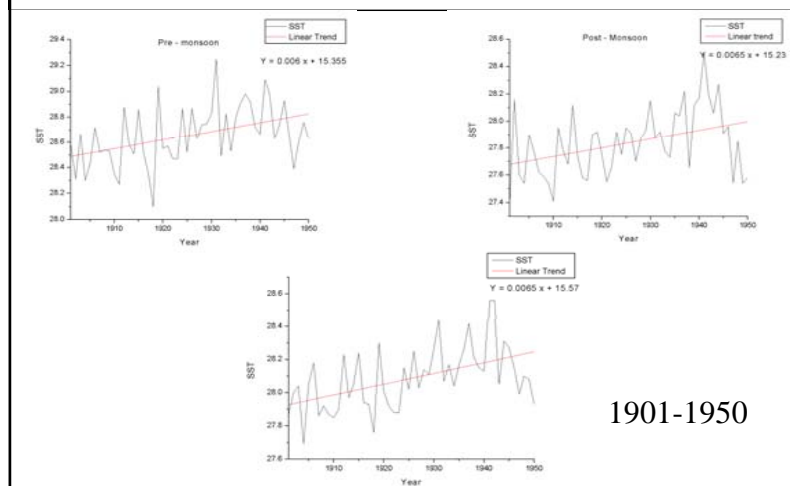
Summary

- The relationship between SST over the Bay of Bengal and the maximum wind speed of the cyclonic systems is complex.
- Results clearly indicate that warm SST's and heat content in the surface to 50 m alone are not sufficient for initiation of convective systems.
- Environmental parameters such as RV, MTRH and VWS, also play an equally important role.

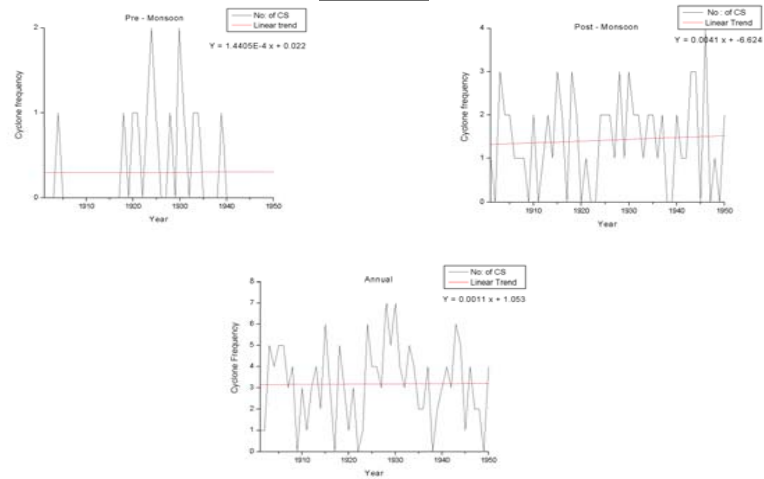
Summary

- These results are preliminary in nature and we propose to look into more recent data sets such as Argo and moored buoy data and satellite data over the Bay of Bengal region.
- We also see that the Monsoon Depressions are showing a significant decreasing trend over the BoB in recent decades.

Trend in SST over BB for different seasons.



Trend of CS in BB for 1901-1950.



SARAL-ALTIKA - SCIENCE & APPLICATIONS

R.M. Gairola

Meteorology and Oceanography Group

Space Applications Centre – ISRO

Ahmedabad 3800 015

SARAL (Satellite with ARGOS and ALTIKA)

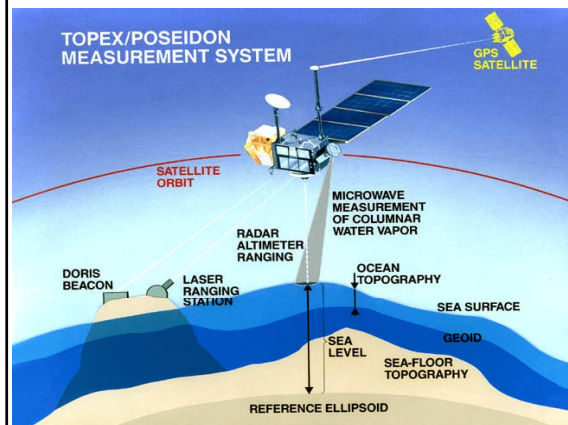
SARAL is an cooperation between CNES and ISRO, will embark the ALTIKA altimeter (working in Ka-band, 35 GHz), as well as a Doris instrument. Signal frequencies in the Ka-band will enable better observation of oceans, ice, rain, coastal zones, land masses, and wave heights.

The SARAL mission is complementary to Jason-2.

To ensure, in association with Jason-2, the continuity of the service given today by the altimeters onboard Envisat and Jason-1,

To answer the need expressed by the ocean and climate study international programs, and contribute to the building of a global ocean observing system.

Altimetric Measurement System



1. Satellite range
2. Orbital height
3. Radar Data Processing
4. Geophysical corrections

SARAL-ALTIKA: SCIENCE & APPLICATIONS

AltiKa Payload:

- **Ka-band altimeter with enhanced bandwidth**
 - ↳ ionospheric effects are negligible
 - ↳ better vertical resolution (0.3m)
 - ↳ Ka-band (35 GHz) authorizes a compact, lightweight instrument easier to accommodate on a wide range of satellite buses
- **Dual-frequency radiometer (24/37 GHz)**
 - ↳ required for tropospheric correction
 - ↳ derived from Madras (Megha-Tropiques) developments
- **Laser Retro-reflector Array**
 - ↳ useful for orbitography and system calibration
- **DORIS**
 - ↳ for adequate orbitography performances in low earth orbit
 - ↳ enable to have similar performance as reference missions like T/P, JASON, ENVISAT
 - ↳ required for mean sea level analysis and coastal/inland applications

ALTIKA Science Plan

Central Objectives:

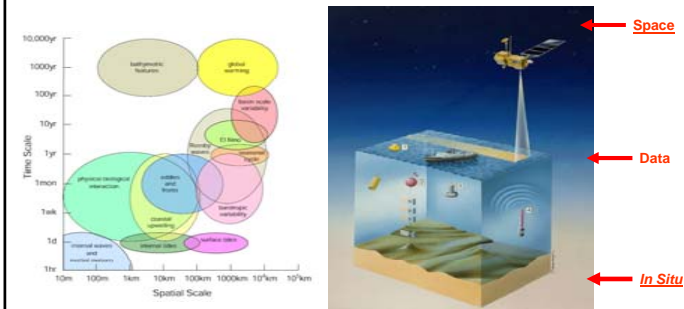
- Ocean Mesoscale variability
- Data assimilation in a global ocean model

Contribution To:

- Operational oceanography
- Coastal Altimetry
- Mean Sea Level and climate Change
- Sea State Observation and forecasting
- Light rainfall and cloud climatology
- Geophysical Investigations & Geodetic Referencing

Other Objectives: Inland water, Ice, sea ice,

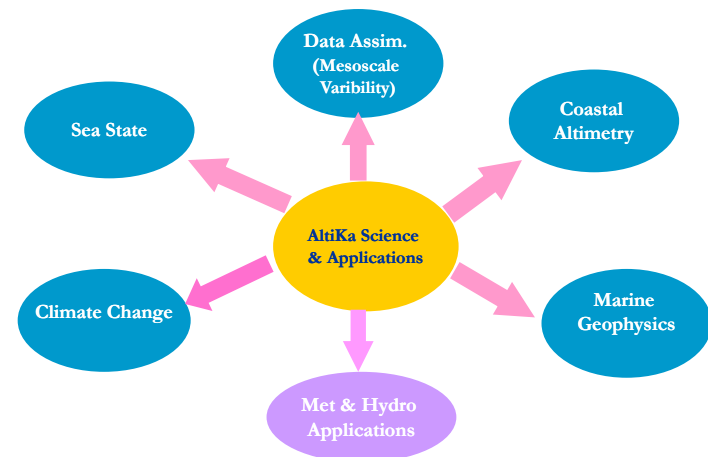
Integrated Oceanography Science, Applications and Operational



Science & Applications: Experiences

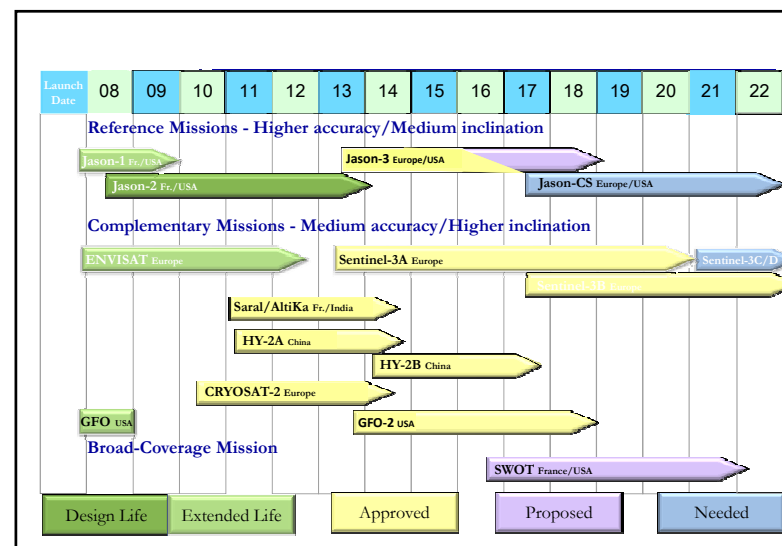
- Altimeter wave and wind retrievals & Applications
- Characterization of Oceanic Eddies
- Mixed layer depth estimation
- Indian Ocean Rossby/Kelvin waves
- Assimilation of altimeter data in models
- Rainfall estimation from dual frequency T/P
- Effectiveness of range corrections
- Tsunamis
- Cyclone Heat Potential
- Seamount detection & charting
- Marine Geoid Mapping and Gravity

AltiKa: Science & Application Plans



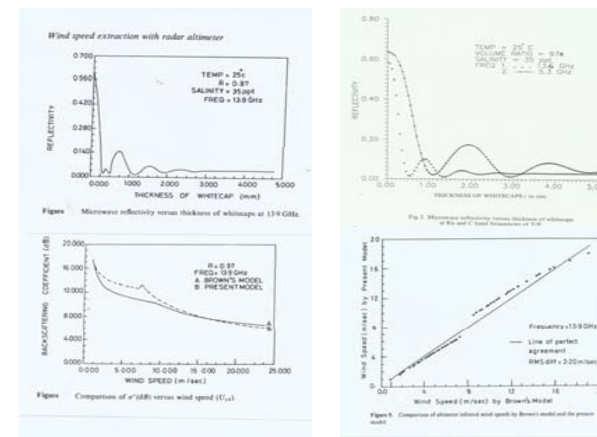
Value Additions

- Characterization of Oceanic upwelling zones
- Western boundary currents
- Ocean bottom topography
- Other Coastal Applications



Consolidation Towards SARAL Science Plan

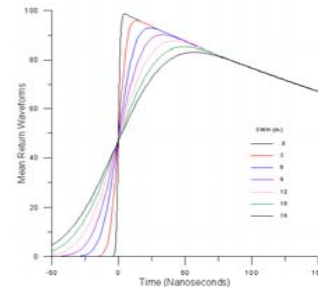
1. National SARAL Workshop 16-17 Sept. 2008, Ahmedabad, India
2. First ISRO-CNES Joint Workshop, 22-23 April, 2009, Ahmedabad, India
3. ISRO-CNES JSWG, 24 April, 2009, Ahmedabad, India
4. ISRO-CNES JSWG, 1 April, 2010, Ahmedabad, India
5. National Scientific Proposals Finalized
6. Global Proposals under Joint ISRO-CNES AOs Finalized



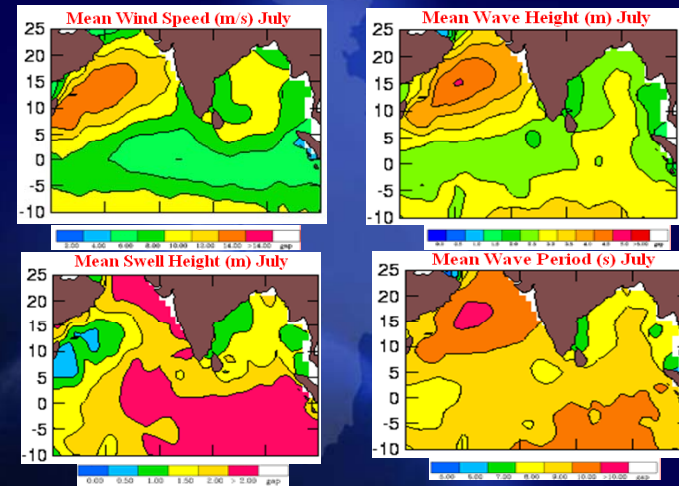
Retrievals of Sea Level from Altimeter

Approach: (a) Simulation of Sea Level
(b) Corrections to the range measurements

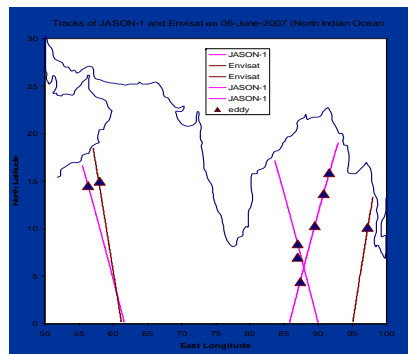
R&D Effort so far: waveform generation for a given SWH
Various corrections to the range measurements



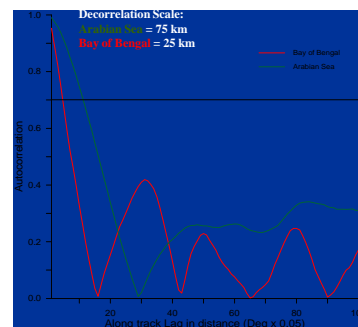
Climatology of wind speed, SWH, wave period and Swells from T/P



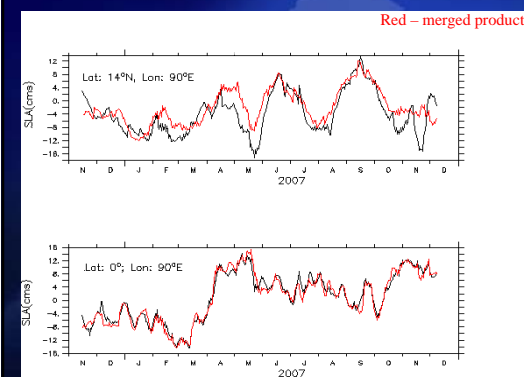
Altimetry: Use in studies of Indian Ocean Eddies



SLA anomalies are passed through a matched filter designed to detect Gaussian signals embedded in noise



Sea level Anomaly (merged and mono-mission) in the Indian Ocean



The two products differ largely in magnitude in Bay, however the large-scale patterns are same. Dominated by small scale eddies and waves.

In the EEIO region, the two products have almost same magnitude and pattern.

Mixed layer depth (MLD) studies

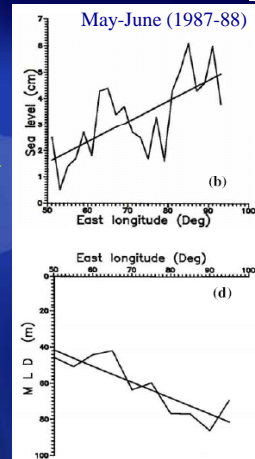


In the equatorial Indian Ocean:
Approximated as 2 Layer System

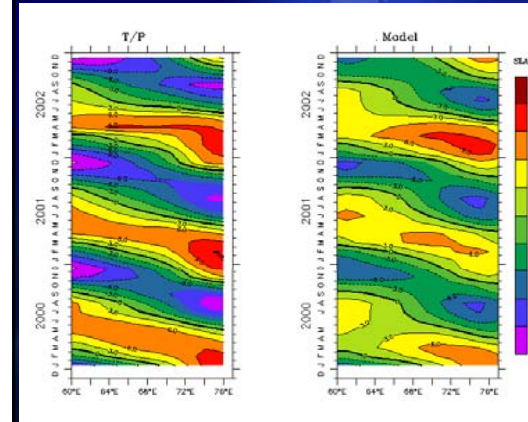
Study using GEOSAT and TOGA XBT data

SLA data for the year 1987-88 used for
estimating MLD

Adjoining diagram shows that in response
to rising SLA towards eastern side (Wyrtki
Jet) MLD slopes down.



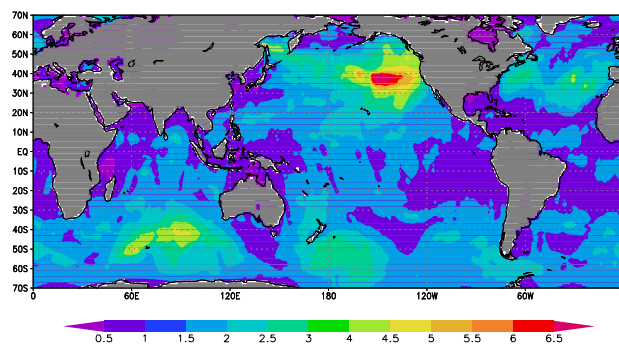
Rossby waves from Ocean model and T/P SLA



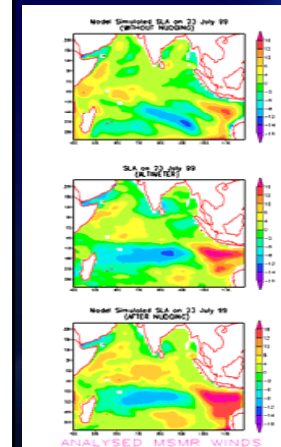
Estimated speed:
18 cm/s (T/P) and 14 cm/s
(Model) at 8 N



WAM Model Control Run Dec 15, 2002
3 Altimeter Data Assimilated



Assimilation of T/P SLA in Reduced gravity model



T/P SLA data assimilated in a in-house
developed reduced gravity model using
nudging technique.

Model was forced with ISRO's Oceansat-I
MSMR winds.

Correlation improved from 0.3 to 0.8 after
Assimilation

SLA data is being assimilated in an OGCM
using Ensemble Kalman Filter technique



Rainfall Climatology from TOPEX/POSEIDON Altimeter

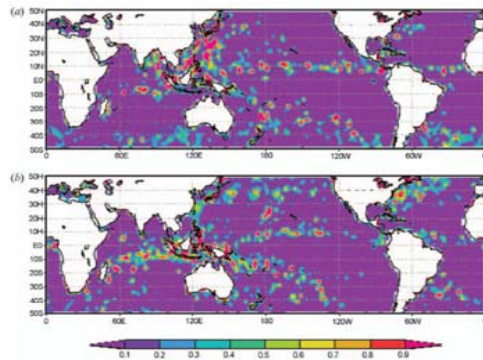
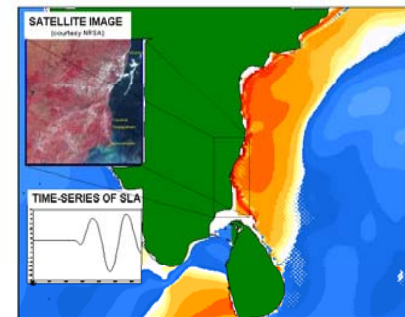


Figure 8. (a) Monthly average rain rate (mmh^{-1}) from TMR and RA for July 2000. (b) Monthly total rainfall (mm/month) from TMR and RA for January 2000.



Simulation of great Indian Ocean tsunami

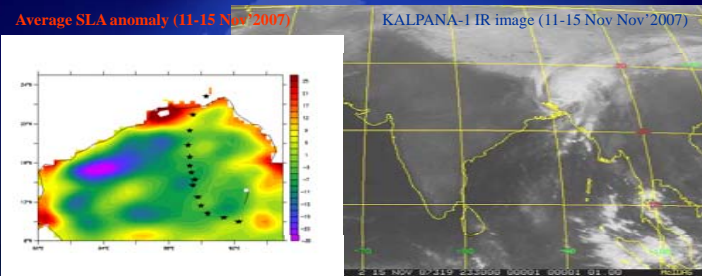


MODEL SIMULATIONS OF 26th DECEMBER 2004 INDIAN OCEAN TSUNAMI

Shows runaway of tsunami to Indian Coast after 2½ hrs of its generation. The inset picture shows the IRS coverage of the devastated area in South India. The line graph shows the time variation of the sea level anomaly created by the tsunami corresponding to the area in IRS image. The range of sea level is 50-60 cm elevation (dark orange) to depression of 20-30 cm (light blue).



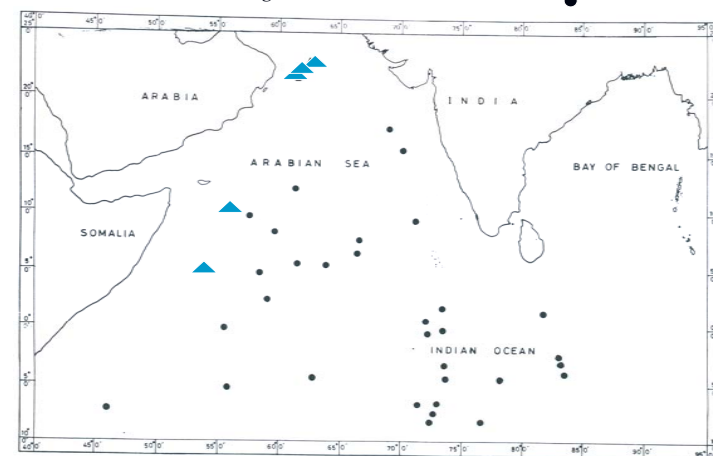
Sea level anomaly and Cyclone “Sidr”



The above picture shows that there is a tendency for the cyclone to move towards the positive sea level anomaly (indicative of large heat potential). In this type of application (near real time), timeliness of the altimeter data is more important.

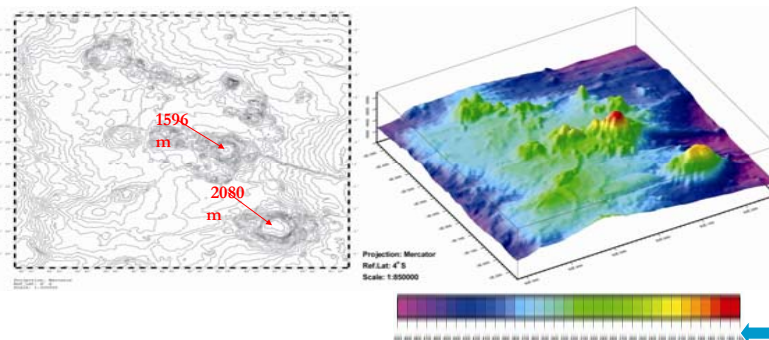


Detection of Seamounts Using GEOSAT RA

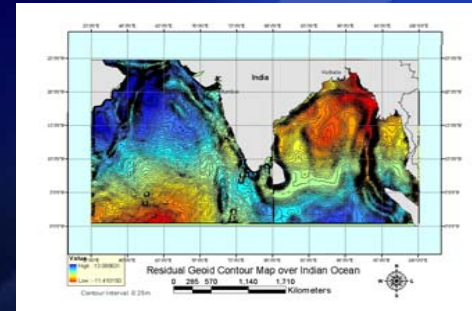


Cobalt-Rich Crust Programme

Mapping of Afanasiy-Nikitin Seamounts (Sudhakar et al. 2008)



Marine Geoid Mapping: Geophysical Information Extraction



Marine Geoid derived from Geosat GM/ERS-1/TOPEX/Poseidon altimeters with resolution of 3.5 km near equator.

Altimeter data over Indian offshore region with a height accuracy of ~ 5 cm and cross-track resolution of 5 km: Optimum for measurements of static parameters (Geoid/gravity)



Operational Cyclone Predictions

S.K. Roy Bhowmik

New Delhi

भारत मौसम विज्ञान विभाग
INDIA METEOROLOGICAL DEPARTMENT



MAJOR ASPECTS IN CYCLONE PREDICTIONS

- CYCLOGENESIS
- TRACK PREDICTION
- INTENSITY PREDICTION
- HEAVY RAINFALL AND STRONG WIND
- STORM SURGE

Natural Hazards, 2009, 50,389-402

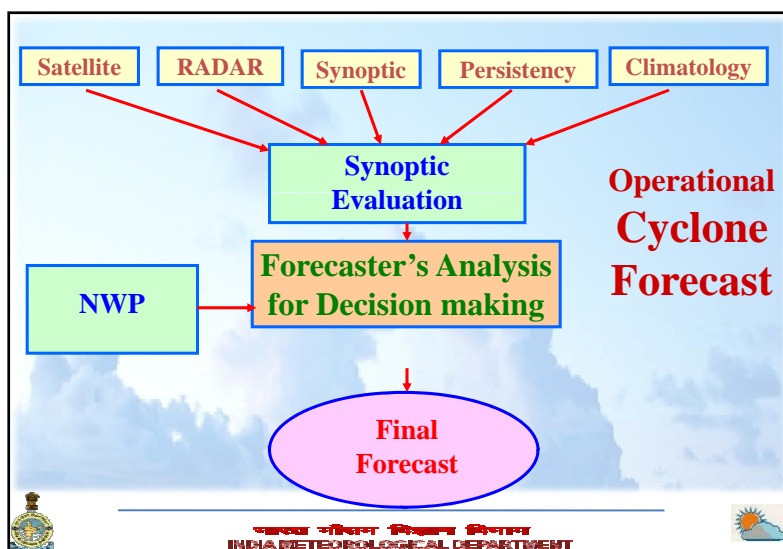
Met Application, 2009 16,169-177

Earth Sc. System, 2008, 117(2), 157-168

J Appl Met, 2005, 44, 179-185



भारत मौसम विज्ञान विभाग
INDIA METEOROLOGICAL DEPARTMENT



भारत मौसम विज्ञान विभाग
INDIA METEOROLOGICAL DEPARTMENT



GENESIS POTENTIAL PARAMETER (GPP)



भारत मौसम विज्ञान विभाग
INDIA METEOROLOGICAL DEPARTMENT



The GPP is defined as:

$$GPP = \frac{\xi_{850} \times M \times I}{S} \quad \text{if } \xi_{850} > 0, M > 0 \text{ and } I > 0$$

$$= 0 \quad \text{if } \xi_{850} \leq 0, M \leq 0 \text{ and } I \leq 0$$

Where, ξ_{850} = Low level relative vorticity (at 850 hPa) in $10^{-5} s^{-1}$
 S = Vertical wind shear between 200 and 850 hPa (ms^{-1})

$$M = \frac{[RH - 40]}{30} = \text{Middle troposphere relative humidity}$$

Where RH is the mean relative humidity between 700 and 500 hPa
 $I = (T_{850} - T_{500}) \cdot C = \text{Middle-tropospheric instability (Temperature difference between 850 hPa and 500 hPa)}$

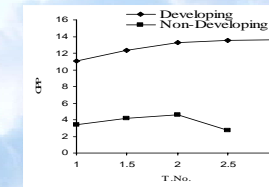


भारत मौसम विज्ञान विभाग
INDIA METEOROLOGICAL DEPARTMENT



Genesis potential parameter for developing versus non-developing systems:

GPP(x10 ⁻⁵) →					
T.No. →	1.0	1.5	2.0	2.5	3.0
Developing	11.1	12.3	13.3	13.5	13.6
Non-Developing	3.4	4.2	4.6	2.7	-



भारत मौसम विज्ञान विभाग
INDIA METEOROLOGICAL DEPARTMENT



Genesis potential parameter (GPP) for Developing System, Non-Developing System and Cyclone "BIJLI"

GPP (x10 ⁻⁵) →				
T.No. →	1.0	1.5	1.5	2.5
Developing	11.1	12.3	12.3	13.5
Non-Developing	3.4	4.2	4.2	2.7
Cyclone "BIJLI"	13.8 (0000 UTC /14.04.2009)	12.4 (1200 UTC /14.04.2009)	10.6 (0000 UTC /15.04.2009)	9.9 (1200 UTC /15.04.2009)



भारत मौसम विज्ञान विभाग
INDIA METEOROLOGICAL DEPARTMENT



**GENESIS OF BAY OF BENGAL
SEVERE CYCLONE 'AILA' OF May
2009**



भारत मौसम विज्ञान विभाग
INDIA METEOROLOGICAL DEPARTMENT



**Genesis potential parameter (GPP) for Developing System,
Non-Developing System and Cyclone "AILA"**

GPP ($\times 10^{-5}$) →					
T.No. →	1.0	1.0	1.0	1.0	1.5
Developing	11.1	11.1	11.1	11.1	12.3
Non-Developing	3.4	3.4	3.4	3.4	4.2
Cyclone "AILA"	20.0 (00UTC /22.05.2009)	20.0 (1200UTC /22.05.2009)	14.3 (0000UTC /23.05.2009)	14.9 (1200UTC /23.05.2009)	16.3 (00UTC /24.05.2009)



भारत मौसम विज्ञान विभाग
INDIA METEOROLOGICAL DEPARTMENT



TRACK PREDICTION



भारत मौसम विज्ञान विभाग
INDIA METEOROLOGICAL DEPARTMENT



TRACK PREDICTION BY NWP MODELS AND MME

- MM5 / WRF
- QLM
- JMA
- ECMWF
- NCEP GFS

MME



भारत मौसम विज्ञान विभाग
INDIA METEOROLOGICAL DEPARTMENT



MME Cyclone Track Prediction

12-hourly forecast latitude (LAT^f) and longitude (LON^f) positions at time t is defined as:

$$LAT_t^f = a_0 + a_1 ECMWF_t^{lat} + a_2 GFS_t^{lat} + a_3 JMA_t^{lat} + a_4 MM5_t^{lat} + a_5 QLM_t^{lat}$$

$$LON_t^f = a'_0 + a'_1 ECMWF_t^{lon} + a'_2 GFS_t^{lon} + a'_3 JMA_t^{lon} + a'_4 MM5_t^{lon} + a'_5 QLM_t^{lon}$$

for t = forecast hour 12, 24, 36, 48, 60 and 72



भारत मौसम विज्ञान विभाग
INDIA METEOROLOGICAL DEPARTMENT



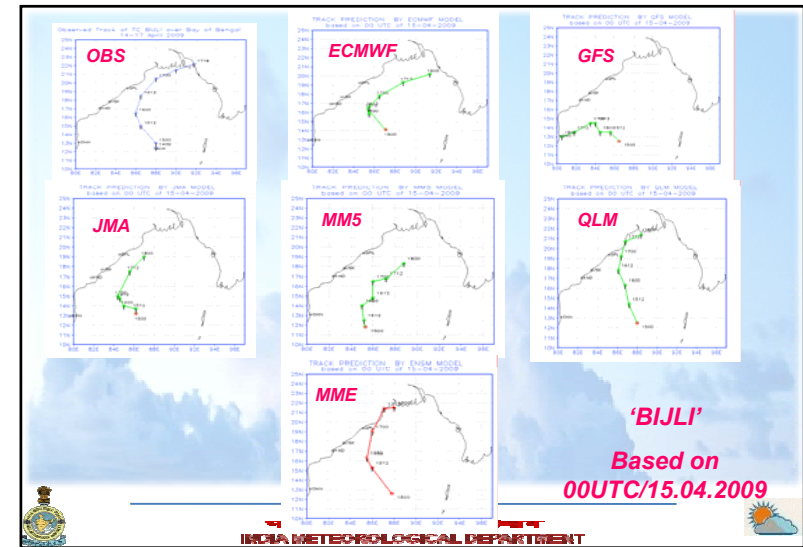
Bay of Bengal Cyclone BIJLI

14 - 17 April 2009

TRACK PREDICTION



भारतीय मетеороलॉजिकल डिपार्टमेंट
INDIA METEOROLOGICAL DEPARTMENT

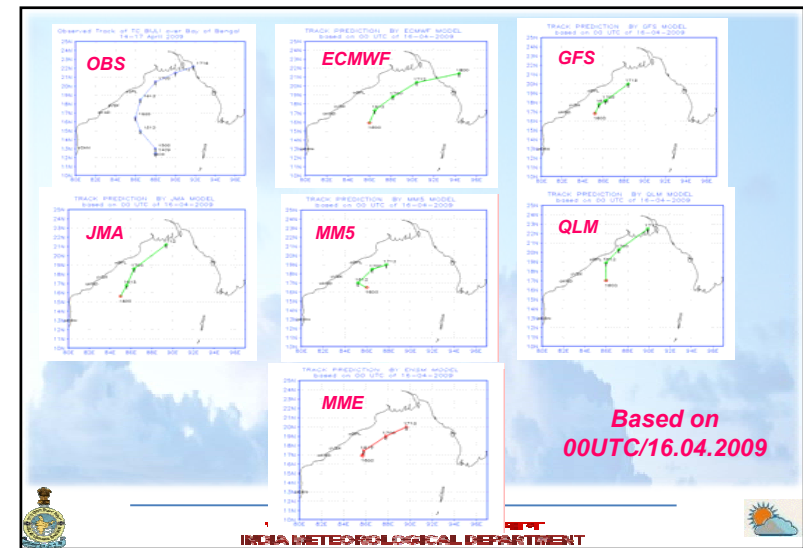


Track forecast error (km) of multimodel ensemble(MME) and its member models based on 00 UTC/15.4.2009

HOUR	ECMWF	GFS	JMA	MM5	QLM	MME
12	195	193	148	311	101	56
24	94	370	298	298	88	60
36	236	472	458	415	89	173
48	339	820	720	420	221	263
60	275	1242	640	599	343	261
Land Fall ERROR	NO LF	NO LF	NO LF	NO LF	582 km 9 hr early	601 km 10 hr early



भारतीय मетеороलॉजिकल डिपार्टमेंट
INDIA METEOROLOGICAL DEPARTMENT



Track forecast error (km) of multimodel ensemble(MME) and its member models based on 00 UTC/16.4.2009

HOUR	ECMWF	GFS	JMA	MM5	QLM	MME
12	133	123	212	216	69	143
24	190	318	276	272	86	168
36	129	235	71	360	112	170
LF ERROR	167km 2h delay	Dissipated	Dissipated	Dissipated	292km 8h early	Dissipated



भारत मौसम विज्ञान विभाग
INDIA METEOROLOGICAL DEPARTMENT



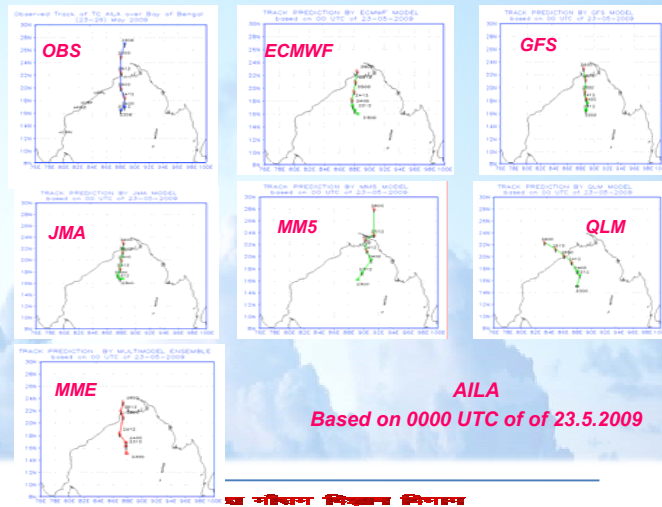
Bay of Bengal Severe Cyclone AILA

23-26 May 2009

TRACK PREDICTION



भारत मौसम विज्ञान विभाग
INDIA METEOROLOGICAL DEPARTMENT



भारत मौसम विज्ञान विभाग
INDIA METEOROLOGICAL DEPARTMENT



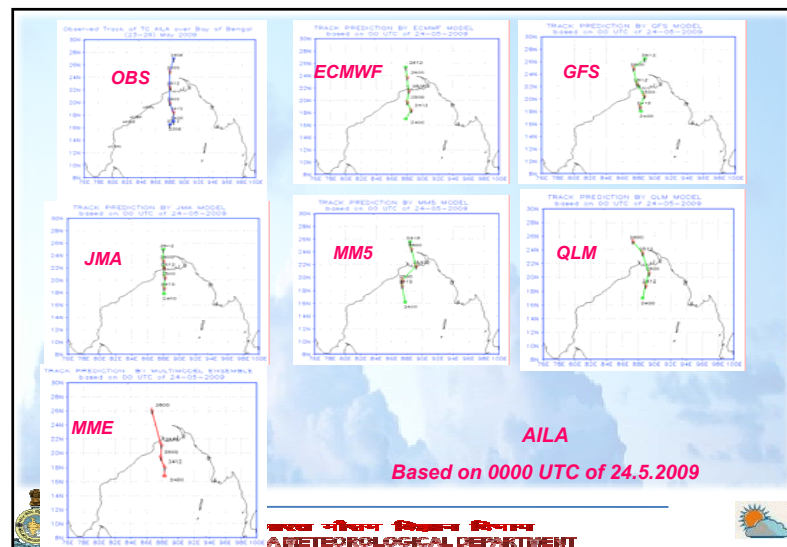
Track forecast error (km) of multimodel ensemble(MME) and its member models based on 00 UTC/23.5.2009

HOUR	ECMWF	GFS	JMA	MM5	QLM	MME
12	15	86	40	216	61	31
24	81	94	115	383	85	75
36	91	33	75	341	115	67
48	50	76	0	303	199	127
60	168	152	124	372	346	114
72	270	226	224	475	559	295
LF ERROR	20 km 10 hr delay	62 km 8 hr delay	40 km 6 hr delay	227 km 8 hr early	275 km 11 hr delay	83 km 2 hr delay



भारत मौसम विज्ञान विभाग
INDIA METEOROLOGICAL DEPARTMENT





Track forecast error (km) of multimodel ensemble(MME) and its member models based on 00 UTC/24.5.2009

HOUR	ECMWF	GFS	JMA	MM5	QLM	MME
12	0	46	54	120	61	49
24	20	70	59	77	156	70
36	102	20	56	146	132	145
48	120	60	180	82	78	129
LF ERROR	10km 5h delay	23km 1h delay	10km 1h delay	124km 4h delay	175km 8h early	20km 7h delay

भारत मौसम विज्ञान विभाग
INDIA METEOROLOGICAL DEPARTMENT

Average Track forecast error (km) of the member models and MME during the year 2009

HOUR	ECMWF	GFS	JMA	MM5	QLM	MME
12 hr	72	83	86	153	77	70
24 hr	111	191	167	234	124	90
36 hr	114	193	142	320	143	147
48 hr	93	117	86	246	242	199
60 hr	168	126	85	351	447	242
72 hr	217	151	152	415	577	293

भारत मौसम विज्ञान विभाग
INDIA METEOROLOGICAL DEPARTMENT

Track Position Error (km)
Final Operational Forecast

system	Forecast period					
	12	24	36	48	60	72
BIJLI	71	248	285	394	--	--
AILA	75	114	123	--	--	--
PHYAN	91	151	--	--	--	--
WARD	129	225	305	429	503	483
Average	91	185	238	411	503	483

भारत मौसम विज्ञान विभाग
INDIA METEOROLOGICAL DEPARTMENT

Landfall forecast error during 2009 Final Operational Forecast

Forecast period (Hrs)	12	24	36	48
BIJLI	20	40	30	155
AILA	55	110	110	110
PHYAN	75	250	-	-
WARD	78	78	78	78
Average	57	120	73	114



भारत मौसम विज्ञान विभाग
INDIA METEOROLOGICAL DEPARTMENT



INTENSITY PREDICTION



भारत मौसम विज्ञान विभाग
INDIA METEOROLOGICAL DEPARTMENT



Statistical Tropical Cyclone Intensity Prediction (SCIP) Model

Intensity change (dv_t) during the time interval t is defined as:

$$dv_t = a_0 + a_1 IC12 + a_2 SMS + a_3 VWS + a_4 D200 + a_5 V850 + a_6 ISL + a_7 SST + a_8 ISI$$

for t = forecast hour 12, 24, 36, 48, 60 and 72

The predictors:

(a) Persistence:

- (i) Initial storm intensity (ISI)
- (ii) Previous 12 hours change in the intensity (IC12)

(b) Thermodynamical factors :

- (i) Storm motion speed (SMS)
- (ii) Sea surface temperature (SST)

(c) Dynamical factors :

- (i) Initial storm latitude position (ISL)
- (ii) Vertical wind shear (850-200) hPa averaged along storm track (VWS)
- (iii) Vorticity at 850 hPa (V850)
- (iv) Divergence at 200 hPa (D200)



भारत मौसम विज्ञान विभाग
INDIA METEOROLOGICAL DEPARTMENT



BIJLI

INTENSITY PREDICTION



भारत मौसम विज्ञान विभाग
INDIA METEOROLOGICAL DEPARTMENT



Intensity Prediction

BIJLI

Model (SCIP) performance based on 0000 UTC of 15 April 2009

Forecasts hours →	00 hr	12 hr	24 hr	36 hr	48 hr	60 hr
Observed (knots)	30	35	40	40	40	25
Forecasts (knots)	30	33	35	41	45	60
Error (knots)	-	-2	-5	+1	+5	+35



भारत मौसम विभाग
INDIA METEOROLOGICAL DEPARTMENT



Intensity Prediction

BIJLI

Model (SCIP) performance based on 0000 UTC of 16 April 2009

Forecasts hours →	00 hr	12 hr	24 hr	36 hr
Observed (knots)	40	40	40	25
Forecasts (knots)	40	44	49	60
Error (knots)	-	+4	+9	+35

Model (SCIP) performance based on 0000 UTC of 17 April 2009

Forecasts hours →	00 hr	12 hr
Observed (knots)	40	25
Forecasts (knots)	40	47
Error (knots)	-	+22



भारत मौसम विभाग
INDIA METEOROLOGICAL DEPARTMENT



AILA

INTENSITY PREDICTION



भारत मौसम विभाग
INDIA METEOROLOGICAL DEPARTMENT



Intensity Prediction

AILA

Model (SCIP) performance based on 0000 UTC of 23 May 2009

Forecasts hours →	00 hr	12 hr	24 hr	36 hr	48 hr	60 hr
Observed (knots)	20	25	25	35	40	50
Forecasts (knots)	20	25	31	43	50	55
Error (knots)	-	0	+6	+8	+10	+5

Model (SCIP) performance based on 0000 UTC of 24 May 2009

Forecasts hours →	00 hr	12 hr	24 hr	36 hr
Observed (knots)	25	35	40	50
Forecasts (knots)	25	32	38	49
Error (knots)	-	-3	-2	-1



भारत मौसम विभाग
INDIA METEOROLOGICAL DEPARTMENT



Model (SCIP) performance based on 0000 UTC of 25 May 2009

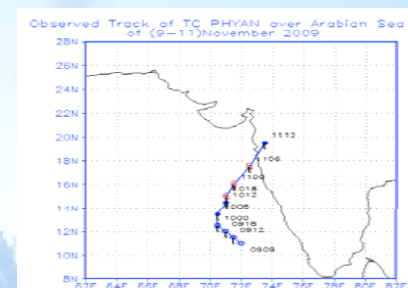
Forecasts hours →	00 hr	12 hr
Observed (knots)	40	50
Forecasts (knots)	40	48
Error (knots)	-	+2



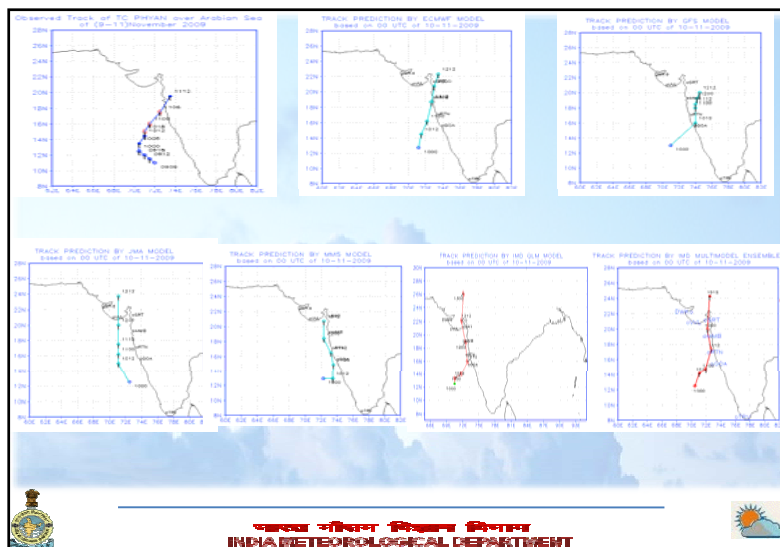
भारत मौसम विज्ञान विभाग
INDIA METEOROLOGICAL DEPARTMENT



Arabia Sea Cyclonic storm “PHYAN ” of (9-11) November 2009



भारत मौसम विज्ञान विभाग
INDIA METEOROLOGICAL DEPARTMENT



भारत मौसम विज्ञान विभाग
INDIA METEOROLOGICAL DEPARTMENT



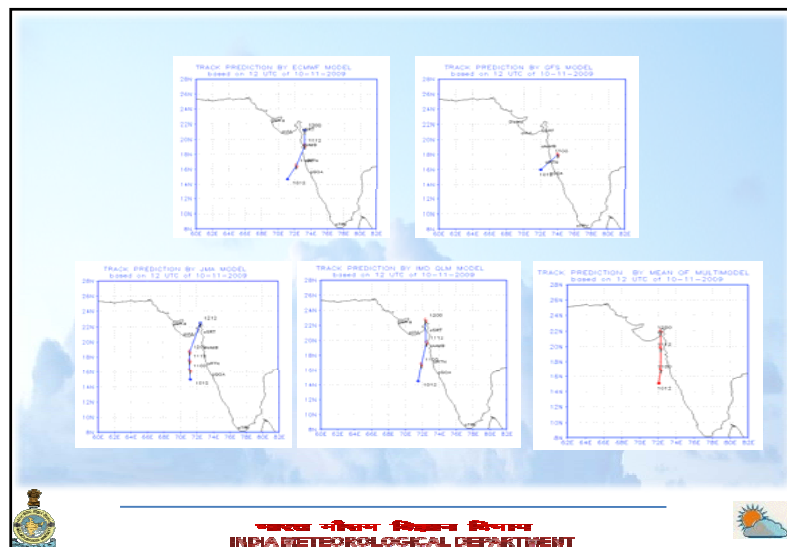
Track forecast error (km) of MME and its member models based on 0000 UTC of 10 November 2009

HOUR	ECMWF	GFS	JMA	MM5	QLM	MME
12	55	362	62	322	144	35
24	85	346	38	248	223	154
36	115	123	325	339	406	277
LF ERROR	38 km 2 hr delay	468 km 27 hr early	271 km 16 hr delay	NO LF Till 72 hr	303 km 12 hr delay	344 km 20 hr delay



भारत मौसम विज्ञान विभाग
INDIA METEOROLOGICAL DEPARTMENT





Track forecast error (km) of MME and its member models based on 1200 UTC of 10 November 2009

HOUR	ECMWF	GFS	JMA	QLM	MME
12	94	346	38	99	131
24	38	-	325	107	130
LF ERROR	Close to LF 1 hr early	220 km 15 hr early	220 km 24hr delay	265 km 10 hr delay	272 20hr delay



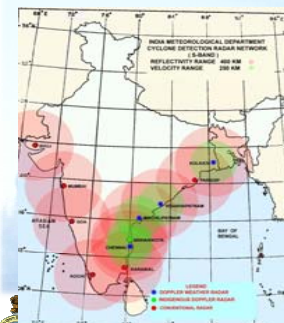
Model (SCIP) performance based on 0000 UTC of 10 November 2009

Forecasts hours →	00 hr	12 hr	24 hr	At landfall Time
Observed (knots)	25	30	40	40
Forecasts (knots)	25	32	37	41
Error (knots)	-	+2	-3	+1



Meso-scale Applications of Doppler Weather RADAR (DWR) Observations

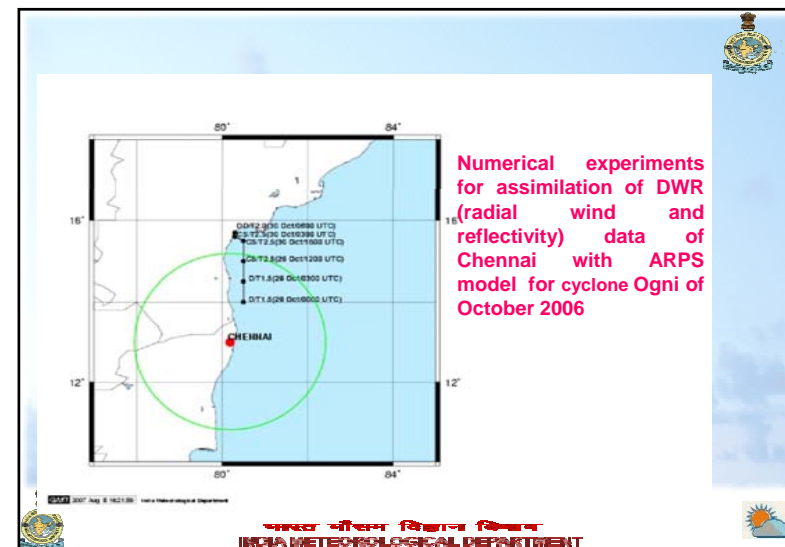
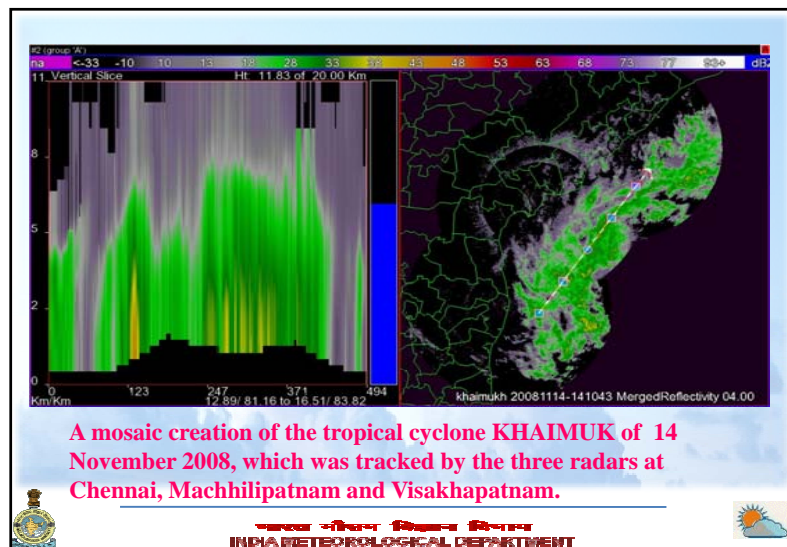
- Processing for Nowcasting Applications
- Ingest into assimilation cycle of NWP models



Parameters: radial wind, reflectivity and spectrum width

DWR Stations: Chennai (2002), Machalipatnam (2004), Vishakapatnam (2006) and Kolkata (2003), Sriharikota (ISRO)

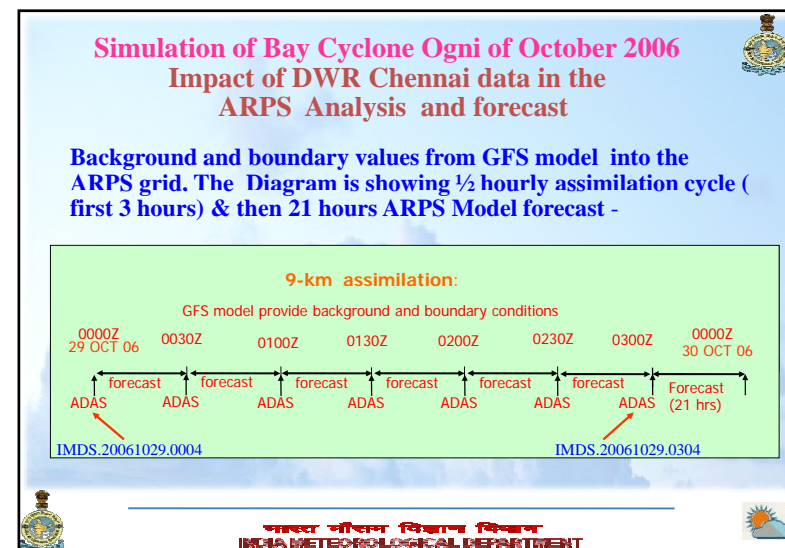




Design of Experiments

No. of grids (x,y,z)	99, 99, 38
Grid spacing	9 km x 9 km
Time step	30 sec
Model initialization	ARPS Data Assimilation System (ADAS) with GFS inputs
Turbulent mixing option	1.5 TKE
Micro Physics	Kain Fritsch warm rain
Convective Cumulus parameterization	Kain Fritsch Cumulus parameterization

INDIA METEOROLOGICAL DEPARTMENT



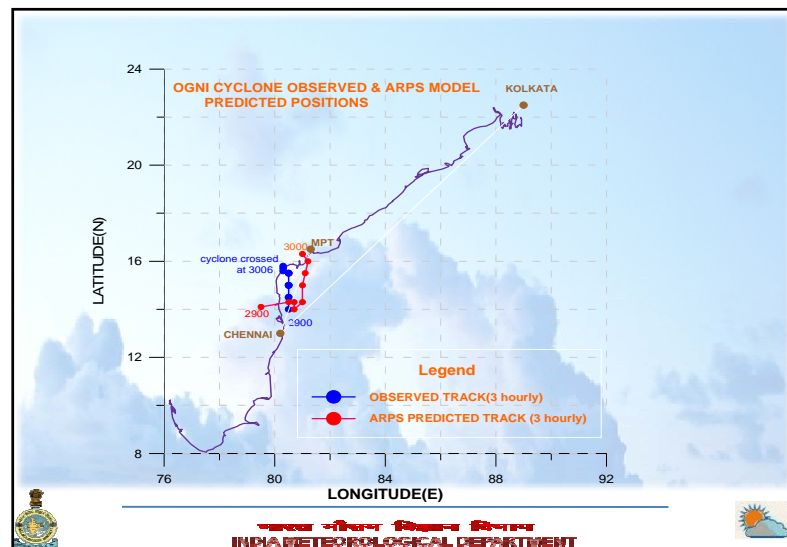
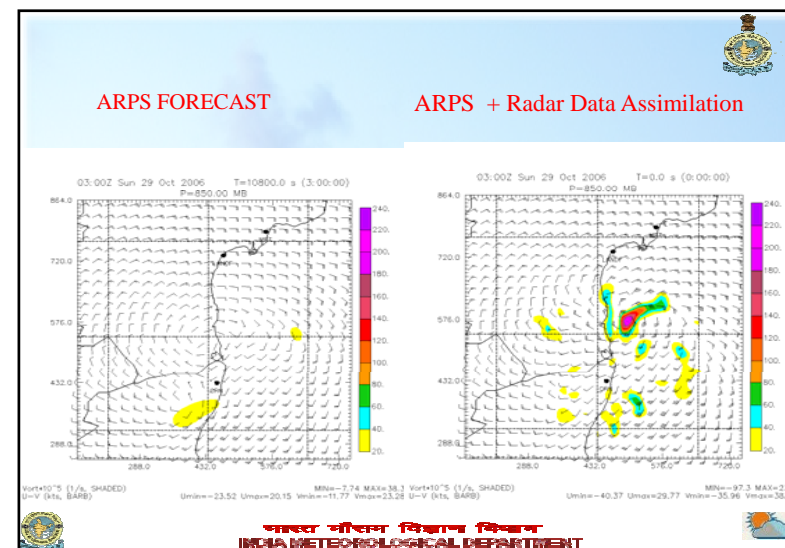
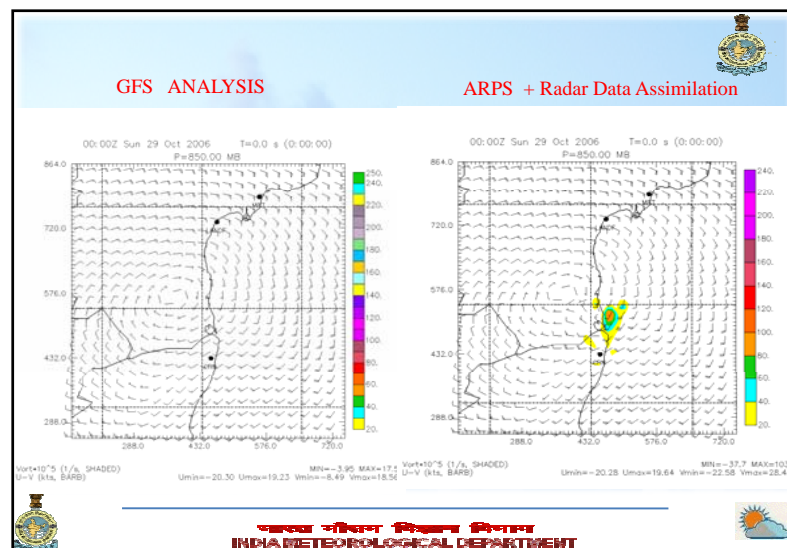


Table: Inter-comparison of three hourly forecast track positions and errors (km), with in the brackets, for the cyclone "Ogní" of 29 October 2006

Time > UTC	0000	0300	0600	0900	1200	1500	1800	2100	2400
Control run	14.1°N / 79.5°E (108.3)	14.1°N / 80°E (69.8)	14.1°N / 80.8°E (55.0)	14.1°N / 80.6°E (100.5)	14.5°N / 81°E (77.3)	15°N / 80.9°E (42.9)	15.6°N / 81°E (54.6)	15.9°N / 81°E (69.5)	16.5°N / 81°E (123.2)
dwr run	14.1°N / 79.5°E (108.3)	14.3°N / 80°E (22.2)	14.3°N / 80.7°E (30.9)	14°N / 80.7°E (113.2)	14.3°N / 81°E (94.5)	15°N / 81°E (53.6)	15.5°N / 81.1°E (64.2)	16°N / 81.2°E (93.2)	16.3°N / 81°E (103.7)
Observed track position	14°N / 80.5°E	14.5°N / 80.5°E	15°N / 80.5°E	15°N / 80.5°E	15°N / 80.5°E	15°N / 80.5°E	15.5°N / 80.5°E	15.5°N / 80.5°E	15.5°N / 80.5°E



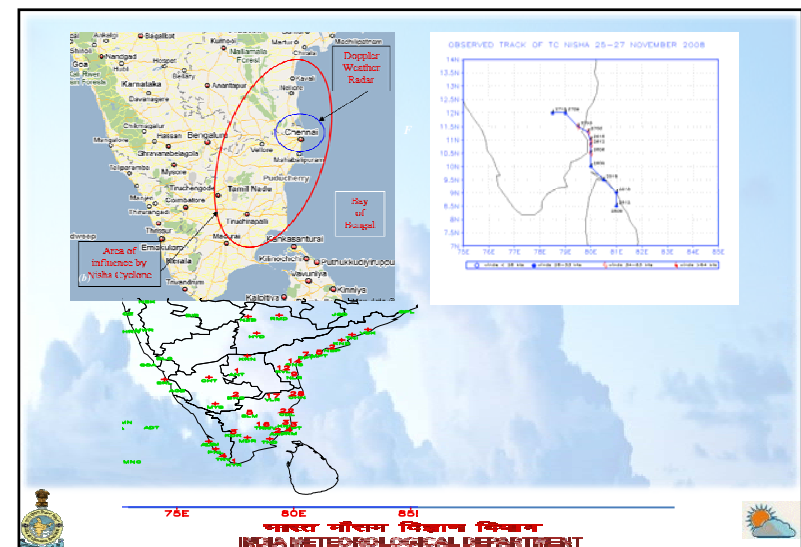
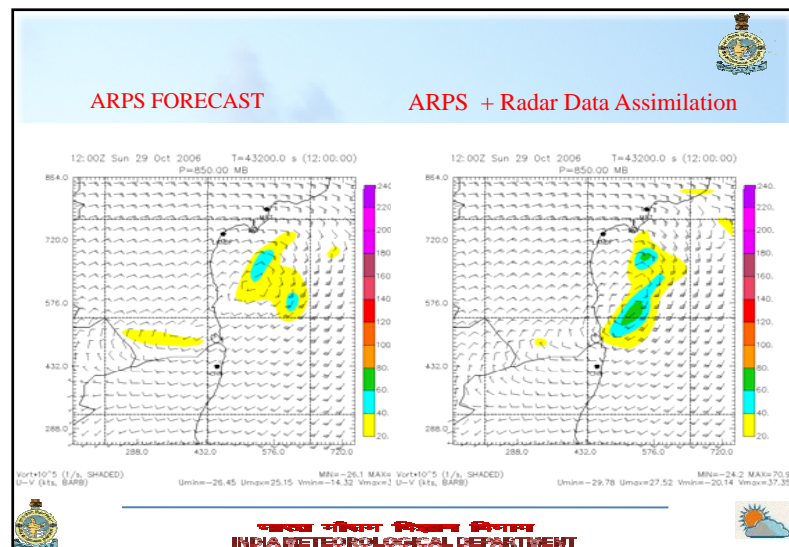
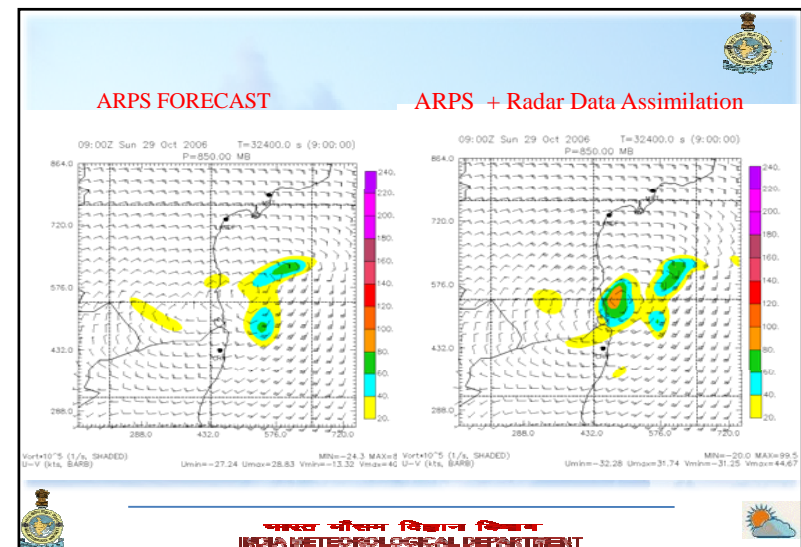
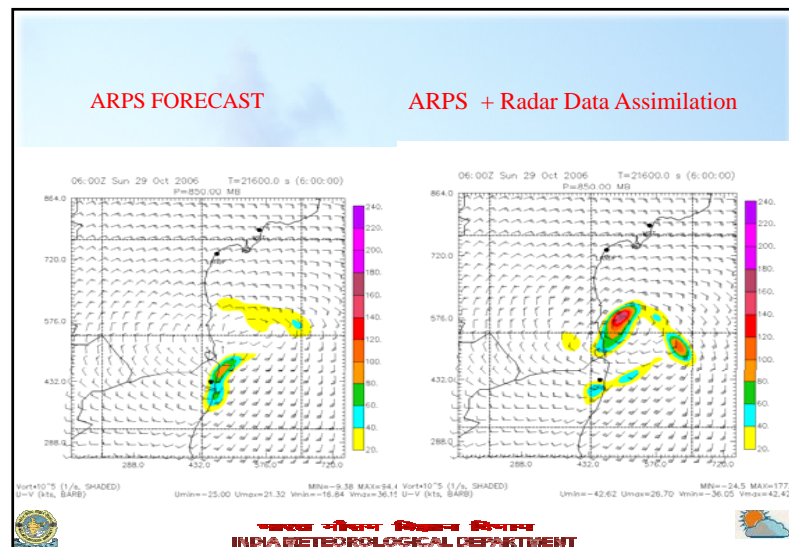
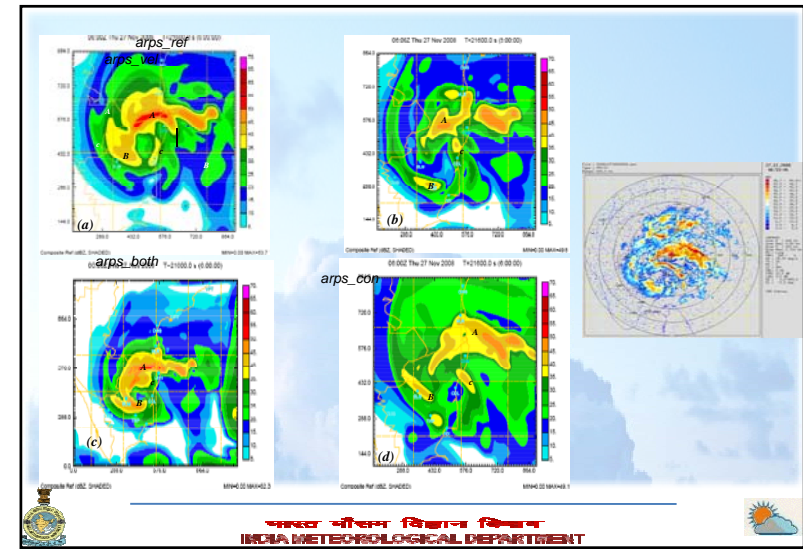


Table: Description of experiments

S.N O.	Experiments	Name of Experiments
1	ARPS control run	arps_con
2	ARPS run using Radial velocity only	arps_vel
3	ARPS run using Reflectivity only	arps_ref
4	ARPS run using both Radial velocity & Reflectivity	arps_both



भारत मौसम विज्ञान विभाग
INDIA METEOROLOGICAL DEPARTMENT



भारत मौसम विज्ञान विभाग
INDIA METEOROLOGICAL DEPARTMENT

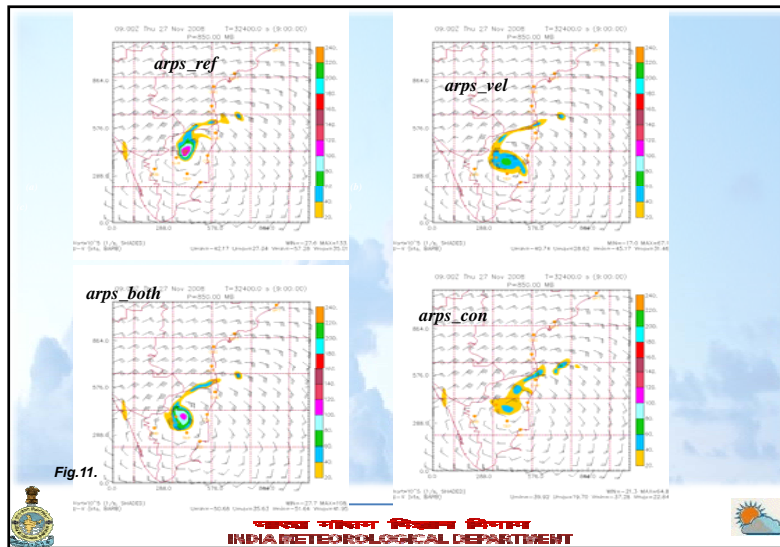
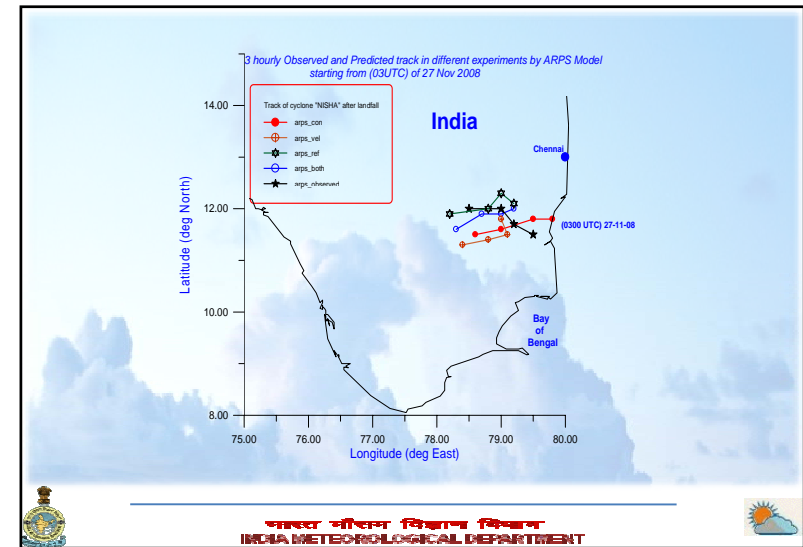


Fig.11.



भारत मौसम विज्ञान विभाग
INDIA METEOROLOGICAL DEPARTMENT



भारत मौसम विज्ञान विभाग
INDIA METEOROLOGICAL DEPARTMENT



Table: Inter-comparison of three hourly track positions and errors (km) with in brackets for the cyclone “Nisha” of 27 November 2008

Time > UTC	0300	0600	0900	1200
arps_con	11.8 / 79.8 (46.6)	11.8 / 79.5 (34.4)	11.6 / 79.0 (44.5)	11.5 / 78.6 (56.6)
arps_vel	11.8 / 79.0 (63.8)	11.5 / 79.1 (24.8)	11.4 / 78.8 (70.1)	11.3 / 78.4 (78.5)
arps_ref	12.1 / 79.2 (74.2)	12.3 / 79.0 (70.1)	12.0 / 78.8 (21.6)	11.9 / 78.2 (34.4)
arps_both	12.0 / 79.2 (64.4)	11.9 / 79.0 (31.0)	11.9 / 78.7 (34.4)	11.6 / 78.3 (49.5)
Observed position	11.5 / 79.5	11.7 / 79.2	12.0 / 79.0	12.0 / 78.5



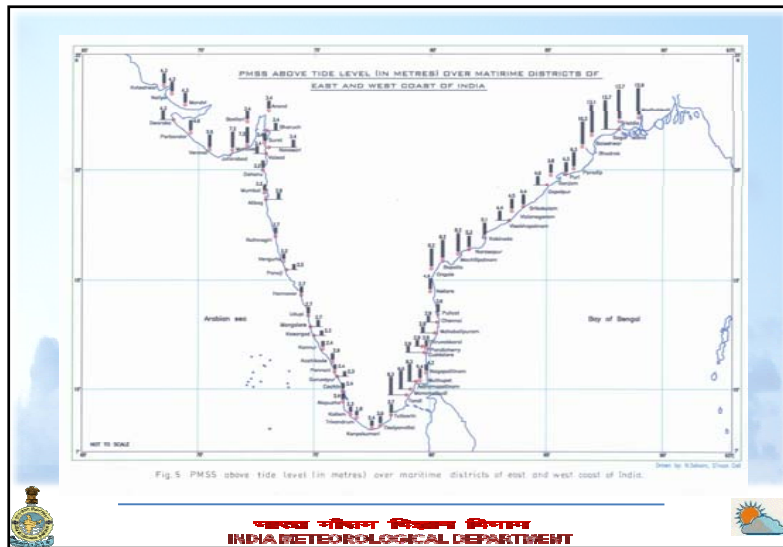
भारत मौसम विज्ञान विभाग
INDIA METEOROLOGICAL DEPARTMENT



Time	Rainfall (c.m.) at 00UTC 28-11-08						Remarks
Name of station	Chennai	Vellore	Nellore	Cuddalore	Trichy	Salem	
Name of Experiment							
arps_both	30	30	10	10	0	10	1. Maximum rainfall (81 cm) is in east west rain band between Chennai & Nellore corresponding to spiral reflectivity band. 2. One more rain cell (maximum rainfall 40 cm) between Trichy & Salem. Matching with observation.
arps_ref	20	20	10	0	0	0	Maximum rainfall (54 cm) is in east west rain band between Chennai & Nellore corresponding to spiral reflectivity band.
arps_vel	10	10	10	10	0	0	Maximum rainfall (32 cm) is in east west rain band between Chennai & Nellore corresponding to reflectivity band.
arps_con	10	10	10	10	0	0	
Observed	28	17	9	22	16	5	



भारत मौसम विज्ञान विभाग
INDIA METEOROLOGICAL DEPARTMENT



भारत मौसम विज्ञान विभाग
INDIA METEOROLOGICAL DEPARTMENT



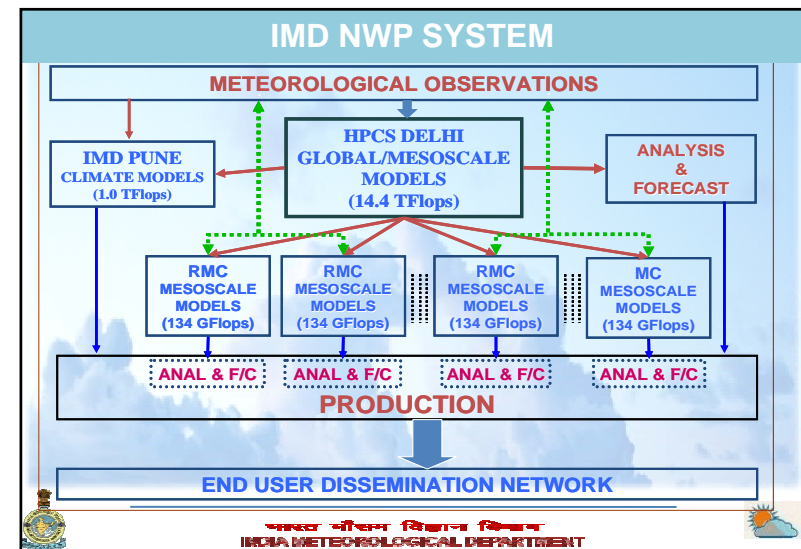
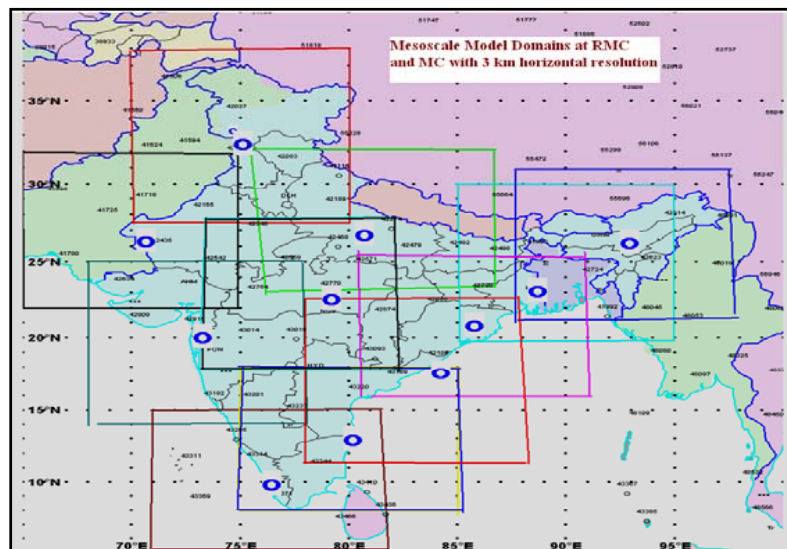
NWP System in IMD Medium range to Nowcast

- GFS T-382/L64 GSI
- WRF – VAR (27 km, 9km, 3 km)
- WRF (3 km) at 12 MCs
- Location specific forecast
- Nowcast



भारत मौसम विज्ञान विभाग
INDIA METEOROLOGICAL DEPARTMENT





FDP Cyclone

- To improve the observational network
- To develop data assimilation strategies
- To improve the accuracy of cyclone intensity and track forecasts for cyclones over north Indian Ocean (1-5 days)



भारत मौसम विज्ञान विभाग
INDIA METEOROLOGICAL DEPARTMENT



Role of eddies and upper ocean heat content in the intensification and movement of storms in Bay of Bengal from satellite data

Dr. Y. Sadhuram
Deputy Director



National Institute of Oceanography, Regional Centre
176, Lawsons Bay colony, Visakhapatnam – 530017

E-mail: sadhuram@nio.org



The frequency of the cyclones is 3 to 4 times higher over Bay of Bengal compared with the Arabian sea, and most of the storms hit east coast of India and some of the severe storms generate storm surges. Since the slopes are less on the east coast of India particularly near the estuaries, these regions are vulnerable for the damages due to cyclones and storm surges.

Storm surge of 8m height due to the “Super Cyclone” which hit Paradeep on 29th October ,1999,killed more than 10,000people.

This was the severe most cyclone during the last 114 years.

The total damage estimated was Rs 5,000 crores.

Number of cyclones (I) and severe cyclones (II) in the Bay of Bengal and Arabian Sea.

Month	Bay of Bengal				Arabian Sea			
	I		II		I		II	
	a	b	a	b	a	b	a	b
January	05	01	01	01	02	00	00	00
February	01	00	01	00	00	00	00	00
March	04	00	02	00	00	00	00	00
April	20	02	09	02	06	01	04	00
May	49	11	32	09	23	04	14	02
June	42	03	04	03	20	03	09	02
July	48	03	07	00	05	00	01	00
August	30	04	03	02	02	00	00	00
September	44	07	16	04	07	02	02	02
October	76	11	29	08	22	05	10	05
November	86	27	43	20	26	01	18	01
December	42	08	18	05	06	01	02	01
Total	449	82	165	52	119	17	60	13

The conditions favorable for the genesis of cyclones are

- (1) Large values of low level relative vorticity
- (2) Coriolis parameter (at least few degrees poleward of equator)
- (3) Weak vertical shear of horizontal winds
- (4) High SST >26°C and deep thermocline
- (5) Conditional instability through a deep atmospheric layer
- (6) Large values of relative humidity in the lower and middle troposphere

It is not clearly known which one of the above parameters is playing a dominant role over Bay of Bengal .It is now realized that the upper ocean thermal structure rather than the SST,plays a vital role in the intensification of storm

Upper Ocean Heat content (UOHC), which is defined as the integrated heat content upto the depth of 26°C isotherm, gives an idea of the available heat energy for the genesis and intensification of a cyclone. An average CHP of 32 kJ/cm² over 28°C can sustain an intense storm for a week with an assumed evaporation rate of 2 cm/day.

$$\text{UOHC} = \rho C_p \int_{D_{26}}^{D_{28}} \Delta T dz$$

Where ρ is the density of water column above 26°C

C_p is the specific heat of sea water at a constant pressure

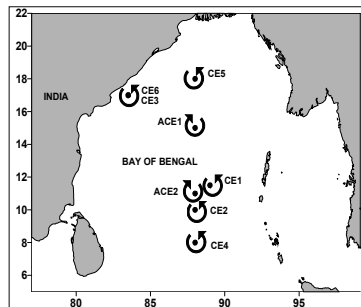
ΔT is the temperature difference between mean temperature of 2 consecutive layers and 26°C

dz is the depth increment and D_{26} is the depth of 26°C isotherm

The role of UOHC in the storm tracks has been examined for few storms and noticed that storm tracks preferred to move over the regions where CHP is high and weakened/dissipated or recurved over the sea when they encountered with low UOHC (<40 kJ/cm²).

S.No	Period of cyclone/depression	CHP (kJ/cm ²)	Track
1	16-19 Sept 2005	60 along the track and <40 in the WNW direction	Moved in SWly direction instead of a WNW direction and crossed at Kalingapatnam
2	26-28 Nov 2005	< 40 where it is dissipated	Dissipated over the sea, a few km off Tamilnaadu
3	6-10 Dec 2005	<40 where it is weakened	Weakened over the sea before hitting Tamilnadu coast
4	24-29 April, 2006	>150 where the storm took a recurve and moved NE	Took a recurve and moved in NEly direction and hit Myanmar coast

Variability of D_{26} (m) and UOHC (KJ/cm²) in the meso scale eddies in Bay of Bengal. CE – Cyclonic Eddy; ACE : Anti Cyclonic Eddy



S.No	Date	Eddy	D26	UOHC
1	28/05/96	ACE1	130	125
2	19/4/2003	ACE2	074	081
		average	102	103
1	9/06/96	CE1	060	067
2	13/07/01	CE2	019	018
3	26/07/01	CE3	027	023
4	18/09/02	CE4	040	028
5	25/09/02	CE5	032	030
6	30/04/03	CE6	042	043
		average	037	035

El-Nino and storm tracks

It is observed that 33 out of 38 storms (about 87%) formed during the El-Nino years have not recurved and crossed the coast south of 17° N.

38 out of 48 storms (79%) formed during the year previous to the El-Nino either recurved or crossed north of 17° N.

During severe El-Nino years 15 out of 16 storms (about 94%) have crossed south of 17° N whereas during the year previous to severe El-Nino years 17 out of 19 (about 89%) have either recurved or crossed north of 17° N.

The above points indicate the strong link between El-Nino and storm tracks in the Bay of Bengal.

UOHC in the Andaman sea during post-monsoon, 1996 I – from CTD data II: Shay et.al , 2000 (using SSHA&SST) III present method

Grid No.	I	II	III
1	38.7	35.6	59.2
2	44.9	38.0	60.7
3	73.1	34.4	69.6
4	46.0	35.7	58.4
5	54.3	37.9	59.8
6	64.8	33.1	64.6
7	75.2	37.5	70.0
8	48.1	33.1	58.0
9	65.8	31.1	66.1
10	75.2	40.0	77.4
11	50.2	34.3	59.8
12	56.4	31.6	71.0
13	65.8	37.1	92.9
14	55.4	38.2	64.5
15	44.9	31.5	70.7
16	43.9	31.0	88.6
17	55.4	39.5	68.2
18	42.8	27.0	66.0
19	41.8	33.3	70.0
20	61.6	39.7	69.0
21	52.2	33.8	70.0
22	56.4	34.4	77.9

I--- CTD data

II--- Shay et.al (2000)

III--- Sadhuram et.al (2006)

$$\text{UOHC} = 64.1 + 1.41 \cdot \text{SSHA} + 0.08 \cdot \text{SSHA}^2$$

$$\text{D26} = 63.84 + 1.39 \cdot \text{SSHA} + 0.044 \cdot \text{SSHA}^2$$

UOHC (kJ/cm²) and D26 (m) during the storm

Date	Position of Argo float	UOHC	D26
12.11.2007	11.04N;89.41E	37	57
13.11.2007	14.48N;89.07E	62	65
14.11.2007	17.612N;90.616E	81	65
15.11.2007	16.36N;91.21E	84	78

SHF,LHF and total enthalpy flux (SHF+LHF) (w/m²) in the region during Sidr and rapid intensification of Nargis

	SHF	LHF	Total
Nargis* I	-20 to -169	445-1036	415- 867
II	-23 to -299	291-627	115-396
Sidr	112	810	922

*Line et al.(2008)

I: numerical experiments during rapid intensification of Nargis with warm ocean observations

II: same as above but with climatological conditions

Lin et.al (2009) , have done extensive work for the western north Pacific Ocean and proposed some relationships between Translation speed of the storm (Uh) vs D26 and Uh Vs UOHC for category-5 storms . The following equations are suggested.

$$\text{Uh} = -0.06 \cdot \text{D26} + 12.1 \quad \text{--- (1)}$$

$$\text{Uh} = -0.065 \cdot \text{D26} + 11.1 \quad \text{--- (2)}$$

$$\text{Uh} = -0.05 \cdot \text{UOHC} + 9.4 \quad \text{--- (3)}$$

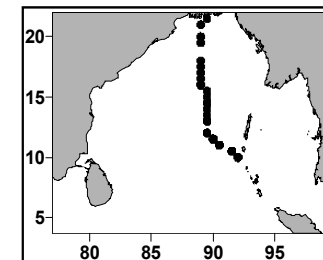
$$\text{D26} = -11.9 \cdot \text{Uh} + 158 \quad \text{--- (4)}$$

Eq.4 considers stratification also ($N^2 < 4 \times 10^{-4} \text{ sec}^{-2}$). Though we are aware that the above equations may differ for Bay of Bengal, we have just computed Uh from the above equations on 15th November when the storm intensity reached category.4 as per IMD and compared with the observed Uh.

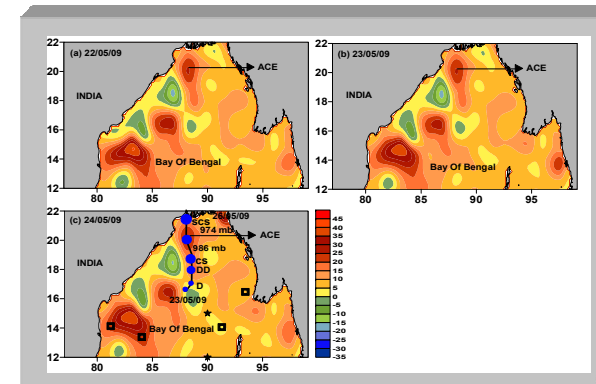
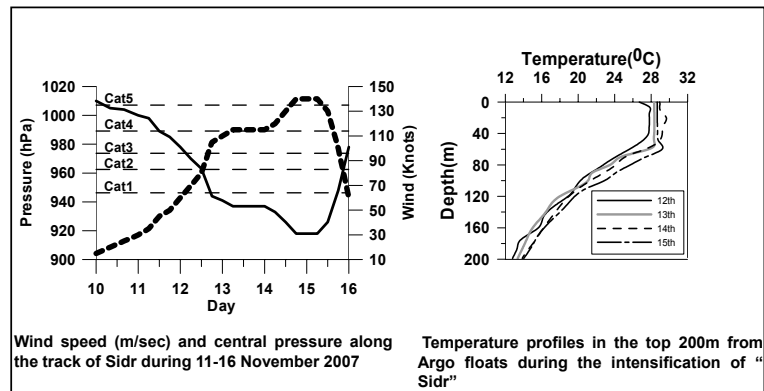
Observed (Uh) (m/sec) and estimated Uh (eqs.1-4) using UOHC (kJ/cm²) and D26 (m) for Sidr (15.11.2007) and Nargis (1.5.2008)

	Sidr (15.11.2007)	Nargis* (1.5.2009)
UOHC	84	82
D26	78	88
Uh-obs	7.5	5.8
Uh(from eq.1)	7.4	6.8
(fromeq.2)	6.0	5.4
(fromeq.3)	5.2	5.3
(fromeq.4)	6.7	5.9

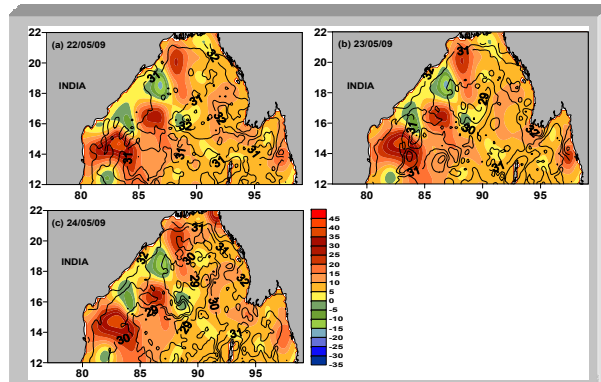
* UOHC and D26 are taken from Lin.et.al³



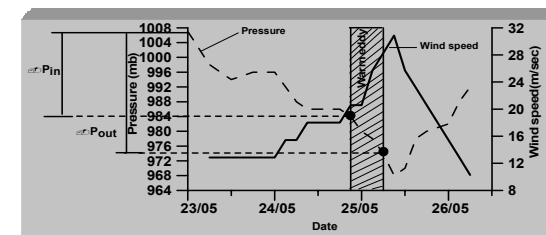
Track of the severe cyclone (Sidr) during 11-16 November in Bay of Bengal



Sea Surface Height Anomalies (SSHA)(cm) during (a) 22-05-09 (b) 23-05-09 and (c) 24-05-09. Track of 'Aila' is shown. Positions of Argo floats (Squares) and Rama Buoys (stars) are also shown in the figure



Sea Surface Height Anomalies (SSHA)(cm) and Sea Surface Temperature (°C) (contours are drawn at 0.5°C interval) during (a) 22-05-09 (b) 23-05-09 and (c) 24-05-09.



Central pressure (mb) and wind speed(m/sec) of 'Aila' during 23rd -26th May 2009. The positions of the storm entering and leaving the warm eddy are shown(●).

The eddy feedback factor , $F_{\text{EDDY-T}}$, is defined as

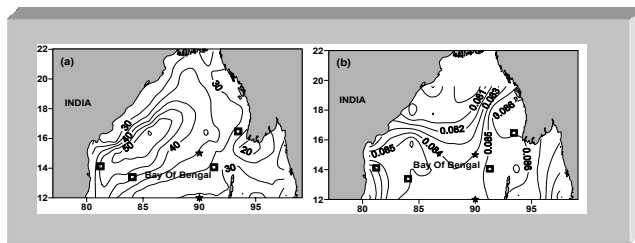
$$F_{\text{EDDY-T}} = \frac{\Delta p_{\text{out}} - \Delta p_{\text{in}}}{\Delta p_{\text{in}}} \text{-----}(1)$$

Where Δp in (Δp out) is the amount of sea level central pressure deepening at the moment when the storm encounters (leaves) the ocean eddy. The subscript “-T” indicates the TC only passes an ocean eddy for a finite (transient) period. Likewise , $F_{\text{EDDY-T}}$ could be positive (warm eddy) or negative (cold eddy).

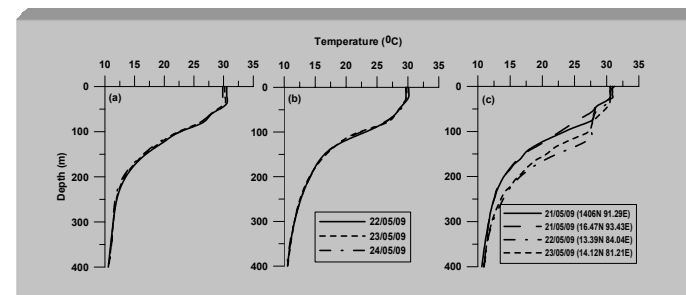
After conducting several numerical experiments over north west Pacific Ocean , Wu et.al (2007) , suggested a best fit line with 8 parameters and a very high correlation (0.97) was found between the model results and the following equation (2).

$$F_{\text{EDDY-T}} = 0.38 \left(\frac{SST_{\text{EDDY}} - 26^\circ\text{C}}{SST - 26^\circ\text{C}} \right)^{1.88} \times (SST_{\text{EDDY}} - 26^\circ\text{C})^{0.2} (ML_{\text{EDDY}})^{0.98} \times (ML)^{-0.97} (\eta)^{0.22} \times (1 - RH)^{-0.74} (\Gamma)^{0.45} (U_H)^{-0.83} \text{-----}(2)$$

Where SST and mixed layer (ML) represent large scale steady ocean. SST_{eddy} and ML_{eddy} are inside the eddy, η is the storm size , RH is ambient relative humidity, Γ is the thermal stratification below mixed layer and U_H is the translation speed (m/sec) of the storm.



Distribution of Mixed Layer Depth (MLD) (m) and (b) Stratification below mixed layer (Γ)($^\circ\text{C}/\text{m}$) in the Bay of Bengal during May 2009.



Vertical temperature profiles ($^\circ\text{C}$) at (a) $12^\circ\text{N}; 90^\circ\text{E}$ (b) $15^\circ\text{N}; 90^\circ\text{E}$ from RAMA buoys and (c) Argo floats .

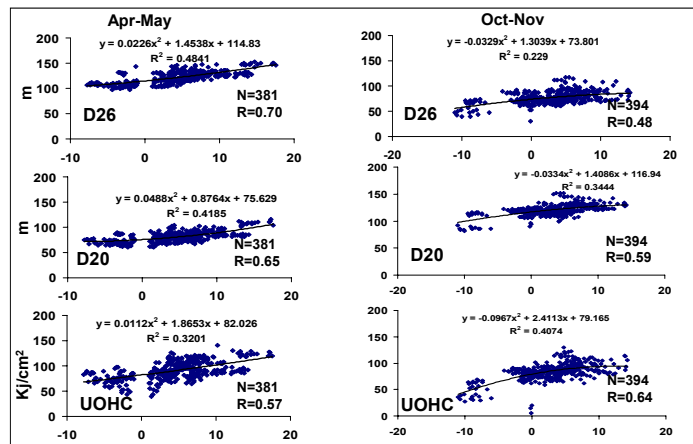
Details of parameters and the data used in the best fit equation (2)
(Wu. et al, 2007)

S.No	parameter	value
1	SST (°C)	30.0
2	SST _{eddy} (°C)	31.0
3	ML (large scale ocean) (m)	40
4	ML _{eddy} (m)	56
5	Ambient RH (%)	83
6	Storm size (η)	0.3
7	Thermal Stratification below mixed layer(Γ) (°C. m ⁻¹)	0.084
8	Translation speed of the storm (Uh) (m/s)	4.0
9	F _{eddy-T} (observed-eq.1)	0.43
10	F _{eddy-T} (estimated-eq.2)	0.34

Different parameters derived from Argo and RAMA buoy profiles

Parameter/Date	Argo				RAMA Buoys			
	21/5	21/5	22/5	23/5	15°N 90°N	12°N 90°N	12°N 90°N	24/5
SST(°C)	30.59	30.90	31.21	30.52	30.52	30.18	29.85	30.13 29.81 29.66
MLD(m)	36	32	36	55	29	29	29	29 29 29
Γ (°C/m)	0.083	0.080	0.078	0.082	0.091	0.09	0.089	0.081 0.082 0.082
D26 (m)	85	70	127	109	83	79	80	80 82 79
D20 (m)	122	125	166	155	122	118	116	118 113 115
UOHC(Kj/cm ²)	111	97	149	147	118	106	103	99 96 94

Computation of D26 and UOHC from SSHA



Values (min, max, avg) of D20, D26 and UOHC from RAMA buoys data (8°N,90°E;12°N,90°E;15°N,90°E) during pre-monsoon (Apr-May) and Post-Monsoon (Oct-Nov) seasons

	D20			D26			UOHC		
	Min	Max	Avg	Min	Max	Avg	Min	Max	Avg
Pre - Monsoon	97.00	152.00	123.00	60.00	116.00	82.09	40.00	131.00	91.00
Post- Monsoon	82.00	152.00	120.07	30.00	117.00	76.47	6.00	129.00	83.00

Conclusions

- ❖ UOHC is about 3 times higher in ACE compared with that of CE .This large variability in UOHC plays a vital role in the intensification/ weakening of storms in Bay of Bengal
- ❖ Intensity of "Aila " enhanced by 43% due to it's interaction with the warm core ACE in the central Bay of Bengal .This is close to the estimated(34%) from the best fit line.
- ❖ Translation speed of (Uh) of Sidr and Nargis estimated from UOHC and D26 are in good agreement with the observed speed.
- ❖ Simple equations to compute UOHC & D26 from SSHA have been developed using RAMA buoys data during pre-monsoon (Apr-May) and post-monsoon (Oct-Nov) Seasons. The methodology has to be tested

Heat Content from ocean circulation models

C. Gnanaseelan



INDIAN INSTITUTE OF TROPICAL METEOROLOGY
PUNE 411008, INDIA

OUTLINE

- Motivation
- Different data sets and models used for the study
- Importance of heat content estimation
- Its feed back on sea level
- Impact of Indian Ocean warming

Why Look at Ocean Heat Content?

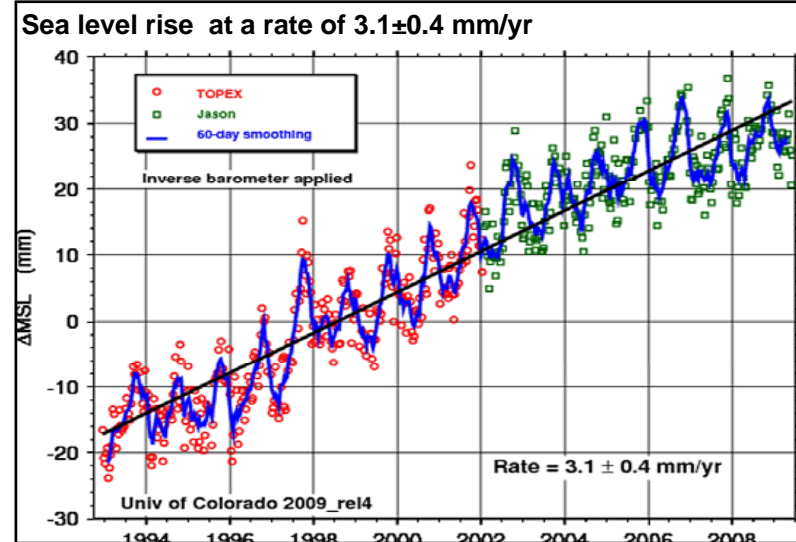
Directly relates to “Transient climate Response”

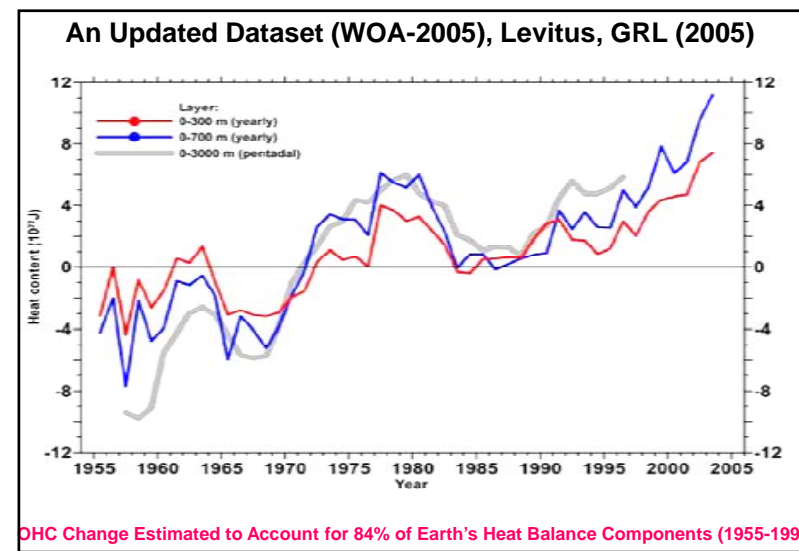
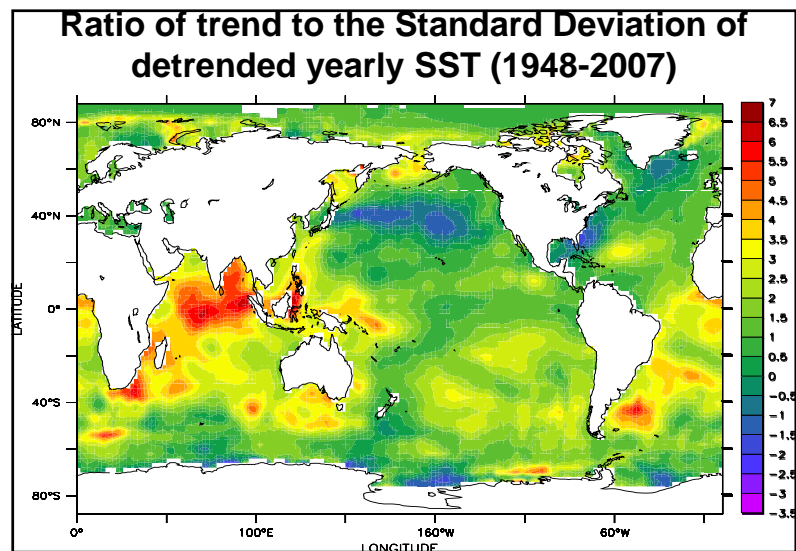
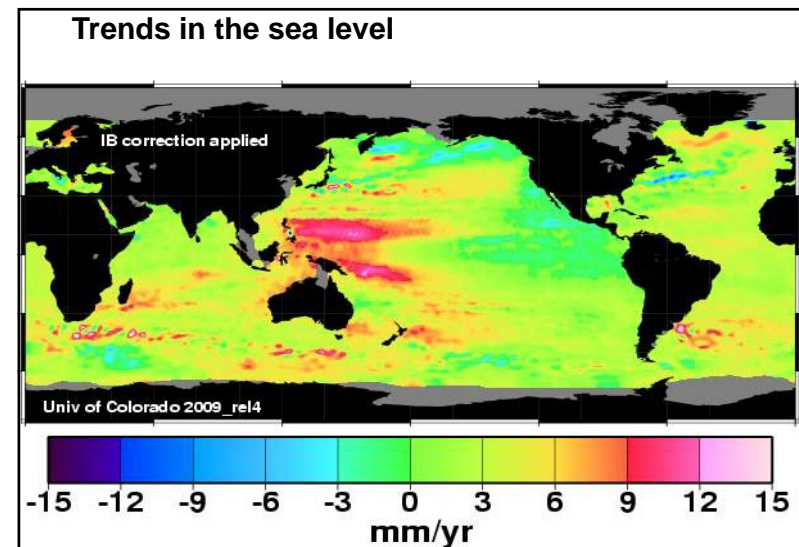
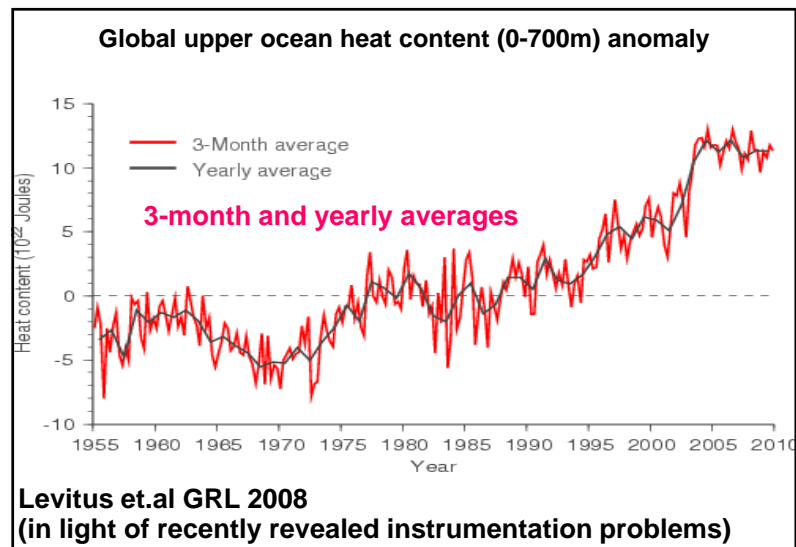
Climate Change “Detection and Attribution”

Sea level rise

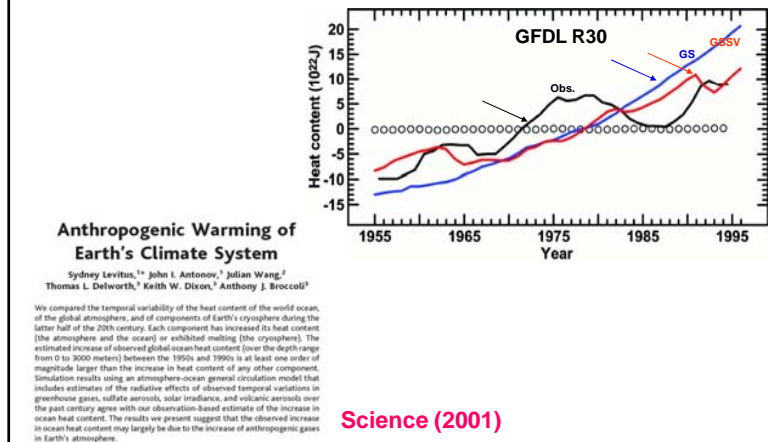
Critical for climate prediction

It influences the marine life as well





Do climate models simulate this ?



Can a stand alone ocean model then be able to simulate the OHC

If so, how good is the vertical thermal structure?

Do we actually expect the models to give D20 (D26) heat content ?

Or we expect the accurate thermal structure?

Two important issues:

1. Models often do not give the accurate vertical structure.
2. How do we incorporate the vertical profiles in a cyclone forecast model.

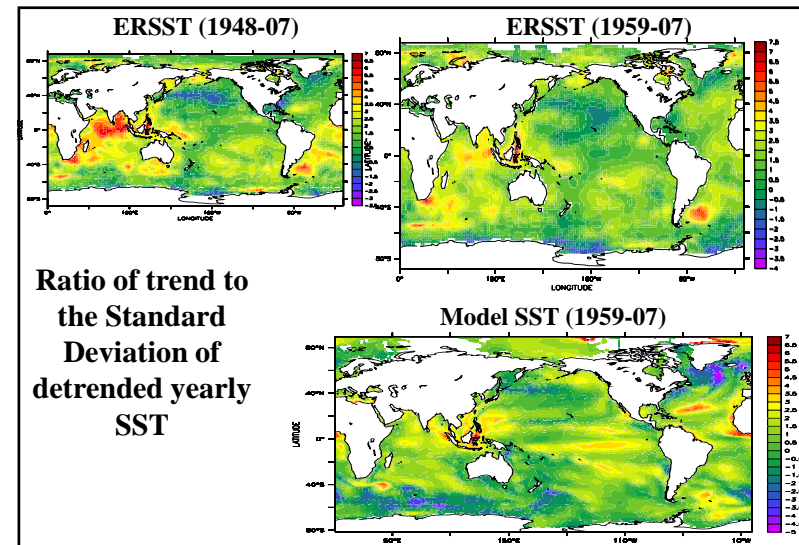
Data and models used

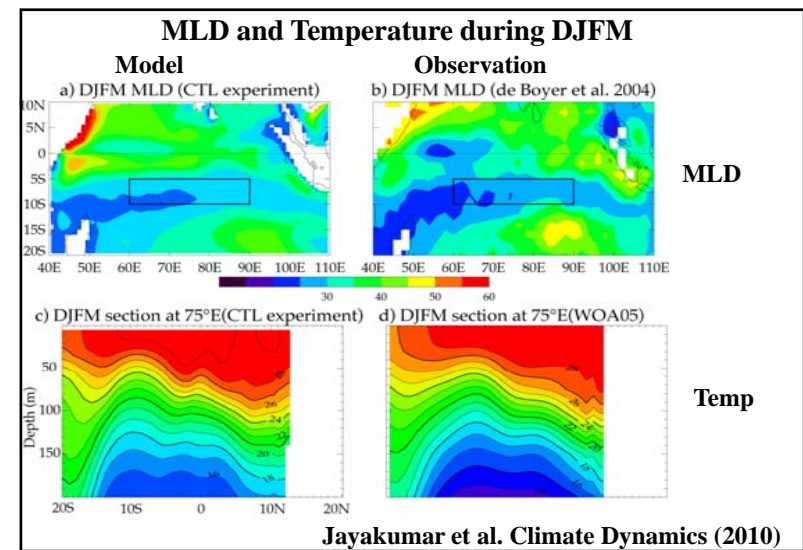
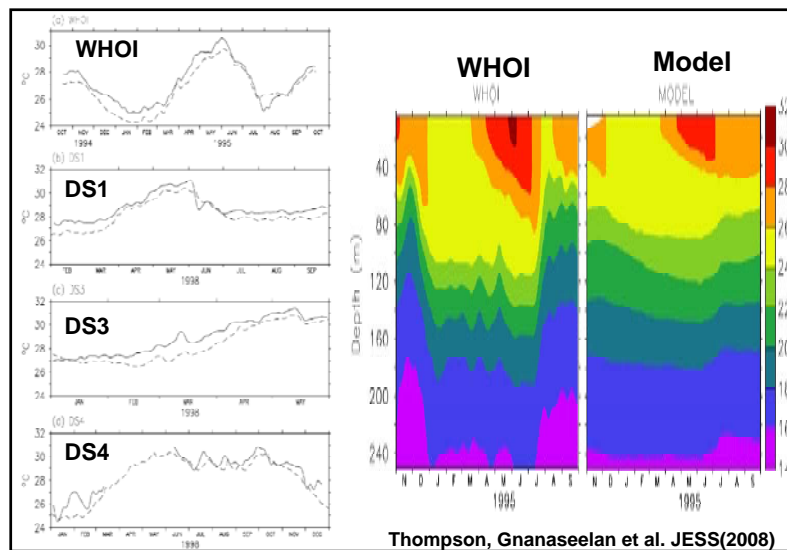
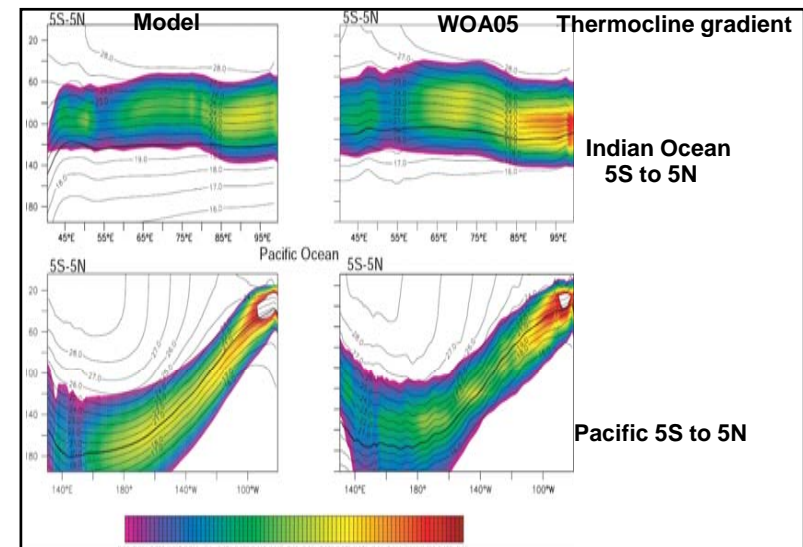
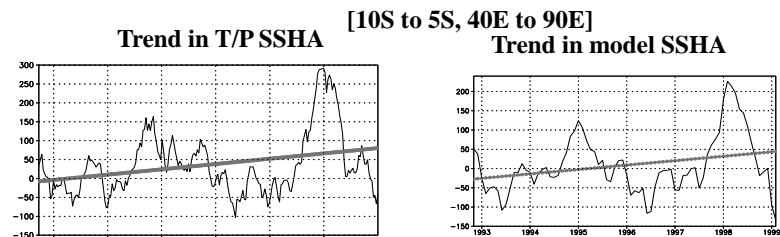
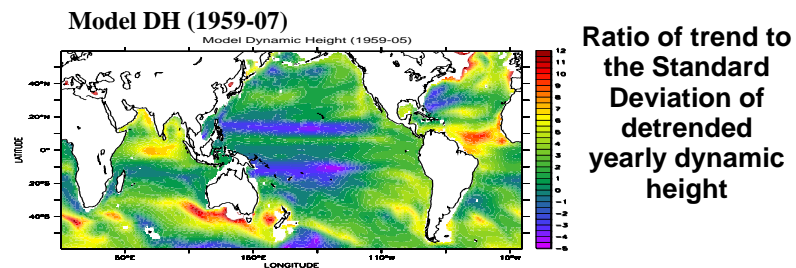
GFDL Modular Ocean Model, MOM4 (both Indian Ocean and Global ocean)

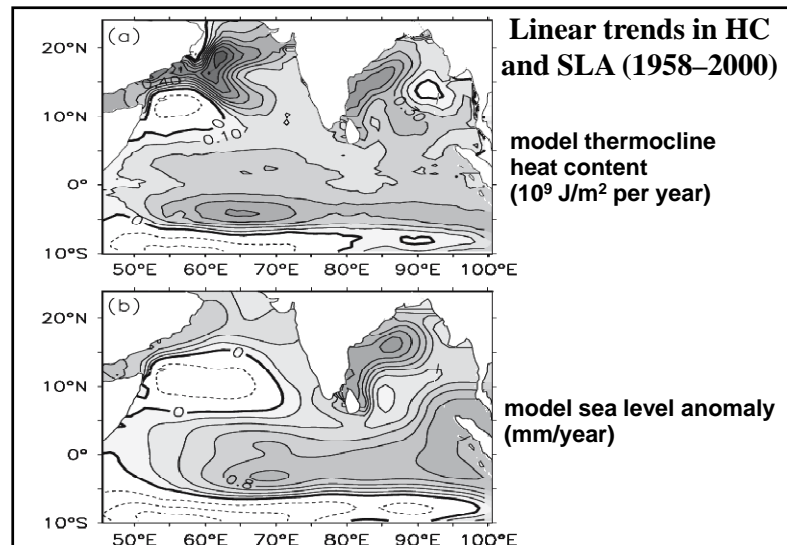
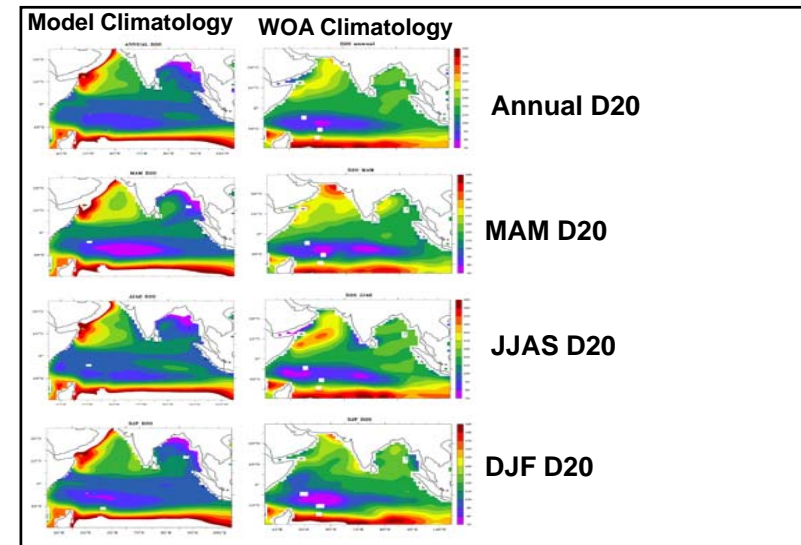
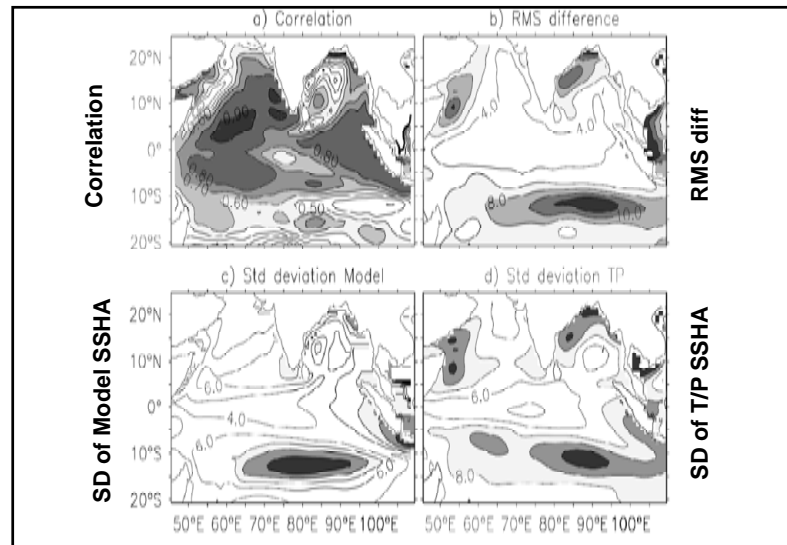
Satellite Altimetry data

Tide gauge data

Forcing data from NCAR







The sea level rise can be contributed by

Steric change (changes in thermal and haline structure of the oceans)

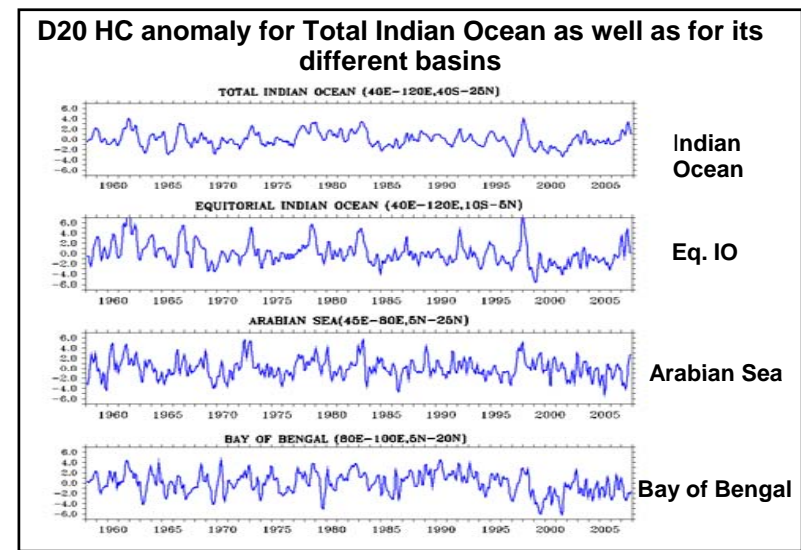
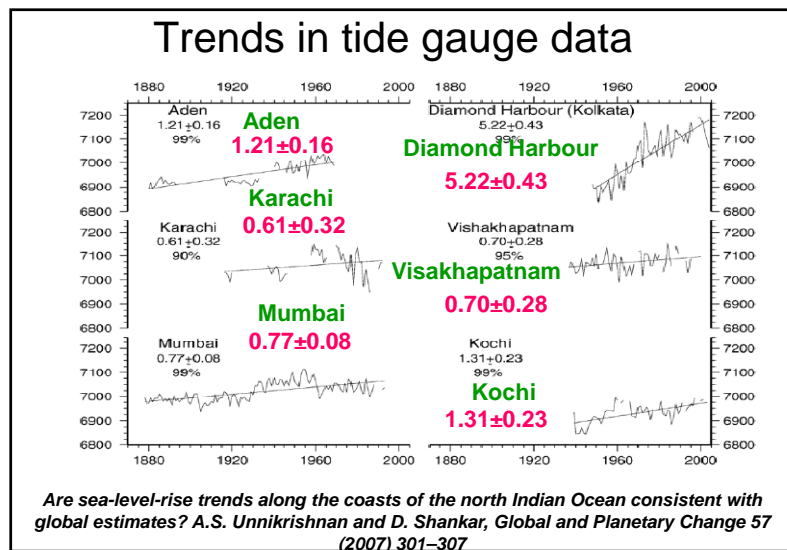
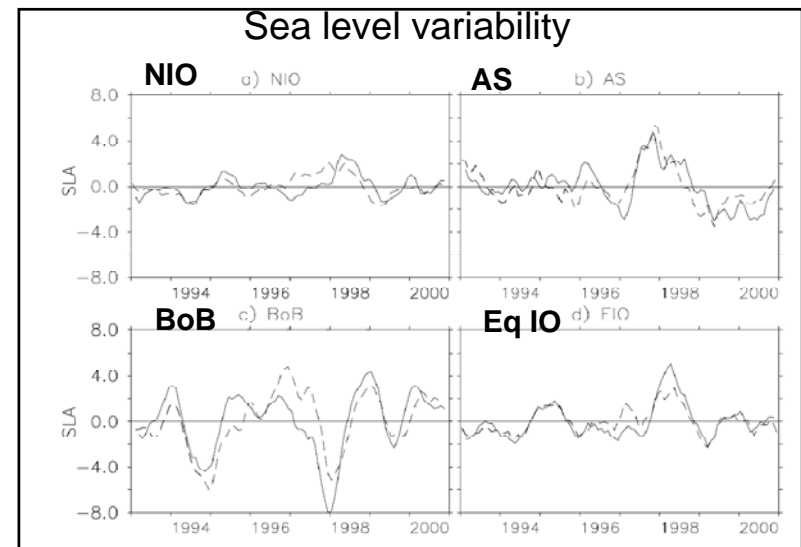
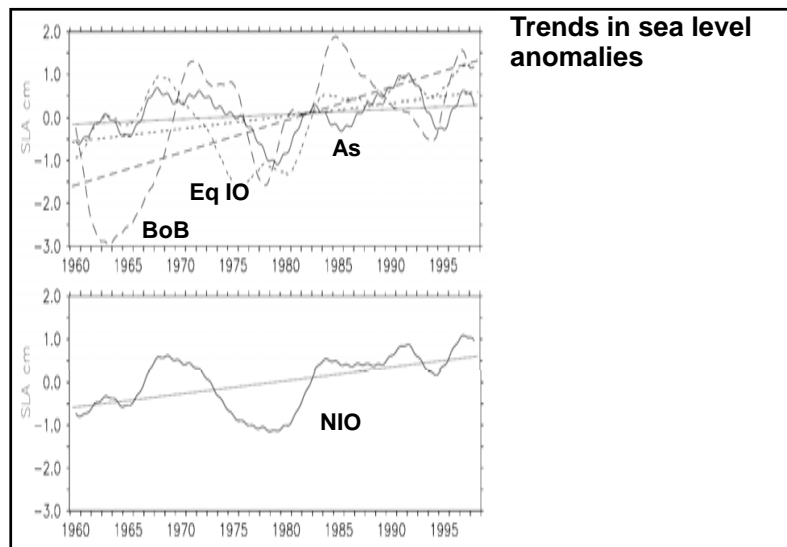
Mass change (melting of continental ice and filling of continental reservoirs)

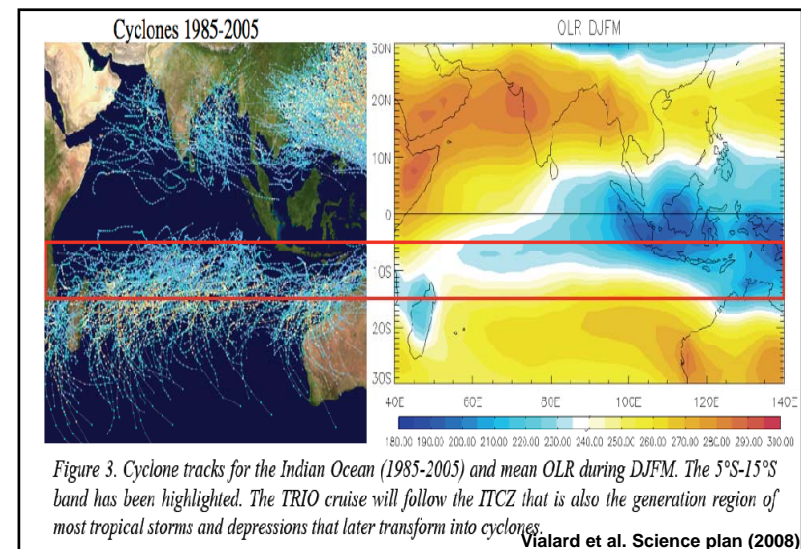
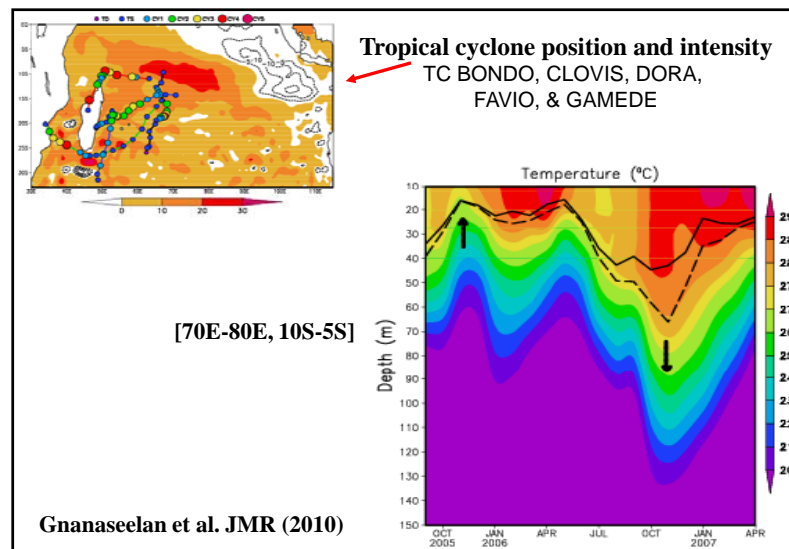
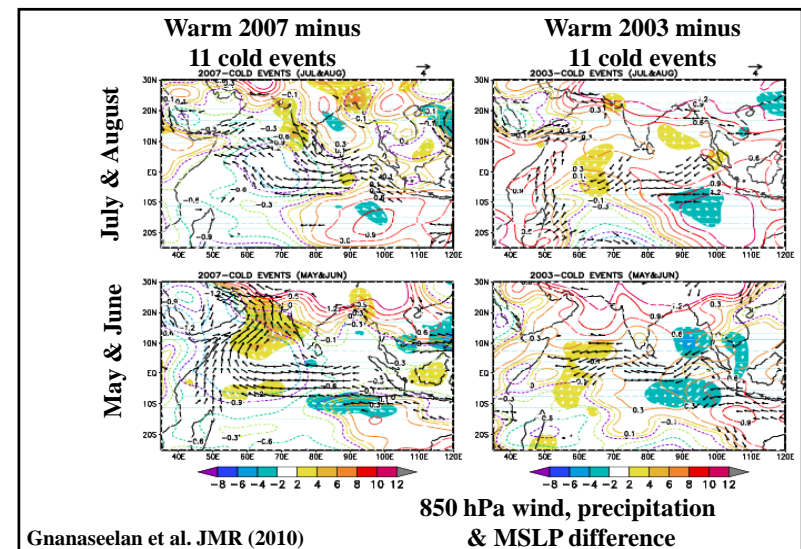
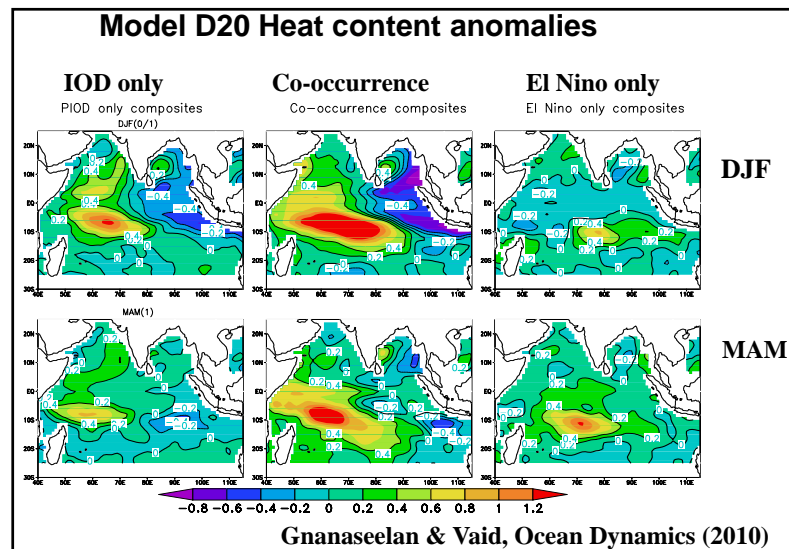
Geologic changes

Global average sea level rise 1.8 mm/year (1961-2003)

Contribution from thermosteric term $0.42 \pm 0.12 \text{ mm/year}$

Global average during 1993-2003 is 3.1 mm/year





Summary

There is a strong warming of the Indian Ocean in climate scale.

The ocean model is able to simulate the vertical thermal structure well.

The model thermocline heat content (of the north Indian Ocean) shows a linear increasing trend at the rate of 1.8×10^8 J/m² per year.

Thermosteric component of the North Indian Ocean sea level anomaly shows a linear increasing trend of 0.31 mm/year, is close to the global value.

Acknowledgements

Prof. B.N. Goswami, Director, IITM

Dr. M.M. Ali and NRSC

INCOIS and SAC

S. Rahul, A. Jayakumar, B. Thompson and S. Chakravorty

Simulation of Tropical cyclones over Indian seas: Impact of Remote Sensing Data

Prof. U. C. Mohanty
Centre for Atmospheric Sciences

Outlines

- ❖ Simulation of TCs with Different Initial and boundary Conditions
- ❖ Data impact studies
 - Satellite derived winds
 - DWR data impact
- ❖ Conclusions

INTRODUCTION

cyclone
requires accurate representation of the vortex in the
model initial conditions.

- ❖ The scarcity of observations both near and in the surrounding of vortex, causes ill defined centers/locations and poor structure of the storm.
- ❖ High resolution meso-scale models with variational data assimilation system plays an important role in improving model initial conditions and hence the forecast.

Contd...

- ❖ With the advancements of remote sensing observations (Satellite & Doppler Weather Radars), tropical cyclones can be monitored efficiently and hence can be used for more accurate prediction of extreme weather events.

Simulation of Tropical Cyclones with Different Initial and boundary Conditions (GFS, FNL and NCMRWF)

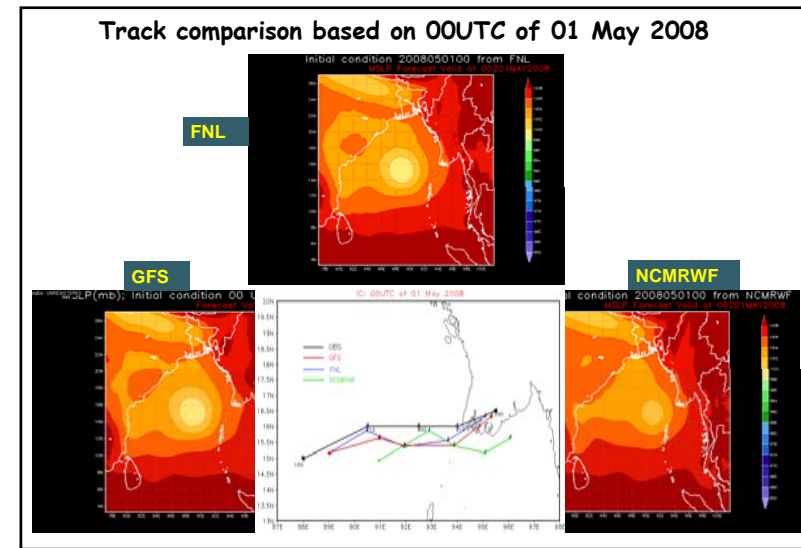
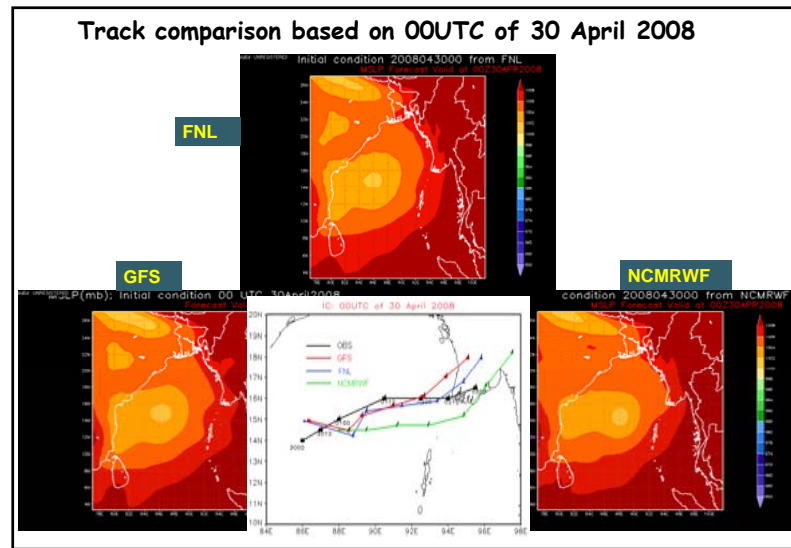
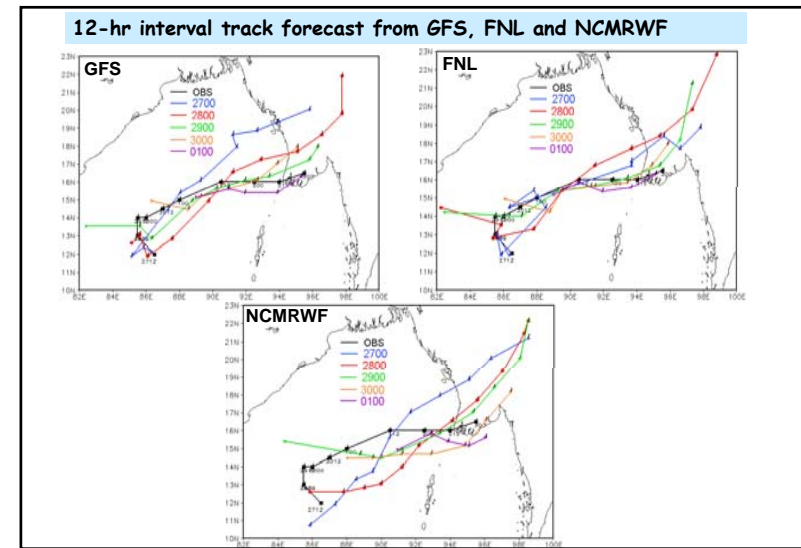
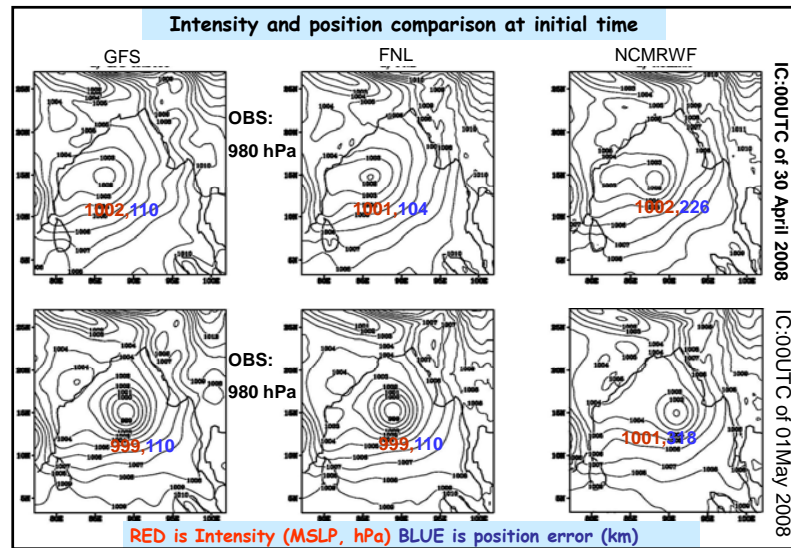
Overview of the WRF model

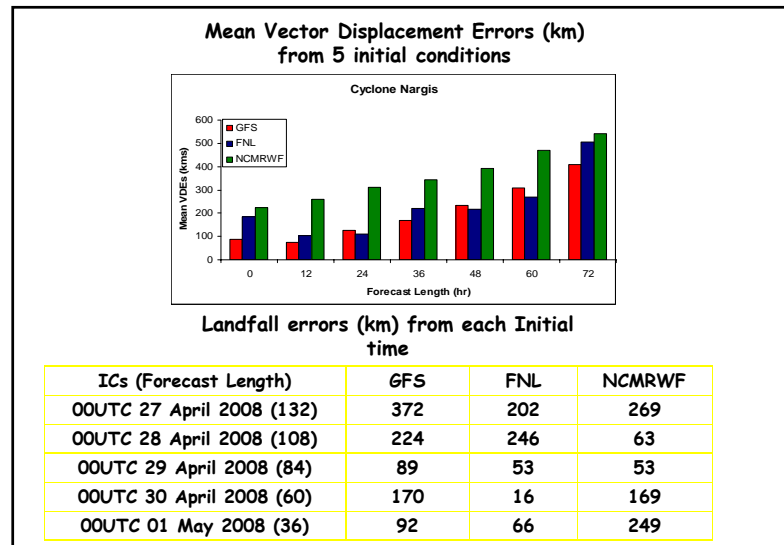
Dynamics	Non -hydrostatic
Domain	78E - 103 E and 3 N - 28 N
Number of domain	1
Horizontal grid distance	9 km
Map Projection	Mercator
Horizontal grid distribution	Arakawa C-grid
Vertical co-ordinate	Terrain-following hydrostatic-pressure co-ordinate (51 levels)
Time Integration	3 rd order Runge-Kutta
Spatial differencing scheme	6 th order centered differencing
Initial & boundary conditions	3-dimensional real data(FNL:1°X1°)
Microphysics	WSM-3 class simple ice scheme
Radiation Scheme	RRTM longwave and Dudhia's short wave radiation
Surface layer parameterization	Thermal diffusion scheme
Cumulus parameterization schemes	Kain Fristch
PBL parameterization	YSU scheme

Numerical Experiments with Different Initial Conditions

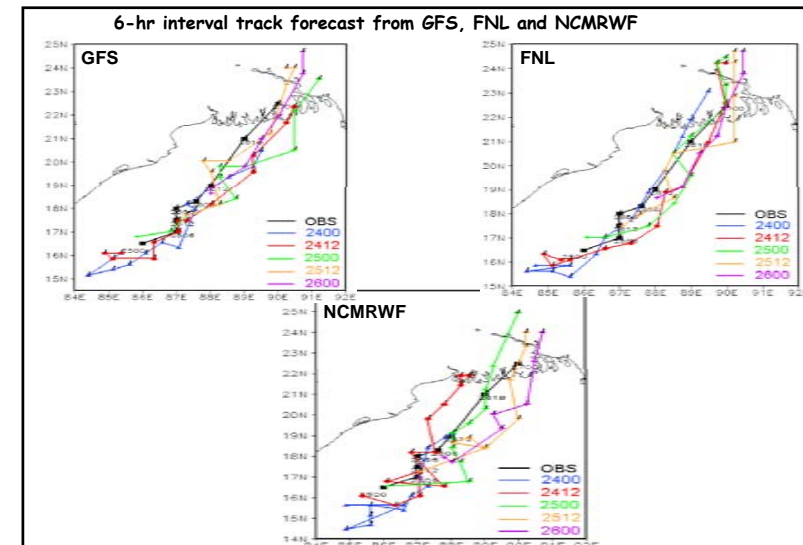
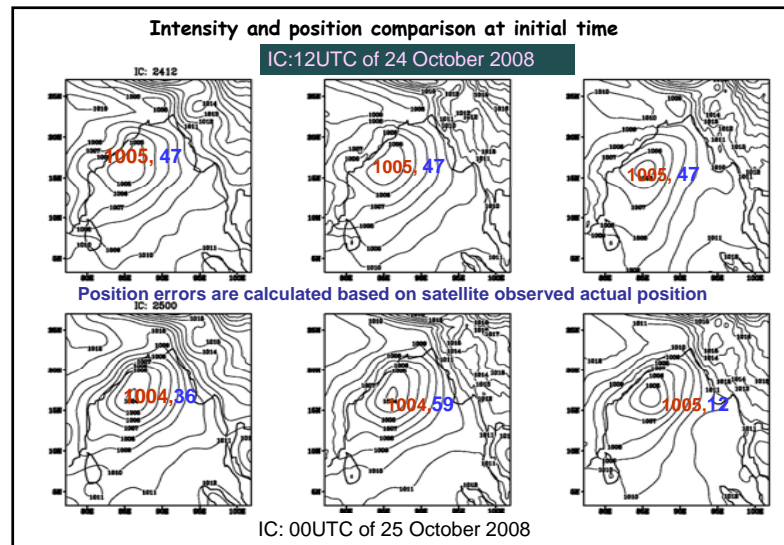
Initial Condition	Horizontal Resolution	Vertical Level	Lateral Boundary Condition
GFS Analysis	0.5° X 0.5°	27	NCEP GFS Forecast
FNL Analysis	1.0° X 1.0°	27	FNL Analysis
NCMRWF Analysis	0.5° X 0.5°	27	NCMRWF T-256L64 Operational Forecast

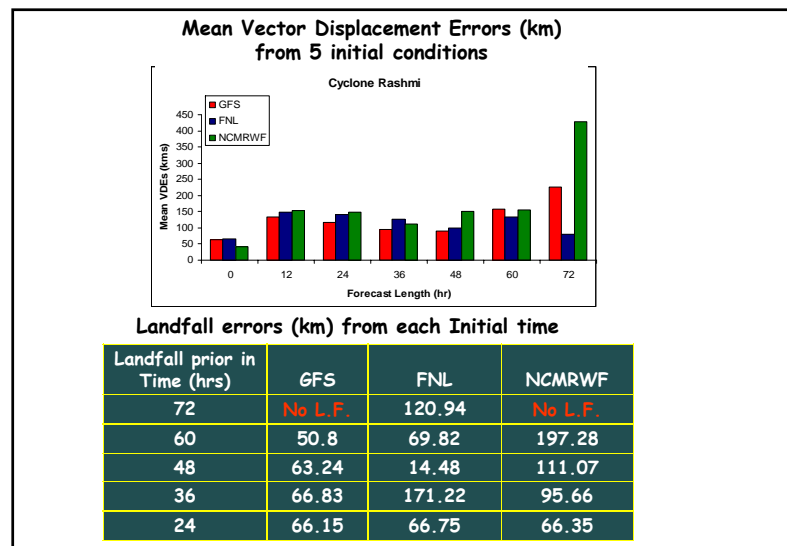
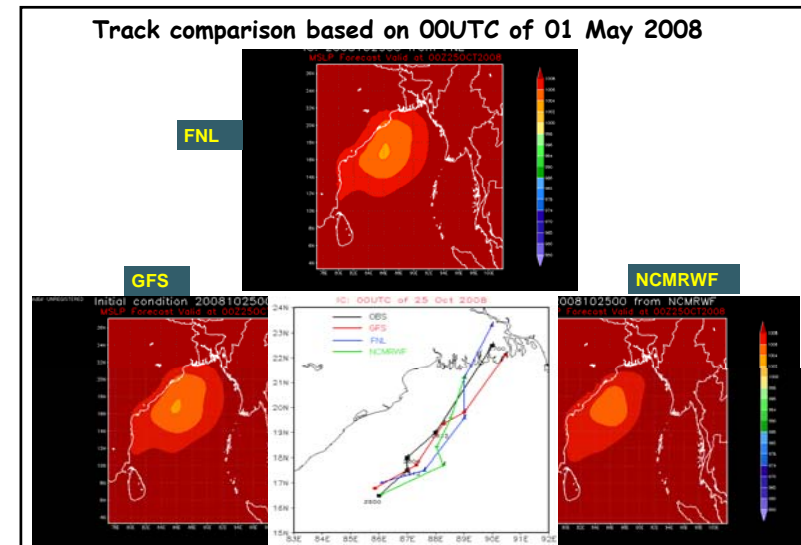
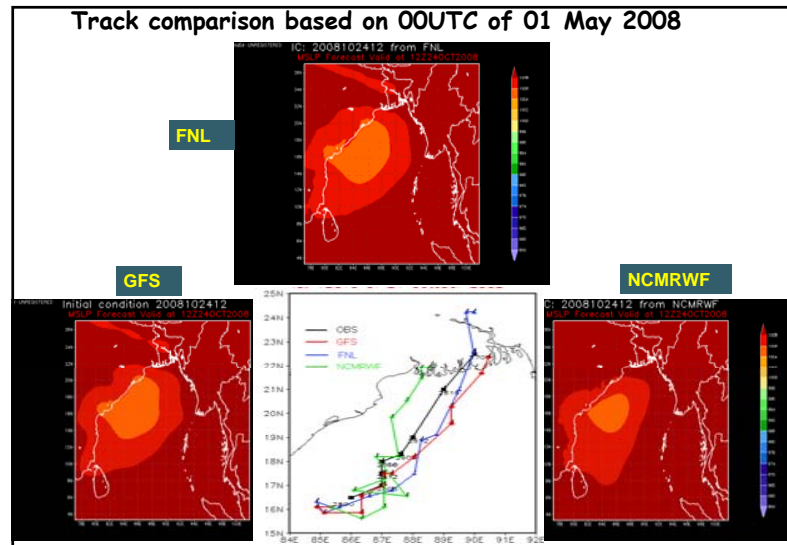
Nargis
(27 April to 3 May 2008)



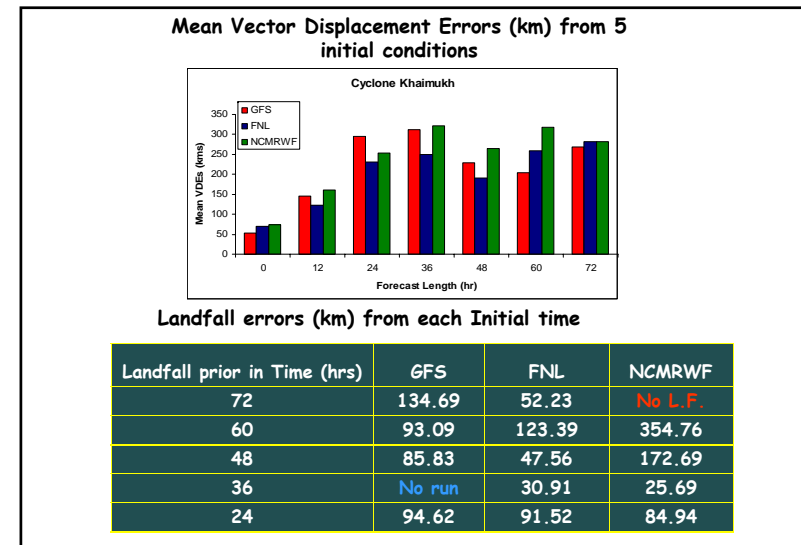
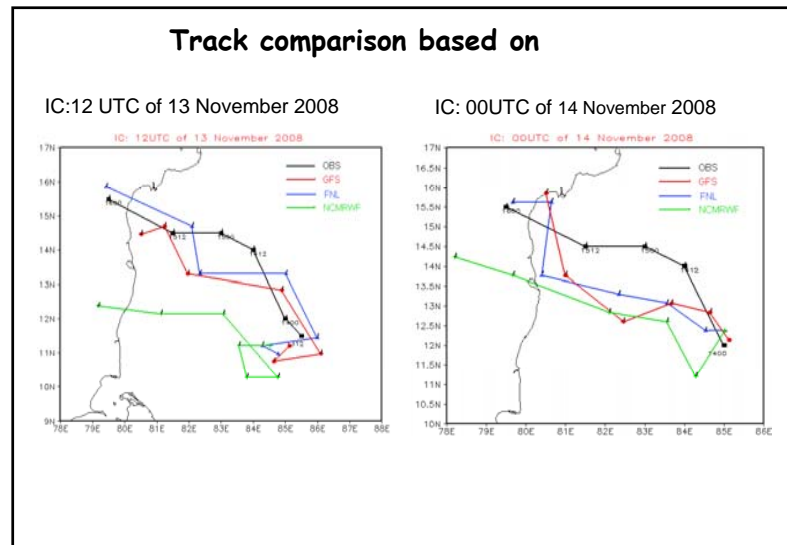
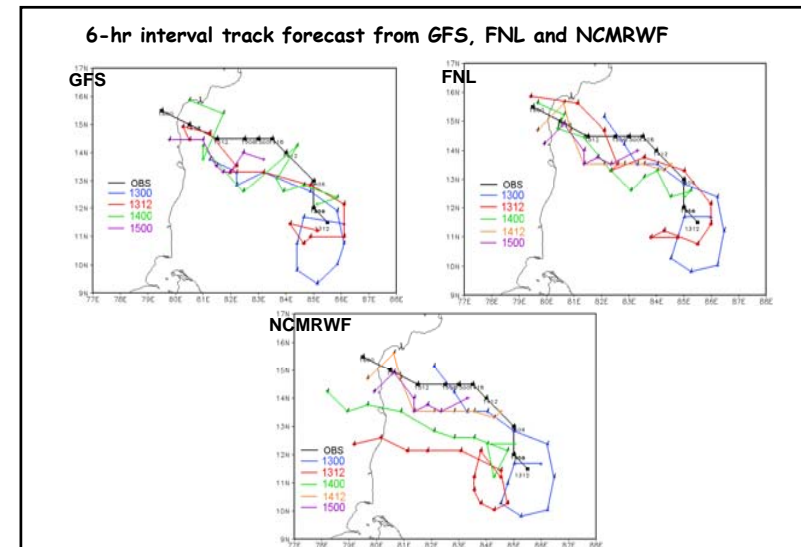
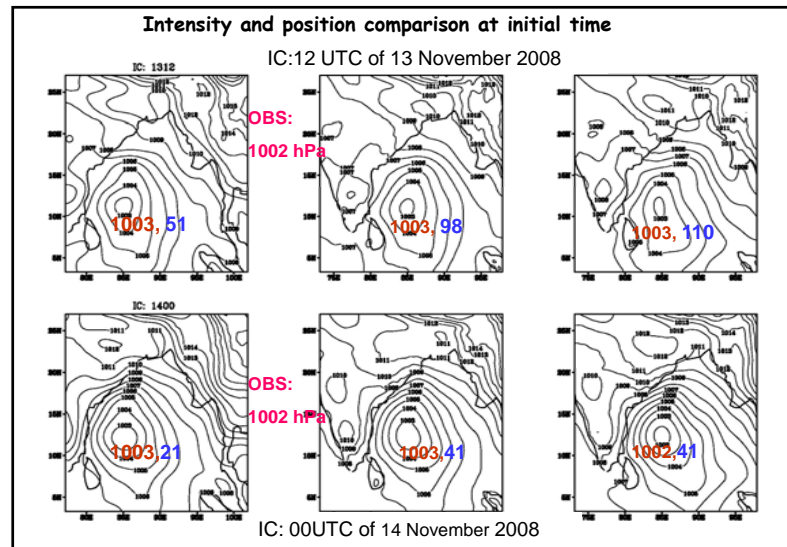


Rashmi (25 – 27 October, 2008)





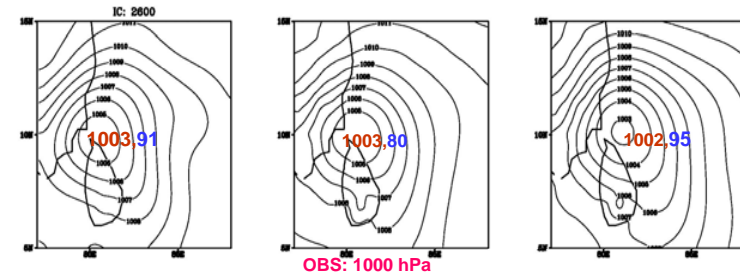
Khai-muk
(13 – 16 November 2008)



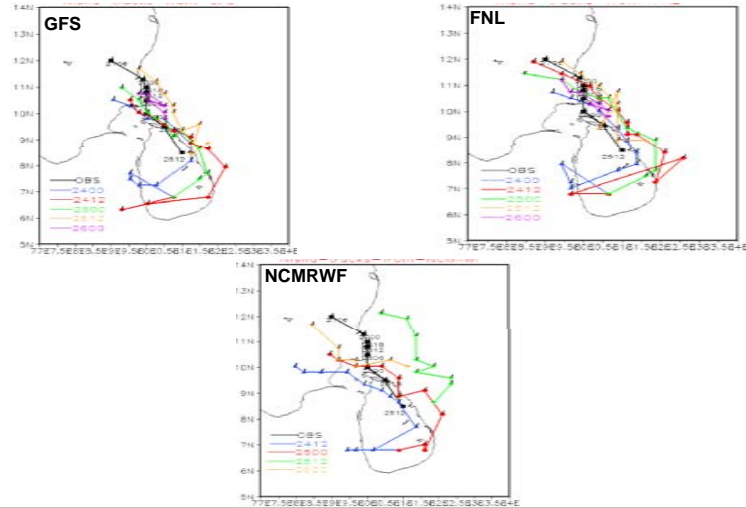
Nisha (25 – 27 November 2008)

Intensity and position comparison at initial time

IC:00UTC of 26 November 2008



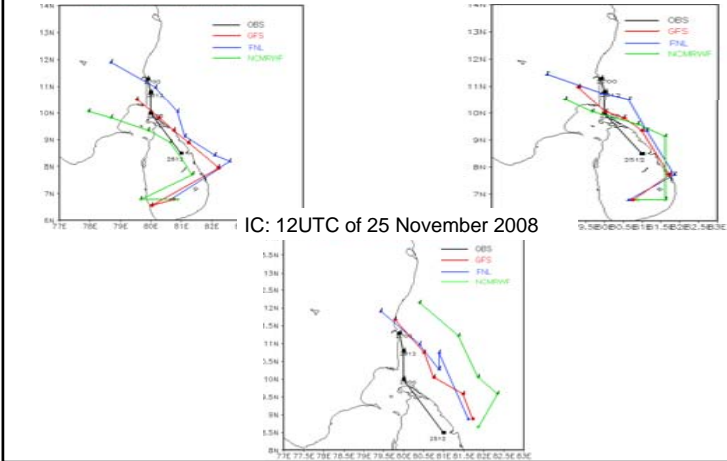
6-hr interval track forecast from GFS, FNL and NCMRWF

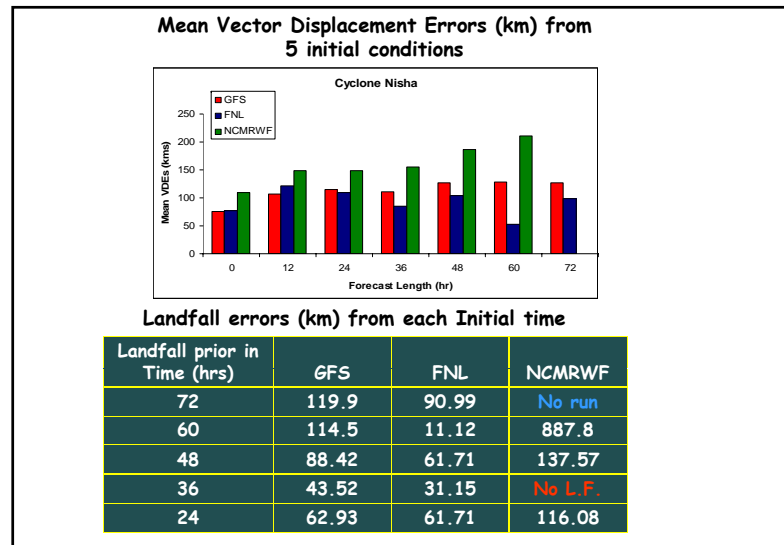


Track comparison based on

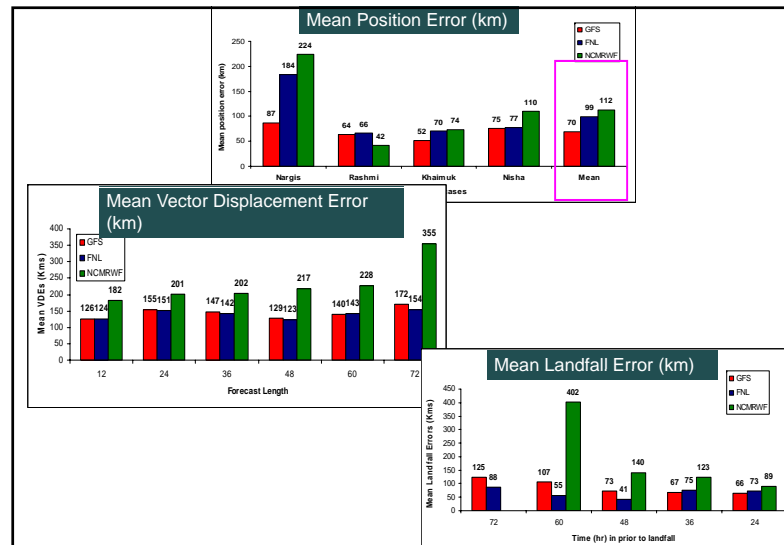
IC: 12UTC of 24 November 2008

IC: 00UTC of 25 November 2008





Mean Error Statistics of Track Forecast (GFS-19, FNL-20, NCMRWF-19)



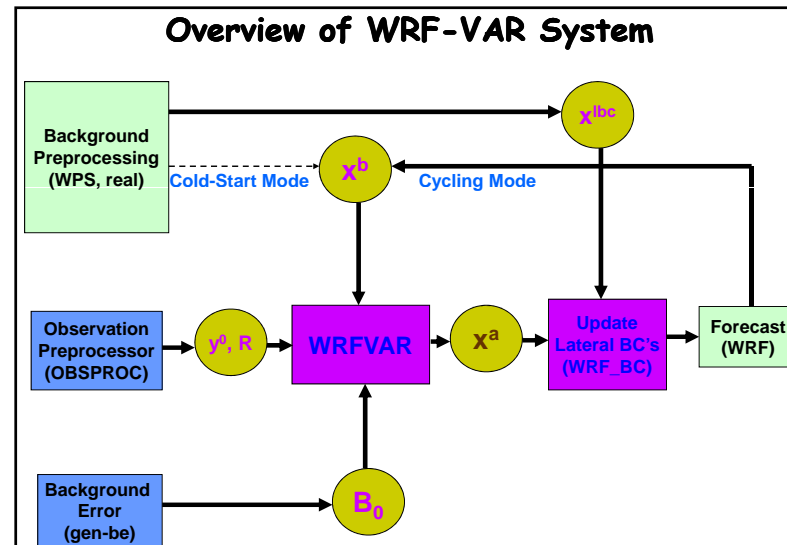
Conclusions

- FNL as initial and boundary conditions could predict the tracks up to landfall with minimum errors and the mean track errors valid for 24-hr, 48-hr and 72-hr forecast are 151, 162 and 242 km respectively.
- The landfall errors in FNL experiment is also quite less compared to GFS and NCMRWF experiments.
- The use of NCMRWF analyses/forecast fields, the model could predict the intensity better for the cyclones with extreme eastward re-curvature.

Impact of Satellite derived winds Assimilation on Track and Intensity

WRF-ARW modeling systems
with 9km resolution

1. Initial vortex position
2. Track and intensity
3. Precipitation

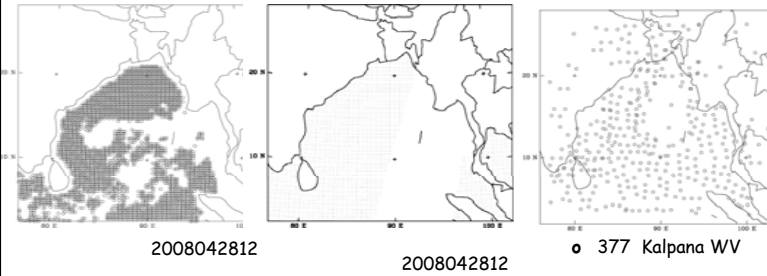


➤ Data used in the Assimilation
Derived winds of
QSCAT (wind speed and direction)
SSM/I (wind speed) and
Kalpana water vapor wind and CMVs

Cyclone	Location	Initial condition (GFS)
NARGIS (27 April - 3 May 2008) (5 Cases)	BOB	00UTC of 28 April 2008 12UTC of 28 April 2008 00UTC of 29 April 2008 12UTC of 29 April 2008 00UTC of 30 April 2008
GONU (2 - 7 June 2007) (4 Cases)	Arabian Sea	00UTC of 2 June 2007 12UTC of 2 June 2007 00UTC of 3 June 2007 12UTC of 3 June 2007

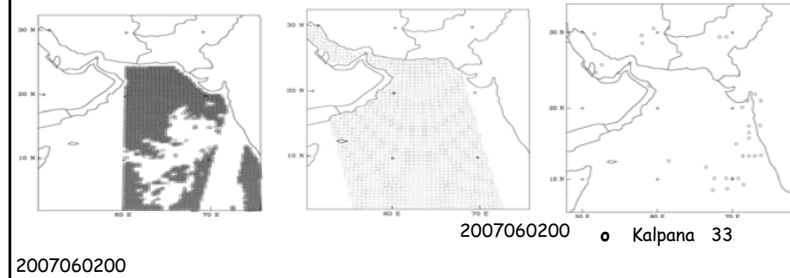
model initial condition of TC NARGIS

SSM/I, QSCAT and Kalpana winds for 12 UTC of 28 April 2008

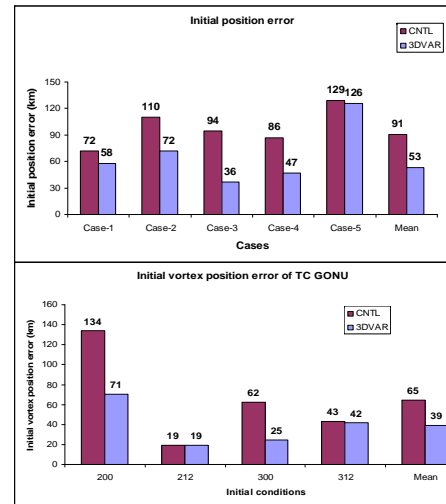
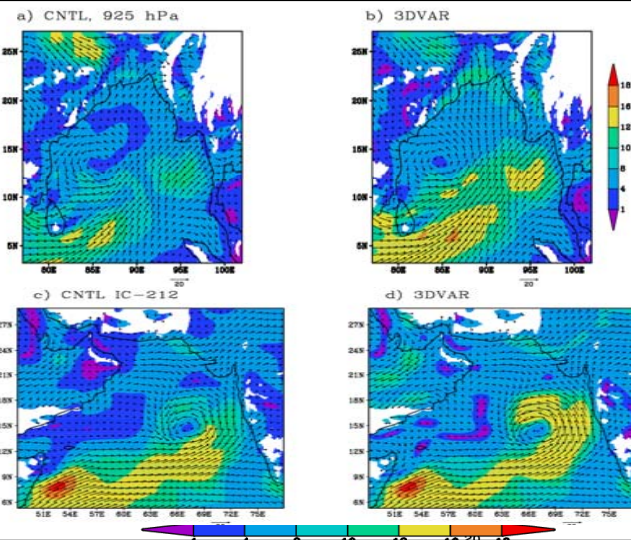


model initial condition of TC GONU

SSM/I, QSCAT and Kalpana winds for 00UTC of 2 June 2007

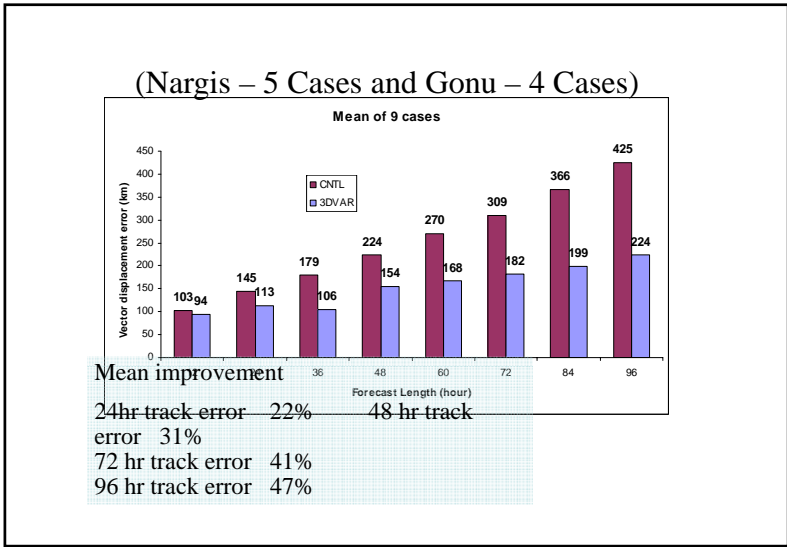
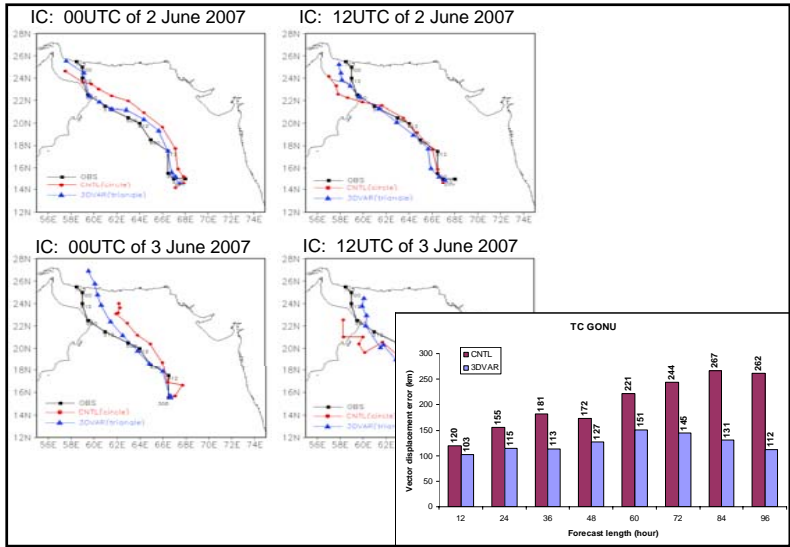
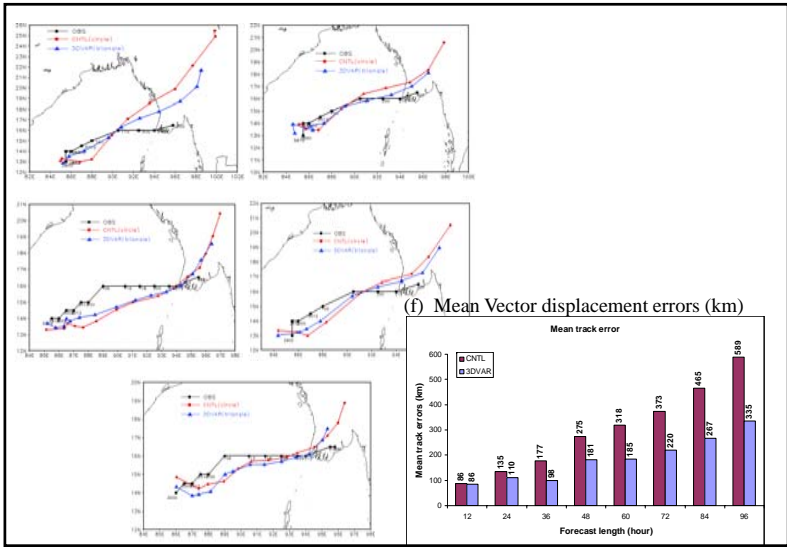
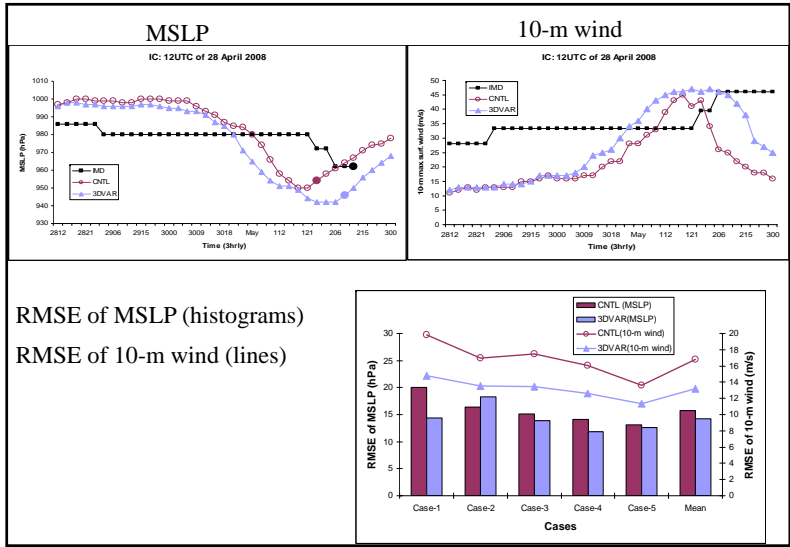


Improvement in initial wind field
NARGIS IC: 12UTC
of 28 April 2008



41 % Improvement

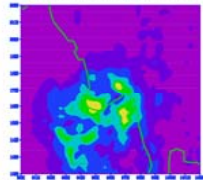
39 % Improvement



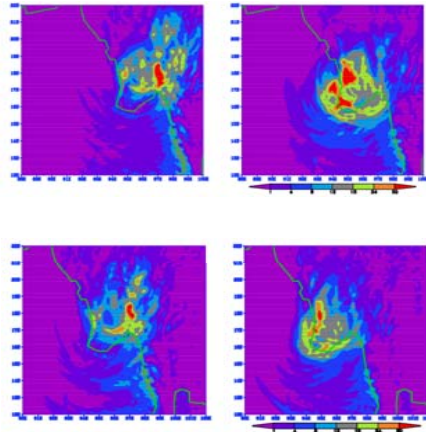
24-hr accumulated rainfall valid at landfall for TC NARGIS

IC: 12UTC of 28 April

d) TRMM (03UTC of 02-03)



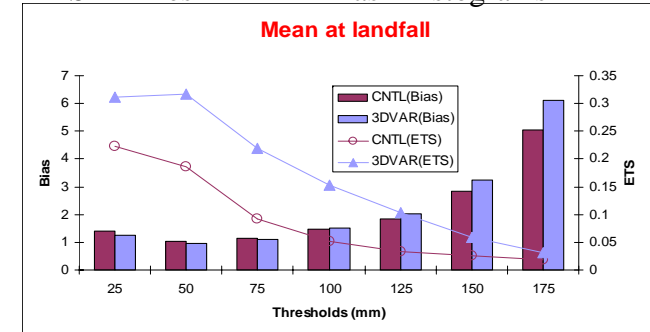
IC: 12UTC of 29 April



Mean (of 5 cases) ETS and Bias of 24-hr accumulated rainfall (mm) valid for landfall

ETS - Lines

Bias - histograms



Conclusions

- The inclusion of satellite derived winds through 3DVAR data assimilation system contributes significant improvement in simulation of intensity, structure and track of tropical cyclones.
- Out of 9 cases (5 cases from TC Nargis & 4 cases from TC Gonu), the initial position of vortex improves in 7 cases by about 35%.
- The 24, 48, 72 and 96 hours mean track forecast improves by 22%, 31%, 41% and 47% respectively.

Impact of DWR data on Track and Intensity Prediction

Experiments and Data used

Three numerical experiments are carried out

CNTL - With out Data Assimilation

GTS - With Assimilation of GTS data

DWR - Assimilation of GTS + DWR data

GTS includes : SYNOP, AWS, SHIP, TEMP, PILOT,
BUOYS, SATOB, SATEM, AIREP etc.

DWR includes : Reflectivity and Radial velocity of Kolkata
DWR

DWR Data thinning procedure

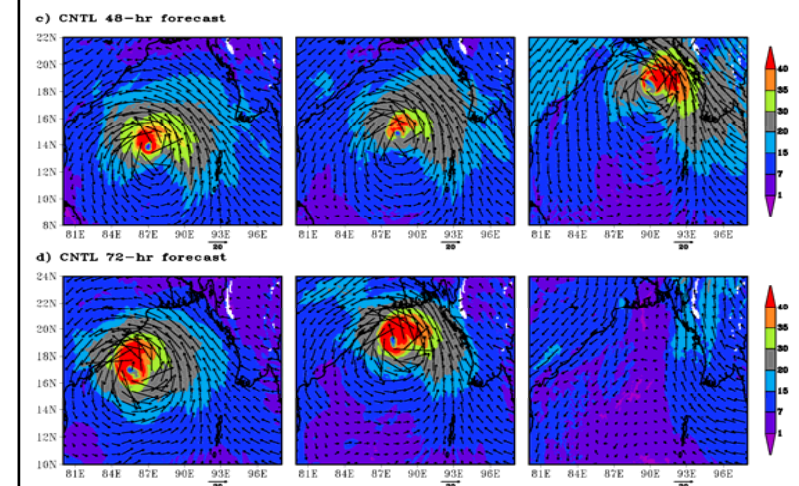
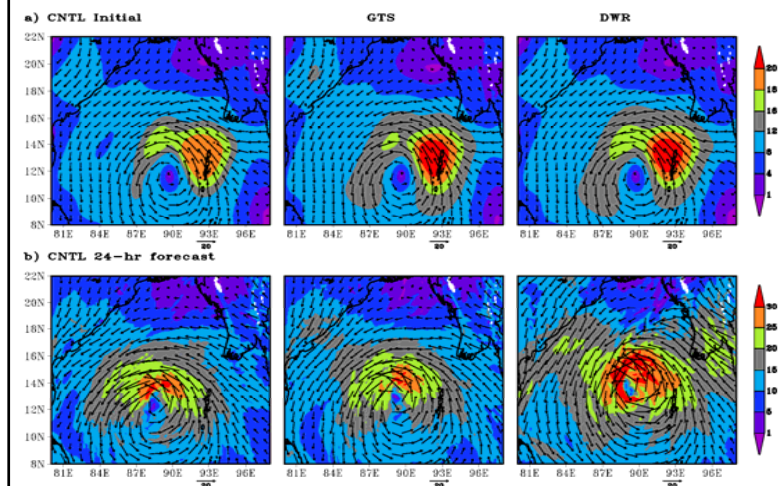
DWR provides very dense data (0.5 km resolution)

The thinning procedure for radial velocity and reflectivity is:

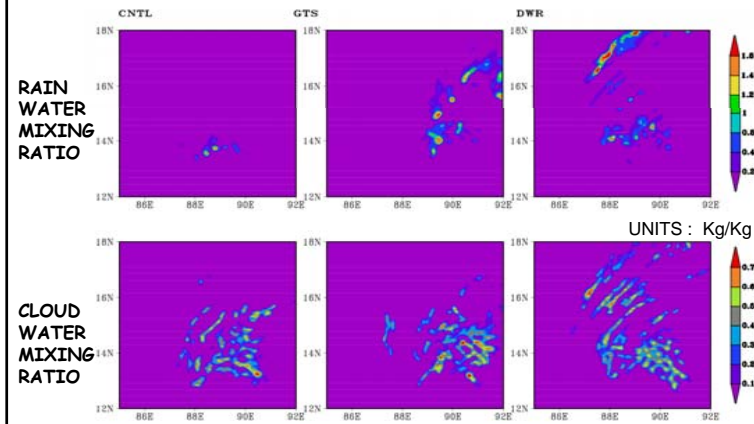
Reflectivity= 10 to 60 dBz

Radial Velocity (Absolute value)= 2 to 30 m/s

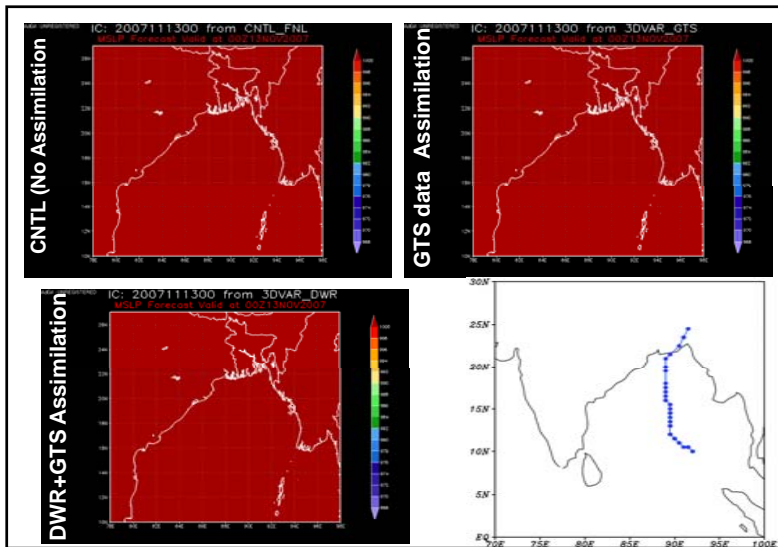
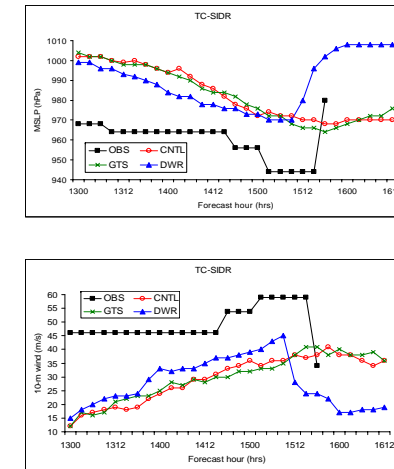
Structure changes in 850-hPa wind field



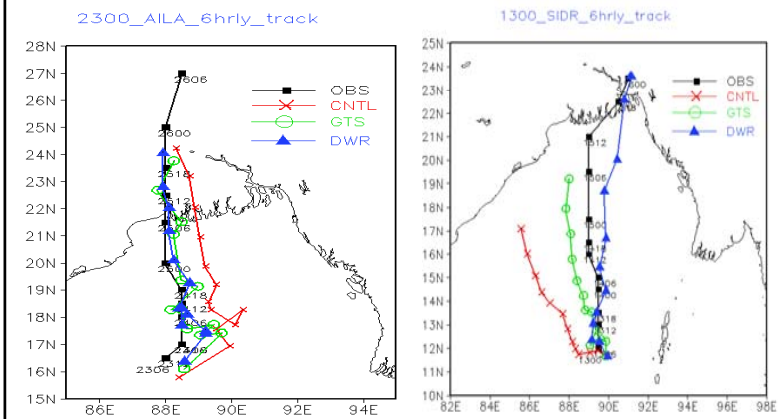
Simulation of hydrometeors (6-hr forecast)

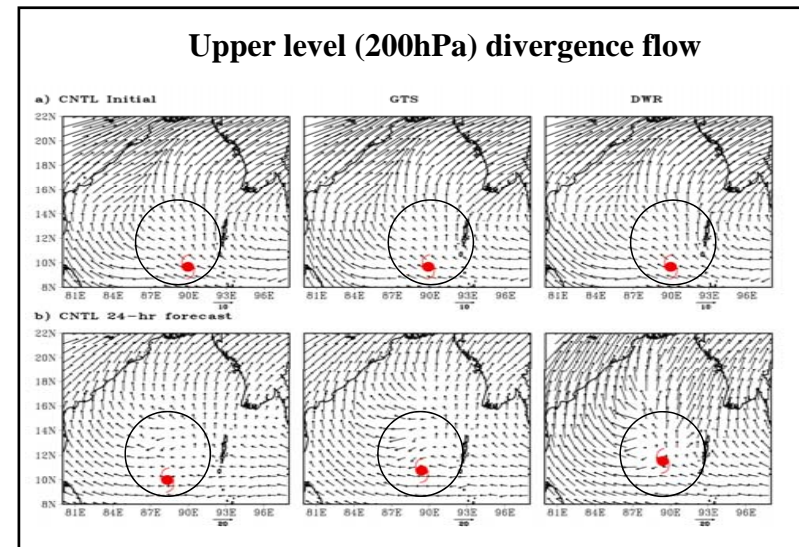
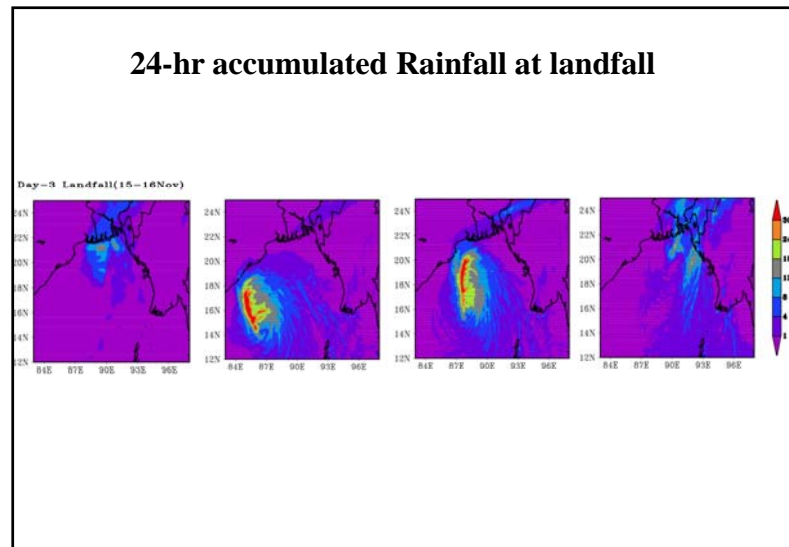
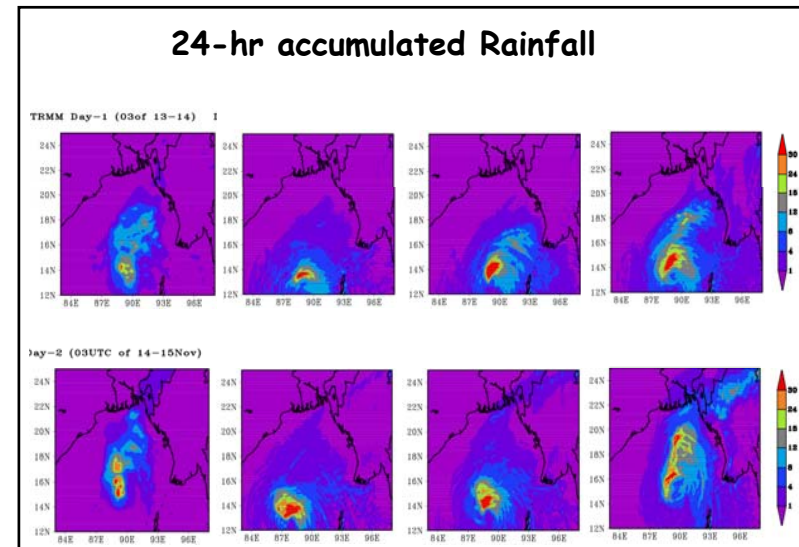
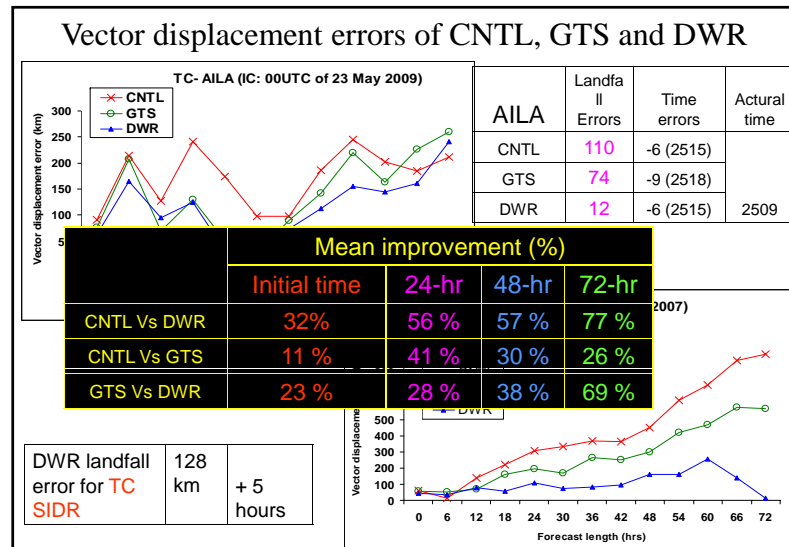


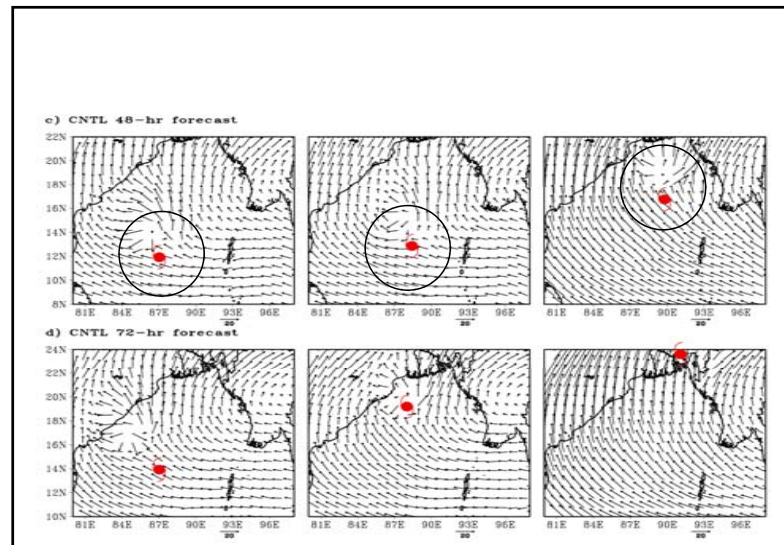
3-hrly intensity prediction



Track Prediction in 6-hr interval



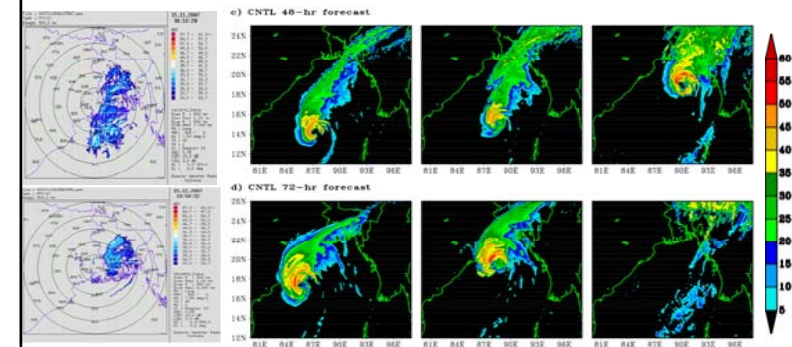




Conclusions

- ❖ The initial structure of TC vortex is significantly well simulated with the DWR data assimilation compared to FNL initial values.
- ❖ DWR data improves the hydrometeors (rain water and cloud water) prediction. Hence, the intensity is also improved in first 24-30 hr forecasts.
- ❖ It is very clear that the track prediction improves significantly (particularly in the case of SIDR) with GTS and DWR data assimilation. However, the experiment with DWR indicates the need of high dense data over the oceanic region for predicting the track.
- ❖ With the improved intensity and track, the rainfall is also well predicted in DWR assimilation experiment.

Model simulated Radar Reflectivity



Overall Conclusions

- ❖ FNL as initial and boundary conditions could predict the tracks up to landfall with minimum errors and the mean track errors valid for 24-hr, 48-hr and 72-hr forecast are 151, 162 and 242 km respectively.
- ❖ The inclusion of satellite derived winds through 3DVAR data assimilation system contributes significant improvement in simulation of intensity, structure and track of tropical cyclones.
- ❖ The 24, 48, 72 and 96 hours mean track forecast improves by 22%, 31%, 41% and 47% respectively.
- ❖ The storm is better represented in terms of intensity and precipitation with satellite derived SST.

- ❖ It is very clear that the track prediction improves significantly (particularly in the case of SDR) with GTS and DWR data assimilation. However, the experiment with DWR indicates the need of high dense data over the oceanic region for predicting the track.
- ❖ The influence of SST gradient is significant not only in intensification and movement but important also for the genesis of the storm.

Future Scope

- Further improvement in track & intensity prediction can be achieved with more satellite products (such as radiance data assimilation).
- The use of multi radar data may be the future step towards DWR data assimilation.
- Vortex re-location and initialization can further improve the initial position of the vortex and hence the

Oceanic heat content studies using insitu and satellite data

V. V. Gopalakrishna¹, M. M. Ali², P.V. Nagamani²,
Nisha Kurian¹, Amit Naik¹, Gustavo Goni³ and Pedrov³

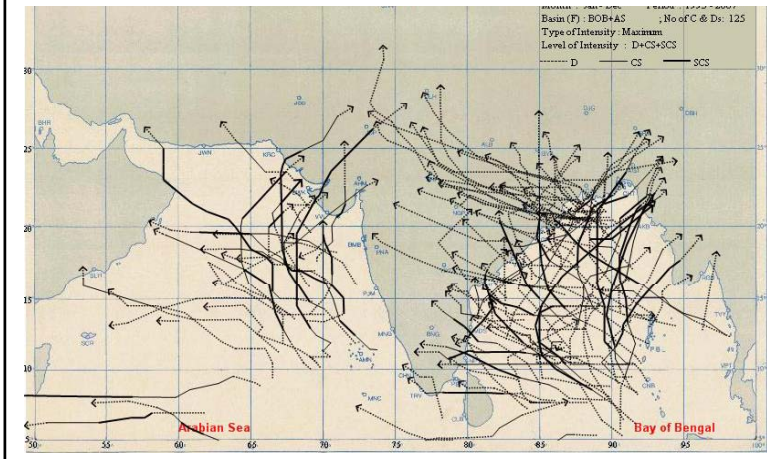
1 National Institute of Oceanography, Goa India

2 National Remote Sensing Centre

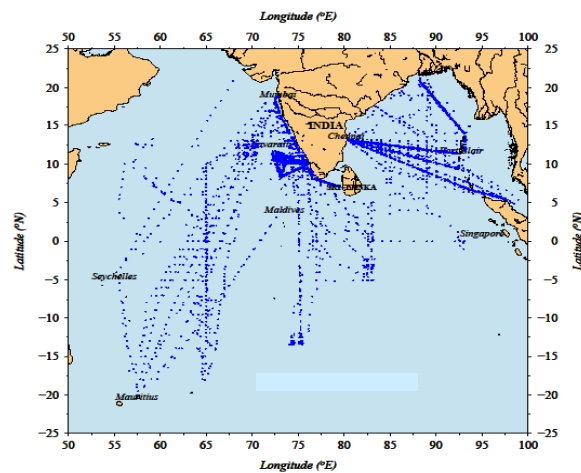
3 AOML, NOAA ,USA



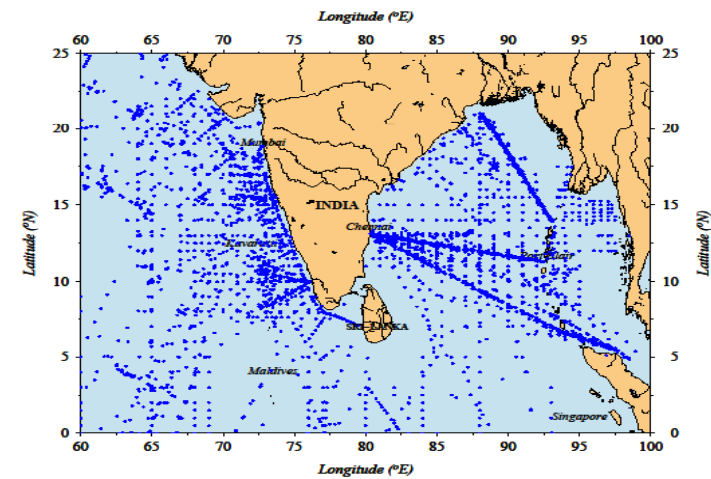
Tracks of severe cyclonic storms during 1993-2009



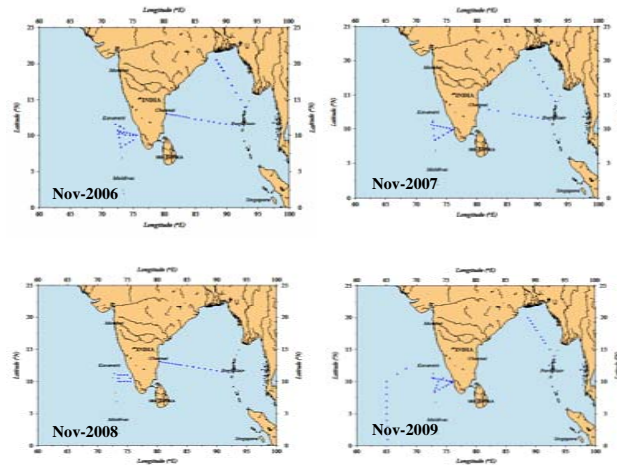
XBT/XCTD data density under the Indian program



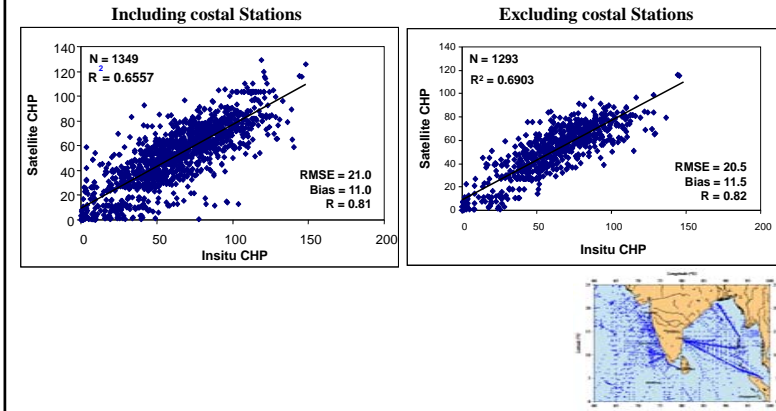
Data used for the present study



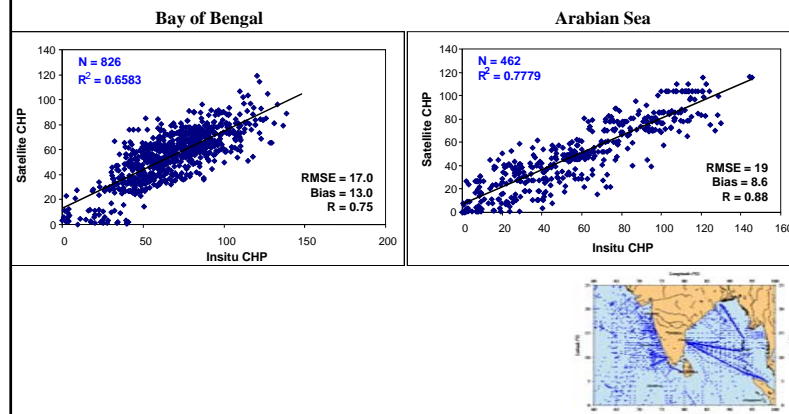
Typical data density for the month of November



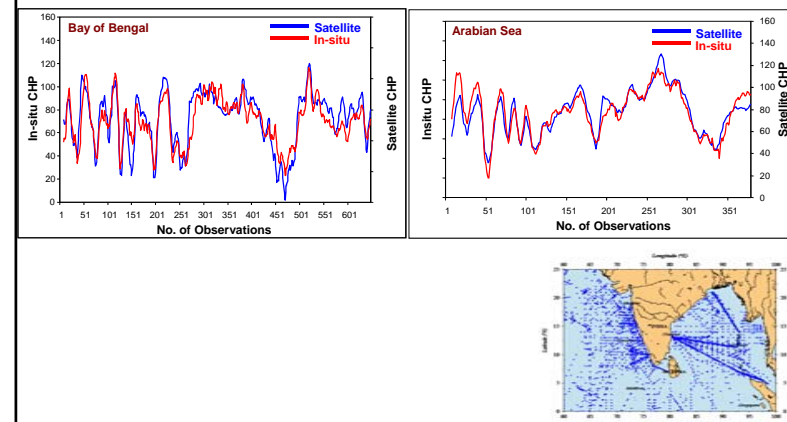
Comparison of Insitu and Satellite measured CHP values for the Indian Ocean

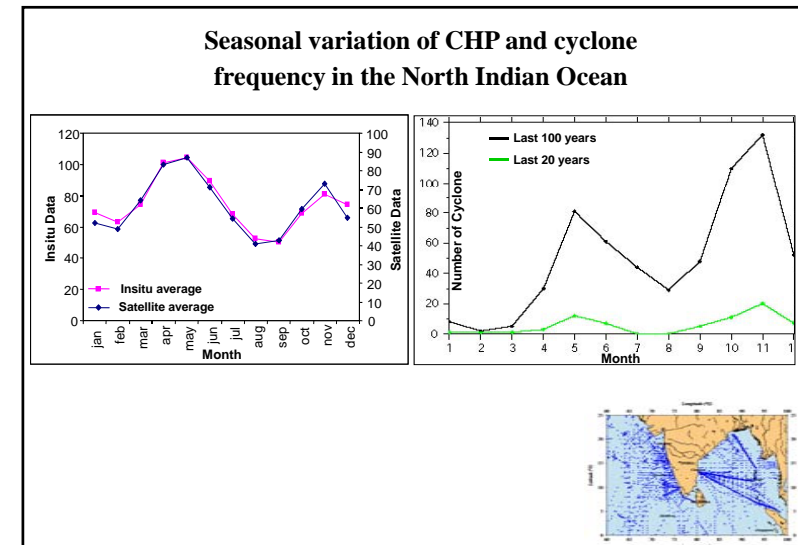
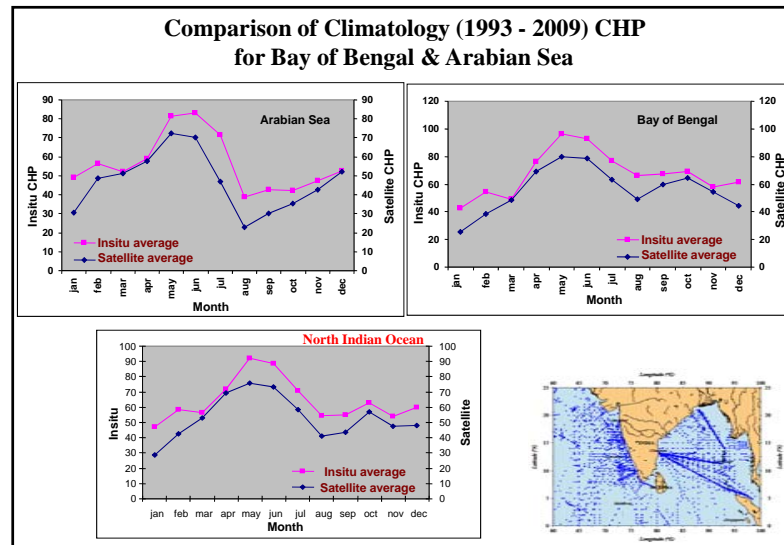


Comparison of Insitu and Satellite measured CHP values for the Bay of Bengal & Arabian Sea



Moving averages between Satellite & Insitu CHP





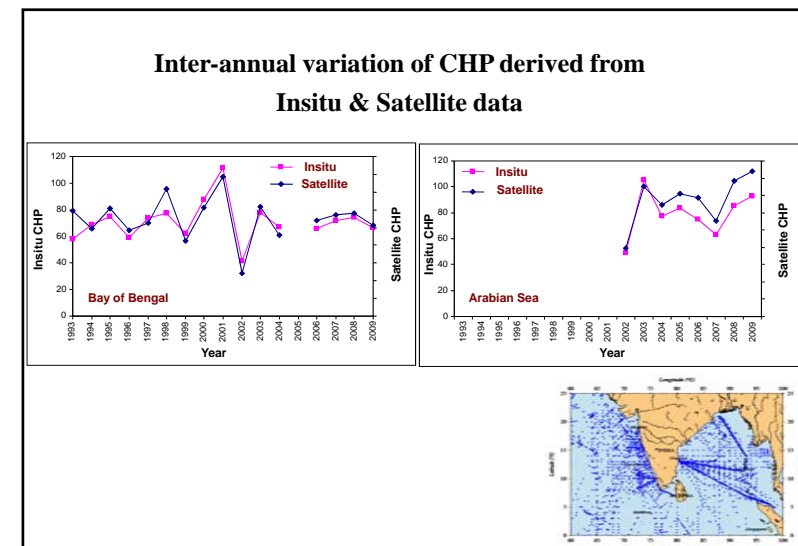
SUMMARY

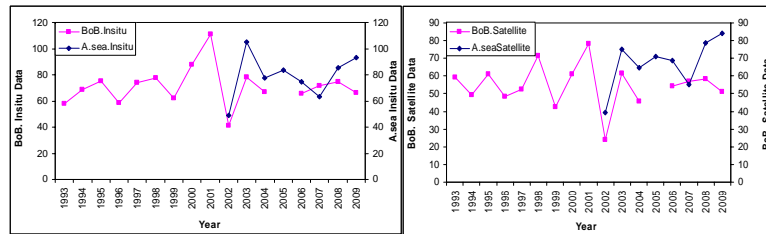
- ❖ Compared the CHP computed using Insitu & Satellite data.
- ❖ Estimations match well for the North Indian Ocean.
- ❖ However, a few satellite derived CHP values do not match with the Bay values.

	Arabian Sea	Bay of Bengal
R^2	0.7779	0.6583
RMS	19	17
Slope	0.74	0.6193
Bias	0.88	0.75

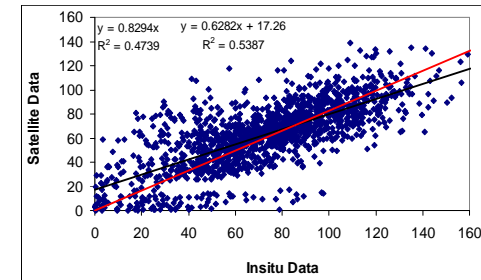
- ❖ Satellite derived CHP values can be conveniently used to study the temporal & spatial variability.

11





Comparison of Insitu and Satellite measured TCHP values for Indian Ocean



Before Removing the Coastal stations data

Annexure-5

Invitees and Resource Persons

List of Invitees and resource persons

Sl. No.	Name of the Invitee	Designation	Institute	
International				
1	Dr. Gustavo Goni	Director, POD	AOML, NOAA	Could not attend, but lecture notes available
2	Prof. Lynn Shay	Professor	University of Miami	
National				
1	Dr. S. K. Roy Bhowmik	Director (NWP)	IMD, New Delhi	
2	Dr.Y.Sadhuram	Scientist-F	NIO-RC	
3	Prof. U.C. Mohanty	Professor	IIT-delhi	
4	Prof. Debasis Sengupta	Professor	CAS	
5	Dr. C. Gnanaseelan	Scientist	IITM	
6	Dr. M. R. Ramesh kumar	Scientist-G	NIO, Goa	
7	Dr. V. V. Gopalakrishna	Scientist-G	NIO, Goa	
8	Dr. C.M. Kishtawal	Scientist	MOG	
9	Dr. R.M. Gairola	Scientist	MOG	
10	Dr. Ajit Tyagi	DG,	IMD, New Delhi	
11	Dr. Sathish C Shenoi	Director	INCOIS	
12	Dr. G. V. Rama	DGM, MF & RO	SDSC, Sriharikota	
13	Dr. L. V. G. Rao	D D (Rtd), NIO, Goa	AS Rao Nagar, Hyd.	
14	Dr. R. V. Madala	Scientist, Rtd.	Kondapur, Hyd.	
15	Dr. J. V. Thamos	Scientist, NNRMS	ISRO, HQ	
16	JAYARAMAN V DR.	Director	NRSA, Hyderabad	
17	P. S. ROY DR.	Deputy Director	NRSA, Hyderabad	
18	KRISHNAMURTHY Y V N DR.	Deputy Director	NRSA, Hyderabad	
19	BEHERA G.	Group Director	NRSA, Hyderabad	
20	Ali M M DR.	HOD	NRSA, Hyderabad	
21	Bhanumurthy V	Head, DMSD	NRSA, Hyderabad	
22	Dr. P N Sridhar	Oceanography	NRSA, Hyderabad	
23	Shri. Bishwadeep Gharai	Oceanography	NRSA, Hyderabad	
24	Shri. K. H. Rao	Oceanography	NRSA, Hyderabad	
25	Dr. Anitha Gera	Oceanography	INCOIS, Hyd.	

Annexure-6

Committee Members

LIST OF COMMITTEE MEMBERS – OHC WORKSHOP

1. Dr. M M Ali - Convener
2. Shri. M. V. Rao - Coordinator
3. Shri. K. H. Rao
4. Dr. K. V. S. Badhrinath
5. Dr. P N Sridhar
6. Shri. I. V. Ramana
7. Dr. T. Anasuya
8. Dr. S. K. Sasmal
9. Shri. Bishwadeep Gharai
10. Dr. S. B Chaudury
11. Dr. P. V. Nagamani
12. Dr. Neeraja Sharma
13. Shri. V.B Sastry
14. Smt. A. Sita Ratnam
15. Shri. M. Ramu.
16. Shri. D. P. Sashikantha Rao
17. Shri. K. Sanathanan.
18. Ms. Anu Rani Sharma
19. Shailesh Kumar Karol
20. Sri. R. V. R. K. Raju
21. Shri E. Sai Baba
22. D. N. Rao
23. Solomon John
24. T. R. Narasimha Kumar
25. K. Narayana Rao
26. N. Raghunandan
27. S. Sudhakara Rao
28. D.V. Mahalakshmi

Annexure-7

Group Photo



Left to right: Sitting: 1. N. Sravanthi, 2. P. L. N. Murthy, 3. T. V. S. Udayabhasker, 4. P. S. Roy, 5. V. V. Gopalakrishna, 6. V. Jayaraman, 7. Gustavo Jorge Goni, 8. M. M. Ali, 9. G. Anitha, 10. T. Anasuya, 11. P. V. Nagamani, 12. Neeraja Sharma, 13. P. N. Sridhar, 14. G. V. Rama, 15. Rabindra Nayak

Standing: first row: 1. P. Yunus Ali, 2. Palash Sinha, 3. M. G. Keerthi, 4. Anil Kumar, 5. M. V. Rao, 6. Y. V. N. Krishna Murthy, 7. P. D. Kunte, 8. C. M. Kishtawal, 9. K. H. Rao, 10. M. R. Ramesh Kumar, 11. R. M. Gairola, 12. C. Gnanaseelan, 13. Roy Bhowmik, 14. D. V. Bhaskara Rao, 15. A. Smitha, 16. I. V. Ramana, 17. S. K. sasamal, 18. G. Behera, 19. C. S. Thomas, 20. M. V. Ramana Murthy, 21. S. B. Choudhury

Second row: 1. Stephen Paul, 2. S. Rahul, 3. V. P. Akil, 4. R. V. Madala, 5. P. S. V. Jagadeesh, 6. P. B. Rao, 7. P. V. Ramana Murthy, 8. G. Prasada Rao, 9. Krishna Kishore, 10. Suneel Vasimalla, 11. B. B. V. S. Vara Prasad